



Grinter, Rhys W. (2014) *Discovering colicin and lectin-like bacteriocins for the creation of disease resistant transgenic plants*. PhD thesis.

<https://theses.gla.ac.uk/5879/>

Copyright and moral rights for this work are retained by the author

A copy can be downloaded for personal non-commercial research or study, without prior permission or charge

This work cannot be reproduced or quoted extensively from without first obtaining permission in writing from the author

The content must not be changed in any way or sold commercially in any format or medium without the formal permission of the author

When referring to this work, full bibliographic details including the author, title, awarding institution and date of the thesis must be given

Enlighten: Theses

<https://theses.gla.ac.uk/>
research-enlighten@glasgow.ac.uk



University
of Glasgow

**Discovering Colicin and Lectin-like
Bacteriocins for the Creation of Disease
Resistant Transgenic Plants**

Submitted to the University of Glasgow for the degree of Doctor of
Philosophy

Rhys W. Grinter, Bbt (Hons)

Submitted 29/08/2014

Institute of Infection, Immunity and Inflammation
College of Medical, Veterinary and Life Sciences
University of Glasgow

Abstract

The colicin and lectin-like bacteriocins are a broad class of antimicrobial proteins produced by Gram-negative bacteria. They are generally narrow spectrum, killing or inhibiting the growth of closely related bacteria. Numerous Gram-negative bacteria that are important pathogens of both animals and plants produce and are susceptible to these bacteriocins. As such, these proteins represent an attractive alternative to traditional small molecule antibiotics for controlling bacterial infection.

Very little is known about bacteriocins produced by Gram-negative plant pathogens and so the aim of this work was to discover novel bacteriocins active against globally important plant pathogens from the genera *Pectobacterium* and *Pseudomonas*. The bacteriocins discovered in this study were then structurally and functionally characterised and assessed for their ability to impart disease resistance when expressed in a model transgenic system.

This study presents the discovery and characterisation of the bacteriocins syringacin M, syringacin L1 and pyocin L1 from the genus *Pseudomonas*, As well as the discovery and characterisation of the unusual ferredoxin containing pectocins from the genus *Pectobacterium*. Also presented is the discovery of a novel virulence related ferredoxin/iron-uptake system in *Pectobacterium*, which is parasitised by the pectocins for cell entry. Additionally, the transgenic expression of the bacteriocin putidacin L1 in both *Arabidopsis thaliana* and *Nicotiana benthamiana* was shown to provide these plants with resistance to infection by strains of the plant pathogen *P. syringae*.

Acknowledgements

The period of research encompassing the results I am presenting here has truly been a journey of scientific discovery. Before I started my PhD studies at Glasgow, I'd never done cloning or protein expression and only had the vaguest of ideas of how to apply things like X-ray crystallography, NMR or Mass Spec to the analysis of biomolecules. Needless to say this journey would have been incomplete and a lot less exciting without the people who I've worked with and been mentored by along the way. There isn't room to personally thank the many people who have assisted me with this project, but I am extremely grateful to all of you.

First and foremost I'd like to thank my supervisor Dr Daniel Walker for his enthusiasm and guidance at every stage of my project. It's a rare combination to have a supervisor who is incredibly supportive, interested and invested in a student's research, while also being comfortable giving them almost total free rein.

I would also like to thank my supervisor Dr Joel Milner, who guided the plant related aspects of the project, providing excellent advice based on decades of experience and was always up for a chat.

Next there is team Walker, namely: Kesha, Laura, Cameron, Carla and the late edition of Sharon. Without your ideas, inspiration, hard work and friendship my PhD would have been nowhere near as successful or enjoyable. I'm sure once we part ways, all of you will do very well, best of luck with the future.

Finally, I'd like to thank Dr Aleks Roszak for his extensive guidance on my journey from purified protein to crystal structure. Without your help and sometimes protracted discussions, it would have been impossible to gain the practical knowledge of how to solve a crystal structure.

Declaration

Unless explicitly states otherwise, all of the experimental work presented in this thesis was performed by me, either independently or in conjunction with others. No part of this research or any part of this document has or will be presented for the fulfilment of any other degree or qualification.

Rhys Grinter

29/08/2014

Abbreviations

AA – Amino acid	IUTD – Intrinsically unstructured translocation domain
ASU – Asymmetric unit	KB – Kings B media
ATP – Adenosine triphosphate	KO - Knockout
BCCM – Belgian coordinated collection of microorganism	LB – Lysogeny Broth
CD – Circular dichroism	LC-MS/MS – Liquid chromatography tandem mass-spectrometry
CPA – Common polysaccharide antigen	LDAO - N,N-Dimethyldodecylamine N-oxide
CSP – Chemical shift perturbation	LPS - Lipopolysaccharide
DDM – n-Dodecyl- β -D-maltopyranoside	MAD – Multiple wavelength anomalous dispersion
DLS – Diamond Lightsource	MBPR – Pectocin M2
DMD – Discrete molecular dynamics	MDC – Syringacin M
DMSO – Dimethyl sulfoxide	MES – 2-(N-morpholino)ethanesulfonic acid
DNA – Deoxyribonucleic acid	MIC – Minimum inhibitory concentration
DTT – Dithiothreitol	MMBL – Monocot mannose binding lectin
EDTA - Ethylenediaminetetraacetic acid	MME – Monomethyl ether
EGTA - ethylene glycol tetraacetic acid	MOPS – 3-(N-morpholino)propanesulfonic acid
FPP-MUB – N-acetylmuramic acid farnesyl pyrophosphate	MPCI – Pectocin M1
GFP – Green fluorescent protein	MPD – 2-Methyl-2,4-pentanediol
GM – Genetically Modified	MR – Molecular replacement
GNA - <i>Galanthus nivalis</i> agglutinin	MS (agar) - Murashige and Skoog agar
HAD - Haloacid dehydrogenase	MS/MS – Tandem mass spectrometry
HEPES - 4-(2-hydroxyethyl)-1-piperazineethanesulfonic acid	Mw – Molecular weight
HSQC – Heteronuclear single quantum coherence spectra	NCPPB – National collection of plant pathogenic bacteria
INDEL – Insertion/deletion mutation	
IPTG - Isopropyl β -D-1-thiogalactopyranoside	
ITC – Isothermal titration calorimetry	

NMR – Nuclear magnetic resonance

NZD – New Zealand dollar

OM – Outer membrane

ORF – Open reading frame

PBP – Penicillin binding protein

PCR – Polymerase chain reaction

PDB – Protein databank

PEG – Polyethylene glycol

PL1 – Putidacin L1

PMF – Proton motive force

PVP – Polyvinylpyrrolidone

RE – Restriction enzyme

RMSD – Root mean square deviation

RNA – Ribonucleic acid

rRNA – Ribosomal ribonucleic acid

SAD – Single wavelength anomalous dispersion

SAXS – Small angle X-ray scattering

SCRI – Scottish crop research institute

SDS-PAGE – Sodium dodecyl sulphate polyacrylamide gel electrophoresis

SEC – Size exclusion chromatography

SL1 – Syringacin L1

SLS – Swiss Lightsource

SNI – Single nucleotide insertion

SNP – Single nucleotide polymorphism

SNV – Single nucleotide variation

SV – Sedimentation velocity

TLC – Thin layer chromatography

TRIS - Tris(hydroxymethyl)

aminomethane

tRNA – Transfer ribonucleic acid

USD – United states dollar

UV – Ultraviolet

β-OG - n-Octyl-β-D-glucoside

1	Introduction	1
1.1	Aim of this study.....	2
1.2	Plant disease and bacterial phytopathogens	2
1.3	Phytopathogenic bacteria targeted in this work.....	3
1.3.1	Pseudomonas syringae	4
1.3.2	Pectobacterium	6
1.4	Bacteriocins: structure function and mechanism of action	8
1.4.1	Overview	8
1.4.2	Colicin-like bacteriocin domain structure and evolution.....	14
1.4.3	Genetic structure and regulation.....	14
1.4.4	Cytotoxic mechanisms of colicin-like bacteriocins	16
1.4.5	Lectin-like bacteriocins	23
1.4.6	Cell surface binding and entry by colicin and lectin-like bacteriocins.....	26
1.5	Colicin and lectin-like bacteriocins produced by phytopathogenic bacteria	30
1.6	Utilisation of bacteriocins to combat bacterial disease in plants	31
1.6.1	Current implementation of bacteriocins in the bio-control of phytopathogenic bacteria	31
1.6.2	Utilising bacteriocins to create transgenic plants.....	32
2	Materials and Methods.....	34
2.1	Chemicals and growth media	35
2.2	Bacterial strains, plasmids and growth conditions	35
2.3	DNA manipulations.....	41
2.3.1	Polymerase chain reaction.....	41
2.3.2	DNA Ligation.....	47
2.3.3	Electrophoresis.....	47
2.3.4	Extraction of genomic DNA	47

2.3.5	Plasmid DNA extraction	48
2.3.6	Bacterial transformation	48
2.3.7	Creation of deletion mutants in <i>Pectobacterium</i>	48
2.4	Determination of protein concentration	49
2.5	Bacteriocin toxicity assays.....	50
2.5.1	Overlay spot plate method	50
2.5.2	Liquid growth assays	50
2.6	Identification of bacteriocins by ammonium sulphate precipitation	51
2.7	Isolation of bacteriocin tolerant mutants	51
2.8	Lipid II cleavage assay.....	52
2.9	SDS-PAGE, silver staining and immunoblotting	52
2.10	LPS purification and isolation of LPS-derived polysaccharide.....	53
2.11	Whole genome sequencing	53
2.12	Isothermal titration calorimetry	54
2.13	Identification of FupA by pull down	54
2.14	Recombinant protein expression and purification	56
2.14.1	Syringacin M.....	56
2.14.2	Pectocin M1, M2 and P	57
2.14.3	Putidacin and syringacin L1.....	57
2.14.4	FupA	58
2.15	Crystallisation, data collection and structure solution.....	59
2.15.1	Syringacin M.....	59
2.15.2	Pectocin M2	62
2.15.3	Pyocin L1	64
2.15.4	FupA crystallisation	66
2.15.5	Crystallisation of syringacin L1 and pectocins P	67

2.16	NMR	68
2.16.1	For pyocin L1	68
2.16.2	For FupA	68
2.17	Analytical ultracentrifugation	69
2.18	SAXS data collection and analysis	69
2.19	Lipid II docking simulations.....	70
2.20	Plant transformation and infection	70
2.20.1	Transient expression of bacteriocins in <i>Nicotiana benthamiana</i>	70
2.20.2	<i>P. syringae</i> infection of <i>N. benthamiana</i>	71
2.20.3	Stable transformation of <i>Arabidopsis thaliana</i> with bacteriocins	72
2.20.4	<i>P. syringae</i> infection of transgenic <i>Arabidopsis</i>	73
3	Discovery and characterisation of syringacin M from <i>Pseudomonas syringae</i> pv. tomato DC3000	74
3.1	Introduction.....	75
3.2	Screening of <i>P. syringae</i> isolates for bacteriocin production and the identification of syringacin M	75
3.3	Domain structure of syringacin M.....	78
3.4	The crystal structure of syringacin M.....	79
3.5	Structural description of syringacin M	80
3.6	The receptor binding domains of colicin M and syringacin M show extensive structural similarity	82
3.7	Comparison of the syringacin M and colicin M active sites	84
3.8	Isolation and characterisation of syringacin M resistant mutants.....	88
3.9	Discussion	90
4	Discovery and characterisation of pectocins from <i>Pectobacterium spp</i>	94
4.1	Introduction.....	95
4.2	Identification of pectocin M genes in the genomes of <i>Pectobacterium spp</i>	96

4.3	Evolution of the pectocin M1 gene through gene duplication and recombination	98
4.4	Purification and characterisation of pectocin M1 and M2	99
4.5	The ferredoxin domain of pectocins M1 and M2 mediate receptor binding	101
4.6	Growth enhancement under iron limiting conditions by pectocins and spinach ferredoxin.....	102
4.7	The crystal structure of pectocin M2	104
4.8	Pectocin M2 is conformationally flexible	108
4.9	Pectocin M2 can adopt a highly extended conformation and exists as two distinct subpopulations in solution.....	109
4.10	The ferredoxin domain is a generic module for the delivery of cytotoxic domains to the periplasm	114
4.11	The pectocin M2 cytotoxic domain has well defined substrate binding site	115
4.12	Isolation and characterisation of pectocin M1 resistant mutants	121
4.13	Discussion	124
5	Identification and characterisation of the ferredoxin uptake (Fup) receptor in <i>Pectobacterium</i>	126
5.1	Introduction.....	127
5.2	Identification of the pectocin receptor (FupA)	128
5.3	Genetic confirmation of FupA as the pectocin/ferredoxin receptor	131
5.4	Expression purification and characterisation of FupA	133
5.5	Analysis of FupA-ferredoxin interaction by NMR.....	135
5.6	Plant ferredoxins of different origin enhance <i>Pectobacterium</i> growth to a variable extent	140
5.7	Crystallisation of FupA.....	143
5.8	Discussion	144

6	Characterisation and identification of cell surface receptor of lectin-like bacteriocins from <i>Pseudomonas spp.</i>	149
6.1	Introduction.....	150
6.2	Putidacin L1 and syringacin L1 are active against multiple strains of <i>P. syringae</i> 151	
6.3	Characterisation of effect of putidacin L1 on bacterial cells.....	155
6.4	Phenotypic and genetic analysis of putidacin L1 tolerant <i>P. syringae</i> strains.....	157
6.5	Pyocin L1 targets the common polysaccharide antigen (CPA) of <i>P. aeruginosa</i> LPS 161	
6.6	Pyocin L1 binds the monosaccharide D-rhamnose	164
6.7	D-rhamnose binds to the C-terminal QxDxNxVxY motifs of pyocin L1	167
6.8	Putidacin L1 binds to <i>P. syringae</i> LPS and D-rhamnose	175
6.9	Discussion	177
7	Expression of bacteriocins in plants to provide resistance against bacterial pathogens 180	
7.1	Introduction.....	181
7.2	Transient expression of bacteriocins in <i>N. benthamiana</i> leaves using agroinfiltration	182
7.3	Creation of signal peptide bacteriocin fusion proteins for extracellular targeting 187	
7.4	<i>P. syringae</i> infection of transiently transformed <i>N. benthamiana</i>	187
7.5	Creation and characterisation of stable <i>A. thaliana</i> expressing putidacin and syringacin L1	190
7.5.1	Vector construction and characterisation	190
7.5.2	Transformation and characterisation of Arabidopsis	191
7.6	Putidacin L1 expressing Arabidopsis displays resistance to susceptible <i>P. syringe</i> strains.....	197
7.7	Discussion	201

8	Concluding Remarks.....	204
8.1	Key findings of this study.....	205
8.2	Future work	206
8.2.1	Analysis of the M-class active site.....	207
8.2.2	Conformation of the syringacin M receptor	207
8.2.3	Characterisation of the Fup operon and its role in iron acquisition.....	208
8.2.4	Determination of the molecular target of lectin-like bacteriocins.....	208
8.2.5	Optimisation of lectin-like bacteriocin production in plants.....	209
9	Supplemental Data.....	210
10	References.....	219
11	Publications related to this work	239

List of Figures

Figure 1-1 Trunk lesions on Kiwifruit (<i>Actinidia spp.</i>) as a result of infection by <i>Pseudomonas syringae</i> pv. <i>actinidiae</i>	5
Figure 1-2 Cut potato tuber inoculated with <i>P. carotovorum</i> LMG2410 and incubated at 30°C degrees for 72 hours,.....	8
Figure 1-3 Colicins with different cytotoxic mechanisms share a common modular domain structure, and conserved structural features	11
Figure 1-4 Pyocin domain structure mirrors that found in the colicins	12
Figure 1-5 Colicins are constituted by distinct combinations of structurally related cell entry and cytotoxicity domains.....	14
Figure 1-6 The structure of the colicin H-N-H nuclease domain.....	19
Figure 1-7 2D-schematic of peptidoglycan precursor molecule lipid II from Gram-negative bacteria (93)	21
Figure 1-8 Pore forming colicins utilise receptor binding and translocation domains of diverse structure to deliver a common cytotoxic domain to the periplasm.	23
Figure 1-9 The lectin-like bacteriocins share a common structure and evolutionary origin with plant MMBL lectins.....	25
Figure 1-10 Binding of colicin E3 to its cell surface receptor BtuB	29
Figure 1-11 Cell entry and cytotoxicity of A- and B-group colicins	29
Figure 2-1: Outline of pull down experiment for the identification of FupA	56
Figure 3-1 Identification of the bacteriocin produced by <i>Pss.</i> LMG1247	77
Figure 3-2 Purification and characterization of wildtype syringacin M and deletion mutants	78
Figure 3-3 Crystal structure of syringacin M.....	80
Figure 3-4 Sequence alignment of colicin and syringacin M.	82
Figure 3-5 The receptor binding and cytotoxic domains of syringacin M and colicin M show structural homology	84
Figure 3-6 Comparison of the syringacin M and colicin M active sites.....	85
Figure 3-7 Dependence of syringacin M activity on divalent metal ions.....	87
Figure 3-8 Susceptibility of wildtype and mutant <i>P. syringae</i> LMG5456 strains to syringacin M	90
Figure 3-9 Graphical representation of mechanisms of diversification of bacteriocins.	93
Figure 4-1 Domain structure, homology and molecular phylogeny of Pectocins M1 and M2	97
Figure 4-2 Genomic context of the pectocin M1 gene	99
Figure 4-3 Purification and characterisation of pectocin M proteins.	100
Figure 4-4 Interference of pectocin M1 killing by inactive pectocins and plant ferredoxin but not human adrenodoxin.	103
Figure 4-5 Growth enhancement of <i>P. carotovorum</i> subspp. <i>carotovorum</i> LMG 2410 by plant-like ferredoxin containing proteins.....	104

Figure 4-6 The crystal structure of pectocin M1 reveals a ferredoxin-containing colicin-like bacteriocin that lacks an IUTD.....	107
Figure 4-7 Conformational difference between ferredoxin domains in the P2 ₁ crystal form....	107
Figure 4-8 SAXS shows pectocin M2 is flexible.....	111
Figure 4-9 Analysis of conformational heterogeneity of pectocin M2 reveals compact and extended ensembles in solution.	112
Figure 4-10 Pectocin M2 P3 ₁ 21 structure confirms extended conformation predicted by solution scattering.	113
Figure 4-11 Growth inhibition of purified pectocins.....	114
Figure 4-12 Pectocin M1 and M2 cleave lipid II.	115
Figure 4-13 The flexible active site of M-class bacteriocins.....	118
Figure 4-14 The lipid II substrate model utilised for docking into the active site of pectocins M2 and syringacin M.....	119
Figure 4-15 <i>In silico</i> docking of lipid II analogue reveals active-site binding site in an open and closed conformation.....	121
Figure 4-16 Mutations in the histidine sensor kinase EnvZ in <i>Pba</i> . LMG2386 conferring resistance to pectocins M1.....	123
Figure 5-1 Co-purification of <i>Pectobacterium</i> membranes with pectocin M1 identifies the ferredoxin receptor FupA.....	130
Figure 5-2 FupA knockout confers resistance to pectocin M1 in <i>Pbc</i> . LMG2386,.....	132
Figure 5-3 Purified FupA separated on an 8% SDS-PAGE gel, visualised by coomassie staining.	133
Figure 5-4 Validation of refolding of FupA.	134
Figure 5-5 1H-15N HSQC spectrum of ¹⁵ N labelled Arabidopsis ferredoxin.	136
Figure 5-6 Interaction of pectocin M1 with the ferredoxin receptor (FupA) from <i>Pectobacterium atrosepticum</i> SCRI1043,	137
Figure 5-7 Mapping of NMR chemical shift data and sequence variation onto a model of the pectocin M1 ferredoxin domain.....	139
Figure 5-8 Plant ferredoxin enhance growth of <i>Pectobacterium</i> strains to varying extent.	141
Figure 5-9 Sequence alignment of plant ferredoxins and pectocin M1 ferredoxin domain.....	142
Figure 5-10 The ferredoxin uptake operon (<i>fup</i>) <i>Pectobacterium</i>	146
Figure 5-11 The extended conformation of pectocin M2 has dimensions compatible with passage through the lumen of a TonB-dependent receptor.	147
Figure 6-1 Purified of putidacin and syringacin L1.....	152
Figure 6-2 Sequence alignment of reported MMBL-like bacteriocins. Dark blue shading designates sequence identity; light blue designates chemically conserved residues. The three conserved MMBL sugar-binding motifs (N1, C1 and C2) and the partially conserved motif (N2) are boxed in red.	155
Figure 6-3 Change in OD ₆₀₀ of <i>P. syringae</i> LMG2222 treated with putidacin L1,	156
Figure 6-4 Phenotypic changes in <i>P. syringae</i> LMG2222 induced by putidacin L1 treatment ..	157

Figure 6-5 Isolation and characterisation of putidacin L1 resistant mutants.....	159
Figure 6-6 CPA production correlates with pyocin L1 killing.	162
Figure 6-7 Pyocin L1 binds strongly to CPA from <i>P. aeruginosa</i> PAO1.	163
Figure 6-8 Pyocin L1 shows specificity for D-rhamnose compared with D-mannose.	165
Figure 6-9 1H-15N HSQC spectra of 15N-labelled pyocin L1 in presence (red) and absence (black) of 100 mM (A) D-rhamnose and (B) D-mannose	167
Figure 6-10 Crystal structure of pyocin L1 reveals tandem MMBL domains and sugar-binding motifs.	169
Figure 6-11 Small angle X-ray scattering of pyocin L1.....	169
Figure 6-12 C-terminal MMBL-sugar binding motifs of pyocin L1 bind D-rhamnose and D- mannose. Electron density (at 1.3 σ) with fitted stick model of pyocin L1 MMBL-sugar binding site C1	171
Figure 6-13 Hydrogen-bonding interactions between pyocin L1 MMBL sugar-binding motif C1 with D-rhamnose and D-mannose.....	172
Figure 6-14 Coordination of D-rhamnose in C1, C2 and N2 binding sites of pyocin L1.....	173
Figure 6-15 Binding of the CPA at the C-terminal sugar binding motifs, C1 and C2, is critical to pyocin L1 cytotoxicity.	174
Figure 6-16 Putidacin L1 binds strongly to LPS-derived polysaccharides from susceptible but not tolerant or resistant <i>P. syringae</i> isolates.	176
Figure 6-17 Putidacin L1 shows specificity for D-rhamnose, compared with D-mannose.....	177
Figure 7-1 Confocal fluorescence microscopy of GFP-bacteriocin fusions transiently expressed in <i>N. benthamiana</i> leaves	183
Figure 7-2 Confirmation of bacteriocin expression in <i>N. benthamiana</i> leaves by western blotting	185
Figure 7-3 Growth inhibition of <i>P. syringae</i> by leaf extracts from bacteriocin transformed <i>N.</i> <i>benthamiana</i> ,.....	186
Figure 7-4 Infection of transiently transformed <i>N. benthamiana</i> leaves with <i>P. syringae</i> LMG 5084,.....	190
Figure 7-5 Expression and activity of C or N-terminally 4xMyc tagged putidacin L1 in <i>N.</i> <i>benthamiana</i>	191
Figure 7-6 Phenotypic differences between wildtype and putidacin L1/syringacin L1 transformed Arabidopsis seedlings, selected on hygromycin agar.....	192
Figure 7-7 Expression of putidacin L1 N-Myc by T0 generation transformed Arabidopsis	194
Figure 7-8 Expression putidacin L1 N-Myc by T1 generation transgenic Arabidopsis, assessed by spot test of leaf extract on LMG 5084.	196
Figure 7-9 Putidacin L1 expression by putidacin L1 N-Myc T2 transgenic Arabidopsis	197
Figure 7-10 Infection by leaf infiltration of wildtype and putidacin L1 N-Myc (Line 1(2)) Arabidopsis, with <i>P. syringae</i> LMG5084.....	200
Figure 9-1 Images of protein crystals produced during this study.	211
Figure 9-2 Examples of diffraction produced by protein crystals produced during this study.	212

Figure 9-3 Structure and CD spectra of syringacin M D232A mutant	213
Figure 9-4 The relationship between OD ₆₀₀ and Cf.u.ml ⁻¹ for <i>P. syringae</i> strain LMG2222	214

List of Tables

Table 2-1 Strains utilised, isolated or derived during this study	35
Table 2-2 Plasmids utilised or created in this study	37
Table 2-3 Primers utilised and created during this study	41
Table 2-4 Standard PCR Reaction Components	45
Table 2-5 Standard PCR Reaction Components	45
Table 2-6 Mutagenesis PCR Conditions.....	46
Table 2-7 Mutagenesis PCR Reaction Components	46
Table 2-8 Data collection and refinement statistics for syringacin M.....	61
Table 2-9 Data collection and refinement statistics for pectocins M2	63
Table 2-10 Data collection and refinement statistics for pyocin L1	65
Table 2-11 Data collection statistics for FupA.....	67
Table 5-1 Growth enhancement of <i>Pectobacterium</i> strains by plant ferredoxin.	142
Table 6-1 Susceptibility and sensitivity of <i>P. syringae</i> strains tested to putidacin and syringacin L1.	153
Table 7-1 Analysis of hygromycin resistance of T1 generation putidacin L1 N-Myc transformed Arabidopsis.....	195
Table 7-2 Qualitative assessment of disease symptoms on leaves of wildtype and putidacin L1 N-Myc Arabidopsis, infected with 10 ⁷ cfu.ml ⁻¹ of <i>P. syringae</i> LMG5084	201
Table 9-1 Production of antimicrobial compounds by <i>P. syringae</i> strains antagonistic to <i>P. syringae</i> growth.....	215
Table 9-2 Susceptibility of <i>Pectobacterium</i> strains to pectocin M1 at different concentrations of bipryidine	216
Table 9-3 Susceptibility of <i>Pectobacterium</i> strains to pectocin M2 at different concentrations of bipryidine	216
Table 9-4 Growth enhancement of <i>Pectobacterium</i> strains by spinach ferredoxin at different concentrations of bipryidine	217
Table 9-5 Killing spectrum of leaf extracts from transiently transformed <i>N. benthamiana</i> leaves	217

1 Introduction

1.1 Aim of this study

The broad objective that formed the basis of this study was to investigate the potential of colicin- and lectin-like bacteriocins, highly potent, narrow spectrum protein antibiotics, as a tool for combating bacterial disease in plants.

Bacteriocins are widely produced by Gram-negative bacteria for intra-species competition and have potential for the treatment of bacterial disease of both plants and animals. Despite this potential, very little research has been performed on the structure and mechanisms of bacteriocins produced by (and thus active against) plant pathogens or their potential application to disease prevention in crops.

As such, the aims of this study were to:

1. Identify novel bacteriocins produced by the plant pathogenic bacteria, *Pseudomonas syringae* and *Pectobacterium spp.*
2. To characterise these bacteriocins, providing information about their structure, mechanism of action and host range
3. To express suitable proteins identified in aims 1 and 2, in the model plants *Nicotiana benthamiana* and *Arabidopsis thaliana* to provide a preliminary indication of the ability of bacteriocin expressing transgenic plants to resist bacterial infection

1.2 Plant disease and bacterial phytopathogens

Feeding a rapidly growing world population is one of this century's key scientific challenges. Currently humanity relies on just fourteen crop plants to provide more than 90% of its basic nutritional requirements. This number is further reduced when it is considered that the big four; rice, wheat, maize and potato constitute the vast majority of this 90% (19). Modern crop plants are grown over wide areas, distant from their geographic origins and have been bred to near genetic homogeneity through the selection of individuals producing the greatest yield (20). The results of this genetic homogeneity and the large scale monocultures of modern agriculture make plant crops prone to disease, often with devastating consequences (21). Additionally, the

vulnerability of crop plants to disease in some regions is likely to be exacerbated by climate change, creating a further challenge to food security (22). Bacteria are responsible for a significant proportion of the > £100 billion *per annum* lost worldwide to disease and spoilage of crops caused by plant pathogens (19). Gram-negative bacterial pathogens account for much of these losses and cause disease in all of the major plant-crops (23). Significant Gram-negative plant pathogens include:

- Enterobacterial soft-rot pathogens of the genus *Pectobacterium* and *Dickeya* which cause significant damage to potato and other field vegetables across Europe and worldwide, with losses as high as 25 % reported for some potato cultivars (24).
- *Xanthomonas oryzae pv. oryzae* the causal agent of bacterial blight and bacterial leaf spot in rice constrains the growth of this crop over much of Africa and Asia, with losses as high as 75% reported (25). *Xanthomonas* species also cause diseases with analogous symptoms in maize, sugar cane and plantain (26,27).
- *P. syringae* which causes serious disease in a number of major plant crops, with major recent outbreaks in New Zealand threatening the kiwifruit industry and in the UK threatening the horse chestnut. (28,29)

1.3 Phytopathogenic bacteria targeted in this work

The phytopathogenic bacterial species *Pseudomonas syringe*, *Pectobacterium atrosepticum* and *Pectobacterium carotovorum* were selected as the target organisms for this study as they represent globally distributed, economically significant pathogens of multiple agricultural crops that are known to produce bacteriocins (30,31). Because of their importance they have been the focus of relatively intensive study, with a considerable number of annotated genome sequences available in public databases. These genome sequences allow rapid identification of putative bacteriocin genes and operons, based on homology to previously characterized bacteriocins from other Gram-negative bacteria. In order to determine how bacteriocins can best be applied to combat infection by these pathogens, it is important to understand the bacteria's physiology and pathogenic mechanisms, and as such these are discussed briefly below.

1.3.1 *Pseudomonas syringae*

The phytopathogen *P. syringae* is a Gram-negative, rod-shaped, obligate aerobe, belonging to the γ subclass of the Proteobacteria. The first *P. syringae* strain was isolated from diseased lilac (lilac genus name = *Syringa*) in 1899, hence the species name (32). Historically, *P. syringae* had been divided into pathovars based on the host plant from which it was isolated, as well as the disease symptoms it causes. This classification scheme has led to the designation of approximately 57 pathovars (33).

Although it is still in use, the use of pathovars to classify *P. syringae* has been shown to be inconsistent with contemporary genetic and biochemical studies, which have found a pattern of relatedness different to pathovar classification (34,35). Phylogenetic analysis based on multilocus sequence typing shows that *P. syringae* can be broadly divided into 4 groups, with strains assigned to the same pathovar frequently distributed among different phylogenetic groups (36). Consequently, predictions of relatedness based on pathovar designation are unreliable, and there is significant contention in the literature about the best method for classification of members of this diverse species (34).

As indicated by the wide range of pathovars classified, *P. syringae* causes disease in a wide range of economically important plant species, including 'bacterial speck' on tomato, 'leaf spot' of soy bean, and trunk cankers and 'blast' diseases on woody tree fruits and olive (37). Individual pathogenic strains are generally specialized and are pathogenic only to a single or small number of plant species (32). *P. syringae* has a hemibiotrophic mode of infection, causing disease in the leaves of the host plant by invading the apoplast of the leaf through the stomata. Once it has invaded the leaf it multiplies intercellularly without invading the host plant cells. In this intercellular phase it subverts host defences by injecting numerous effectors into the host cells, via the type III secretion system (38). This most aggressive phase of intercellular growth occurs in the absence of cell death. However, in the later stages of disease, as the plant succumbs to infection, infection is associated with extensive necrosis of infected tissues (38,39). *P. syringae* also infects the ligneous tissues of woody plants, leading to the formation of characteristic lesions or cankers (40).

In addition to its pathogenic lifestyle, *P. syringae* is widely present in the environment and is a common isolate from the epidermis of plant leaves, where it can exist and grow

in a non-pathogenic state (32). It has also been suggested that *P. syringae* has an important role in global weather by stimulating cloud formation through the production of ice nucleation proteins (32).

An illustration of the importance of *P. syringae* as a disease causing agent in global agriculture is the epidemic infection of kiwifruit by strains of *P. syringae* *pv.* *actinidiae*. Serious outbreaks of infection of kiwifruit by this strain were first reported in Japan in the 1980's, and subsequently serious losses to kiwifruit production have been reported in continental Asia, Europe and New Zealand (41). A recent review of this disease suggested that losses of up to \$410 million NZD (209 million GBP) are predicted over the next 5 years (42). Antibiotics such as streptomycin, kanamycin or tetracycline and copper salts have been used extensively to treat *P. syringae* *pv.* *actinidiae*, however they rarely succeed in eradicating infection and high levels of resistance to these compounds are now endemic in pathogen populations (29). The development of new control strategies are urgently required, both to decrease losses due to *P. syringae*, but also to provide an alternative to the use of valuable antibiotics required to treat human infection.



Figure 1-1 Trunk lesions on Kiwifruit (*Actinidia* spp.) as a result of infection by *Pseudomonas syringae* *pv.* *actinidiae*.

(Source: <http://www.infojardin.com/foro/showthread.php?p=6960593&posted=1>)

1.3.2 *Pectobacterium*

The genus *Pectobacterium* contains Gram-negative plant pathogens of the family *Enterobacteriaceae* that exhibit both broad and restricted host ranges. Members of this genus cause soft rot, stem rot, bacterial wilt, and black leg disease in angiosperm species representing over 35% of plant orders (including the economically important crop plants, potato, sugar beet, maize, pineapple and cabbage). The genus has been divided into four species (*Pectobacterium atrosepticum*, *betavasculorum*, *carotovorum* and *wasabiae*) based on multiple genetic and phenotypic factors. However, these classifications are inconsistently applied and somewhat contentious (43,44). Generally, strains from *carotovorum*, *wasabiae* and *carotovorum subsp. brasiliensis* (discussed below) are all broad host range, with *atrosepticum* being restricted to potato and *betavasculorum* to sugar beet (45). A study by Ma et al (2007) using multilocus sequence analysis of a number of housekeeping genes of 36 members of these species found that species designations correlated cladistically for these genes, with the exception of recently identified *P. carotovorum subsp. brasiliensis* which formed a separate Clade (I) (45). Based on this evidence the authors suggested that the classification of *brasiliensis* warrants a separate species designation and is sometimes reported as such (46,47).

Members of the genus *Pectobacterium* were previously assigned to the genus *Erwinia* and like *Erwinia* species more generally they are distinguished by the production of large quantities of pectin and cellulose degrading enzymes that enable them to macerate parenchymatous tissues of plants. This leads to a characteristic soft rot disease phenotype (Figure 1-2) (45). Geographically only *P. carotovorum* and *P. atrosepticum* have been reported in the same environments. *P. carotovorum* strains are found worldwide, while *P. atrosepticum* is generally found in cool climates (43). Ecologically and genetically much more information is available about *P. carotovorum* and *atrosepticum* than other species. *P. atrosepticum* is of specific interest to this study as it causes black leg and soft rot disease in the stems and tubers of potato during growth and storage and together with the closely related soft rot pathogen *Dickeya dadantii*, is the most damaging bacterial pathogen of potato in Europe (30). Recent estimates place losses as high as 22 % of total potato production due to these pathogens and associated diseases (48).

The main virulence mechanism of *P. atrosepticum* and *D. dadantii* in potato is the quorum sensing coordinated production of a prolific variety of plant cell wall degraded enzymes, which are secreted into the extracellular environment by the Type I and Type II secretion systems (49). In addition, the delivery of the cognate effector DspA/E and helper/hairpin proteins (HrpN/HrpW) by the Type III secretion system have been shown to be required for full virulence (50). In potato, *P. atrosepticum* and *D. dadantii* cause black leg in plants in the field and soft rot of tubers post-harvest. They are also known to live asymptotically as epiphytes or saprophytes in the soil or groundwater, making their control difficult (51). During the early stages of infection, plants begin to yellow and wilt in the absence of environmental stress (i.e. water shortage). Blackleg lesions then can develop *de novo* in the stem well above ground level; however in the vast majority of cases lesions start at the base of the stem at the point of contact with an already infected and decaying mother tuber. Soft rot *Pectobacterium spp.* are primarily vascular pathogens when inoculated directly into stems and progressive decay of stem tissue follows movement of the bacteria through the vascular system. In tubers, rotting initially starts in small pockets, generally under wet anaerobic conditions and rapidly consumes the tuber (52).

Current strategies for the control of these and other pathogens are limited to the application of copper compounds and high levels of sanitation during handling of food tuber and seed stock. Copper compounds can be effective in preventing infection but are ineffective once infection is established (53). Prevention and control of *Pectobacterium* and *Dickeya* infection remains challenging due to their wide environmental distribution and latent infection of tubers, weeds and rotation crops (53). The development of alternative strategies, are required for the control of this significant agricultural pathogen (54,55).

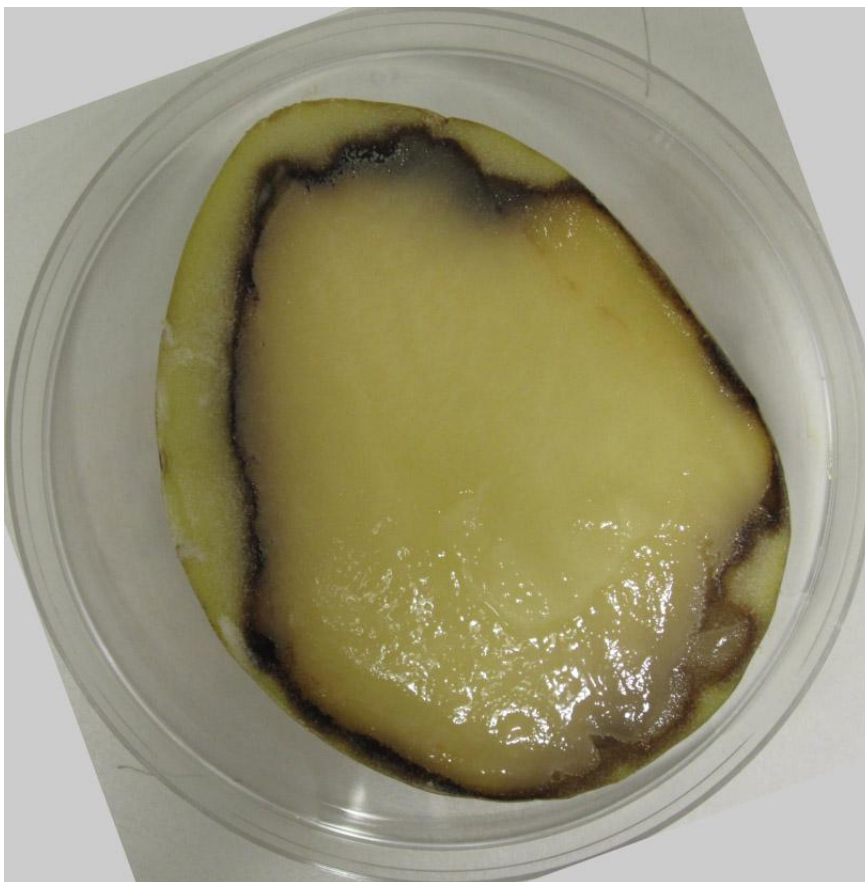


Figure 1-2 Cut potato tuber inoculated with *P. carotovorum* LMG2410 and incubated at 30°C degrees for 72 hours,
Over 70% of the tuber was macerated at this point.

1.4 Bacteriocins: structure function and mechanism of action

1.4.1 Overview

Life is a competitive business. Not least for bacteria who being single celled and tiny have limited capacity as individuals to modify their environment. Energy and nutrients required for growth and the environments in which they are found are limited, and as such competition between microbes occupying the same environmental niche is fierce. This competition results in a dynamic struggle for survival. This struggle provides the impetus for the evolution of systems that prevent the growth of competitor organisms directly by interfering with their cellular machinery or structure in a way which inhibits metabolism and growth, and/or leads to lysis and cell death. This struggle is as old as life itself, and the results of more than 3.8 billion years of evolution (56) are seen in the considerable

variety of anti-microbial compounds that have been discovered and the certain existence of a wealth of systems and compounds still to be discovered and characterized (57).

These compounds range from small molecule antibiotics, such as those currently used in clinical practice, to antimicrobial peptides and proteins, through to large multi protein complexes which appear to result from the genetic debris of phage infection (58).

Bacteriocins are loosely defined as: biologically active proteins or peptides with a bactericidal or bacteriostatic mode of action (59). This definition is applied across the literature to describe a variety of compounds from small peptide anti-microbials to the large phage tail complexes such as the R and F-type pyocins (58,60). Bacteriocins are generally produced during times of nutrient and environmental stress as weapons to kill close competitors, increasing the proportion of available resources and thus the chances of survival for the bacterial population producing them (57).

Colicin- and lectin-like bacteriocins which form the focus of this study represent a subclass of bacteriocins, consisting of proteins between 25-80 kDa with a modular domain structure and a variety of cytotoxic mechanisms, including nucleic acid degradation, inner-membrane pore formation or interference with peptidoglycan synthesis (59). This class of bacteriocin is typified by the intensively studied colicins of *Escherichia coli* and the S-type pyocins of *Pseudomonas aeruginosa*. The colicins of *E. coli* are the most extensively studied group of these proteins, with a domain structure generally consisting of an N-terminal translocation domain, which facilitates transport of the protein into the target cells, followed by a receptor binding domain which interacts with receptors on the surface the target cell, forming the initial contact between the bacteriocin and its target. The C-terminal domain of these proteins contains a functional domain with killing activity and for nuclease colicins, the region to which an associated immunity protein binds (4). The killing activity of this domain varies between colicins displaying; membrane pore forming activity, endonuclease activity (DNase, tRNase, and rRNase) or a phosphatase directed against lipid II which abolishes peptidoglycan synthesis (61).

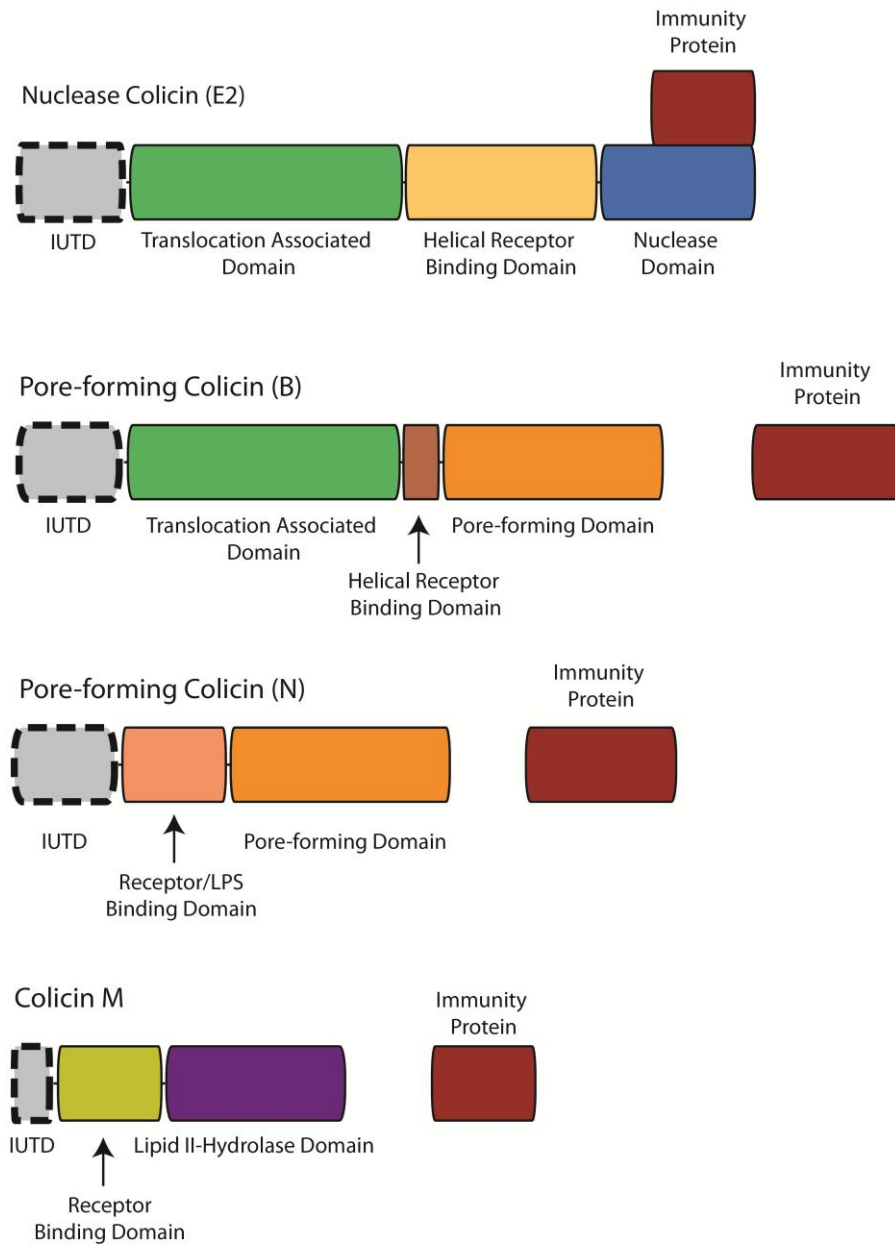
The pyocins of *P. aeruginosa* are evolutionarily related to colicins, share a modular domain structure and have C-terminal cytotoxic domains homologous in structure and function. However, while pyocins share a similar modular structure and are composed of structurally analogous domains the order of the domains is different to that of the

colicins. In addition, colicins are often encoded on 'colicinogenic' plasmids, whereas the pyocins discovered to date are chromosomally encoded (62).

Putative bacteriocins with a similar structure to the colicins and pyocins have been identified in numerous other members of the γ -proteobacterial family including;

Pseudomonas fluorescens, *Pseudomonas putida*, *P. syringae*, *Klebsiella pneumonia*, *Yersinia pestis*, *Photobacterium luminescens*, *P. atrosepticum* and *P. carotovorum* (11,58).

Information available about the various structural and functional features of this class of bacteriocin are reviewed below, primarily using data available for colicins as they constitute the best characterised examples. A schematic showing the size and domain structure of representative colicins and pyocins is provided in Figure 1-3 and Figure 1-4.

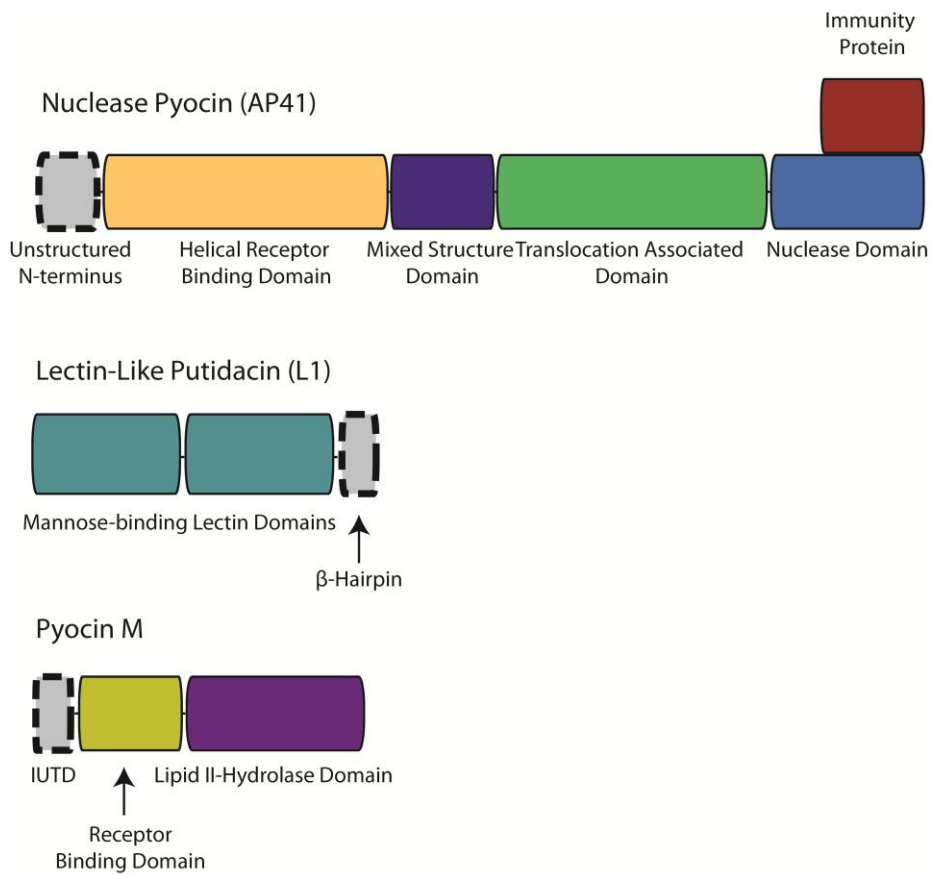


500 Amino Acids

1000 Amino Acids

Figure 1-3 Colicins with different cytotoxic mechanisms share a common modular domain structure, and conserved structural features

Analysis of the domain structure of notable colicin shows conserved domains and features shared between bacteriocins. Nuclease colicins (see colicin E2) have a tightly associated immunity protein that binds to and inactivates the nuclease domain, while pore forming colicins (colicin B and N) and colicin M have immunity proteins which protect the cell without strong interactions with the bacteriocin. As illustrated by E2, B and N, various colicins combine different cytotoxic or cell entry associated modules to create active toxins. IUTD = Inherently unstructured translocation domain (6)



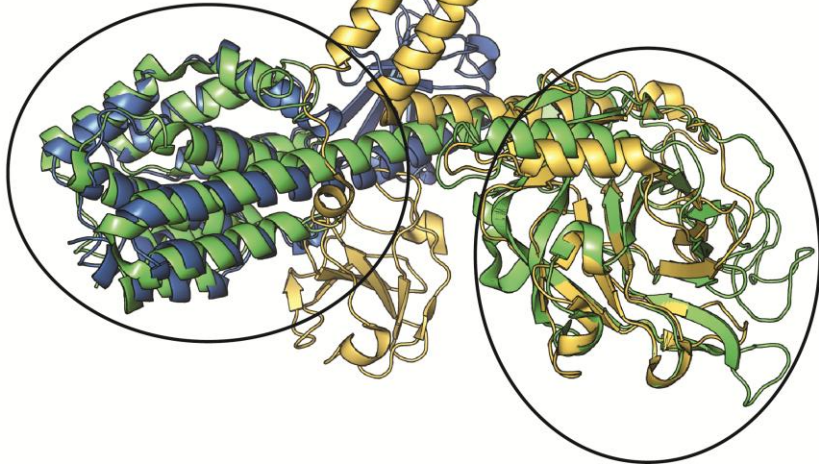
500 Amino Acids

1000 Amino Acids

Figure 1-4 Pyocin domain structure mirrors that found in the colicins

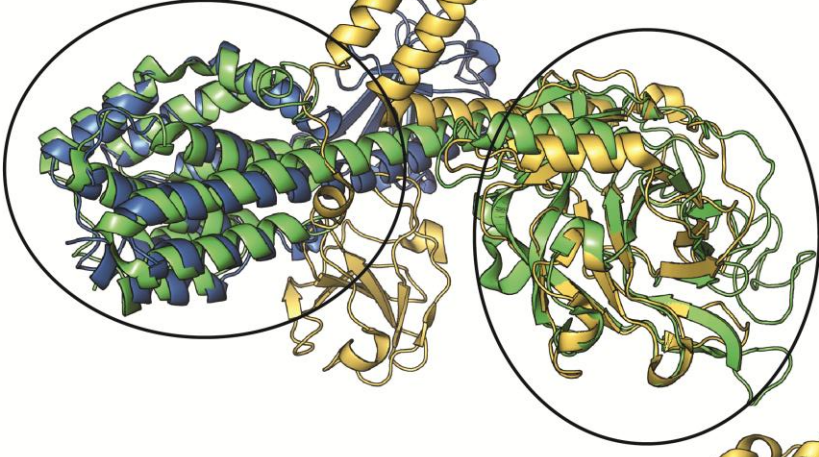
Nuclease pyocins (see colicin AP41) possess structurally analogous nuclease domains to colicins. They also possess structurally analogous receptor binding and translocation domains; however the order of these domains appears to be reversed. Structural analysis of M-class bacteriocins from *Pseudomonas spp.* (see pyocin M) shows that they share structural homology throughout the entire length of the protein, despite no detectable sequence identity in the receptor binding and translocation domains (1,2). Homologues of the recently identified lectin-like bacteriocins (see putidacin L1) are unrepresented in the colicins, they have unique tandem MMBL β -prism domains (11)

Pore Forming
Cytotoxic Domain



'Translocation' Domain

Pore Forming
Cytotoxic Domain



'Translocation' Domain

Colicin N = Blue
Colicin B = Green
Colicin E3 = Yellow

Figure 1-5 Colicins are constituted by distinct combinations of structurally related cell entry and cytotoxicity domains

A stereo view of the structural alignment of the colicins N, B and E3 illustrates the modular structure of colicins. Colicins N and B both share a structurally homologous pore forming cytotoxic domain, but unrelated receptor binding and translocation domain. Colicin B and E3 share a large globular domain implicated in colicin translocation, despite unrelated pore forming and RNA degrading cytotoxic domains (18,63,64).

1.4.2 Colicin-like bacteriocin domain structure and evolution

The highly modular domain structure of colicin-like bacteriocins, with distinct functional domains for: binding to the cell surface, translocation across the outer-envelope and cell killing, allow for the generation of new bacteriocin specificities through genetic recombination (65). As discussed in detail below, different receptor binding domains bind to specific receptors on the surface of the bacterial cell, with translocation domains targeting either the Ton or Tol machinery, inner-membrane complexes with related but distinct function, for cell entry (4,66). Susceptible bacterial cells can escape killing by a specific bacteriocin through mutation in the cell surface receptor or translocation machinery, or by acquiring the gene encoding the corresponding immunity protein for a bacteriocin. Genetic recombination creating new combinations of receptor binding, translocation and cytotoxic domains provides a means circumventing this immunity (57). As a result, the vast majority of colicin-like bacteriocins identified consist of mosaics of structurally and evolutionarily related domains (Figure 1-5). Analysis of the genetic context of colicin-like bacteriocins shows them to be hot spots of genetic recombination, confirming it as a major force in the evolution of these proteins (65).

1.4.3 Genetic structure and regulation

In *E. coli*, the majority of colicins that have been characterised are produced by strains containing a 'colicinogenic' plasmid. They are found on two types of plasmids, type I plasmids are small (6-10 kb) in size, having around 20 copies per cell and are mobilisable. Type II plasmids are large (40 kb) monocopy plasmids which are conjugative (4). For nuclease type colicins the first gene is the colicin gene, followed by the immunity protein gene directly downstream. Transcription of the immunity protein gene is under

the control to two promoters: an SOS induced promoter and a constitutive promoter. The constitutive promoter provides a constant low level expression to ensure immunity to incoming colicin molecules (67). Often colicinogenic plasmids also contain additional genes encoding immunity proteins with different colicin specificities. These genes are constitutively expressed and provide additional protection to the plasmid harbouring strain. The last gene encodes a lysis protein, the production of which causes cell lysis and allows release of the colicin from the cell (68). Colicin production is induced by DNA damage, and as such it is generally induced in the laboratory by physical DNA damaging agents like UV or mitomycin C. Transcription of colicin operons is strongly repressed by LexA, with the LexA binding site (SOS box) located immediately upstream of the Pribnow box. In the SOS response RecA becomes activated and cleaves LexA, activating transcription of the colicin operon and other genes of the SOS regulon (4).

In contrast to the plasmid encoded colicins, all pyocins identified thus far are chromosomally encoded, consisting of a pyocin gene followed by one or more immunity protein genes (11). No pyocin associated lysis protein encoding genes have been identified and the mechanism through which pyocins are secreted from the producing cell remains to be discovered. Pyocins are also inducible in response to DNA damage. Despite this regulation pyocins have no upstream SOS box, but instead an upstream consensus sequence named a 'P box' has been identified which is bound by the activator protein PrtN. Under normal conditions the PrtN protein is transcriptionally repressed by a partner protein PrtR. When DNA damage activates RecA, it cleaves PrtR, enabling transcription of *prtN* with its product PrtN then activating pyocin transcription (69).

As with the pyocins, all bacteriocins identified in *P. syringae*, *P. atrosepticum* and *P. carotovorum* are chromosomally encoded, often in conjunction with a downstream immunity protein. Production of a number of bacteriocins in *Pectobacterium sp.* has been shown to be induced by UV and mitomycin C (70). However detailed information on the mechanisms of the regulation of bacteriocin production has not been elucidated for these species.

1.4.4 Cytotoxic mechanisms of colicin-like bacteriocins

Colicin-like bacteriocins target cells using a variety of cytotoxic mechanisms. The most prevalent of which are pore formation and the degradation of nucleic acids. However, other modes of action including degradation of peptidoglycan or inhibition of peptidoglycan synthesis have been reported (4). The mechanism through which the recently described lectin-like bacteriocins kill cells remains to be discovered (15).

1.4.4.1 Nuclease type bacteriocins

The cytotoxic domain of the nuclease type bacteriocins degrades target cell nucleic acids leading to cell death. A number of colicins and pyocins with nuclease domains have been experimentally characterised degrading either DNA, tRNA or rRNA (71). Almost all DNA degrading pyocins and colicins described at the time of writing (colicins E2, E7, E8 and E9 and pyocins S1, S2 and AP41) belongs to the H-N-H nuclease super family (4). The exception to this is pyocin S3, which has a DNA degrading catalytic domain with no obvious homology to studied proteins. Structurally these enzymes consist of a central three-stranded antiparallel-sheet surrounded by helices. The DNA degrading H-N-H motif of the enzyme is approximately 34 AA in length, and contains 4 conserved histidine residues. Three of these residues are involved in coordinating a catalytic metal ion (Figure 1-6-A), with the fourth most N-terminal histidine acting as a general base in the DNA cleavage reaction (71). The H-N-H motif is a versatile DNA binding domain, which has been identified in over 500 enzymes of divergent function, including mobile intron homing, DNA repair, mammalian apoptosis and DNA restriction. The H-N-H site architecture is related to a superfamily of nucleases distributed across all kingdoms of life (72). H-N-H DNase colicins non-specifically nick DNA, with multiple nicking events cumulating in double stranded breaking of the DNA (4). Coordination of a metal ion in the active site is essential for enzymatic activity with, Mg^{2+} being the likely physiological metal ion cofactor for DNA cleavage, although certain members of this family have been shown to be active with a variety of metal ion cofactors including Zn^{2+} and Ni^{2+} (Figure 1-6-B) (71,73). The nuclease domains of the colicins (E2, E7, E8 and E9) share 65%

approximately AA identity, with pyocin (S1, S2 and AP41) and colicin domains sharing approximately 50% identity (11).

In order to prevent cell suicide upon bacteriocin production, H-N-H bacteriocins (and nuclease bacteriocins more generally) are co-transcribed with an immunity protein. This protein, which also serves to protect the cell against incoming nuclease domains, binds with extremely high affinity to the nuclease domain and inactivates it. The immunity protein for H-N-H bacteriocins binds adjacent to the active site of the nuclease domain, inactivating it through steric hindrance of the substrate, rather than directly blocking the active site (Figure 1-6-A) (74). This exosite binding has the consequence of allowing divergent selection to occur at the immunity protein nuclease domain interface while retaining catalytically important residues, facilitating the generation of new bacteriocin/immunity protein pairs. This has led to rapid diversification of DNase bacteriocin immunity protein specificities, and provides a possible explanation for the identification of a larger number of DNase type colicin-immunity protein complexes (57). As a result of this most of the amino acid variation in the DNase domains occurs at the immunity protein binding interface (3). The C-terminal domains of non-DNAase, nuclease colicin-like bacteriocins elicit cell death through the inhibition of protein synthesis by cleaving specific phosphodiester bonds of RNA. These enzymes do not require metal ion cofactors and can be separated into two groups based on activity, those that cleave the 16S rRNA subunit (colicins E3, E4 and E6 and pyocin S6) and those that cleave the anticodon loop of specific tRNAs (colicins E5 and D and pyocin S4) (4,71).

Colicins E3, E4 and E6 all share significant homology over the length of their C-terminal domains, which suggests a common evolutionary origin. They specifically attack the 30S ribosomal subunit of the target cells, cleaving 16S rRNA towards the 3' end between nucleotides A1493 and G1494 (75).

Although the tRNAse colicins E5 and D (pyocin S4 is homologous to colicin E5) both have very similar cytoplasmic targets (E5 targets tRNAs carrying Tyr, His, Asn and Asp, D targets 4 different tRNAs for Arg), sequence and structural comparisons suggest that the C-terminal domains of these proteins have acquired similar functions through convergent evolution (76). Crystal structures of the catalytic domains of these proteins show recognizable RNA binding domains which lack structural similarity, suggesting a distinct evolutionary ancestry (4).

In order to prevent cell suicide the immunity proteins for RNase type bacteriocins are also co-transcribed with the bacteriocin. As is the case for the H-N-H bacteriocins, rRNase immunity proteins inactivate the toxin domain by binding adjacent to the active site (77). Alternatively, the immunity proteins for the structurally unrelated tRNase colicins E5 and D bind directly to the active site, through substrate mimicry. This more classic mode of enzyme inhibition is similar to the inhibition mechanisms of other RNase inhibitors, such as the barstar the inhibition of barnase (78).

Nuclease colicins are released from cells as a heterodimer, complexed with an immunity protein. As affinity between the immunity protein and cognate bacteriocin is very high (the K_d for colicin E9+Im E9 is 10^{-16} M) and removal of the immunity protein is required to activate the toxin, a significant energy input and/or partial unfolding of the complex is required for separation and activation of the nuclease (79). Current evidence suggests the this energy for dissociation is provided during translocation of the bacteriocin into the target cell (74).

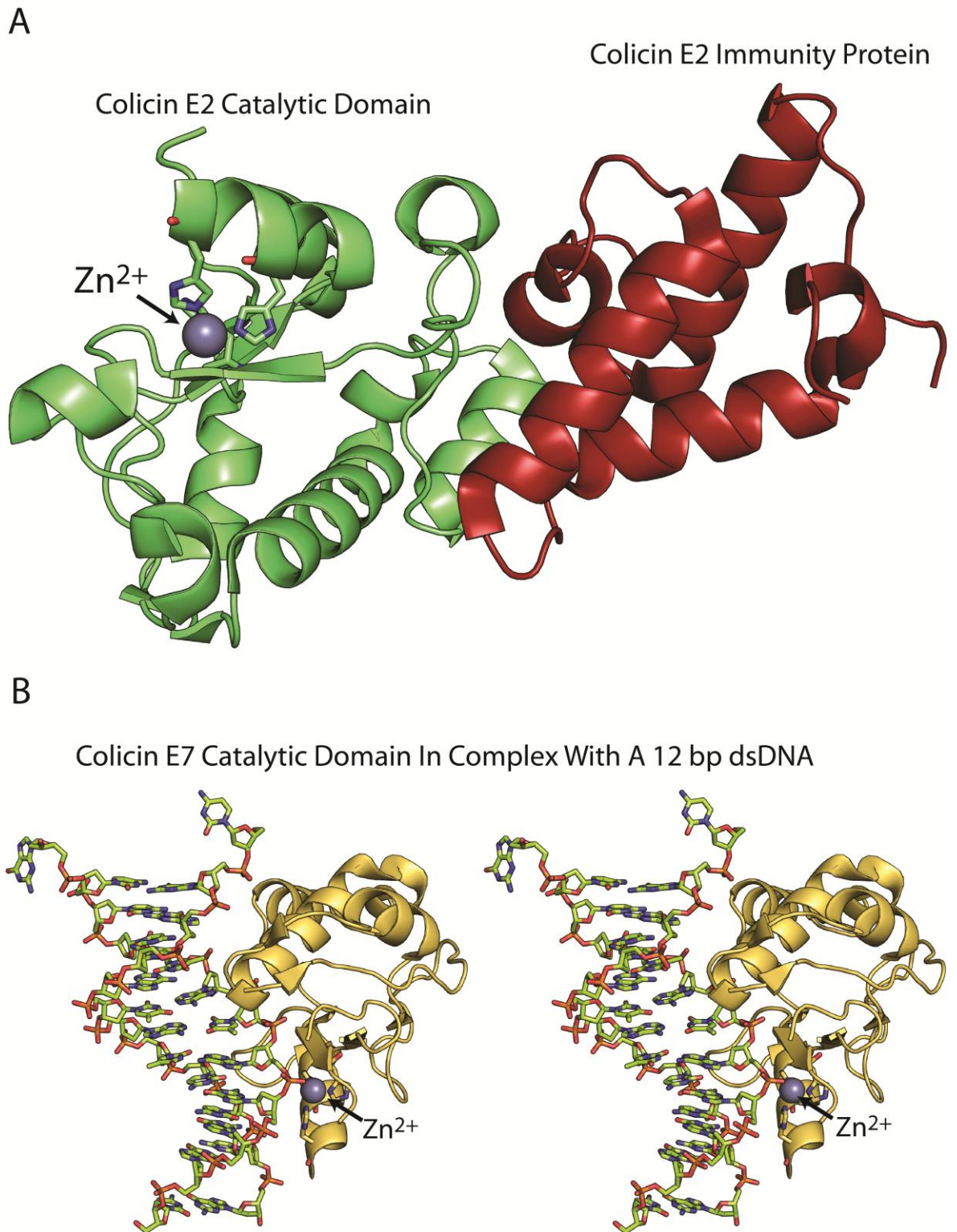


Figure 1-6 The structure of the colicin H-N-H nuclease domain.

A) The crystal structure of colicin E2 in complex with its immunity protein. The immunity protein binds to nuclease domain adjacent to the active site, inactivating the domain by steric hindrance and electrostatic effects (3). B) A stereo representation of the crystal structure of the colicin E7 H-N-H DNase domain in complex with 12 bp of double stranded DNA, showing the extended DNA binding interface, with the DNA in close proximity to the divalent metal ion (in this case zinc) in the active site (17).

1.4.4.2 Lipid II-hydrolysing, M-class bacteriocins

Colicin M the initial member of the M-class bacteriocins was first described and characterised in the 1970s (80). Subsequently, a number of homologues from other Gram-negative bacterial species, for example pyocin M (PaeM) from *P. aeruginosa* and fluoricin M from *P. fluorescens* have subsequently been identified (81,82). The cytotoxic domain of M-class bacteriocins is a metal dependent phosphatase that elicits its lethal effect through hydrolysis of lipid II between its pyrophosphate and undecaprenyl moieties (83,84). Lipid II resides in the inner membrane and functions in the transport of peptidoglycan subunits of the bacterial cell wall from their site of synthesis in the cytoplasm, to the periplasm where the cell wall is assembled (Figure 1-7) (85,86). Cleavage of lipid II by the M-class bacteriocins occurs at the periplasmic face of the inner membrane and prevents recycling of the carrier lipid. Ordinarily during cell wall synthesis the peptidoglycan subunit of lipid II is removed by the penicillin binding proteins (PBPs) and is incorporated into the cell wall, leaving undecaprenyl-pyrophosphate embedded in the inner membrane. Undecaprenyl-pyrophosphate is then modified to a monophosphate in the periplasm, before being transported to the cytoplasm where it is regenerated to lipid II (86). The lipid II cleavage reaction catalysed by M-class bacteriocin leads to the dephosphorylation of undecaprenyl moiety, decoupling the lipid II synthetic process, and ultimately to an arrest of cell wall synthesis and lysis of the cell (83,87). In order to protect the producing cell from the lethal effects of the toxin, the colicin M operon encodes an immunity protein (Cmi), directly downstream of the gene for colicin M (88). Unlike the immunity proteins from nuclease bacteriocins a strong interaction between colicin M and its immunity protein has not been demonstrated. Cmi possesses a signal anchor transmembrane helix, which directs it to the periplasmic face of the inner membrane where it mitigates the effect of colicin M on the cell. While the crystal structure of Cmi has been determined, how it confers immunity to colicin M remains unknown (89,90). Recent work by Helbig et. al., showed that in addition to Cmi conferred immunity, the level of expression on the cytoplasmically localised flavin containing protein CbrA also modulates the sensitivity of *E. coli* to colicin M (91). Interestingly, pyocin M and other predicted M-class bacteriocins from *Pseudomonas* and *Burkholderia*

sp. are not associated with an immunity protein gene homologous to Cmi, suggesting diverse mechanisms of immunity for M-class bacteriocins. (1,82,92)

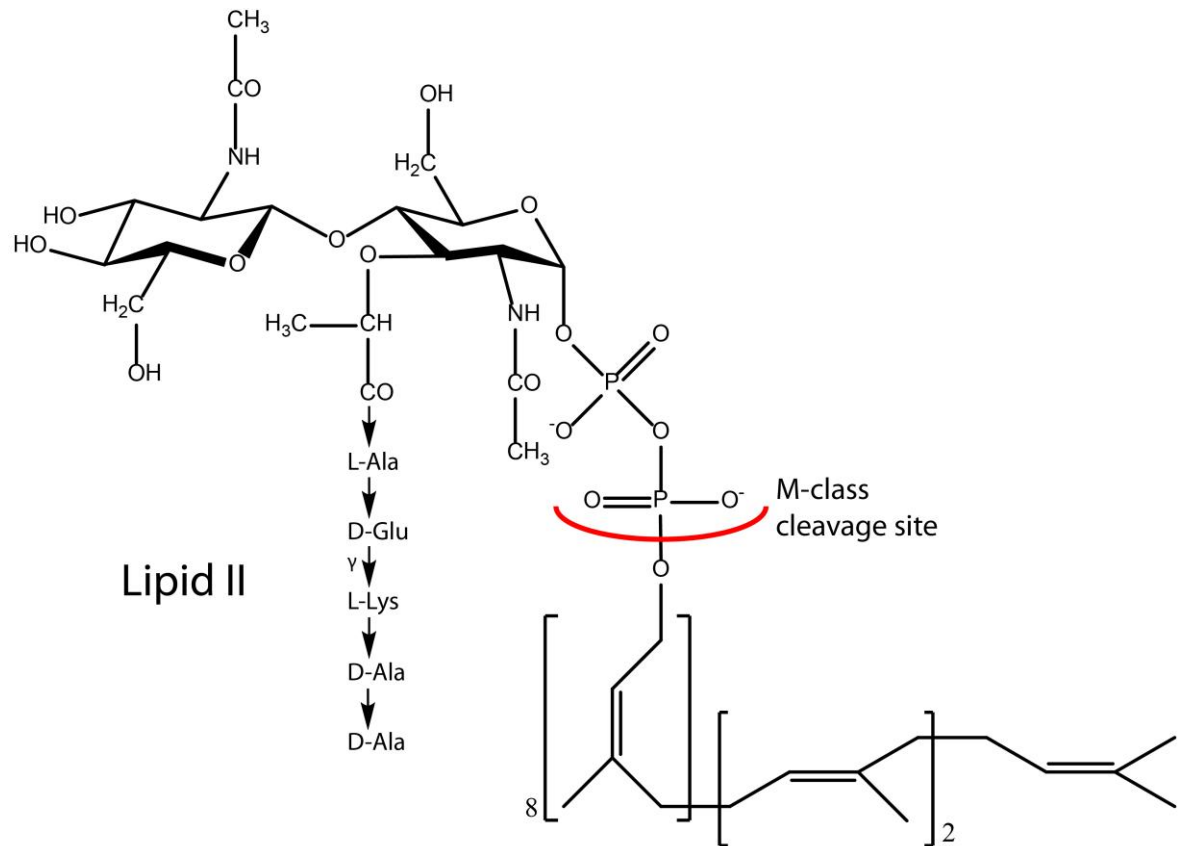


Figure 1-7 2D-schematic of peptidoglycan precursor molecule lipid II from Gram-negative bacteria (93)

1.4.4.3 The lysozyme-like pesticin cytotoxic domain

Pesticin, a colicin-like bacteriocin produced by *Yersinia pestis*, the causal agent of the bubonic plague, possesses a cytotoxic domain which is structurally related to bacteriophage T4 lysozyme (94,95). Pesticin, like its phage lysozyme homologue, has been shown to degrade the peptidoglycan cell wall, leading to cell lysis due to the cells internal osmotic pressure. Interestingly, an engineered pesticin protein, in which the cytotoxic domain was replaced with either T4 or chicken egg white lysozyme was cytotoxic to cells which possessed the pesticin receptor FyuA (96).

1.4.4.4 Pore forming bacteriocins

The cytotoxic domains of the pore forming bacteriocins are structurally homologous in all colicin-like bacteriocins studied to date and consists of a compact 9-helix bundle. Pore forming bacteriocins target cells by creating a pore in the cytoplasmic membrane, dissipating the proton gradient across this membrane and thus disabling the cell (97). Studies have shown that these toxins act with single molecule kinetics, indicating that multimerisation of the protein is not required to achieve this (97,98). The central helices of the pore forming domain are hydrophobic and this has led to the postulation of an umbrella model of pore formation, in which the initial insertion of the central helices into the inner membrane, is followed by rearrangement or 'opening' of the bundle to form the pore (99). Interestingly the crystal structures of colicins B, N and Ia show that pore forming domains exist conjugated to structurally diverse receptor binding and translocation domains to form active bacteriocins, with these bacteriocins ranging in size from colicin N at 387 AA to colicin IA at 624 AA (Figure 1-8).

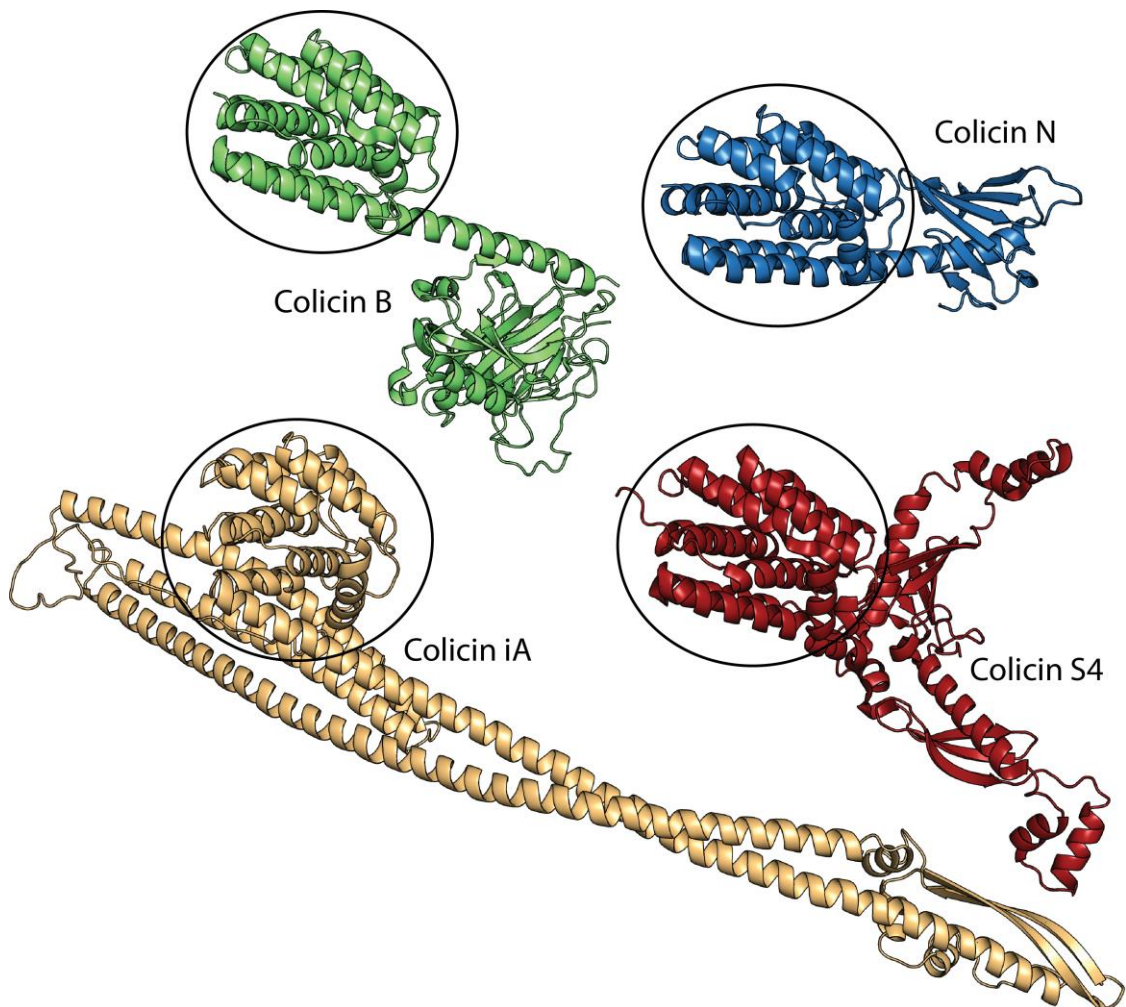


Figure 1-8 Pore forming colicins utilise receptor binding and translocation domains of diverse structure to deliver a common cytotoxic domain to the periplasm.

The crystal structures of pore forming colicins illustrate the structural diversity of colicin cell entry domains. Pore forming colicins S4 and N both belong to group A colicins that gain entry to the cell through interactions with TolA or TolB, however they possess receptor binding domains with different specificities. The colicin S4 receptor binding domain interacts with OmpW, whereas the colicin N receptor binding domain binds to cell surface LPS. Similarly, the B group pore formers Colicin B and colicin IA enter the cell through interactions with TonB, but bind to different TonB-dependent nutrient receptors on the cell surface. Colicin B binds FepA, while colicin IA binds Cir (7) (9,10) (12,13).

1.4.5 Lectin-like bacteriocins

The lectin-like bacteriocins are a recent and interesting addition to the bacteriocin family. Unlike the generally asymmetric domain structure of the colicin-like bacteriocins, they consist of two carbohydrate-binding domains of the monocot mannose-binding lectin (MMBL) family, and a C-terminal β -hairpin extension (100-104). Lectin-like bacteriocins from *Pseudomonas* spp. *BW11M1* (putidacin L1 or LlpA_{BW}) *P. syringae* (LlpA_{PSS642}) and *P. fluorescens* (LlpA_{1pf-5}) have been characterised and have the unprecedented ability to kill strains from a broad range of bacterial species within the genus *Pseudomonas*, but are not active outside this genus (101,103,104). Similarly the lectin-like bacteriocins LlpA_{Xcm761} and LlpA_{AU1054} from *Xanthomonas citri* pv. *malvacearum* LMG 761 and *Burkholderia cenocepacia* AU1054, respectively, have the ability to kill various species within their respective genus (101,105). The molecular basis of this unusual genus specific activity has yet to be determined. Lectins are a structurally and evolutionarily diverse class of proteins produced widely by prokaryotes and eukaryotes and are defined by their ability to recognise and bind carbohydrates. This binding is specific and mediates a range of diverse functions, including cell-cell interaction, immune recognition and cytotoxicity (106,107). MMBLs represent a structurally conserved lectin subclass, of which the mannose-binding lectin *Galanthus nivalis* agglutinin (GNA) was the first to be characterised (108). The MMBL-fold consists of a three sided β -prism; each face of which contains a sugar binding motif with the conserved sequence QxDxNxVxY (5). While originally identified in monocots such as *G. nivalis* and *Allium sativum*, it is now recognised that proteins of this class are distributed widely throughout prokaryotes and eukaryotes, where they have

evolved to mediate diverse functions (108-111). Structural and biochemical analysis of MMBLs have shown that they are generally translated as a single polypeptide chain containing tandem β -prism domains that are then proteolytically processed into monomers. These domains often form homo- or hetero-dimers by strand exchange and π -stacking (Figure 1-9-A)(112). Unusually, the lectin-like bacteriocins are not proteolytically processed and thus consist of a single peptide chain, containing tandem β -prism domains (Figure 1-9-A/B). Sequence alignments of members of this class from *Pseudomonas* spp. show complete conservation of two QxDxNxVxY sugar binding motifs on the C-terminal domain and partial conservation of two sites on the N-terminal domain (100). Recent work by Ghequire *et al* (100) on the characterisation of putidacin L1 shows these motifs to be important for cytotoxicity. Mutagenesis of the first C-terminal motif has the most dramatic effect on activity, while mutagenesis of the second C-terminal and first N-terminal sugar binding motifs leads to a synergistic reduction in activity. This study also showed low-affinity binding between putidacin L1 and methyl- α -D-mannose or a range of mannose containing oligosaccharides. However, K_d s for these protein-carbohydrate complexes were reported in the range from 46 mM for methyl- α -D-mannoside to 2 mM for a mannose containing pentasaccharide (100). An extensive search for high affinity carbohydrate binding through the use of glycan arrays failed to detect high affinity carbohydrate binding for this lectin-like bacteriocin (100).

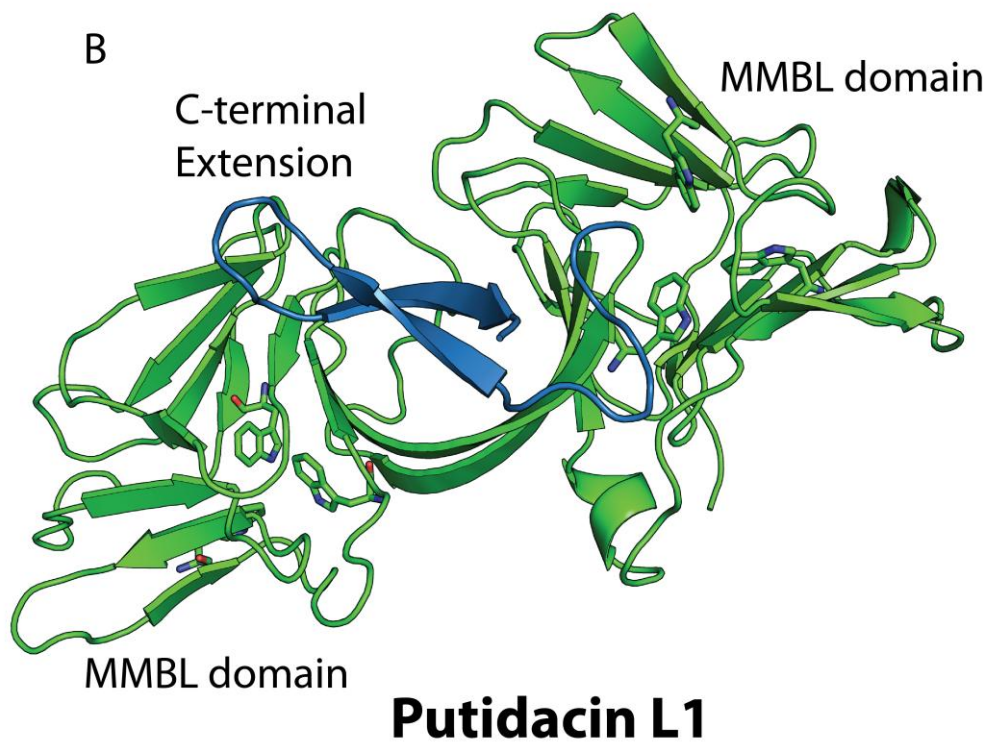
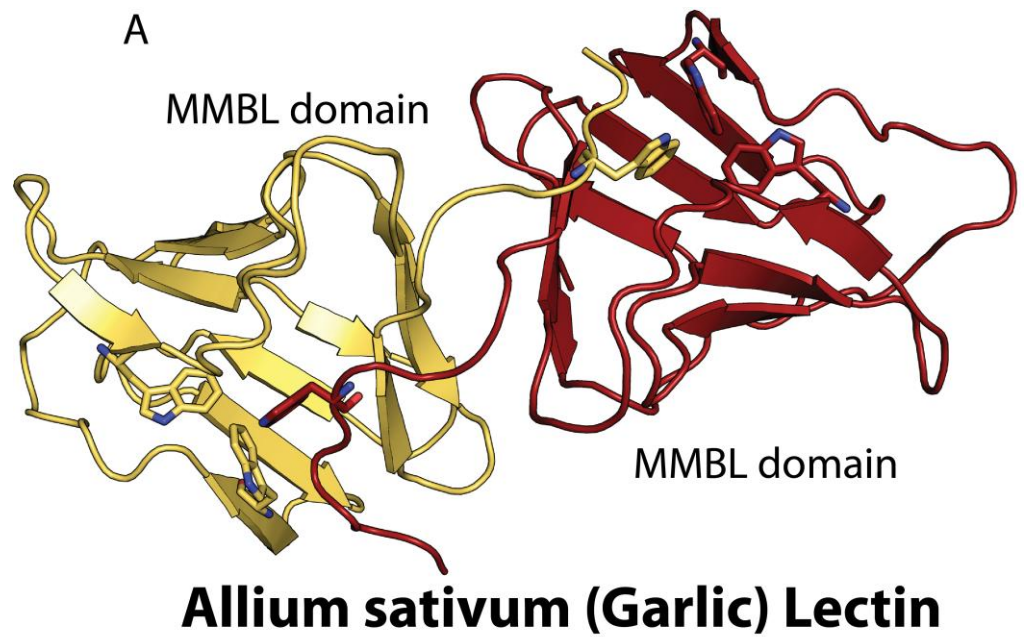


Figure 1-9 The lectin-like bacteriocins share a common structure and evolutionary origin with plant MMBL lectins

A) The crystal structure mannose binding lectin from *A. sativum* (Garlic), a protein of unknown physiological function present at high concentrations in garlic tubers (5), B) The crystal structure of putidacin L1 produced by *Pseudomonas spp.* BW11M1, with killing activity against other *Pseudomonas spp.*. Structurally the tandem β -prism domains with the π -stacking tryptophan motif are conserved, however putidacin L1 consists of a single peptide chain whereas plant like lectins are homo or heterodimers. Lectin-like bacteriocins also possess a C-terminal extension shown to be essential for activity of the protein (14-16).

1.4.6 Cell surface binding and entry by colicin and lectin-like bacteriocins

In order to deliver the cytotoxic domain to its site of action in the target cell, colicin-like bacteriocins must first penetrate the Gram-negative cell envelope. To achieve this, these proteins possess additional domains, termed receptor binding and translocation domains, which deliver the cytotoxic domain to its site of action (6).

As the name suggests, the receptor binding domain of colicin-like bacteriocins mediates a high affinity interaction between the bacteriocin and its outer membrane receptor. For most bacteriocins studied thus far this is a TonB-dependent nutrient receptor, however two bacteriocins (colicin N and pyocin L1; pyocin L1 discussed in chapter 6) have recently been shown to utilise lipopolysaccharide (LPS) as a cell surface receptor (12,15). TonB-dependent receptors have a physiological role in the uptake of valuable nutrient substrates (for example iron siderophores or cobalamin) too large to enter the cell by diffusion through outer membrane pores (113). The specific receptor utilised varies between different groups of bacteriocins, with for example, the E colicins utilising BtuB, colicin IA utilising Cir, colicin M utilising FhuA and the S-type pyocins, S2, S3 and S4, which use receptors involved in uptake of the siderophore pyoverdine (Figure 1-10) (4,114). Despite the variety of receptors used, what is invariably true is that the interaction between the colicin-like bacteriocin and its receptor is highly specific, with disassociation constants of low μM to nM reported (6). Binding to its cell surface receptor serves to remove the bacteriocin from the three dimensional milieu, fixing it to the surface of the outer membrane (115). The bacteriocins then needs to enter the target cell, the mechanism by which colicins-like bacteriocins achieve this crossing or 'translocation' can be used to divide these proteins into different groups, based on the domains utilised and the interacting partners required to gain entry to the cell (66). Early genetic screens were able to broadly classify colicins into two groups, A and B based on their requirement for components of either Tol or Ton complexes (116). The Ton and Tol systems are evolutionarily related protein complexes, with divergent functions, that both play a physiological role in transducing stored energy from the proton gradient across the inner membrane to performed functions at the outer membrane (117,118). While the exact function of the Tol system is unknown, it has been shown to be recruited to the septation apparatus during cell division, where it plays a role in stabilizing the outer

membrane (113,119). More generally, mutants in genes encoding its components or its interacting partner Pal have been found to display defects in outer membrane permeability and stability (120). The Ton complex provides the energy required for the import of iron containing siderophores and related substrates through TonB-dependent receptors. This occurs through interaction with a specific binding epitope (the TonB box) at the N-terminus of the receptor plug domain subsequent to binding of the substrate on the outer surface of the receptor (113). Subsequent to binding, it has been postulated though not conclusively proven that energy provided by the Ton complex through TonB causes removal or rearrangement of the receptor plug domain allowing ingress of the substrate into the cell (121).

It was subsequently discovered that colicins (and potentially colicin-like bacteriocins more generally) possess an intrinsically unstructured translocation domain at their N-terminus (IUTD). Removal of this domain, leads to a bacteriocin unable to kill cells, but still active in receptor binding and cytotoxic domain activity *in vitro* (66). The IUTD of both A and B group bacteriocins has been shown to deliver a binding epitope to the periplasm, which directly mediates binding to the Tol or Ton complexes. While the specific details of the process are still poorly understood, this interaction presumably allows the bacteriocin to access the energy transduced by these complexes to cross the outer membrane (122). In group B colicins this binding epitope has been shown to be analogous to the epitope which mediates interaction between TonB and the TonB-dependent receptors, suggesting molecular mimicry is involved in colicin-TonB interactions (123).

Colicin-like bacteriocins studied structurally adopt both highly elongated and more compact structures. The elongated colicins (E colicins and colicin Ia) bind to their TonB-dependent receptor via an elongated helical receptor binding domain, while the IUTD searches for a secondary receptor/translocator, the abundant outer membrane porin OmpF for the nuclease colicins (E2, E7, E8 and E9), and in the case of colicin E1 and Ia, TolC and Cir, respectively (4). The IUTD of the nuclease E-group colicins has been shown experimentally to thread through the pore of OmpF to deliver its binding epitope to the periplasm (122). Compact colicins like colicins M, B, D and pesticin have only been shown to bind to a single TonB-dependent receptor, which likely serves both receptor binding and translocator function (6,96). Interestingly, while different colicins recruit different receptor and translocation proteins, Tol/Ton dependence for importation can for some

colicins be switched by changing the epitope on the IUTD from a Ton to a Tol specific sequence (124). This suggests colicins bind to cell surface receptors regardless of their endogenous function in order to capture transmembrane systems that transduce the PMF to the outer membrane. Upon entering the periplasm pore forming colicins, colicin M and pesticin, can exert their toxic effects, however the nuclease colicins still need to cross the inner membrane and enter cytoplasm of the cell. Limited experimental evidence on this process is available, however work by Walker et al in 2007, showed that both the net positive charge on the colicin E9 nuclease domain and the presence of anionic phospholipids in the outer membrane were important for colicin killing. Additionally, the authors demonstrated that FtsH, an inner membrane ABC transporter responsible for the retro-translocation of misfolded membrane proteins was necessary for colicin toxicity. The model proposed by the authors to explain this data suggests that interactions between the colicin DNase domain and the inner membrane lead to destabilisation and partial unfolding of the protein, which facilitates its translocation into the cytoplasm via FtsH (125). A schematic of the colicin translocation process is presented in (Figure 1-11).

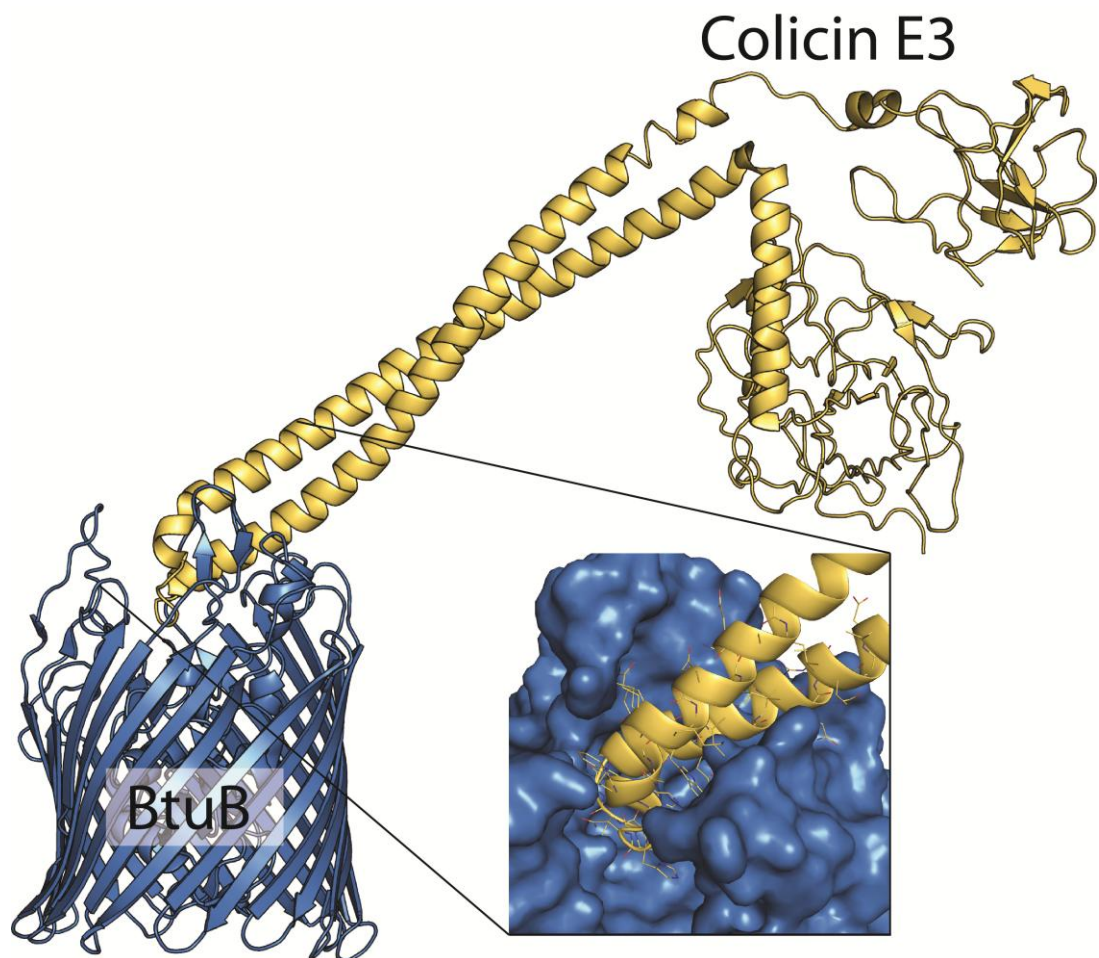


Figure 1-10 Binding of colicin E3 to its cell surface receptor BtuB

The crystal structure of BtuB in complex with the colicin E3 receptor binding domain show in atomic detail where the colicin interacts with BtuB. An overlay of the crystal structure of full length colicin E3, with the receptor binding domain from this complex shows the position and conformation of colicin E3 (and other E colicins which share its domain architecture) on the bacterial cell surface (8).

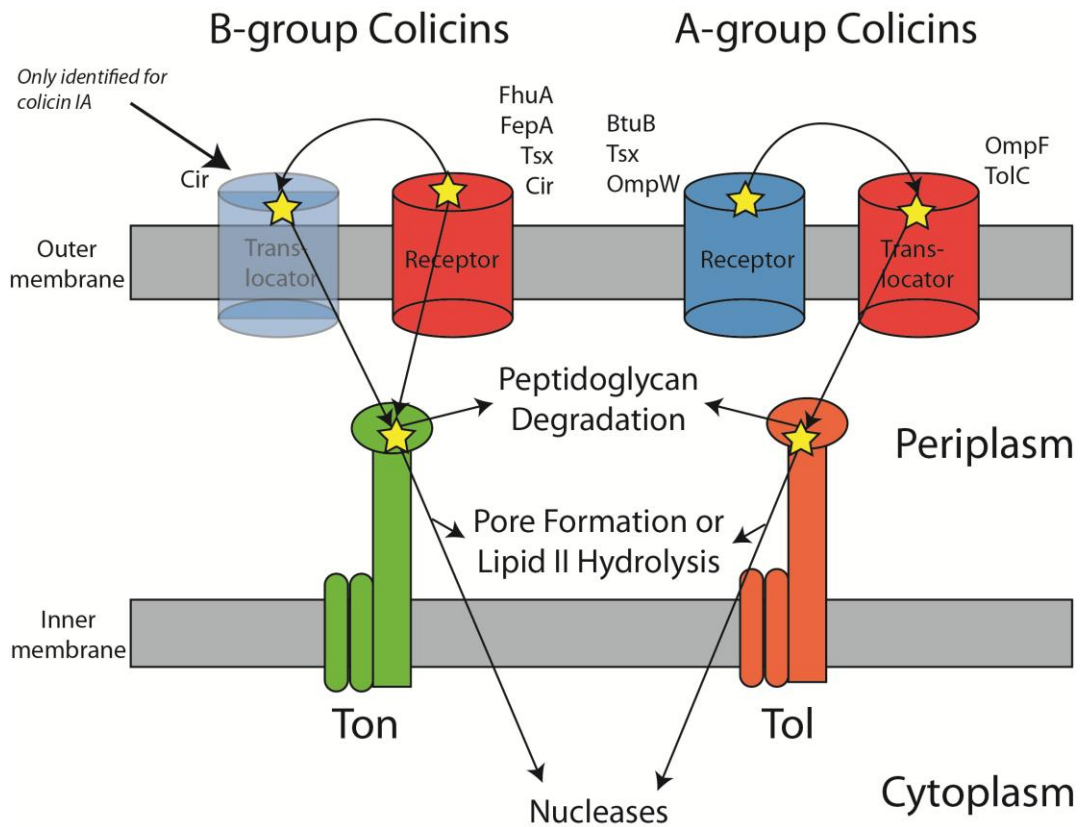


Figure 1-11 Cell entry and cytotoxicity of A- and B-group colicins

A-group colicins bind to their cell surface receptor, before recruiting the porin OmpF as a translocator. The IUTD of the colicins threads through the lumen of OmpF interacting with the Tol complex in the periplasm. This interaction with Tol facilitates entry of the bacteriocin, with energy provided by the proton motive force (4).

B-group also interact with a cell surface receptor, however with the exception of colicin IA which utilises a second copy of its receptor Cir as it's translocator, a secondary translocator has not been identified. B-group colicins interact with TonB via a TonB-binding epitope to gain entry to the target cell (18).

1.5 Colicin and lectin-like bacteriocins produced by phytopathogenic bacteria

Limited experimental work has been performed characterising colicin-like bacteriocins from phytopathogens. However, genes encoding putative bacteriocins can be readily identified in the available genome sequences of the economically important plant pathogens such as *P. syringae*, *P. atrosepticum*, *P. carotovorum*, *D. solani*, *Xanthomonas spp.* and *Agrobacterium spp.* indicating that bacteriocin production is widespread among phytopathogenic bacteria. (58,126). Despite this potential wealth of bacteriocins, to date only a handful of bacteriocins produced by phytopathogens have been described. Three bacteriocins from *Pectobacterium spp.* with catalytic domains homologous to colicin-like bacteriocins have recently been characterised. These proteins were designated 'carocins' based on the identity of the producing species, *P. carotovorum*. All three proteins have catalytic domains with nuclease activity, with the first protein identified, carocin S1, possessing a DNase domain homologous to the cytotoxic domain of pyocin S3 (127). Similarly, carocin S2 possesses a tRNase domain homologous to the cytotoxic domain of colicin D, while carocin D possesses DNase activity (70,128). Previous experimental and bioinformatic analysis show that strains of *P. syringae* also produce bacteriocins homologous to the colicin-like bacteriocins. However, characterization of these proteins has been limited (126,129). Syringacin M produced by *P. syringae pv. tomato* DC3000, which is a focus of this study was first reported by Barreteau et. al.. This protein, which has a catalytic domain homologous to that of colicin M, was purified and shown to have catalytic activity against the lipid II. However, no cytotoxic activity was observed against the *Pseudomonas* strains tested (82). Other studies on bacteriocin production in *P. syringae* and closely related plant-associated pseudomonads have identified high molecular weight phage tail-type bacteriocins and bacteriocins analogous to recombination hot spot (*rhs*) proteins (105,130). Lectin-like bacteriocins active against phytopathogens, have also been identified (105). The initial member of this class, putidacin L1 (LlpA1) was isolated from a rhizosphere dwelling *Pseudomonas* isolate from the *P. putida* cluster and was found to have cytotoxic activity against a number of phytopathogenic *Pseudomonad* species (103). Further studies identified and cloned

lectin-like bacteriocins from the plant pathogenic/commensal bacteria *P. fluorescens*, *P. syringae*, *Xanthomonas citri*. Limited characterization of these bacteriocins has been performed. However, they have been shown to possess cytotoxicity at comparable concentrations to putidacin L1 and possess a genus level killing spectrum (104,105,131,132).

1.6 Utilisation of bacteriocins to combat bacterial disease in plants

1.6.1 Current implementation of bacteriocins in the bio-control of phytopathogenic bacteria

To date, bacteriocins have not been used extensively to prevent or limit the effects of bacterial disease in plants. However, this is predominantly due to lack of research into the diversity and mechanisms of action of these proteins in phytopathogenic bacteria, rather than their potential (60). A number of studies have shown bacteriocins to be effective agents in the treatment of bacterial disease. *Lavermicocca et. al.*, reported the use of an uncharacterized bacteriocin from *P. syringae pv. ciccaronei* in the prevention of olive knot disease. This study showed a 60-80% reduction in knot formation when stem wounds were pretreated with a crude bacteriocin preparation prior to infection with the casual-agent of the disease *P. syringae pv. savastanoi*. Additionally, a 350-400 fold decrease in the epiphytic numbers of the pathogen was observed when unwounded olive plants were treated with a crude preparation of the bacteriocin (40). A study by *Kerr and Htay*, showed that co-inoculation of a non-pathogenic bacteriocin producing strain *Agrobacterium radiobacter* strain 84, with pathogenic *Agrobacterium* strains led to attenuation of gall formation relative to only inoculation with the pathogenic strain (133). This attenuation was shown to be due to bacteriocin production, with only one bacteriocin sensitive pathogenic strain not subject to biological control. It transpired that this strain produced a bacteriocin active against *A. radiobacter* 84 (133). Based on this work, *A. radiobacter* strain 84 and the bacteriocin it produces, identified as the leucyl-

tRNA synthetase inhibiting agrocin 84, have been used extensively for the bio-control of pathogenic *Agrobacterium spp.* (134-136).

It is well established that bacteriocin resistant mutants arise upon treatment of a susceptible population. This is often stated as a counter case to the use of bacteriocins as disease control agents. However, it should be noted that the majority of mutants isolated are defective in either the outer membrane receptor responsible for bacteriocin binding or the periplasmic machinery involved in its uptake (137). The normal physiological function of bacteriocin outer membrane receptors and the periplasmic uptake machinery is frequently the uptake of nutrients such as iron, required during infection for growth, and as such these mutations may represent a fitness cost to the bacteria (6). As nutrient limitation represents a key defense strategy in many host pathogen interactions, it might be expected and has in fact been observed that bacteriocin resistant mutants are also attenuated in virulence (133,138).

1.6.2 Utilising bacteriocins to create transgenic plants

The ultimate aim of this work is the utilisation of bacteriocins in disease control through the creation of transgenic plants expressing multiple bacteriocins. Colicin and lectin-type bacteriocins are attractive targets for this approach for a number of reasons. Firstly, bacteriocins of this class are unmodified monomeric proteins encoded by a single open reading frame, making the creation of transgenic plants expressing one or a number of bacteriocins a relatively simple procedure. Secondly, the narrow spectrum of these toxins allows for the targeting of specific pathogens without disturbing the wider microbial community. This narrow spectrum also means the consumption of transgenic food crops expressing bacteriocins, is unlikely to negatively impact the health of humans or their gut flora. Finally these proteins are highly potent, often only requiring a single molecule to kill a bacterial cell (4).

The genetic modification of crop plants is an attractive option for introducing desirable genes, which are outside of the species range of the plant and thus inaccessible to regular breeding techniques. GM technology provides the ability to create crop plants with additional agriculturally or nutritionally desirable traits (139). While the technology required for creating transgenic plants has been under-development since the mid-1980s,

significant regulatory and social pressures have limited the diversity of its application. In 2012, the estimated cost of developing and obtaining approvals for a transgenic plant is \$134 million USD, with the estimated cost of obtaining regulatory approvals alone estimated at \$34 million USD (140). The requirement of such a significant investment has largely limited the application of the technology in commodity crops, such as maize and soybean and to traits which provide a significant commercial benefit (140). As such, the two most successful applications of the technology are the addition of genes providing resistance to the herbicide glyphosate (so called Roundup Ready® plants) and for the production of toxins from *Bacillus thuringiensis* (Bt crops) to provide resistance to insect pests (141). Genes imparting these traits have been engineered into a number of important crop plants and are grown over large areas. In 2012, genetically modified crops were grown in 28 countries and on more than 170 million hectares of land, consisting mainly of corn, soybean, canola, and cotton (140), with 77 % of soybean and 50 % of cotton grown globally being genetically modified (141). Despite the dominance of Bt and Roundup ready crops in terms of area, numerous other beneficial traits have been engineered into crop plants. These include resistance to genes for viral or oomycete pathogens, in papaya and potato respectively and the addition of the β -carotene biosynthetic pathway to create so called Golden Rice (142,143). The diversity of crop species to which GM technology has been applied and the variety of traits that have been engineered provides proof of concept for the creation of bacteriocin expressing transgenic plants.

Focusing future work on the identification and characterisation bacteriocins that target economically important plant pathogens will contribute towards the creation of a library of bacteriocins suitable for the creation of disease resistant transgenic plants. Delineating the functional domains and dissecting the catalytic mechanisms of these proteins will provide data required for protein engineering to create novel bacteriocins with an expanded host range. Multiple bacteriocin genes can then be 'stacked' into host plants to provide robust resistance to a broad spectrum of pathogenic strains under field conditions. In addition, expression of bacteriocins in tubers will provide an ideal agent for preventing tuber rot during storage This kind of application using small peptide bacteriocins from 'lactic acid' bacteria has gained attention in the food industry (58).

2 Materials and Methods

2.1 Chemicals and growth media

All chemicals used in this study were analytical grade and were purchased from Melfold, Sigma Aldrich or Fischer Scientific unless stated otherwise.

2.2 Bacterial strains, plasmids and growth conditions

Strains and plasmids utilised in this study are presented in Table 2-1 and Table 2-2 respectively. Strains of *P. aeruginosa* and *E. coli* were grown in LB (10 g tryptone, 5 g yeast extract, 10 g NaCl) at 37 °C. *P. syringae* were grown in Kings B Media (KB) (20 g peptone, 10 g glycerol, 1.5 g MgSO₄, 1.5 g K₂HPO₄ per liter adjusted to pH 7.5) at 28 °C. *Pectobacterium* strains were grown in LB at 28 °C. *A. tumefaciens* was grown in LB at 28 °C. Bacteria were maintained short term at 4 °C on agar plates and long term in 30-50% glycerol at -80 °C

Table 2-1 Strains utilised, isolated or derived during this study

Strain or Plasmid	Relevant Characteristic(s)	Source
<i>E. coli</i>		
DH5α	F ⁻ , φ80dlacZΔM15, Δ(lacZYA-argF)U169, deoR, recA1, endA1, hsdR17(rk ⁻ , mk ⁺), phoA, supE44, λ ⁻ , thi-1, gyrA96, relA1	Invitrogen
BL21DE3	F ⁻ ompT hsdSB(rB ⁻ , mB ⁻) gal dcm (DE3)	Invitrogen
BL21(DE3)pLysS	F ⁻ ompT hsdSB (rB ⁻ mB ⁻) gal dcm (DE3) pLysS (Cam ^R)	Invitrogen
SM10 (λpir)	Km ^R , thi-1, thr, leu, tonA, lacY, supE, recA::RP4-2-Tc::Mu, pir.	BCCM
<i>A. tumefaciens</i>		
GV3101	Rif ^r , Gent ^r , contains helper plasmid for binary vector mobilisation	(144)
<i>P. syringae</i>		
pv. tomato DC3000	isolated from <i>Solanum lycopersicum</i>	BCCM

<i>pv. tomato</i> NCPPB 1107	isolated from <i>Solanum lycopersicum</i>	NCPPB
<i>pv. tomato</i> NCPPB 2563	isolated from <i>Solanum lycopersicum</i>	NCPPB
<i>pv. tomato</i> NCPPB 3160	isolated from <i>Solanum lycopersicum</i>	NCPPB
<i>pv. coronafaciens</i> LMG 5060	isolated from <i>Avena sativa</i>	BCCM
<i>pv. lachrymans</i> LMG 5456	isolated from <i>Cucumis sativus</i>	BCCM
<i>pv. maculicola</i> LMG 2208	isolated from <i>Brassica oleracea</i>	BCCM
<i>pv. morsprunorum</i> LMG2222	isolated from <i>Prunus avium</i>	BCCM
<i>pv. syringae</i> LMG1247	isolated from <i>Syringa vulgaris</i> , type strain	BCCM
<i>pv. syringae</i> LMG 5082	isolated from <i>Zea mays</i>	BCCM
<i>pv. syringae</i> LMG 5084	isolated from <i>Pyrus communis</i>	BCCM
Carlise 1	isolated from <i>Tilia tomentosa</i>	This study
Carlise 2	isolated from <i>Tilia tomentosa</i>	This study
LMG2222 lmut	derived from <i>pv. LMG2222 morsprunorum</i> , putidacin L1 tolerant mutant	This study
LMG2222 In50	derived from <i>pv. LMG2222 morsprunorum</i> , putidacin L1 tolerant mutant	This study
LMG2222 20(1)	derived from <i>pv. LMG2222 morsprunorum</i> , putidacin L1 tolerant mutant	This study
LMG5456 MDC2	derived from <i>pv. LMG5456 morsprunorum</i> , syringacin M resistant mutant	This study
LMG5456 MDC3	derived from <i>pv. LMG5456 morsprunorum</i> , syringacin M resistant mutant	This study
<i>P. aeruginosa</i>		
PAO1	Clinical isolate	(145)
E2	Environmental isolate	(15)
P8	Clinical isolate	This study
<i>P. carotovorum subsp. carotovorum</i>		
LMG 2378	Isolated from <i>Solanum tuberosum</i>	BCCM
LMG 2383	Isolated from <i>Solanum tuberosum</i>	BCCM
LMG 2384	Isolated from <i>Solanum tuberosum</i>	BCCM
LMG 2385	Isolated from <i>Solanum tuberosum</i>	BCCM
LMG 2394	Isolated from <i>Solanum tuberosum</i>	BCCM
LMG 2410	Isolated from <i>Cucumis sativus</i>	BCCM
LMG 2412	Isolated from <i>Hyacinthus orientalis</i>	BCCM
LMG 2442	Isolated from <i>Brassica oleracea</i>	BCCM

LMG 2444	Isolated from <i>Solanum tuberosum</i> (tuber soft rot)	BCCM
LMG 2913	Isolated from soil	BCCM
<i>P. atrosepticum</i>		
LMG 2374	Isolated from <i>Apium graveolens var. dulce</i>	BCCM
LMG 2375	Isolated from <i>Solanum tuberosum</i> (tuber soft rot)	BCCM
LMG 2386	Isolated from <i>Solanum tuberosum</i> (stem rot)	BCCM
LMG 2390	Isolated from soil	BCCM
LMG 2391	Isolated from soil	BCCM
LMG 2413	Isolated from soil	BCCM
LMG 2443	Isolated from <i>Brassica oleracea</i>	BCCM
LMG 2454	Isolated from <i>Chrysanthemum morifolium</i>	BCCM
SCRI 1043	Isolated from <i>Solanum tuberosum</i> (tuber soft rot)	SCRI
LMG2386 ΔFupA	derived from LMG2386 with 1000bp deletion of FupA gene	This study
LMG2386 MPC11 to 7	derived from LMG2386, 7 isolates tolerant or resistant to pectocin M1	This study

Table 2-2 Plasmids utilised or created in this study

Plasmid	Relevant Characteristic(s)	Source
Cloning/Knockout		
Vectors		
pJexpress411	Kan ^r cloning/expression vector, T7 promoter	DNA 2.0
pJexpress404	Amp ^r cloning/expression vector, T5 promoter	DNA 2.0
pET21-a(+)	Amp ^r cloning/expression vector, T7 promoter	Novagen
pET28-a(+)	Kan ^r cloning/expression vector, T7 promoter	Novagen
pENTR	Kan ^r Gateway cloning entry vector, No promoter	Invitrogen
pMRS101	Amp ^r , Str ^r , Suc ^S , Suicide Vector based on pKNG101	(146)
pENTRPL1	pENTR with putidacin L1 inserted using gateway system	This study
pENTRSL1	pENTR with syringacin L1 inserted using gateway system	This study

pENTRMDC	pENTR with syringacin M inserted using gateway system	This study
Agrobacterium Binary Vectors		
pGWB5	Kan ^r Hyg ^r , Gateway binary vector, 35s promoter, C terminal-sGFP fusion	(147)
pGWB6	Kan ^r Hyg ^r , Gateway binary vector, 35s promoter, N terminal-sGFP fusion	(147)
pGWB17	Kan ^r Hyg ^r , Gateway binary vector, 35s promoter, C terminal-sGFP fusion	(147)
pGWB18	Kan ^r Hyg ^r , Gateway binary vector, 35s promoter, N terminal-sGFP fusion	(147)
pJO530	Kan ^r Hyg ^r , Binary vector, 35s promoter, No-tag	(148)
pG5PL1	pGWB5 with Putidacin L1 inserted by gateway recombination	This study
pG6PL1	pGWB6 with Putidacin L1 inserted by gateway recombination	This study
pG17PL1	pGWB17 with Putidacin L1 inserted by gateway recombination	This study
pG18PL1	pGWB18 with Putidacin L1 inserted by gateway recombination	This study
pG5SL1	pGWB5 with Syringacin L1 inserted by gateway recombination	This study
pG6SL1	pGWB6 with Syringacin L1 inserted by gateway recombination	This study
pG17SL1	pGWB17 with Syringacin L1 inserted by gateway recombination	This study
pG18SL1	pGWB18 with Syringacin L1 inserted by gateway recombination	This study
pG5MDC	pGWB5 with Syringacin M inserted by gateway recombination	This study
pG6MDC	pGWB6 with Syringacin M inserted by gateway recombination	This study
pG17MDC	pGWB17 with Syringacin M inserted by gateway recombination	This study
pG18MDC	pGWB18 with Syringacin M inserted by gateway	This study

recombination		
pJOPL1-Cmyc	pJO530 with Putidacin L1 plus C-terminal 4xMyc tag inserted into KpnI site	This study
pJOPL1-Nmyc	pJO530 with Putidacin L1 plus N-terminal 4xMyc tag inserted into KpnI site	This study
pJOSL1	pJO530 with Syringacin L1 untagged inserted into KpnI site	This study
pJOP19	pJO530 with bushy stunt virus silencing repressor P19 ligated into KpnI site	(149)
Protein Expression		
Vectors		
pETMDC	pET21-a(+) with syringacin M inserted into NdeI/XhoI sites, C-term 6X his tag	This study
pETMDC-10	As pETMDC, with -10 N-terminal amino acids of syringacin M	This study
pETMDC-20	As pETMDC, with -20 N-terminal amino acids of syringacin M	This study
pETMDC_D232A	As pETMDC, with Aspartate 232 mutated to Alanine of syringacin M	This study
pJMPCI	pJexpress411 with Pectocin M1 inserted into NdeI/XhoI sites, No tag	DNA 2.0
pETMPCI	pET21-a(+) with Pectocin M1 inserted into NdeI/XhoI sites, C-term 6X his tag	This study
pETMPCI_D226A	As pETMPCI, with Aspartate 226 mutated to Alanine of pectocin M1	This study
pJMBPR	pJexpress411 with Pectocin M2 inserted into NdeI/XhoI sites, No tag	DNA 2.0
pETMBPR	pET21-a(+) with Pectocin M2 inserted into NdeI/XhoI sites, C-term 6X his tag	This study
pJPP1	pJexpress404 with Pectocin P inserted into NdeI/XhoI sites, C-term 6X his tag	DNA 2.0
pETMPCifer	pET21-a(+) with Pectocin M1 amino acids 1-92, inserted into NdeI/XhoI sites, C-term 6X his tag	This study
pETARAfer	pET21-a(+) with Arabidopsis ferredoxin 1, inserted into NdeI/XhoI sites, C-term 6X his tag	This study
pETMAZfer	pET21-a(+) with Maize ferredoxin 1, inserted into NdeI/XhoI	This study

	sites, C-term 6X his tag	
pETPOTfer	pET21-a(+) with Potato ferredoxin 1, inserted into NdeI/XhoI sites, C-term 6X his tag	This study
pETSPNfer	pET21-a(+) with Spinach ferredoxin 1, inserted into NdeI/XhoI sites, C-term 6X his tag	This study
pJPL1	pJexpress411 with Putidacin L1 inserted into NdeI/XhoI sites, No tag	DNA 2.0
pETPL1	pET21-a(+) with Putidacin L1 inserted into NdeI/XhoI sites, C-term 6X his tag	This study
pJSL1	pJexpress411 with Putidacin L1 inserted into NdeI/XhoI sites, No tag	DNA 2.0
pETSL1	pET21-a(+) with Syringacin L1 inserted into NdeI/XhoI sites, C-term 6X his tag	This study
pET28SL1	pET28-a(+) with Syringacin L1 inserted into NdeI/XhoI sites, N-term 6X his tag	This study
pETPyoL1	pET21-a(+) with Pyocin L1 inserted into NdeI/XhoI sites, C-term 6 his tag + RRRRAVV linker	(15)
pETPyoL1_N1	As pETPyoL1 with Aspartate 31 mutated to Alanine	(15)
pETPyoL1_N2	As pETPyoL1 with Aspartate 97 mutated to Alanine	(15)
pETPyoL1_C1	As pETPyoL1 with Aspartate 150 mutated to Alanine	(15)
pETPyoL1_C2	As pETPyoL1 with Aspartate 180 mutated to Alanine	(15)
pETFR1043	pET21-a(+) with FupA1043 inserted into NdeI/XhoI sites, No-tag	This study
pT5FR1043	pJexpress404 with FupA1043 inserted into NdeI/XhoI sites, No-tag	This study
pETFR2913	pET21-a(+) with FupA2913 inserted into NdeI/XhoI sites, No-tag	This study
pT5FR2913	pJexpress404 with FupA2913 inserted into NdeI/XhoI sites, No-tag	This study
pETFRIB1043	pET28-a(+) with FupA1043 -20 N-terminal amino acids, inserted into NdeI/XhoI sites, N-terminal 6x his tag	This study
pETFRIB2913	pET28-a(+) with FupA2913 -20 N-terminal amino acids, inserted into NdeI/XhoI sites, N-terminal 6x his tag	This study
pETFRIB2386	pET28-a(+) with FupA2386 -20 N-terminal amino acids, inserted into EcoRI/HindIII sites, N-terminal 6x his tag	This study
pETFRKO1_2386	pET21-a(+) with FupA2386 first 1000bp inserted into Sall, XbaI	This study

	sites, Ending with stop codon	
pETFRKO2_2386	pET21-a(+) with FupA2386 last 1000bp inserted into XbaI, Sall sites, Ending with stop codon	This study
pMRFRKO2386	pMRS101 with FRKO1 and FRKO2 fragments ligated at Xba site, ligated into vector Sall site	This study
pKNFRKO2386	pMRFRKO2386 with Col1 origin of replication containing NdeI fragment removed	This study

2.3 DNA manipulations

2.3.1 Polymerase chain reaction

Primers utilised for cloning in this study are outlined in Table 2-3. These primer sets were utilised to create all the vectors in the plasmid table and for sequencing and diagnostic purposes where necessary.

Table 2-3 Primers utilised and created during this study

Name	RE Site	Sequence 5' to 3'	Purpose
FupA₂₃₈₆ F KO	Sall	GCATCGTTCGACATGAATAA GAACGTCTATTTAATGATG	FupA ₂₃₈₆ knockout construction forward gene start
FupA₂₃₈₆ R KO	Sall	GCATCGTTCGACTTACCAGG TGTAAGCGACGC	FupA ₂₃₈₆ knockout construction reverse gene end
FupA₂₃₈₆ R KO	HindIII	GCATCAAGCTTTTACCACCG CCGTTATTGGTATAAG	FupA ₂₃₈₆ knockout construction forward middle
FupA₂₃₈₆ F KO	HindIII	GCATCAAGCTTGCGTGCGT GTCACATATGATGA	FupA ₂₃₈₆ knockout construction reverse middle
FupA₂₃₈₆ F IB	EcoRI	GCATCGAATTCATGACACCT CTGCCGATGAAA	FupA ₂₃₈₆ Δ20 cloning forward
FupA₂₃₈₆ R IB	HindIII	GCATCAAGCTTTTACCAGGT	FupA ₂₃₈₆ Δ20 cloning reverse

GTAAGCGACGC			
FupA₁₀₄₃ F	NdeI	GCATCCATATGAATAAGAAC	FupA ₁₀₄₃ and FupA ₂₉₁₃ cloning forward
		GTCTATTTAATGATGATT	
FupA₁₀₄₃ F IB	NdeI	GCATCCATATGCAGCAAAA	FupA ₁₀₄₃ and FupA ₂₉₁₃ Δ20 cloning forward
		CGACACCTCTGC	
FupA₁₀₄₃ R IB	XhoI	GCATCCTCGAGTTACCAGG	FupA ₁₀₄₃ and FupA ₂₉₁₃ cloning reverse
		TGTAAGCGACGC	
GTAAGCGACGC			
Maz Fer F	NdeI	GCATCCATATGGCTACCTAC	Maize ferredoxin cloning forward
		AATGTGAAAC	
Maz Fer R	XhoI	GCATCCTCGAGCAGCAGGT	Maize ferredoxin cloning reverse
		CGTCTTCTTTGTG	
Pot Fer F	NdeI	GCATCCATATGGCGAGCTA	Potato ferredoxin cloning forward
		CAAGGTG	
Pot Fer R	XhoI	GCATCCTCGAGAGCGGTCA	Potato ferredoxin cloning reverse
		GTTCTTCTTCTTTATG	
Spin Fer F	NdeI	GCATCCATATGGCGGCTTA	Spinach ferredoxin cloning forward
		CAAGGTC	
Spin Fer R	XhoI	GCATCCTCGAGTGCCGTCA	Spinach ferredoxin cloning reverse
		GTTCTTCTTCTTTATG	
Ara Fer F	NdeI	GCATCCATATGGCTACCTAC	Arabidopsis ferredoxin cloning reverse
		AAGGTCAAGTTC	
Ara Fer R	XhoI	GCATCCTCGAGCATAATGG	Arabidopsis ferredoxin cloning reverse
		CTTCTTCTTTGTGGG	
MPCI Fer R	XhoI	ATCCCTCGAGCATCTCTTCC	Pectocin M1 ferredoxin domain cloning reverse
		ACGCCCGTTTT	

PL1 F	KpnI	GCTTAGGTACCATGGCAGG TCGTACCCGC	Putidacin L1 cloning forward (for pJO530)
PL1 R	KpnI	GCATCGGTACCTTAGAAGT GCCAGGTCCAGATG	Putidacin L1 cloning reverse (for pJO530)
PL1 CACC F	-	CACCATGGCAGGTCGTACC CGC	Putidacin L1 cloning forward (Gateway)
PL1 F	NdeI	GGTTCCATATGGCAGGTCG TACCCGC	Putidacin L1 cloning forward
PL1 R	XhoI	GCATCCTCGAGTTAGAAGT GCCAGGTCCAGATG	Putidacin L1 cloning reverse
Myc F	KpnI	GCATCGGTACCATGAGCGG GTTAATTAACGGTG	N-term Myc tag cloning forward (for pJO530)
Myc R	KpnI	GCATCGGTACCTAAGCGCT ACCGTTCAAGTC	C-term Myc tag cloning reverse (for pJO530)
SL1 F	KpnI	GCTTAGGTACCATGGCTGT AAATTACAAACCGCTC	Syringacin L1 cloning forward (for pJO530)
SL1 R	KpnI	GCATCGGTACCTTAAACTC GTAGCCGATATGACC	Syringacin L1 cloning reverse (for pJO530)
SL1 CACC F	-	CACCATGGCTGTAAATTACA AACCGCTC	Syringacin L1 cloning forward (Gateway)
SL1 F	NdeI	CATATGGCTGTAAATTACAA ACCGCTC	Syringacin L1 cloning forward
SL1 R stop	XhoI	CTCGAGAAACTCGTAGCCG ATATGACCG	Syringacin L1 cloning reverse (No stop codon)
SL1 R No stop	XhoI	CTCGAGTTAAACTCGTAGC CGATATGACC	Syringacin L1 cloning reverse (No stop codon)

MPCI F	NdeI	GCATCCATATGGCTACGTA CAAATCAAGGATC	Pectocin M1 cloning forward
MPCI R	XhoI	GCATCCTCGAGTAAACGTT GACCGCGACCGC	Pectocin M1 cloning reverse
MBPR F	NdeI	GCATCCATATGGCGACGTA CAAAGTTAAGTTAA	Pectocin M2 cloning forward
MBPR R	XhoI	GCATCCTCGAGTTTCTTACC ATTTTCTTTAATCTTCAATTC	Pectocin M2 cloning reverse
MDC -10	NdeI	GCATCCATATGACCCCTTAT CCTGAAATTAGCG	Syringacin M -10 truncation cloning forward
MDC -20	NdeI	TGCAGCATATGAATGGTAC CTATCGTGGTCAAG	Syringacin M -20 truncation cloning forward
MDC CACC F		CACCATGGCAGGTCGTACC CGC	Syringacin M cloning forward (Gateway)
MDC F	NdeI	GCTACCATATGCCTATTGAG CTTCCTCC	Syringacin M cloning forward
MDC R	XhoI	GCTACCTCGAGGTTGCCAC TAACCGTAACCG	Syringacin M cloning reverse
MPCI D226A F	-	GCATCCGCGCATATAACGC TCTGTATGATGCTAATCCG	Pectocin M1 D222A mutagenesis forward
MPCI D226A R	-	CGGATTAGCATCATACAGA GCGTTATATGCGCGGATGC	Pectocin M1 D222A mutagenesis reverse
MDC D232A F	-	GCGCCTTCAATGCTGTCTA CGATGCCAATCCGTC	Syringacin M D232A mutagenesis forward
MDC	-	GACGGATTGGCATCGTAGA	Syringacin MD232A mutagenesis

D232A R	CAGCATTGAAGGCGC	reverse
----------------	------------------------	---------

Amplification PCR reactions were performed with the following range of conditions:

Table 2-4 Standard PCR Reaction Components

	Step	Duration (s)
Temperature (°C)		
95	Initial Denaturing	300
95	Denaturing*	45
52-60	Annealing*	45
72	Extension*	60(/kb)
72	Final Extension*	600
10	Hold!	Indefinite

* steps repeated for 30 cycles

With the following reaction composition:

Table 2-5 Standard PCR Reaction Components

	Concentration	Volume
Component		
Pfu Turbo	Stock	1 µl
Reaction Buffer	10X	5 µl
Reverse Primer	1 nM	5 µl
Reverse Primer	1 nM	5 µl
Template	Variable	1-5 µl
dNTPs	5mM	1 µl
H₂O	100%	28-32 µl
		50 µl

For colony PCR a small amount of a bacterial colony on agar from plate was transferred to 50 µl of 10 mM Tris [pH 7.5] and heated for 5 minutes at 96°C. The resulting solution was

clarified by centrifugation and diluted 1:10 into distilled H₂O. 5 µl was used as template for PCR reaction. For PCR from plasmid template or PCR product, the stock was diluted 1:10 and 1 µl was used as reaction template.

If initial PCR conditions did not yield the desired product the reaction was optimized by the inclusion of 5-10 % DMSO and variation of the annealing temperature.

Mutagenic PCR reactions were performed with the following conditions:

Table 2-6 Mutagenesis PCR Conditions

	Step	Duration (s)
Temperature (°C)		
95	Initial Denaturing	30
95	Denaturing*	30
55	Annealing*	60
68	Extension*	60/kb
72	Final Extension*	600

* steps repeated for 18 cycles

Table 2-7 Mutagenesis PCR Reaction Components

	Concentration	Volume
Component		
Pfu Turbo	Stock	1 µl
Reaction Buffer	10X	5 µl
Reverse Primer	1 nM	5 µl
Reverse Primer	1 nM	5 µl
Template Plasmid	2.5 µl	1 µl
dNTPs	5mM	1 µl
H₂O	100%	32 µl
		50 µl

A negative control reaction lacking polymerase was run to assess transformation background. 10 µl of reaction was run on an agarose gel (see below) to assess the success of amplification. 1 µl of DpnI was added to the reaction mixture and this was incubated at 37 °C for 1-2 hours to remove methylated template plasmid. 2-5 µl was used to transform competent DH5α with appropriate selection (see below).

2.3.2 DNA Ligation

PCR and vector fragments were ligated by first digesting plasmid and insert DNA with the appropriate restriction enzymes. Generally 10 µl of PCR product and 10 µl of 100 µg/ml vector were digested. Digested DNA was run on an agarose gel; the bands were excised and cleaned up by gel extraction. Resulting DNA fragments were used for the ligation reaction with the following composition: 8 µl insert, 3 µl vector, 2 µl 10x ligation buffer, 1 µl T4 Ligase, H₂O to 20 µl. When a ligation was performed with two insert fragments 6 µl of each insert and 3 µl of vector was used, in a final volume of 25 µl. Ligation reaction was performed for 3 hours on the bench and then 2-5 µl was used to transform DH5α with appropriate selection (see below).

2.3.3 Electrophoresis

DNA was separated on a 0.8-2 % agarose gel in 2x TBE buffer and visualized with GelRED (Cambridge Biosciences, UK), SYBR Safe (Life Technologies) gel stains.

2.3.4 Extraction of genomic DNA

Genomic DNA for genome sequencing was extracted from 1 ml of overnight bacterial culture using the QIAamp DNA Mini Kit (Qiagen) following the manufacturer's supplied protocol.

2.3.5 Plasmid DNA extraction

Plasmid DNA was prepared from 5 ml of overnight culture of the plasmid bearing strain using a plasmid mini-prep kit (Qiagen) and the standard protocol. It is important to note that for non-*endA* minus strains (i.e. *E. coli* SM10 or *Pectobacterium* sp.) the PB wash must be performed to remove the contaminating nuclease. For standard cloning strains i.e. DH5 α , this step can be omitted.

2.3.6 Bacterial transformation

Commercially prepared chemically competent *E. coli* DH5 α and BL21 derivatives were used for transformations using the manufacturer supplied protocol. The electroporation method was utilized for non-standard strains of *E. coli*, *Pectobacterium* and *A. tumefaciens*. 50 ml of cells were cultured in LB to an approximate OD₆₀₀ of 0.6, chilled on ice for 10 minutes and harvested by centrifugation at 4500 g for 10 minutes. Cells were then rinsed twice in 40 ml of ice cold sterile H₂O, and then resuspended in 1 ml of ice cold sterile 10 % (v/v) glycerol. 100 μ l of cells and 2-5 μ l of DNA were added to an electroporation cuvette and 2.5 kV applied at a capacitance of 25 μ F using an electroporator (Invitrogen, UK). Cells were recovered immediately in 700 μ l of LB at 37 or 28 °C, before plating on LB agar with the appropriate selection.

2.3.7 Creation of deletion mutants in *Pectobacterium*

The suicide pMRS101 plasmid was utilized in the creation of deletion mutants in *Pectobacterium* spp.(146). This vector is derived from pKNG101 with the addition of the high copy number Col0 origin of replication on an NdeI fragment to increase plasmid yield and to allow initial manipulations in DH5 α . pKNG101 has a conditional origin of replication requiring the replication factor λ pir for propagation and thus is unable to replicate in most Gram-negative bacteria.(150) The initial and final 1000bp of the target gene were fused with a stop codon inserted at the fusion site. This cassette was inserted

into pMRS101 at the unique Sall site and the ColO origin of replication excised by NdeI digestion. After this step the vector (designated pKNFRKO2386) needed to be propagated in *E. coli* SM10 λ pir with 50 $\mu\text{g}.\text{ml}^{-1}$ streptomycin as the selection agent.

The vector was then transformed into the *Pectobacterium* knockout target (LMG2386) by electroporation and cells were selected on 50 $\mu\text{g}.\text{ml}^{-1}$ streptomycin. It was found to be important to use 50 $\mu\text{g}.\text{ml}^{-1}$ streptomycin rather than the published 25 $\mu\text{g}.\text{ml}^{-1}$ to prevent the isolation of spontaneously resistant colonies. Isolated streptomycin resistant colonies had the entire pKNFRKO2386 plasmid recombined into the *Pectobacterium* genome via recombination in one 1000 bp gene fragment.

pMRS101 possesses the *sacB* gene which imparts sucrose sensitivity on Gram-negative bacteria (150). Recombination in the second 1000 bp fragment, which leads to excision of the plasmid and either regeneration of the whole gene or creation of the knockout was selected for by growth in NaCl free LB broth +10 % sucrose (LB sucrose), followed by serial dilutions onto LB sucrose agar (and LB streptomycin agar to test for completeness of plasmid excision). Sucrose resistant colonies were screened by PCR using primers for the target gene, with PCR products truncated to 2000 bp indicative of a successful knockout.

2.4 Determination of protein concentration

Concentration of purified protein was determined by the spectroscopic method, using the absorbance of the protein solution at 280 nm. The webtool 'Protparam' (current weblink = <http://web.expasy.org/protparam/>) was used to estimate the molar extinction coefficient for the protein and this was utilised to calculate the protein concentration using the following equation. The ratio of absorbance between 280 and 260 nm was monitored to assess for contamination of the sample with nucleic acids.

$$C = A/\epsilon$$

Where:

C = Protein concentration

A = Absorbance of sample (over a path length of 1 cm)

ϵ = The molar absorptivity of the protein (i. e. $\frac{\text{extinction coefficient @ 280 nm}}{\text{molar mass}}$)

To determine the protein concentration of non-homogenous samples the Bradford assay was employed (ref). The Biorad Quick Start Bradford Protein assay kit was employed, using the standard manufacturer supplied protocol.

2.5 Bacteriocin toxicity assays

2.5.1 Overlay spot plate method

Soft agar overlay spot plates were performed using the method of Fyfe et. al.(151). 150 μ l of test strain culture at $OD_{600\text{ nm}} = 0.6$ was added to 6 ml of 0.8% soft agar and poured over an LB or KB agar plate, as appropriate. 5 μ l of neat or serially diluted bacteriocin solution was spotted onto the plates and incubated for 20 hours at 37 or 28 °C, as appropriate. After incubation plates were inspected for zones of inhibition, growth enhancement (in the case of pectocins or ferredoxins) or interference between proteins. To assess bacterial strains directly for the production of bacteriocins the colony antagonism agar overlay assay was utilised. Individual colonies were grown on an agar plate under appropriate inducing conditions (i.e. 200 μ M mitomycin C) and lysed using chloroform vapours, by exposure of the plate face down to filter paper disk (2 cm by 2 cm) soaked in chloroform. The chloroform was allowed to dissipate for 15-30 minutes and then soft agar containing the strain to be tested for sensitivity was overlaid, as above.

2.5.2 Liquid growth assays

For inhibition of growth in liquid culture, cells were grown in LB or KB broth with or without 200 μ M 2,2'-bipyridine. Purified bacteriocin was added at an appropriate time point and the OD_{600} , along with phenotypic changes and cell lysis was monitored throughout the experiment.

2.6 Identification of bacteriocins by ammonium sulphate precipitation

Bacteriocins responsible for the cytotoxicity of strains of *P. syringae* showing inhibition in colony antagonism agar overlay assay were identified by ammonium sulphate precipitation of clarified stationary phase culture of the producing strain. Strains were grown for 24-48 h in 2 × 625 ml of Kings B media with mitomycin C (50-200 µM). The culture was clarified by centrifugation and the supernatant concentrated by ammonium sulfate precipitation; 3 M ammonium sulfate was added to the supernatant and precipitation was allowed to proceed at 4 °C with stirring for 1 h. Precipitate was collected via centrifugation (3000 g for 20 minutes) and resuspended in sample buffer (50 mM Tris, 20 mM NaCl, 1 mM DTT, 1 mM EDTA, pH 7.5) with protease inhibitor tablets (Complete EDTA free, Roche) and was dialyzed against sample buffer and tested for killing activity by spotting onto a KB agar plate overlaid with soft agar containing 200 µl of 0.6 OD₆₀₀ culture of a test strain. Proteins were separated by native PAGE at 4 °C. Samples were run in duplicate, gels were halved and killing activity was tested via soft agar overlay of half the gel. The other half was stained with Coomassie Brilliant Blue 250, the band corresponding to zones of inhibition in the soft agar overlay assay were excised and identified via tandem mass spectrometry (MS/MS), with trypsin as the fragmentation step.

2.7 Isolation of bacteriocin tolerant mutants

1.5 ml of a culture of appropriate bacterial strain (OD_{600 nm} = 0.6 to 1) was centrifuged and resuspended in 100-500 µl of 50mM Tris, 50mM NaCl [pH7.5], containing purified bacteriocin at a concentration of 50-300 µM. The bacteria and bacteriocin mixture was then incubated with shaking at 28 °C for 30 minutes to 1 hour. The mixture then spread on appropriate nutrient agar plate and incubated for between 20 and 48 hours at 28 °C. Isolated colonies were initially screened to exclude contamination by PCR amplification of 16S DNA followed by sequencing. Mutants were then subjected to phenotypic characterization and genome sequencing.

2.8 Lipid II cleavage assay

Lipid II hydrolysis assays were performed using a modified version of the assay described by Barreteau *et al.* (82), with non-radiolabeled lipid II substrate obtained from the UK Bacterial Cell Wall Biosynthesis Network (152,153). Assays were carried out in 100 mM Tris, 150 mM NaCl, 0.2% n-dodecyl-D-maltoside with 5 µg of lipid II and 10 µg of wildtype or mutant M-class bacteriocins. To test the metal dependence of the M-class bacteriocins, assays were performed in the presence of MgCl₂, CaCl₂, MnCl₂, CoCl₂, ZnCl₂ or NiSO₄ at 20 mM or with 1 mM EGTA. Reactions were performed at 30 °C for 0-120 minutes and terminated by heating at 100 °C. Reaction products were separated by thin-layer chromatography on LK6D silica gel plates with 2-propanol: ammonium hydroxide: water (6:3:1) as the mobile phase and visualised by staining with 20% phosphomolybdic acid solution in ethanol and heating. A band corresponding to lipid II was observed with an R_f of 0.7 as reported previously.(82)

2.9 SDS-PAGE, silver staining and immunoblotting

Purified proteins and LPS in this study resolved by electrophoresis on 10 to 18 % SDS-polyacrylamide gels. Proteins resolved by the gels were visualised by coomassie blue staining (0.1 % Coomassie Blue R250 in 10 % acetic acid, 50 % methanol, in H₂O) for 30 minutes, followed by destaining (10 % acetic acid, 10 % methanol, in H₂O). Low concentration protein or LPS was visualised by silver staining using the Invitrogen ultrafast silver staining method. For immunoblotting protein was transferred onto nitrocellulose membranes blocked in TN tween (0.1% Tween 20, 100 mM Tris, 150 mM NaCl pH7.5) with 20% milk powder and then visualised using appropriate primary (incubation in 1:2000 dilution in TN tween for 30 minutes) and secondary antibody (incubation in 1:5-10000 dilution in TN tween for 30 minutes) combinations, with 1 x 30 followed by 5 x 5 minute washes with TN tween between blocking and antibody incubation steps. The blots were developed using Clarity Western ECL Substrate (Life Science Research).

2.10 LPS purification and isolation of LPS-derived polysaccharide

LPS was purified from *P. aeruginosa* and *P. syringae* strains as described previously, with modifications (154). Cells were grown for 20 hours at 37 °C and 28 °C for *P. aeruginosa* and *P. syringae* respectively, pelleted by centrifugation at 6000 g for 20 minutes, and resuspended in 50 mM Tris, pH 7.5 containing lysozyme (2 mg ml⁻¹) and DNase I (0.5 mg ml⁻¹). Cells were lysed by sonication and the cell lysate was incubated at 20 °C for 30 minutes before EDTA was added to a final concentration of 2 mM. An equal volume of aqueous phenol was added and the solution was heated at 70 °C for 20 minutes, with vigorous mixing. The solution was then cooled on ice for 30 minutes, centrifuged at 7000 g for 20 minutes and the aqueous phase extracted. Proteinase K was added to a final concentration of 0.05 mg ml⁻¹ and dialysed for 12 hours against 2 x 5 L dH₂O. LPS was pelleted by ultracentrifugation at 100,000 g for 1 hour, resuspended in dH₂O and heated to 60°C for 30 minutes to remove residual proteinase K activity. LPS-derived carbohydrates were isolated by heating LPS in 2% acetic acid for 1.5 hours at 96 °C. Lipid A was removed by centrifugation at 13,500 g for 3 minutes followed by extraction with an equal volume of chloroform. The aqueous phase was then lyophilised.

2.11 Whole genome sequencing

The genomes of wildtype bacterial strain and bacteriocin tolerant mutants were sequenced at the Glasgow Polyomics Facility, generating paired-end reads on an Illumina MiSeq Personal Sequencer. Reads from wildtype strain were trimmed using quality scores and assembled *de novo* using the CLC genomics workbench. Assembled contigs were then annotated by the Xbase webserver (155), using the most closely related available genome sequence as a reference. To identify genetic changes in mutant strains, reads were trimmed and mapped to annotated wildtype genome, probabilistic variant detection was utilized to identify potential SNPs and INDELS using CLC genomics workbench. Variations from wildtype were inspected manually to verify authenticity.

2.12 Isothermal titration calorimetry

ITC experiments were performed on a VP-ITC microcalorimeter (MicroCal LLC). For monosaccharide binding, titrations were carried out at 298 K with regular 15 μl injections of ligands into 60-100 μM pyocin L1 or putidacin L1 at 300 second intervals. 50 mM D-mannose and D-rhamnose were used as titrants and reactions were performed in 0.2 M sodium phosphate buffer, pH 7.5. Proteins were dialysed into reaction buffer overnight and sugar solutions were made using this dialysis buffer. For O-antigen-pyocin L1 binding reactions, pyocin L1 was used as titrant at 150 μM with cleaved O-antigen sugars dissolved at 1 mg ml^{-1} in the chamber. For curve fitting we estimated the molar concentration of LPS-derived CPA containing carbohydrate chains at 20 μM based on an estimated average molecular weight of 10 kDa for CPA containing polysaccharides and estimating the percentage of total LPS represented by CPA containing carbohydrates as 20% of the total by weight (156). This value may not be accurate and as such the stoichiometry implied by the fit is likely to be unreliable. However, the use of this estimated value has no impact on the reported parameters of ΔH , ΔS and K_d . For O-antigen-putidacin L1 binding reactions, O-antigen was used as the titrant at 3 mg ml^{-1} with 60 μM putidacin L1 in the chamber. Reactions were performed in 20 mM HEPES buffer pH 7.5. All samples were degassed extensively prior to the experiments. Calorimetric data were calculated by integrating the area under each peak and fitted with a single-site binding model with Microcal LLC Origin software. The heats of dilution for each titration were obtained and subtracted from the raw data.

2.13 Identification of FupA by pull down

A 2 L suspension culture of *Pba* LMG 2386 was grown in LB with 200 μM bipryidine until stationary phase was reached. Cells were harvested by centrifugation, resuspended in 20 ml of 50 mM Tris, 10 mM EDTA, pH 7.2. Protease inhibitors and 2 mg ml^{-1} lysozyme were added and cells were lysed by sonication. Cellular debris were removed by centrifugation at 8000 g for 10 minutes and membranes were then pelleted by ultracentrifugation at 100,000 g at 4°C, for 1 h. Pelleted membranes were resuspended with a tight fitting homogeniser in 20 ml of 50 mM Tris, 0.5% sarkosyl pH 7.2, left to solubilise for 20

minutes at room temperature and the outer membrane fraction pelleted by centrifugation at 100,000 g at 4 °C, for 1 h. The pellet was resuspended as before in 20 ml of 20 mM Tris, 1% n-octyl- β -D-glucoside (β -OG) pH 7.2 and solubilised for 12 hours at 4°C. Purified pectocin M1 in 50 mM Tris, 50 mM NaCl, pH 7.5 was immobilised on a 1 ml His-trap column. Bound pectocin M1 was washed with 20 column volumes of Tris buffer (50 mM Tris, 500 mM NaCl, 10 mM imidazole, pH 8.0). The solubilised OM fraction from *Pba* LMG 2386 was passed through the column, which was subsequently washed with 20 column volumes of Tris buffer as above. Proteins were eluted from the column with Tris buffer containing an increasing concentration of imidazole (20, 50, 100 and 150 mM with pectocin M1 eluting at 100 mM imidazole). Control experiments were performed in which the *Pba* LMG 2386 solubilised OMs were passed down a column with no pectocin bound and imidazole elutions were undertaken for a column to which no OM fraction had been added (Figure 2-1). Proteins were visualised by Coomassie and silver staining of SDS-PAGE gels and bands unique to the pectocin M1 plus OM fraction experiment were excised and identified by peptide mass fingerprinting.

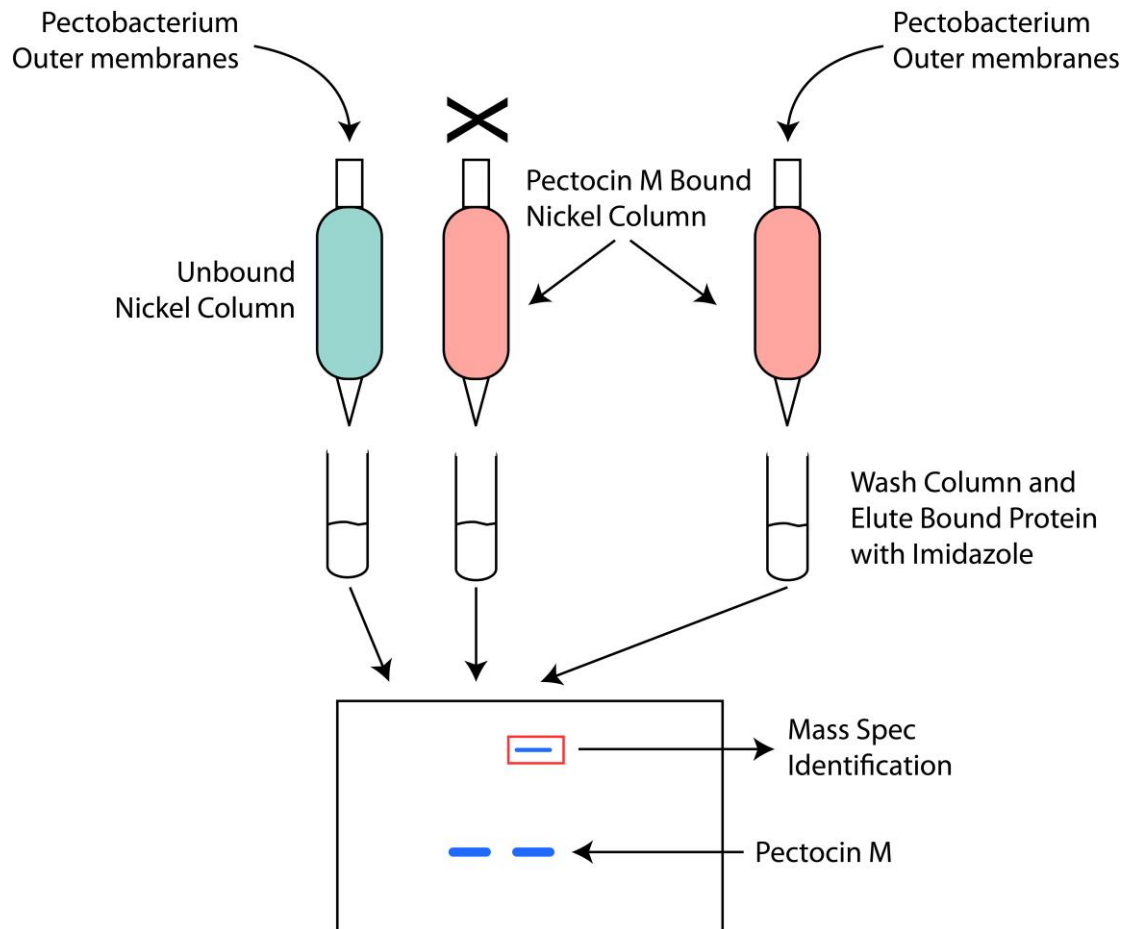


Figure 2-1: Outline of pull down experiment for the identification of FupA

2.14 Recombinant protein expression and purification

2.14.1 Syringacin M

Syringacin M was overexpressed from *E. coli* BL21 (DE3) carrying the plasmid pETMDC. 5 L of LB broth was inoculated (1:100) and overnight culture and cells were grown at 37 °C in a shaking incubator to an $OD_{600} = 0.6$. Protein production was induced by the addition of 0.3 mM IPTG, the cells were grown for a further 12 hours at 24 °C and harvested by centrifugation. The cell pellet was resuspended in 20 mM Tris-HCl and 100 mM NaCl containing 5 mM imidazole (pH 7.5). Selenomethionine derivative protein was produced by expressing syringacin M in the methionine auxotrophic *E. coli* strain B834 (DE3), grown

in M9 minimal media supplemented with 2 mg l⁻¹ thiamine, 40 mg l⁻¹ of each of 9 essential amino acids (excluding methionine) and 50 mg ml⁻¹ selenomethionine. Cells were grown to 0.4 OD₆₀₀, induced with 1 mM IPTG and grown for a further 8 hours at 28 °C. Cells were lysed using a MSE Soniprep 150 (Wolf Laboratories, UK) and the cell debris separated by centrifugation. The cell-free lysate was applied to a 5 ml His Trap™ HP column (GE Healthcare, USA) and the protein eluted over a 0-350 mM imidazole gradient. Syringacin M containing fractions were dialysed overnight into 20 mM Tris-HCl, 20 mM NaCl (pH 8.0) and the protein was further purified by gel filtration chromatography on a Superdex S75 26/60 column (GE Healthcare) equilibrated in the same buffer. The protein was concentrated to 10-15 mg.ml⁻¹ stored at -80 °C in this buffer until required.

2.14.2 Pectocin M1, M2 and P

Expression and purification of His-tagged proteins was as for syringacin M, using plasmids pETMBPR, pETMPCI and pJPP1 in *E. coli* BL21 (DE3) pLysS. 5% glycerol was added to all buffers when purifying pectocin M1 and pectocin P as it was found to enhance protein stability. Expression of untagged pectocin M1 and M2 was performed in the pectocin resistant strain *P. carotovorum subsp. carotovorum* LMG2410, containing pJMPCI or pJBMPR. 5 L of LB broth was inoculated (1:100), cells were grown at 28 °C to OD₆₀₀ = 0.6 and then induced with 0.3 mM IPTG and growth for an additional 12 hours at 28 °C. Cells were lysed and clarified as for syringacin M and supernatant applied to a DE-52 anion exchanged column (Whatman) equilibrated in 50 mM Tris-HCl, pH 7.5, 20 mM NaCl. Bound protein was eluted with a linear gradient of 20-600 mM NaCl in lysis buffer. Protein was then purified by gel filtration and concentrated and frozen as for syringacin M.

2.14.3 Putidacin and syringacin L1

Expression and purification of His-tagged proteins was performed as described for syringacin M, using plasmids pETPL1, pETSL1 and pET28SL1 in *E. coli* BL21 (DE3) for putidacin L1 and *E. coli* BL21 (DE3) pLysS for syringacin L1.

2.14.4 FupA

The FupA open reading frames (ORF) from *Pba* SCRI1043 (FupA₁₀₄₃), *Pbc* LMG2913 (FupA₂₉₁₃) and *Pba* LMG2386 (FupA₂₃₈₆) were amplified by PCR in their entirety or lacking the region coding for the 20 amino acid N-terminal signal sequence (Δ 20) (For *Pba* LMG2836 for only the Δ 20 construct was made). The full-length ORF was ligated into pET21a at the *Nde*I and *Xho*I restriction sites. The Δ 20 ORF was ligated into pET28a at the *Nde*I and *Xho*I (or *Eco*RI and *Hind*III for *Pba* LMG2386) restriction sites to encode a protein with an N-terminal His₆-tag. Plasmids were transformed into *E. coli* BL21 (DE3) for expression. Cells expressing full-length FupA were induced at OD₆₀₀ = 0.6 with 0.1 mM IPTG and grown at 28 °C for 12 h. The outer membrane fraction from these cells was isolated and co-elution experiments performed as described in section 2.12.

Cells expressing FupA Δ 20 constructs as inclusion bodies were grown at 37 °C for 36 h in auto-inducing super broth (157). Inclusion bodies were refolded using the method of Saleem et. al. with modifications (158). Cells were harvested and lysed as for syringacin M, the insoluble fraction (containing the inclusion bodies) was isolated by centrifugation at 18,000 g for 25 minutes and homogenised using a tight fitting homogeniser in with 50 mM Tris, 1.5% LDAO, pH 7.5 and incubated at room temperature with shaking for 30 minutes. Inclusion bodies were pelleted by centrifugation at 18,000 g for 25 minutes and homogenised once more in 50 mM Tris, 1.5% LDAO (v/v), pH 7.5, pelleted and washed once in 50 mM Tris pH 7.5 before pelleting a final time. Inclusion bodies were then denatured in denaturing buffer (10 mM Tris, 1 mM EDTA, 8 M Urea, 1 mM DTT pH 7.5) at a ratio of 0.5 g of inclusion body to 40 ml of buffer using a tight fitting homogeniser, followed by incubation with shaking at 56 °C for 30 minutes. Insoluble material was then removed by centrifugation at 8000g for 10 minutes.

FupA in denaturing buffer was then added drop wise to an equal volume of rapidly stirring refolding buffer (20 mM Tris, 1M NaCl, 5% (v/v) LDAO pH 7.9), followed by stirring for 1.5 h. Refolded FupA was then dialysed (10-15,000 Mw cut off membrane) into 2 x 5L of dialysis buffer (20 mM Tris, 0.5 M NaCl, 0.1% (v/v) LDAO pH 7.9) over 16 hours at 4 °C. Refolded FupA was then purified by Ni-affinity chromatography, with dialysis buffer used for binding FupA to the nickel column and dialysis buffer with 0.5 M imidazole used to

elute the protein. The protein was further purified using a superdex S200 26/60 column equilibrated in 50 mM Tris, 200 mM NaCl, 0.1 % (v/v) LDAO pH 7.9.

For crystallisation experiments in β -OG, FupA was exchanged into buffer containing 0.8-1 % β -OG, by immobilisation on a nickel column followed by washing with 10 column volumes of 50 mM Tris, 200 mM NaCl, 0.8-1 % (v/v) β -OG pH 7.9 and eluted with the same buffer with 0.5 M imidazole. The protein was then concentrated to 10-15 mg.ml⁻¹ before dialysis (10-15,000 Mw cut off membrane) for 20 h against 50 mM Tris, 200 mM NaCl, 0.8-1 % (v/v) β -OG, pH 7.9, to remove imidazole and normalise β -OG concentration. Successful refolding of FupA was confirmed by analytical gel filtration and circular dichroism. Refolded FupA₁₀₄₃ was concentrated and dialysed against a final buffer of 50 mM Tris, 50 mM NaCl, 0.1% LDAO pH 7.5, for storage or 50 mM sodium phosphate, 0.1% LDAO for NMR experiments.

2.15 Crystallisation, data collection and structure solution

2.15.1 Syringacin M

Initial crystallisation trials were performed using a Cartesian Honeybee 8+1 dispensing robot into 96 well plates via the sitting drop method (reservoir volume of 80 μ l, drop size: 0.5 μ l protein, 0.5 μ l reservoir solution) by vapour diffusion with syringacin M at a final concentration of 6 mg ml⁻¹. Hexagonal shaped crystals that diffracted to 6-7 Å at a home X-ray source were obtained in 10 % w/v PEG 8000, 20 % v/v ethylene glycol, 0.03 M CaCl₂, 0.03 M MgCl₂, 0.1 M Bicine/Trizma base pH 8.5 at 20 °C from the MORPHEUS crystallisation screen (159). This crystal form had a symmetry of the space group *P*6₃22 and an unusually high solvent content of approximately 80%. Optimisation was performed in sitting drop plates around this condition for both wildtype and D232A mutant protein. The best hexagonal crystals (Figure 9-1-A) were obtained in 7% w/v PEG 8000, 30% v/v ethylene glycol 0.03 M CaCl₂, 0.03 M MgCl₂, 5% dimethyl sulfoxide, 0.1 M Bicine/Tris base pH 8.5 at 16 °C, and used for data collection at Diamond Light Source, Oxfordshire (DLS) with diffraction to 2.83 Å and 3.12 Å for wildtype and mutant proteins, respectively (Figure 9-2-A). All data sets collected at the DLS were processed with the programs XDS (160) and Scala (161). Phasing was attempted by molecular replacement

(MR) using PHASER (162), with the catalytic domain from colicin M as the search model. This proved unsuccessful and selenomethionine labelled protein (SeMet) was prepared and crystallised in the above conditions. A SeMet labelled crystal, producing diffraction to 3.1 Å, was used to collect multiple-wavelength anomalous dispersion (MAD) data near the selenium absorption edge at the DLS. Phases were determined by MAD/SAD techniques using programs SHARP/autoSHARP (163,164), SHELXC/D/E (165), and a partial model was built using ARP/wARP (166) and BUCCANEER (167). Further modelling and refinement against the wildtype or mutant data was performed with programs COOT (168), REFMAC (169) and various other programs from the CCP4 suite (170). Quality control of the geometry of the model was performed using RAMPAGE (171).

The limited resolution of data from the hexagonal crystal form resulted in difficulty in modelling of the β -strands and connecting loops and so *in situ* trypsin digestion/crystallisation was performed to change the crystal packing (172). Trypsin was added to syringacin M (15 mg ml⁻¹) at a ratio of 1:200 on ice, immediately prior to addition to drop. Stacks of thin plates, diffracting to 2.1 Å at a home X-ray source, were grown in 8% w/v PEG 8000, 30% v/v ethylene glycol, 0.13 M CaCl₂, 0.03 M MgCl₂, 0.1 M Bicine/Tris base pH 8.5 at 4 °C. To obtain single crystals, crystals grown under these conditions were crushed in the above reservoir buffer and 3-fold serial dilutions of this solution were used to seed sitting drops of the same composition at 16 °C. Single rhombic crystals formed after two days (Figure 9-1-B). These crystals had symmetry of the $P2_1$ space group and a solvent content of 52 %. Diffraction data were collected for the crystal of this form at DLS, reaching a resolution of 1.46 Å (Figure 9-2-B). This data was phased by MR using PHASER (162) and the model previously built against the data for the hexagonal crystal form, excluding the N-terminal 38 amino acids. High resolution data allowed for improved structure modelling in COOT (168) and final refinement with the use of individual atom anisotropic thermal parameters performed by REFMAC (169). Model based on monoclinic data was subsequently used to improve the full-length wildtype and mutant models from the hexagonal form. The N-terminal residues 2-38 were also modelled using the hexagonal form data for both wildtype and the D232A mutant. Features of the N-terminal electron density suggested some degree of conformational disorder, which limited the quality of the modelling of this region. Despite this, numerous interactions between N-

terminus and the rest of the protein were observed. Data collection and refinement statistics for both crystal forms of syringacin M are presented in Table 2-8.

Table 2-8 Data collection and refinement statistics for syringacin M

	Monoclinic	Hexagonal	Hexagonal D232A
Data Collection^a			
Space group	<i>P</i> 2 ₁	<i>P</i> 6 ₃ 22	<i>P</i> 6 ₃ 22
Cell dimensions			
<i>a</i>, <i>b</i>, <i>c</i> (Å)	55.81, 96.60, 64.27	159.69, 159.68, 100.17	160.35, 160.35, 100.74
<i>α</i>, <i>β</i>, <i>γ</i> (°)	90, 114.17, 90	90, 90, 120	90, 90, 120
Resolution (Å)	50.92 - 1.46 (1.50 - 1.46)	46.34 - 2.83 (2.91 - 2.83)	40.09 - 3.12 (3.20 - 3.12)
Solvent content	~50%	~80%	~80%
No. of unique observations	106648 (7853)	17330 (1337)	13347 (1018)
Multiplicity	6.2 (6.0)	8.2 (8.6)	15.5 (16.2)
Completeness (%)	99.7 (99.7)	99.12 (100)	99.53 (100)
<i>R</i>_{merge} (%)	5.2 (96.6)	5.9 (69)	4.8 (78.7)
<i>R</i>_{pim} (%)^b	2.5 (51.5)	2.2 (25.7.8)	1.8 (28.4)
Mean <i>I</i>/σ(<i>I</i>)	13.6 (2.9)	19.5 (3.1)	26.9 (4.3)
Refinement Statistics			
<i>R</i>_{work}/<i>R</i>_{free} (%)	15.2/20.1	20/23.9	18.2/22.4
Non-hydrogen atoms	4412	2139	2123
RMSD of bond length (Å)	0.020	0.020	0.012
RMSD of angle (°)	2.097	2.028	1.513
Waters	551	35	27
Mean/Wilson plot B-value (Å²)	28.94/23.1	84.27/102.3	98.7/107.9
Ramachandran plot (%)^c			

Favoured/Allowed/O	97.9/2.1/0	88.3/9.9/1.8	89.1/8.4/2.6
Outliers			
PDB identifier	4FZL	4FZN	4FZM

^a Values in parentheses refer to the highest resolution shell.

$$^b R_{\text{pim}} = \frac{\sum_{\text{hkl}} [1/(N - 1)^{1/2} \sum_i |I_i(\text{hkl}) - \langle I(\text{hkl}) \rangle| / \sum_{\text{hkl}} \sum_i I_i(\text{hkl})]}{}$$

^c Percentages of residues in favoured/allowed regions calculated by the program RAMPAGE (27)

2.15.2 Pectocin M2

Initial crystallisation trials were performed at the high throughput crystallization facility of the University of Zurich using the vapour diffusion method (reservoir volume of 50 μl , drop size: 100 nl protein, 100 nl reservoir solution) with pectocin M2 at a final concentration of 15 mg ml^{-1} . Pectocin M2 formed crystals or spherulites in a number of conditions containing ammonium sulphate and PEG 3350. Crystals were extracted from one of these conditions (15 % PEG 3350, 0.2 M ammonium sulphate, 3 % 2-methyl-2,4-pentanediol (MPD), 0.1 M bis-tris pH 6.5), cryoprotected by increasing PEG 3350 to 30 % and data were collected at 100 °K to 2.3 Å in the space group $P2_1$, at the SLS (Zurich). Re-crystallisation screening of pectocin M2 was performed, using a custom screen with variations in the concentration/ratio of precipitants from the original condition (ammonium sulphate and PEG 3350), pH and additives. Clusters of large rod-shaped crystals formed at high ammonium sulphate concentrations (Figure 9-1-C). This was optimised giving a final condition of 1.8 M ammonium sulphate, 3 % MPD, 0.1 M MES, pH 6.5. These crystals were manually separated and cryoprotected with 15-20 % glycerol. Data were collected at 100 K on beamlines I02 and I03 at the Diamond Light Source (Oxfordshire, UK) to a resolution of 1.86 Å (Figure 9-2-C). Automatic data-processing was performed with Xia2 within the EDNA package (173). Datasets for experimental phasing using the iron-sulphur cluster of pectocin M2 were collected at the iron K-edge (1.7433 Å) and high-resolution data were collected at 0.9796 Å.

Phases for the $P2_1$ and $P3_121$ datasets, were obtained from the anomalously scattering substructure from the pectocin-ferredoxin domain iron-sulphur cluster, determined for the iron-edge dataset using the Hybrid Substructure Search from the Phenix package (174). Four positions were located per ASU corresponding to two iron-sulphur clusters

(correlation coefficient = 0.5) from two pectocin M2 molecules. These positions were then utilised by Phaser-EP to determine initial phases for the map (162,170,174). Phases were improved by density modification using RESOLVE density modification from the Phenix package, and the initial model was built and refined using Phenix Autobuild (174). In the $P3_121$ form the autobuilt model was then utilised by Phaser to obtain phases for the high-resolution dataset and the model was further built and refined manually using Coot 0.7 and Refmac5 (162,168,169). Validation of refined structures was performed using the Molprobit web server and Procheck from CCP4i (175,176). Data collection and refinement statistics for both crystal forms of pectocin M2 are presented in Table 2-9.

Table 2-9 Data collection and refinement statistics for pectocins M2

	High Resolution Data		Iron Edge Data
Data Collection ^a			
Space Group	$P2_1$	$P3_121$	$P3_121$
Cell Dimensions			
a, b, c (Å)	44.65, 116.75, 60.78	117.45, 117.45, 128.45	117.26, 117.26, 128.53
α, β, γ (°)	90, 94.96, 90	90, 90, 120	90, 90, 120
Resolution (Å)	50.00-2.30 (2.44-2.30)	64.22-1.86 (1.91 - 1.86)	43.31-2.01 (2.06-2.01)
Rmerge (%)	5.0 (59.9)	3.4 (68.3)	3.8 (69.3)
Rpim (%)^b	-	0.9 (15.7)	2.0 (31.0)
Mean $I/\sigma(I)$	12.41 (1.85)	47.1 (5.5)	28.9 (3.1)
Completeness (%)	96.6 (95.7)	100.0 (99.9)	99.4 (98.7)
Redundancy	3.2 (2.8)	20 (20.8)	8 (6.6)
Refinement			
Resolution (Å)	50.00-2.30 (2.44-2.30)	64.22-1.86 (1.91 - 1.86)	
No. Reflections	52652 (8438)	86092 (6304)	
Rwork / Rfree (%)	21.0/27.2	16.8/19.1	
No. Atoms			
Protein	4093	4175	
Ligand/ion	34	388	

<i>Water</i>	49	438
B factors		
<i>Protein</i>	69.1	45.5
<i>2Fe-2S</i>	74.6	35.4
<i>SO₄²⁻ / Cl⁻</i>	95	68.2
<i>Glycerol / MPD</i>	-	70.7
<i>Water</i>	42.4	56.0
r.m.s deviations		
<i>Bond lengths (Å)</i>	0.016	0.024
<i>Bond angles (°)</i>	1.757	2.55
PDB identifier	4N59	4N58

^a Values in parentheses refer to the highest resolution shell

$$^b R_{\text{pim}} = \frac{\sum_{hkl} [1/(N-1)]^{1/2} \sum_i |I_i(hkl) - \langle I(hkl) \rangle|}{\sum_{hkl} \sum_i I_i(hkl)}$$

^c Percentages of residues in favoured/allowed regions calculated by the program RAMPAGE (68)

2.15.3 Pyocin L1

Purified pyocin L1 at a concentration of 15 mg ml⁻¹ was screened for crystallisation conditions using the Morpheus and PGA crystallisation screens (Molecular Dimensions) (177). Clusters of needle shaped crystals grew in a number of conditions in each screen over 3 to 7 days. Two of these conditions, condition 1 (20% v/v ethylene glycol, 10% w/v PEG 8000, 0.03 M CaCl₂, 0.03 M MgCl₂, 0.1 M Tris/Bicine, pH 8.5) and condition 2 (20% PEG 550 MME, 20% PEG 20K, 0.03 M CaCl₂, 0.03 M MgCl₂, 0.1 M MOPS/HEPES, pH 7.5) from the Morpheus screen were selected for optimisation in 24 well plates. Clusters of needles from these trays were mechanically separated. The un-soaked crystals were from condition 1, while soaked crystals were from condition 2. Un-soaked crystals were looped and directly cryo-cooled to 110 K; D-mannose and D-rhamnose soaked crystals were soaked for 2-12 minutes in artificial mother liquor containing 4 M D-mannose or 2 M D-rhamnose, before cryo-cooling to 110 K. X-ray diffraction data were collected at the Diamond Light Source, Oxfordshire, UK at beam lines I04, I04-1 and I24. Automatic data processing was performed with Xia2 within the EDNA package (173).

A dataset from an un-soaked pyocin L1 crystal was submitted to the Balbes pipeline along with the amino acid sequence for pyocin L1 (178). Balbes produced a partial molecular

replacement solution based on the structure of *Galanthus Nivalis* agglutinin (PDB ID: 1MSA). Initial phases from Balbes were improved via density modification and an initial model was built using Phase and Build from the Phenix package.(179) The model was then built and refined using REFMAC5 and Coot 0.7 (180,181). Validation of all models was performed using the Molprobity web server and Procheck from CCP4-I (175,176). Two structures of sugar soaked pyocin L1 were solved by molecular replacement using Phaser (182), with the sugar-free pyocin L1 as the search model. Additional electron density corresponding to bound sugars, was observed in both $2F_o-2F_c$ and F_o-F_c maps (183). Sugars were fitted and structures refined using Coot 0.7 and REFMAC5. β -D-mannose (PDB ID: BMA) corresponded best to the density of bound D-mannose. The density in the D-rhamnose complex best corresponded to α -D-rhamnose, for which no PDB ligand exists; a model for α -D-rhamnose was prepared by removing the oxygen from carbon 6 of α -D-mannose and submitting these PDB coordinates to the Prodrgr server, which generated the model and modelling restraints (183). The resultant α -D-rhamnose was designated with the PDB ID: XXR. Data collection and refinement statistics for pyocin L1 apo and sugar bound crystals are presented in Table 2-10 .

Table 2-10 Data collection and refinement statistics for pyocin L1

	Sugar Free Form	D-Rhamnose Soak	D-Mannose Soak
Data collection ^a			
Space group	C222 ₁	C222 ₁	C222 ₁
Cell dimensions, <i>a</i> , <i>b</i> , <i>c</i> (Å)	53.41, 158.40, 147.67	52.99, 160.65, 150.57	53.42, 162.1, 152.5
Resolution (Å)	36.42 - 2.09 (2.14 - 2.09)	54.99 - 2.37 (2.43 - 2.37)	55.53 - 2.55 (2.67 - 2.55)
Solvent content (%)	56	55	56
No. of unique observations	37131 (2751)	26242 (1922)	22096 (2901)
Multiplicity	4.8 (4.9)	4.4 (4.5)	5.5 (5.7)
Completeness (%)	99.0 (99.8)	99.1 (99.5)	99.9 (100.0)
R _{merge} (%)	7.2 (59.2)	5.9 (83.0)	7.1 (85.6)
R _{pim} (%) ^b	4.1 (33.0)	3.4 (44.9)	3.3 (39.2)

Mean I/sigma (I)	14.3 (2.1)	19.0 (2.1)	13.3 (2.3)
Refinement statistics			
R_{work}/R_{free} (%)	17.8/22.2	20.9/25.7	19.4/24.8
No. of non-hydrogen atoms	4505	4178	4138
RMSD of bond lengths (Å)	0.02	0.015	0.013
RMSD of bond angles (°)	1.96	1.63	1.70
No. of waters	344	95	27
Mean/Wilson plot B-value (Å²)	40.2/33.8	54.2/43.6	65.9/59.1
Ramachandran plot (%)^c			
Favoured/Allowed/Outliers	97.2/2.2/0.6	97.4/2.2/0.4	96.6/3.0/0.4
PDB identifier	4LE7	4LED	4LEA

^a Values in parentheses refer to the highest resolution shell

$$^b R_{\text{pim}} = \frac{\sum_{hkl} [1/(N-1)]^{1/2} \sum_i |I_i(hkl) - \langle I(hkl) \rangle|}{\sum_{hkl} \sum_i I_i(hkl)}$$

^c Percentages of residues in favoured/allowed regions calculated by the program RAMPAGE (68)

2.15.4 FupA crystallisation

Crystallisation trials for FupA were conducted on refolded FupA₁₀₄₃ in a buffer containing 50 mM Tris, 200 mM NaCl and 1 % β-OG, approximately 800 conditions from commercial screens (Memplus, Memgold I/II, Morpheus, JCSG +, Midas, PACT, PGA, Memstart) were tested (159). Very small needle like crystals (5-20 μM) grew in a number of conditions, with the best forming in Midas condition H12 (15 % PVP-K15, 25 % PEG MME 5500, 0.1 M Tris, pH 8.0. Crystals from the initial screen failed to diffract and so were subjected to extensive optimisation. The results of this optimisation yielded conditions (11-14 % PVP, 14 % PEG 2000 MME, 0.1 Tris, 0.05 M MgCl₂ pH 7.5, with a FupA concentration of 15 mg.ml⁻¹ in 50 mM Tris, 200 mM NaCl, 0.8-1 % (v/v) β-OG, 0.4 % LDAO pH 7.9) producing crystals with somewhat improved morphology, still possessing a long needle-like structure, but being thicker and much larger (100-700 μm) (Figure 9-1-E). Crystals were cryoprotected with 20% ethylene glycol and data collected at DLS at 100 K. The crystals were in the space group *P2*₁ and diffracted with extreme variability, with the best data recorded reflections to 2.8 Å and the best autoprocessed dataset to 3.76 Å (Table 2-11)

(Figure 9-2-E). Selenomethionine labelled FupA was expressed and refolded, but despite extensive screening and optimisation failed to crystallise reproducibly, with the best examples diffracting to 7 Å.

Table 2-11 Data collection statistics for FupA

Data collection ^a	
Space group	<i>P2₁</i>
Cell dimensions, <i>a</i>, <i>b</i>, <i>c</i> (Å)	137.4, 78.36, 137.93
Resolution (Å)	68.95-3.76 (3.86-3.76)
Solvent content (%)	45-65
No. of unique observations	30209 (2221)
Multiplicity	3.4 (3.5)
Completeness (%)	99.8 (99.8)
R_{merge} (%)	11.3 (52.7)
R_{pim} (%)^b	8.6 (39.8)
Mean <i>I</i>/sigma (<i>I</i>)	9.2 (2.0)

2.15.5 Crystallisation of syringacin L1 and pectocins P

During the course of this study crystallisation of a number of other targets was attempted. Hits were obtained for both syringacin L1 and pectocin P.

Syringacin L1 was purified from BL21 pLysS (DE3) containing pET28SL1, by nickel affinity chromatography followed by size exclusion on an S75 column, as for syringacin M. The N-terminal 6xhis tag was subsequently cleaved by overnight incubation in SEC buffer, with thrombin conjugated to agarose beads (Sigma). The cleavage tag was removed by passage through a nickel column and the protein was concentrated to approximately 20 mg/ml. Sitting drop crystal trails were set up with 100 nl + 100 nl protein to precipitant, in Morpheus, JCSG and PACT crystallisation screens. Hexagonal shaped crystals formed in condition A10 of JCSG (0.2 M potassium formate, 20 % w/v PEG 3350) that appeared proteaceous in nature. However these crystals were destroyed during looping and so

their diffraction potential remains unknown. Due to the difficulty experienced in consistently obtaining syringacin L1 these crystallisation trials were not repeated in this study.

Pectocin P was purified from BL21 pLysS (DE3) containing pJPP1, and purified by nickel affinity chromatography and size exclusion on an S75 column, as for syringacin M. the protein was concentrated to approximately 15 mg.ml⁻¹ and approximately 1000 conditions were screened. A number of characteristically red crystals grew after 8 months in wells B12, D12 and E12 of the Morpheus screen (159). Crystals from B12 were shot at Diamond Lightsource beamline I24 producing diffraction to approximately 3 Å, the crystal was of the space group *P1*, with unit cell parameters of 58.0, 71.3, 74.5 Å and 71.3, 66.9, 89.5 °, however due to radiation damage and robot malfunction a complete dataset could not be collected. Optimisation trays for these conditions were set however no crystals were obtained during this study.

2.16 NMR

2.16.1 For pyocin L1

NMR chemical shift perturbation analysis of sugar binding by pyocin L1 and putidacin L1 was carried out at 305 K and 300 K respectively. Fast-HSQC spectra (184) were recorded using ¹⁵N labelled proteins (0.1-0.2 mM) and unlabelled ligands, D-rhamnose and D-mannose (100 mM), on a Bruker AVANCE 600 MHz spectrometer. Protein samples were prepared with and without the sugars present and volumes were exchanged at fixed ratios, making sure the protein concentration remained unchanged. The spectra were processed with Topspin and analysed with CCPNmr analysis (185).

2.16.2 For FupA

Fast-HSQC spectra (186) were recorded for ¹⁵N-labelled *Arabidopsis* ferredoxin and pectocin M1 ferredoxin (100 μM) on a Bruker AVANCE 600 MHz spectrometer. The interaction of these proteins with FupA was explored by acquiring spectra for 1:1 ratio

mixtures. LDAO (0.1%)-containing buffer was used as a negative control to ensure that chemical shifts were not caused by the presence of the zwitterionic detergent. In the case of the *Arabidopsis* ferredoxin-FupA complex, TROSY spectra were acquired to try to detect ^{15}N -labelled ferredoxin in slow exchange with FupA. All spectra were processed with AZARA (W. Boucher, www.bio.cam.ac.uk/azara) and analysed with CCPNmr analysis (187).

2.17 Analytical ultracentrifugation

Sedimentation velocity (SV) was carried out in a Beckman Coulter Optima XL-I analytical ultracentrifuge using an An-50 Ti 4-hole rotor. Sample (90 μl) was loaded into a 3 mm path-length centrepiece and spun at 49,000 rpm for 12 h at 15°C. Scans were collected every 7 minutes using absorbance optics (at 280 nm; a radial range of 5.8 - 7.2 cm, and radial step-size of 0.005 cm). 50 mM Tris, 200 mM NaCl, 2 mM α -sulfo myristic acid (C14SF), pH 7.5 was used as the buffer and this buffer lacking C14SF as a reference. Data were analysed with SEDFIT⁽¹⁸⁸⁾ using the continuous c(s) distribution model. SEDNTERP was used to calculate the partial specific volume, the buffer density and viscosity at 15 °C and 20 °C.

2.18 SAXS data collection and analysis

SAXS data were collected on the X33 beamline at the Deutsches Elektronen Synchrotron (DESY, Hamburg, Germany). A range of pectocin M2 and pyocin M concentrations between 0.4-4.0 mg ml^{-1} was used. The scattering from buffer was acquired before and after each sample and an average of the buffer scattering was subtracted from the sample scattering. The first 200 points (low angle data) of the scattering curve obtained for 1 mg ml^{-1} protein were merged with the rest of the high angle data from the 4 mg ml^{-1} sample to avoid the influence on the data of any inter-particle interference. All data processing was performed using PRIMUS (189). Porod-Debye ($I(q)q^4$ vs q^4) and normalised Kratky ($I(q)q^2$ vs q) plots were used to assess particle flexibility as described in

the Results section^{(190),(191)}. The distance distribution function, $p(r)$, was obtained by indirect Fourier transform of the scattering intensity using GNOM (192). A Guinier plot ($\ln I(s)$ vs s^2) was used to determine the radius of gyration, R_g , of pectocin M2 and pyocin M. US-SOMO (193) was used to determine hydrodynamic parameters based on the crystal structures of pectocin M2. CRY SOL (194) was used to compute theoretical scattering curves from high-resolution X-ray structures.

2.19 Lipid II docking simulations

To simulate the active form of the enzyme the structure of pectocin M2 was modified to include a Mg^{2+} ion coordinated by the D226 side chain and backbone carbonyls from L202 and N204, no modifications were performed on the syringacin M structure. The docked model for lipid II was derived from the Nisin-Lipid II complex structure (158) (PDB =1WCO), the pentapeptide and N-acetylglucosamine groups were removed to create the model used in docking simulations. Autodock vina (195) embedded in UCSF Chimera (196) molecular viewer was utilised to perform docking simulations. A search volume of 67 by 36 by 32 Å was defined containing the catalytic domain of either pectocin M2 or syringacin M. The docking simulation was run with charges normalised and non-polar hydrogen atoms removed, water molecules were ignored. The number of binding modes was set to 9 with the best scored docking, in which the full lipid II molecule (i.e. with the pentapeptide and N-acetylglucosamine groups) would not cause major clashes (solution 1/9 for pectocin M2, solution 2/9 for syringacin M) was selected. Search exhaustiveness was set to 8, with a maximum energy difference of 3 kcal/mol.

2.20 Plant transformation and infection

2.20.1 Transient expression of bacteriocins in *Nicotiana benthamiana*

The leaves of *N. benthamiana* plants between 4 to 8 weeks of age were syringe infiltrated with 0.2 OD₆₀₀ *A. tumefaciens* GV3101 containing the desired binary vector in 10 mM sterile $MgCl_2$. To activate the *A. tumefaciens* DNA transfer machinery the plant wounding

hormone acetosyringone was added to the solution at 200 μ M 2 hours prior to infiltration. Infiltration was achieved by filling a 1 ml syringe with bacterial solution, applying the tip to the leaf underside while holding the top of the leaf and ejecting the syringe. To limit silencing of the transiently expressed bacteriocins *A. tumefaciens* GV3101 with a binary vector containing the bushy stunt virus P19 silencing repressor was co-inoculated in the same MgCl₂ solution for all constructs at an OD₆₀₀ of 0.2 (149). Expression of bacteriocins was monitored from 2 and 7 days by grinding transformed leaf material, snap frozen in liquid nitrogen, in extraction buffer (50 mM Tris, 200 mM NaCl, pH 7.5, with protease inhibitor cocktail (Roche)). Buffer was then clarified and tested for expression using the soft agar overlay assay or western blotting. Expression of GFP-tagged proteins was visualised by confocal microscopy. A 1cm² leaf section of transformed *N. benthamiana* was excised and infiltrated with H₂O by repeated application of suction in a water filled syringe. The leaf section was then immobilised on a microscope slide under a cover slip secured with contact adhesive. GFP fluorescence was observed using a GFP filter set with the excitation laser at to 485 nm, and emission detected at 520-560 nm.

2.20.2 *P. syringae* infection of *N. benthamiana*

A solution of 10⁴-10⁷ cfu/ml of *P. syringae* in sterile 10 mM MgCl₂ was syringe infiltrated into the leaves of *N. benthamiana*, the extent of the infiltration area was marked on leaf. Bacterial growth and lesion formation was monitored visually and by cfu/cm counts from the infected area. Triplicate 0.7 mm leaf disks from infected plants were homogenised separately in 1.5 ml Eppendorf tubes using a tissue homogeniser in 100 μ l of sterile H₂O. Lysate was clarified by centrifugation and 10 fold serial dilutions in sterile H₂O were performed, 3x10 μ l spots of each dilution were plated on KB agar. Plates were incubated at 28°C for 16 hours and colonies at the highest dilution with >4 colonies per spot were used to determine leaf bacterial concentration.

2.20.3 Stable transformation of *Arabidopsis thaliana* with bacteriocins

For stable transformation of *A. thaliana* with gene for putidacin L1 or syringacin L1 the vector pJO530 (pJOPL1-Nmyc or pJOSLI) was utilised. The floral dip method was used as per Zhang et. al. 2006 with modifications (197). *Arabidopsis* plants (approximately 4 per pot) were grown in pots covered with fabric mesh, and grown under long day conditions to induce flowering. When approximately 10-20 % of flower heads had formed green seed pods, the entire flower head was submerged for 30 seconds in 500 ml of a stationary phase culture of *A. tumefaciens* containing pJO530 derived binary vector dissolved in 500 ml 5 % sucrose and 0.02% Silwet L-77 (Momentive). Plants were kept in high humidity (i.e. plastic bag) for 12 hours and dipping repeated after 24 hours. Plants were then grown until flower heads formed mature seed pods.

Seeds from transformed plants were harvested and sterilised by suspension in: 70 % ethanol for 1 minute, followed by suspension for 10 minutes in a seed sterilisation solution consisting of: 5 ml of a solution of a chlorine tablet sterilisation tablet dissolved in 20 ml of H₂O plus 5 drops of triton X-100, added to 45 ml of 100 % ethanol. Seeds were then washed for 2 minutes in 70 % ethanol, followed by washing for 3 x 1 minutes in sterile H₂O. Sterilised seeds were then plated onto MS agar (4.3 g Murashige & Skoog salts, 10 g sucrose, 0.5 g MES, 8 g agar per liter; pH 5.7) with 25 µg.ml⁻¹ hygromycin B (the selection for pJO530). Plates were incubated at 4 °C for 72 hours and maintained in the dark for 5 days. For collection of seed from T0 to T2 generations plants were then grown under long day conditions. Plates were inspected for successful transformants after approximately 2-3 weeks. All seeds are capable of germination and chlorophyll production under hygromycin selection, however sensitive plants are able to not exhibit normal growth and are unable to undergo significant root development or production of a second set of leaves. Resistant plants were transferred to soil and grown until the formed mature seeds for collection. Leaves from resistant plants were harvested and tested for bacteriocin expression as for *N. benthamiana* experiments.

Seeds from initial transformations (T0 generation) were selected for hygromycin resistance on MS agar with 25 µg.ml⁻¹ hygromycin B as above and the ratio of resistant to sensitive plants assessed to identify lines with a single insertion event. Resistant plants

from lines displaying a 3:1 resistant to sensitive ratio were grown to maturity and seeds collected (T1 generation).

Seeds from multiple plants from each line of T1 generation were selected for hygromycin resistance and those producing progeny with a 100 % resistant phenotype, thus possessing a homozygous transgenic phenotype, were utilised for future study.

2.20.4 *P. syringae* infection of transgenic *Arabidopsis*

The leaves of wildtype and transgenic *Arabidopsis* growth under short day conditions in individual pots were utilised for infection assays. Plants between 4 and 6 weeks of age were infiltrated with 10^5 to 10^7 cfu/ml of *P. syringae* in sterile 10 mM $MgCl_2$, using the syringe infiltration method described above. Plants were maintained at high humidity (i.e. by covering growth trays with a clear plastic lid) for 16 hours post infiltration as it was found to assist in successful infection. Disease phenotype and bacterial growth in the leaf tissue was monitored as for *N. benthamiana* infections.

3 Discovery and characterisation of syringacin M from *Pseudomonas syringae* pv. tomato DC3000

Results from this section are included in:

Grinter, R.*, Roszak, A. W.*, Cogdell, R. J., Milner, J. J., and Walker, D. (2012) The Crystal Structure of the Lipid II-degrading Bacteriocin Syringacin M Suggests Unexpected Evolutionary Relationships between Colicin M-like Bacteriocins. **J. Biol. Chem.** 287, 38876-38888

* Denotes joint first authorship

Disclaimer on work performed:

Data collection from syringacin M crystals, structural solution and model building in this chapter were performed in conjunction with and under the guidance of Dr. Aleksander Roszak.

3.1 Introduction

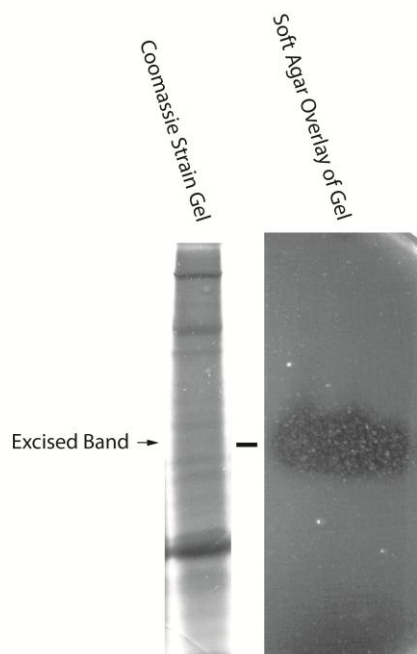
At the outset of this study a number of *P. syringae* strains of UK origin, isolated from a diverse array of plant species, were obtained from the Belgian Coordinated Collection of Microorganisms (BCCM) and National Collection of Plant Pathogenic Bacteria (NCPPB) in the UK. Along with these strains, for which genome sequences were unpublished, the well-studied *P. syringae* isolate, pv. tomato DC3000 was obtained. As discussed in this chapter, these strains were tested for the production of bacteriocins, which resulted in the identification of the novel M-class bacteriocin syringacin M. Syringacin M, which is produced by the *P. syringae* isolates DC3000 and LMG1247, was previously cloned by Barreteau et. al. in 2009, however it was not shown to exhibit any cytotoxic activity against strains tested (82). The data presented in this chapter shows that this protein is indeed an active bacteriocin and provides insight into the catalytic mechanism and evolution of M-class bacteriocins. Prior to this work the crystal structure of colicin M, the first M-class bacteriocin to be identified, had been solved and the cytotoxicity of M-class bacteriocins has been shown to be due to the degradation of Lipid II in the periplasm (83,198). However, limited information was available about M-class bacteriocins from other species. The structural and biochemical analysis of syringacin M presented in this chapter significantly expands our knowledge of this class of antimicrobial protein.

3.2 Screening of *P. syringae* isolates for bacteriocin production and the identification of syringacin M

In order to identify potential bacteriocins to use to combat *P. syringae* infection, a soft agar overlay assay of chloroform lysed colonies of *P. syringae* was used to screen a number of diverse pathovars of *P. syringae* for the production of bacteriocins in the presence of the DNA damaging agent mitomycin C (Table 2-1, Table 9-1). Of these potential bacteriocin producing strains, *P. syringae* pv. *syringae* LMG1247 (the type strain for this pathovar) produced a large diffuse zone of inhibition, reminiscent of the S-type pyocins from *P. aeruginosa*, against two indicator strains (*P. syringae* LMG5456 and LMG5084) in soft agar overlay experiments. In order to identify this bacteriocin a 1 L

culture of *Pss.* LMG1247 was grown in the presence of mitomycin C and subjected to ammonium sulphate precipitation to isolate secreted proteins. Secreted proteins were then separated by native-PAGE and the native gel was used in a soft agar overlay assay against a sensitive indicator strain. A band which correlated with cytotoxicity was excised, trypsinised and subjected to LC-MS/MS (Figure 3-1-A). Analysis and database searching of MS/MS data using the MASCOT search engine matched the secreted bacteriocin through 5 peptides to a predicted colicin M-like bacteriocin, ZP_07266212 from *Pss.* 642 for which the genome sequence is available (Figure 3-1-B). Primers were designed based on this sequence to amplify and identify the corresponding gene from *Pss.* LMG1247. Successful amplification and sequencing of this gene showed that *Pss.* LMG1247 harbours a bacteriocin encoding gene that shares 99 and 94 % sequence identity at the amino acid level to ZP_07266212 from *Pss.* 642 and a close homologue Q88A25 from *Pto* DC3000, respectively. This homologue from *Pto*. DC3000 has been purified previously and shown to have lipid II degrading activity *in vitro*; the study however did not find any cytotoxic activity associated with the bacteriocin when tested against 24 strains of *P. syringae* or isolates of *P. aeruginosa* and *P. fluorescens* (82). To support the idea that Q88A25 from *Pto* DC3000 and the trivially different homologous bacteriocin from *Pss.* LMG1247 are in fact active bacteriocins, we cloned the Q88A25 gene from *Pto* DC3000 into the *E. coli* expression vector pET21a and produced and purified recombinant C-terminally His₆-tagged protein (Figure 3-2-A). The spectrum of activity of this recombinant protein was identical to the secreted bacteriocin from *Pss.* LMG1247, supporting the MS/MS identification data (Figure 3-2-B). To standardize the nomenclature for bacteriocins from *P. syringae*, this bacteriocin was named syringacin M. In addition to the 10 *P. syringae* test strains, the activity of syringacin M was tested against various strains of *P. aeruginosa*, *Pectobacterium* spp, *P. fluorescens* and *P. putida* (Table 2-1). Killing of these bacterial species was not detected. Thus, syringacin M is an active bacteriocin, whose targets, like other colicin-like bacteriocins are bacterial strains that are closely related to the producing strain.

A



B

```

1  MPIELPPTYI TPYPEISTGG NGTYRGQDLN AGQSFPRGMQ NPVATVLLIQ
51  GDLYCSPNCL ATFQDQAMRD GFGIQSRVAL KTLAAADQRE AEGRDLRTAY
101 NEIATDIGRT QQINEHIIKY PPANHVLSGG LMTPFHALAH GMFGLGAPVM
151  FPIQNVGLNV DIRGIPDVMN AIQSARPVGT SSLDVNFAYD VGKDSNASWL
201  TLGNITLRLV GTIDKSSSGA WTFSGEIRAF NDVYDANPSN HRGWLGENLT
251  SVLSAVPFTS YSIEIPGSLP VTVSGN
  
```

Start	End	Observed Mr (expt)	Mr (calc)	Delta	Miss Sequence	
M . PIELPPTYITPYPEISTGGNGTYR . G						
2	25	879.393	2635.1572	2635.317	-0.1598	0
R . TAYNEIATDIGR . T						
98	109	662.284	1322.5534	1322.6466	-0.0932	0
R . TQQINEHIK . Y						
110	119	612.278	1222.5414	1222.667	-0.1255	0
K . SSSGAWTFSGEIR . A						
216	228	692.775	1383.4954	1383.6419	-0.1464	0
R . AFNDVYDANPSNHR . G						
229	242	810.262	1618.5094	1618.7124	-0.203	0

Figure 3-1 Identification of the bacteriocin produced by Pss. LMG1247

Native-PAGE gel (8%) of DEAE anion exchange purification fraction from concentrated culture medium of Pss. LMG1247, coomassie stained and overlaid with soft agar seeded with test strain Psl. LMG 5456. Band corresponding to zone of growth clearing excised and identified using tandem mass spectrometry.

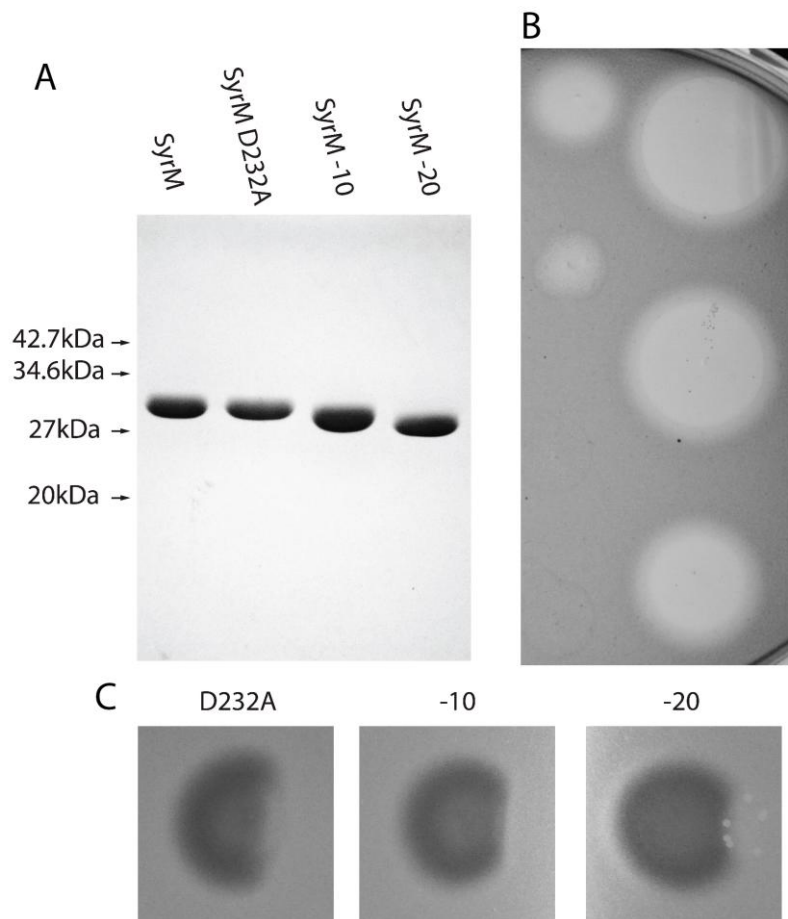


Figure 3-2 Purification and characterization of wildtype syringacin M and deletion mutants

A) 15% SDS-PAGE gel showing purified syringacin M (SyrM) and mutant proteins generated in this study, B) Light field image of five-fold serial dilutions ($37.5 \mu\text{M}$ to 1 nM , MIC = 60 nM) of syringacin M spotted onto a soft agar overlay of susceptible strain *P. syringae* pv. *lachrymans* LMG 5456, C) Dark field image of interference of killing activity of syringacin M on soft agar overlay by adjacent spotting of inactive mutants (proteins spotted at $100 \mu\text{M}$).

3.3 Domain structure of syringacin M

For colicin M and other colicins the N-terminal domain of the protein, which is often fully or partially disordered, corresponds to the translocation domain, and the central domain is involved in receptor binding (4). However, for the closely related S-type pyocins of *P. aeruginosa* the literature reports that the order of these domains is reversed and the receptor binding functionality resides within the N-terminal domain (69). To

unambiguously assign functionality to the N-terminal and central domains of syringacin M we created truncated syringacin M variants lacking the first 10 or 20 amino acids. Both deletion mutants lacked discernible bactericidal activity, indicating an essential functional role for the N-terminal domain of syringacin M. In order to determine whether these mutants possessed an intact receptor binding domain competition experiments were performed by spotting syringacin M Δ 10 and Δ 20 protein within the diffusion zone of wildtype protein in a soft agar overlay experiment, both proteins inhibited killing by the wildtype syringacin M (Figure 3-2-C). This inhibition is attributable to competition for binding to the cell surface receptor required for entry of syringacin M into the target cell and indicates that the mutants possess a functional receptor binding domain. The N-terminal domain is therefore a translocation domain, while the globular central domain is the receptor binding domain. These data suggest that syringacin M displays a colicin-like arrangement of domains with an N-terminal translocation domain, a central receptor binding domain and a C-terminal cytotoxic domain.

3.4 The crystal structure of syringacin M

Crystals were obtained and intensity data collected for two crystal forms of purified syringacin M, one of full length protein in the hexagonal form diffracting to 2.83 Å and another resulting from *in situ* trypsin digested protein, in the monoclinic form diffracting to 1.46 Å. Hexagonal crystal data produced electron density corresponding to residues 2-276, although quality of density corresponding to residues 2-38 suggested partial disorder in this region, with some sections having a high degree of conformational flexibility (Figure 3-3-A). Threading of this region was attempted but the Ramachandran geometry was imperfect (171). The monoclinic crystal contained two molecules per asymmetric unit related by a non-crystallographic 2-fold symmetry with only minor differences due to crystal packing. Electron density from this data allowed unambiguous modelling of residues 38-276, which correlates well with the presence of a predicted trypsin cleavage site between R37 and G38. Figure 3-3-B presents a cartoon representation of molecule A. Alignment of residues 38-276 from hexagonal wildtype and monoclinic trypsin-digested models gave a backbone RMSD of 0.47 Å and showed that the conformation of the

protein is the same in both crystal forms. As such, the high resolution model will be used in the further discussion except for where the N-terminus is discussed.

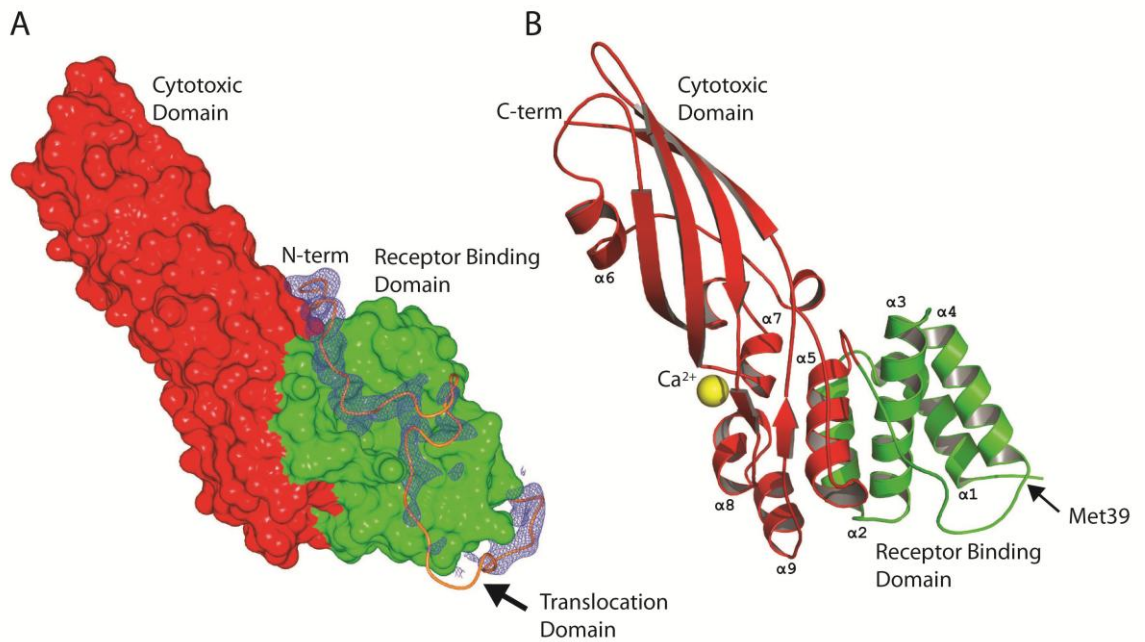


Figure 3-3 Crystal structure of syringacin M

A) Full length structure of syringacin M showing AA 38-276 as a surface model and the unstructured N-terminus (AA 2-37) is a ribbon model. The $F_o - F_c$ omit map of electron density at 2.7σ for AA 2-37 is shown as a chicken wire model B) cartoon representation of high resolution structure of syringacin M (AA 38-276) showing receptor binding domain (green), cytotoxic domain (red) and Ca²⁺ ion (orange).

3.5 Structural description of syringacin M

The structure of syringacin M reveals a protein with a compact mixed sheet/helix structure and a partially disordered N-terminus consisting of 39 amino acids. Disordered or partially disordered translocation domains are also observed in a number of other colicin structures and like the N-terminal 39 amino acids of syringacin M they are rich in Pro, Ala, Ser and Gly residues. In colicin E3, where the first 83 amino acids of the protein are disordered, an unstructured N-terminal domain is required to enable threading of this region of the protein through the lumen of the OmpF porin to deliver the TolB interacting region of the protein into the periplasm (64,66). Similarly, in colicin M, the N-terminal 35 residues, although visible in the crystal structure display markedly higher temperature

factors than other regions of the protein and lack regular secondary structure (198). Thus syringacin M possesses an N-terminal translocation domain that is typical of colicin-like bacteriocins. As with colicin M the receptor binding domains and catalytic domains of syringacin M do not form obviously distinct structural entities. However, on the basis of truncation experiments Barreteau et. al. reported that the minimum catalytically active region of colicin M corresponds to amino acids 122-271 and that helix 1 (37-46) is required for receptor binding. This delineates the receptor binding domain as a compact bundle of 5 helices spanning residues 37-122 (40-127 in syringacin M) (199). As expected from the extensive sequence similarity (Figure 3-4) the structures of the colicin M and syringacin M catalytic domains are structurally homologous (RMSD 2.6 Å). However, for syringacin M well defined electron density for a single metal ion is present in the active site. This density correlates well with the presence of Ca^{2+} which is present at high concentration in the crystallization buffer. In the syringacin M model, Ca^{2+} is coordinated by backbone carbonyl groups of residues L202, N204 and the side chain of a highly conserved aspartic acid, D232. The corresponding aspartic acid in colicin M (D226) is critical for catalytic activity in colicin M with mutation to a number of chemically similar residues (including glutamic acid) abolishing activity (200) .

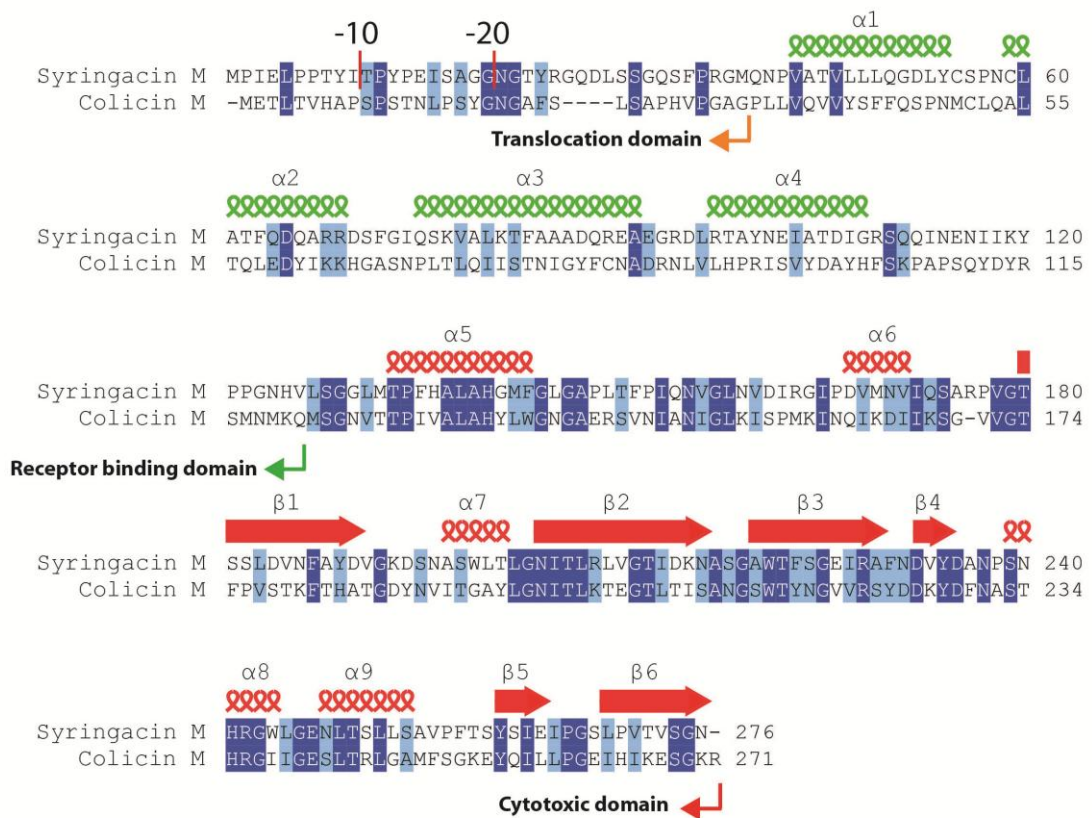


Figure 3-4 Sequence alignment of colicin and syringacin M.

Sequence alignment of syringacin M and colicin M, showing conserved (dark blue) and similar (light blue) residues, secondary structure (sheets and helices) for syringacin M (top) and colicin M (bottom), location of truncation for -10 and -20 deletion mutants of syringacin M generated in this study.

3.6 The receptor binding domains of colicin M and syringacin M show extensive structural similarity

Outside the C-terminal cytotoxic domain there is no clear sequence similarity between colicin M and syringacin M (Figure 3-4). However, using the DALI server (201) to search for proteins in the PDB that are structurally homologous to syringacin M revealed not only the expected structural homology between the cytotoxic domains of colicin M and syringacin M, but also extensive similarity within the respective receptor binding domains of these proteins. Indeed, structural homology extends from the C-terminus of the proteins and spans the entirety of the cytotoxic and receptor binding domains, with the exception of helix 1 in syringacin M (43-54) that adopts a more compact conformation.

The RMSD for the alignment of the receptor binding and cytotoxic domains (residues 43-276 of syringacin M) with those of colicin M (entry 2XTR) is 3.3 Å with a Z score of 16.9. A structural alignment of the two proteins is illustrated in Figure 3-5. The superposition of colicin M and syringacin M structures shown in Figure 3-5-A/B is based on alignment of the catalytic domain half β -barrels, while Figure 3-5-C shows the alignment based on helices 2-4 of the receptor binding domains. These alignments illustrate a difference in angle between the receptor binding and cytotoxic domains in colicin and syringacin M. Alignment of the relevant regions (helices 2-4) of the receptor binding domains of colicin M and syringacin M are shown in Figure 3-5-D/E. Given the lack of discernible sequence homology between the receptor binding domains of these proteins this structural similarity was unexpected. Indeed, it has been previously postulated that these first 126 amino acids of syringacin M represent receptor binding and translocation domains that are specific to *P. syringae* and unrelated to those of colicin M (198). The observed similarity in tertiary structure suggests a hitherto undetected divergent evolutionary relationship between the receptor binding domains of colicin M and syringacin M and suggests that the novel receptor binding function of these colicin M-like bacteriocins has been generated through diversifying selection and not through diversifying recombination as previously suggested (200). This is discussed further in section 3.9.

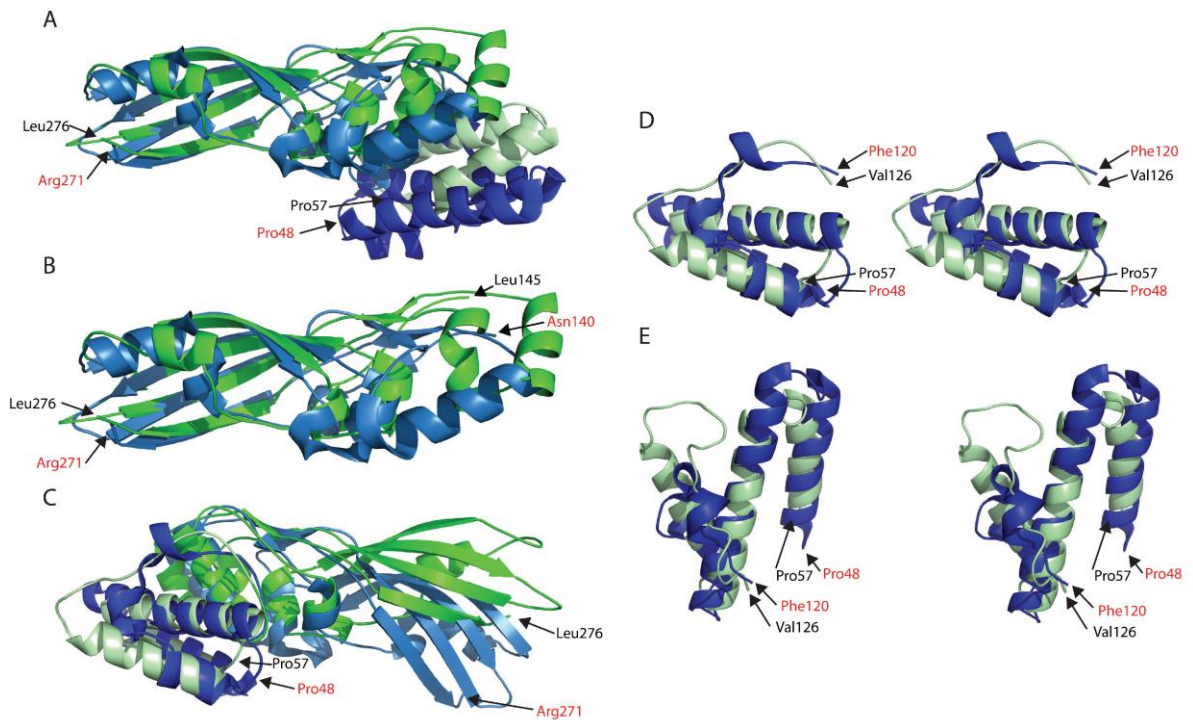


Figure 3-5 The receptor binding and cytotoxic domains of syringacin M and colicin M show structural homology

A) Structural alignment of syringacin M 57-276 (green) and colicin M 48-271 (blue) based on the catalytic domain β -barrel, residues 180-190, 204-216, 220-229, 269-275 (minus 6 for colicin M residue numbers) (RMSD 1.765 Å). B) As for A but truncated to residues 145-276 for syringacin M and residues 140-271 for colicin M, C) Structural alignment as A, based on of receptor binding domain helices 2-4, residues 58-70 (53-65), 73-92 (73-92), 95-101 (97-103) (colicin M residues in brackets) (RMSD 2.051 Å). D/E) Stereo view overlay of receptor binding domains of syringacin M residues 57-125 (green) and colicin M residues 48-119 (blue) showing structurally conserved core helices and random coil (RMSD 3.3 Å).

3.7 Comparison of the syringacin M and colicin M active sites

The syringacin M cytotoxic domain consists of residues 129-276 and forms the mixed helix/sheet structure, incorporating a half β -barrel structure in an overall fold that is unique to colicin M type bacteriocins (198). Previous mutational studies on colicin M have identified the conserved residues D226 (D232), D229 (D235), H235 (H241) and R236 (R242) (syringacin M numbering in brackets) as essential for activity. These residues are surrounded by additional conserved residues and together these likely constitute the active site of these enzymes (Figure 3-6). In the syringacin M structure a Ca^{2+} ion is present, coordinated by the side chain of D232, backbone carbonyl groups from L202 and N204, two water molecules and an ethylene glycol molecule Figure 3-6-B.

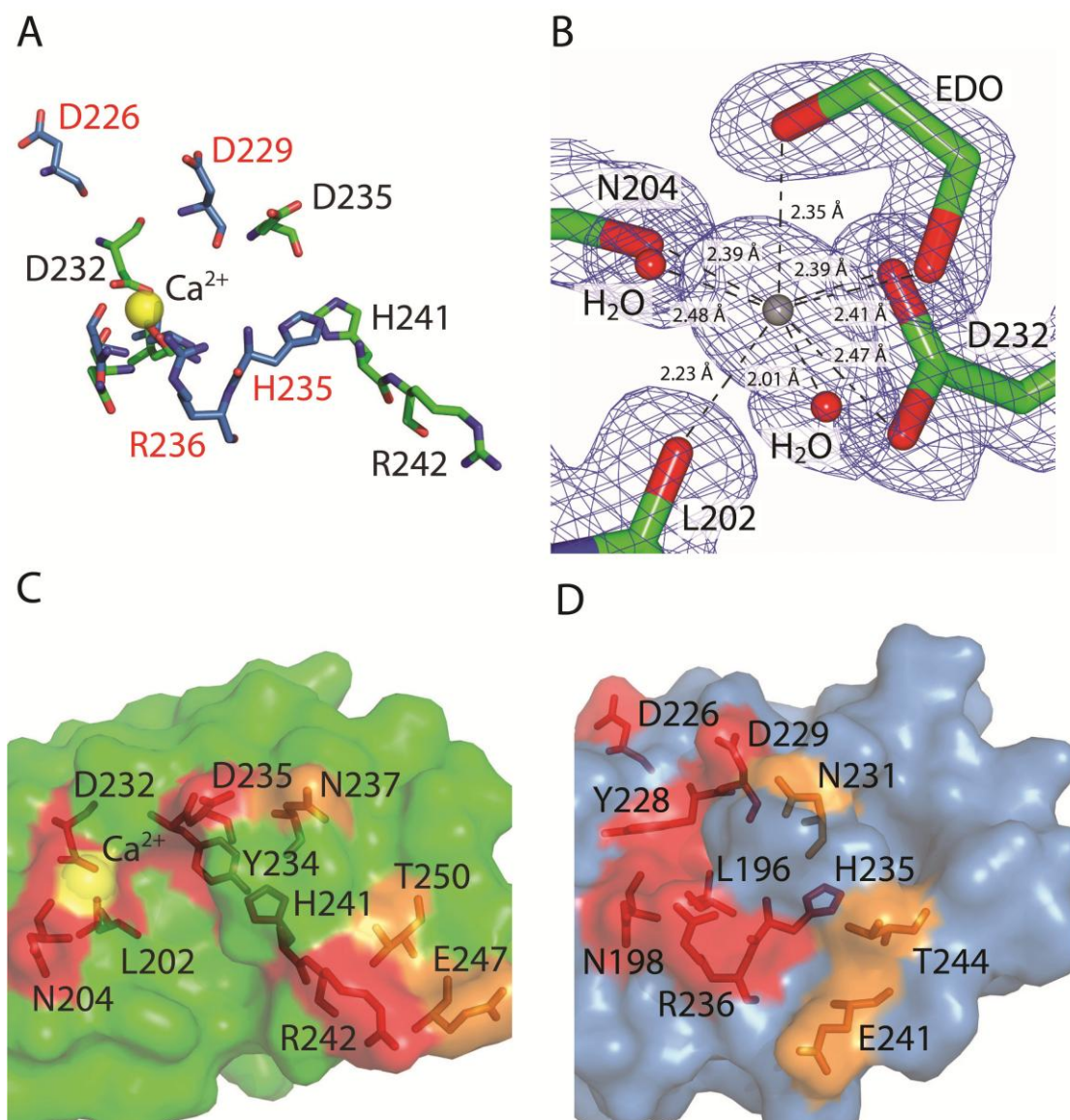


Figure 3-6 Comparison of the syringacin M and colicin M active sites.

A) Superimposition of the active site of syringacin M (green) and colicin M (blue) showing location (stick representation) of key conserved residues (colicin M = red, syringacin M = black) and Ca^{2+} ion from syringacin M. B) Coordination of Ca^{2+} ion in the active site of syringacin M, residues and monomers involved in coordination shown as a stick model, $2F_o - F_c$ electron density map shown as chicken wire model at 1.71σ . C) Surface representation of syringacin M active site showing conserved residues essential (red) and important (orange) for cytotoxicity. D) Surface representation of colicin M active site showing conserved residues essential (red) and important (orange) for activity in colicin M.

The assignment of Ca^{2+} to this density as opposed to Mg^{2+} , which is also a cofactor for the enzyme and is present in the crystallization buffer is based on a number of factors. Firstly, the difference Fourier $F_o - F_c$ map shows insufficient electron density has been attributed

to the metal ion when Mg^{2+} is fitted but not when Ca^{2+} is fitted. Secondly, the B-factors obtained for the metal ion when Mg^{2+} is fitted to this density (19.1 and 21.4 \AA^2 for molecules A and B, respectively) are significantly lower than the surrounding environment (average B-factor for coordinating protein oxygens in molecules A and B are 23.6 and 25.1 \AA^2 , respectively) suggesting that an insufficient number of electrons have been attributed to the metal ion when Mg^{2+} is modelled. However, with Ca^{2+} modelled the metal ion B-factors (25.0 and 27.5 \AA^2 for molecules A and B, respectively) are in the expected range. Thirdly, the average bond length of the coordinating oxygen atoms to the metal ion is 2.34 \AA , close to the average value of 2.39 \AA calculated from consideration of 3818 high resolution Ca^{2+} containing protein structures. The average bond length for magnesium-oxygen bonds from 2310 high resolution structures is 2.16 \AA (202). Finally, the metal ion has a coordination number of eight. This coordination is common for Ca^{2+} but is not favoured by Mg^{2+} , which rarely has a coordination number higher than six (203,204). The presence of this active site metal ion, which is absent in the colicin M structure, likely orientates the side chain of D232 close to the side chains of the other putative active site residues. In the structure of syringacin M a break in helix 8 within the cytotoxic domain results in the side chain of R242 being orientated away from the putative active site, whereas in the colicin M structure the equivalent arginine lies closer to the active site pocket. The surface model representation of syringacin M 40-276 shown in Figure 3-6-C reveals a potential active site binding pocket, formed by the essential Ca^{2+} and its coordinating residues on one side and key catalytic residues Y234, D235 and H241 on the other. In contrast, in the colicin M structure 37-271 the unbroken confirmation of helix 9 and the loop extended due to the confirmation of D226 results in a pocket too narrow to accommodate the substrate (Figure 3-6-D). Colicin M activity has been shown to be dependent on the presence of Mg^{2+} although it has not been reported whether Ca^{2+} and other metal ions are capable of supporting activity. To determine if the Ca^{2+} bound structure of syringacin M likely represents a physiologically relevant cofactor and to determine the ability of other metal ions to support activity the ability of syringacin M to cleave lipid II in the presence of a range of metal ions was tested.

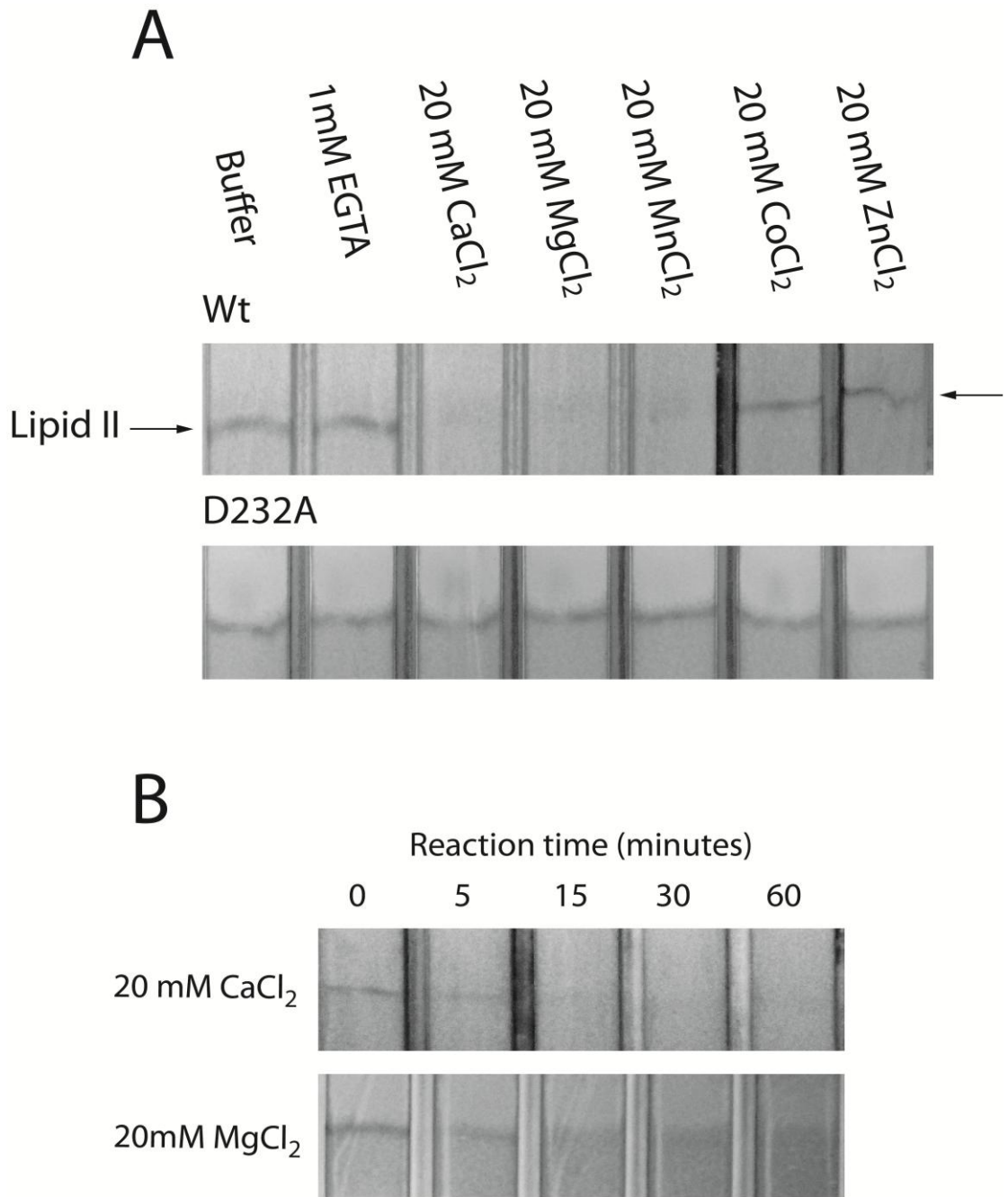


Figure 3-7 Dependence of syringacin M activity on divalent metal ions.

A) Thin layer chromatography (TLC) visualization of reaction of syringacin M (wildtype top panel or D232A mutant bottom panel) and lipid II in the presence and absence of various divalent cations, all reactions identical except for labelled component (buffer = no additional reagents added). B) TLC visualization of time course reaction of syringacin M and lipid II in the presence of CaCl₂ or MgCl₂.

In addition to activity in the presence of Mg^{2+} , both Ca^{2+} and Mn^{2+} ions were also able to support activity, while other divalent cations tested, Zn^{2+} , Ni^{2+} and Co^{2+} were not (Figure 3-7-A). Semi-quantitative time course experiments show that syringacin M displays comparable catalytic activity in the presence of either Ca^{2+} or Mg^{2+} (Figure 3-7-B). The syringacin M D232A mutant which displays no bactericidal activity was also found to be catalytically inactive under all conditions (Figure 3-7-A). The structure of the D232A mutant was also determined and shown to lack the Ca^{2+} ion found in the active site of the wildtype protein, indicating that this side chain is critical to Ca^{2+} binding. However, despite the loss of Ca^{2+} from the active site of syringacin M D232A the crystal structure and circular dichroism spectra of the mutant show the overall secondary structure and conformation of active-site side chains were analogous (Figure 9-3). These data indicate that the lack of activity of the D232A mutant is due to its role in the coordination of a catalytically essential metal ion.

While Ca^{2+} was identified as the metal ion bound in the active site of syringacin M, both Mg^{2+} and Ca^{2+} have been shown to be relatively abundant in the periplasm of Gram-negative bacteria, at least under the conditions tested (204,205). Ca^{2+} ions have been shown to be concentrated in the periplasm relative to the cytoplasm or extra-cellular environment (205). As the ionic composition of the periplasm, where colicin M-like bacteriocins are active, is highly dependent on external conditions, flexibility in the use of metal ion cofactors could be advantageous and so this class of bacteriocins may have evolved to utilize both Mg^{2+} and Ca^{2+} as a cofactor. Interestingly, published work on colicin M and our observations with syringacin M, show that cytotoxicity in liquid culture is dependent on the presence of Ca^{2+} , suggesting that at least under some conditions Ca^{2+} acts as the metal cofactor (206).

3.8 Isolation and characterisation of syringacin M resistant mutants

In order to determine genetic factors involved in *P. syringae* susceptibility to syringacin M, *P. syringae* LMG5456, a syringacin M susceptible strain, was treated with purified syringacin (10mg ml^{-1}) and resistant colonies isolated. Ten resistant isolates characterised

could be broadly divided into two groups, one group displayed normal colony morphology and the other displayed a highly mucoid phenotype (Figure 3-8). Representative isolates were selected from each group (*P. syringae* LMG 5456 MDC2 and MDC3, respectively). The stability of the syringacin M resistant phenotype was tested after growth in King's B media. Both isolates showed a stable syringacin M resistant phenotype and so genomic DNA from the mutant and the wildtype strains was sequenced, using an Illumina MiSeq platform. Reads from wildtype LMG5456 were assembled *de novo* into 180 contigs ranging in size from 260,000 to 1000 bp in length. These contigs were then annotated and used as a scaffold to which the mutant reads were mapped. Analysis of genetic variation between MDC2 and wildtype LMG5456 revealed two verifiable genetic changes, the first a single nucleotide polymorphism (SNP) in *algE* a gene encoding a putative outer membrane alginate transporter. The second was a single nucleotide insertion (SNI) in an open reading frame encoding a putative outer-membrane ferric siderophore receptor, the closest homologue in *P. syringae* of the *E. coli* ferrichrome receptor FhuA. The mutation in *algE* leads to the substitution of leucine 385 for phenylalanine and as both these residues are hydrophobic and relatively large, this mutation may not have a significant effect on the function of this protein. In contrast, the SNI into the gene for the FhuA homologue causes a frame shift at AA 389, leading almost certainly to a non-functional protein. Interestingly, colicin M is known to utilise FhuA as its cell surface receptor/translocator with FhuA knockout mutants entirely resistant to the colicin (207). This suggests that it is the truncation of the FhuA homologue rather than the mutation in *algE* which is providing syringacin resistance, however this remains to be tested by complementation of the knockouts.

Comparing the MDC3 sequence with wildtype LMG5456 revealed a four nucleotide deletion in an open reading frame encoding a homologue of the periplasmic glucan synthesis protein MdoG. This deletion causes a frame shift at AA 356 (of 621 AA total length) and almost certainly inactivates the protein. The broader cellular function of MdoG has yet to be elucidated, however along with its paralogue MdoD it has been shown to be necessary for the synthesis of membrane derived oligosaccharides in the periplasm (208). MdoG knockouts have been shown to be associated with diverse phenotypes, including phage resistance, an enlarged periplasm and increased outer-

membrane permeability (208-210), and so the observed resistance to syringacin M may be due to pleiotropic effects (211).

The results from the genomic analysis of the syringacin M resistant mutants are preliminary, and while the authenticity and uniqueness of the mutations discussed were verified as well as possible, further validation by complementation and phenotypic characterisation is required. (*Raw genomic data and analysis is contained in supplementary electronic data*).

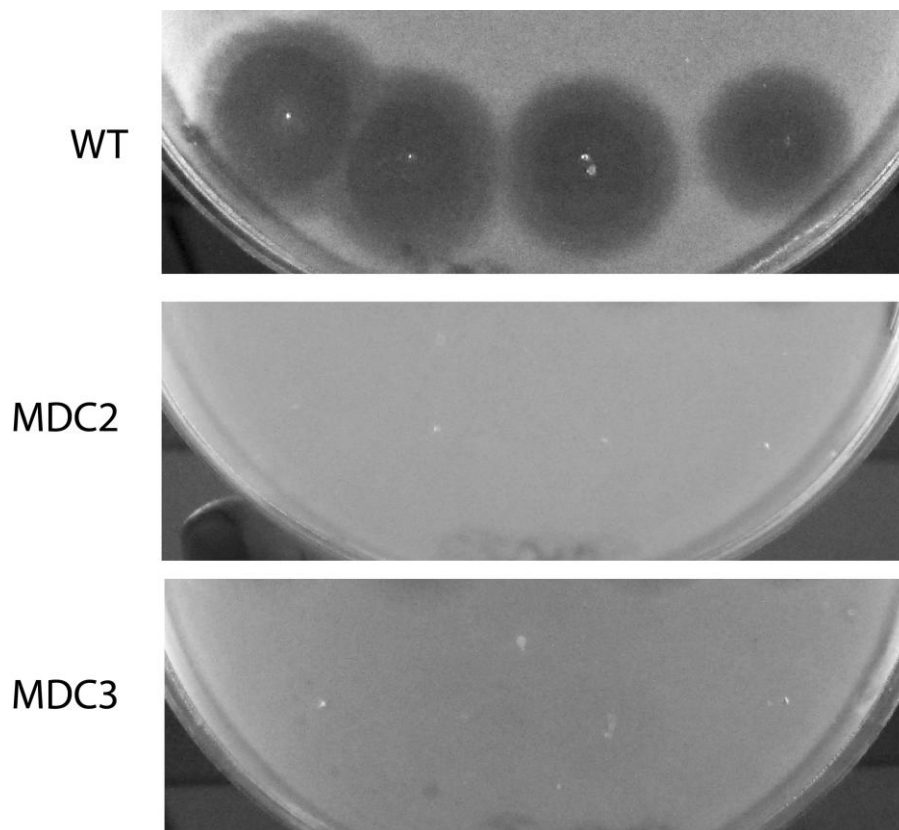


Figure 3-8 Susceptibility of wildtype and mutant *P. syringae* LMG5456 strains to syringacin M

Purified syringacin M (starting concentration 5 mg.ml^{-1} with 5 fold dilution from left to right) was spotted onto a soft agar overlay seeded with either wildtype or mutant *P. syringae* LMG5456.

3.9 Discussion

The overall structure of syringacin M shows that this bacteriocin shares an analogous arrangement of structural domains to colicin M with a partially disordered N-terminal

translocation domain that is a characteristic of colicins. Colicin M binds to the FhuA receptor and utilizes TonB in order to gain entry into target cells. The translocation domain of colicin M spans the N-terminal 37 amino acids, with binding to TonB mediated by the first 7 amino acids that constitute the TonB box. Mutation or deletion of the TonB box results in a protein that does not possess cytotoxicity, but is not deficient in receptor binding and catalytic activity (212). A similar loss of cytotoxicity is also observed for $\Delta 10$ syringacin M and so it is reasonable to postulate that this region of syringacin M contains a binding box which is equivalent in binding the TonB orthologue of *P. syringae*. Adding further weight to this hypothesis, a putative colicin M homologue from *P. syringae* pv. *morsprunorum* str. M302280, has overall sequence identity with syringacin M of only 18%, but shares a nearly identical N-terminal 8 amino acids (MPIELPPTY/MPVELPPTY). Diversifying recombination is a major evolutionary mechanism in generating bacteriocins that are able to exploit novel receptors or that possess novel cytotoxic activities, and clear examples of the results of recombination events can be observed through comparative sequence or structural analysis (4). For example, colicin E3 and E9 share almost identical translocation and receptor binding domains but their cytotoxic domains share no sequence, structural or functional similarities, with the former possessing an rRNase domain and the latter a DNase domain. Similarly, the M-class pectocins (discussed in Chapter 4) and colicin M both share homologous lipid II cleaving catalytic domains but there is no sequence or structural similarity between their receptor binding domains, with the pectocin receptor binding domain closely related to 2Fe-2S plant ferredoxins and possessing an intact iron-sulphur cluster (92). Given that diversifying recombination has been shown to be the major mechanism for the acquisition of novel receptor binding, translocation and cytotoxic functionalities and that the receptor binding domains of colicin M and syringacin M share no obvious sequence identity, the observed structural similarity between these proteins within their receptor binding domains is unexpected. However, as protein structure is conserved over much longer evolutionary distances than amino acid identity (213), the observed structural similarity, suggests that colicin M and syringacin M have evolved divergently from a common ancestor. This hypothesis is supported by our preliminary genomic data suggesting that the receptor for syringacin M is the FhuA homologue in *P. syringae*, suggesting that these bacteriocins have maintained their relationship with the ferrichrome receptor over an evolutionary time scale.

Furthermore, we have observed that the receptor binding and cytotoxic domains of colicin M homologues, which show clear sequence homology, show distinctly different levels of sequence identity in their cytotoxic and receptor binding domains. For example, a putative homologue from *Salmonella* identified bioinformatically shares a conserved receptor binding domain and an overall sequence identity of 43% with colicin M. This sequence identity is however distributed unevenly, with the receptor binding and cytotoxic domains sharing 31% and 51% identity, respectively. An analogous level of sequence divergence between the two domains is also observed in homologues from *Burkholderia* spp. and suggests different levels of selection pressure for mutation within the two domains.

While it is worth considering that the structurally analogous receptor binding domains of colicin or syringacin M may have evolved through convergent evolution, it seems unlikely that such structural homology would have arisen independently given the structural diversity of receptor binding domains from other colicins, which essentially share the same function (9,64,214). Secondly, structural conservation is unlikely to have evolved in order to stabilize the catalytic domain or overall structure of colicin M-like bacteriocins, as the receptor binding domains of pectocin M1 and M2 consists of a ferredoxin-like protein with no structural similarity to the receptor binding domains of colicin M or syringacin M (92). Therefore, we suggest that diversifying selection, in addition to its role in the generation of novel cytotoxic domain-immunity protein pairs, may be an important evolutionary mechanism in the genesis of novel receptor-binding function in colicin-like bacteriocins. Interestingly and perhaps not unexpectedly, considering the data presented here, positive selection has also been detected in the outer membrane receptors of some colicin-like bacteriocins (215,216). The main documented evolutionary pathways of colicin-like bacteriocins are summarized in Figure 3-9.

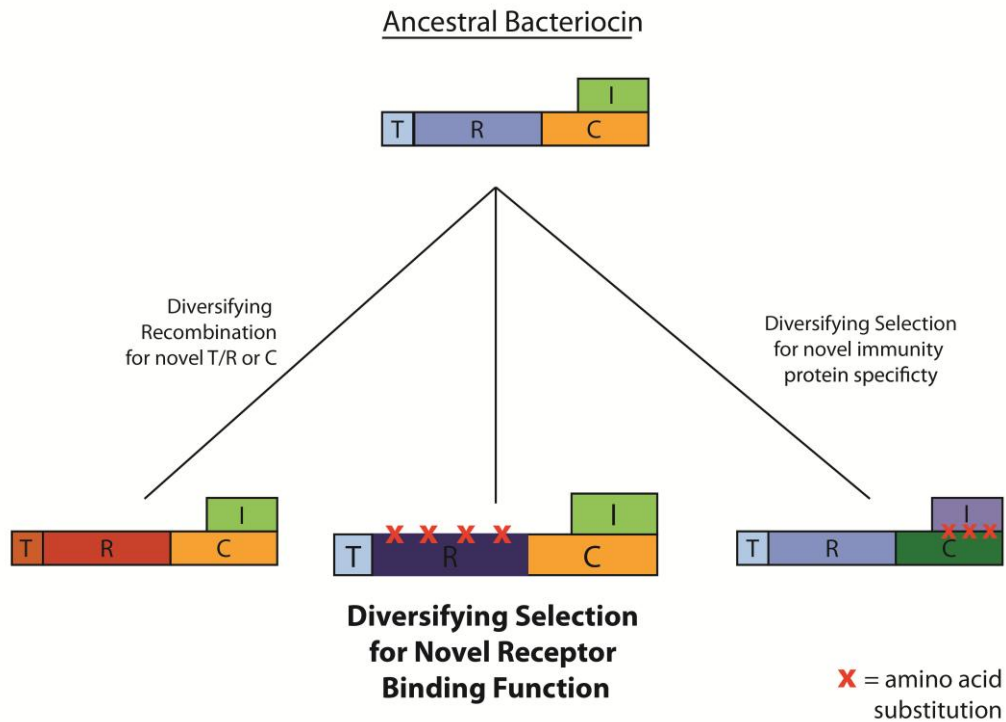


Figure 3-9 Graphical representation of mechanisms of diversification of bacteriocins.

Diversifying recombination for novel translocation (T), receptor binding (R) or cytotoxic domain (C) functions has been widely observed in colicin-like bacteriocins and diversifying selection is the mechanism through which novel cytotoxic-immunity protein (I) specificities are generated in the DNase and rRNase type colicins (16),(13). The structural similarity between the receptor binding domains of colicin M and syringacin M suggest diversifying selection may also be important in the generation of novel receptor binding specificities.

In the case of colicin M and syringacin M comparative sequence analysis is therefore not a reliable indicator of the evolutionary relationship between the receptor binding domains of these bacteriocins. As with other groups of proteins, direct structural comparison is required to detect this relationship (217).

On a methodological note, in this work we improved the resolution of syringacin M crystals from 2.83 to 1.46 Å by removing the N-terminal 37 amino acids by utilizing the *in situ* trypsin digest method of Dong et al., 2007 (172,218). Flexible or disordered regions of a protein often limit resolution or prevent crystallization and as a disordered translocation domain is a hallmark of colicin-like bacteriocins, this technique may prove useful to a structural biologist working on these proteins.

4 Discovery and characterisation of pectocins from *Pectobacterium spp*

Results from this section are included in:

Grinter, R., Milner, J., and Walker, D. (2012) Ferredoxin containing bacteriocins suggest a novel mechanism of iron uptake in *Pectobacterium spp.*, **PLoS ONE** 7, e33033

Grinter, R.*, Josts, I.*, Zeth, K., Roszak, A. W., McCaughey, L. C., Cogdell, R. J., Milner, J. J., Kelly, S., Byron, O., and Walker, D. (2014), Structure of the atypical bacteriocin pectocin M2 implies a novel mechanism of protein uptake, **Molecular Microbiology**, Jul;93(2):234-46

* Denotes joint first authorship

Disclaimer on work performed:

SAXS data presented in this section was collected and analysed by Mr Inokentijis Josts. DMD modelling was also performed by I. Josts. These data are presented here for completeness as they provide additional and complimentary insight to that from the crystal structure.

Initial screens for pectocins crystallisation conditions were conducted in conjunction with Dr. Kornelius Zeth, data for the P2₁ form was collected and phased by K. Zeth, models for both forms were built and refined by me.

4.1 Introduction

In the initial stages of this study, culture collection derived *Pectobacterium* strains were tested for the production of bacteriocins under mitomycin C induction. However, the production of colicin-like bacteriocins was not observed under these conditions and as such a genome mining strategy was adopted to identify bacteriocins in *Pectobacterium*. As discussed in detail below, the bacteriocins pectocin M1, M2, P were identified using this approach. These proteins consist of either an M-class cytotoxic domain or a lysozyme-like pesticin cytotoxic domain, fused to a plant-like ferredoxin domain. Ferredoxins are iron containing redox proteins (219) and this unusual structure provides insight not only into bacteriocin translocation but also how *Pectobacterium* obtains the essential nutrient iron during infection of its plant host. Due to its role in the creation of oxygen radicals via the Fenton reaction and to limit its availability to invading pathogens the vast majority of intracellular iron in plants is sequestered by haem or iron-sulphur-proteins, or the iron storage protein ferritin (220) (221). In order to successfully infect its host plant *Pectobacterium* needs to obtain this iron. Experimental studies into the iron acquisition systems possessed by *Pectobacterium*, their regulation and role in virulence are limited. However, analysis of data from existing studies along with the genome sequences of a number of strains suggests the genera uses multiple systems for obtaining iron during infection (222). For example, the genome of *P. carotovorum* SCRI1043 contains a gene cluster for the biosynthesis and transport of the siderophore enterobactin, which has been shown to be regulated by quorum sensing (51,223). Genes encoding the transport machinery, but not biosynthesis machinery of achromobactin are also present, suggesting it may be utilised as a xenosiderophore (222). The role of these systems in virulence is yet to be tested but as *Pectobacterium* can adopt a saprophytic, soil dwelling lifestyle, iron acquisition during infection may not be their prominent role (224). *Pectobacterium* possesses other iron-uptake systems more likely to be involved in virulence such as the ferric citrate uptake system and the HasA/HasR system. Plants utilise citrate to transport ferric iron to photosynthetic tissues via the xylem, meaning uptake of this complex may be important during vascular colonisation by the pathogen (225). As our understanding of pathogenesis related iron-uptake systems in

Pectobacterium is still limited, it is quite possible that the genus has evolved unique mechanisms to obtain iron from its host.

4.2 Identification of pectocin M genes in the genomes of *Pectobacterium* spp

In order to identify bacteriocins for use as biocontrol agents we searched the available genome sequences of *Pectobacterium* species for genes encoding putative colicin-like bacteriocins. Two putative colicin M-like bacteriocin genes were identified in the genomes of *P. carotovorum* sub spp. *carotovorum* PC1 (*Pcc* PC1) and *P. carotovorum* subspp. *brasiliensis* BPR1692 (*Pcb* BPR1692). The genes encode proteins that were named pectocin M1 and pectocin M2, respectively. Pectocin M1 and M2 have an N-terminal domain with approximately 60% identity to spinach ferredoxin I and a C-terminal domain with approximately 46% identity to the catalytic domain of colicin M (Figure 4-1). The colicin M-like domains of both proteins contain all residues that have previously been shown to be important for the catalytic activity and consequently cytotoxicity of colicin M (200). A linker region of approximately 20 amino acids, which is not conserved between pectocin M1 and M2 connects the two domains and overall these proteins share 58% sequence identity.

Phylogenetic analysis of the ferredoxin domains of these pectocins show they cluster with a number of other ferredoxin and ferredoxin-domain containing proteins from *Pectobacterium* species. This cluster of sequences is most similar to [2Fe-2S] ferredoxins from plants and cyanobacteria, with ferredoxins from the genus *Arabidopsis* sharing the highest sequence identity. The domains are much more distantly related to typical bacterial ferredoxins. The cysteine residues of plant ferredoxins that coordinate the [2Fe-2S] cluster in the active centre of these proteins are conserved in the pectocins, indicating that these proteins also contain the [2Fe-S2] cluster (Figure 4-1) .

The domain structure of pectocins M1 and M2 consisting of a fusion between an M-class bacteriocin cytotoxic domain and a plant-like ferredoxin is unprecedented and highly unusual. It implies that the ferredoxin domain is somehow contributing to the receptor

a) Domain structure of pectocin M1 and relationship to colicin M and plant ferredoxin. b) Sequence alignment of pectocin M1, M2 and pectocin P (see discussion) with [2Fe-2S] ferredoxin type proteins and colicin M. For clarity of presentation prior to alignment pectocin P was truncated to amino acids 1-101 (N-terminal domain) and colicin M was truncated to amino acids 128-271 (C-terminal domain).

Genbank/PDBaccession numbers are as follows: Ferredoxin I [*S. oleracea*] 1704156A, plant-like ferredoxin [Pcc PC1] YP_003017870, pectocin M1 [Pcc PC1] YP_003017875, pectocin M2 [Pcb BPR1692] ZP_03825528, colicin M [*E. coli* SMS-3-5] YP_001739994, pectocin P [Pcc WPP14] ZP_03830397. Invariant residues are highlighted in black, residues with similar properties in gray b) nearest neighbour joining molecular phylogenetic tree of [2Fe-2S] ferredoxins and pectocin ferredoxin domains. Bootstrap values (%) at major nodes are indicated. Species names represent independent ferredoxin proteins from listed species, typifying the class of ferredoxin. Proteins discussed in the study are named with species designation in brackets. Plant ferredoxins and adrenodoxin were aligned with signal peptides removed, pectocin sequences were trimmed to minimum region on homology with plant-like ferredoxin from Pcc PC1. Ellipses designate the following: blue = plant-type ferredoxins, red = ferredoxins found predominately in γ -Proteobacteria, yellow = ferredoxins involved in electron transport to cytochrome P450. Scale represents substitutions per amino acid site.

4.3 Evolution of the pectocin M1 gene through gene duplication and recombination

Analysis of the genomic context of pectocin M1 gives clues to its evolutionary origin. As shown in Figure 4-2-A, approximately 3000 bp upstream of the gene coding for pectocin M1, is a predicted open reading frame encoding a plant-like ferredoxin with approximately 52% amino acid identity to the ferredoxin domain of pectocin M1. Alignment of the nucleotide sequences of these regions (Figure 4-2-B) shows high nucleotide conservation (>50%) that encompasses the area of sequence similarity between pectocin M1 and the plant-like ferredoxin, as well as part of a hypothetical open reading frame present in both regions, but truncated in the pectocin M1 region. High levels of similarity and truncation of the adjacent open reading frame in the pectocin M1 region strongly suggests a gene duplication event. Evolution of the gene encoding the active bacteriocin is therefore likely to have occurred after this gene duplication event, through recombination between the duplicated ferredoxin gene and an ancestral bacteriocin carrying a colicin M-like cytotoxic domain. An open reading frame directly

upstream of the pectocin M1 gene encodes a likely pectocin M1 immunity protein, which shares 24% amino acid identity with the immunity protein of colicin M. Pectocin M2 does not share this genomic context, however the open reading frame directly upstream codes for a bacteriocin closely related to the RNA degrading carocin S2 (128), suggesting it may have been recruited to a genomic island.

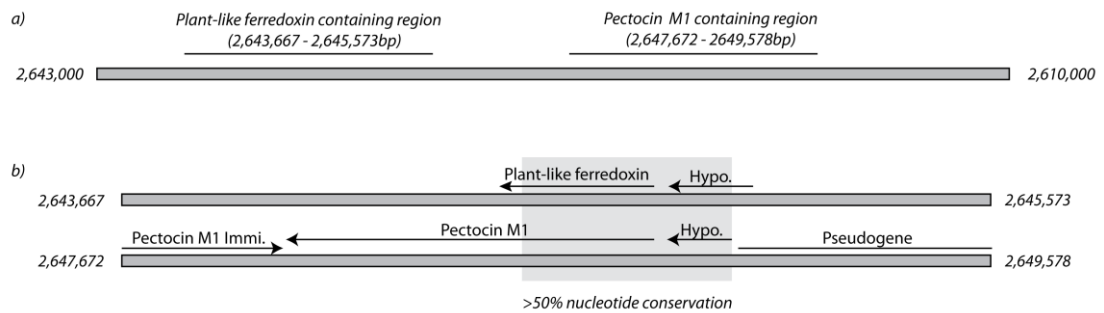


Figure 4-2 Genomic context of the pectocin M1 gene

a) Position of genomic regions on the chromosome of *Pcc* PC1 containing the pectocin M1 gene and a related plant-like ferredoxin gene. b) Alignment of genomic regions from above, containing the pectocin M1 gene and the related plant-like ferredoxin gene showing annotated open reading frames and nucleotide homology shared between the two regions

4.4 Purification and characterisation of pectocin M1 and M2

Pectocin M1 and M2 were expressed in *E. coli* BL21 (DE3) and purified by anion exchange chromatography and gel filtration to >90% homogeneity based on analysis by SDS-PAGE (Figure 4-3-A). The purified recombinant proteins were red-brown in colour and the absorption spectra of both proteins displayed maxima at 330 nm, 423 nm, and 466 nm (Figure 4-3-B), which are characteristic of plant ferredoxins (219). These data show both pectocins M1 and M2 contain a [2Fe-2S] cluster.

Initially the killing spectrum of pectocin M1 and pectocin M2 was tested against five *P. atrosepticum* and five *P. carotovorum* isolates using the agar overlay spot test method on LB agar. Under these experimental conditions pectocin M1 was found to be active against three *P. atrosepticum* strains and one *P. carotovorum* strain. The zones of inhibition in this experiment while distinct were hazy and varied in size upon repetition. Pectocin M2 did not show activity against any of the strains tested under these conditions.

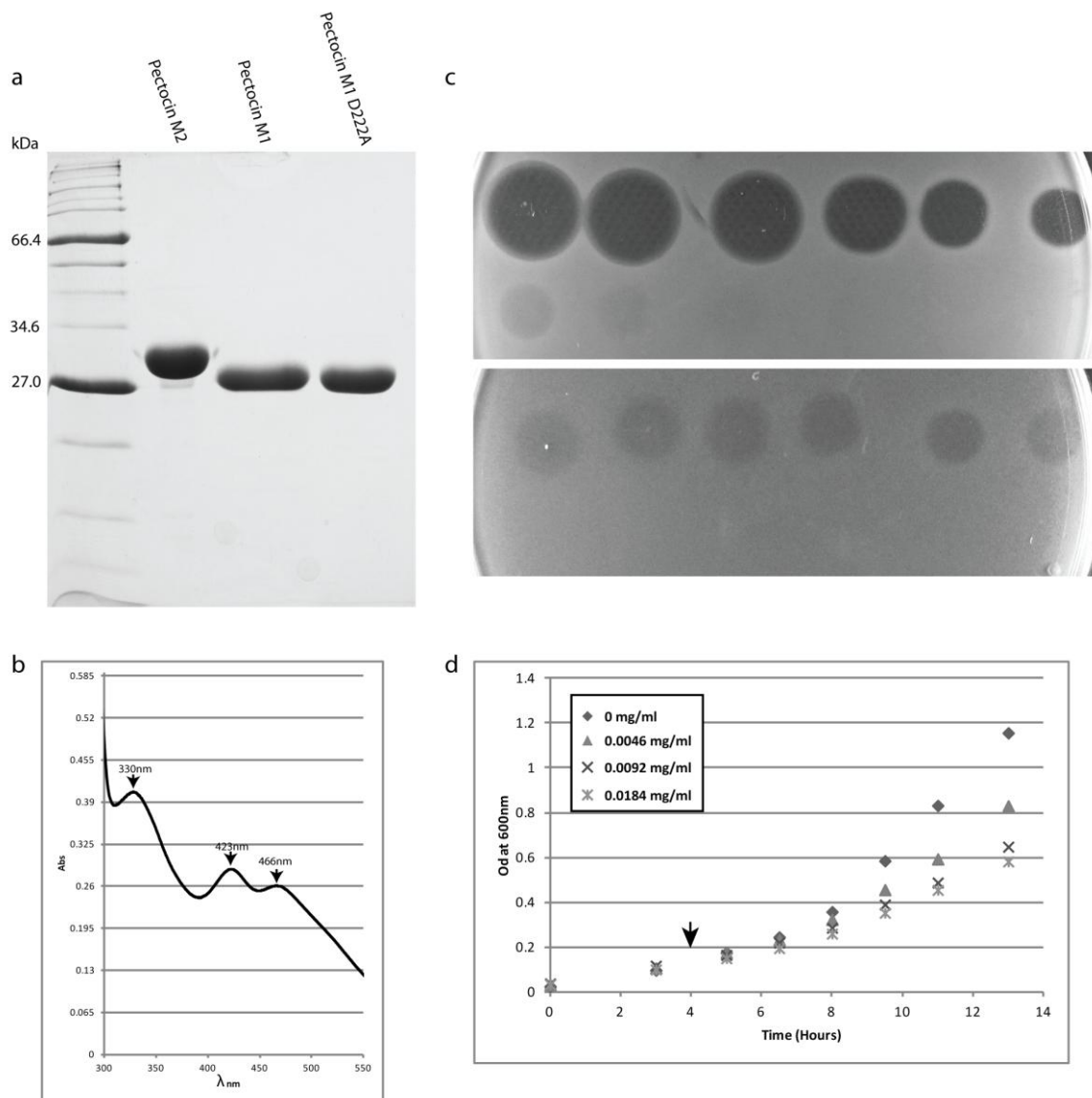


Figure 4-3 Purification and characterisation of pectocin M proteins.

a) SDS-PAGE of purified pectocin M2, M1 and M1 D222A b) Absorbance spectrum of pectocin M1 at a concentration 1.2 mg ml^{-1} . Maxima at 330, 423 and 466 nm, identical to those observed in plant ferredoxins, indicate the presence of a [2Fe-2S] cluster in pectocin M1. Spectra with identical absorbance peaks were obtained for the pectocin D222A mutant and pectocin M2. c) Agar overlay spot tests of a 10-fold serial dilution ($7.5 \mu\text{M}$ - 7.5 nM) of pectocin M1 spotted onto overlay of *P. atrosepticum* LMG 2386 cells grown in the presence of the iron chelator 2,2'-bipyridine ($200 \mu\text{M}$). d) Liquid growth inhibition assay, test strain LMG 2386, grown in LB broth with $200 \mu\text{M}$ 2,2'-bipyridine. Purified PM1 was added when indicated.

Since a number of bacteriocins utilise outer membrane receptors involved in iron uptake (4) we tested the activity of the pectocins under iron limiting conditions, induced by addition of the iron chelator 2,2'-bipyridine to the LB agar. Under these conditions the activity of pectocin M1 was greatly enhanced (Figure 4-3-C), with seven of ten *Pectobacterium spp.* being inhibited. For pectocin M2, three of the ten strains were weakly inhibited (Table 9-2, Table 9-3). The minimum inhibitory concentration of pectocin M1 under iron-limiting conditions was calculated, using the above method with serial dilutions of pectocin M1, varying from 14.5-145 nM among susceptible strains. The cytotoxic effect of pectocin M1 in liquid culture was tested by adding varying concentrations of pectocin M1 to an iron limited log-phase culture of the susceptible strain *P. atrosepticum* LMG 2386. A concentration-dependent reduction in growth was observed upon the addition of pectocin M1 (Figure 4-3). To determine if pectocin M1 and M2 were active against more distantly related bacterial species, pectocin M1 and pectocin M2 were tested for inhibitory activity against strains of *E. coli*, *Pseudomonas syringae*, *Pseudomonas aeruginosa* and *Erwinia rhapontici* (Table 2-1). None of these more distantly related bacteria showed any susceptibility to pectocin M1 or M2 (at 1.2 and 10mg.ml⁻¹ respectively) suggesting that the activity of these pectocins is limited to species of *Pectobacterium* closely related to the producing strain.

4.5 The ferredoxin domain of pectocins M1 and M2 mediate receptor binding

As ferredoxin is a potential iron source for phytopathogenic *Pectobacterium* species one possibility that pectocins M1 and M2 are parasitising an existing iron uptake system by using their ferredoxin domain to bind to a cell surface receptor, which has a normal physiological role in iron acquisition from ferredoxin. If this is the case, the addition of a plant ferredoxin at sufficient concentration should abolish pectocin M1 binding to its receptor and therefore abolish its cytotoxic activity. To test this hypothesis spinach ferredoxin was spotted adjacent to pectocin M1 in an agar overlay spot test. Clear inhibition of cell killing was observed in the region where the diffusion zone of spinach ferredoxin overlaps with the pectocin M1 diffusion zone (Figure 4-4). Indeed, for all 7

susceptible strains cytotoxicity of pectocin M1 could be abolished to a similar extent by the addition of spinach ferredoxin. This effect was not observed with adrenodoxin, a more distantly related mammalian [2Fe-2S] cluster containing ferredoxin, indicating specificity for plant ferredoxins (Figure 4-4). Additionally, in five pectocin M1 susceptible strains that are not sensitive to pectocin M2 the cytotoxicity of pectocin M1 could be abolished by the addition of pectocin M2, indicating these two bacteriocins utilise the same receptor. To determine if the activity of the colicin M-like domain of pectocin M1 is essential for its cytotoxicity, mutant pectocin M1 was generated in which Asp226 is replaced by Ala. As discussed in chapter 3 the equivalent Asp of colicin M and syringacin M has been shown to be essential for the catalytic activity and consequent cytotoxicity (1,200). Purified pectocin M1 Asp226Ala had no detectable cytotoxicity, but was able to inhibit cytotoxicity of wildtype pectocin M1 in a competition assay, indicating that it is fully functional in binding to its receptor (Figure 4-4). Taken together, these data indicate that receptor recognition occurs through the ferredoxin domain of pectocin M1 and M2 and that the normal physiological role of pectocin M1/M2 receptor is to bind plant ferredoxins.

4.6 Growth enhancement under iron limiting conditions by pectocins and spinach ferredoxin

During spot tests on iron limiting media to determine the killing spectrum of pectocin M1 and M2 it was observed that the growth of a number of insensitive *Pectobacterium* strains was enhanced where the pectocins were spotted onto the plate. Additionally, some strains that were inhibited by pectocin M1 displayed a zone of enhanced growth peripheral to the zone of inhibition. Four and five of the ten *Pectobacterium* isolates exhibited enhanced growth in the presence of pectocin M1 and M2, respectively. The enhancement of growth due to pectocin M1 was significantly more pronounced than that due to pectocin M2, with strongest enhancement present at 200 μ M 2,2'-bipyridine for both pectocin M1 and pectocin M2 (Table 9-2, Table 9-3). This observation led to the hypothesis that *Pectobacterium* strains are able to utilise these ferredoxin domains as an iron source under iron limiting conditions. To test this idea further, and to test the

specificity of this growth enhancement, related plant and mammalian ferredoxin-type proteins (spinach ferredoxin I and human adrenodoxin) as well as syringacin M, a colicin M homologue from *Pseudomonas syringae* which contains an active colicin M catalytic domain but an unrelated N-terminal region (82) were tested for their ability to enhance the growth of *Pectobacterium* spp. under iron-limiting conditions. Five strains exhibited strongly enhanced growth due to the spinach ferredoxin at either 20 or 2 mg ml⁻¹ (Figure 4-5), this enhanced growth was dependent on the concentration of the iron chelator 2,2'-bipyridine, with the strongest enhancement at 400 μM (Table 9-4). No enhanced growth was observed with the [2Fe-2S] cluster containing protein adrenodoxin at 30 mg ml⁻¹ or syringacin M at 5 mg ml⁻¹.

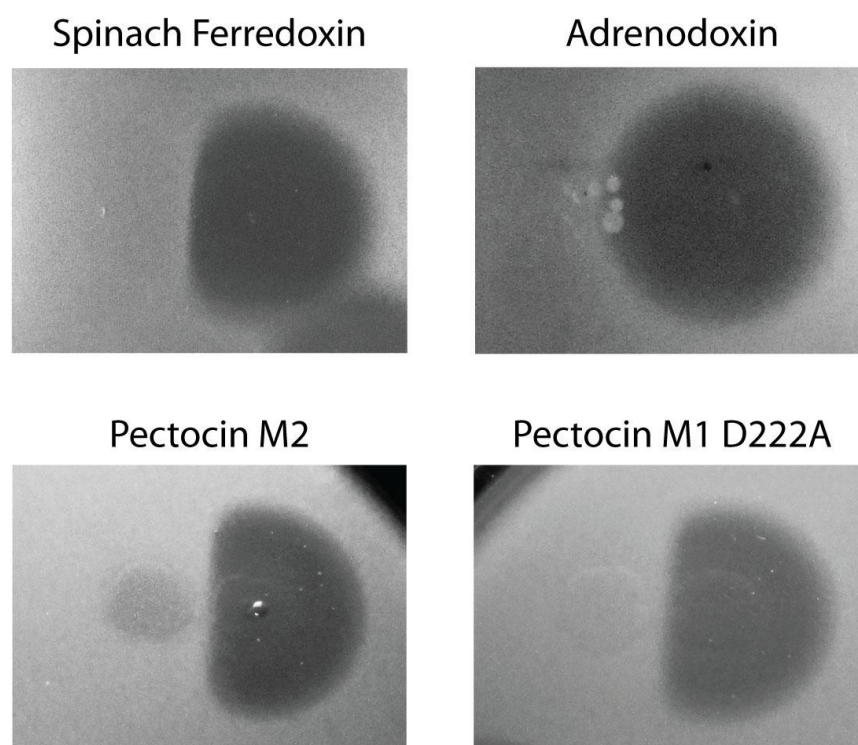


Figure 4-4 Interference of pectocin M1 killing by inactive pectocins and plant ferredoxin but not human adrenodoxin.

Interference of pectocin M1 growth inhibition zones against agar seeded with *P. atrosepticum* LMG2386, due to plant-like ferredoxin containing proteins, but not adrenodoxin. Protein concentration for spots were as follows: pectocin M1 1.2 mg ml⁻¹, spinach ferredoxin 20 mg ml⁻¹, adrenodoxin 30 mg ml⁻¹, pectocin M2 10 mg ml⁻¹, pectocin M1 D222A 5.6 mg ml⁻¹

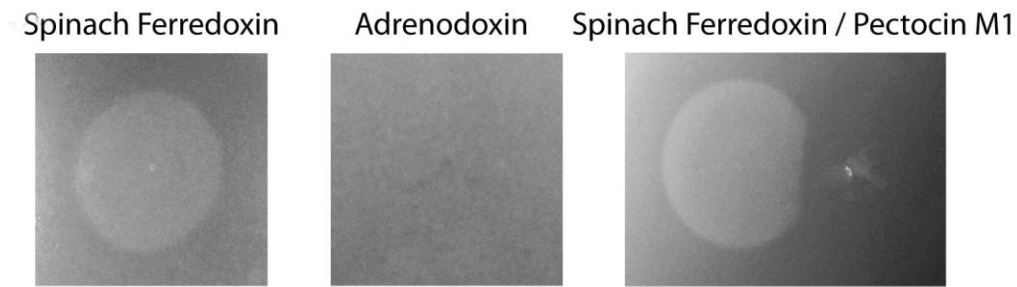


Figure 4-5 Growth enhancement of *P. carotovorum subsp. carotovorum* LMG 2410 by plant-like ferredoxin containing proteins.

Protein concentrations for spots were as follows: spinach ferredoxin 20 mg ml⁻¹, adrenodoxin 30 mg ml⁻¹, Spinach ferredoxin 20 mg ml⁻¹:pectocin M1 1.2 mg ml⁻¹. Pectocin M1 causes asymmetry in zone of enhancement due to spinach ferredoxin.

4.7 The crystal structure of pectocin M2

To provide structural insight into these unusual ferredoxin containing bacteriocins, crystallisation trials for pectocins M1 and M2 were setup. Despite extensive screening no crystals were obtained for pectocin M1, however, in initial crystallisation trials for pectocin M2, characteristic red-brown crystals formed with PEG 3350 and ammonium sulphate as precipitants (Figure 9-1-C). Data from these crystals were collected to 2.3 Å in the space group $P2_1$ and phased using anomalous scattering data from the metal centres of the [2Fe-2S] iron-sulphur cluster. The structure of pectocin M2 revealed an N-terminal domain with the predicted ferredoxin-fold (residues 2-94, in red), separated from the colicin M-like cytotoxic domain (residues 116-271, in blue) by a linker region (residues 95-115, in green) that forms an α -helix (Figure 4-6-A/B). There is a significant difference in the orientation of the cytotoxic and ferredoxin domains of the two pectocin M2 molecules in the asymmetric unit (ASU) with a root mean square deviation (r.m.s.d) of 3.4 Å, between main chain atoms (Figure 4-7). The fold of the pectocin M2 ferredoxin domain is highly homologous (r.m.s.d 0.60 Å) to that of spinach ferredoxin (PDB ID = 1A70) and the C-terminal cytotoxic domain is highly similar to the lipid II-cleaving catalytic domain of colicin M (PDB ID = 2XMX, r.m.s.d 1.7 Å) (Figure 4-6-C/D) (198). In contrast to the compact structures of the homologous bacteriocins, colicin M, pyocin M and syringacin M, where the receptor binding and catalytic domains are not separated by linker regions and do not

form obviously structurally distinct elements (1,81,198), the catalytic and receptor binding domains of pectocin M2 do not form extensive interactions. The relative orientation of the ferredoxin domain, linker region and cytotoxic domain gives rise to a non-linear dog-leg structure. Interestingly, and again in contrast to colicin M, pyocin M and syringacin M, the N-terminal region of pectocin M2 lacks a disordered or flexible IUTD that is otherwise characteristic of the colicin-like bacteriocins, with the entire N-terminus being integral to the globular ferredoxin domain. Thermal unfolding indicates that this iron-sulphur cluster containing domain is highly stable (Figure 4-6-E). These data suggest a mechanism of uptake distinct from closely related colicin-like bacteriocins.

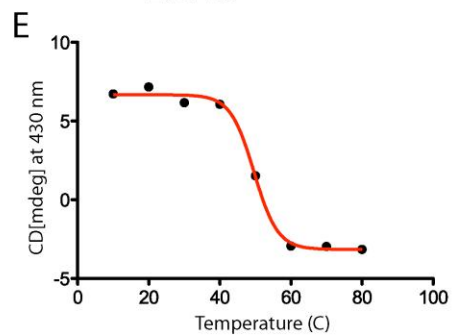
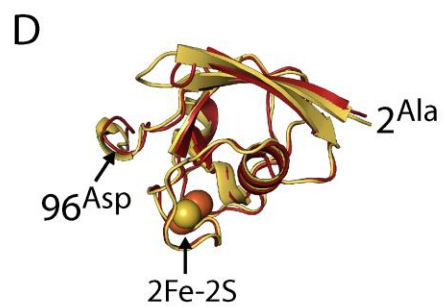
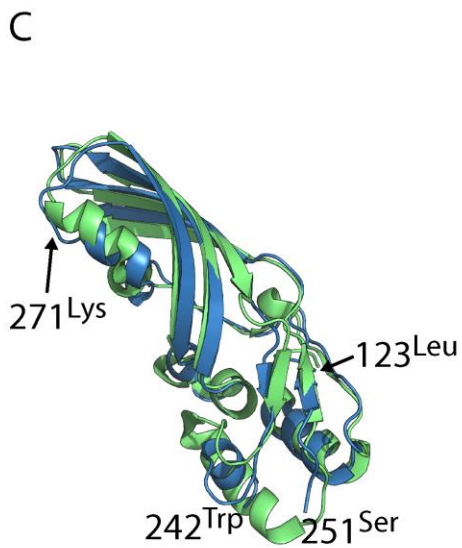
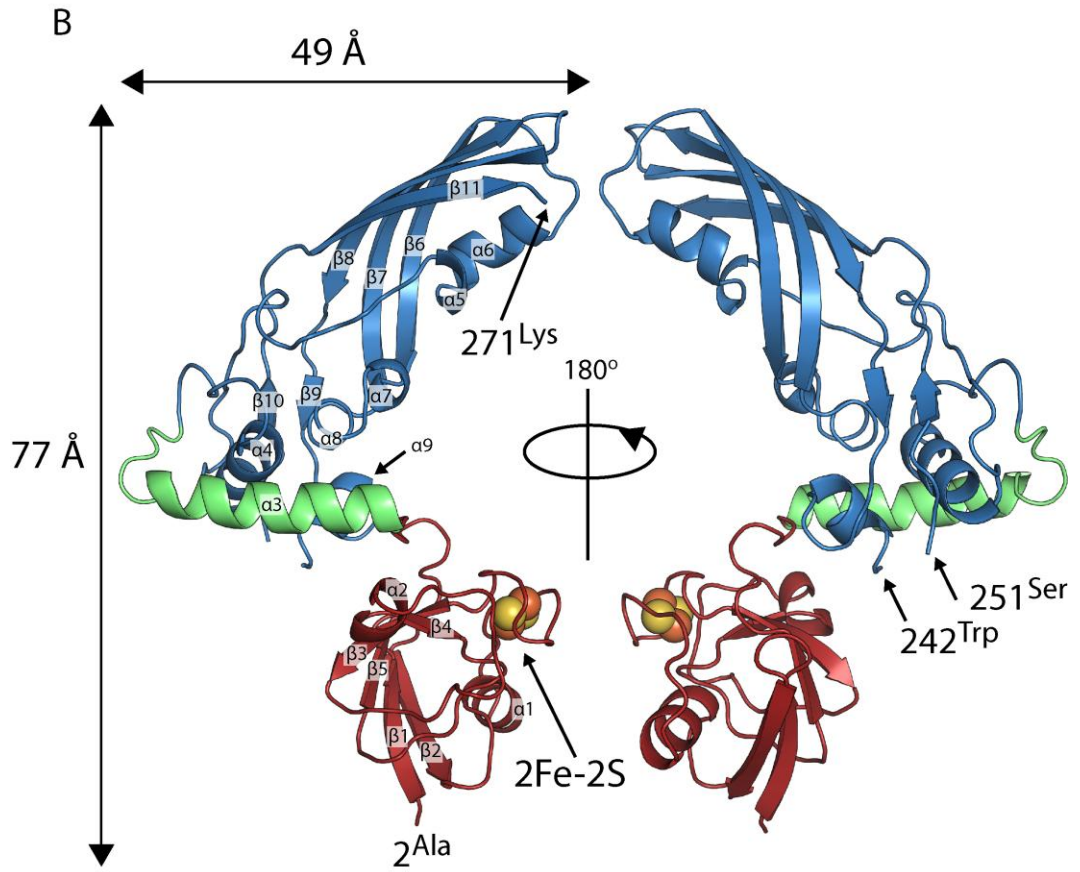
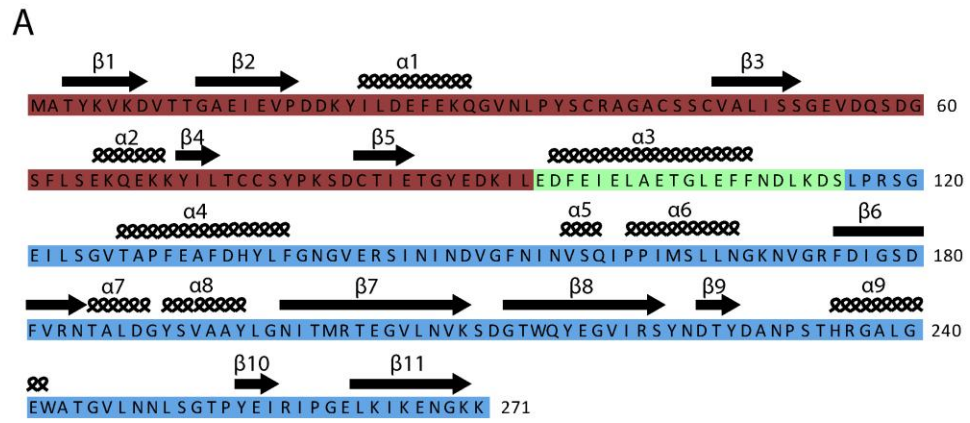


Figure 4-6 The crystal structure of pectocin M1 reveals a ferredoxin-containing colicin-like bacteriocin that lacks an IUTD.

A) Amino acid sequence of pectocin M2, showing structural domains (ferredoxin domain = red, linker helix = green, catalytic domain = blue) and annotated with secondary structure. B) Schematic of the crystal structure of pectocin M2 observed in the P2₁ crystal form, with the cytotoxic domain in blue, plant-like ferredoxin domain in red and linker helix in green. The [2Fe-2S] iron-sulphur cluster is represented by spheres. C) Schematic of cytotoxic domain of pectocin M2 aligned with that of colicin M (PDB ID = 2XMX) (backbone r.m.s.d = 1.65 Å, pectocin M2 residues = 123-271, colicin M residues = 123-271). D) Schematic of the ferredoxin domain of pectocin M2 aligned with that of spinach ferredoxin (PDB ID = 1A70) (backbone r.m.s.d = 0.6 Å, pectocin M2 residues = 2-96, spinach ferredoxin residues 2-96). E) Unfolding of the ferredoxin domain of pectocin M2 shown by change in circular dichroism spectra at 430 nm, with increasing temperature (T_m = 50°C).

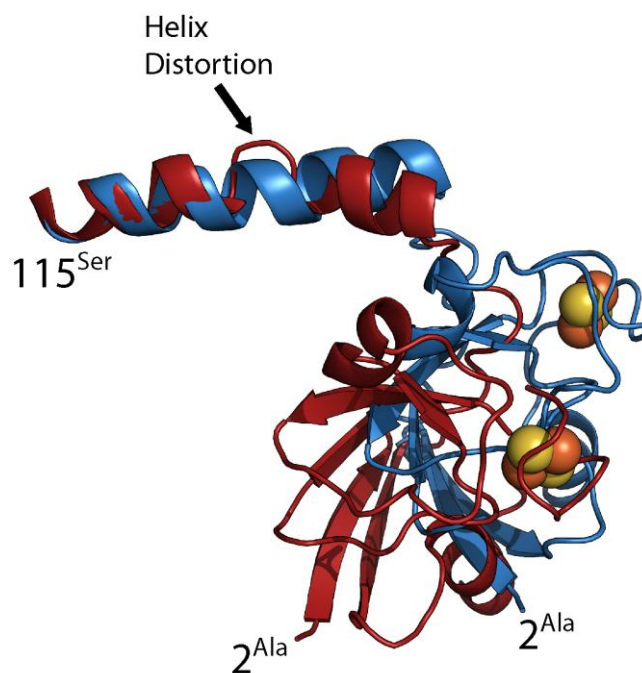


Figure 4-7 Conformational difference between ferredoxin domains in the P2₁ crystal form

The difference in orientation of ferredoxin domains between the two molecules in the asymmetric unit of the P2₁ crystal form, alignment of molecules was based on the catalytic domain AA 116-271. Distortion in the linking helix of one of the molecules leads to the majority of the difference.

4.8 Pectocin M2 is conformationally flexible

Given that pectocin M2 lacks an IUTD required to contact the Tol or Ton complexes in the periplasm and mediate translocation of this protein across the outer membrane, alternative mechanisms of uptake must be considered. One possibility is that the entire bacteriocin passes through the lumen of its OM receptor. Since proteins involved in iron uptake are invariably TonB-dependent receptors that possess large 22-stranded β -barrels this hypothesis is plausible. However, such a mechanism would only be feasible if pectocin M2 were flexible and significant rearrangement of the dog-leg configuration observed in the crystal structure could be achieved. The observation that there is a relatively large difference in orientation between the cytotoxic and ferredoxin domains in the monomers of the ASU is suggestive of such flexibility and indicates that the crystal structure may not be wholly representative of pectocin M2 in solution.

To assess the conformational flexibility of pectocin M2 small angle X-ray scattering (SAXS) was performed. SAXS data were obtained for a range of pectocin M2 concentrations. Comparison of these data with a theoretical scattering curve generated, using CRY SOL (194), from the pectocin M2 crystal structure shows there are obvious differences between the theoretical curve and experimental scattering data (Figure 4-8-A). In addition, the radius of gyration ($R_g = 27 \text{ \AA}$) obtained from Guinier analysis of the experimental scattering data is somewhat larger than that calculated from the pectocin M2 crystal structure ($R_g = 24 \text{ \AA}$) using SOMO (193) (Figure 4-8-B). Consistent with this, the $P(r)$ function, which describes the paired set of vectors between all the electrons within the protein, indicates a maximum particle size ($D_{\max} = 96 \text{ \AA}$, Figure 4-8-C) that is much greater than the maximum dimension of the pectocin M2 crystal structure (77 \AA , Figure 4-6-B). These data suggest that the pectocin M2 crystal structure is not wholly representative of the conformational ensemble present in solution and that this protein adopts an elongated conformation, implying inter-domain flexibility.

To test this idea further, the Porod-Debye plot of pectocin M2, where scattering decay is examined as q^4 versus $I(q)q^4$, was examined. Typically, for compact globular particles a plateau is reached within a limited q^4 region of the curve. However, for pectocin M2 no discernible plateau was observed (Figure 4-8-D). For comparison, scattering data for

pyocin M which, as with colicin M and syringacin M, forms a compact structure were obtained and similarly analysed (81). In contrast to the curve obtained for pectocin M2, the Porod-Debye plot for pyocin M reached a plateau confirming its rigidity and compactness (Figure 4-8-D). In addition, the Kratky plot ($I(q)q^2$ versus q) for pectocin M2 normalised to the scattering intensity $I(0)$ and R_g , has two maxima with increasing scattering at higher angles, consistent with a two-domain protein connected by a flexible linker (Figure 4-8-E). In comparison, there is a single maximum in the pyocin M Kratky plot, consistent with its single domain-like globular structure. Taken together these analyses indicate that pectocin M2 is flexible and adopts conformations distinct from that observed in the crystal structure.

4.9 Pectocin M2 can adopt a highly extended conformation and exists as two distinct subpopulations in solution

To determine if the SAXS data for pectocin M2 could be better described by an ensemble of conformations we first used discrete molecular dynamics (DMD) simulations (226) to explore the accessible conformational states of pectocin M2 and generated a random pool of 5,000 possible conformations using the crystal structure of pectocin M2. Next, a genetic algorithm was implemented in the program GAJOE (227) to select for ensembles of these models that would better describe our SAXS data. Model selection was successful as judged by the close correlation of the theoretical scattering curve generated from the selected ensemble with the experimental SAXS data (Figure 4-9-C), indicating that those scattering data are best described by an ensemble of pectocin M2 conformers in solution. Interestingly, the selected ensembles show a bimodal distribution in comparison with the random pool of DMD-generated pectocin M2 models when the population frequency is plotted against R_g or D_{max} (Figure 4-8-A/B). Thus, in the population of selected conformations, a compact conformation is frequently found, described by the first peak (with maxima at approximately 23 and 75 Å for R_g and D_{max} , respectively) that approximates closely to the conformation found in the pectocin M2 $P2_1$ crystal structure for which R_g and D_{max} were calculated as 24 and 77 Å, respectively. The second peak represents an ensemble of pectocin M2 conformers in an extended

conformation with D_{\max} values ranging up to 98 Å which correlates closely with the experimentally determined value of D_{\max} (96 Å). These analyses suggest that pectocin M2 can adopt both bent and elongated linear conformations in solution. The bimodal distribution of the selected ensembles suggests discrete populations in solution, the more compact of which is similar to the conformation observed in the $P2_1$ crystals of pectocin M2. In an attempt to capture the more elongated conformation *in crystallo*, thus validating the solution scattering and modelling data, crystallisation of pectocin M2 was repeated. A custom re-crystallisation screen was devised exploiting information from the initial trials. Crystals were obtained in a number of conditions from this screen and were tested for diffraction as well as space group and unit cell variation, which is indicative of novel packing. A form with the radically different space group of $P3_121$ was chosen for optimisation, which yielded crystals diffracting to 1.86 Å. As an alternative domain arrangement to the $P2_1$ form was expected, data from this crystal form were again phased using anomalous data from the metal centres of the [2Fe-2S] cluster. During model building from these data it was immediately apparent that in this crystal form pectocin M2 did indeed adopt an elongated conformation (Figure 4-10-A). The calculated R_g and D_{\max} for this structure were 28 and 97 Å, respectively. These values correlate well with the extended population from the DMD simulation, suggesting that this structure is representative of the second elongated pool identified by modelling. Alignment of this elongated $P3_121$ form and the original $P2_1$ form, based on their cytotoxic or ferredoxin domains, show a major difference in the relative orientations of these domains (Figure 4-10-B/C).

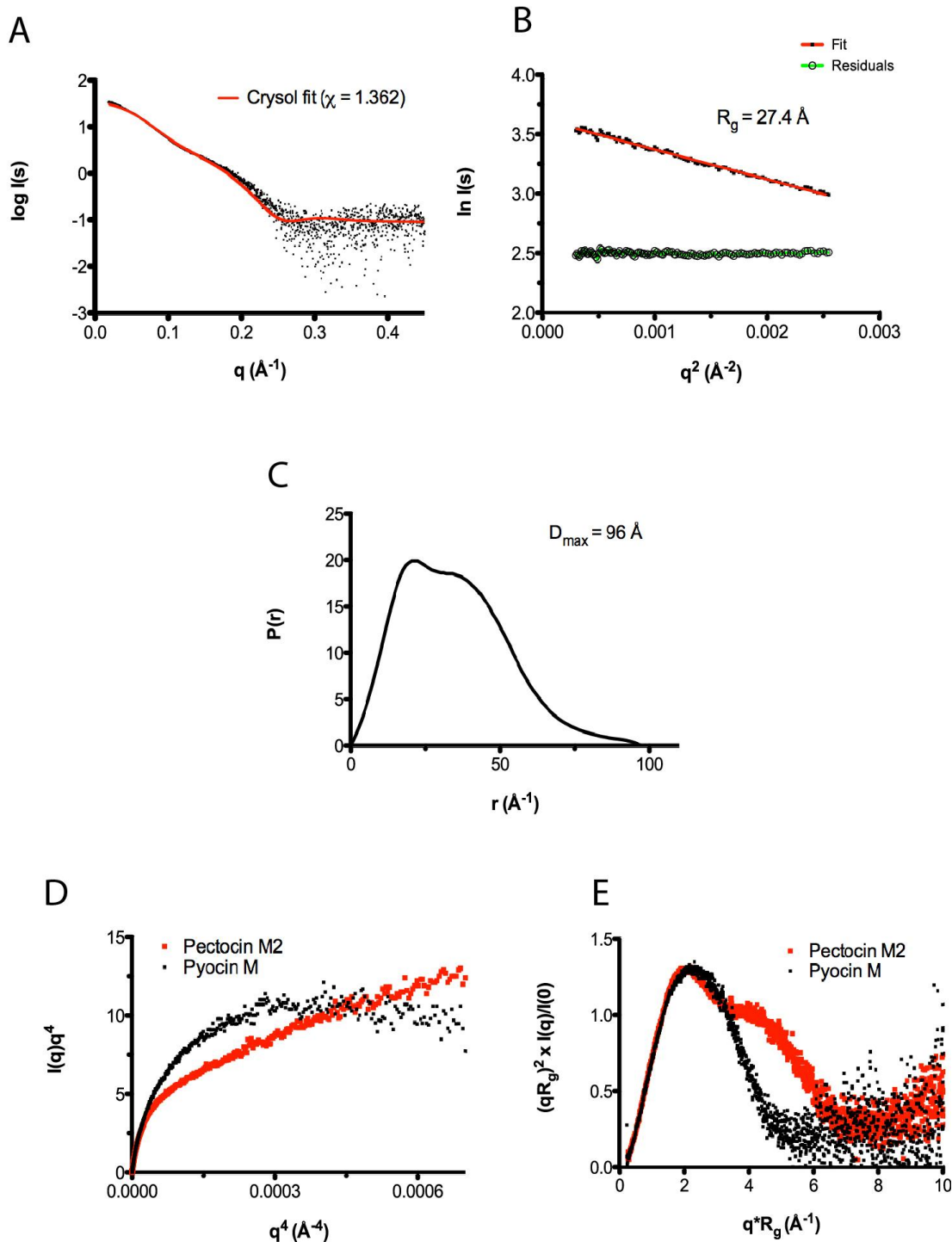


Figure 4-8 SAXS shows pectocin M2 is flexible.

A) Overlay of the experimentally determined pectocin M2 SAXS curve (black points) with the scattering curve computed with CRYSOLOG from the P21 crystal structure (red line) produces a fit ($\chi=1.362$) with visible deviations between the data, especially evident at low angles, suggesting that the crystal structure is more compact than that of pectocin M2 in solution. B) Derivation of R_g from a Guinier analysis (red) of the scattering curve; residuals of the fit are in green. C) Pair-distance distribution plot from experimental scattering data for pectocin M2 exhibiting two maxima which highlights the bimodal character of the molecule in solution. The D_{max} of the particle is 96 Å. D) Porod-Debye and (e) normalised Kratky plots for pectocin M2 imply increased flexibility of the protein in solution (red). Pyocin M (black), a protein of similar molecular weight with a relatively rigid structure and strong inter-domain contacts is used as a control.

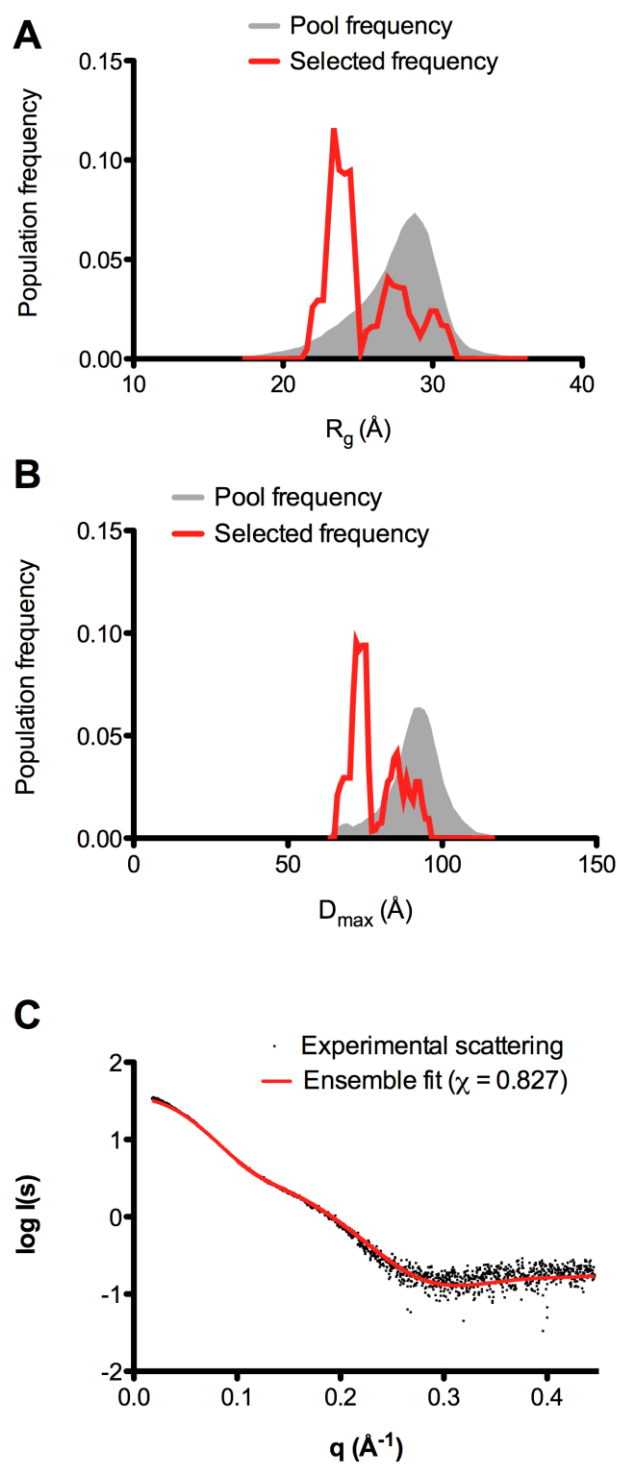


Figure 4-9 Analysis of conformational heterogeneity of pectocin M2 reveals compact and extended ensembles in solution.

R_g A) and D_{max} B) distribution of solution ensembles selected by a genetic algorithm using GAJOE from a pool of 5000 random conformers of pectocin M2. Compact and elongated molecule were both selected implying that the protein is conformationally heterogeneous in solution allowing for significant inter-domain re-arrangements about the linker helix (residues 96-115). C) Overlay of scattering curves of pectocin M2 between experimental data and the best ensemble selected by GAJOE indicates improved fit to the scattering data ($\chi = 0.827$).

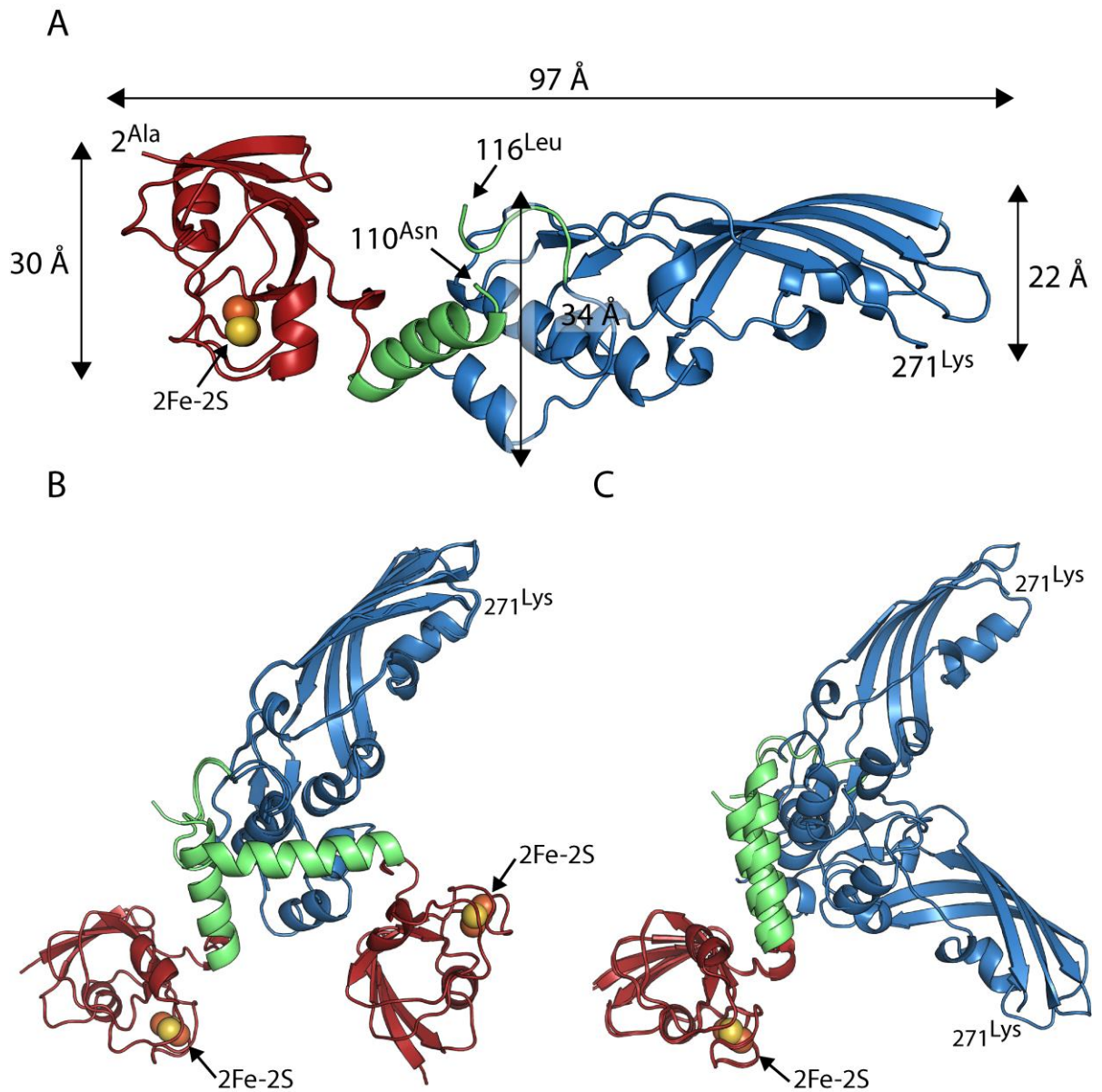


Figure 4-10 Pectocin M2 P₃₁2₁ structure confirms extended conformation predicted by solution scattering.

A) Pectocin M2 in P₃₁2₁ crystal form is highly elongated, consistent with the extended conformation predicted from solution scattering and DMD simulations. (B) Alignment of the catalytic domains of the P₂₁ and P₃₁2₁ crystal forms of pectocin M2, illustrating the difference in orientation between the ferredoxin and linker regions. (C) Alignment of the ferredoxin domains of the P₂₁ and P₃₁2₁ crystal forms of pectocin M2, illustrating the difference in orientation of the catalytic domains.

4.10 The ferredoxin domain is a generic module for the delivery of cytotoxic domains to the periplasm

In addition to pectocin M1 and M2, a putative third member of the ferredoxin-containing bacteriocin family, designated pectocin P was identified through bioinformatic analysis (92). The open reading frame for pectocin P, identified in the genome of *Pectobacterium carotovorum* subsp. *carotovorum* WPP14, consists of an N-terminal ferredoxin domain, connected to a pesticin-like cytotoxic domain, which is analogous to T4 lysozyme. Similar to pectocins M1 and M2, there is no sequence N-terminal of the ferredoxin domain, so this bacteriocin also lacks an IUTD. To confirm that this open-reading frame encodes an active bacteriocin, the cytotoxic activity of recombinantly expressed and purified pectocin P was tested against diverse *Pectobacterium* isolates. For this test a solid growth inhibition assay was conducted in parallel with pectocins M1 and M2 (151). As with pectocins M1 and M2, limited inhibition of growth was observed under iron-replete conditions (LB agar). However, under iron-limiting conditions, inhibition of growth was observed for 17 of the 19 strains (Figure 4-11). The existence of pectocin P, an additional ferredoxin-containing bacteriocin with no N-terminal IUTD and a pesticin-like cytotoxic domain, provides strong supporting evidence that the ferredoxin domain acts as a generic module for the delivery of cytotoxic domains to the periplasm in *Pectobacterium* spp. The cytotoxic domains of both M-class bacteriocins and pesticin have been studied extensively and there is no indication that they possess any intrinsic capacity to cross the OM (94,96,199,200), indicating that ferredoxin uptake represents an unprecedented example of receptor-mediated protein uptake for nutrient acquisition in bacteria.

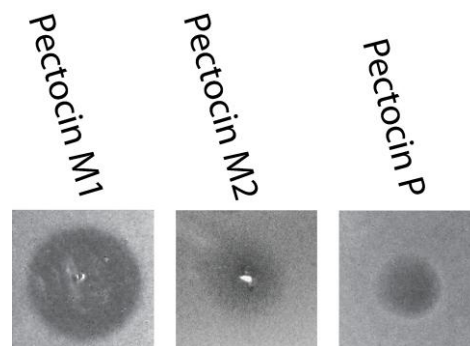


Figure 4-11 Growth inhibition of purified pectocins.

Zones of inhibition by pectocins M1, M2 and P after spotting onto a soft agar overlay seeded with Pba LMG 2386.

4.11 The pectocin M2 cytotoxic domain has well defined substrate binding site

The crystal structure of pectocin M2 adds to a growing body of structural and biochemical data on the colicin M-like cytotoxic domain, which is delivered to the periplasm by the ferredoxin domains of pectocin M1 and M2 (1,81,198-200). The enzymatic activity of pectocin M1 and M2 was confirmed by a lipid II hydrolysis assay. As expected, both proteins were able to cleave the substrate in a metal dependent fashion, with pectocin M2 exhibiting higher relative activity (Figure 4-12). In the recently solved structures of pyocin M (PaeM) and syringacin M a divalent metal ion (Ca^{2+} or Mg^{2+}) is coordinated by a key catalytic aspartic acid side chain in conjunction with two backbone carbonyls. The metal ions, Mg^{2+} , Ca^{2+} or Mn^{2+} are required for catalytic activity of M-class bacteriocins, and analysis of these proteins has shown coordination at this position to be essential for activity (1,2). In the pectocin M2 structure this key aspartate (D226) adopts an analogous conformation to syringacin M, however no density for a metal ion is observed in this position, which is occupied by a water molecule (Figure 4-13-A). This absence of a metal ion is unsurprising however, given the lack of divalent ions and the high ionic strength of the crystallisation conditions.

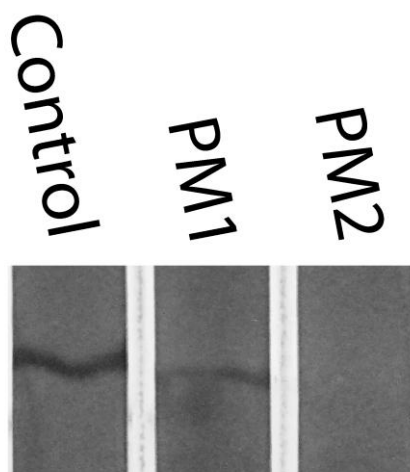


Figure 4-12 Pectocin M1 and M2 cleave lipid II.

Thin layer chromatography plate showing degradation of lipid II after incubation with either pectocin M1 (PM1) or pectocin M2 (PM2). Control reaction contained no protein. The observed band corresponding to lipid II migrated at the expected R_f of 0.7, compared to the solvent front.

Comparative analysis of the catalytic domains of colicin M homologues reveals significant variation between the structures. In the structures of pyocin M and syringacin M the key conserved arginine is located distant from other conserved residues creating an open active-site cleft. In contrast, in the pectocin M2 structure this residue (R236) is orientated towards the other key catalytic residues (Figure 4-13-B). The electron density for R236 permitted modelling of two conformations, one within hydrogen bonding distance of the aspartic acid coordinated water and the other forming a hydrogen bond with N184. In both conformations, R236 creates a defined active site tunnel capable of coordinating the lipid II pyrophosphate group in close proximity to all key catalytic residues (Figure 4-13). To test the capacity of this active site tunnel to accommodate lipid II, docking simulations were performed using Autodock Vina (195) with the N-acetylmuramic acid farnesyl pyrophosphate (FPP-MUB) portion of lipid II and the catalytic domain of pectocin M2. The best scored docking solution (score = -8.5) from this simulation threaded the hydrophobic farnesyl-chain into the hydrophobic cleft adjacent to the putative active site, positioning the phosphoester bond attacked by the enzyme within 3 Å of D226 and the Mg²⁺ cofactor (Figure 4-14-A/B). The binding of lipid II to an open conformation of the enzyme, was then simulated by docking FPP-MUB and catalytic domain of syringacin M (PDB ID = 4FZL). The best scored docking solution (score = -7.2) placed FPP-MUB in a very similar relative position and orientation to that in the simulation with pectocin M2, with a difference in the relative positions of the two phosphorous atom of 4.1 and 2.2 Å, in the superimposed docked structures. Interestingly, the farnesyl-chain fitted into an analogous hydrophobic cleft (Figure 4-14-C/D). As Autodock Vina docking is performed without the aid of external restraints, these docking results are validated by knowledge of catalytically important residues (2,200) and suggestive of a major conformational change upon substrate binding, which orientates the lipid II molecule for catalysis. A morphing simulation of the catalytic domain from the syringacin M to pectocin M2 docking simulations provides a plausible model for how this conformational change occurs upon substrate binding (228) (Movie S1).

The cleavage of lipid II by M-class bacteriocins yields undecaprenol (C₅₅-OH) and 1-pyrophospho-MurNAc(pentapeptide)-GlcNAc. In most phosphatases, catalysis occurs in two steps with an initial attack by a nucleophilic side chain leading to the formation of a covalent enzyme-substrate intermediate and a subsequent phosphoryl-group transfer to

a water molecule. The role of the metal cofactor is generally to bind the phosphate group of the substrate, correctly orientating the phosphorus atom for nucleophilic attack. In the phosphatases of the large haloacid dehydrogenase (HAD) family attack by the Asp nucleophile leads to the formation of an aspartylphosphate intermediate, which is hydrolysed by nucleophilic attack of a water molecule (229,230).

In silico docking suggests that the lipid II phosphoester bond attacked by the enzyme is in the immediate vicinity of both the essential divalent cofactor and catalytically essential residues. D235 which has been shown to be essential for catalytic activity in M-class bacteriocins, would be a likely candidate for the attacking nucleophile (200). The essential role of D232 in Ca^{2+} binding and the bidentate coordination of this metal ion likely preclude it from acting as a nucleophile. Also by analogy with the mechanism of the HAD phosphatases, H241 may act a general acid in the first step of this mechanism by donating a proton to the leaving undecaprenol group on formation of the aspartylphosphate intermediate and then as a general base through abstraction of a proton from the attacking water molecule in the second step. Alternatively, H241 could act as a nucleophile and D235 as a general acid/base. While comparative analysis of structures and *in silico* docking provides valuable information for hypothesis generation, a clear view of the mechanism of lipid II cleavage will require further biochemical analysis and structures of colicin M-like bacteriocins in complex with substrate or substrate analogues.

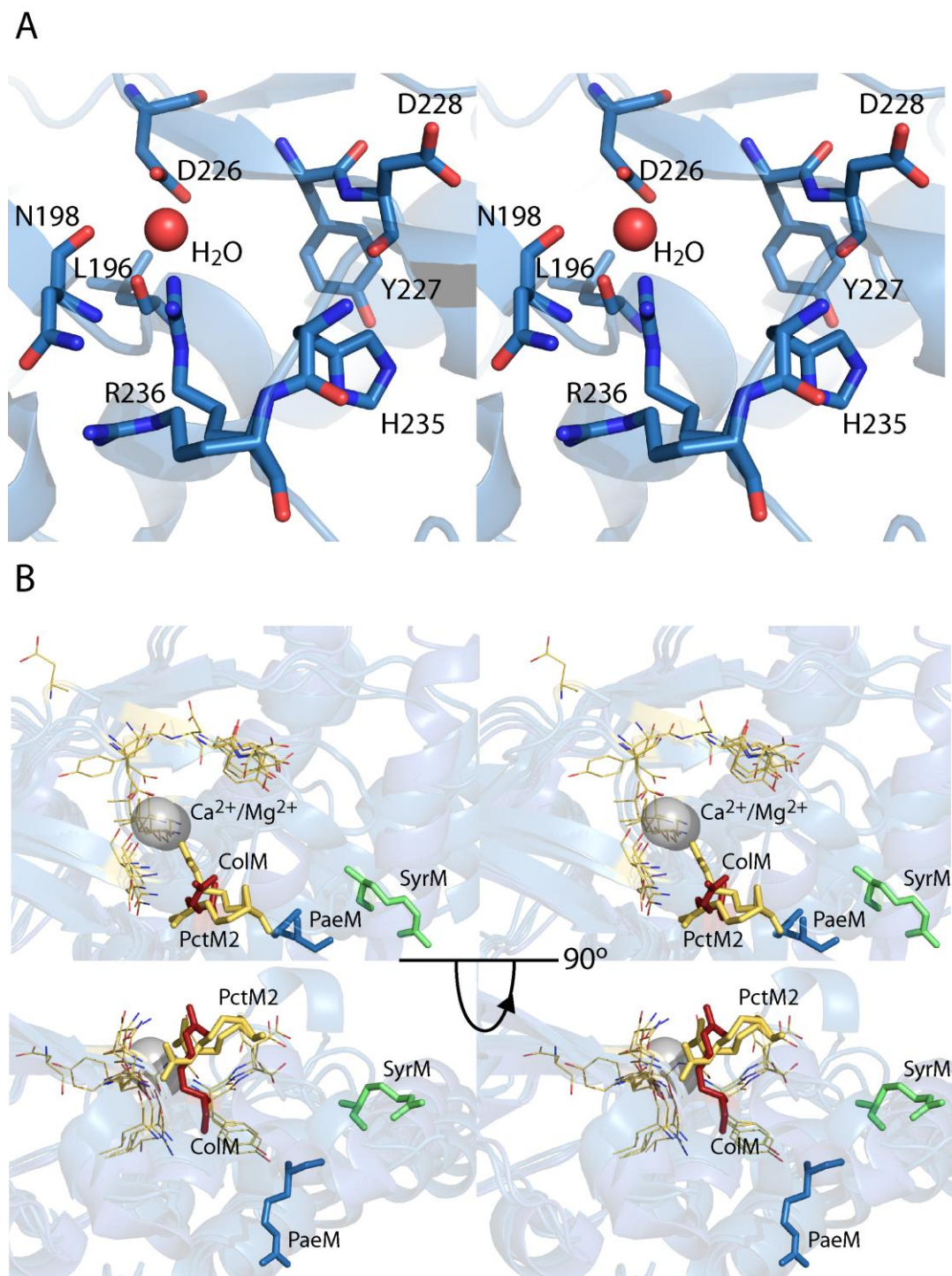


Figure 4-13 The flexible active site of M-class bacteriocins

A) A stereo view of a stick model of the key active site residues of pectocin M2, showing a water molecule occupying the key metal binding site of the enzyme. B) A stereo view of the overlay of the catalytic site from all structurally characterised colicin-M class bacteriocins, showing conformational variability of the key catalytic arginine. Key arginine shown as sticks and colour coded according to structure; green = syringacin M (PDB ID = 4FZL), blue = pyocin M (PDB ID = 4G75), red = colicin M (PDB ID = 2XMX) and yellow = pectocin M2 (PDB ID = 4N58), All other catalytically important residues shown as lines in yellow.

Lipid II

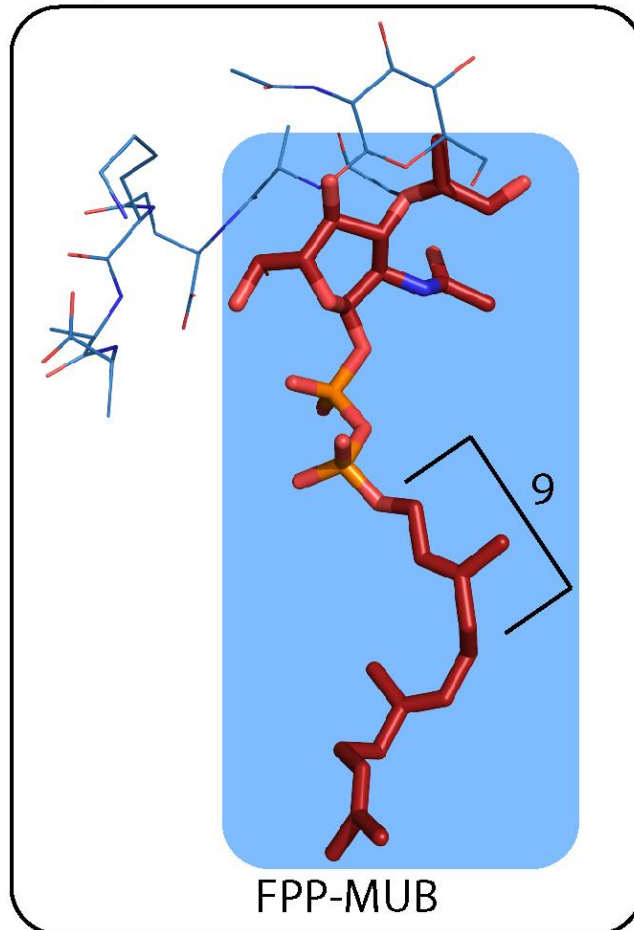


Figure 4-14 The lipid II substrate model utilised for docking into the active site of pectocins M2 and syringacin M.

The section in red sticks represents the trimmed molecule used for docking simulations. The addition of the N-acetyl glucosamine and penta-peptide motif, along with the 9x carbon repeat represents the full lipid II molecule.

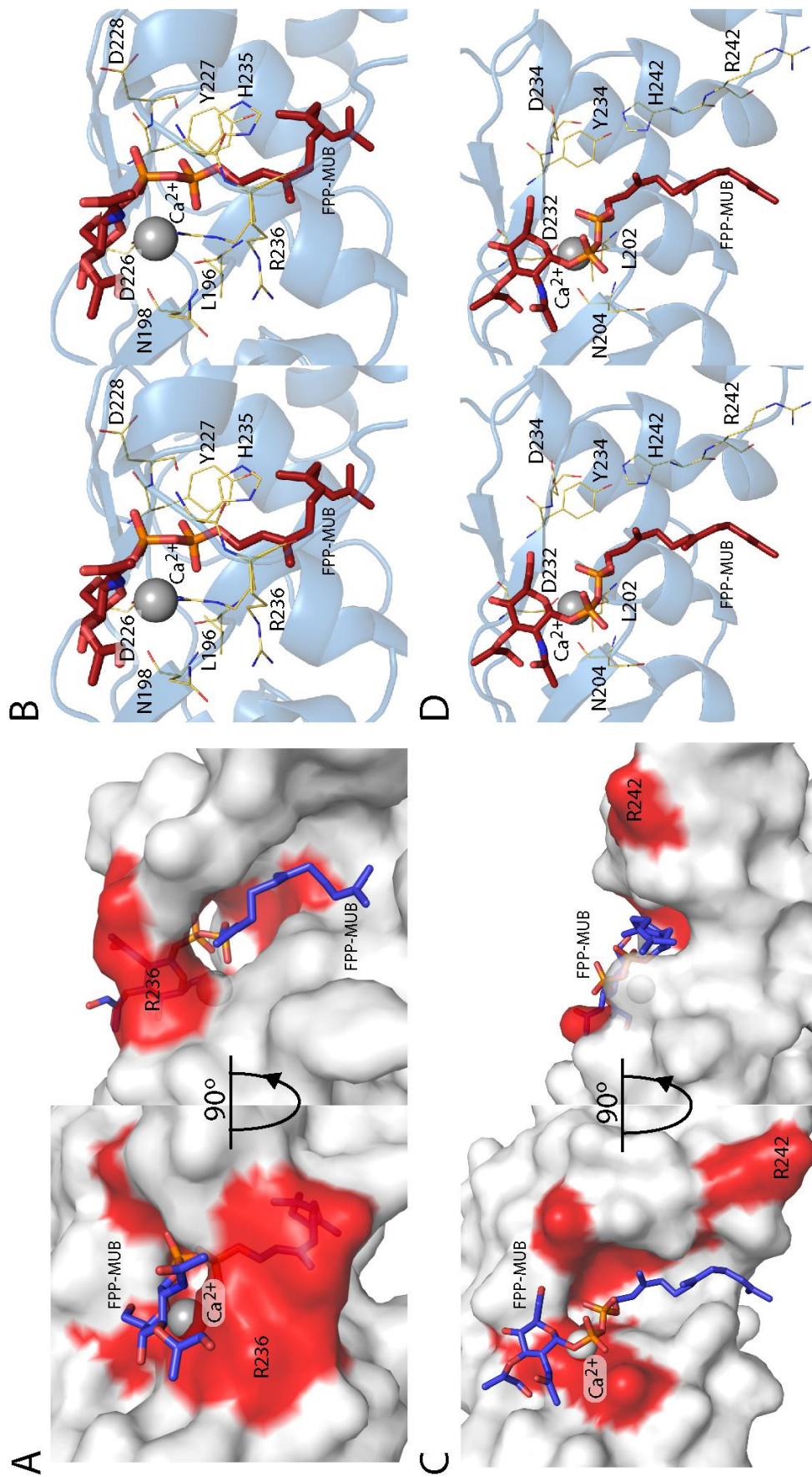


Figure 4-15 *In silico* docking of lipid II analogue reveals active-site binding site in an open and closed conformation.

A) Surface representation of pectocin M2 catalytic domain docked with FPP-MUB, catalytically important residues shown in red. B) Stereo schematic of docking from (a) showing important residues as lines. C) Surface representation of syringacin M catalytic domain docked with FPP-MUB, catalytically important residues shown in red. D) Stereo schematic of docking from (c) showing important residues as lines.

4.12 Isolation and characterisation of pectocin M1 resistant mutants

In an attempt to determine the gene(s) encoding the receptor and associated molecular machinery responsible for ferredoxin and pectocin uptake, the pectocin M1 susceptible strain *Pca*. LMG 2386 was incubated with purified pectocin M1 and plated onto iron limiting LB agar (+ 200 µM bipyridine) to isolate pectocin resistant mutants. Resistant colonies were confirmed as *Pectobacterium* by 16S rRNA sequencing, and as having a stable pectocin M1 resistant or tolerant phenotype after repeat propagation in LB broth. The majority of colonies isolated were entirely resistant to pectocin M1, with some showing a very low level of sensitivity. In order to determine the genetic basis for this resistance the genomic DNA of 6 independently isolated resistant lines and wildtype LMG 2386 was extracted and sequenced on an Illumina MiSeq platform. The phenotype and genetic polymorphisms between the mutant and wildtype strains were as follows:

200(1) = Resistant to pectocin M1 (Possibly very faint inhibition)

- SNV in putative gene for AFG-1 Family ATPase, leading to mutation Glu 342 to Gly
- SNV in gene for histidine sensor kinase EnvZ, leading to mutation Gln 45 to Pro

200(2) = Tolerant to pectocin M1 (faint zone of inhibition half the size of wildtype)

- SNV in gene for histidine sensor kinase EnvZ, leading to mutation Gln 283 to Leu
- Two base pair deletion in putative dTDP-glucose 4-6-dehydratase, leading to frame shift from Asp 120

200(3) = Resistant to pectocin M1

- Genetically identical to 200(1)

400(1) = Resistant to pectocin M1 (Possibly very faint inhibition)

- Two base pair deletion in putative dTDP-glucose 4-6-dehydratase, leading to frame shift from Asp 120
- SNV in gene for histidine sensor kinase EnvZ, leading to mutation Arg 253 to Pro
- SNV in gene for Lipoprotein NPLA, leading to mutation Phe 110 to Tyr

400(2) Tolerant to pectocin M1 (Faint zone of inhibition the same size at wildtype)

- SNV in putative gene for AFG-1 Family ATPase, leading to mutation Glu 342 to Gly
- SNV in gene for histidine sensor kinase EnvZ, leading to mutation Leu 135 to Pro

400(3) Resistant to pectocin M1

- Genetically Identical to 400(2)

Of the 6 mutant strains selected for genome sequencing, 4 were genetically unique. Somewhat curiously, none of the mutations identified in these strains were in open reading frames encoding proteins expected to be involved in outer membrane nutrient uptake (i.e. TonB dependent receptors). As shown above, mutant strains had a limited number of genetic differences compared to the wildtype, with identical mutations occurring in open reading frames in two strains, encoding a putative AFG-1 Family ATPase and dTDP-glucose 4-6-dehydratase. As it is less likely that identical mutations would arise multiple times in response to bacteriocin selection, these mutations may represent pre-existing polymorphisms in the population of wildtype cells unrelated to the bacteriocin resistant phenotype. However, this needs to be confirmed by experimentation. Interestingly, all four resistant strains isolated had accrued unique SNVs in the sensor histidine kinase EnvZ, leading to amino acid substitutions in the protein. The location and nature of these substitutions is shown in Figure 4-16. EnvZ in *Pectobacterium* shares 88 % AA sequence identity with its homologue in *E. coli*, in which it is known to be involved in the regulation of OmpF and OmpC in response to osmotic changes in the external environment (231,232). Mutations in EnvZ are also associated with more general pleiotropic effects on the Gram-negative outer envelope, which may explain the association with a pectocin M1 resistant phenotype (233). While the details of the mechanism by which the observed EnvZ mutations lead to pectocin M1 resistance needs to be characterised, it is interesting to note that none of the mutations occur in the enzymatic kinase 2 domain and 3 of the 4 mutations lead to the inclusion of a proline

residue. The general mechanism by which bacterial sensor kinases transmit a signal across the inner membrane is thought to occur by a conformational change in response to an environmental stimulus (234). It seems plausible that the inclusion of conformationally restrictive residue like proline could lock the sensor in an active (or inactive) conformation, forcing the cell into a regulatory state conducive to bacteriocin resistance.

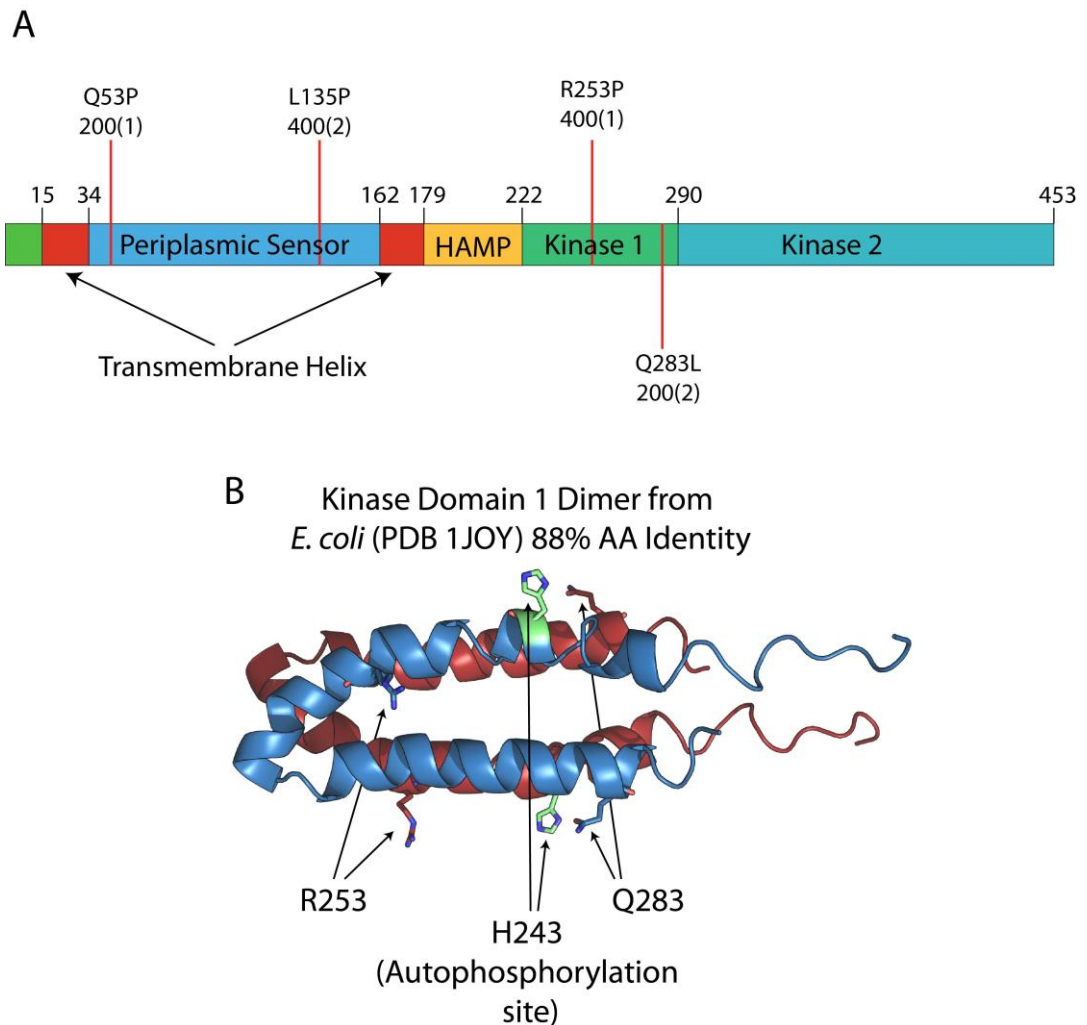


Figure 4-16 Mutations in the histidine sensor kinase EnvZ in *Pba*. LMG2386 conferring resistance to pectocins M1.

A) Schematic of the histidine sensor kinase EnvZ showing its predicted domain structure and the location and effect of point mutations in *Pba*. LMG2386 mutants resistant to pectocins M1. B) The crystal structure of the Kinase 1 domain from EnvZ from *E. coli* showing the location of the histidine auto-phosphorylation site in relation to the mutations in EnvZ from 400(1) and 200(2)

4.13 Discussion

The work presented in this chapter has identified the pectocins. A family of colicin like-bacteriocins consisting of a fusion between cytotoxic domains analogous to previously identified colicin-like bacteriocins and a plant-like ferredoxin, which has horizontally acquired by *Pectobacterium spp.*. This structural arrangement is unprecedented for a colicin-like bacteriocin, with the receptor binding and translocation domains for previously characterised proteins sharing common characteristics, but without obvious structural homology to proteins which perform an unrelated function (4). Despite this unusual and unprecedented domain structure, there are interesting parallels and contrasts between colicin-like bacteriocin receptor binding and translocation domains and how the pectocin's ferredoxin domain appears to function.

As discussed previously the majority of colicin-like bacteriocins bind to the surface of their target cell and often gain entry to the cell through the parasitisation of TonB-dependent nutrient receptors and their associated uptake machinery (4,10,18,235-237). In conjunction with the identification of the pectocins the work performed in this chapter demonstrates that *Pectobacterium* possesses a receptor and import machinery necessary to utilise plant ferredoxin as an iron source. Indeed, it appears to be this system which the pectocins exploit to gain entry to the periplasm. As all iron-uptake systems identified to date in Gram-negative bacteria, either siderophore based or targeting a protein substrate, utilise a TonB-dependent receptor to transport iron across the outer membrane it is likely that the ferredoxin receptor belongs to this class of protein (238). Therefore, like other colicin-like bacteriocins it seems that a TonB-dependent receptor is responsible for mediating ferredoxin iron and pectocin uptake. Structural analysis of pectocin M2 revealed that unlike all other colicin-like bacteriocins identified thus far the pectocins lack an IUTD. In bacteriocins the IUTD normally functions to deliver an epitope to the periplasm, which mediates binding to the Tol or Ton complexes. This direct interaction occurs between the colicins and TolB for group A colicins and TonB for group B colicins and is essential for uptake of these bacteriocins. Since pectocin M1 and M2 lack an IUTD they are unable make direct contact with the Tol or Ton complexes in the periplasm and thus are unable to directly utilise the pmf for cell entry. However, the fact

that the pectocins parasitise a system for which the receptor binding and translocation domains are structurally analogous to the substrate provides an intuitive solution to this problem. A number of TonB-dependent receptors have been identified, which obtain iron from host proteins during infection. In all of these systems the iron or iron containing compound is liberated from the protein on the cell surface and transported into the cell, potentially because all of the proteins identified are too large to pass through the lumen of their receptor (238-240). Plant ferredoxin, however, is a small globular protein, which is in fact comparable in dimensions to the plug domain that ordinarily occludes the pore of a TonB-dependent receptor. This creates the possibility that the ferredoxin is imported intact into the periplasm. If this were the case it could readily explain the pectocins lack of an IUTD as the energy required for cell entry would still be provided by the Ton complex, but transduced through receptor plug domain, as with ordinary substrate importation.

5 Identification and characterisation of the ferredoxin uptake (Fup) receptor in *Pectobacterium*

Disclaimer on work performed:

NMR spectra of labelled ferredoxin discussed in the chapter were collected and analysed in conjunction with Mr Inokentijis Josts and Dr Brian Smith. Preliminary assignment of the pectocin M1 ferredoxin domain discussed in Section 5.4 was performed predominantly by I. Josts.

CD analysis was performed in conjunction with Dr Sharon Kelly.

5.1 Introduction

The results presented in this chapter relate to the discovery of the Fup operon, encoding the protein machinery required for pectocin import and plant-like ferredoxin based iron acquisition by *Pectobacterium*. The outer membrane receptor for this system is identified as FupA and is a TonB-dependent receptor. While this is the first description of a TonB-dependent receptor obtaining iron from a host protein in a phytopathogen, the utilisation of TonB-dependent receptors for obtaining iron from host proteins is well described for a number of mammalian Gram-negative pathogens. As such, before proceeding to the details of the discovery and characterisation of FupA it is worth reviewing what is currently known about these systems.

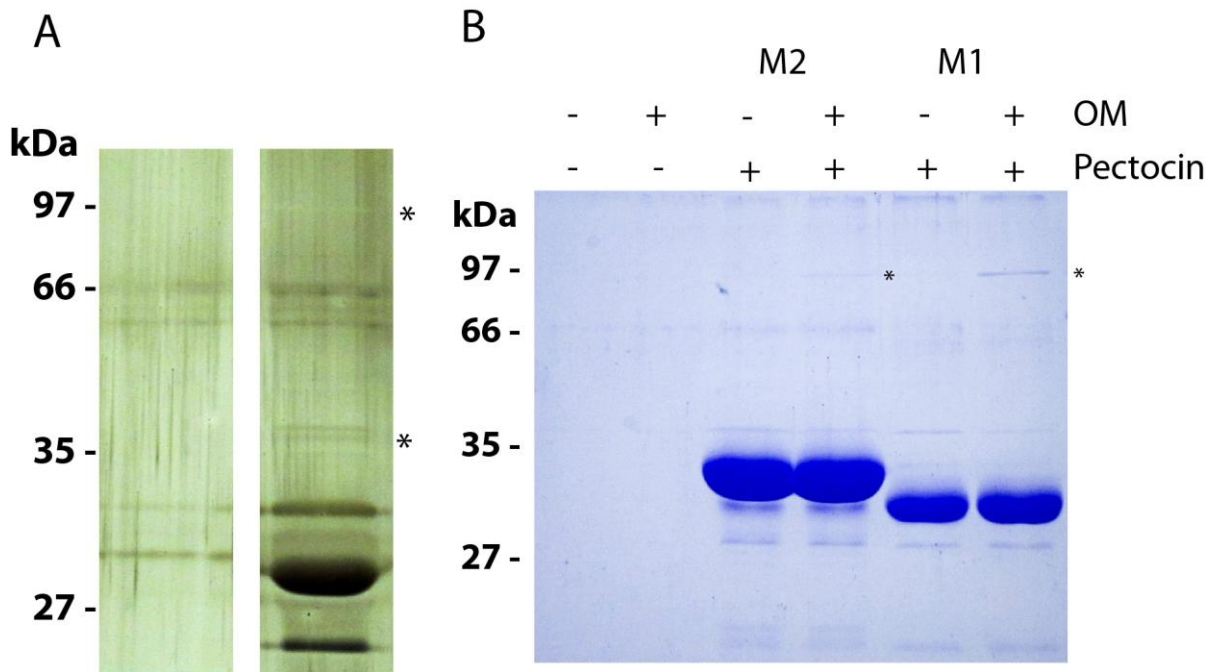
A number of bacterial pathogens specific to mammalian hosts possess systems for directly obtaining iron from host proteins such as transferrin and lactoferrin that sequester free iron in the body's extracellular fluids. The most thoroughly characterised of these systems is the transferrin iron-acquisition system of *Neisseria gonorrhoeae* and *Neisseria meningitidis* (239). Transferrin-binding protein A (TbpA), a 100 kDa integral outer membrane protein and transferrin-binding protein B (TbpB) an 80 kDa membrane anchored co-receptor form the basis of this system. TbpA, a TonB-dependent receptor strongly binds transferrin and acts as the conduit for transport of the liberated ferric iron across the outer membrane. However, it lacks the ability to distinguish between the apo and holo forms of the protein (241). The co-receptor TbpB has a strong affinity for the iron loaded transferrin only and acts synergistically with TbpA, considerably increasing the efficiency of iron import (242). Following binding and extraction of iron, apo-transferrin is released from the complex (243). The importance of this system for fitness is demonstrated by the fact that its inactivation renders *N. gonorrhoeae* avirulent (244). The majority of iron in a mammalian host is stored intercellularly as haemoglobin (245). As such haemoglobin and the haem it contains represent an important iron source for invading pathogens (240). As a result, pathogenic bacteria commonly secrete haemolysins and cytolytins that lyse host cells and release haemoglobin and other haemoproteins (246). Uptake of the liberated haem is then achieved by a number of specialised systems, which in addition to the TonB-dependent outer membrane receptor consist of a periplasmic binding protein and an inner membrane ABC transporter (247). An example

of such a system is the HpuA/B system of *N. meningitides*, which is evolutionarily and mechanistically related to the transferrin binding system discussed above (245). A second system identified in a number of Gram-negative bacteria and characterised from the opportunistic pathogens *Pseudomonas aeruginosa* and *Serratia marcescens* involves the TonB-dependent receptor HasR and HasA, a secreted haem binding protein termed the 'haemophore' (248,249). Structural and biochemical studies of this system have demonstrated that HasA is able to bind free haem or wrest it directly from host proteins, HasA then binds to HasR to deliver its cargo. HasR is also able to obtain haem directly from the environment in the absence of HasA, however its presence greatly enhances the efficiency of haem uptake (250). Interestingly, members of the genus *Pectobacterium*, which possesses a highly lytic mode of infection (discussed below) also possess genes encoding HasA and HasR homologues (222). While not as abundant as in a mammalian host, haemoproteins still represent a potentially important source of iron for an invading phytopathogen (251,252).

5.2 Identification of the pectocin receptor (FupA)

The discovery of the pectocins, their characterisation and the ability of *Pectobacterium* to specifically utilise plant ferredoxin as an iron source, strongly suggested that *Pectobacterium* possesses an outer membrane nutrient receptor and associated periplasmic machinery for the import of ferredoxin derived iron. Additionally, the pectocins lack of an IUTD suggests that the mechanism through which the pectocins are translocated across the outer membrane is fundamentally different from other colicin-like bacteriocins, which deliver a Tol or Ton binding epitope to the periplasm via the IUTD (4). The fact that the ferredoxin domain of the M-class pectocins shares a common receptor with ferredoxin, through which *Pectobacterium* spp. are able to acquire iron, suggests that these bacteriocins parasitise an existing ferredoxin uptake system to deliver their cytotoxic domains to the periplasm. To confirm this hypothesis, it was necessary to identify the receptor for ferredoxin and the ferredoxin-containing bacteriocins. As initial experiments performing genetic analysis on pectocin M1 resistant mutants, described in chapter 4, failed to identify the ferredoxin/pectocin receptor, a co-purification experiment with His₆-tagged pectocin M1, using nickel affinity

chromatography was performed. Isolated OMs of *Pba* LMG 2386 were applied to a nickel affinity column pre-loaded with His₆-tagged pectocin M1 or, in control experiments, to an identical column that did not contain pre-bound proteins. After imidazole elution of bound protein and subsequent SDS-PAGE, bands corresponding to two proteins were observed, with molecular weights of approximately 100 and 40 kDa, which co-purified with pectocin M1 and were absent in control samples (Figure 5-1-A). Peptide mass fingerprinting identified the closest matches to these proteins as a 97 kDa TonB-dependent receptor PCC21_007820 from *Pbc* subsp. *carotovorum* PCC21 and the 37 kDa OM protein OmpA. As TonB-dependent receptors are invariably responsible for iron uptake and OmpA is highly expressed and a common contaminant in the preparation of OM proteins, we thought it likely that PCC21_007820 (which we designated FupA for ferredoxin uptake protein) represents the ferredoxin receptor. The peptides identified as matching PCC21_007820 are shown in Figure 5-1-C.



C

Match to: **WP_010301353.1** Mascot Score: **433**
 TonB-dependent receptor [Pectobacterium cartovorum]

1	MNKNVYLMMI	LSLLSGPALA	QQNDTSADEN	QQKNNAEETEE	EQQGDSSSEN
51	SEDTILVRST	PTSQSMGTQI	LNAEQIKKMP	TGNGSVTELL	KNNAAVQFSN
101	TANSSNIPGE	LAPENVSFHG	EK FYN NNFMI	DGLSNNSNIN	PGANK GQMDG
151	DPDGYSPTDL	PAGGPQSFWI	NSELIETLEV	FDSNISAK YG	DFTGGVVDAR
201	LMDPKLDNVF	GKISYRTSRD	SWTSYHVDGG	ISEDIFYSATN	LYYQPKFKK Q
251	FYSATFNQPL	SDKAGFI FAY	NR QQSDIPYY	HSYMGQWDDQ	NRISETYLLK
301	GTYLADNGDI	IRMTGMYS PH	ESK YYKKNIK	NGAFTNTGGG	YRFNMEWEHN
351	ASWGKMVSLA	GYQYEQNKTE	HEANEFVQWV	YSTRVPGGF	ISPSLDWQSA
401	ATNSQIGGYG	TFSTEKKTTT	LKQDYELNPK	FLLGMTHQID	FGWQADFAST
451	QYRRFQDSYT	ASVAANATYI	NPNVVCLPGD	SLCIPGEQFA	GTRTLFPARS
501	VQASYSYAA	YLQNSMSYGR	LEVTPGVRAS	YDDFLENLNF	APR FAASYDV
551	FGDR STRFLG	GANRYYAANM	LAYKLREGIG	MNISQRRRTSS	TGPWVSNQPR
601	MGTNYTVSDL	NTPYSDEVTL	GLSQRVMNTV	WTAKWVNRQG	KEQFGRESIT
651	ANGESYRVMN	NKGSTEGNTL	SLEVQPISPH	RFSFAE VNWK	LGASMAKNKA
701	NSIAYYDDTD	TDESRVIVDG	KLMYKGDMDA	MDFNTPWTAF	LSVDTYFPTI
751	RVNWXQRVGY	TSGYKGYMTA	SIQTVCPGGS	PACNADPSFS	GSAAEHVSTK
801	YDDFISYDWR	LSYSQPIYKN	QTLDF'TLDVL	NVLDNVVETQ	QISRFNSTIV
851	TYKPGRQFWL	GVAYTW			

Figure 5-1 Co-purification of *Pectobacterium* membranes with pectocin M1 identifies the ferredoxin receptor FupA.

A) Silver stained SDS-PAGE gel showing co-elution of FupA with pectocin M1 from Ni²⁺ affinity column with 100 mM imidazole through which solubilised outer-membranes from Pba LMG 2386 had been passed in the

absence (lane 1) and presence (lane 2) of bound pectocin M1. Stars represent proteins which co-eluted in the presence of pectocin M1; the upper band at approximately 97 kDa was identified as FupA, B) Coomassie stained SDS-PAGE gel showing co-elution of FupA with pectocin M1 and M2 when recombinantly expressed in *E. coli* BL21(DE3), elution as in presence or absence of bound pectocins and in the presence or absence of added OM fraction, C) Peptides identified by tandem MS from the approximately 97 kDa band of the gel from (a), identifying the protein as a TonB dependent receptor of unknown function, designated FupA.

To test this further *fupA* from *Pba*. SCRI1043 was cloned into the *E. coli* expression vector pET21a and overexpressed the protein in *E. coli* BL21(DE3). To determine if recombinant FupA overexpressed in *E. coli* was able to bind the ferredoxin domains a pull-down assay was utilised, using nickel-affinity beads charged with His₆-tagged pectocin M1 and pectocin M2 and the solubilised OMs from *E. coli* BL21(DE3) cells containing this vector and overexpressing FupA and from cells harbouring the empty pET21a vector. As shown in Figure 5-1-B interaction between pectocin M1/M2 and FupA was demonstrated (identity of FupA confirmed by mass spectrometry), further indicating that FupA is the *Pectobacterium* ferredoxin receptor. Interestingly, despite a higher concentration of pectocin M2, being used in this experiment, a significantly fainter FupA band was observed compared to pectocin M1. Pectocin M1 has much higher activity than pectocin M2 against *Pba*. SCRI1043, the strain from which the receptor used in the experiment originates and against the isolates tested in this study more generally. This observed difference in affinity for the receptor may in part be explained by this.

5.3 Genetic confirmation of FupA as the pectocin/ferredoxin receptor

The co-precipitation experiments with native and recombinant FupA provide evidence of an interaction with pectocin M1. However, to unambiguously prove that FupA is indeed the ferredoxin receptor additional genetic evidence was sought through the creation of a Δ FupA mutant of *Pba*. LMG2386, using the suicide vector pMRS101. To create the Δ FupA strain, a mutagenesis cassette was created in which the middle 1 kb of the coding sequence of FupA from LMG2386 was removed and replaced with the stop codon TAA (Figure 5-2-A). When the suicide vector containing this cassette is introduced into LMG2386 it undergoes recombination with chromosomal copy of *fupA* inserting the

entire vector into this gene. This recombination event is selected for using the streptomycin resistance gene contained on the plasmid. The vector also contains the *sacB* gene, which confers sucrose sensitivity to Gram-negative bacteria. By growing cells harbouring the recombined plasmid in media containing sucrose a second recombination event is selected for, which excises the plasmid from the genome, leaving either the full length gene or the truncated cassette (146). Successful mutants from this process were confirmed as having a sucrose resistant, streptomycin sensitive phenotype, with PCR using primers for *fupA* resulting in the amplification of a truncated 2000 bp product compared to that from wildtype LMG2386. *Pba*. LMG2386 Δ FupA was found to be resistant to pectocin M1, with sensitivity restored by complementation with a T5 expression vector containing full length *fupA* from *Pbc*. LMG2913. The pectocin M1 susceptible phenotype in the complemented strain was most pronounced when FupA was induced by IPTG, under iron limiting conditions. This suggests that other iron regulated proteins play a role in activating FupA for bacteriocin uptake. These data unambiguously show that Δ FupA is the ferredoxin receptor.

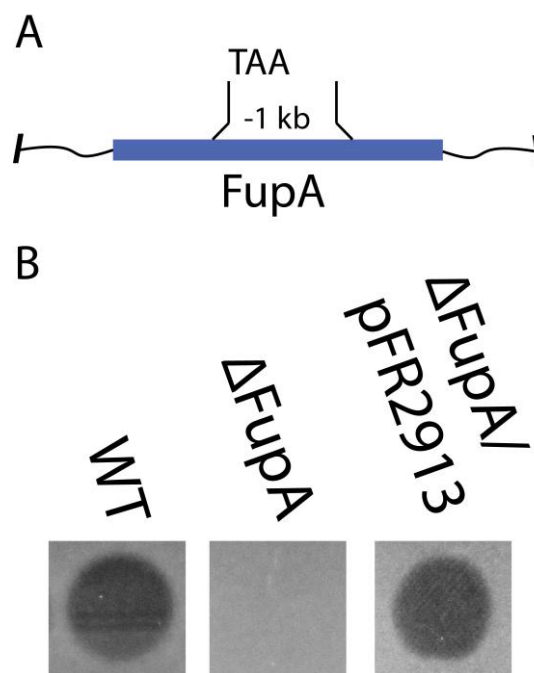


Figure 5-2 FupA knockout confers resistance to pectocin M1 in *Pba*. LMG2386,

A) Schematic of the FupA mutation introduced by recombination of suicide vector. B) Inhibition of growth by pectocin M1 spotted onto a lawn of *Pba*. LMG2386 is observed for WT, but not for the FupA knockout strain (Δ FupA), the ability of pectocin M1 to inhibit growth is restored by plasmid based complementation of FupA from *Pbc*. LMG2913.

5.4 Expression purification and characterisation of FupA

In order better characterise FupA and its interaction with the pectocins and ferredoxin a FupA expression vector (derived from pET28a) was created in which the signal sequence was replaced with an N-terminal His₆-tag. Overexpression using this construct gave large amounts of protein that could be isolated as inclusion bodies. After solubilisation and refolding in buffer containing LDAO, FupA was purified by nickel affinity chromatography and gel filtration and analysed by SDS-PAGE (Figure 5-3). FupA purified by this method was observed to be monodisperse by sedimentation velocity analytical ultracentrifugation and eluted from a gel filtration column as a single symmetrical peak (Figure 5-4-A/D). Thermal denaturation curves of FupA, monitored by the change in far UV circular dichroism, showed a sharp transition with a midpoint at 75 °C, indicating that purified FupA is folded (Figure 5-4-B/C).

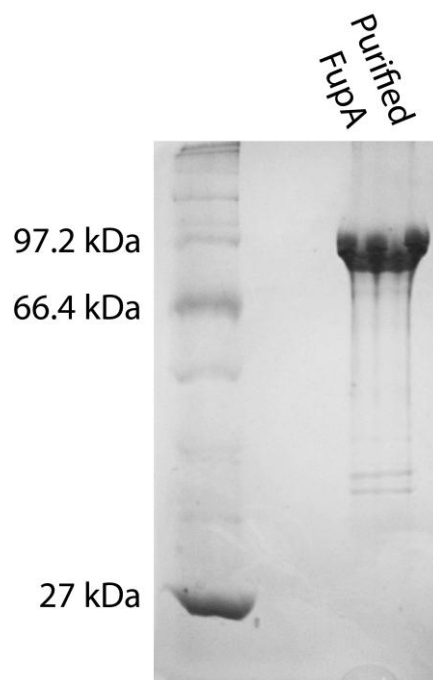


Figure 5-3 Purified FupA separated on an 8% SDS-PAGE gel, visualised by coomassie staining.

FupA was expressed in *E. coli* BL21 DE3 as inclusion bodies before refolding and purification using Ni²⁺ affinity chromatography and SEC. Purified FupA, ran at an expected molecular weight of approximately 97 kDa

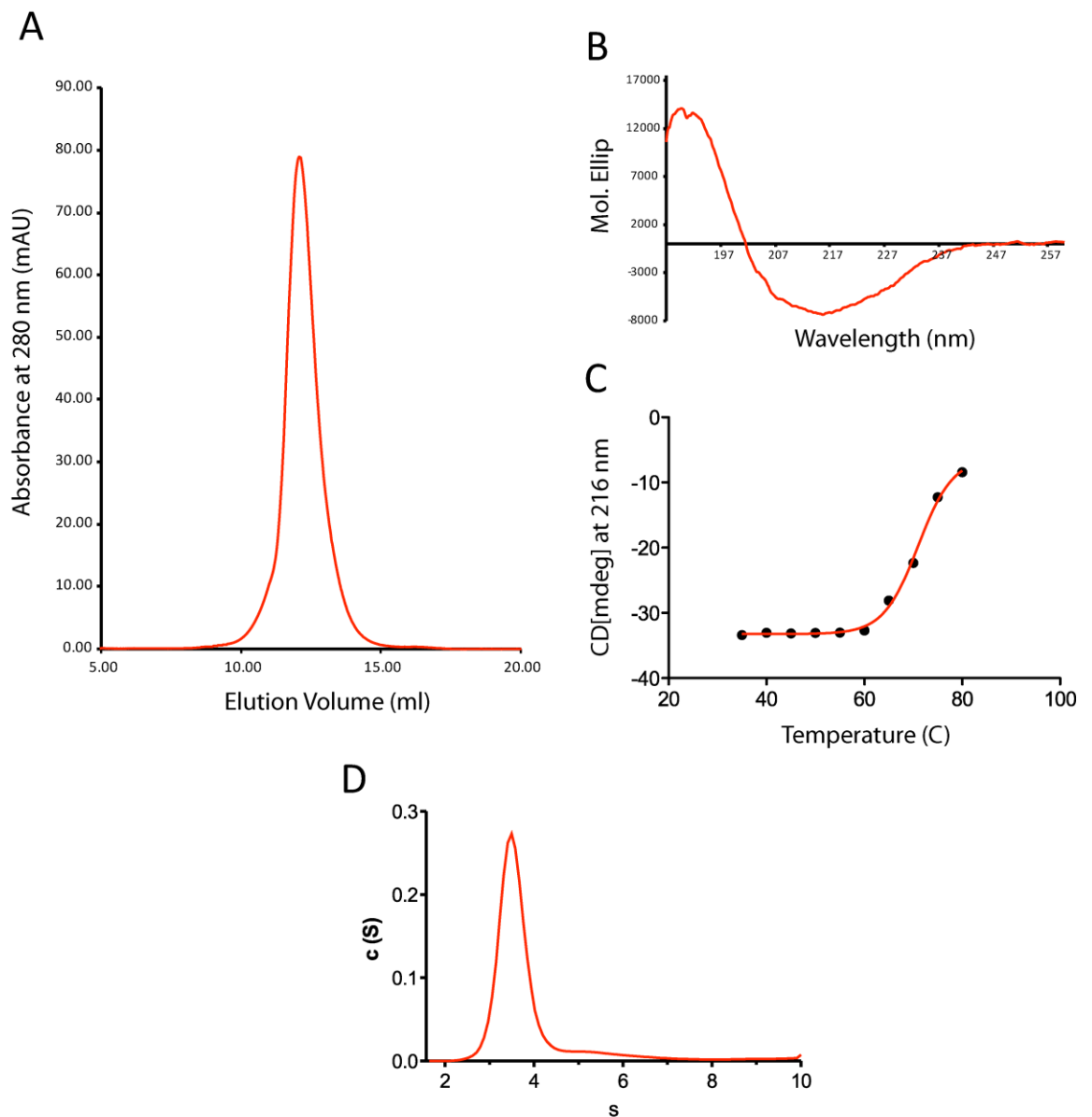


Figure 5-4 Validation of refolding of FupA.

A) Analytical Superdex S200 gel filtration profile of purified FupA, shows a single species with Gaussian elution profile. B) Far-UV CD spectrum for purified FupA suggests a predominantly β -barrel structure. C) The melting profile with a discrete unfolding mid-point of 72.5°C suggests a folded, highly stable structure. D) Sedimentation velocity data for purified and refolded FupA (10 μ M) shows that the protein is monodisperse and monomeric in solution, with a sedimentation coefficient ($s_{20, w}$) of 5.05 S.

5.5 Analysis of FupA-ferredoxin interaction by NMR

NMR represents a powerful technique for characterising the binding between FupA and plant ferredoxin or the isolated pectocin M1 ferredoxin. To probe interactions between the two molecules we produced recombinant ^{15}N -labeled *Arabidopsis* ferredoxin and the isolated ferredoxin domain from pectocin M1 (pectocin M1_{fer}). Both labelled ferredoxins gave rise to well dispersed and resolved ^1H - ^{15}N HSQC spectra with cross-peaks of uniform line-shape. Spectra for *Arabidopsis* ferredoxin presented are in Figure 5-5. Despite the presence of the paramagnetic [2Fe-2S] cluster, which broadens resonances within a 5-8 Å radius (253), we could resolve in excess of 70 peaks for both ferredoxins in the HSQC spectrum, suggesting that only approximately 20% of the peaks were broadened beyond detection. To observe the effect of FupA binding on the ferredoxin spectra we acquired the ^1H - ^{15}N HSQC spectrum for labelled ferredoxin domains in the presence and absence of the receptor. We observed the complete disappearance of *Arabidopsis* ferredoxin cross-peaks from the ^1H - ^{15}N HSQC spectrum on incubation with FupA (mixed in a 1:1 stoichiometry), which was not remedied through acquisition of TROSY spectra, indicating slow exchange and high affinity binding to the 97 kDa receptor. In contrast, for pectocin M1_{fer} we observed concentration-dependent chemical shift and intensity changes in a discrete subset of cross-peaks in the presence of FupA, again indicative of binding but showing that in this case exchange is fast and that FupA binds to pectocin M1_{fer} (Figure 5-6).

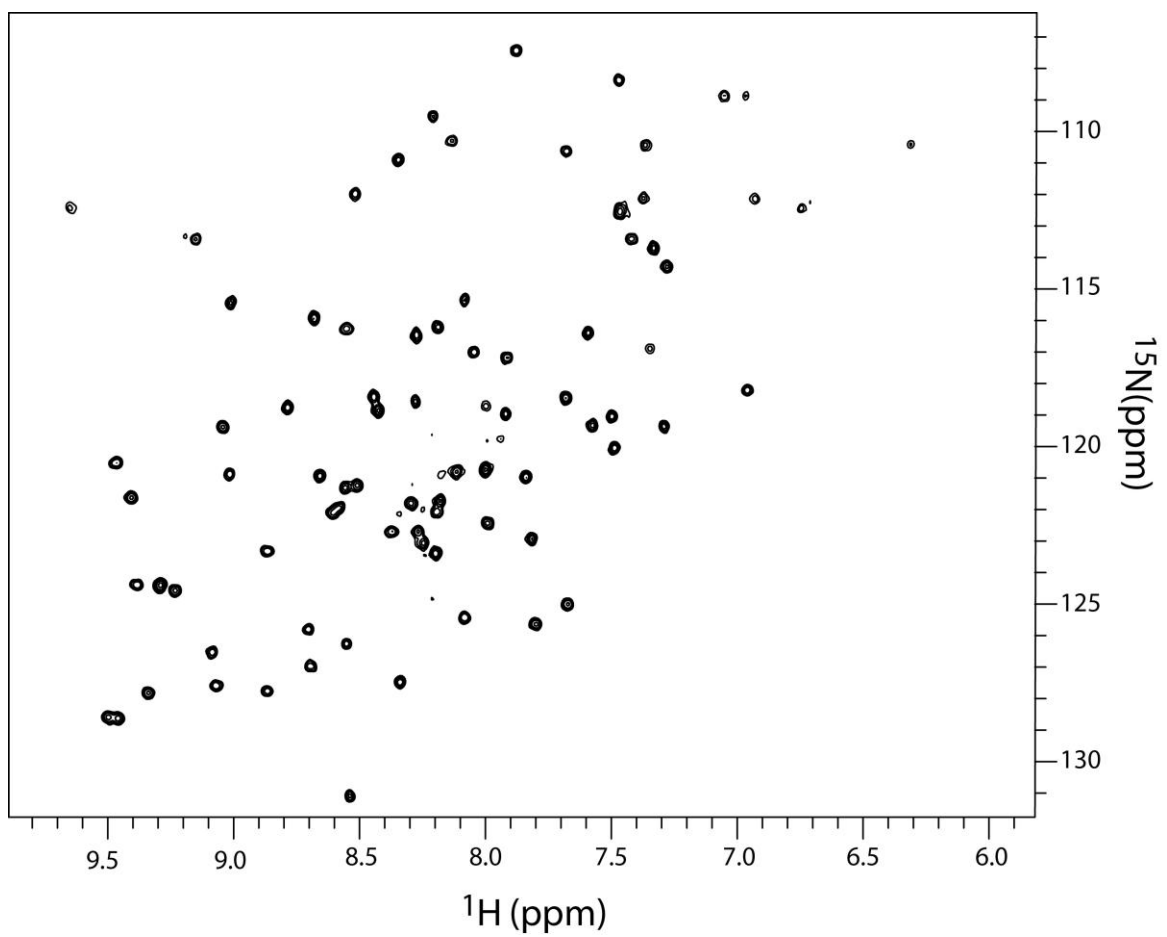


Figure 5-5 ^1H - ^{15}N HSQC spectrum of ^{15}N labelled Arabidopsis ferredoxin.

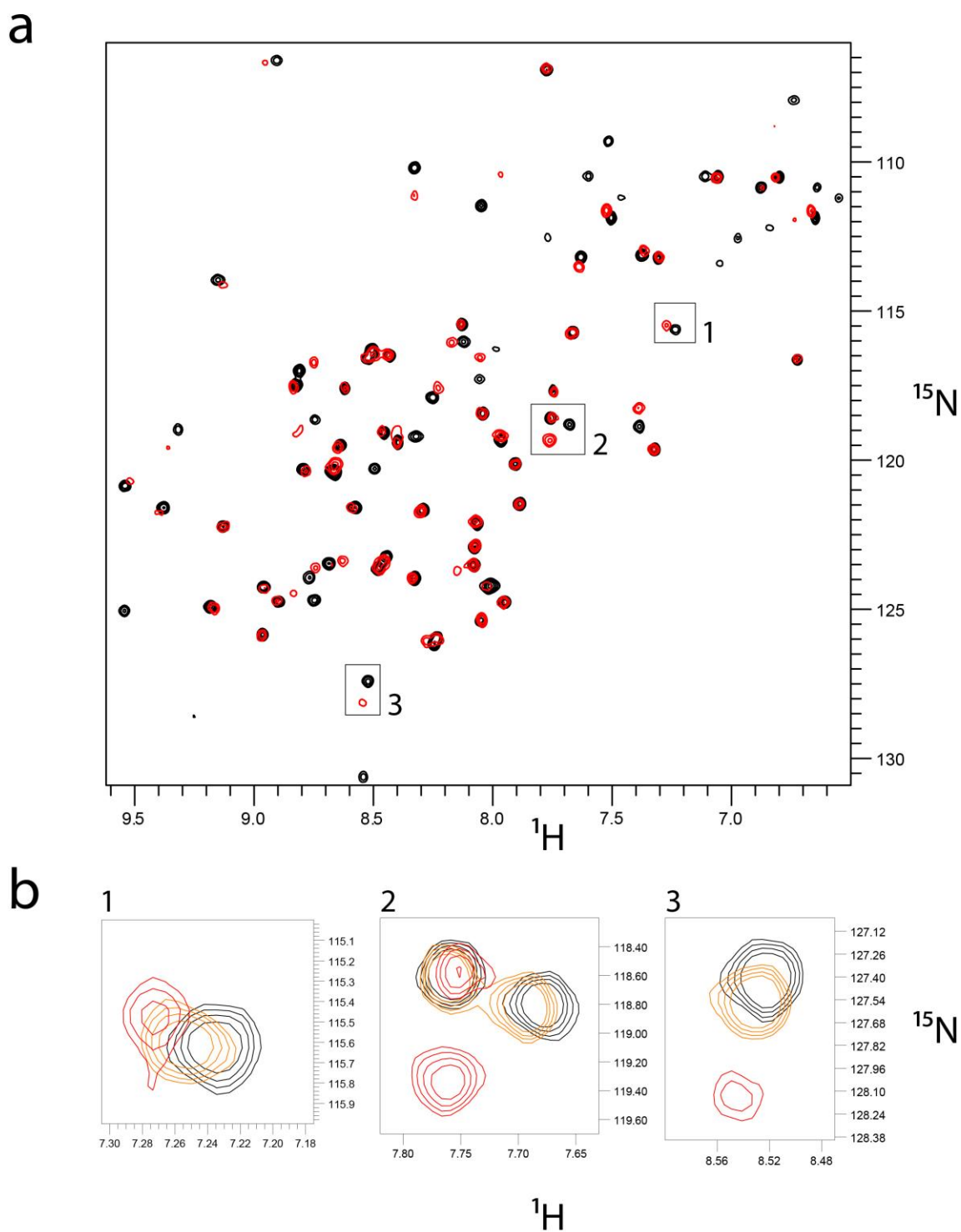


Figure 5-6 Interaction of pectocin M1 with the ferredoxin receptor (FupA) from *Pectobacterium atrosepticum* SCRI1043,

A) ^1H - ^{15}N HSQC spectrum of ^{15}N labelled pectocin M1fer in the absence (black) and presence (stoichiometry 1:1) of FupA (red) shows concentration-dependent changes (B) in chemical shift positions and intensity. The interaction with FupA causes shifts in a subset of cross-peaks in ^{15}N pectocin M1fer suggesting a localised binding site within this domain.

As the binding between FupA and pectocin M1_{fer} is in fast exchange and discrete chemical shift are observable in a subset of peaks on the HSQC spectra, by assigning each of the peaks of the spectra to a specific amide bond of pectocin M1_{fer}, the FupA binding site of the protein can be mapped. To achieve assignment of peaks on the HSQC spectra ¹⁵N/¹³C-labeled pectocin M1_{fer} was prepared and additional spectra (NOSEY, HSQC TOCSY, HNCOCACB, HNCACB, HNCACO) were recorded. At the time of writing full assignment protein is in progress with assignment of a number of peaks shifted in the +FupA HSQC spectra providing a preliminary picture of the FupA binding site of pectocin M1. These residues are outlined in Figure 5-7-A and when mapped onto a model of pectocin M1_{fer} (generated using the Phyre2 server (254)), reveal a relatively compact binding site localised to the β-sheet portion of the molecule remote from the iron sulphur cluster. It should be noted that due to signal broadening it is impossible to detect interactions directly with or adjacent to the iron sulphur cluster with this technique. As the NMR analysis of FupA/ferredoxin interactions shows that FupA has stronger affinity for Arabidopsis ferredoxin than for the pectocin ferredoxin domain, correlating the amino acid variation between the two ferredoxins with the assigned residues shifting upon FupA binding should provide a preliminary indication of ferredoxin residues important for FupA interaction. A sequence alignment between the two ferredoxins is shown in Figure 5-9-B and these variations are mapped onto the surface of the pectocin M1 ferredoxin model in Figure 5-7-B. A number of residues that form the preliminary binding interface vary between the two proteins, mutagenesis of these residues as well those which vary between the plant ferredoxins, coupled with binding and growth enhancement experiments can be utilised in future work to determine the importance of individual residues at the binding interface.

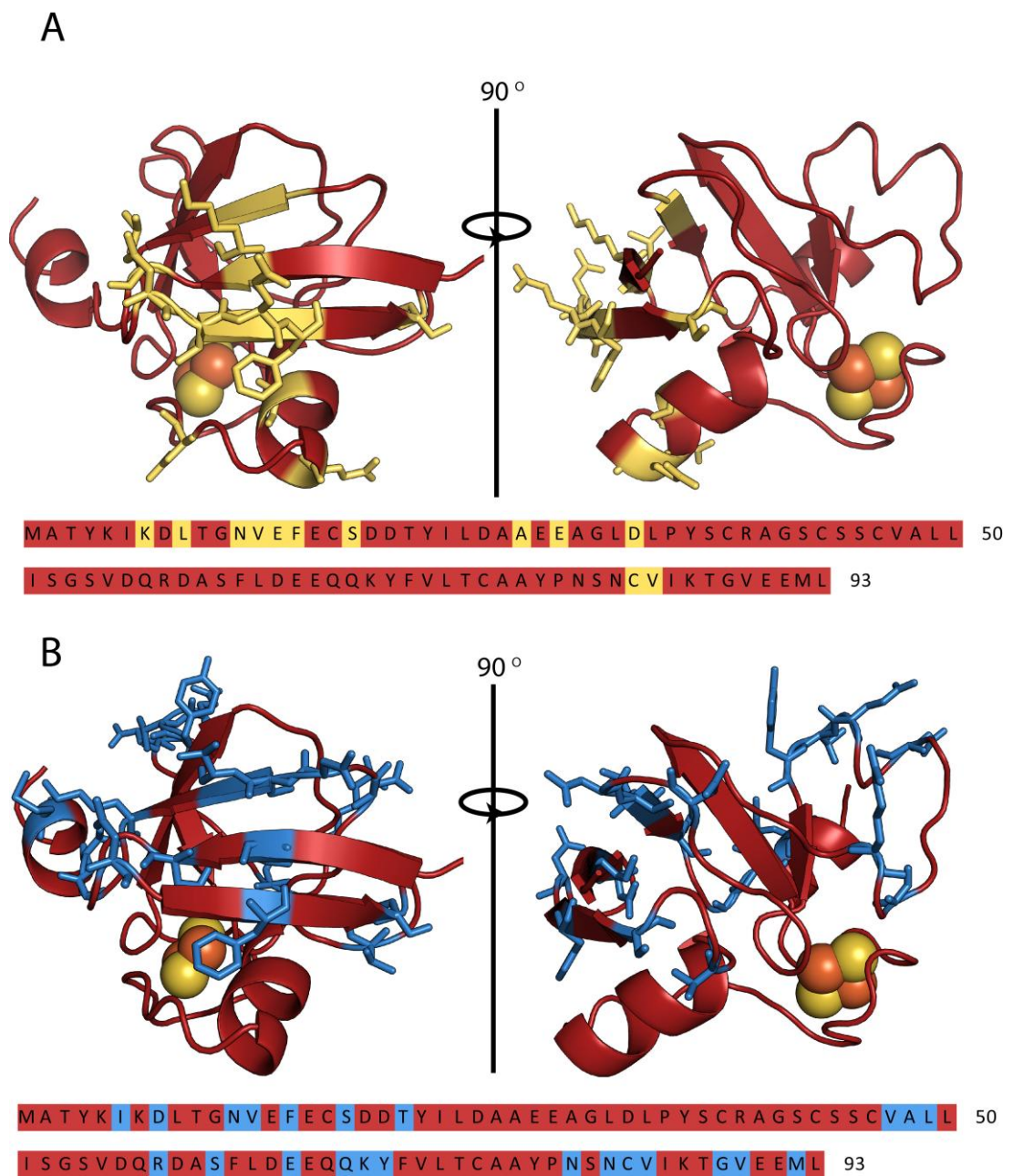


Figure 5-7 Mapping of NMR chemical shift data and sequence variation onto a model of the pectocin M1 ferredoxin domain

A) The preliminary FupA-ferredoxin binding surface of the pectocin M1 ferredoxin domain, defined by assigned residues exhibiting chemical shifts on the HSQC spectra (shown in yellow) in the presence of FupA,
 B) Sequence variation between the pectocin M1 ferredoxin domain and Arabidopsis ferredoxin, mapped onto a model of the ferredoxin domain of pectocin M1 (shown in blue).

5.6 Plant ferredoxins of different origin enhance *Pectobacterium* growth to a variable extent

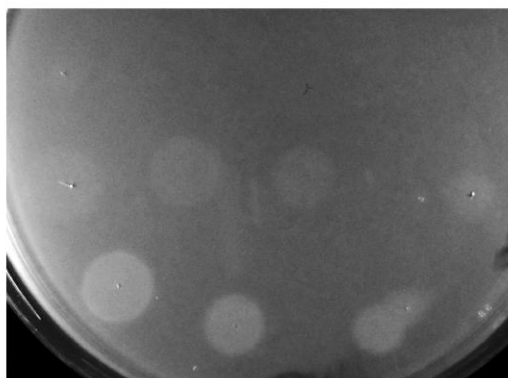
In order to further characterise the ability of *Pectobacterium* to utilise ferredoxin as an iron source plant ferredoxin from Maize, Potato and Arabidopsis were cloned and expressed. These proteins were purified and their ability to enhance a *Pectobacterium* overlay on iron limited agar (400 μ M bipryidine) was tested. Three fold serial dilutions of ferredoxin at a starting concentration of 1 mg ml⁻¹ were spotted onto the plates. The growth of different strains of *Pectobacterium* was enhanced by the ferredoxin to differing degrees, with the strains exhibiting the strongest enhancement (LMG2410 and LMG2442) shown in Figure 5-8. An amino acid sequence alignment of the three ferredoxins is presented in Figure 5-9-A for reference. Table 5-1 shows the minimum concentration at which enhancement was observed for the strains tested, along with the relative strength of enhancement. This experiment clearly demonstrates that ferredoxins originating from different plants were able to enhance growth to differing degrees. Arabidopsis ferredoxin was able to enhance growth in nearly all strains tested, although the degree of enhancement varied widely. In contrast, potato ferredoxin enhanced only half the strains tested and those strains to a lesser degree, while maize ferredoxin only enhanced LMG2442 weakly. Interestingly, these ferredoxins share a high level of AA sequence identity (approximately 70 %); all contain a two iron-atom payload and almost certainly share the same overall structure. One may therefore postulate that the differences in their ability to enhance growth in *Pectobacterium* derive from amino acid variation at the binding interface between the ferredoxin and FupA or another component of the ferredoxin iron uptake machinery.

P. cartovorum LMG 2410

Maize Ferredoxin

Potato Ferredoxin

Arabidopsis
Ferredoxin



P. cartovorum LMG 2442

Maize Ferredoxin

Potato Ferredoxin

Arabidopsis
Ferredoxin

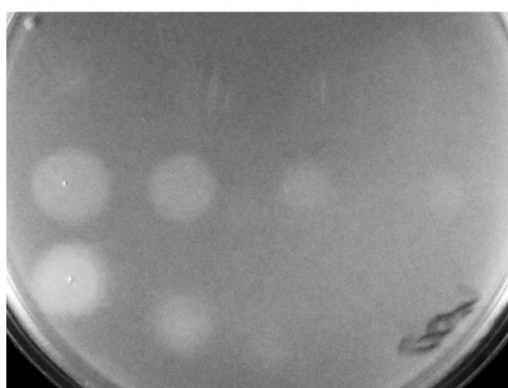


Figure 5-8 Plant ferredoxin enhance growth of *Pectobacterium* strains to varying extent.

Three fold serial dilutions of purified plant ferredoxin starting at 1 mg/ml was spotted on a lawn of *Pectobacterium* cells on LB + 400 μM)

A

Maize	MATYNVKLITPEGEMELQVPPDDVYLDFAEEEGI	DLPFSCRAGSCSSCAG	50	
Potato	MASYKVKLITPDGPIEFECPPDDVYLDAQAEEEGH	DLPYSCRAGSCSSCAG	50	
Arabidopsis	MATYKVKFITPEGELVEECD	DDVYVLDAAEEAGI	DLPYSCRAGSCSSCAG	50
Maize	KVVSGSVDQSDQSFLNDNQVADGWVLTCAAYPTS	DVVIETHKEDDLL	97	
Potato	KVTAGTVDQSDGKFLDDDDQEAAGFVLTCAVAYPKC	DVTIETHKEEELTA	98	
Arabidopsis	KVVSGSVDQSDQSFLDDEQIGEGFVLTCAAYPTS	DVTIETHKEEAIM	97	

B

Arabidopsis	MATYKVKFIFITPEGELVEECD	DDVYVLDAAEEAGI	DLPYSCRAGSCSSCAG	50
Pectocin M1	MATYKIKDLT--GNVEFEC	SDDTYILDAEEAGL	DLPYSCRAGSCSSCVA	48
Arabidopsis	KVVSGSVDQS	DQSFLDDEQIGEGFVLTCAAYPTS	DVVTIETHKEEAIM	97
Pectocin M1	LLISGSVDQR	DASFLDDEQQ-KYFVLTCAAYPNS	NCVIKTGV EEMLL	94

Figure 5-9 Sequence alignment of plant ferredoxins and pectocin M1 ferredoxin domain

(A) Amino acid sequence alignment of plant ferredoxins, (B) Amino acid sequence alignment of Arabidopsis ferredoxin and the pectocin M1 ferredoxin domain.

Table 5-1 Growth enhancement of Pectobacterium strains by plant ferredoxin.

Ferredoxin species of origin listed at top of table, dilution is the lowest spot on plate at which enhancement was observed; strength is the relative strength of the growth enhancement compared to the strongest observed spot.

Collection	Strain #	Arabidopsis		Potato		Maize	
		Dilution (mg/ml)	Strength	Dilution (mg/ml)	Strength	Dilution (mg/ml)	Strength
SCRI	1043	0.04	Weak	0.33	Weak	-	-
LMG	2374	-	-	-	-	-	-
LMG	2378	0.33	Weak	-	-	-	-
LMG	2383	-	-	-	-	-	-
LMG	2384	0.04	Medium	0.11	Weak	-	-
LMG	2385	0.04	Weak	0.33	V Weak	-	-
LMG	2386	0.04	Weak	-	-	-	-
LMG	2390	0.11	Weak	-	-	-	-
LMG	2391	0.33	Weak	-	-	-	-
LMG	2410	0.04	Strong	0.04	Medium	-	-
LMG	2412	0.04	Strong	0.04	Medium	-	-
LMG	2442	0.04	Strong	0.04	Strong	0.33	Weak
LMG	2443	0.04	Strong	0.04	Weak	-	-
LMG	2444	0.04	Weak	1.00	Weak	-	-
LMG	2454	0.33	Weak	-	-	-	-
LMG	2686	-	-	-	-	-	-

5.7 Crystallisation of FupA

High resolution structural information on FupA would provide invaluable insight into how this protein functions in ferredoxin/iron uptake and would also provide complementary data to the binding information obtained by NMR. As such and due to the availability of relatively large quantities of purified FupA (Figure 5-3) crystallisation of this protein was attempted. The purification and refolding protocol for FupA utilises LDAO as the detergent for shielding the hydrophobic regions of the protein. However, as LDAO is often described as less than optimal detergent for crystallisation, due to its relatively large micelle size of approximately 20 kDa and tendency to denature some proteins (255). Therefore crystallisation with β -OG and DDM was also attempted. Crystals were initially obtained in a number of conditions from commercial screens in which protein had been transferred from LDAO to β -OG by dialysis utilising a 40-50,000 Mw cut off membrane. These crystals were of poor quality (small thin needles). However, this result was taken as an indication that β -OG was a useful detergent for crystallisation of FupA.

For optimisation, the condition producing the best crystals from the MIDAS crystallisation screen containing PVP and PEG5000 MME as the precipitant was chosen (256). In order to more rigorously exchange FupA from LDAO to β -OG, purified protein was bound to a nickel column and the LDAO buffer was exchanged for one containing 0.8-1 % β -OG. The protein was then eluted and concentrated, before dialysis to remove excess imidazole and β -OG.

Controlling and monitoring detergent concentration when purifying and concentrating membrane proteins is known to be problematic, concentration of purified membrane proteins leads to concentration of detergent especially in the case of detergents with a large micelle size (257). Due to micelle formation dialysis is often insufficient to remove this excess detergent. Because of this, when optimisation trials were set, FupA was buffer exchanged into a 0.8-1% β -OG containing buffer by immobilisation on a nickel column. When crystallisation trials were performed however, this protein precipitated in the crystallisation drops and failed to form crystals. A screen of 96 chemical additives was performed, in addition to the original MIDAS condition and it was found that the addition of either LDAO or DDM led to crystal formation while in all other wells of the screen the

protein precipitated. This result showed that β -OG was necessary for crystallisation of FupA, but that an additional detergent was required for stabilisation.

Optimisation performed on the precipitant buffer and detergent composition improved the diffraction and morphology of the crystals (see section 2.15.4, Figure 9-1-E Figure 9-2-E) with the best crystals diffracting to 2.8 Å. Selenomethionine labelled protein was prepared but failed to produce crystals of acceptable quality, using the above crystallisation conditions (or others from extensive screening) and so preparation of platinum, gold and samarium derivative crystals is currently in progress.

5.8 Discussion

Analysis of the genetic context of *fupA*, reveals that it exists in a putative operon with four other open reading frames, encoding proteins of hypothetical but unconfirmed function (Figure 5-10-A). The hypothetical function to these proteins based on homology to known proteins, provides an intriguing picture of the ferredoxin uptake (*fup*) operon (Figure 5-10-B). The first gene in the operon designated *fupB* encodes a homologue of TonB. TonB is an inner membrane anchored protein, which spans the periplasm and in conjunction with the inner membrane proteins ExbB and ExbD, energises TonB-dependent receptors for nutrient import with energy provided by the proton motive force (258). Interestingly, while *E. coli* has been shown to possess only one version of the TonB protein, which energises the importation of substrates by a number of TonB receptor proteins, other Gram-negative bacteria, including *Pseudomonas aeruginosa* and *Serratia marcescens* have been shown to possess a number of TonB proteins often specialised to a specific receptor (259-261). It seems likely that FupB, a homologue of TonB, interacts uniquely with FupA to provide energy for substrate import.

TonB dependent nutrient acquisition systems, for example the haemin uptake system from *Yersinia enterocolitica*, utilise a periplasmic binding protein (PBP) which binds the incoming substrate and delivers it to an inner-membrane ABC transporter for transport to the cell cytoplasm (262). While *fupD* encodes a putative ABC transporter, *fupC* the other open reading frame in the operon does not encode a PBP but rather a M16 family zinc protease. M16 proteases are large (100 kDa+) and consist of two domains forming a clam shell structure, with an internal cavity capable of engulfing their substrate during

proteolysis. The M16 proteases are a diverse family represented in both prokaryotes and eukaryotes, including mitochondrial and chloroplastic signal peptidases, which function in removing the signal peptides from proteins imported into these vesicles (263).

As ferredoxin is a small and globular protein of approximately 100 amino acids, it is entirely feasible and indeed structurally plausible that the role of FupC is to cleave ferredoxin as part of the mechanism of liberating iron from this protein. For this to occur however, the ferredoxin would need to be imported along with its iron payload into the periplasm. If this proves to be the case, it is to our knowledge the first example of protein import to obtain nutrients in Proteobacteria.

The liberated iron-sulphur cluster, or its degradation product, may represent the iron-containing substrate for the ABC transporter FupD to transport across the inner membrane to the cytoplasm. Based on the hypothetical function we can assign to its components it is our hypothesis that the putative *fup* operon encodes the proteins necessary for uptake of ferredoxin, the liberation of its iron and for the transport of iron across the cytoplasmic membrane. The hypothesis that ferredoxin is imported into the periplasm by the Fup system prior to the liberation of its iron provides an intriguing solution to the pectocins lack of an IUTD. If this importation hypothesis was correct, then presumably the energy required for ferredoxin import would be provided by the Ton system and mediated by interactions between ferredoxin and the plug domain. The ferredoxin domain of pectocin M2 and its flexible nature could allow it to follow the same importation route as the independent ferredoxin domain. In support of this hypothesis, ferredoxin and pectocins M2 in its extended confirmation adopt dimensions comparable with the plug domain of TonB-dependent receptors (Figure 5-11).

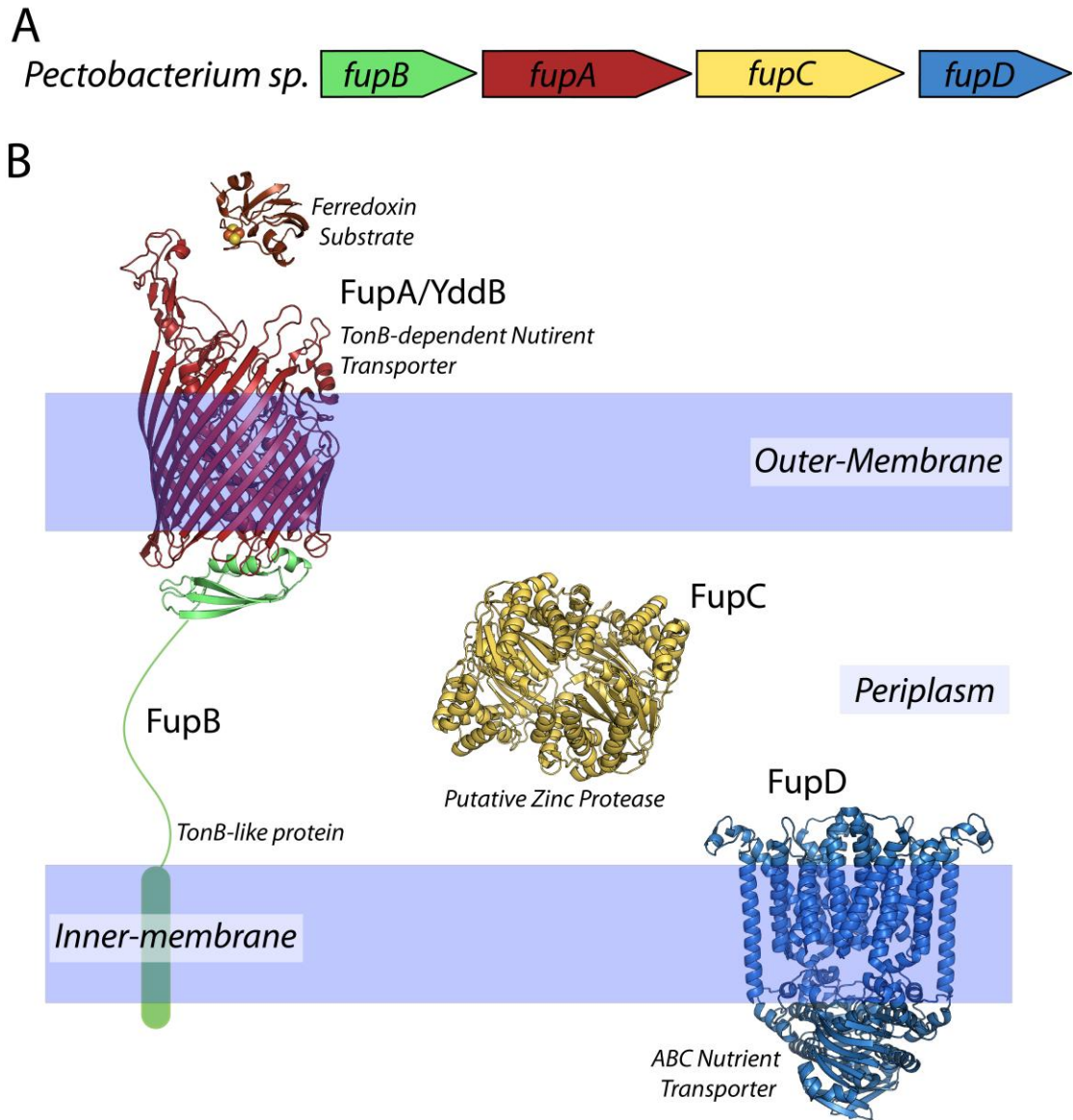


Figure 5-10 The ferredoxin uptake operon (*fup*) *Pectobacterium*

(A) The genetic constituents of the *fup* operon from *Pectobacterium* (B) The predicted cellular location and function of the products of the *fup*, based on the assigned function of homologues. Models of proteins in (B) are drawn using structural homologues available in the PDB.

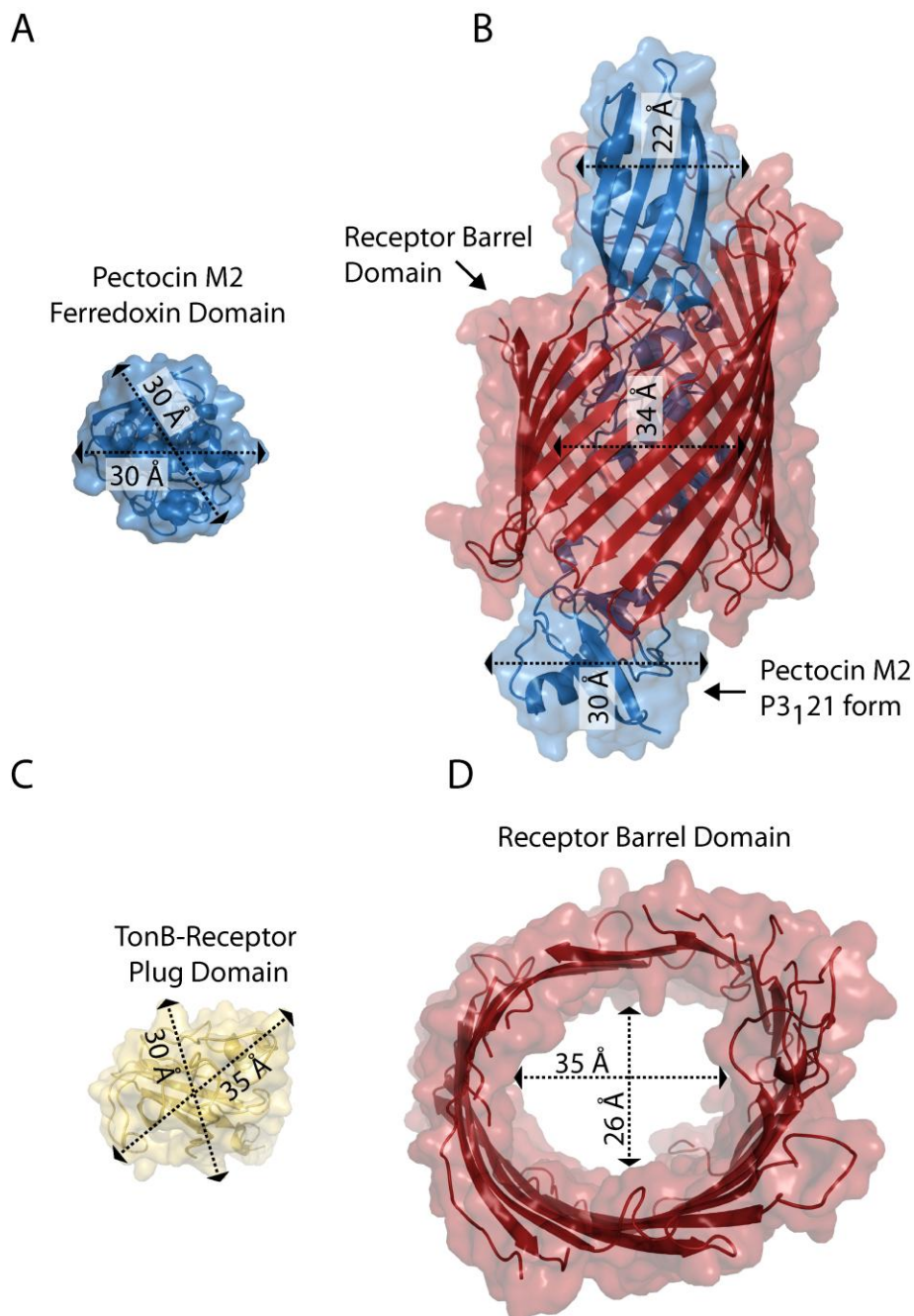


Figure 5-11 The extended conformation of pectocin M2 has dimensions compatible with passage through the lumen of a TonB-dependent receptor.

A) The extended conformation of pectocin M2 (blue cartoon and surface), fitted into the pore of the barrel of HasR from *Serratia marcescens* PDB ID = 3CLS, illustrating that the extended conformation of pectocin M2 is conducive to transport through the lumen of a TonB-dependent receptor without unfolding. B) Dimensions of the ferredoxin domain of pectocin M2. C) Top-down view of the HasR barrel showing the internal dimensions of the barrel domain. D) The width of the plug domain, which ordinarily blocks the lumen of the receptor barrel, is similar to that of the elongated conformation of pectocin M2.

Searching the genomes of other Gram-negative bacteria reveals that closely related homologues of *fupA* are found in all other sequenced strains of *Pba* and *Pbc* (76-85% amino acid sequence identity) and all strains of the related soft rot pathogens of the genus *Dickeya* (63-64% identity). In all cases, *fupA* is invariably found in a putative operon with the 3 additional *fup* genes (*fupB*, *fupC* and *fupD*). More distantly related homologues of *fupACD* can also be readily identified in a range of important human and plant pathogens including *E. coli*, *Pasteurella* spp., *Yersinia* spp., *Actinobacillus* spp., *Neisseria* spp. and *Campylobacter* spp. In a number of these bacteria the FupA and FupC homologues have been shown to be both upregulated during infection and important for virulence and persistence in animal models (264,265). Specifically, in *D. dadantii* (formerly *Erwinia chrysanthemi*), homologues of *fupA* and *fupC* are among the most highly upregulated genes during plant infection and in *Pasteurella multocida* the *fupC* homologue is upregulated in response to iron limitation and during infection of chicken. Taken together our results suggest a role for the Fup and homologous proteins in virulence, potentially functioning to obtain iron from host proteins during infection (266-268).

The identification of the Fup operon during this project is consistent with the colloquialism that the scientific process often leads to unexpected outcomes. The initial aim of the project was to discover and characterise bacteriocins from plant pathogens as targets for creating transgenic plants to combat disease. The discovery and characterisation of the unusually structured pectocins, with a ferredoxin receptor binding domain, inadvertently led to the discovery that *Pectobacterium* exploits plant ferredoxin as an iron source using the products of the Fup operon.

6 Characterisation and identification of cell surface receptor of lectin-like bacteriocins from *Pseudomonas spp.*

Results from this section are included in:

McCaughey, L. C.*, **Grinter, R.***, Josts, I., Roszak, A. W., Waløen, K. I., Cogdell, R. J., Milner, J., Evans, T., Kelly, S., Tucker, N. P., Byron, O., Smith, B., and Walker, D. (2014) Lectin-Like Bacteriocins from *Pseudomonas spp.* Utilise D-Rhamnose Containing Lipopolysaccharide as a Cellular Receptor. **PLoS Pathog.** 10, e1003898

* Denotes joint first authorship.

Disclaimer on work performed:

*Structural and biochemical analysis of pyocin L1 discussed in this chapter was conducted in conjunction with Mrs Laura McCaughey and Mr Inokentijis Josts. Specifically: Isolation and characterisation of pyocin L1 and pyocin L1 tolerant mutants was performed by L. McCaughey. Purification of *P. aeruginosa* LPS and pyocin L1 mutants was performed in conjunction with L. McCaughey. ITC analysis of wildtype and mutant pyocin L1 binding to LPS and hexose sugars was performed in conjunction with L. McCaughey and I Josts. Crystals of pyocin L1 were produced by L. McCaughey. Data collection, structural solution, refinement and sugar soaks were conducted by me.*

Production of labelled pyocin L1 and collection of NMR spectra of pyocin L1 in the presence and absence of sugars and data analysis was performed in conjunction with I. Josts, L. McCaughey and B. Smith.

SAXS data on pyocin L1 was collected by and analysed in conjunction with I. Josts.

6.1 Introduction

On first observation the tandem β -prism architecture seems an unlikely scaffold for an extremely potent family of bacteriocins. However, even prior to the structural solution of putidacin L1 by Ghequire et. al., secondary structure prediction strongly suggested that the lectin-like bacteriocins shared direct common ancestry with MMBLs proteins from plants (14,103). Further analysis of this protein family reveals that the MMBL fold is widely distributed in plant, animal and prokaryotic kingdoms and this versatile scaffold has been adapted to perform diverse and unrelated functions. Interestingly, these functions may not make usage of the MMBL's canonical mannose binding motifs (107). For example, in addition of the lectin-like bacteriocins, the MMBL fold is represented in: the S-receptor kinase protein of pollen incompatibility system in *Brassicaceae*, the sweet taste-modifying protein curculin and in pufflectin a protein produced by the pufferfish (*Fugu rubripes*) for parasite defence (110,269,270). Ironically, the biological function of the originally discovered MMBL lectins, which are produced in large quantities in the bulbs of garlic (*A. sativum*) and snowdrop lectin (*G. nivalis*) has not been definitively determined (271). During the experimental phase of this work, a paper presenting structural and functional analysis of putidacin L1 was published by Ghequire et. al.. In addition to the presentation of the crystal structure of the putidacin L1, this work showed that the two C-terminal sugar binding sites of putidacin L1 were synergistically important for cytotoxic activity. When the first site (designated III^C) was inactivated the killing activity of the protein was reduced 5-6 fold. While inactivation of the second site (II^C) alone didn't affect activity of the protein, inactivation of both sites decreased activity 35-fold. As discussed below, this result is in agreement with role of these sites in the activity of pyocin L1. This work also showed, through the creation of chimeric lectin like bacteriocins, that the N-terminal MMBL domain is at least partially responsible for the specificity of lectin like bacteriocins (14). Lectin-like bacteriocins were first identified in 2003 and subsequent work and bioinformatics analysis has shown them to be widely distributed throughout the proteobacteria (15,104,105,132). The potency and stability of these proteins, along with their genus level specificity makes them attractive targets for inhibiting the growth of pathogenic bacteria. The work presented in this chapter

identifying LPS as the lectin-like bacteriocin cell surface receptor takes the first step towards characterising this fascinating protein family (15).

6.2 Putidacin L1 and syringacin L1 are active against multiple strains of *P. syringae*

As discussed in the introductory section of this thesis, previous work by Parret *et. al.* identified a novel family of lectin-like bacteriocins with genus specific activity, produced by *Pseudomonas* species (103,104,272). Because of their stability, potency and relatively broad spectrum this class of bacteriocin represent potentially useful targets for engineering bacteriocin expressing disease resistant transgenic plants, therefore their activity and mode of action was investigated. The previously characterised putidacin L1 was shown to have activity *against P. syringae* isolates, and as such its gene and an open reading frame encoding a putative lectin like bacteriocin from *Pss. 642* (designated syringacin L1) were obtained by gene synthesis (103). The proteins, putidacin L1 and syringacin L1, were expressed, purified and tested for activity against a range of *P. syringae* and other Gram-negative bacterial isolates (Figure 6-1) (Table 2-1). Expression and purification of syringacin L1 was problematic, with expression in *E. coli* leading to the accumulation of large quantities of inclusion bodies and a low yield ($1-5 \text{ mg ml}^{-1}$) of protein that precipitated during purification and concentration. Putidacin L1 which was highly stable and expressed at a yield of greater than 50 mg L^{-1} Both proteins were found to be active against a number of *P. syringae* strains tested, but not against other Gram-negative bacterial species tested. The spectrum of killing of putidacin L1 and syringacin L1 and their potency on a soft agar overlay is presented in Table 6-1. Syringacin L1 was found to kill the majority of isolates (10/12 tested) to a low μM concentration, with LMG5084 the most susceptible strain, killed down to a concentration of $0.27 \mu\text{M}$. Putidacin L1 inhibited less strains (5/12 tested) but was generally more potent with killing activity at nM concentrations. The most susceptible strain LMG2222 was killed at concentrations down to 0.85 nM .

Subsequent to the expression and preliminary characterisation of syringacin L1, a description of the cytotoxicity of this bacteriocin was published by Ghequire *et. al.* (105).

In parallel to this work L. McCaughey (University of Glasgow), isolated and characterised an additional lectin-like bacteriocin, designated pyocin L1, produced by *P. aeruginosa* C1433 which was shown to have activity against a range of *P. aeruginosa* isolates. See Figure 6-2 for a sequence alignment of these proteins

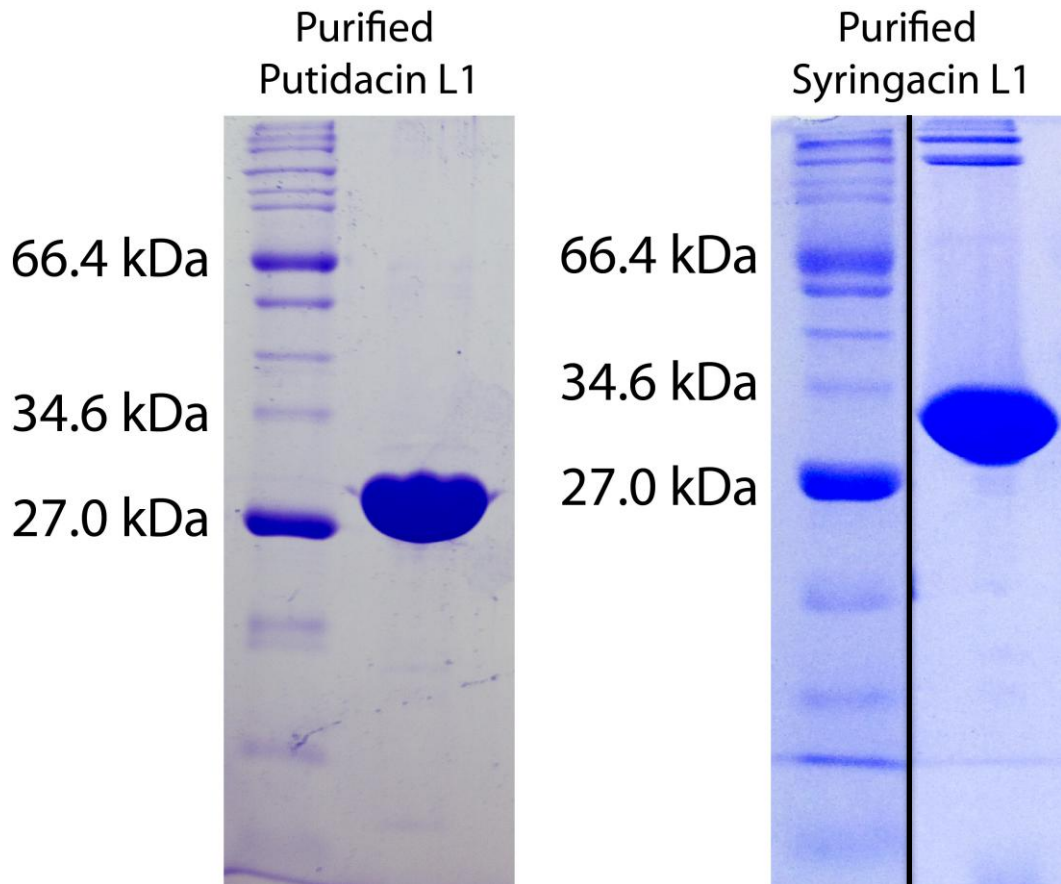


Figure 6-1 Purified of putidacin and syringacin L1.

Coomassie stained 15 % SDS-PAGE gel showing purified putidacin L1 (left) and syringacin L1 (right), utilised for toxicity assays, biochemical characterisation and crystallisation trials. *The syringacin L1 gel is derived from two lanes of the same gel, loaded with Mw marker and purified syringacin L1 respectively, the intervening lanes have been cropped for simplicity.*

Pathovar	Strain	Inhibition	MIC (nM)	Inhibition	MIC (μ M)
tomato	NCPPB3160	No	-	Yes	64.81
syringae	LMG5082	Yes	8.3	Yes	0.27
morsprunorum	LMG2222	Yes	0.85	Yes	2.40
tomato	NCPPB2563	No	-	Yes	21.60
tomato	NCPPB1107	No	-	Yes	7.20
tomato	DC3000	No	-	Yes	2.40
lachrymans	LMG5456	Yes	22.9	Yes	7.20
syringae	LMG5084	Yes	5.6	Yes	0.27
coronafaciens	LMG5060	No	-	Yes	583.33
syringae	LMG1247	Yes	1851.85	No	-
maculicola	LMG2208	No	-	No	-
unknown	Carlise1/2	No	-	Yes	N/D

Table 6-1 Susceptibility and sensitivity of *P. syringae* strains tested to putidacin and syringacin L1.

Inhibition was tested with purified protein up to a concentration of 600 μ M using the soft agar overlay; MICs listed are the lowest bacteriocin concentration as which a zone of inhibition was observed in this assay.

Figure 6-2 Sequence alignment of reported MMBL-like bacteriocins. Dark blue shading designates sequence identity; light blue designates chemically conserved residues. The three conserved MMBL sugar-binding motifs (N1, C1 and C2) and the partially conserved motif (N2) are boxed in red.

6.3 Characterisation of effect of putidacin L1 on bacterial cells

The phenotype induced by putidacin L1 treatment was investigated, cells grown in liquid culture (Kings B media, with shaking) were treated with varying concentrations of putidacin L1 at an OD₆₀₀ of between 0.1 or 0.3. After the addition of the bacteriocin the OD₆₀₀ of treated cultures initially increased more rapidly than untreated cultures, however after 5 hours the OD₆₀₀ increased more slowly than for untreated cells (Figure 6-3). Analysis of treated cells by light microscopy showed that this rapid increase in OD₆₀₀ was not due to an increased rate of bacterial growth, but rather to agglutination and filamentation of treated cells (Figure 6-4-A). Larger particles scatter light at 600 nm more effectively creating an artefact in the use of optical density for measuring cell growth. Cells treated with putidacin L1 became immobile and settled to the bottom of the culture flask in a dose dependent manner (Figure 6-4-B), most likely as a consequence of the agglutination observed after treatment. Treated cells remained viable until approximately 12 hours after treatment and could be recovered by transfer to putidacin free media or by spotting on KB agar, however after 12 hours cells became spherical and by 18 hours extensive cell lysis was apparent. While this phenotypic characterisation does not provide direct evidence of the mechanism of action of the lectin-like bacteriocins, the inability of treated cells to divide normally (i.e. filamentation), combined with the clumping observed suggests some function in disruption of the cell-envelope or cell division machinery (273). The delayed lysis of treated bacteria may be a direct consequence of the bacteriocin or downstream autolysis in response to a more general cellular effect on physiology due to bacteriocin treatment (274).

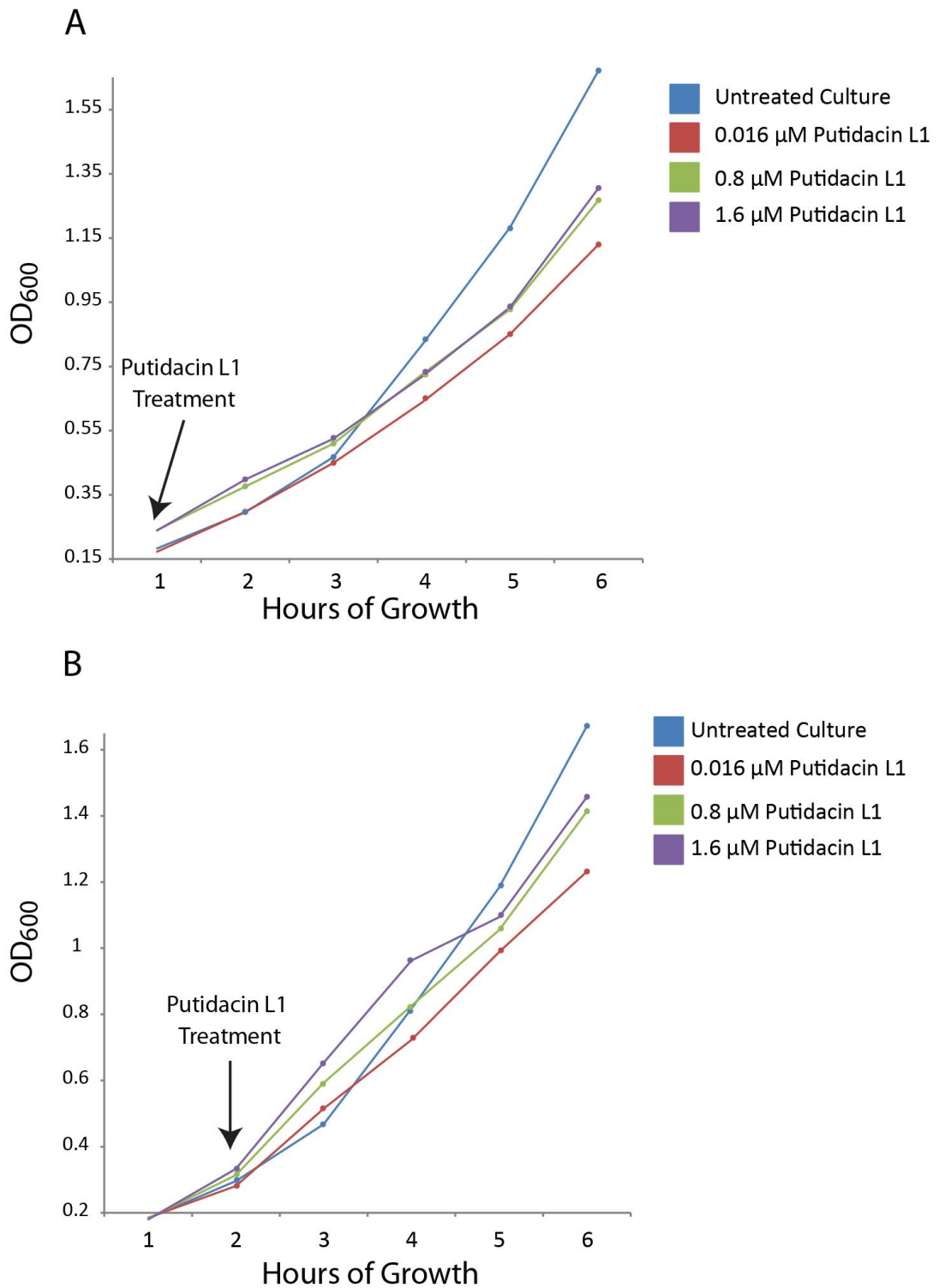


Figure 6-3 Change in OD₆₀₀ of *P. syringae* LMG2222 treated with putidacin L1,

Change in absorbance at OD₆₀₀ of LMG2222 cultures treated with differing concentrations of putidacin L1 at 1 or 2 hours post inoculation. The OD₆₀₀ of cultures treated with putidacin L1 initially increased more rapidly than wildtype cells, before falling behind wildtype growth rate at approximately 2 hours after the addition of putidacin L1.

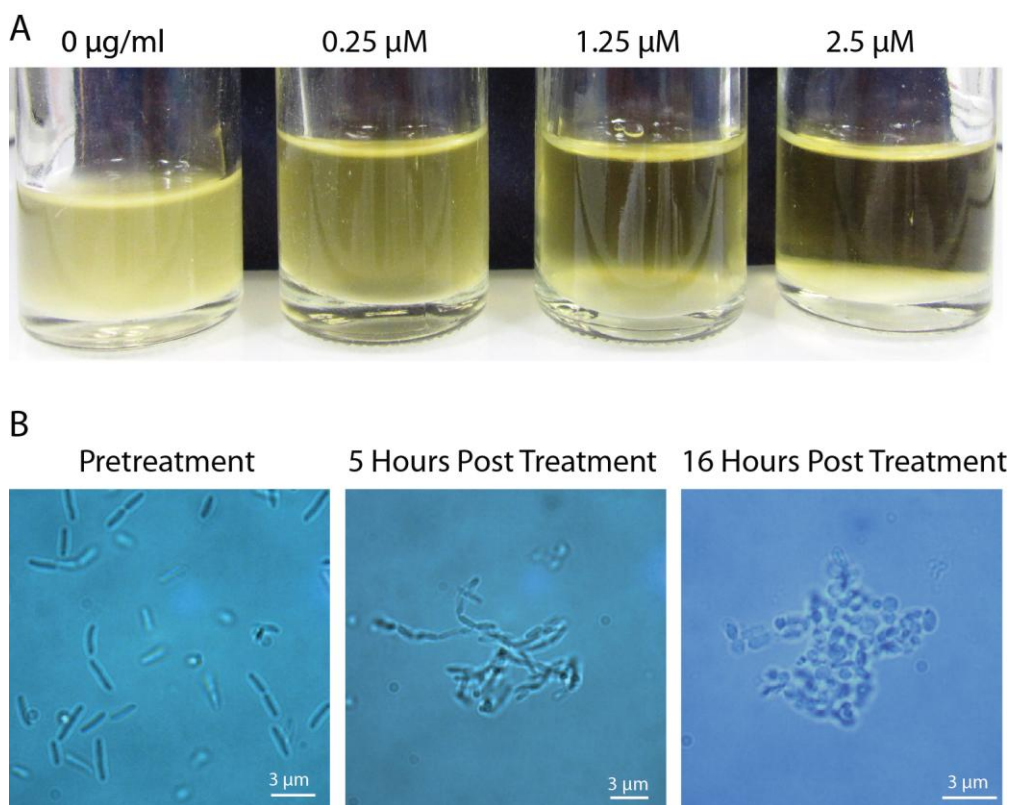


Figure 6-4 Phenotypic changes in *P. syringae* LMG2222 induced by putidacin L1 treatment

A) Reduction of mobility of stationary cultures of LMG2222 treated with varying concentrations of putidacin L1, photos taken 8 hours after treatment. B) Phenotype of unstained/fixed LMG2222 cells treated with putidacin L1 at a concentration of 2.5 µM, visualised by light microscopy at 1000x magnification.

6.4 Phenotypic and genetic analysis of putidacin L1 tolerant *P. syringae* strains

To shed light on the function of the lectin-like bacteriocins, LMG2222 was incubated with putidacin L1 and colonies which survived the treatment were isolated. A number of different mutant colonies were isolated and tested for increased resistance to putidacin L1. None of the colonies isolated were found to be completely resistant to putidacin L1, but rather exhibited greatly increased tolerance. Three mutants designated, IN50, Imut and 20(1) were chosen as representative tolerant phenotypes for further study. Both Imut and 20(1) exhibited an approximately a 30-fold higher resistance to putidacin L1, relative to wildtype LMG2222, on an agar overlay spot test, with hazy zones of inhibition observed at all concentrations suggesting tolerance to putidacin L1 even at high concentrations. Zones of inhibition of IN50 by putidacin L1 were clear, but the strain was

over 250 times more tolerant to putidacin L1 relative to wildtype LMG2222 (Figure 6-5-A/B). Phenotypically both Imut and 20(1) were normal, with cells motile and of a size and shape analogous to wildtype LMG2222. Alternatively, IN50 cells were non-motile and grew in long filaments (Figure 6-5-C). On KB agar wildtype LMG2222 colonies display a smooth colony morphology. Both Imut and 20(1) shared this morphology, whereas IN50 had a rough colony type. A rough to smooth colony type transition is often due to a change in cell-envelope LPS production and as the lectin like bacteriocins possess well defined sugar binding motifs, it was postulated that LPS binding is involved in cell entry or killing. To test if the change in morphology of IN50 was due to a change in LPS production, LPS was purified from wildtype and mutant LMG2222 and visualised by SDS-PAGE and silver staining. As shown in Figure 6-5-D, although the LPS profile of Imut and 20(1) were comparable to wildtype, IN50 lacks O-antigen LPS. This lack of O-antigen LPS in the IN50 mutant may indicate that LPS recognition may play some role in putidacin L1 killing. Furthermore, phenotypic differences between IN50 and Imut/20(1) indicate that the tolerance of these mutants is due to a different mechanism.

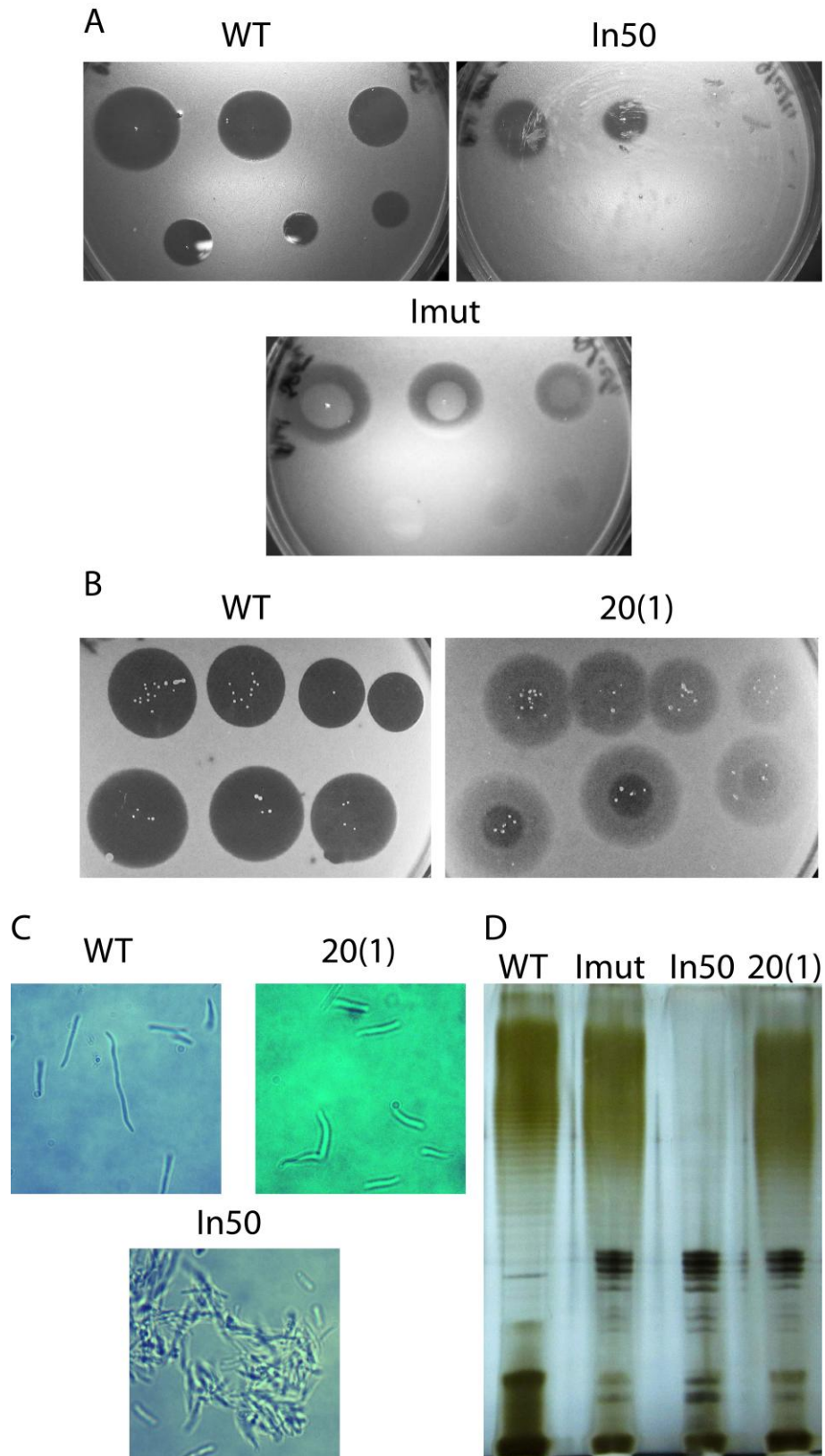


Figure 6-5 Isolation and characterisation of putidacin L1 resistant mutants

A/B) Difference in sensitivity of putidacin L1 tolerant and wildtype LMG2222 to putidacin L1, shown by soft agar overlay assay, C) morphology of untreated putidacin L1 tolerant mutants compared to wildtype visualised by light microscopy at 1000x magnification, D) Composition of purified LPS from wildtype and putidacin L1 tolerant LMG222, separated by 10 % SDS-PAGE gel and visualised by silver staining.

In order to determine the genetic basis the tolerant phenotype observed in the mutants, genomic DNA from wildtype LMG2222 as well as Imut, 20(1) and IN50 was extracted and sequenced. The sequencing reactions produced good data; the reads from wildtype LMG2222 were assembled *de novo* into approximately 150 contigs, for which the consensus sequence was extracted and annotated. These contigs then served as the reference sequence for the mutant data, with verifiable genetic differences outlined below:

Imut, 30-fold more tolerant to putidacin L1, with hazy zones of inhibition

- 2 nucleotide deletion in open reading frame encoding histidine sensor kinase related to CpxA, leading to frame shift at Leu 149
- SNV in putative open reading frame encoding histidine sensor kinase related to CheY/GacS, leading to mutation of residue 253 from Ala to Thr

20(1), 30-fold more tolerant to putidacin L1, with hazy zones of inhibition

- 4 nucleotide insertion in open reading frame encoding histidine sensor kinase related to CpxA, leading to frame shift at Ala 66

IN50, 250-fold more tolerant to putidacin L1, with clear zones of inhibition and an aberrant phenotype

- SNV in putative open reading frame encoding histidine sensor kinase related to CheY/GacS family, leading to mutation of residue 490 from Gly to Ser
- Dinucleotide deletion in open reading frame encoding a homologue of WbpM LPS biosynthesis, leading to frame shift at Glu 565
- Single nucleotide insertion in open reading frame encoding a homologue of Wtz LPS ABC export protein, leading to a frame shift at Gly 256

Interestingly, as with the pectocin M1 resistant mutants described in chapter 4, variant histidine sensor kinases featured prominently in the putidacin L1 tolerant mutants isolated. Both Imut and 20(1) acquired distinct frame shift mutations in a homologue of the *E. coli* kinase sensor CpxA, which functions in sensing and responding to outer-membrane stress (275). As this was the only mutation identified in 20(1) it likely plays a significant role in the in tolerance of both mutants to putidacin L1. In both strains the frame shift mutation occurs in the N-terminal periplasmic sensor domain, leading to the production of a truncated protein lacking the cytoplasmic kinase domain.

Imut and IN50 both acquired a distinct SNV in a homologue of a sensor kinase of the CheY/GacS family, leading to A253T and G490S variants, respectively. As both strains acquired mutations in this gene it seems likely it contributes towards the tolerant phenotype. CheY and GacS have been shown to be involved in regulating chemotaxis, virulence factor and siderophore production and so a putative role in putidacin L1 tolerance is not immediately obvious (276,277).

Two further mutations were identified in IN50, both leading to frame shifts in core components of the bacterial LPS synthesis and transport machinery. WbpM is a highly conserved integral inner membrane C₆ dehydratase essential for LPS synthesis and Wzt is an ABC transporter responsible for transport of synthesised LPS across the inner membrane. Strains deficient in either gene are unable to produce the O-antigen component of LPS (278,279), explaining the O-antigen deficient phenotype of IN50. The fact that lectin-like bacteriocins have well defined sugar binding motifs for hexose sugars, which are also utilised to construct LPS O-antigens and the correlation between lack of production of LPS in the LMG2222 mutant IN50, with tolerance to putidacin L1 suggests the mechanism of action of these bacteriocins involves interaction with LPS at the bacterial cell surface (14).

6.5 Pyocin L1 targets the common polysaccharide antigen (CPA) of *P. aeruginosa* LPS

Concurrently with the isolation of putidacin L1 resistant *P. syringae* LMG2222, *P. aeruginosa* E2 was subjected to high concentrations of recombinant pyocin L1 and mutants were recovered with greatly increased tolerance (Figure 6-6-A). The genomes of two of these mutants were sequenced and comparative analysis with the genome of wildtype E2 revealed a dinucleotide deletion (CT) at 710-11 bp of the 1146 bp *wbpZ*. This deletion was common to both mutants. WbpZ a glycosyltransferase of 381 amino acids that plays a key role in lipopolysaccharide synthesis, specifically in the synthesis of the common polysaccharide antigen (CPA) also known as A-band LPS (280). Most strains of *P. aeruginosa* produce two distinct LPS-types that differ in their O-antigen, but share the same core oligosaccharide. The CPA is a homopolymer of D-rhamnose and the O-specific

antigen contains a heteropolymeric repeating unit that varies widely among strains (281). Consistent with mutation of *wbpZ*, we found that production of CPA, as determined by immunoblotting with a CPA-specific monoclonal antibody (282), in both M4(E2) and M11(E2) was reduced to undetectable levels (Figure 6-6-B).

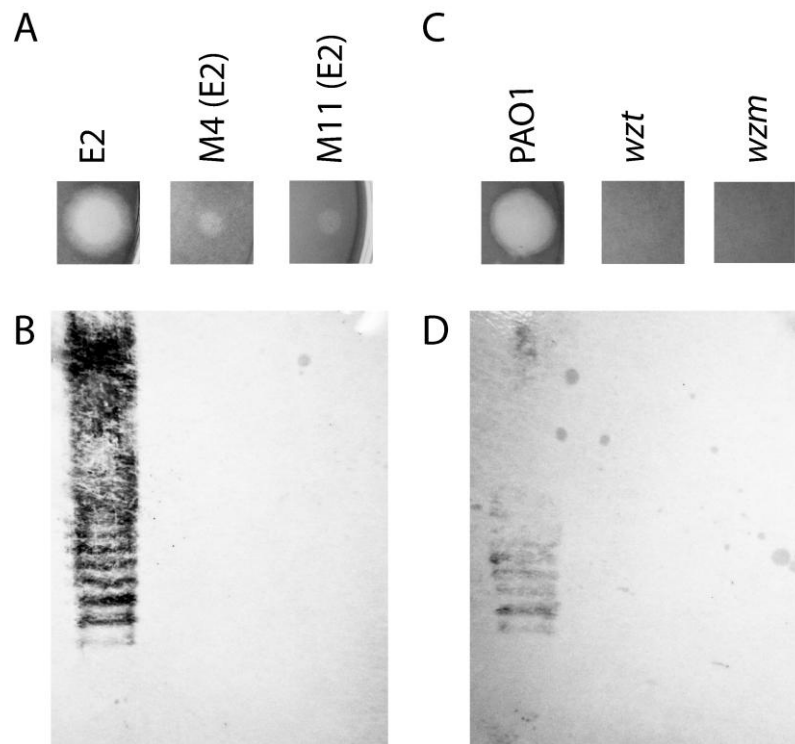


Figure 6-6 CPA production correlates with pyocin L1 killing.

A) Inhibition of growth of *P. aeruginosa* E2 and tolerant mutants M4 and M11 by pyocin L1, as shown by a soft agar overlay spot-test. 5 μ l of purified pyocin L1 (1.5 mg ml⁻¹) was spotted onto a growing lawn of cells. Clear zones indicate cell death. B) Expression of CPA by *P. aeruginosa* E2 and tolerant mutants, visualised by immunoblotting with the CPA specific antibody N1F10. C) Inhibition of growth of *P. aeruginosa* PAO1 and PAO1 *wzm* and *wzt* mutants by pyocin L1 (details as for A). D) Expression of CPA by PAO1 and *wzm* and *wzt* strains (details as for B). (Experimental data produced by L McCaughey)

These observations correlate well with the LPS deficient phenotype of IN50 and suggest that pyocin L1 may utilise LPS, specifically the CPA as a cellular receptor. To test this idea further, two transposon insertion mutants of *P. aeruginosa* PAO1, which is sensitive to pyocin L1, with insertions in the genes responsible for the transport of CPA to the periplasm were obtained (283). These two genes, *wzt* and *wzm*, encode the ATP-binding component and membrane component of a CPA dedicated ABC transporter (281). Pyocin L1, which shows good activity against PAO1 showed no activity against strains with

insertions in *wzm* and *wzt* (Figure 6-6-C) and immunoblotting with a CPA-specific antibody confirmed the absence of the CPA in these pyocin L1 resistant strains (Figure 6-6-D). Thus, the presence of CPA on the cell surface is required for pyocin L1 killing. In order to determine if the requirement for CPA is due to a direct interaction with pyocin L1, LPS from wildtype PAO1 and from the pyocin L1 resistant, *wzm* and *wzt* mutants (which produce no CPA but do produce the O-specific antigen) was purified and the pyocin-CPA interaction was analysed by isothermal titration calorimetry (ITC). Titration of pyocin L1 into isolated LPS-derived polysaccharides (a mixture of CPA and the O-specific antigen containing polysaccharides) from PAO1 gave rise to strong saturable exothermic heats of binding with an apparent K_d of 1.6 μM (Figure 6-7-A), whereas no binding was detected on titration of pyocin L1 into an equivalent concentration of LPS carbohydrates from PAO1 *wzt*, which produces the O-specific antigen but not the CPA (Figure 6-7-B). These data show that pyocin L1 binds directly to the CPA and that this interaction is required for killing. The CPA is therefore likely to be the cellular receptor for pyocin L1.

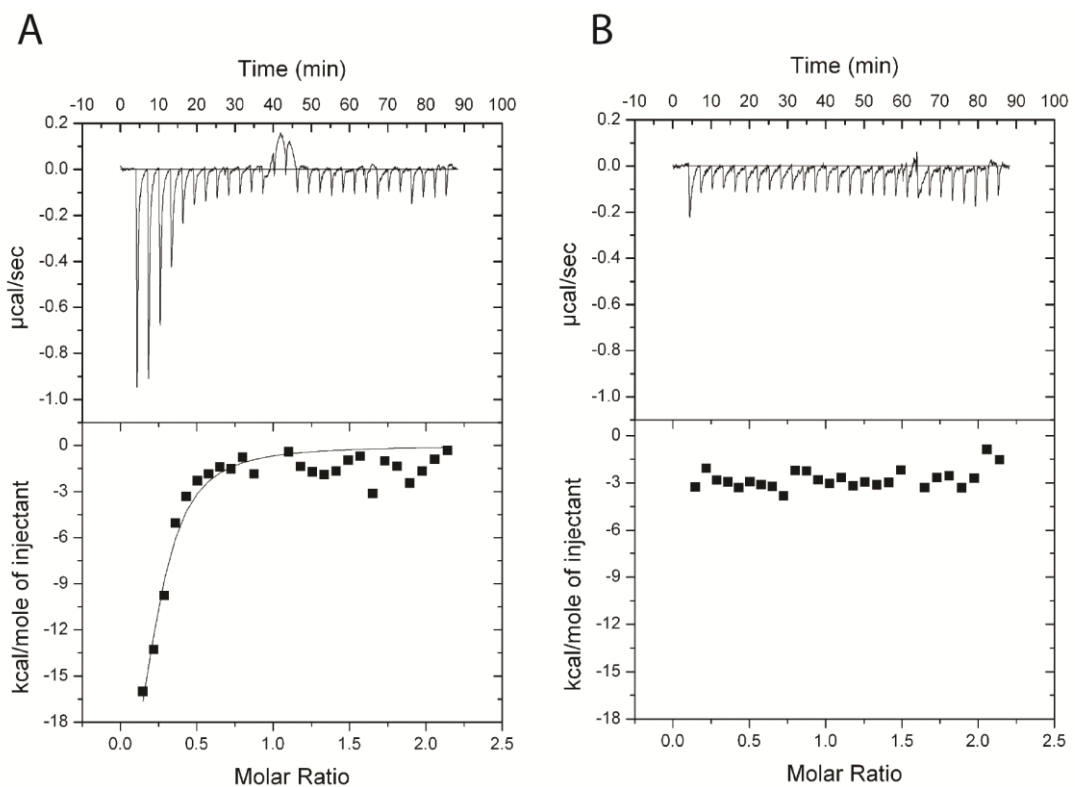


Figure 6-7 Pyocin L1 binds strongly to CPA from *P. aeruginosa* PAO1.

A) ITC binding isotherm of pyocin L1 (150 μM) titrated into isolated LPS-derived polysaccharide (1 mg ml^{-1}) from wildtype *P. aeruginosa* PAO1. Strong, saturable heats were observed indicative of a strong interaction. Curve fitted with a single binding site model. B) ITC isotherm of pyocin L1 (150 μM) titrated into isolated LPS-derived polysaccharide (1 mg ml^{-1}) from PAO1 *wzt*. No saturable binding isotherm was observed. (Experimental data produced by L. McCaughey)

6.6 Pyocin L1 binds the monosaccharide D-rhamnose

The evolutionary relationships between MMBL-like bacteriocins and the originally identified mannose-binding members of this protein family, led to the assumption that carbohydrate binding of polysaccharides by the lectin-like bacteriocins is primarily mediated through binding of D-mannose at one or more of their conserved QxDxNxVxY carbohydrate binding motifs. Indeed, the recent structures (100) of putidacin L1 bound to mannose-containing monosaccharides show this protein has at least some affinity for the sugar, although measured affinities between polysaccharides and putidacin L1 are weak (mM) and so may not be physiologically relevant. However, the strong interaction between pyocin L1 and the CPA, which does not contain mannose, is incompatible with this and suggests that D-rhamnose and not D-mannose is the likely physiological substrate for the QxDxNxVxY carbohydrate binding motifs.

To determine the affinity of pyocin L1 for D-rhamnose and D-mannose, isothermal titration calorimetry (ITC) was performed. Titration of pyocin L1 into D-rhamnose gave rise to weakly saturable heats of binding that are significantly larger than the heats observed on titration of pyocin L1 into an identical concentration of D-mannose. From this experiment an apparent K_d of 5-10 mM was estimated for the interaction of pyocin L1 with D-rhamnose with apparently weaker binding for D-mannose, $K_d > 50$ mM (Figure 6-8-A/B). The interaction between pyocin L1 and these monosaccharides was also probed using NMR with ^{15}N labelled pyocin L1, monitoring changes to its ^{15}N -HSQC spectra on addition of D-rhamnose or D-mannose. In the absence of added monosaccharide ^{15}N -HSQC spectra of pyocin L1 were well dispersed, indicative of a folded protein. Addition of either D-rhamnose or D-mannose up to a concentration of 100 mM did not give rise to large global changes in chemical shifts but on addition of D-rhamnose strong and discrete chemical shift changes were observed for a number of peaks including the NH_2 region of the ^{15}N -HSQC spectra, with changes of a smaller magnitude observed on the addition of D-mannose (Figure 6-9-A/B). Plotting chemical shifts on addition of D-rhamnose for peaks showing strong chemical shift changes allows estimation of a K_d for the pyocin L1-D-rhamnose complex in the range of 5 - 20 mM (Figure 6-8-C-F). It should be noted however that as saturation of the pyocin L1 binding sites with D-rhamnose was not achieved, this K_d is not regarded as precise. These data correlated well with the ITC sugar binding data,

with low mM binding of pyocin L1 to D-rhamnose and much weaker binding to D-mannose.

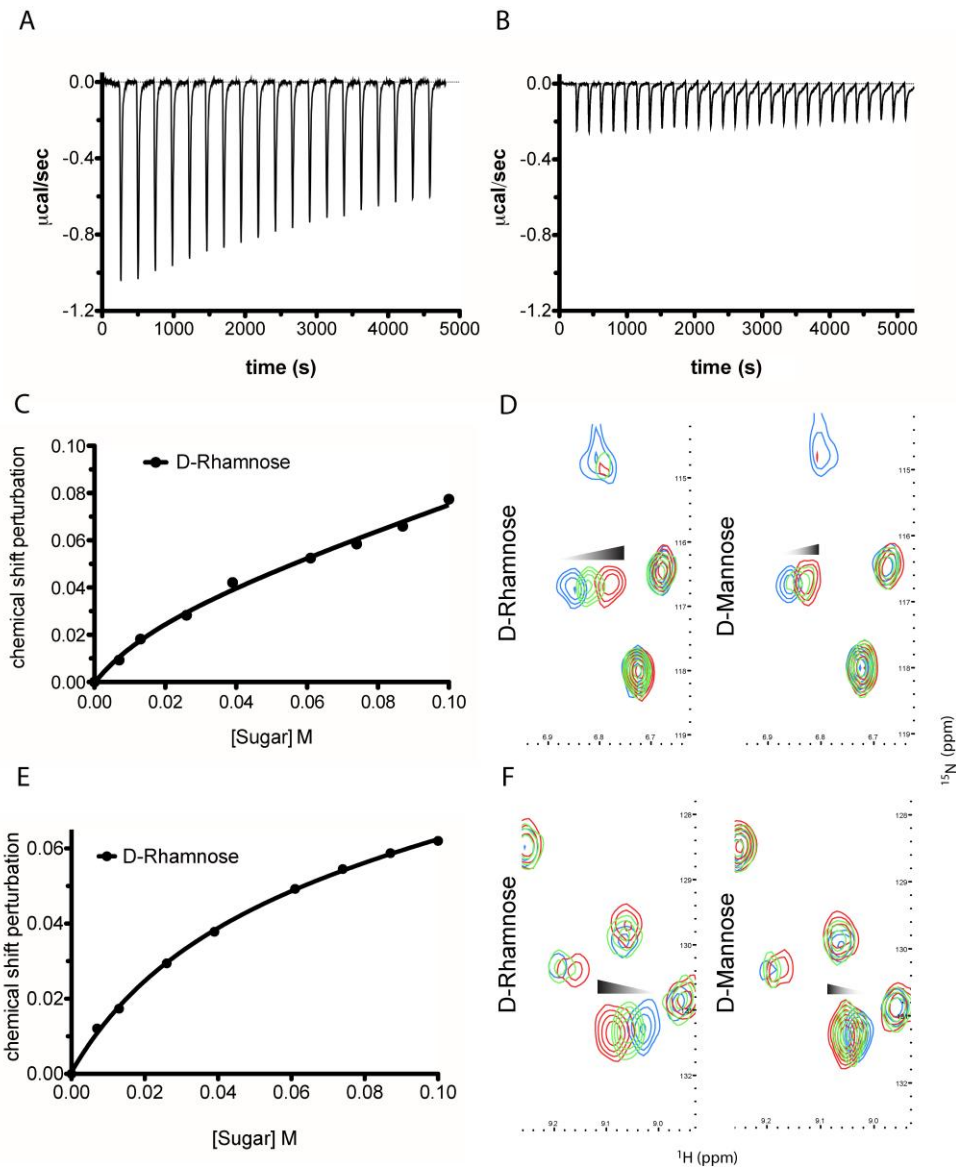
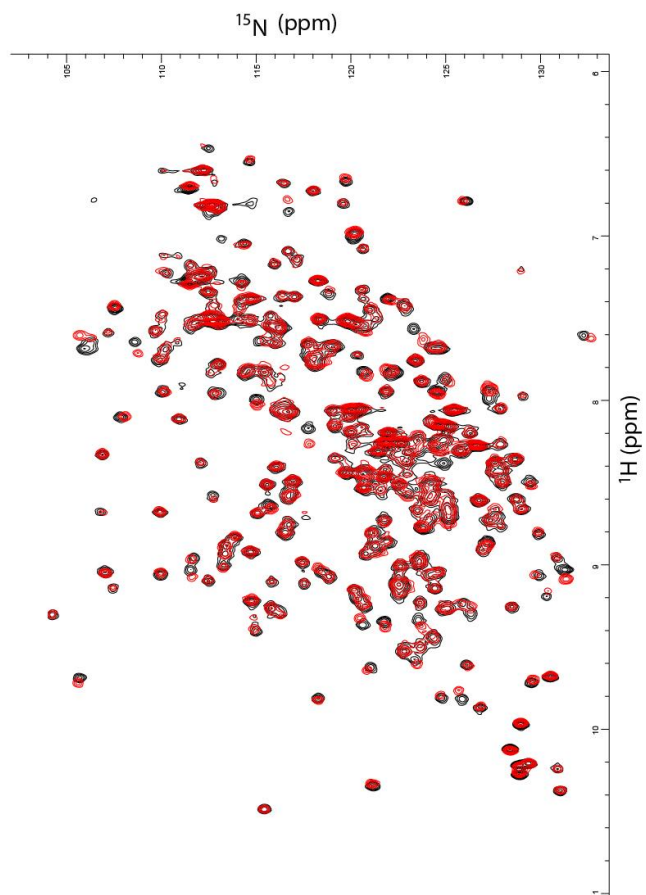


Figure 6-8 Pyocin L1 shows specificity for D-rhamnose compared with D-mannose.

A) ITC binding isotherm of D-rhamnose (50 mM) titrated into pyocin L1 (100 μM). Weakly saturable heats were observed, indicative of binding with weak affinity ($K_d \sim 5-10$ mM). B) ITC binding isotherm of D-mannose (50 mM) titrated into pyocin L1 (100 μM). Small-weakly saturable heats were observed, indicative of very weak interaction ($K_d \sim 50$ mM). Titration of monomeric sugars into ^{15}N -labelled pyocin L1, monitored using ^1H - ^{15}N HSQC NMR spectroscopy. Shifts within spectra were converted to chemical shift perturbation (CSP) values using equation $\Delta\text{ppm} = \sqrt{[\Delta\delta\text{HN} + (\Delta\delta\text{N} \cdot \alpha\text{N})^2]}$. CSP values are plotted against sugar concentration in C) and E) and visualised in D) and F). Peak positions, which correspond to backbone amide signals, at selected sugar concentrations (blue: no sugar, green: 60 mM, red: 100 mM) are shown. Perturbation of peak position (ppm) is indicative of association between ligand and protein molecules in solution.

A 100 mM D-rhamnose



B 100 mM D-mannose

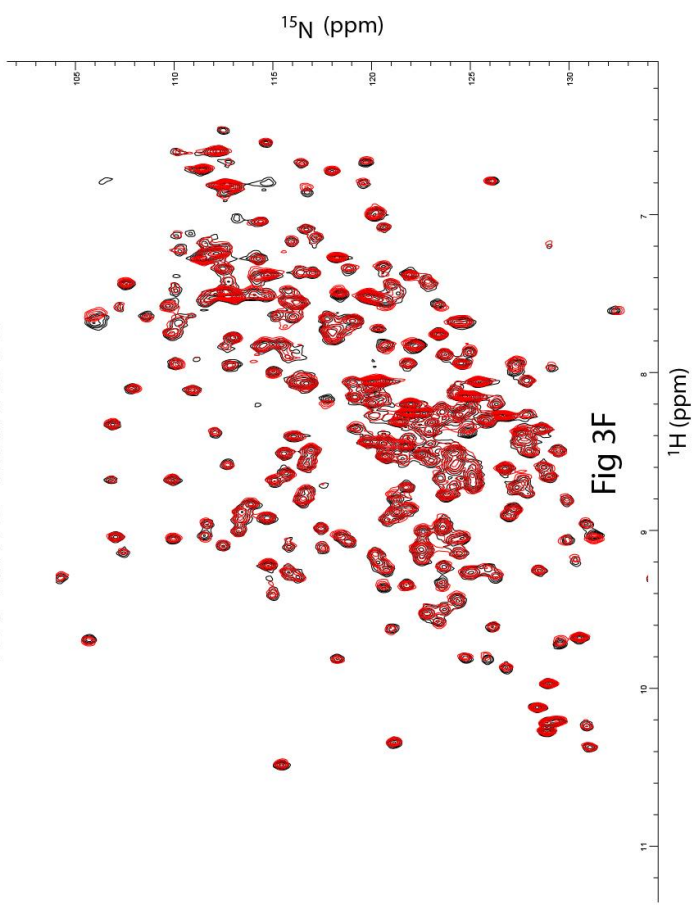


Figure 6-9 1H-15N HSQC spectra of 15N-labelled pyocin L1 in presence (red) and absence (black) of 100 mM (A) D-rhamnose and (B) D-mannose

Showing distinctive chemical shifts upon addition of associating sugars. Chemical shift changes specific to a small number of cross-peaks illustrates association of the sugars with a small subset of amino acids, which likely correspond to the residues within the binding sites. Analogous changes are observed for D-rhamnose and D-mannose titrations indicative that the same sites are binding both ligands. Greater shift magnitude is observed for D-rhamnose, indicative of a greater affinity towards this monosaccharide. Boxed regions include cross-peaks used for chemical shift perturbation analysis as shown in Figure 6-8.

6.7 D-rhamnose binds to the C-terminal QxDxNxVxY motifs of pyocin L1

In an attempt to determine the location of the pyocin L1, D-rhamnose binding site(s) and the structural basis of the D-rhamnose specificity of pyocin L1 the X-ray structures of pyocin L1 with bound D-mannose, D-rhamnose and in the unbound form were determined (Table 2-10). Pyocin L1, as predicted by sequence homology to MMBL proteins, consists of two tandem β -prism domains characteristic of MMBLs, connected by antiparallel strands propagating from the end of each MMBL domain and lending a strand to the reciprocal β -prism. The strands contain a tryptophan residue which forms π -stacking interactions with two other tryptophans in the β -prism to stabilise the structure (Figure 6-10-A). This interaction is conserved throughout MMBLs, with most members of the class utilising it to form either homo- or hetero-dimers of single MMBL subunits. However, in pyocin L1, as with the recently described structure of putidacin L1, both domains are from a single polypeptide chain (100). Other structural elements are also common between the two bacteriocins, namely a C-terminal extension of 30 amino acids and a two-turn α -helix insertion into loop 6 of the N-terminal MMBL domain (Figure 6-10-B). The overall rmsd for pyocin L1 and putidacin L1 is 7.5 Å, which is relatively high due to a difference in the relative orientation of the two MMBL domains. In contrast, the relative orientation of the tandem MMBL domains of pyocin L1 matches those of the dimeric plant lectins very closely, with alignment of pyocin L1 with the snowdrop lectin homodimer (pdb ID: 1MSA) giving an rmsd of 4.81 Å. Comparison of the respective N- and C-terminal domains from pyocin L1 and putidacin L1 shows they possess very similar folds with rmsds of 2.77 Å and 2.02 Å, respectively (Figure 6-10-C/D). The higher value for

comparison of the N-terminal domains is due to the presence of a 2-strand extension to β -sheet two of the putidacin L1 N-terminal MMBL domain, which is absent from pyocin L1 and other MMBLs. A DALI search for structures similar to pyocin L1 reported significant hits for only putidacin L1 and proteins with the MMBL fold such as the snowdrop lectin. MMBL dimers of plant origin often form higher order structures, however small angle X-ray scattering of pyocin L1 showed it to be monomeric in solution (Figure 6-11).

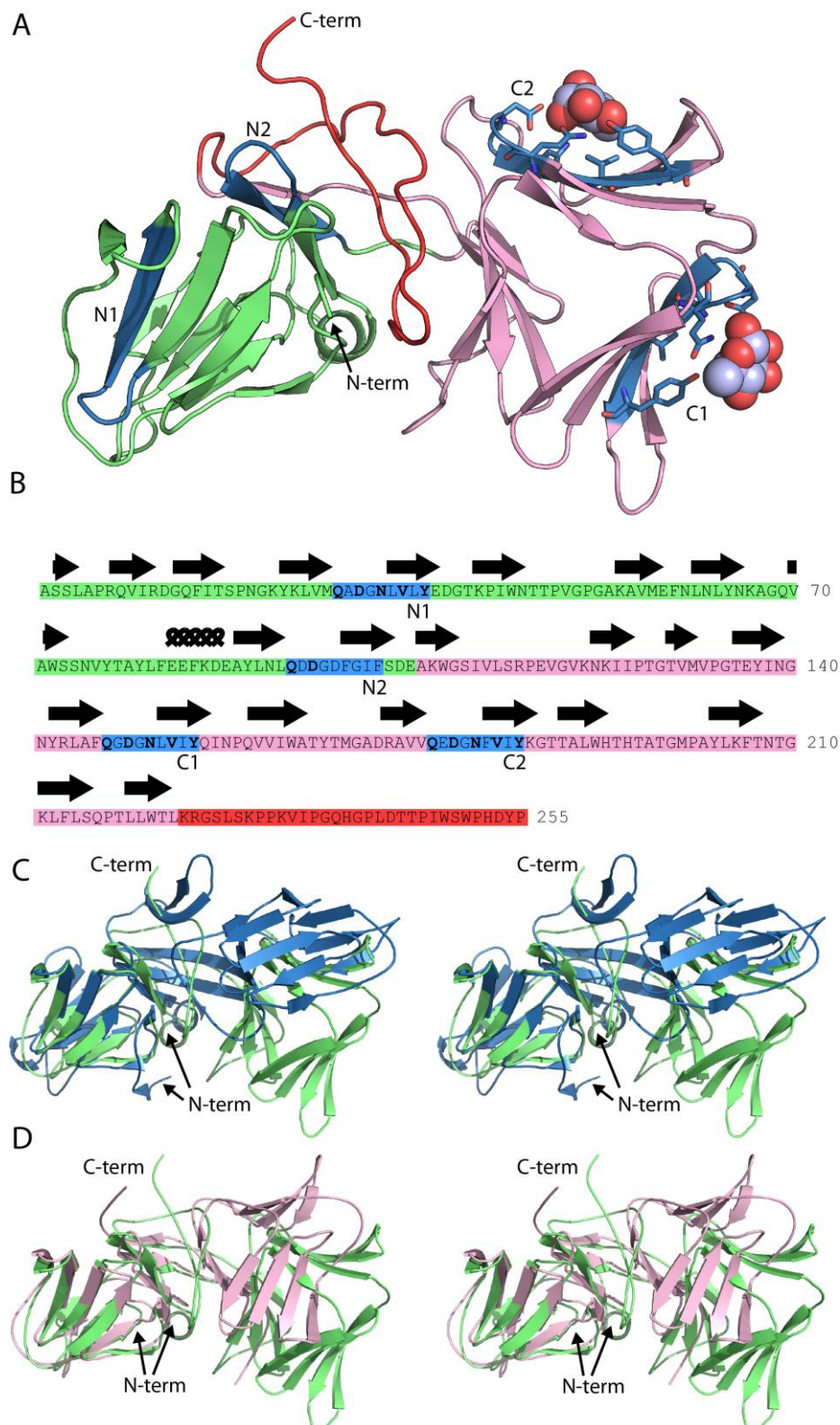


Figure 6-10 Crystal structure of pyocin L1 reveals tandem MMBL domains and sugar-binding motifs.

A) Ribbon diagram of structure of pyocin L1 in complex with α -D-rhamnose, amino acids 2-256. N-terminal domain (green), C-terminal domain (pink), C-terminal extension (red), α -D-rhamnose (spheres) and sugar binding sites containing the conserved or partially conserved QxDxNxVxY motif are highlighted (blue) and are designated N1, N2 and C1, C2 according to order of appearance in the primary sequence of the N- and C-terminal domains, respectively. Pyocin L1 residues involved in hydrogen bonding with α -D-rhamnose are shown in stick representation. B) Sequence and secondary structure (β -sheets = arrows, α -helices = coils) of pyocin L1 with colours corresponding to the structure in (A). Residues conserved in sugar binding motifs are shown in bold. C) Structural alignment of pyocin L1 (green) and putidacin L1 (blue) based on N-terminal MMBL domain in wall-eyed stereo. D) Structural alignment of pyocin L1 (green) and *Allium sativum* agglutinin (1BWU) (pink) based on N-terminal MMBL domain in wall-eyed stereo.

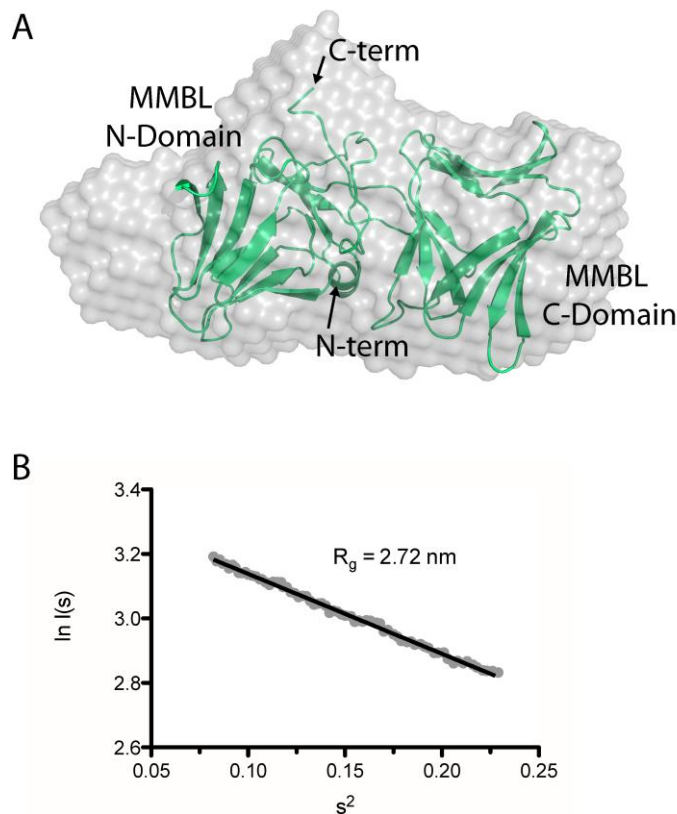


Figure 6-11 Small angle X-ray scattering of pyocin L1.

A) Ab initio model of pyocin L1 computed with DAMMIF overlaid with the crystal structure. B) Guinier plot of scattering data indicates that the protein is monomeric in solution ($I(0)$ gives a molecular mass of 29.53 kDa) by extrapolation of scattering intensity to zero scattering angle. Radius of gyration is 2.72 nm, indicative of a folded, globular monomeric particle in solution.

In order to determine which 4 conserved sugar binding motifs are important for binding LPS sugars, pyocin L1 crystals were soaked with both D-mannose and D-rhamnose. Electron density maps, derived from both D-mannose and D-rhamnose soaked crystals show clear density for sugar moieties in both sites, C1 and C2 (Figure 6-13). The sugars refined well in these densities at full occupancy, giving B-factors comparable to the surrounding protein side chains. The canonical MMBL hydrogen bonds observed for both D-mannose and D-rhamnose were the same: Gln to O3, Asp to O2, Asn to O2 and Tyr to O4. In addition, O6 of D-mannose forms a hydrogen bond with Tyr169 in C1 and His194 in C2. As D-rhamnose is C6 deoxy D-mannose, it lacks these interactions (Figure 6-13). The fact that D-mannose forms an additional hydrogen bond is counter-intuitive given that pyocin L1 has a significantly stronger affinity for D-rhamnose, however Val154, Val163 and Ala166 of C1 and Val184 and Ala191 of C2 form a hydrophobic pocket to accommodate the C6-methyl group of D-rhamnose (Figure 6-14). Weak density was observed for both sugars at site N1, however given the high concentrations used in the soak and the overall low binding affinity of pyocin L1 for monomeric sugars, it is unlikely that N1 represents a primary binding site for D-rhamnose (Figure 6-14). The conserved residues in site N2 form interactions with the C-terminal extension of the protein and as such are inaccessible. Weak density was also observed adjacent to the binding site C1 of mol B in both the soaks and in mol A of the D-rhamnose form. This density may correspond to a peripheral binding site utilised in binding to the carbohydrate chain of LPS, as is observed in the structure of putidacin L1 bound to oligosaccharides (100).

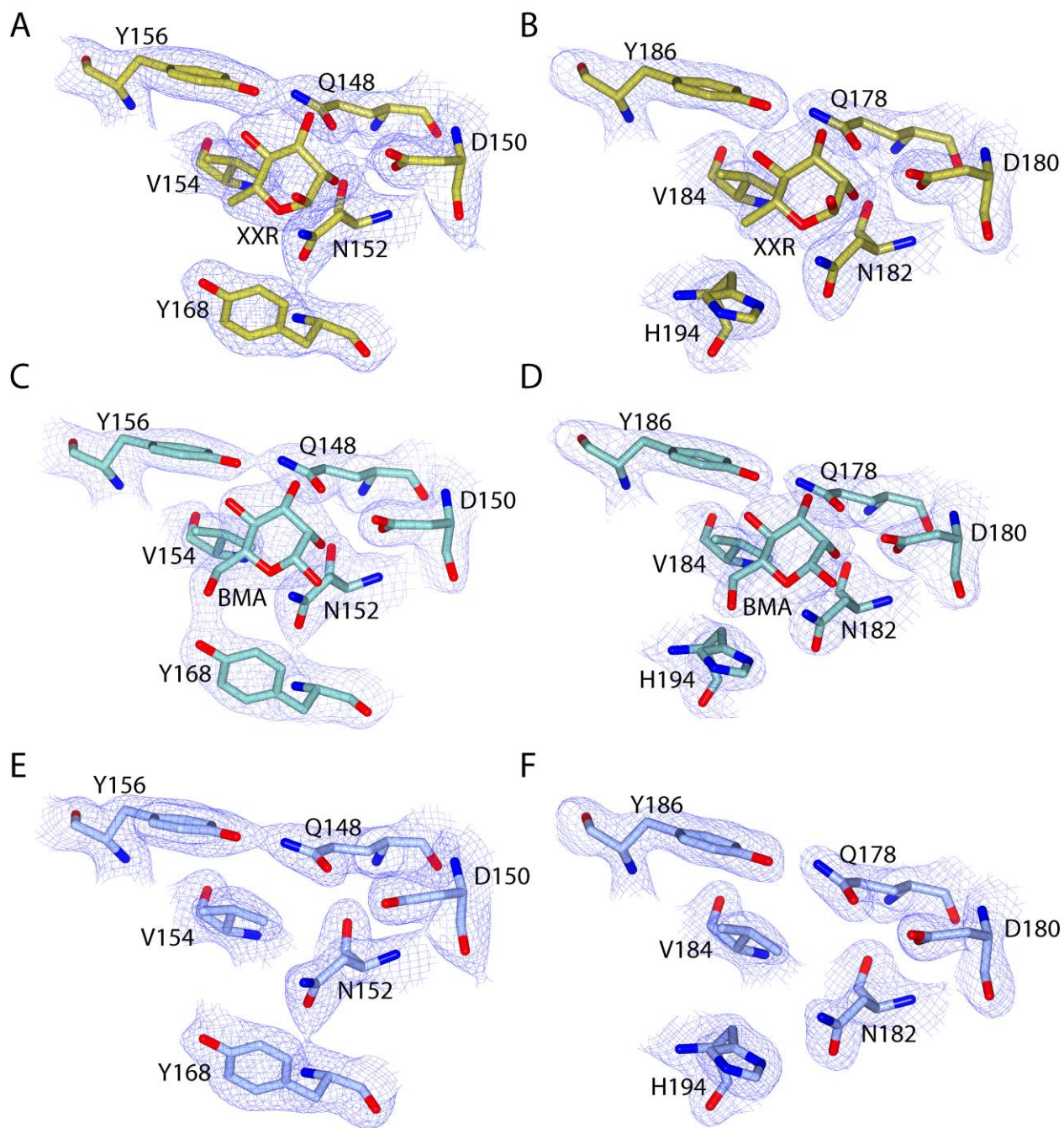


Figure 6-12 C-terminal MMBL-sugar binding motifs of pyocin L1 bind D-rhamnose and D-mannose.

Electron density (at 1.3 σ) with fitted stick model of pyocin L1 MMBL-sugar binding site C1

(A) D-rhamnose (XXR), (C) D-mannose (BMA), (E) no bound sugar, and sugar binding site C2 with: (B) D-rhamnose, (D) D-mannose, (F) no bound sugar. For clarity, electron density is clipped to within 1.5 Å of visible atoms.

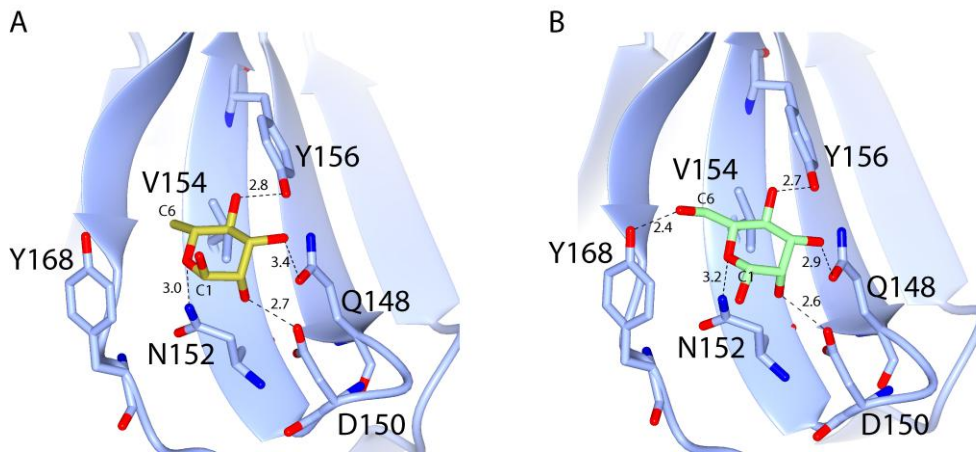


Figure 6-13 Hydrogen-bonding interactions between pyocin L1 MMBL sugar-binding motif C1 with D-rhamnose and D-mannose

Hydrogen bonds between protein side chains with (A) D-rhamnose and (B) D-mannose are shown; all distances are in Å.

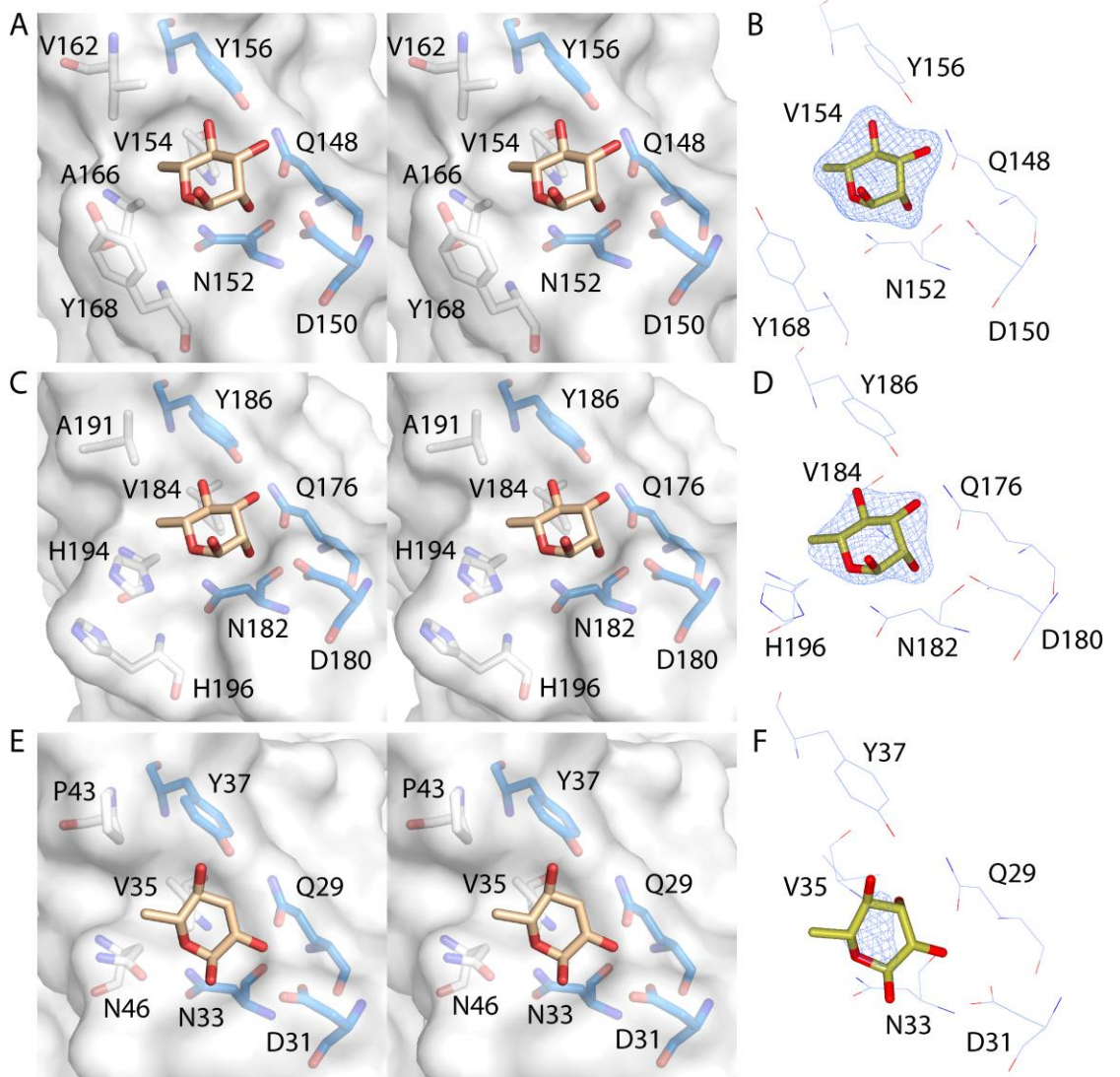
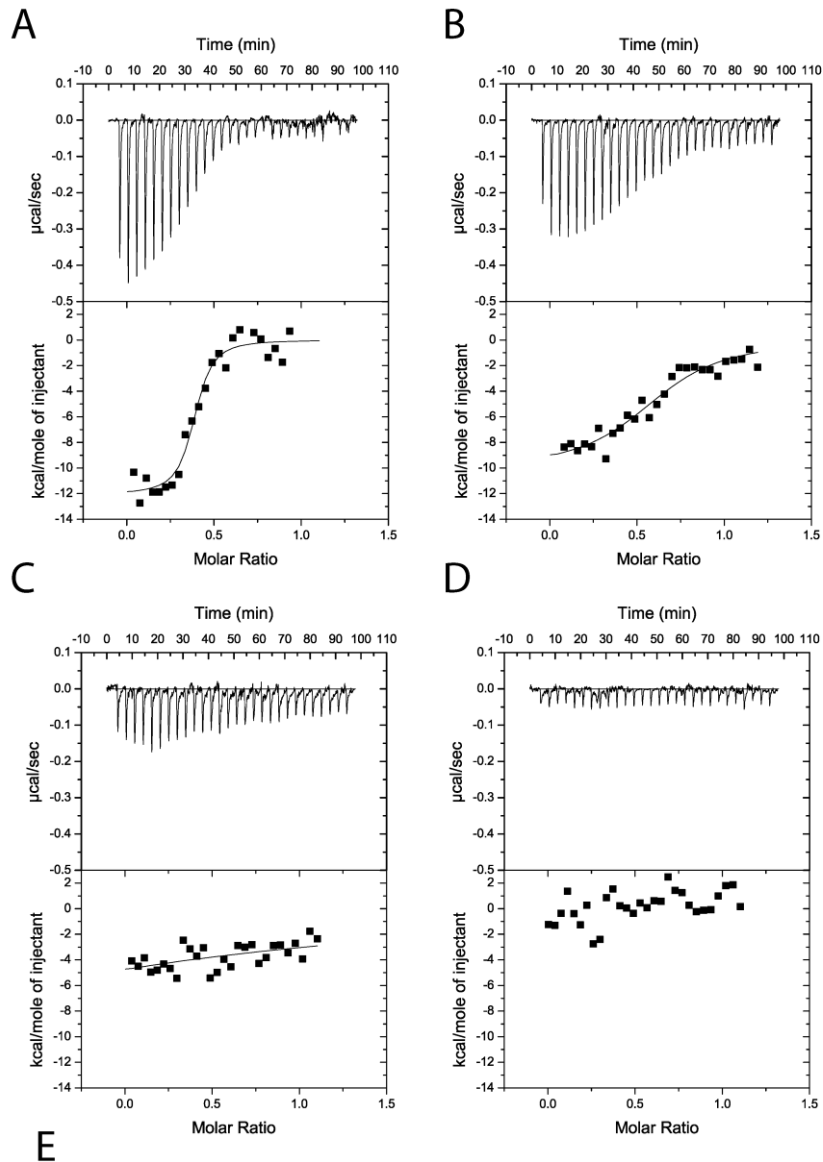


Figure 6-14 Coordination of D-rhamnose in C1, C2 and N2 binding sites of pyocin L1

A) Stereo view of D-rhamnose coordination by binding site C1 A), C2 C) and N1 E), from D-rhamnose soak data. Core binding motif residues (blue) and additional residues contributing to the pocket (white) are shown. Omit map density for D-rhamnose in binding site C1 B), C2 D), N1 F) calculated by refinement of data from D-rhamnose soaked crystal with model built from unsoaked crystal. Density for all sites contoured to $0.15e/\text{\AA}^3$.

To test the idea that the observed binding of D-rhamnose to sites C1 and C2 is reflective of CPA binding and that this binding is critical to pyocin L1 cytotoxicity, pyocin L1 variants were created in which the conserved aspartic acids of the QxDxNxVxY motifs of the C1 and C2 sugar binding sites were mutated to alanine and compared their cytotoxicity and ability to bind the CPA by ITC was compared with the wildtype protein. Titrations with wildtype pyocin L1 and the D150A (C1) and D180A (C2) variants were performed by titrating protein at a concentration of 100 μM into a solution of LPS-derived polysaccharide (1 mg ml^{-1}) from strain PAO1 (Figure 6-15). Under these conditions binding isotherms were generated that enabled us to accurately determine an apparent K_d of $0.15 (\pm 0.07) \mu\text{M}$ for the wildtype pyocin L1-CPA complex. For both the D150A (C1) and D180A (C2) variants, affinity for CPA was reduced. For the pyocin L1 D180A-CPA complex a K_d of $1.52 (\pm 0.51) \mu\text{M}$ was determined, a 10-fold increase in K_d relative to the wildtype pyocin L1-CPA complex. However, CPA binding to the D150A variant was severely weakened and although heats of binding were still observed the K_d for this complex, which could not be accurately determined, is likely $> 500 \mu\text{M}$. We also produced a double mutant in which both D150A and D180A mutations were present. For this double mutant, no binding to CPA was observed by ITC. These data show that both the C1 and C2 sugar binding motifs are required for full CPA binding, but that the C1 binding site is the major CPA binding determinant. The killing activity of these sugar binding motif variants showed a good correlation with their ability to bind the CPA. Both the D150A and D180A variants showed reduced cytotoxicity against PAO1 relative to pyocin L1, with the D150A showing a greater reduction in activity and for the D150A/D180A variant very low levels of cytotoxicity were observed (Figure 6-15).



2-fold dilution series

WT
D150A/D180A
D180A
D150A

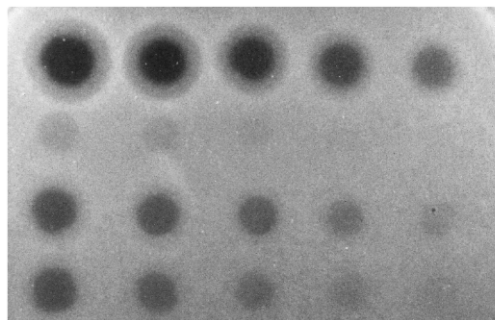


Figure 6-15 Binding of the CPA at the C-terminal sugar binding motifs, C1 and C2, is critical to pyocin L1 cytotoxicity.

ITC binding isotherms of A) wildtype B) D180A C) D150A and D) D150A/D180A pyocin L1 all at (100 μM) titrated into isolated LPS-derived polysaccharide (1 mg ml^{-1}) from wildtype *P. aeruginosa* PAO1. Fit to a single binding site model is shown. E) Spot tests to determine cytotoxic activity of wildtype and pyocin L1 variants against of *P. aeruginosa* PAO1. Purified protein (starting concentration $400 \mu\text{g ml}^{-1}$ with 2-fold sequential dilutions) was spotted onto a growing lawn of *P. aeruginosa* PAO1. Clear zones indicate pyocin L1 cytotoxicity.

6.8 Putidacin L1 binds to *P. syringae* LPS and D-rhamnose

The crystal structure of pyocin L1 and the sugar binding data clearly demonstrates that pyocin L1 targets sensitive strains of *P. aeruginosa* through binding to LPS and utilises this as a cell surface receptor. Our isolation of IN50 a mutant rendered tolerant to putidacin L1 due to its inability to produce LPS O-antigen strongly suggests that putidacin L1 also utilises LPS as its cell surface receptor. However, the fact that putidacin L1 is not active against *P. aeruginosa* strains containing CPA suggests that it targets a structurally distinct LPS polymer. To confirm that LPS binding is common to putidacin L1, susceptibility of a number of strains of *P. syringae* was correlated with the ability of putidacin L1 to bind to LPS-derived carbohydrates from these strains. From the five strains of *P. syringae* tested, LMG 2222 and LMG 5456 were found to be highly susceptible to putidacin L1 with killing down to concentrations of 8.3 and 22 nM, respectively. DC3000 and NCPPB 2563 showed complete resistance to putidacin L1 and LMG1247 was highly tolerant (killing down to 0.6 μ M). Binding of putidacin L1 to the isolated LPS-derived polysaccharides of the above mentioned strains was tested by ITC. Large saturable heats of binding were observed for putidacin L1 and the LPS-derived polysaccharides from LMG 5456 and LMG 2222, while no binding was observed between putidacin L1 and the LPS-derived polysaccharides from LMG 1247, 2563 or DC3000 (Figure 6-16). Thus, there is excellent correlation between putidacin L1 cell killing and the binding of LPS-derived polysaccharide indicating that like pyocin L1, putidacin L1 utilises LPS as a surface receptor. Although *P. syringae* O-antigens are diverse relative to CPA, the incorporation of D-rhamnose is widespread and seemingly almost universal in strains of this species (284,285). Interestingly, in cases where D-rhamnose is not a component of *P. syringae* LPS, L-rhamnose is present (284). As with pyocin L1 we utilised ITC to characterise the binding affinity of putidacin L1 for D-rhamnose, in comparison with D-mannose and L-rhamnose.

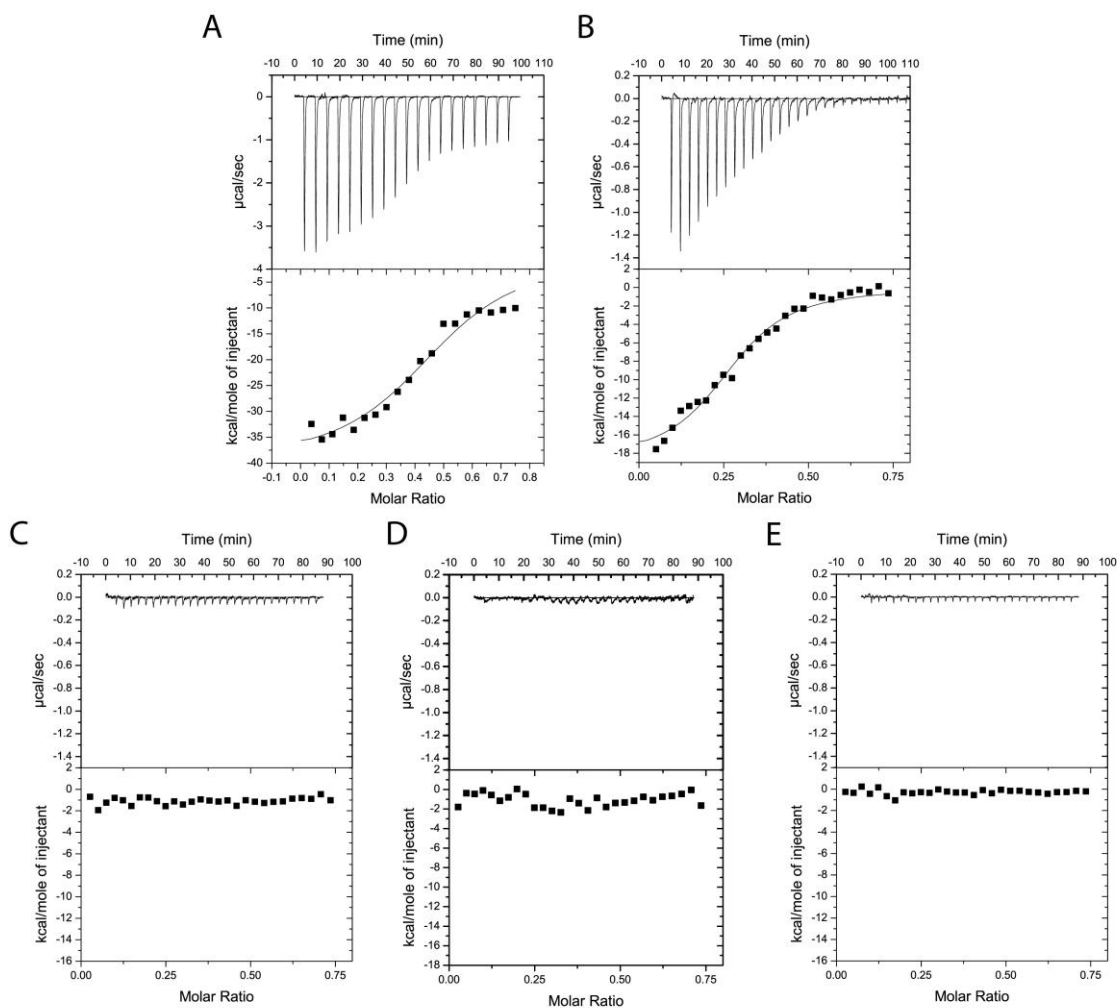


Figure 6-16 Putidacin L1 binds strongly to LPS-derived polysaccharides from susceptible but not tolerant or resistant *P. syringae* isolates.

ITC isotherm of LPS-derived polysaccharides (3 mg ml^{-1}) from strains highly sensitive to putidacin L1: A) *P. syringae* LMG 2222, B) *P. syringae* LMG 5456 titrated into putidacin L1 ($60 \mu\text{M}$). Large, saturable heats are indicative of binding. LPS-derived polysaccharides (3 mg ml^{-1}) from strains non-sensitive to putidacin L1: C) *P. syringae* NCPPB 2563, D) *P. syringae* DC3000, or highly tolerant E) *P. syringae* LMG 1247 to putidacin L1, show no heats of binding when titrated into putidacin L1 ($60 \mu\text{M}$).

Putidacin L1 exhibited an affinity of 5-10 mM for D-rhamnose, which is comparable to that of pyocin L1, and approximately 10-fold stronger than its affinity for D-mannose (Figure 6-17-A/B). No binding of L-rhamnose to putidacin L1 was observed (Figure 6-17-C).

Interestingly, it was found that pyocin L1 is able to weakly inhibit strains of *P. syringae*, and the killing spectrum (but not the potency) of pyocin L1 and putidacin L1 is identical. This observation combined with the specificity of putidacin L1 for D-rhamnose, strongly suggests that it also binds to a D-rhamnose containing O-antigen, which is structurally

distinct from CPA. Indeed branched D-rhamnose O-antigens are common in *P. syringae* (284,285). Our data for both pyocin L1 and putidacin L1 indicate that D-rhamnose containing O-antigens are utilised as surface receptors for lectin-like bacteriocins from *Pseudomonas* spp. This is an attractive hypothesis since the inclusion of D-rhamnose in the lipopolysaccharides from members of this genus is widespread and could form an important component of the genus specific activity of this group of bacteriocins.

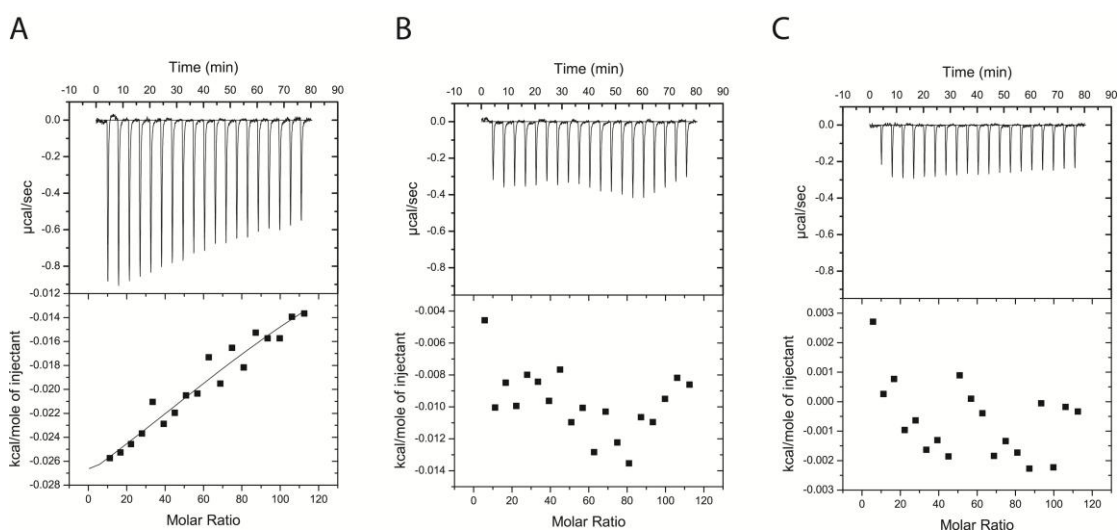


Figure 6-17 Putidacin L1 shows specificity for D-rhamnose, compared with D-mannose.

A) ITC isotherm of D-rhamnose (50 mM) titrated into putidacin L1 (0.1 mM). Weakly saturable heats are indicative of binding with modest affinity ($K_d \sim 5\text{-}10$ mM). B) ITC isotherm of D-mannose (50 mM) titrated into putidacin L1 (0.1 mM). Binding is undetectable under reaction conditions. C) ITC isotherm of L-rhamnose (50 mM) titrated into putidacin L1 (0.1 mM). Binding is undetectable under reaction conditions.

6.9 Discussion

In this work it was shown that pyocin L1 targets susceptible cells through binding to the CPA component of LPS and that primary recognition of the CPA occurs through binding of D-rhamnose at the conserved QxDxNxVxY sugar binding motifs of the C-terminal lectin domain. These data show the ability of both pyocin L1 and putidacin L1 to recognise D-rhamnose containing carbohydrates is an important component of their ability to target sensitive strains of *Pseudomonas* spp. The use of the O-antigen as a primary receptor differentiates the lectin-like bacteriocins from other multidomain bacteriocins such as colicins and S-type pyocins (colicin-like bacteriocins) which generally utilise outer

membrane proteins as their primary cell surface receptors (66). However, the recent discovery that the pore forming colicin N, which binds core LPS sugars as a cell surface receptor, suggests this may be a more widespread phenomena (12).

The colicin-like bacteriocins also possess a flexible, or natively disordered N-terminal region that is thought to pass through the lumen of a co-receptor and interact with the periplasmic Tol or Ton complexes that mediate translocation of the bacteriocin across the outer membrane (1,66). The lack of such a flexible N-terminal region in the lectin-like bacteriocins suggests that either they do not need to cross the outer membrane in order to mediate their cytotoxicity or they do so by a mechanism that is fundamentally different to the diverse family of colicin-like bacteriocins. Given the extensive structural homology between the lectin-like bacteriocins and plant lectins it seems likely that these bacteriocins share a common ancestor with plant lectins and from an evolutionary perspective are unrelated to the colicin-like bacteriocins.

In addition to O-antigen recognition, additional factors, as yet to be determined, are clearly also important in strain and species specificity among the lectin-like bacteriocins. Indeed, recent work from Ghequire et. al. has shown through domain swapping experiments that for putidacin L1 (LlpA_{BW}) and the homologous lectin-like bacteriocin LlpA_{1PF-5} from *Pseudomonas fluorescens*, species specificity is governed by the identity of the N-terminal lectin domain (100). Thus, in view of these and our own data it seems likely that the C-terminal lectin domain of this class of bacteriocins plays a general role in the recognition of D-rhamnose containing O-antigens, with the N-terminal domain interacting with species-specific factors and thus determining the precise species and strain specificity of these bacteriocins. Although there are few clues as to how the lectin-like bacteriocins ultimately kill susceptible cells, this work has established a clear role for the C-terminal MMBL domain of these proteins. The roles of the N-terminal MMBL domain and the C-terminal extension, which are conserved in pyocin L1 and putidacin L1, remain to be discovered (100). However, from the previous work of Ghequire et. al., it is clear that all three of these regions are required for killing of susceptible cells.

Interestingly, although rhamnose is frequently a component of plant and bacterial glycoconjugates, such as the rhamnolipids of *P. aeruginosa* (286) and pectic polysaccharides of plant cell walls (287), it is generally the L-form of this sugar that is found in nature. Although otherwise rare, D-rhamnose is found frequently as a

component of the LPS of plant pathogens and plant associated bacteria such as *P. syringae* (284,285), *P. putida* (288), *Xanthomonas campestris* (289) and *Burkholderia spp.* (290), but is a relatively rare component of the O-antigens of animal pathogens such as *E. coli*, *Salmonella* and *Klebsiella* where D-mannose is a predominant component (291). It is interesting to speculate that since D-rhamnose is a common component of the LPS of bacterial plant pathogens, that some of the many lectins produced by plants may have evolved to target D-rhamnose as part of plant defence to bacterial pathogens. It is also interesting to note that *P. aeruginosa* which produces distinct LPS species containing the CPA or an O-specific antigen is an opportunistic pathogen of both plants and animals (292).

The specificity of lectin-like bacteriocins suggests that these protein antibiotics may be useful in combating plant pathogenic bacteria, either through the use of bacteriocin expressing biocontrol strains or by the production of transgenic plants engineered to express these proteins. The specific targeting mechanism described here, binding of D-rhamnose containing polymers, indicates that the lectin-like bacteriocins would not interact with either plant or animal cells, since these lack D-rhamnose containing glycoconjugates. In addition, these narrow spectrum antibiotics would leave the majority of the soil microbiome and the gut microbiome of plant-eating animals intact and so would be likely to have minimal environmental impact and minimal impact on animal health. The former property makes these proteins ideal for utilisation in the generation of bacterial resistant transgenic plants, while the latter property and the potency of these protein antibiotics could also make the use of lectin-like bacteriocins in the treatment of chronic multidrug-resistant *P. aeruginosa* infections in humans an attractive proposition.

7 Expression of bacteriocins in plants to provide resistance against bacterial pathogens

7.1 Introduction

The expression of non-endogenous proteins in plants, using GM technology, has created crop plants with resistance to a number of prokaryotic and eukaryotic pathogens (140). The most notable and widely utilised strategy is the creation of insect resistant plants expressing the Cry or Cyt toxins, naturally produced by the insect pathogen *B. thuringiensis* (293). Cry and Cyt toxins, form a crystalline coating around the *B. thuringiensis* spore, which dissolves upon ingestion of the spore by the insect gut. The Cry and Cyt toxins then oligomerise to form pores in the gut membrane, facilitating infection by the bacteria and ultimately killing the insect (294). These proteins have been engineered into a number of different crop plants, of which maize, cotton and soybean represent the most prominent examples (141). Crops expressing these toxins have been highly successful in decreasing the level of insect predation and the levels of chemical pesticides required to control this predation (295,296). While Cry and Cyt are utilised to combat insect pathogens rather than bacteria, like colicin and lectin-like bacteriocins these toxins are of bacterial origin and are expressed as a single polypeptide. Additionally, like these bacteriocins, Cry and Cyt toxins bind to specific receptors on the surface of their target cells (297). A variety of different Cry and Cyt toxins have been identified, with different ranges of activity towards different insect pathogens, relating to the natural host range of the *B. thuringiensis* from which they were isolated. These natural toxins have then been further engineered to enhance their host range and activity. Transgenic plants expressing these toxins are generally engineered to simultaneously produce multiple toxin variants, maximising the range of insect pests to which the plant is resistant and minimising the chance of insect pests developing toxin resistance (298). Similar strategies will ultimately need to be applied in the generation of bacteriocin expressing plants.

In addition to the commercially applied Cry and Cyt toxins, a number of studies in model plant systems have shown the engineering of plants to produce ribosomally encoded antimicrobial peptides, such as defensins has led to at least partial resistance to bacterial pathogens (299,300). However, no studies in which colicin or lectin-like bacteriocins have been used to create transgenic plants have been reported. The aim of the work presented in this chapter was to test the ability of the model plants *N. benthamiana* and

A. thaliana to express the bacteriocins discovered in chapters 3 and 6. These transgenic plants were then assessed for their ability to resist infection of bacteriocin susceptible strains of *P. syringae*.

7.2 Transient expression of bacteriocins in *N. benthamiana* leaves using agroinfiltration

To quickly assess the ability of the plants to produce active bacteriocins, the model plant *N. benthamiana* was used as a transient expression system. In order to achieve transformation, a culture of *Agrobacterium tumefaciens* GV3-101 (0.2-0.4 OD₆₀₀) containing the desired gene in a binary expression vector (see chapter 2 for details) was syringe infiltrated into the *N. benthamiana* leaf. The transformation machinery of the *Agrobacterium* cells was activated prior to infiltration by the addition of the plant wounding hormone acetosyringone. In the wild, *Agrobacterium* utilises the large Ti plasmid to genetically transform the host plant and induce gall formation to provide a habitat for the bacteria. The binary vector system developed for the genetic transformation of plants using *Agrobacterium* utilises machinery that was originally encoded by the Ti plasmid. The ability to transform the host is assisted by ingress into the plant tissues through a wound. In order to recognise plant wounding, *Agrobacterium* senses the plant wounding hormone acetosyringone and activates the expression of the Ti plasmid encoded transformation machinery (301).

A series of binary vectors were created for the bacteriocins syringacin M, syringacin L1 and putidacin L1, based on the gateway binary vector set designed by Nakagawa et. al. (147), as either untagged or C- or N-terminally 4xMyc or GFP tagged constructs (see Table 2-2 for details). These constructs were transformed into *N. benthamiana* and protein expression and localisation was monitored by activity assays, confocal microscopy and western blotting. Confocal microscopy of leaves transformed with the GFP tagged bacteriocins revealed strong fluorescence in syringacin M and putidacin L1 transformed leaves for both C and N-terminal fusions. Very low signal was observed for syringacin L1 constructs. Images for syringacin M and putidacin L1 are presented in Figure 7-1. Expression of the fusion protein was evenly distributed throughout the *Agrobacterium*

infiltrated area. However, significant variation in expression between the individual cells was observed, likely due to individual transformation events. Expression of both proteins was cytoplasmic. In epidermal cells, which possess a large central vacuole, expression was localised to the cell edges and surrounding the nucleus (shown in syringacin M-N GFP), while in mesophyll cells expression was generally distributed outside the chloroplasts (shown in syringacin M-C GFP). As the bacteriocin-GFP fusion proteins may be inactive activity assays were not performed.

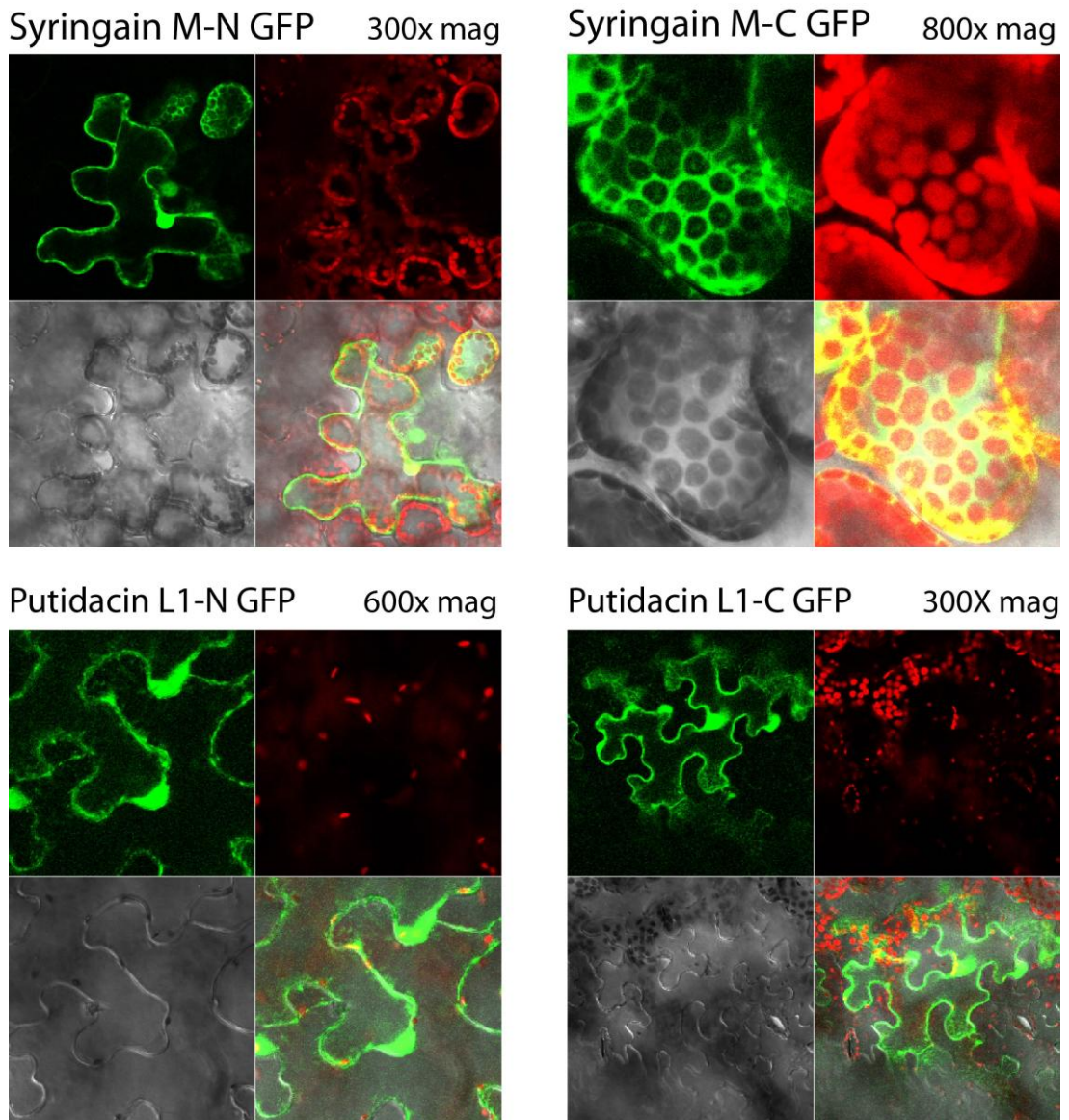


Figure 7-1 Confocal fluorescence microscopy of GFP-bacteriocin fusions transiently expressed in *N. benthamiana* leaves

Top left panel shows distribution of GFP-fusion protein in leaf section, top right panel shows chloroplast fluorescence at GFP excitation wavelength, bottom leaf shows bright field image of leaf, bottom right shows merged view of three images

In order to assess protein expression and cytotoxicity of leaf tissue from transformed *N. benthamiana* leaves were homogenised in buffer and protein concentration was normalised by Bradford assay (302). Clarified leaf homogenate was separated by SDS-PAGE and protein expression was assessed by western blotting. Leaf tissue extract from N- and C-terminally tagged syringacin L1, N-terminally tagged putidacin L1 and untagged syringacin M was tested (Figure 7-2-A). Strong bands were observed at approximately the correct Mw for C-terminally Myc tagged syringacin L1 and N-terminally Myc tagged putidacin L1. However for syringacin L1 an approximately 10 kDa lower band was also observed for the C-terminal construct suggesting some degradation of the protein was occurring. A comparatively weak single band was observed for N-terminal tagged syringacin L1. As expected no bands were observed for untransformed (wildtype) or syringacin M transformed leaf extracts.

Bacteriocin expression by transformed leaf tissue was also tested by *P. syringae* growth inhibition using the soft agar overlay assay. *N. benthamiana* leaf extract from plants transformed with GFP was used as a control. Growth inhibition was observed for all bacteriocin transformed leaf extracts, however the level of inhibition varied markedly between construct and bacteriocin. The level of growth inhibition against *P. syringae* strains tested is presented in Table 9-5 and zones of inhibition from the most sensitive strains are presented in. N-terminally tagged putidacin L1 expressing leaf extracts were highly active at inhibiting growth of the most susceptible strain, LMG 2222, to 1:125 dilution of neat leaf extract Figure 7-3. Syringacin M appeared to be less active or be less well expressed inhibiting growth to only a 1:5 dilution of neat extract. Interestingly, despite the seemingly higher levels of C-terminally tagged syringacin L1 determined by western blotting, extracts from the N-terminally tagged transformed plants were significantly more active, suggesting the location of the epitope tag may be effecting the activity and expression of the protein.

These data validate the ability of plants to express bacteriocins and show that putidacin L1 represents the best of the three proteins tested in terms of cytotoxic activity.

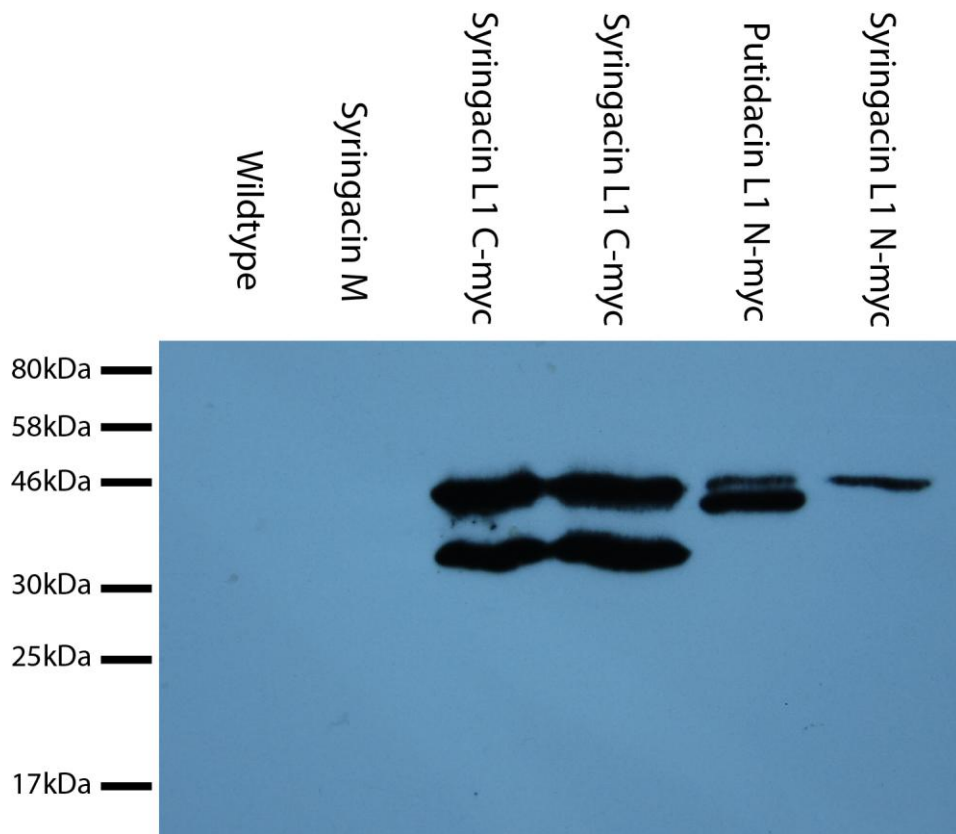
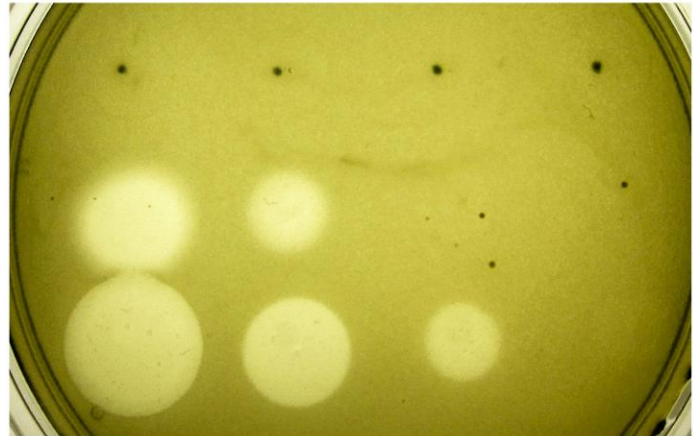


Figure 7-2 Confirmation of bacteriocin expression in *N. benthamiana* leaves my western blotting

cMyc western blot of SDS-PAGE separated leaf extract from *N. benthamiana* leaves transiently transformed with bacteriocin constructs. Band of appropriate size for the lectin-like bacteriocin 4XMyc fusion (35-40 kDa) are present in leaf extracts transformed with Myc fusion constructs.

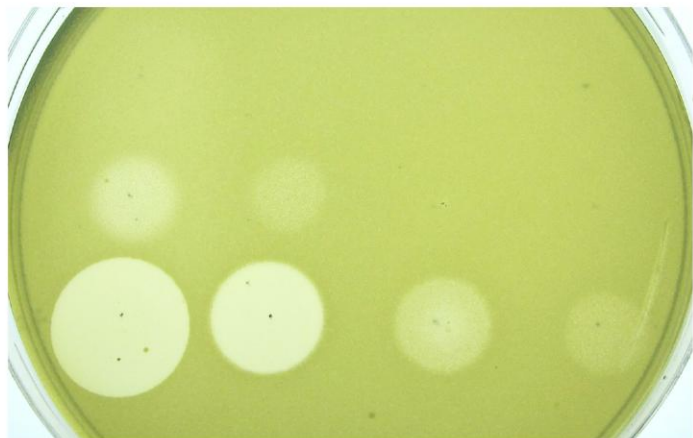
LMG5456

GFP
Syringacin M
Putidacin L1 N-myc



LMG5084

GFP
Syringacin M
Putidacin L1 N-myc



LMG2222

GFP
Syringacin M
Putidacin L1 N-myc

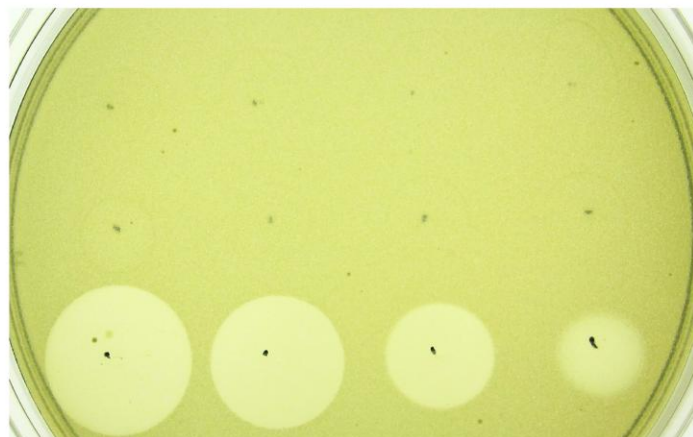


Figure 7-3 Growth inhibition of *P. syringae* by leaf extracts from bacteriocin transformed *N. benthamiana*,

5-fold serial dilutions of extracts from transformed *N. benthamiana* leaves (extract concentration normalised to 2 mg/ml) spotted onto King's B agar plates seeded with an overlay of a susceptible *P.*

syringae strains. Plates were incubated at 28 °C for 12 hours. Zones of inhibition are apparent from transformed leaf extract; the left hand spot is neat leaf extract with dilutions proceeding to the right. The GFP sample is a negative control consisting of extract from leaves transformed with a GFP only expression construct.

7.3 Creation of signal peptide bacteriocin fusion proteins for extracellular targeting

For the majority of its infection cycle *P. syringae* is known to act as an intercellular pathogen, persisting and proliferating in the apoplast without entering or causing widespread lysis of infected tissues (32). As such, it is likely that bacteriocins localised to the apoplast of transgenic plants would be more successful in providing resistance to this pathogen. As such, constructs were designed and created to encode syringacin L1, putidacin L1 and syringacin M fused to signal peptides derived from 4 proteins that are known to lead to successful excretion of proteins in plants. C-terminal GFP fusions and untagged bacteriocin/signal peptide fusions were expressed in *N. benthamiana* to test for expression, localisation and cytotoxic activity. Observation of expression and localisation of the GFP tagged constructs by confocal microscopy showed very low levels of fluorescence and as a result it was impossible to accurately judge if proteins were being transported to the apoplast. Additionally, plant extracts from the untagged and C-Myc tagged signal peptide fusion constructs did not exhibit any cytotoxic activity towards *P. syringae* strains. Consequently, it was decided not to pursue the extracellular targeting of bacteriocins further, but rather focus on assessing the disease resistant phenotype from cytoplasmically expressed bacteriocins. It is plausible however, that protein localisation may prove to be an important parameter for optimisation in future studies.

7.4 *P. syringae* infection of transiently transformed *N. benthamiana*

In order to obtain a preliminary indication of the ability of bacteriocin expressing plants to resist *P. syringae* infection, bacteriocin transformed leaves 72 hours post transformation

with either syringacin M or putidacin L1 constructs, were infected with 10^5 cfu.ml⁻¹ of *P. syringae* LMG5084, a strain that is susceptible to both syringacin and putidacin L1. Bacterial growth was then monitored by determination of the cfu.cm⁻¹ of leaf tissue at 24h, 48h and 8 day post infection (Figure 7-4-A). Both untransformed and GFP transformed leaves were used as a negative control and it was immediately apparent that infiltration with *Agrobacterium* prior to infection with LMG5084, greatly reduced the ability of *P. syringae* to proliferate (Figure 7-4-A). This effect was also apparent upon observation of disease symptoms of infected leaves, with untransformed leaves (wildtype) quickly succumbing to disease in the infected area, while leaves infiltrated with *Agrobacterium* containing either a bacteriocin or GFP expression construct displaying much milder disease symptoms (Figure 7-4-B). This is unsurprising given the known role of bacterial molecules like LPS and flagella proteins in activating the plant innate immune system via the recognition of pathogen associated molecular patterns (PAMPs) (303). The introduction of *Agrobacterium*, which has been shown to activate the innate immune system in *N. benthamiana*, a number of days prior to infection effectively primes the plants immune system to resist the *P. syringae* infection (304). This activation of the immune response makes this transient expression system less than ideal for testing the ability of bacteriocins to combat bacterial infection. Interestingly, while bacterial load isolated from infected plants expressing syringacin M didn't differ significantly from the control, no colonies were recovered from leaves expressing putidacin L1 (Figure 7-4-A). This effect was robust and reproducible over a number of experiments and a plausible explanation is that putidacin L1 is preventing bacterial infection *in planta*. As the colony counting procedure involves homogenisation of the plant tissue to extract the bacterial cells, an alternative explanation is that putidacin L1 is released during this procedure killed the bacterial cells. However, as *P. syringae* remained viable for an extended period (12 hour plus) in liquid culture containing recombinant putidacin L1, this hypothesis is less likely (see Section 6.3).

It should be noted that comparable lesions were observed for putidacin infected leaves compared to those infected with other constructs suggesting some level of infection. This observation is at odds with the lack of viable LMG5084 isolated from the leaf tissue. However the lesions observed may be due to hypersensitive cell death induced by the initial inoculation of bacteria rather than bacterial proliferation (305).

The results from the transient expression of bacteriocins in *N. benthamiana*, combined with the infection assay demonstrate that putidacin L1 represents a good target for the creation of stably transformed plants. It also demonstrates the transient expression system is unsuitable for subsequent infection to assess enhanced disease resistance. Therefore, as the first choice stably transformed Arabidopsis expressing putidacin L1 was selected as a model to assess the ability of putidacin L1 to impart disease resistance against *P. syringae*. Additionally, to test the variability of bacteriocin expression between plant species, the creation of stably transformed Arabidopsis expressing syringacin L1 was also attempted.

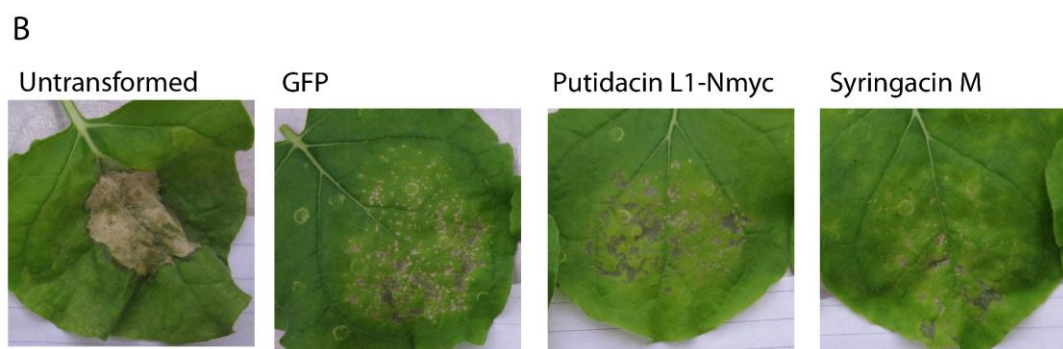
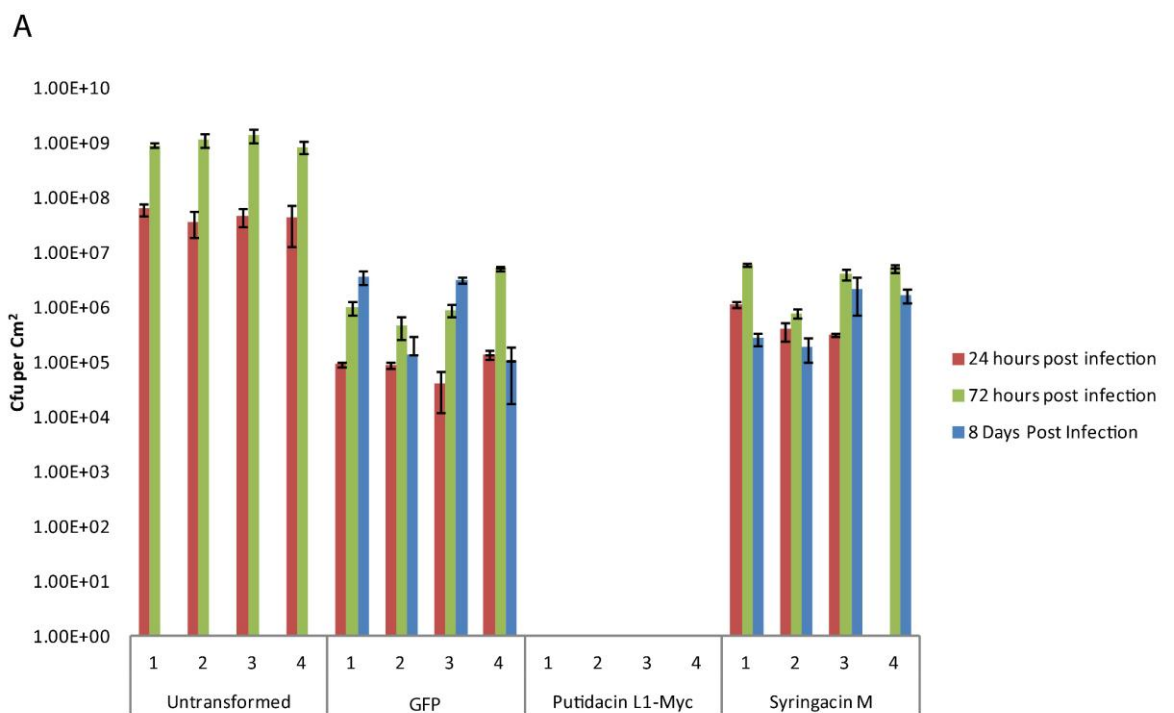


Figure 7-4 Infection of transiently transformed *N. benthamiana* leaves with *P. syringae* LMG 5084,
A) Cfu.cm^{-1} of *P. syringae* LMG 5084, recovered from leaves of untransformed, GFP or bacteriocin expressing *N. benthamiana* infected with 10^5 cfu.ml^{-1} at 24, 72 hours and 8 days post infection. Colony counts from untransformed leaves were impossible at 8 days due to desiccation of the infected area. B) Infection symptoms of leaves 8 days after infection with *P. syringae* LMG 5084.

7.5 Creation and characterisation of stable *A. thaliana* expressing putidacin and syringacin L1

7.5.1 Vector construction and characterisation

The binary vector pJO530 was selected for creating transgenic Arabidopsis (148). pJO530 constructs were created containing putidacin L1 with either a C- or N- terminal 4xMyc tag and tested for activity in *N. benthamiana* as described above. Interestingly, while leaf extracts from both constructs were shown to produce comparable levels of Myc tagged protein by western blot, only extract from leaves transformed with the N-terminally tagged construct showed cytotoxicity (Figure 7-5-A/B). Structural analysis of lectin-like bacteriocins has shown that the C-terminal 30 amino acids form a beta hairpin that are necessary for cytotoxic activity of the protein (14). As the 4xMyc tag consists of 60 amino acids representing 6.5 kDa of additional sequence, the fusion of the 4xMyc epitope to this region of the protein may interfere with its function. Alternatively, the N-terminal of lectin-like bacteriocins starts with a β -prism domain, which is more likely to play a structural role in the protein and may be less susceptible to inactivation by the fusion of the epitope (15). In the transient expression experiments only an N-terminally tagged putidacin L1 fusion was utilised. However, a C-terminally 4xMyc tagged syringacin L1 construct was utilised, which displayed greatly reduced activity compared to the N-terminal fusion. This suggests that C-terminal tags interfere with lectin-like bacteriocin killing. Large epitope tags provide a convenient and specific way of confirming protein expression in transgenic plants, via western blotting or immunofluorescence. However, as bacteriocins need to translocate across at least the outer membrane to elicit their cytotoxic effect, a large epitope tag represents unnecessary 'extra baggage' with the potential to reduce or abolish cytotoxic activity. As the success of transformation of an

untagged bacteriocin can be conveniently assessed with a simple cytotoxicity assay, the creation of untagged bacteriocin constructs, especially for poorly characterised bacteriocins is favourable. As such, for the creation of syringacin L1 expressing *Arabidopsis*, a pJO530 derived vector containing untagged syringacin L1 was created.

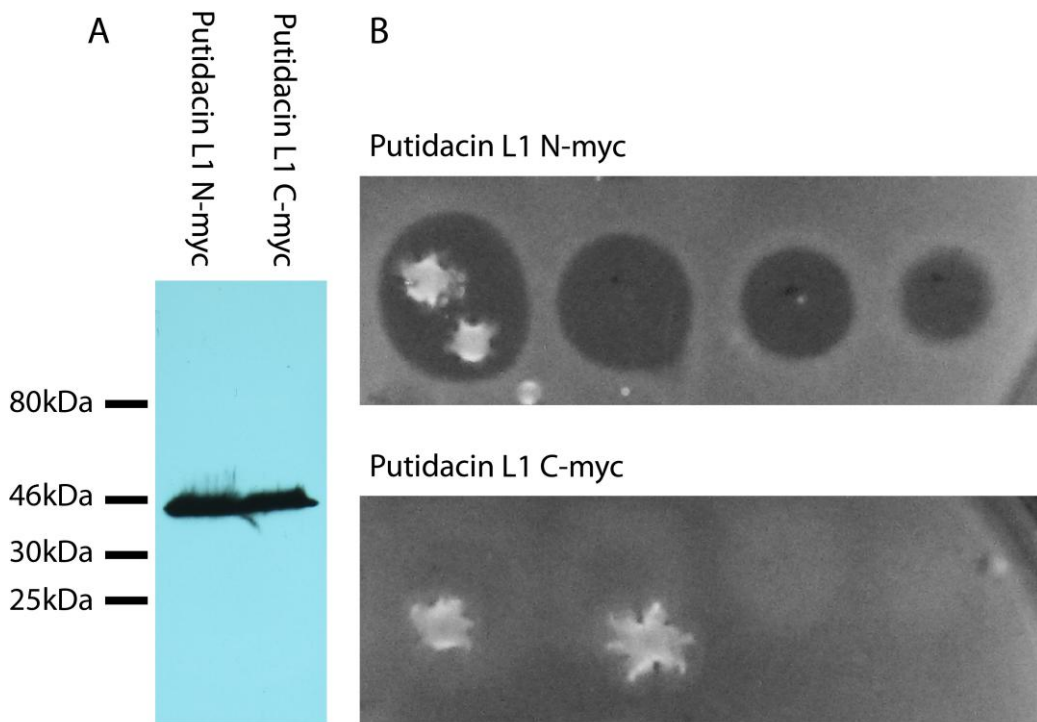


Figure 7-5 Expression and activity of C or N-terminally 4xMyc tagged putidacin L1 in *N. benthamiana*.

A) Anti-Myc Western blot of SDS-PAGE separated leaf extracts from *N. benthamiana* expressing putidacin L1 with either an N- or C-terminal Myc tag. B) Cytotoxic activity of Myc-tagged putidacin L1 expressing leaf extracts against *P. syringae* LMG 5084, visualised by soft agar overlay.

7.5.2 Transformation and characterisation of *Arabidopsis*

The glabrous (i.e. lacking leaf hairs) mutant strain GL-7 of *Arabidopsis thaliana* Col-0 was utilised for the creation of N-terminally 4xMyc tagged putidacin L1 and or untagged syringacin L1 expressing plants, by the floral dip method (197). Plants were grown to anthesis and dipped in *Agrobacterium* harbouring the appropriate pJO530 derived bacteriocin containing vector (Table 2-2). Plants were allowed set seed and dried seeds were collected and transformants selected for on MS-agar containing $25 \mu\text{g ml}^{-1}$ hygromycin B (the selection marker for pJO530). Successful transformants grew with an

analogous phenotype to wildtype seedlings on MS agar in the absence of selection, whereas the hygromycin sensitive seedlings (non-transformants) were visibly stunted and unable to produce a second set of leaves (Figure 7-6). Approximately 1-2 % of total seed from the floral dipped plants (T0 generation) displayed hygromycin resistance.

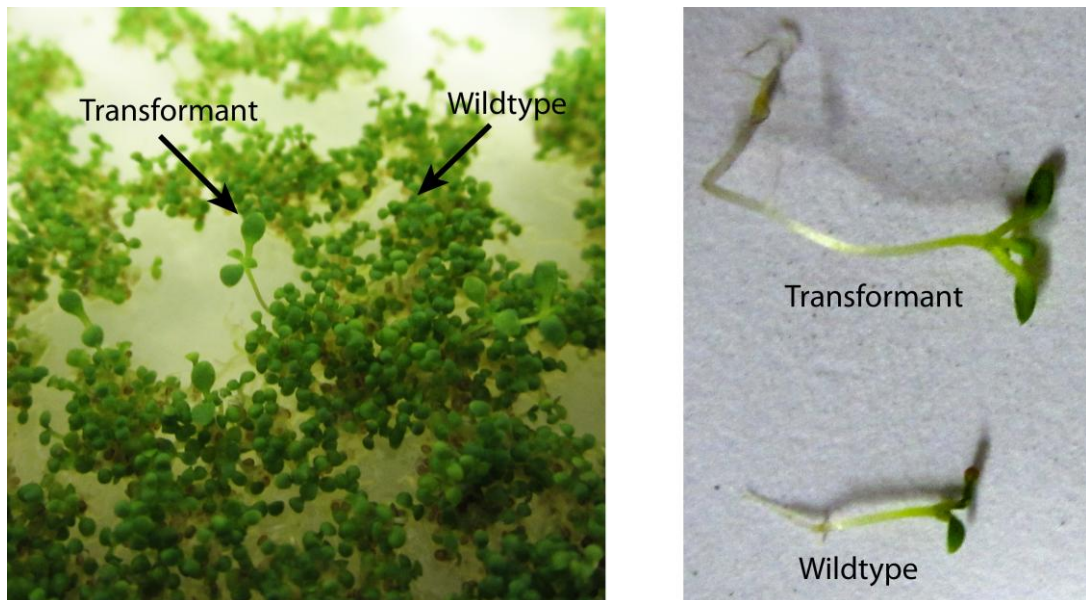


Figure 7-6 Phenotypic differences between wildtype and putidacin L1/syringacin L1 transformed Arabidopsis seedlings, selected on hygromycin agar.

Approximately 2% of seeds from floral dip transformation were resistant to hygromycin and grew normally on nutrient agar plates containing hygromycin. Non-transformed seeds were able to germinate and produce chlorophyll but were stunted and unable to grow significant roots or produce a second set of leaves.

Eight resistant seedlings for each bacteriocin were transferred to soil and grown under long day conditions to induce flowering. Leaf extract from these plants was tested for activity by western blotting and cytotoxicity assay. Plants from the syringacin L1 transformation exhibited only very weak activity against the most susceptible strain *P. syringae* Carlise 1, an environmental isolate isolated during this study, suggesting that only a low level of expression of active protein was occurring. The putidacin L1 transformed lines showed variable levels of expression by western blotting for the C-Myc epitope, with all lines showing significant activity in the cytotoxicity assay (Figure 7-7).

At this point due to their low expression level the syringacin L1 transformed plants were abandoned, while seed from the first 6 putidacin L1 transformed plants was collected, plated onto hygromycin selection as above and the ratio of sensitive to resistant progeny was analysed. As Arabidopsis are naturally self-pollinating these progeny, representing the T1 generation, should display a 3 to 1 resistant to sensitive ratio if transformation occurred through a single insertion event. Resistant/bacteriocin expressing plants from the T1 generation, with a single insertion will be heterozygous or homozygous for the bacteriocin gene. Progeny analysis revealed that lines 1, 2 and 6 displayed ratios sufficiently close to 3 to have resulted from a single insertion event. The 2.4 ratio of line 1 is somewhat lower, but as it appeared to have the best expression of all lines, so it was taken forward for further analysis. Line 4 exhibited a segregation ratio lower than three, suggestive of gene silencing. Lines 3 and 5 possessed morphological defects suggestive of insertion into a developmental gene; these lines were abandoned at this point. See Table 7-1 for progeny analysis.

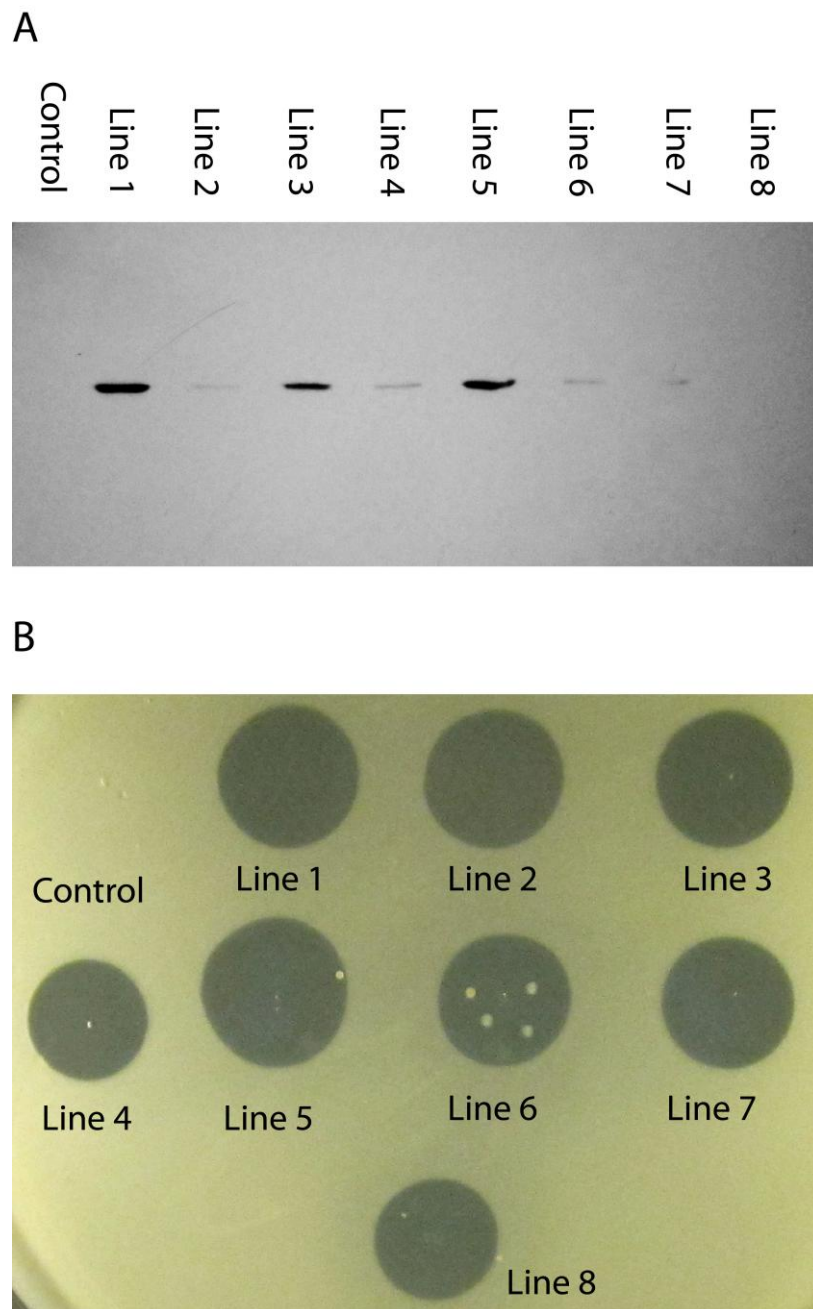


Figure 7-7 Expression of putidacin L1 N-Myc by T0 generation transformed Arabidopsis

A) Anti-Myc western blot of SDS-PAGE separated leaf extract, showing variable levels of expression between various transgenic nMyc-putidacin L1 expressing Arabidopsis lines (protein concentrations normalised by Bradford assay), B) Agar overlay spot test of cell lysate from T1 transgenic lines on LMG5084, showing significant cytototoxicity in all lines.

Table 7-1 Analysis of hygromycin resistance of T1 generation putidacin L1 N-Myc transformed Arabidopsis

Arabidopsis is self-fertilizing so a ratio of resistant to susceptible progeny of approximately 3:1 is indicative of a single cassette insertion event, which is desirable for the analysis of stable transgenic lines.

Line	Resistant	Susceptible	Ratio
1	180	74	2.4
2	366	111	3.3
3	315	83	3.8
4	125	14	8.9
5	-	-	-
6	145	50	2.9

The leaf extract from resistant T1 generation plants was tested for cytotoxicity by agar overlay assay to confirm that hygromycin resistance correlated with putidacin L1 expression Figure 7-9. All lines were found to have significant cytotoxicity towards *P. syringae* LMG5084. T1 generation plants were then grown under long day conditions to induce flowering and seed was collected. This seed representing the T2 generation was plated onto hygromycin selection to isolate lines homozygous for putidacin L1. Lines displaying progeny with a 100% resistant phenotype are homozygous; where as those with a 3:1 resistant to susceptible ratio are heterozygous for the insert. Lines 1(2), Line 2(1) and Line 6(1) were found to be homozygous and as such they were selected for infection assays. The expression of putidacin L1 as a percentage of total leaf protein was estimated by comparing the lowest dilution at which killing was observed on the cytotoxicity assay with the minimum inhibitory concentration of recombinant putidacin L1. Cytotoxicity was averaged over 6 different leaf sections with protein concentrations normalised by Bradford assay. Putidacin L1 was found to constitute between 0.02 and 0.06 % of total leaf protein (Figure 7-9).

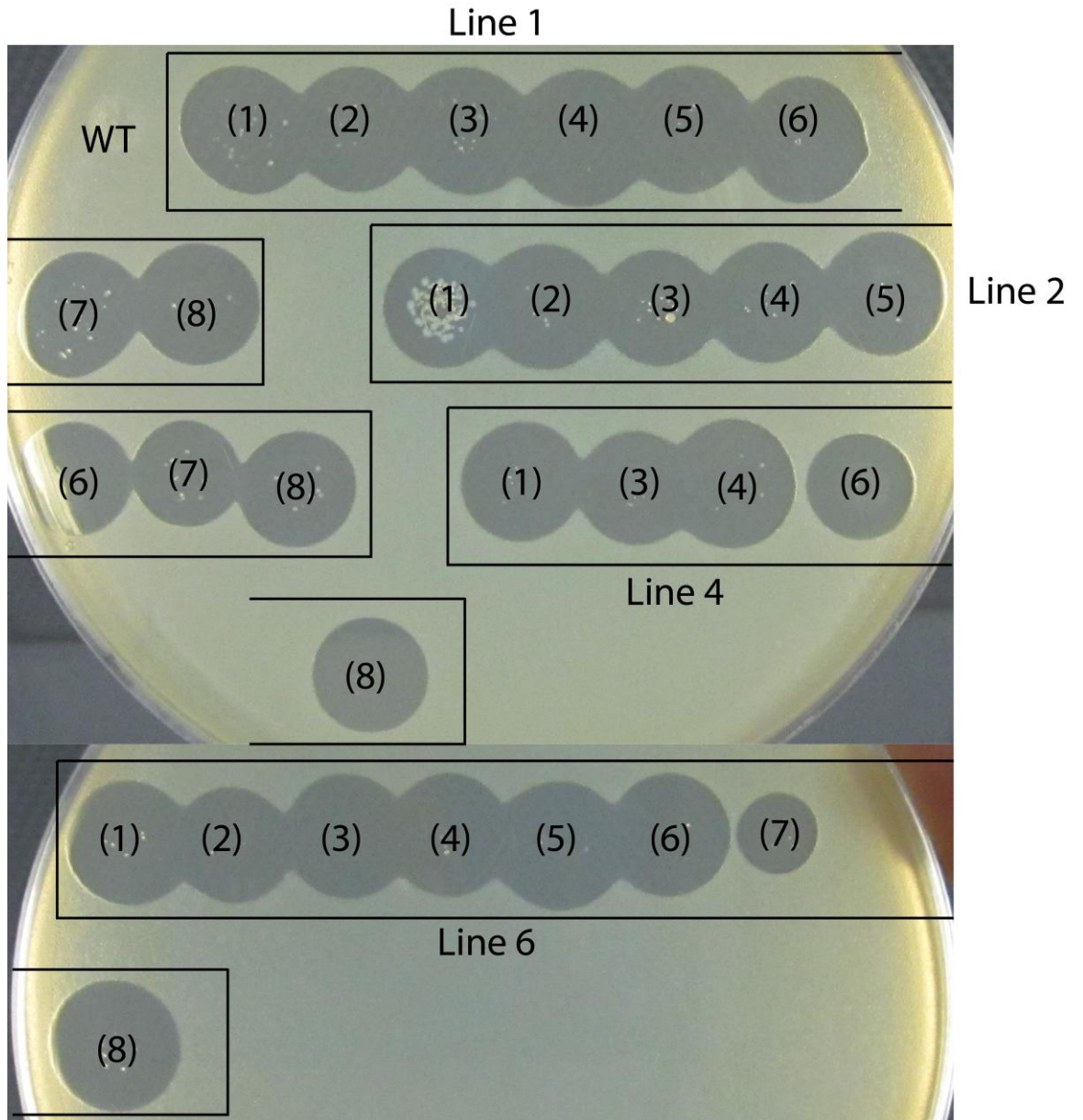


Figure 7-8 Expression putidacin L1 N-Myc by T1 generation transgenic Arabidopsis, assessed by spot test of leaf extract on LMG 5084.

Clarified leaf extract from T1 generation putidacin L1 N-Myc expressing transgenic Arabidopsis plants (lines 1, 2, 4 and 6) was spotted onto a Kings B agar plate overlain with soft agar containing the putidacin L1 susceptible indicator strain LMG5084. Expression of putidacin L1 in these lines was assessed qualitatively by the zone of inhibition produced by the extract. No inhibition was observed for untransformed (WT) extract, while significant activity of observed for all transgenic plants.

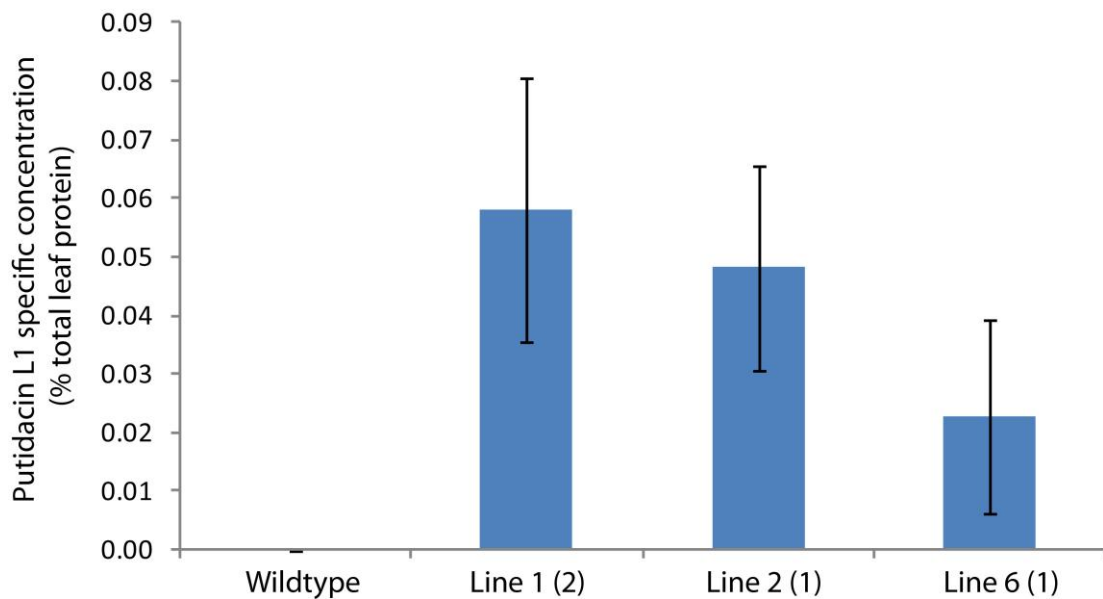


Figure 7-9 Putidacin L1 expression by putidacin L1 N-Myc T2 transgenic Arabidopsis

Expression of putidacin L1 N-Myc as was determined as a percentage of total leaf protein (determined by Bradford assay). 2-fold serial dilutions of transformed leaf extract were spotted on a Kings B agar plate overlain with a sensitive indicator strain. The minimum dilution at which inhibition was observed was compared to that for purified recombinant putidacin L1 to give putidacin L1 content of the extract. This was then normalised to the protein content of the leaf extract.

7.6 Putidacin L1 expressing Arabidopsis displays resistance to susceptible *P. syringae* strains

To assess the ability of the putidacin L1 expressing Arabidopsis to resist *P. syringae* infection, wildtype and transgenic Arabidopsis plants were challenged with infection by the three putidacin L1 susceptible *P. syringae* strains susceptible: LMG2222, LMG5084 and LMG5456. *P. syringae* at 10^5 , 10^6 and 10^7 cfu.ml⁻¹ was syringe infiltrated into Arabidopsis leaves and disease symptoms and bacterial proliferation was monitored. In initial experiments more mature (approximately 6 week old) Arabidopsis seedlings were utilised and plants were incubated at ambient humidity after infiltration. Under these conditions only minor disease symptoms were observed, with no obvious

distinction between wildtype and transformed lines. Additionally, bacterial counts from infected leaf tissue did not increase beyond 10^6 cfu.cm⁻¹, suggesting that the bacteria were incapable of infecting under these conditions.

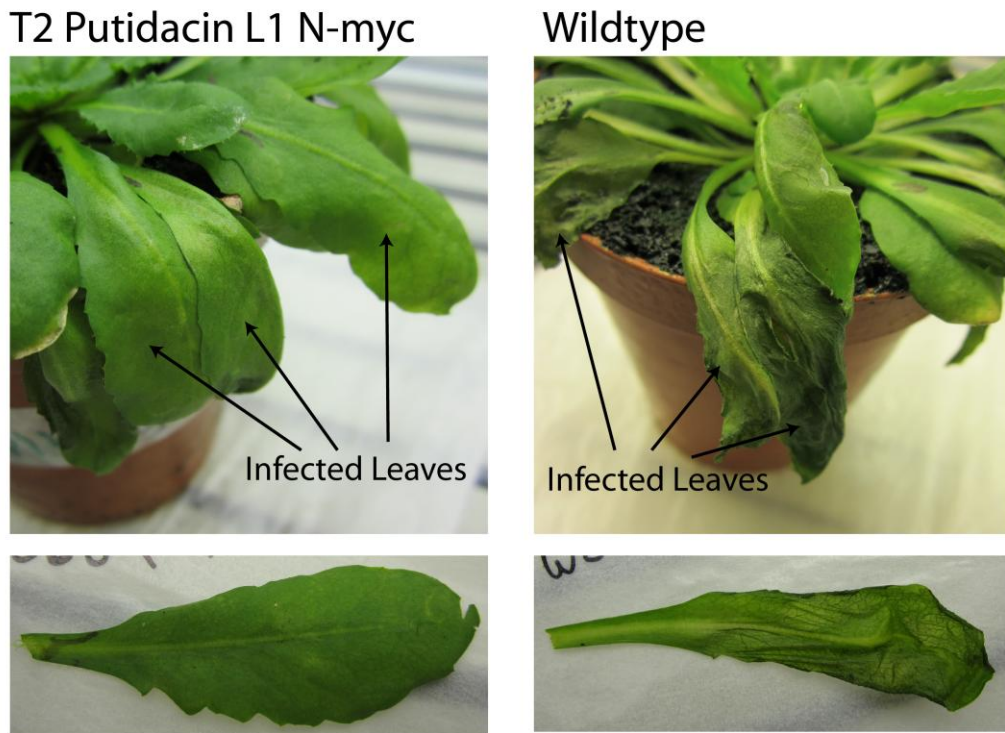
As a result the infection protocol was modified and younger plants (3-4 weeks old) were utilised with the plants kept at >95 % humidity (i.e. in water containing trays with a transparent lid) for 16 hours after infiltration. Under these conditions plants infected with 10^6 and 10^7 cfu.ml⁻¹ of LMG5456 and LMG5084 displayed significant symptoms of disease, whereas LMG2222 infected plants still only displayed a mild symptoms. Despite the lack of disease symptoms as a result of LMG2222 infection, bacterial proliferation was assessed using the colony count method. In agreement with the observed symptoms no significant proliferation was observed beyond inoculation levels in either wildtype or transgenic plants. For this reason infection assays using this strain were not pursued further. Disease symptoms from LMG5456 infection were the same as for wildtype and transgenic plants, potentially due to the relatively low potency of putidacin L1 against this strain (Table 6-1), or due to programmed cell death due to activation of the hypersensitive response (305). As a result of the lack of difference in symptoms between wildtype and transgenic plants, plants infected by LMG5456 were also not investigated further.

Infection of wildtype Arabidopsis by 10^6 or 10^7 cfu.ml⁻¹ LMG5084 resulted in rapid onset of disease symptoms; lesions formed on infected leaves, followed by desiccation and withering of the infected area, the infection was most pronounced in plants infected with 10^7 cfu.ml⁻¹. In contrast, putidacin L1 expressing infected plants showed only mild symptoms and no withering or desiccation of leaves, suggesting that infection was alleviated by expression of the bacteriocin (Figure 7-10-A). Bacterial load in infected leaves was monitored at 0, 24 and 48 hours. After 48 hours, infected leaves from the wildtype plants had desiccated to the point that extraction of material for sampling was difficult and the plant had begun to outgrow the infection.

Figure 7-10-B shows cfu.cm⁻¹ of infected leaf tissue at the sampled time points. At 0 hours (directly after infection), comparable numbers of bacteria were isolated from both wildtype and transgenic plants, showing inoculation levels were consistent. Both wildtype and transgenic plants inoculated at 10^5 cfu.ml⁻¹, did not exhibit bacterial proliferation above 10^5 cfu.cm⁻¹, which is indicative of an unsuccessful infection and consistent with

the lack of disease symptoms observed in the wildtype plants. Consistent with observed disease symptoms only a modest increase in bacterial numbers were observed in putidacin L1 transgenic plants inoculated with 10^6 or 10^7 cfu.ml⁻¹ of LMG5084, with neither surpassing 10^6 cfu.cm⁻¹. In contrast, high levels of proliferation were observed in wildtype plants inoculated with either 10^6 or 10^7 cfu.ml⁻¹ of LMG5084, with both inoculation levels reaching 10^8 cfu.cm⁻¹. This level of bacterial growth in leaf tissue is indicative of successful infection by the pathogen and is consistent with the disease symptoms observed. Lower levels of bacteria were isolated from leaves at the 48 hour time point for wildtype plants inoculated with 10^6 cfu.ml⁻¹, which was inconsistent with the high levels isolated at 24 hours. However, it was observed during this 48 h sampling of the 10^6 cfu.ml⁻¹ infected leaves, that the sampled tissue had begun to desiccate. When colony counts were performed on completely desiccated infected tissues from later time points, no viable *P. syringae* LMG5084 cells were not recovered, suggesting that *P. syringae* LMG5084 is unable to survive in the desiccated leaf tissue. This observation presents an explanation for the decline observed in the 10^6 cfu.ml⁻¹ cell counts. The decline in bacterial numbers from infected tissues at later stages of the infection makes it difficult to ascertain the susceptibility of the plants to bacterial infection by colony counts alone. To provide a qualitative assessment of the difference in susceptibility between wildtype and transgenic plants, the relative disease symptoms of infected plants was scored (Table 7-2). This analysis showed that in all cases wildtype plants exhibited more severe disease symptoms than the transgenic lines, with all infected leaves displaying severe disease symptoms (>40% of the infected leaf area displaying lesions). The three transgenic lines tested varied in the level of disease resistance they displayed, with no plants from line 1(2) displaying more than mild disease symptoms (<20% of the infected leaf area displaying lesions), but a number of infected leaves from lines 2(1) and 6(1) displaying moderate disease symptoms (>20% of the infected leaf area displaying lesions). This may be due to the lower levels of putidacin L1 expression in these lines (Figure 7-9).

A



B

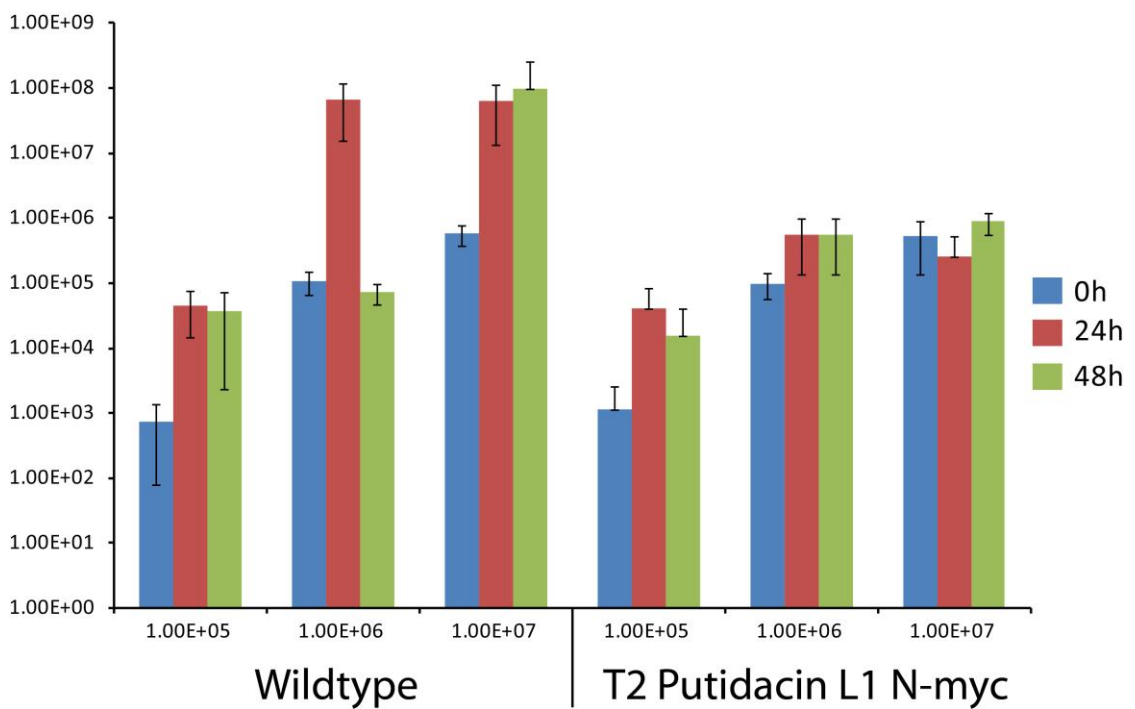


Figure 7-10 Infection by leaf infiltration of wildtype and putidacin L1 N-Myc (Line 1(2)) Arabidopsis, with *P. syringae* LMG5084

A) Difference in disease symptoms between wildtype and putidacin L1 Arabidopsis after 48 hours, when infected with 10^7 cfu.ml⁻¹ of *P. syringae* LMG 5084, obvious wilting and desiccation was observed for

wildtype plants, whereas transgenic plants appear generally healthy, B) cfu.cm⁻¹ recovered from wildtype and putidacin L1 expressing Arabidopsis at various time 0,24 and 48 hours post syringe infiltration with 10⁵ to 10⁷ cfu.ml⁻¹ of *P. syringae* LMG 5084.

Table 7-2 Qualitative assessment of disease symptoms on leaves of wildtype and putidacin L1 N-Myc Arabidopsis, infected with 10⁷ cfu.ml⁻¹ of *P. syringae* LMG5084

Infection was conducted in three replicate plants, all infected leaves were assessed for symptoms, + = leaves displaying at least moderate symptoms, - = leaves displaying less than moderate symptoms, % = total percentage of infected leaves displaying at least moderate disease symptoms, **Symptom notes:** All wildtype leaves exhibited severe symptoms, 1(2) only displayed mild symptoms or no symptoms, 2(1) and 6(1) leaves only displayed moderate symptoms at worst, **Symptoms Key:** Mild = Less than 20% of the leaf affected by lesions, Moderate = More than 20% of the leaf affected by lesions, Severe = Greater than 40% of leaf affected by lesions

10⁷ cfu.ml⁻¹ LMG5084 Infected leaves exhibiting at least moderate symptoms							
	Plant 1		Plant 2		Plant 3		
Line	+	-	+	-	+	-	%
Wt	12	0	12	0	10	0	100
1(2)	0	12	0	11	0	10	8
2(1)	4	8	6	4	5	6	45
6(1)	3	5	6	5	3	6	42

7.7 Discussion

In this work the expression of the bacteriocins syringacin M, syringacin L1 and putidacin L1 were assessed in *N. benthamiana* using a transient expression system. All three bacteriocins were shown to be expressed in this system, albeit to varying degrees. This result definitively shows that *N. benthamiana* is capable of expressing bacterially derived anti-microbial proteins, paving the way for futures studies. While it was outside the scope of this study, *N. benthamiana* represents an excellent model plant for infection studies and the creation of stable bacteriocin expressing lines would provide an ideal system for testing the efficacy of bacteriocins in mediating disease resistance.

Following the transient expression experiments, stably transformed Arabidopsis lines expressing putidacin L1 and syringacin L1 were created. While both these bacteriocins have the same overall structure and presumably a similar mechanism of killing (see chapter 6), they were produced by *in planta* to varying degrees. As putidacin L1 was expressed to high levels in Arabidopsis and is highly effective against a number of strains, the putidacin L1 expressing lines were utilised to test the efficacy of bacteriocin expression in mediating resistance to *P. syringae* infection. The results of these infection assays, in which putidacin L1 susceptible *P. syringae* strains were infiltrated into the leaves of Arabidopsis, showed that the transgenic plants exhibited both reduced disease symptoms and reduced bacterial proliferation compared to the wildtype plants. While expression of putidacin L1 was unable to completely eradicate *P. syringae* infection, these data provide a very positive indication of the ability of bacteriocins to increase disease resistance.

It should be stressed that these results are preliminary and significant further work is required to confirm these findings and improve on the model system utilised in this study. As discussed previously, during infection of leaf tissue *P. syringae* predominantly exists in the intercellular space (28), confocal microscopy of plants expressing GFP-bacteriocin fusion proteins showed bacteriocin expression to be cytoplasmically localised. This means that the bacteriocin produced is effectively partitioned away from the *P. syringae* cells during infection. This suggests that the disease resistance observed is due to the exposure of *P. syringae* to trace levels of putidacin L1 due to lysis of a small percentage of plant cells. Extracellular targeting of bacteriocins was attempted in this study through the fusion of bacteriocins to extracellular targeting peptides, however approach did not prove successful. Optimisation of this approach or development of a novel strategy for targeting bacteriocins to the extracellular space may improve the efficacy of bacteriocins in combatting *P. syringae* infection.

Assessment of disease resistance would also benefit from an improved infection assay. By necessity the *P. syringae* strains utilised for the infection assays needed to be sensitive to the bacteriocins used in the study and also able to cause infection in Arabidopsis. Due to the limited time and resources for this study, it was not possible to create transgenic plants other than Arabidopsis. *P. syringae* LMG5084 was the only putidacin L1 sufficiently susceptible strain available, capable of infecting Arabidopsis via leaf infiltration. *P.*

syringae LMG5084 was not particularly virulent, requiring an inoculum of at least 10^6 cfu.ml⁻¹ and careful control of infection conditions to establish and infection. Additionally, leaves successfully infected with *P. syringae* LMG5084 desiccated quickly with the bacteria not remaining viable. This made assessment of infection by colony counts difficult. The establishment of a model system in which the bacteria was highly susceptible to the bacteriocin utilised and also highly virulence to the host plant, would be highly beneficial for the development of this technology.

8 Concluding Remarks

8.1 Key findings of this study

The aims of this study were to identify bacteriocins produced by plant pathogenic bacteria, to characterise them and to apply this knowledge to the creation of transgenic plants with increased resistance to specific bacterial pathogens. The results presented in chapters 3, 6 do the former, identifying and characterising the novel bacteriocins syringacin M, syringacin L1 and putidacin L1 active against *P. syringae* species. While those in chapter 4 identify pectocins M1, M2 and P active against *Pectobacterium* spp.. Chapter 7 shows that the three bacteriocins active against *P. syringae* can be expressed *in planta* and that the expression of putidacin L1 leads to increased disease resistance. Chapter 6 represents a tangent to the main aims of the thesis, detailing the discovery of the ferredoxin uptake receptor (FupA) possessed by *Pectobacterium* spp.. The unusual ferredoxin receptor binding/translocation domain of the pectocins led to the identification of this system, which allows this phytopathogen to utilise host ferredoxin as an iron source during infection. While tangential to the stated aims of this work, this discovery represents a key finding of the study, with implications for protein import and virulence in both *Pectobacterium* and Gram-negative bacteria more generally. The work in chapters 3 and 4, also provides key insights into the function of the M-class colicin-like bacteriocins. Firstly, the structures of syringacin and pectocin M show that both recombination and diversifying evolution drive the generation of new specificities in this class of bacteriocin. Despite the lack of sequence identity between the receptor binding and translocation domains of colicin M and syringacin M, comparison of their crystal structures show that they both possess the same overall fold derived from a common ancestor. Additionally, preliminary data suggests that syringacin M requires the homologue of FhuA (the colicin M receptor) for killing, suggesting that the cell surface receptor is also conserved. Alternatively, the recombination derived fusion of the M-class cytotoxic domain with a plant-like ferredoxin allows the M-class pectocins to utilise FupA as their receptor. Prior to this study, the crystal structure of colicin M provided a picture of the M-class active site at odds with the mutagenic and biochemical data. The key catalytic residues in the structure are distant from each other and no bound metal ion (known to be essential for activity) was observed in the putative active site. The structure

of syringacin M, revealed the location and coordination of this metal ion and comparison of the active sites of pectocin M2 and syringacin M combined with docking simulations with its lipid II substrate, provide a credible model for substrate binding.

Phenotypic and structural analysis of the lectin-like bacteriocins in this study firmly established LPS as the cell surface receptor for these proteins. For pyocin L1 this was definitively shown to be the D-rhamnose homopolymer CPA, whereas for putidacin L1 while D-rhamnose was shown to be bound by the protein, the story may be more complex. At the time this study was conducted, no colicin-like bacteriocins had been shown to utilise LPS as a receptor, however the concurrent identification of LPS binding in colicin N suggests this may be a more widespread phenomena (12). In addition to the LPS receptor discovery, this study provides clues to the killing mechanism of the lectin-like bacteriocins. The observed septation defect after treatment with putidacin L1 and the increased putidacin L1 resistance of mutants for the outer-membrane stress regulator CpxA, suggests a cytotoxic mechanism localised to the bacterial outer envelope. The data presented in chapter 7 shows, for the first time, that colicin and lectin-like bacteriocins can be expressed *in planta* and that this expression does not lead to reproductive or phenotypic defects. Additionally, this work shows that expression of putidacin L1 in *Arabidopsis* leads to a quantifiable reduction in both the ability of susceptible bacteria to replicate in these plants and in the severity of disease symptoms. These data provide a sound basis for future work on the commercial exploitation of bacteriocins in this context.

In summary, this work represents an important advance in our theoretical and practical understanding of how bacteriocins from plant pathogens function. As illustrated in chapter 7, these proteins have considerable potential in controlling bacterial disease in plants, and that their utilisation for this purpose will require in-depth knowledge of how they function.

8.2 Future work

As with any scientific study of limited duration, there is never enough time or resources to 'finish the story' or characterise a system in adequate detail to satisfy the curiosity of the investigator. As such, future work is necessary to build on and increase our depth of

understanding of subjects of this study. This future work can be broadly classified into investigation of the function of bacteriocins and their associated nutrient uptake systems and development of bacteriocin expressing plants.

8.2.1 Analysis of the M-class active site

While *in silico* docking and analysis of the M-class catalytic domains provides a highly suggestive picture of the lipid II binding site, it would be beneficial to confirm this binding and elucidate the catalytic mechanism of lipid II hydrolysis. Co-crystallisation of M-class bacteriocins, mutated so they retain substrate binding but not hydrolysis activity, with lipid II or a substrate analogue provides a means of achieving this. However, due to the flexible nature of the active site of this enzyme, it may be difficult to capture the bound conformation *in crystallo*. NMR provides an alternative approach. While full length M-class bacteriocins are approximately 30 kDa in length, making NMR analysis non-trivial, a number of studies have shown that the isolated cytotoxic domain, at approximately 17 kDa, in size is still highly active (199,200). Assigning the HSQC spectra of this domain and mapping chemical shifts in the presence and absence of various substrate analogues would provide an alternative means of mapping the binding site.

8.2.2 Conformation of the syringacin M receptor

The syringacin M resistant *P. syringae* LMG5456 line MDC2, was shown by whole genome sequencing to possess a frame shift mutation in the gene encoding a homologue of the TonB-dependent receptor FhuA. FhuA from *E. coli* is the outer-membrane receptor for colicin M and as such it is likely that the homologue is the syringacin M receptor (207). This could be confirmed by complementation of the FhuA homologue mutation in MDC2, via transformation with a plasmid containing the gene or by allelic exchange. If the FhuA homologue proves to be the syringacin M receptor, expression, purification and co-crystallisation with the syringacin M receptor binding domain, would provide insight into receptor binding for this bacteriocin.

8.2.3 Characterisation of the Fup operon and its role in iron acquisition

In this study *Pectobacterium* was shown to utilise plant ferredoxin as an iron source and FupA was identified as the ferredoxin receptor. However, only limited characterisation of this system was performed. As homologues of the Fup operon are present in a number of mammalian pathogens, understanding how this system works in molecular detail has implications for bacterial virulence outside of *Pectobacterium spp.* (264). Determination of the structure of FupA and utilisation of a combination of crystallographic, mutagenic and NMR based approaches will allow for the binding interface between ferredoxin and FupA to be mapped. These data will provide information about the initial steps of iron acquisition, providing clues as to whether the entire ferredoxin or just its iron-sulphur cluster is imported. FupC, a large M16 zinc protease, present in the Fup operon may play a role in liberation of iron from ferredoxin once it has been imported into the periplasm. Expressing recombinant FupC and determining if it interacts with and cleaves plant ferredoxin would provide strong evidence for the importation of ferredoxin to the periplasm. Additionally, determining the localisation of FupC, by tagging and cell fractionation experiments, would confirm its presence in the periplasm. If FupC is shown to both cleave ferredoxin and be localised to the periplasm, analysis of Δ FupC strains for periplasmic ferredoxin accumulation and a lack of growth enhancement phenotype would provide definitive evidence for ferredoxin uptake by this system.

8.2.4 Determination of the molecular target of lectin-like bacteriocins

While this study showed that lectin-like bacteriocins utilise LPS as their cell surface receptor, given the potency of these molecules it seems unlikely that this LPS binding activity is solely responsible for their cytotoxic activity. Identification of the killing mechanism of these proteins would be useful from the point of view of understanding their function and also in potentially identifying a new target for antibiotic development. In addition to identifying genes responsible for LPS production as important for lectin-like bacteriocin killing, isolation of bacteria tolerant to putidacin L1 revealed that tolerance could be inferred by inactivation of CpxA. CpxA is the receptor component of a two-component sensor kinase, which has been extensively implicated in antibiotic sensitivity

(275,306). Investigation of differences in cellular regulation of wildtype and Δ CpxA strains, in the presence and absence of lectin-like bacteriocins, should provide clues to its killing mechanism.

8.2.5 Optimisation of lectin-like bacteriocin production in plants

This study shows that colicin and lectin-like bacteriocins can be successfully expressed in plants and that this expression leads to increased disease resistance. However, in order to pave the way for commercial exploitation of bacteriocins in this way additional work is required. Two immediate aspects which could be focused on are improving the infection model for assessing bacteriocin mediated resistance, and optimising the cellular localisation of expressed bacteriocins. As discussed in chapter 7, the model system developed during this study had a number of short comings. The susceptible *P. syringae* strain utilised was not particularly virulent in the Arabidopsis leaf infiltration assay and didn't survive in leaves which became desiccated due to infection. The infection system could be immediately improved by identifying *P. syringae* strains, which are putidacin L1 sensitive, highly virulent against Arabidopsis and with increased persistence in the leaf post infection. Alternatively, a different infection assay could be utilised. Flood inoculation of Arabidopsis seedlings grown on plant-nutrient agar with *P. syringae* has been shown to be an effective model system for assessing disease resistance and could be applied (307). As *P. syringae* is an intercellular pathogen, extracellular localisation of bacteriocins would put both bacteria and bacteriocin in the same place, intuitively, maximising the chance of disease resistance. As such more effort into engineering bacteriocin constructs facilitating the secretion of active bacteriocins would be beneficial.

9 Supplemental Data

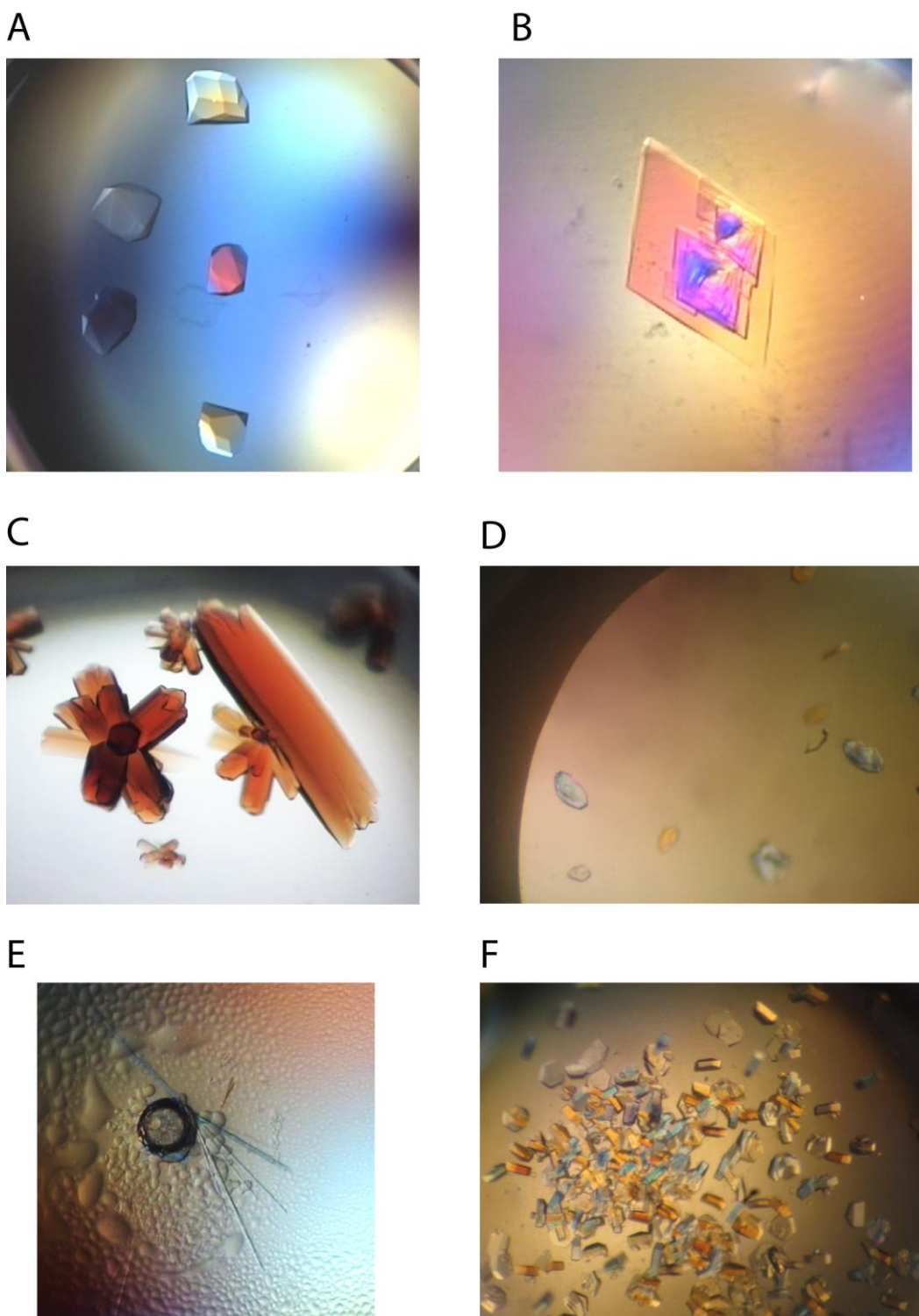


Figure 9-1 Images of protein crystals produced during this study.

A) The $P6_322$ crystal form of syringacin M, B) The $P2_1$ crystal form of syringacin M, C) The $P3_121$ crystal form of Pectocin M2, D) the $C222_1$ crystal form of pyocin L1, E) the $P2_1$ crystal form of FupA, F) crystals of putidacin L1 in the space group $P6_522$.

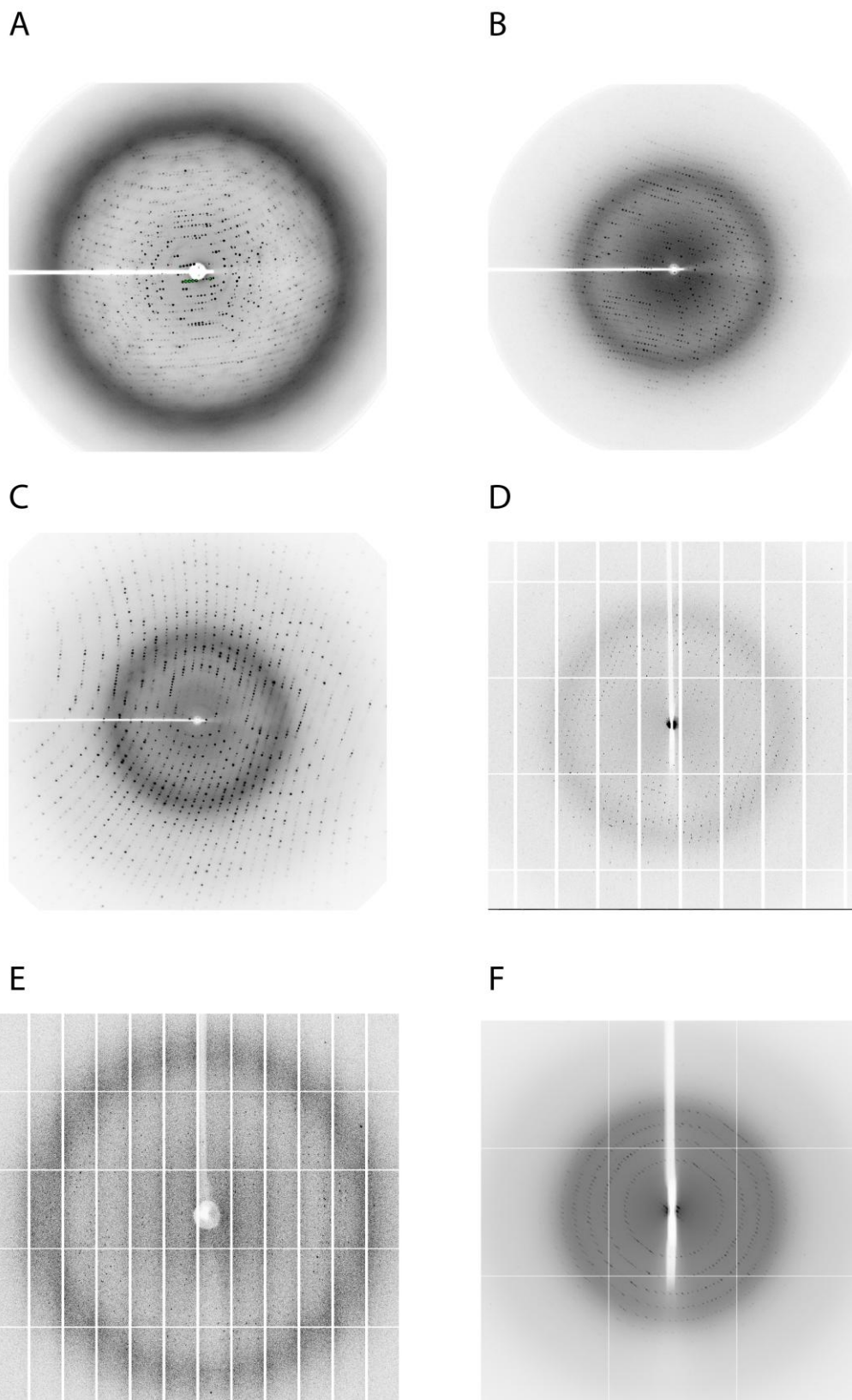


Figure 9-2 Examples of diffraction produced by protein crystals produced during this study.

A) The $P6_322$ crystal form of syringacin M, B) The $P2_1$ crystal form of syringacin M, C) The $P3_121$ crystal form of Pectocin M2, D) the $C222_1$ crystal form of pyocin L1, E) the $P2_1$ crystal form of FupA, F) crystals of putidacin L1 in the space group $P6_522$. (Detector distances and resolution limits vary between images)

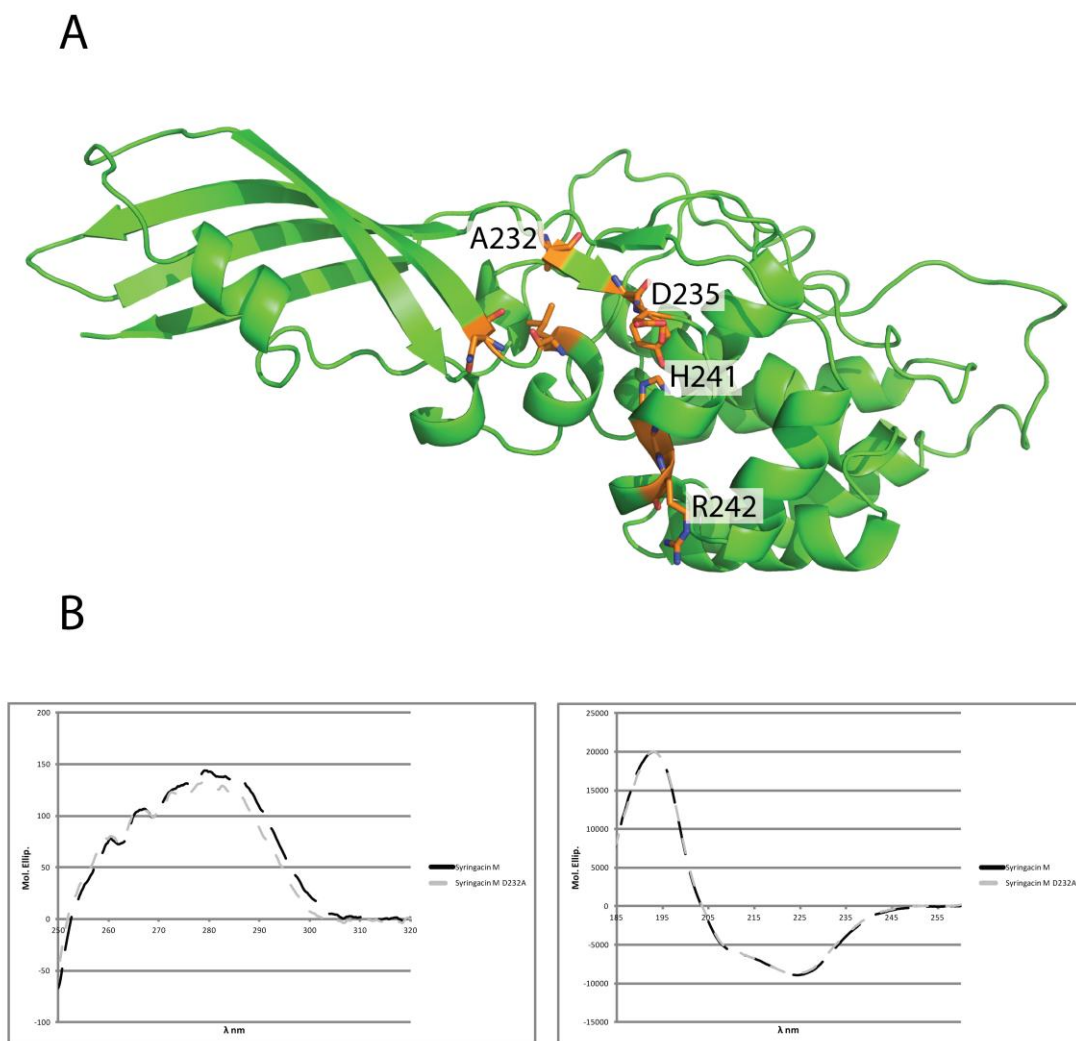


Figure 9-3 Structure and CD spectra of syringacin M D232A mutant

A) A schematic of the crystal structure of syringacin M D232A, at 3 Å, showing key catalytic residues (orange sticks) and the lack of an associated metal ion cofactor. B) Near and far CD spectra of wildtype and D232A mutant syringacin M show unperturbed secondary structure.

A

Hours	OD 600nm	Dilution	1	2	3	Average	cfu.ml
1	0.141	1.00E+05	3	7	3	4.33	4.33E+07
2	0.296	1.00E+05	7	6	8	7.00	7.00E+07
3	0.48	1.00E+06	1	1	4	2.00	2.00E+08
4	0.817	1.00E+06	7	4	3	4.67	4.67E+08
5	1.184	1.00E+06	8.5	14	11	11.17	1.12E+09

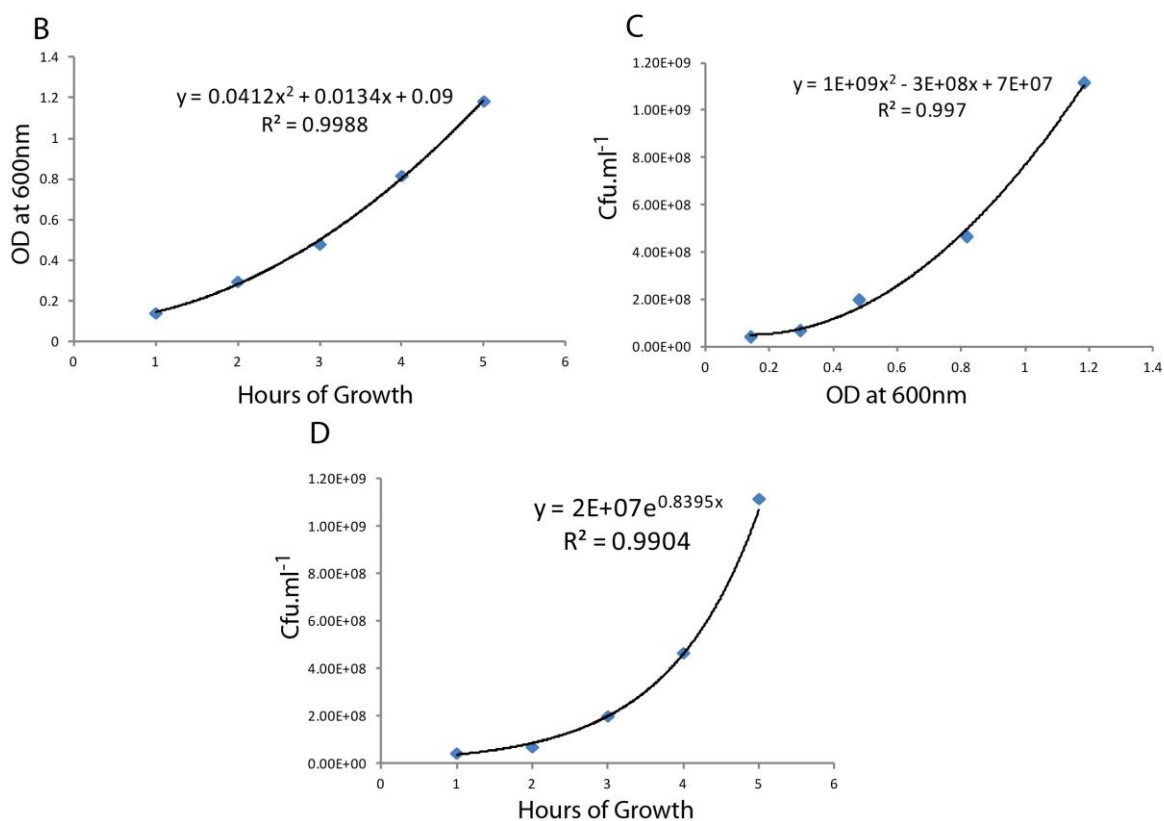


Figure 9-4 The relationship between OD₆₀₀ and Cfu.ml⁻¹ for *P. syringae* strain LMG2222

A) The OD₆₀₀ of an actively growing culture of LMG2222 was determined at hourly time points and cfu.ml⁻¹ were also determined by serial plating on Kings B agar. B to D) Graphical representation of relationship between optical density, hours of growth and Cfu.ml⁻¹. The relationship between Cfu.ml⁻¹ and OD₆₀₀ was used to determine the Cfu.ml⁻¹ for plant infection experiments.

Table 9-1 Production of antimicrobial compounds by *P. syringae* strains antagonistic to *P. syringae* growth

Colonies of *P. syringae* strains, shown in the far left column, were grown on Kings B agar in the presence of 0.25 µM Mitomycin C and lysed using chloroform vapours. Soft agar containing indicator strains was overlain over lysed colonies and zones of inhibition surrounding the colonies was observed after growth at 28 °C for 12 hours. Indicator strains, shown in top and middle rows, inhibited are shown as an X while those uninhibited are shown as an O. Except for the inhibition of LMG5456 by DC3000 and LMG1247 which was diffusible in the agar and shown to be due to syringacin M, all zones of inhibition were non-diffusible and suggestive of large phage tail type bacteriocins.

	DC3000	LMG5456	NCP PB 2563	NCP PB 3160	LMG 5060
DC3000	O	X (8mm)	O	O	O
NCP PB 1107	O	O	O	O	O
NCP PB 2563	O	O	O	O	O
NCP PB 3160	O	O	O	O	O
LMG 5060	O	O	O	O	O
LMG5456	O	O	O	O	O
LMG 2208	O	O	O	O	O
LMG 2222	O	O	O	O	O
LMG 1247	O	X (15mm)	O	O	O
LMG 5082	O	X (6mm)	O	O	O
LMG 5084	O	X (7mm)	X (7mm)	X (7mm)	X (7mm)

	LMG 2208	LMG 2222	LMG 1247	LMG 5082	LMG 5084
DC3000	O	O	O	X (7mm)	O
NCP PB 1107	O	O	O	X (7mm)	X (7mm)
NCP PB 2563	O	X (8mm)	O	X (8mm)	X (7mm)
NCP PB 3160	O	O	O	O	O
LMG 5060	O	O	O	X (7mm)	O
LMG5456	O	O	O	O	O
LMG 2208	O	O	O	O	O
LMG 2222	O	O	O	O	O
LMG 1247	O	X (7mm)	O	X (7mm)	X (7mm)
LMG 5082	O	X (7mm)	O	O	X (7mm)

LMG 5084	X (7mm)	O	X (7mm)	O	O
----------	---------	---	---------	---	---

Table 9-2 Susceptibility of *Pectobacterium* strains to pectocin M1 at different concentrations of bipryidine

LB plates +/- bipryidine were overlain with soft agar seeded with the strain of interest, purified pectocin M1 was spotted onto the plate before incubation at 28 °C for 12 hours. The effect of pectocin M1 was assessed. E = growth enhancement due to pectocin M1, I = inhibition to pectocin M1, I/E = an internal zone of growth enhancement surrounded by growth inhibition, - = pectocin M1 didn't effect growth of the strain. + symbol represents the relative size and clarity of the zone, ranging from + = small hazy zone to ++++ = large pronounced zone

	2,2 Bipryidine concentration						
	0 µM	100 µM		200 µM		400 µM	
LMG2444	-	E	++	-	-	-	-
LMG2374	-	I	++	I	+++	I	++++
LMG2391	-	I	+	I/E	+	I	++++
LMG2442	-	-	-	-	-	-	-
LMG2410	-	-	-	E	+	-	-
LMG2412	-	I/E	++	I	+++	I	++++
SCRI1043	-	-	-	I	+	I	++++
LMG2386	-	I	++	I	+++	I	++++
LMG2913	-	E	++	I/E	++	I/E	+++
LMG2375	-	I	+	I	+	I	++++

Table 9-3 Susceptibility of *Pectobacterium* strains to pectocin M2 at different concentrations of bipryidine

LB plates +/- bipryidine were overlain with soft agar seeded with the strain of interest, purified pectocin M2 was spotted onto the plate and plates before incubation at 28 °C for 12 hours. The effect of pectocin M2 was assessed. E = growth enhancement due to pectocin M2, I = inhibition to pectocin M2, I/E = an internal zone of growth enhancement surrounded by growth inhibition, - = pectocin M2 didn't effect growth of the strain. + symbol represents the relative size and clarity of the zone, ranging from + = small hazy zone to ++++ = large pronounced zone

	2,2 Bipryidine concentration				
	0 µM	100 µM	200 µM		400 µM
LMG2444	-	-	E	++	-
LMG2374	-	-	I	+	-
LMG2391	-	-	-	-	-
LMG2442	-	-	E	+	-

LMG2410	-	-	E	++	-	
LMG2412	-	E	++	E	++	++
SCRI1043	-	-	-		-	
LMG2386	-	-	-		-	
LMG2913	-	E	+	E	++	-
LMG2375	-	-	-			+

Table 9-4 Growth enhancement of *Pectobacterium* strains by spinach ferredoxin at different concentrations of bipryidine

LB plates +/- bipryidine were overlain with soft agar seeded with the strain of interest; purified spinach ferredoxin was spotted onto the plate before incubation at 28 °C for 12 hours. The effect of spinach ferredoxin was then assessed. E = growth enhancement due to spinach ferredoxin, - = spinach ferredoxin didn't effect growth of the strain. + symbol represents the relative size and clarity of the zone, ranging from + = small hazy zone to ++++ = large pronounced zone

	2,2 Bipryidine concentration				
	0 µM	100 µM	200 µM	400 µM	
LMG2444	-	-	-	-	
LMG2374	-	-	-	-	
LMG2391	-	-	-	-	
LMG2442	-	-	E	+ E	++++
LMG2410	-	-	E	+ E	++++
LMG2412	-	-	-	E	++++
SCRI1043	-	-	-	-	
LMG2386	-	-	-	-	
LMG2913	-	-	E	+ E	++++
LMG2375	-	-	-	-	

Table 9-5 Killing spectrum of leaf extracts from transiently transformed *N. benthamiana* leaves

Zone = diameter of zone in millimetres, Killing = clarity or turbidity of killing zone (+ = highly turbid zone, +++++ = no bacterial growth in zone), Purified Putidacin L1 was spotted at 2 mg.ml⁻¹. PL1 = putidacin L1, SL1 = syringacin L1

PL1 purified		GFP-control		Untagged MDC	
Zone	Killing	Zone	Killing	Zone	Killing

LMG 5084	20mm	+++++	-	8mm	++
LMG5456	18mm	++++	-	13mm	+++
LMG1247	12mm	+++	-	-	
LMG 5082	5mm	+	-	-	
LMG2222	20mm	+++++	-	5mm	+
LMG5060	-		-	-	
DC3000	-		-	-	
NCPPB1107	-		-	-	
NCPPB2563	-		-	-	
NCPPB3160	-		-	-	
LMG2208	-		-	-	

	SL1 C-Myc		PL1 N-Myc		SL1 C-Myc	
	Zone	Killing	Zone	Killing	Zone	Killing
LMG 5084	5mm	++	12mm	+++++	9mm	++++
LMG5456	-		13m	++++	6mm	++
LMG1247	-		-		-	
LMG 5082	-		-		-	
LMG2222	5mm	++	12mm	+++++	6mm	+++++
LMG5060	-		-		-	
DC3000	-		-		-	
NCPPB1107	-		-		-	
NCPPB2563	-		-		-	
NCPPB3160	-		-		-	
LMG2208	-		-		-	

10 References

1. Grinter, R., Roszak, A. W., Cogdell, R. J., Milner, J. J., and Walker, D. (2012) The Crystal Structure of the Lipid II-degrading Bacteriocin Syringacin M Suggests Unexpected Evolutionary Relationships between Colicin M-like Bacteriocins. *J. Biol. Chem.* **287**, 38876-38888
2. Barreteau, H., Tiouajni, M., Graille, M., Josseaume, N., Bouhss, A., Patin, D., Blanot, D., Fourgeaud, M., Mainardi, J.-L., Arthur, M., van Tilbeurgh, H., Mengin-Lecreulx, D., and Touzé, T. (2012) Functional and Structural Characterization of PaeM, a Colicin M-like Bacteriocin Produced by *Pseudomonas aeruginosa*. *J. Biol. Chem.* **287**, 37395-37405
3. Wojdyla, J. A., Fleishman, S. J., Baker, D., and Kleanthous, C. (2012) Structure of the ultra-high-affinity colicin E2 DNase–Im2 complex. *J. Mol. Biol.* **417**, 79-94
4. Cascales, E., Buchanan, S. K., Duché, D., Kleanthous, C., Lloubès, R., Postle, K., Riley, M., Slatin, S., and Cavard, D. (2007) Colicin biology. *Microbiol. Mol. Biol. Rev.* **71**, 158-229
5. Chandra, N. R., Ramachandraiah, G., Bachhawat, K., Dam, T. K., Surolia, A., and Vijayan, M. (1999) Crystal structure of a dimeric mannose-specific agglutinin from garlic: Quaternary association and carbohydrate specificity. *J Mol Biol* **285**, 1157-1168
6. Jakes, K. S., and Cramer, W. A. (2012) Border Crossings: Colicins and Transporters. *Annu. Rev. Genet.* **46**, null
7. Jakes, K. S., and Finkelstein, A. (2010) The colicin Ia receptor, Cir, is also the translocator for colicin Ia. *Mol. Microbiol.* **75**, 567-578
8. Kurisu, G., Zakharov, S. D., Zhalnina, M. V., Bano, S., Eroukova, V. Y., Rokitskaya, T. I., Antonenko, Y. N., Wiener, M. C., and Cramer, W. A. (2003) The structure of BtuB with bound colicin E3 R-domain implies a translocon. *Nat. Struct. Mol. Biol.* **10**, 948-954
9. Arnold, T., Zeth, K., and Linke, D. (2009) Structure and function of colicin S4, a colicin with a duplicated receptor-binding domain. *J. Biol. Chem.* **284**, 6403-6413
10. Buchanan, S. K., Lukacik, P., Grizot, S., Ghirlando, R., Ali, M. M. U., Barnard, T. J., Jakes, K. S., Kienker, P. K., and Esser, L. (2007) Structure of colicin I receptor bound to the R-domain of colicin Ia: implications for protein import. *EMBO J.* **26**, 2594-2604
11. Ghequire, M. G. K., and De Mot, R. (2014) Ribosomally encoded antibacterial proteins and peptides from *Pseudomonas*. *FEMS Microbiol. Rev.* **38**, 523-568
12. Johnson, C. L., Ridley, H., Marchetti, R., Silipo, A., Griffin, D. C., Crawford, L., Bonev, B., Molinaro, A., and Lakey, J. H. (2014) The antibacterial toxin colicin N binds to the inner core of lipopolysaccharide and close to its translocator protein. *Mol. Microbiol.* **92**, 440-452
13. Sano, Y. (1993) The inherent DNase of pyocin AP41 causes breakdown of chromosomal DNA. *J. Bacteriol.* **175**, 912-915
14. Ghequire, M. G. K., Garcia-Pino, A., Lebbe, E. K. M., Spaepen, S., Loris, R., and De Mot, R. (2013) Structural Determinants for Activity and Specificity of the Bacterial Toxin LlpA. *PLoS Pathog.* **9**, e1003199

15. McCaughey, L. C., Grinter, R., Josts, I., Roszak, A. W., Waløen, K. I., Cogdell, R. J., Milner, J., Evans, T., Kelly, S., Tucker, N. P., Byron, O., Smith, B., and Walker, D. (2014) Lectin-Like Bacteriocins from *Pseudomonas* spp. Utilise D-Rhamnose Containing Lipopolysaccharide as a Cellular Receptor. *PLoS Pathog.* **10**, e1003898
16. Cheng, Y.-S., Shi, Z., Doudeva, L. G., Yang, W.-Z., Chak, K.-F., and Yuan, H. S. (2006) High-resolution crystal structure of a truncated ColE7 translocation domain: implications for colicin transport across membranes. *J. Mol. Biol.* **356**, 22-31
17. Wang, Y.-T., Yang, W.-J., Li, C.-L., Doudeva, L. G., and Yuan, H. S. (2007) Structural basis for sequence-dependent DNA cleavage by nonspecific endonucleases. *Nucleic Acids Res.* **35**, 584-594
18. Devanathan, S., and Postle, K. (2007) Studies on colicin B translocation: FepA is gated by TonB. *Mol. Microbiol.* **65**, 441-453
19. Strange, R. N., and Scott, P. R. (2005) Plant Disease: A Threat to Global Food Security. *Annual Review of Phytopathology* **43**, 83-116
20. Esquinas-Alcazar, J. (2005) Protecting crop genetic diversity for food security: political, ethical and technical challenges. *Nat. Rev. Genet.* **6**, 946-953
21. Goodwin, S. B., Cohen, B. A., and Fry, W. E. (1994) Panglobal distribution of a single clonal lineage of the Irish potato famine fungus. *Proceedings of the National Academy of Sciences* **91**, 11591-11595
22. Evans, N., Baierl, A., Semenov, M. A., Gladders, P., and Fitt, B. D. L. (2008) Range and severity of a plant disease increased by global warming. *Journal of The Royal Society Interface* **5**, 525-531
23. Setubal, J. C., Moreira, L. M., and da Silva, A. C. R. (2005) Bacterial phytopathogens and genome science. *Curr. Opin. Microbiol.* **8**, 595-600
24. Toth, I. K., van der Wolf, J. M., Saddler, G., Lojkowska, E., Hélias, V., Pirhonen, M., Tsrör, L., and Elphinstone, J. G. (2011) *Dickeya* species: an emerging problem for potato production in Europe. *Plant Pathology* **60**, 385-399
25. Nivo-Liu, D. O., Ronald, P. C., and Bogdanove, A. J. (2006) *Xanthomonas oryzae* pathovars: model pathogens of a model crop. *Molecular Plant Pathology* **7**, 303-324
26. Qhobela, M., Clafin, L. E., and Nowell, D. C. (1990) Evidence that *Xanthomonas campestris* pv. *zeae* can be distinguished from other pathovars capable of infecting maize by restriction fragment length polymorphism of genomic DNA. *Canadian Journal of Plant Pathology* **12**, 183-186
27. Pan, Y. B., Grisham, M. P., and Burner, D. M. (1997) A Polymerase Chain Reaction Protocol for the Detection of *Xanthomonas albilineans*, the Causal Agent of Sugarcane Leaf Scald Disease. *Plant Disease* **81**, 189-194
28. O'Brien, H. E., Thakur, S., and Guttman, D. S. (2011) Evolution of Plant Pathogenesis in *Pseudomonas syringae*: A Genomics Perspective. *Annual Review of Phytopathology* **49**, 269-289
29. Scortichini, M., Marcelletti, S., Ferrante, P., Petriccione, M., and Firrao, G. (2012) *Pseudomonas syringae* pv. *actinidiae*: a re-emerging, multi-faceted, pandemic pathogen. *Molecular Plant Pathology* **13**, 631-640
30. Pérombelon, M. C. M. (2002) Potato diseases caused by soft rot erwinias: an overview of pathogenesis. *Plant Pathology* **51**, 1-12
31. Wilson, A. D., Lester, D. G., and Oberle, C. S. (2004) Development of Conductive Polymer Analysis for the Rapid Detection and Identification of Phytopathogenic Microbes. *Phytopathology* **94**, 419-431

32. Hirano, S. S., and Upper, C. D. (2000) Bacteria in the Leaf Ecosystem with Emphasis on *Pseudomonas syringae*—a Pathogen, Ice Nucleus, and Epiphyte. *Microbiol. Mol. Biol. Rev.* **64**, 624-653
33. Bull, C., De Boer, S., Denny, T., Firrao, G., Saux, M. F.-L., Saddler, G., Scortichini, M., Stead, D., and Takikawa, Y. (2010) Comprehensive list of names of plant pathogenic bacteria, 1980-2007. *Journal of Plant Pathology*, 551-592
34. Gardan, L., Shafik, H., Belouin, S., Broch, R., Grimont, F., and Grimont, P. A. D. (1999) DNA relatedness among the pathovars of *Pseudomonas syringae* and description of *Pseudomonas tremae* sp. nov. and *Pseudomonas cannabina* sp. nov. (ex Sutic and Dowson 1959). *Int. J. Syst. Bacteriol.* **49**, 469-478
35. Gardan, L., Cottin, S., Bollet, C., and Hunault, G. (1991) Phenotypic heterogeneity of *Pseudomonas syringae* van Hall. *Res. Microbiol.* **142**, 995-1003
36. Krzymowska, M., Konopka-Postupolska, D., Sobczak, M., Macioszek, V., Ellis, B. E., and Hennig, J. (2007) Infection of tobacco with different *Pseudomonas syringae* pathovars leads to distinct morphotypes of programmed cell death. *The Plant Journal* **50**, 253-264
37. Feil, H., Feil, W. S., Chain, P., Larimer, F., DiBartolo, G., Copeland, A., Lykidis, A., Trong, S., Nolan, M., Goltsman, E., Thiel, J., Malfatti, S., Loper, J. E., Lapidus, A., Detter, J. C., Land, M., Richardson, P. M., Kyrpides, N. C., Ivanova, N., and Lindow, S. E. (2005) Comparison of the complete genome sequences of *Pseudomonas syringae* pv. *syringae* B728a and pv. *tomato* DC3000. *Proc. Natl. Acad. Sci. U. S. A.* **102**, 11064-11069
38. Nomura, K., Melotto, M., and He, S.-Y. (2005) Suppression of host defense in compatible plant–*Pseudomonas syringae* interactions. *Curr. Opin. Plant Biol.* **8**, 361-368
39. Buell, C. R., Joardar, V., Lindeberg, M., Selengut, J., Paulsen, I. T., Gwinn, M. L., Dodson, R. J., Deboy, R. T., Durkin, A. S., Kolonay, J. F., Madupu, R., Daugherty, S., Brinkac, L., Beanan, M. J., Haft, D. H., Nelson, W. C., Davidsen, T., Zafar, N., Zhou, L., Liu, J., Yuan, Q., Khouri, H., Fedorova, N., Tran, B., Russell, D., Berry, K., Utterback, T., Van Aken, S. E., Feldblyum, T. V., D'Ascenzo, M., Deng, W.-L., Ramos, A. R., Alfano, J. R., Cartinhour, S., Chatterjee, A. K., Delaney, T. P., Lazarowitz, S. G., Martin, G. B., Schneider, D. J., Tang, X., Bender, C. L., White, O., Fraser, C. M., and Collmer, A. (2003) The complete genome sequence of the *Arabidopsis* and tomato pathogen *Pseudomonas syringae* pv. *tomato* DC3000. *Proceedings of the National Academy of Sciences* **100**, 10181-10186
40. Lavermicocca, P., Lonigro, S. L., Valerio, F., Evidente, A., and Visconti, A. (2002) Reduction of Olive Knot Disease by a Bacteriocin from *Pseudomonas syringae* pv. *ciccaronei*. *Appl. Environ. Microbiol.* **68**, 1403-1407
41. Vanneste, J. L., Cornish, D. A., Yu, J., and Stokes, C. A. (2013) First Report of *Pseudomonas syringae* pv. *actinidiae* the Causal Agent of Bacterial Canker of Kiwifruit on *Actinidia arguta* Vines in New Zealand. *Plant Disease* **98**, 418-418
42. Cameron, A., and Sarojini, V. (2014) *Pseudomonas syringae* pv. *actinidiae*: chemical control, resistance mechanisms and possible alternatives. *Plant Pathology* **63**, 1-11
43. Kim, H.-S., Ma, B., Perna, N. T., and Charkowski, A. O. (2009) Phylogeny and Virulence of Naturally Occurring Type III Secretion System-Deficient *Pectobacterium* Strains. *Appl. Environ. Microbiol.* **75**, 4539-4549

44. Kõiv, V., Andresen, L., and Mäe, A. (2010) AepA of *Pectobacterium* is not involved in the regulation of extracellular plant cell wall degrading enzymes production. *Mol. Genet. Genomics* **283**, 541-549
45. Ma, B., Hibbing, M. E., Kim, H.-S., Reedy, R. M., Yedidia, I., Breuer, J., Breuer, J., Glasner, J. D., Perna, N. T., Kelman, A., and Charkowski, A. O. (2007) Host Range and Molecular Phylogenies of the Soft Rot Enterobacterial Genera *Pectobacterium* and *Dickeya*. *Phytopathology* **97**, 1150-1163
46. Glasner, J. D., and Perna, N. T. (2004) Genomics of enterobacteriaceae. in *Encyclopedia of Genetics, Genomics, Proteomics and Bioinformatics* (Jorde, L., Little, P., Dunn, M., and Subramaniam, S. eds.), John Wiley & Sons, Ltd. pp
47. Glasner, J. D., Marquez-Villavicencio, M., Kim, H. S., Jahn, C. E., Ma, B., Biehl, B. S., Rissman, A. I., Mole, B., Yi, X., Yang, C. H., Dangl, J. L., Grant, S. R., Perna, N. T., and Charkowski, A. O. (2008) Niche-Specificity and the Variable Fraction of the *Pectobacterium* Pan-Genome. *Mol. Plant. Microbe Interact.* **21**, 1549-1560
48. Czajkowski, R., Pérombelon, M. C. M., van Veen, J. A., and van der Wolf, J. M. (2011) Control of blackleg and tuber soft rot of potato caused by *Pectobacterium* and *Dickeya* species: a review. *Plant Pathology* **60**, 999-1013
49. Liu, H., Coulthurst, S. J., Pritchard, L., Hedley, P. E., Ravensdale, M., Humphris, S., Burr, T., Takle, G., Brurberg, M.-B., Birch, P. R. J., Salmond, G. P. C., and Toth, I. K. (2008) Quorum Sensing Coordinates Brute Force and Stealth Modes of Infection in the Plant Pathogen *Pectobacterium atrosepticum*. *PLoS Pathog.* **4**, e1000093
50. Holeva, M. C., Bell, K. S., Hyman, L. J., Avrova, A. O., Whisson, S. C., Birch, P. R., and Toth, I. K. (2004) Use of a pooled transposon mutation grid to demonstrate roles in disease development for *Erwinia carotovora* subsp. *atroseptica* putative type III secreted effector (DspE/A) and helper (HrpN) proteins. *Mol. Plant. Microbe Interact.* **17**, 943-950
51. Bell, K. S., Sebaihia, M., Pritchard, L., Holden, M. T. G., Hyman, L. J., Holeva, M. C., Thomson, N. R., Bentley, S. D., Churcher, L. J. C., Mungall, K., Atkin, R., Bason, N., Brooks, K., Chillingworth, T., Clark, K., Doggett, J., Fraser, A., Hance, Z., Hauser, H., Jagels, K., Moule, S., Norbertczak, H., Ormond, D., Price, C., Quail, M. A., Sanders, M., Walker, D., Whitehead, S., Salmond, G. P. C., Birch, P. R. J., Parkhill, J., and Toth, I. K. (2004) Genome sequence of the enterobacterial phytopathogen *Erwinia carotovora* subsp. *atroseptica* and characterization of virulence factors. *Proc. Natl. Acad. Sci. U. S. A.* **101**, 11105-11110
52. Perombelon, M. C., and Kelman, A. (1980) Ecology of the soft rot erwinias. *Annual Review of Phytopathology* **18**, 361-387
53. Marquez-Villavicencio, M. d. P., Groves, R. L., and Charkowski, A. O. (2011) Soft Rot Disease Severity Is Affected by Potato Physiology and *Pectobacterium* taxa. *Plant Disease* **95**, 232-241
54. Balogh, B., Jones, J. B., Momol, M. T., Olson, S. M., Obradovic, A., King, P., and Jackson, L. E. (2003) Improved Efficacy of Newly Formulated Bacteriophages for Management of Bacterial Spot on Tomato. *Plant Disease* **87**, 949-954
55. Rodrigues, C., Takita, M., Coletta-Filho, H., Olivato, J., Caserta, R., Machado, M., and de Souza, A. (2008) Copper resistance of biofilm cells of the plant pathogen *Xylella fastidiosa*. *Appl. Microbiol. Biotechnol.* **77**, 1145-1157
56. Mojzsis, S. J., Arrhenius, G., McKeegan, K., Harrison, T., Nutman, A., and Friend, C. (1996) Evidence for life on Earth before 3,800 million years ago. *Nature* **384**, 55-59

57. Riley, M. A., and Wertz, J. E. (2002) BACTERIOCINS: Evolution, ecology, and application. *Annu. Rev. Microbiol.* **56**, 117-137
58. Parret, A. H. A., and De Mot, R. (2002) Bacteria killing their own kind: novel bacteriocins of *Pseudomonas* and other γ -proteobacteria. *Trends Microbiol.* **10**, 107-112
59. Riley, M. A., and Wertz, J. E. (2002) Bacteriocin diversity: ecological and evolutionary perspectives. *Biochimie* **84**, 357-364
60. Holtsmark, I., Eijsink, V. G. H., and Brurberg, M. B. (2008) Bacteriocins from plant pathogenic bacteria. *FEMS Microbiol. Lett.* **280**, 1-7
61. Chavan, M., and Riley, M. (2007) Molecular evolution of bacteriocins in gram-negative bacteria. in *Bacteriocins: Ecology and Evolution* (Riley, M. A., and Chavan, M. A. eds.), Springer Berlin Heidelberg, Berlin. pp 19-43
62. Majeed, H., Lampert, A., Ghazaryan, L., and Gillor, O. (2013) The Weak Shall Inherit: Bacteriocin-Mediated Interactions in Bacterial Populations. *PLoS ONE* **8**, e63837
63. Baboolal, T. G., Conroy, M. J., Gill, K., Ridley, H., Visudtiphole, V., Bullough, P. A., and Lakey, Jeremy H. (2008) Colicin N Binds to the Periphery of Its Receptor and Translocator, Outer Membrane Protein F. *Structure* **16**, 371-379
64. Soelaiman, S., Jakes, K., Wu, N., Li, C., and Shoham, M. (2001) Crystal structure of colicin E3: Implications for cell entry and ribosome inactivation. *Mol. Cell* **8**, 1053-1062
65. Riley, M. A. (1998) Molecular mechanisms of bacteriocin evolution. *Annu. Rev. Genet.* **32**, 255-278
66. Kleanthous, C. (2010) Swimming against the tide: progress and challenges in our understanding of colicin translocation. *Nat. Rev. Microbiol.* **8**, 843-848
67. Riley, M. A. (1993) Molecular mechanisms of colicin evolution. *Mol. Biol. Evol.* **10**, 1380-1395
68. Braun, V., Patzer, S. I., and Hantke, K. (2002) Ton-dependent colicins and microcins: modular design and evolution. *Biochimie* **84**, 365-380
69. Michel-Briand, Y., and Baysse, C. (2002) The pyocins of *Pseudomonas aeruginosa*. *Biochimie* **84**, 499-510
70. Roh, E., Park, T.-H., Kim, M.-i., Lee, S., Ryu, S., Oh, C.-S., Rhee, S., Kim, D.-H., Park, B.-S., and Heu, S. (2010) Characterization of a new bacteriocin, carocin D, from *Pectobacterium carotovorum* subsp. *carotovorum* Pcc21. *Appl. Environ. Microbiol.* **76**, 7541-7549
71. Papadakos, G., Wojdyla, J. A., and Kleanthous, C. (2012) Nuclease colicins and their immunity proteins. *Q. Rev. Biophys.* **45**, 57-103
72. Pommer, A. J., Cal, S., Keeble, A. H., Walker, D., Evans, S. J., KuÈhlmann, U. C., Cooper, A., Connolly, B. A., Hemmings, A. M., and Moore, G. R. (2001) Mechanism and cleavage specificity of the HNH endonuclease colicin E9. *J. Mol. Biol.* **314**, 735-749
73. Walker, D. C., Georgiou, T., Pommer, A. J., Walker, D., Moore, G. R., Kleanthous, C., and James, R. (2002) Mutagenic scan of the H-N-H motif of colicin E9: implications for the mechanistic enzymology of colicins, homing enzymes and apoptotic endonucleases. *Nucleic Acids Res.* **30**, 3225-3234
74. Kleanthous, C., and Walker, D. (2001) Immunity proteins: enzyme inhibitors that avoid the active site. *Trends Biochem. Sci.* **26**, 624-631

75. Ng, C. L., Lang, K., Meenan, N. A. G., Sharma, A., Kelley, A. C., Kleanthous, C., and Ramakrishnan, V. (2010) Structural basis for 16S ribosomal RNA cleavage by the cytotoxic domain of colicin E3. *Nat. Struct. Mol. Biol.* **17**, 1241-1246
76. Masaki, H., and Ogawa, T. (2002) The modes of action of colicins E5 and D, and related cytotoxic tRNases. *Biochimie* **84**, 433-438
77. Walker, D., Moore, G. R., James, R., and Kleanthous, C. (2003) Thermodynamic consequences of bipartite immunity protein binding to the ribosomal ribonuclease colicin E3. *Biochemistry* **42**, 4161-4171
78. Buckle, A. M., Schreiber, G., and Fersht, A. R. (1994) Protein-protein recognition: Crystal structural analysis of a barnase-barstar complex at 2.0-Å resolution. *Biochemistry* **33**, 8878-8889
79. Farrance, O. E., Hann, E., Kaminska, R., Housden, N. G., Derrington, S. R., Kleanthous, C., Radford, S. E., and Brockwell, D. J. (2013) A Force-Activated Trip Switch Triggers Rapid Dissociation of a Colicin from Its Immunity Protein. *PLoS Biol.* **11**, e1001489
80. Braun, V., Schaller, K., and Wolff, H. (1973) A common receptor protein for phage T5 and colicin M in the outer membrane of Escherichia coli B. *Biochimica et Biophysica Acta (BBA) - Biomembranes* **323**, 87-97
81. Barreteau, H., Tiouajni, M., Graille, M., Josseaume, N., Bouhss, A., Patin, D., Blanot, D., Fourgeaud, M., Mainardi, J.-L., Arthur, M., van Tilbeurgh, H., Mengin-Lecreulx, D., and Touze, T. (2012) Functional and structural characterization of PaeM, a colicin M-like bacteriocin produced by Pseudomonas aeruginosa. *Journal of Biological Chemistry*
82. Barreteau, H., Bouhss, A., Fourgeaud, M., Mainardi, J.-L., Touzé, T., Gérard, F., Blanot, D., Arthur, M., and Mengin-Lecreulx, D. (2009) Human- and plant-pathogenic pseudomonas species produce bacteriocins exhibiting colicin M-like hydrolase activity towards peptidoglycan precursors. *J. Bacteriol.* **191**, 3657-3664
83. El Ghachi, M., Bouhss, A., Barreteau, H., Touzé, T., Auger, G., Blanot, D., and Mengin-Lecreulx, D. (2006) Colicin M exerts its bacteriolytic effect via enzymatic degradation of undecaprenyl phosphate-linked peptidoglycan precursors. *J. Biol. Chem.* **281**, 22761-22772
84. Braun, V., Schaller, K., and Wabl, M. R. (1974) Isolation, characterization, and action of colicin M. *Antimicrob. Agents Chemother.* **5**, 520-533
85. van Heijenoort, J. (2007) Lipid Intermediates in the Biosynthesis of Bacterial Peptidoglycan. *Microbiol. Mol. Biol. Rev.* **71**, 620-635
86. Breukink, E., and de Kruijff, B. (2006) Lipid II as a target for antibiotics. *Nature Reviews Drug Discovery* **5**, 321-323
87. Harkness, R. E., and Braun, V. (1989) Colicin M inhibits peptidoglycan biosynthesis by interfering with lipid carrier recycling. *J. Biol. Chem.* **264**, 6177-6182
88. Ölschläger, T., Turba, A., and Braun, V. (1991) Binding of the immunity protein inactivates colicin M. *Mol. Microbiol.* **5**, 1105-1111
89. Usón, I., Patzer, S. I., Rodríguez, D. D., Braun, V., and Zeth, K. (2012) The crystal structure of the dimeric colicin M immunity protein displays a 3D domain swap. *J. Struct. Biol.* **178**, 45-53
90. Gérard, F., Brooks, M. A., Barreteau, H., Touzé, T., Graille, M., Bouhss, A., Blanot, D., van Tilbeurgh, H., and Mengin-Lecreulx, D. (2011) X-Ray Structure and Site-Directed Mutagenesis Analysis of the Escherichia coli Colicin M Immunity Protein. *J. Bacteriol.* **193**, 205-214

91. Helbig, S., Hantke, K., Ammelburg, M., and Braun, V. (2012) CbrA Is a Flavin Adenine Dinucleotide Protein That Modifies the Escherichia coli Outer Membrane and Confers Specific Resistance to Colicin M. *J. Bacteriol.* **194**, 4894-4903
92. Grinter, R., Milner, J., and Walker, D. (2012) Ferredoxin containing bacteriocins suggest a novel mechanism of iron uptake in *Pectobacterium* spp. *PLoS ONE* **7**, e33033
93. Grinter, R., and Walker, D. (2014) Lipid II-Degrading M-Class Bacteriocins. in *Encyclopedia of Inorganic and Bioinorganic Chemistry*, John Wiley & Sons, Ltd. pp
94. Patzer, S. I., Albrecht, R., Braun, V., and Zeth, K. (2012) Structure and mechanistic studies of pesticin, a bacterial homolog of phage lysozymes. *J. Biol. Chem.*
95. Vollmer, W., Pils, H., Hantke, K., Hölftje, J. V., and Braun, V. (1997) Pesticin displays muramidase activity. *J. Bacteriol.* **179**, 1580-1583
96. Lukacik, P., Barnard, T. J., Keller, P. W., Chaturvedi, K. S., Seddiki, N., Fairman, J. W., Noinaj, N., Kirby, T. L., Henderson, J. P., Steven, A. C., Hinnebusch, B. J., and Buchanan, S. K. (2012) Structural engineering of a phage lysin that targets Gram-negative pathogens. *Proceedings of the National Academy of Sciences* **109**, 9857-9862
97. Parker, M. W., and Feil, S. C. (2005) Pore-forming protein toxins: from structure to function. *Prog. Biophys. Mol. Biol.* **88**, 91-142
98. Zhang, X. Y.-Z., Llobès, R., and Duché, D. (2010) Channel domain of colicin A modifies the dimeric organization of its immunity protein. *J. Biol. Chem.* **285**, 38053-38061
99. Bermejo, Ivan L., Arnulphi, C., Ibáñez de Opakua, A., Alonso-Mariño, M., Goñi, Félix M., and Viguera, Ana R. (2013) Membrane Partitioning of the Pore-Forming Domain of Colicin A. Role of the Hydrophobic Helical Hairpin. *Biophys. J.* **105**, 1432-1443
100. Ghequire, M. G. K., Garcia-Pino, A., Lebbe, E. K. M., Spaepen, S., Loris, R., and De Mot, R. (2013) Structural Determinants for Activity and Specificity of the Bacterial Toxin LlpA. *PLoS Pathog* **9**, e1003199-e1003199
101. Ghequire, M. G. K., Li, W., Proost, P., Loris, R., and De Mot, R. (2012) Plant lectin-like antibacterial proteins from phytopathogens *Pseudomonas syringae* and *Xanthomonas citri*. *Environ Microbiol Rep* **4**, 373-380
102. Ghequire, M. G. K., Loris, R., and De Mot, R. (2012) MMBL proteins: from lectin to bacteriocin. *Biochem. Soc. Trans.* **40**, 1553-U1433
103. Parret, A. H. A., Schoofs, G., Proost, P., and De Mot, R. (2003) Plant lectin-like bacteriocin from a rhizosphere-colonizing *Pseudomonas* isolate. *J Bacteriol* **185**, 897-908
104. Parret, A. H. A., Temmerman, K., and De Mot, R. (2005) Novel Lectin-Like Bacteriocins of Biocontrol Strain *Pseudomonas fluorescens* Pf-5. *Appl. Environ. Microbiol.* **71**, 5197-5207
105. Ghequire, M. G. K., Li, W., Proost, P., Loris, R., and De Mot, R. (2012) Plant lectin-like antibacterial proteins from phytopathogens *Pseudomonas syringae* and *Xanthomonas citri*. *Environmental Microbiology Reports*, no-no
106. Sharon, N. (2001) Lectins. in *eLS*, John Wiley & Sons, Ltd. pp
107. Sharon, N., and Lis, H. (2004) History of lectins: from hemagglutinins to biological recognition molecules. *Glycobiology* **14**, 53R-62R
108. Van Damme, E. J. M., Nakamura-Tsuruta, S., Smith, D. F., Ongenaert, M., Winter, H. C., Rouge, P., Goldstein, I. J., Mo, H., Kominami, J., Culerrier, R., Barre, A.,

- Hirabayashi, J., and Peumans, W. J. (2007) Phylogenetic and specificity studies of two-domain GNA-related lectins: generation of multispecificity through domain duplication and divergent evolution. *Biochem J* **404**, 51-61
109. Vasta, G. R., Nita-Lazar, M., Giomarelli, B., Ahmed, H., Du, S., Cammarata, M., Parrinello, N., Bianchet, M. A., and Amzel, L. M. (2011) Structural and functional diversity of the lectin repertoire in teleost fish: Relevance to innate and adaptive immunity. *Dev. Comp. Immunol.* **35**, 1388-1399
110. Kurimoto, E., Suzuki, M., Amemiya, E., Yamaguchi, Y., Nirasawa, S., Shimba, N., Xu, N., Kashiwagi, T., Kawai, M., Suzuki, E.-i., and Kato, K. (2007) Curculin Exhibits Sweet-tasting and Taste-modifying Activities through Its Distinct Molecular Surfaces. *J. Biol. Chem.* **282**, 33252-33256
111. Shimokawa, M., Fukudome, A., Yamashita, R., Minami, Y., Yagi, F., Tateno, H., and Hirabayashi, J. (2012) Characterization and cloning of GNA-like lectin from the mushroom *Marasmius oreades*. *Glycoconj. J.* **29**, 457-465
112. Hester, G., and Wright, C. S. (1996) The Mannose-specific bulb lectin from *Galanthus nivalis* (snowdrop) binds mono- and dimannosides at distinct sites. Structure analysis of refined complexes at 2.3 angstrom and 3.0 angstrom resolution. *J Mol Biol* **262**, 516-531
113. Noinaj, N., Guillier, M., Barnard, Travis J., and Buchanan, S. K. (2010) TonB-Dependent Transporters: Regulation, Structure, and Function. *Annu. Rev. Microbiol.* **64**, 43-60
114. Elfarash, A., Dingemans, J., Ye, L., Hassan, A. A., Craggs, M., Reimann, C., Thomas, M. S., and Cornelis, P. (2014) Pore-forming pyocin S5 utilizes the FptA ferripyochelin receptor to kill *Pseudomonas aeruginosa*. *Microbiology* **160**, 261-269
115. Kim, Y. C., Tarr, A. W., and Penfold, C. N. (2014) Colicin import into *E. coli* cells: A model system for insights into the import mechanisms of bacteriocins. *Biochimica et Biophysica Acta (BBA) - Molecular Cell Research* **1843**, 1717-1731
116. Hughes, C., Phillips, R., and Roberts, A. P. (1982) Serum resistance among *Escherichia coli* strains causing urinary tract infection in relation to O type and the carriage of hemolysin, colicin, and antibiotic resistance determinants. *Infect. Immun.* **35**, 270-275
117. Lazzaroni, J.-C., Dubuisson, J.-F., and Vianney, A. (2002) The Tol proteins of *Escherichia coli* and their involvement in the translocation of group A colicins. *Biochimie* **84**, 391-397
118. Krewulak, K. D., and Vogel, H. J. (2011) TonB or not TonB: is that the question? *Biochem. Cell Biol.* **89**, 87-97
119. Kleanthous, C. (2010) Translocator hunt comes full Cir-Col. *Mol. Microbiol.* **75**, 529-533
120. Bernadac, A., Gavioli, M., Lazzaroni, J.-C., Raina, S., and Llobès, R. (1998) *Escherichia coli* tol-pal Mutants Form Outer Membrane Vesicles. *J. Bacteriol.* **180**, 4872-4878
121. Grinter, R., Josts, I., Zeth, K., Roszak, A. W., McCaughey, L. C., Cogdell, R. J., Milner, J. J., Kelly, S. M., Byron, O., and Walker, D. (2014) Structure of the atypical bacteriocin pectocin M2 implies a novel mechanism of protein uptake. *Mol. Microbiol.* **93**, 234-246
122. Housden, N. G., Hopper, J. T. S., Lukoyanova, N., Rodriguez-Larrea, D., Wojdyla, J. A., Klein, A., Kaminska, R., Bayley, H., Saibil, H. R., Robinson, C. V., and Kleanthous,

- C. (2013) Intrinsically Disordered Protein Threads Through the Bacterial Outer-Membrane Porin OmpF. *Science* **340**, 1570-1574
123. Udho, E., Jakes, K. S., and Finkelstein, A. (2012) TonB-Dependent Transporter FhuA in Planar Lipid Bilayers: Partial Exit of Its Plug from the Barrel. *Biochemistry* **51**, 6753-6759
124. PilsI, H., and Braun, V. (1998) The Ton system can functionally replace the TolB protein in the uptake of mutated colicin U. *FEMS Microbiol. Lett.* **164**, 363-367
125. Walker, D., Mosbahi, K., Vankemmelbeke, M., James, R., and Kleanthous, C. (2007) The Role of Electrostatics in Colicin Nuclease Domain Translocation into Bacterial Cells. *J. Biol. Chem.* **282**, 31389-31397
126. Vidaver, A. K., Mathys, M. L., Thomas, M. E., and Schuster, M. L. (1972) Bacteriocins of the phytopathogens *Pseudomonas syringae*, *P. glycinea*, and *P. phaseolicola*. *Can. J. Microbiol.* **18**, 705-713
127. Chuang, D.-y., Chien, Y.-c., and Wu, H.-P. (2007) Cloning and expression of the *Erwinia carotovora* subsp. *carotovora* gene encoding the low-molecular-weight bacteriocin carocin S1. *J. Bacteriol.* **189**, 620-626
128. Chan, Y.-C., Wu, J.-L., Wu, H.-P., Tzeng, K.-C., and Chuang, D.-Y. (2011) Cloning, purification, and functional characterization of Carocin S2, a ribonuclease bacteriocin produced by *Pectobacterium carotovorum*. *BMC Microbiol.* **11**, 99
129. Lavermicocca, P., Lonigro, S. L., Evidente, A., and Andolfi, A. (1999) Bacteriocin production by *Pseudomonas syringae* pv. *ciccaronei* NCPPB2355. Isolation and partial characterization of the antimicrobial compound. *J. Appl. Microbiol.* **86**, 257-265
130. Sisto, A., Cipriani, M., Morea, M., Lonigro, S., Valerio, F., and Lavermicocca, P. (2010) An *Rhs*-like genetic element is involved in bacteriocin production by *Pseudomonas savastanoi* pv. *savastanoi*. *Antonie van Leeuwenhoek* **98**, 505-517
131. De Los Santos, P. E., Parret, A. H. A., and De Mot, R. (2005) Stress-related *Pseudomonas* genes involved in production of bacteriocin LlpA. *FEMS Microbiol. Lett.* **244**, 243-250
132. Ghequire, M. G. K., De Canck, E., Wattiau, P., Van Winge, I., Loris, R., Coenye, T., and De Mot, R. (2013) Antibacterial activity of a lectin-like *Burkholderia cenocepacia* protein. *MicrobiologyOpen* **2**, 566-575
133. Kerr, A., and Htay, K. (1974) Biological control of crown gall through bacteriocin production. *Physiological Plant Pathology* **4**, 37-44
134. Ellis, J. G., Kerr, A., Van Montagu, M., and Schell, J. (1979) *Agrobacterium*: genetic studies on agrocin 84 production and the biological control of crown gall. *Physiological Plant Pathology* **15**, 311-319
135. Moore, L. W., and Warren, G. (1979) *Agrobacterium Radiobacter* Strain 84 and Biological Control of Crown Gall. *Annual Review of Phytopathology* **17**, 163-179
136. Agarwal, V., Tikhonov, A., Metlitskaya, A., Severinov, K., and Nair, S. K. (2012) Structure and function of a serine carboxypeptidase adapted for degradation of the protein synthesis antibiotic microcin C7. *Proceedings of the National Academy of Sciences*
137. Davies, J. K., and Reeves, P. (1975) Genetics of resistance to colicins in *Escherichia coli* K-12: cross-resistance among colicins of group A. *J. Bacteriol.* **123**, 102-117
138. Expert, D., and Toussaint, A. (1985) Bacteriocin-resistant mutants of *Erwinia chrysanthemi*: possible involvement of iron acquisition in phytopathogenicity. *J. Bacteriol.* **163**, 221-227

139. Qaim, M. (2009) The Economics of Genetically Modified Crops. *Annual Review of Resource Economics* **1**, 665-694
140. Clive, J. (2012) Global status of commercialized biotech/GM crops: 2012. *ISAAA brief* **44**
141. Prado, J. R., Segers, G., Voelker, T., Carson, D., Dobert, R., Phillips, J., Cook, K., Cornejo, C., Monken, J., Grapes, L., Reynolds, T., and Martino-Catt, S. (2014) Genetically Engineered Crops: From Idea to Product. *Annu. Rev. Plant Biol.* **65**, 769-790
142. Fedoroff, N. V. (2010) The past, present and future of crop genetic modification. *New Biotechnology* **27**, 461-465
143. Paine, J. A., Shipton, C. A., Chaggar, S., Howells, R. M., Kennedy, M. J., Vernon, G., Wright, S. Y., Hinchliffe, E., Adams, J. L., Silverstone, A. L., and Drake, R. (2005) Improving the nutritional value of Golden Rice through increased pro-vitamin A content. *Nat Biotech* **23**, 482-487
144. Otten, L., Piotrowiak, G., Hooykaas, P., Dubois, M., Szegedi, E., and Schell, J. (1985) Identification of an *Agrobacterium tumefaciens* pTiB6S3 vir region fragment that enhances the virulence of pTiC58. *Molec. Gen. Genet.* **199**, 189-193
145. Stover, C. K., Pham, X. Q., Erwin, A. L., Mizoguchi, S. D., Warrenner, P., Hickey, M. J., Brinkman, F. S. L., Hufnagle, W. O., Kowalik, D. J., Lagrou, M., Garber, R. L., Goltry, L., Tolentino, E., Westbrook-Wadman, S., Yuan, Y., Brody, L. L., Coulter, S. N., Folger, K. R., Kas, A., Larbig, K., Lim, R., Smith, K., Spencer, D., Wong, G. K. S., Wu, Z., Paulsen, I. T., Reizer, J., Saier, M. H., Hancock, R. E. W., Lory, S., and Olson, M. V. (2000) Complete genome sequence of *Pseudomonas aeruginosa* PAO1, an opportunistic pathogen. *Nature* **406**, 959-964
146. Sarker, M. R., and Cornelis, G. R. (1997) An improved version of suicide vector pKNG101 for gene replacement in Gram-negative bacteria. *Mol. Microbiol.* **23**, 410-411
147. Nakagawa, T., Kurose, T., Hino, T., Tanaka, K., Kawamukai, M., Niwa, Y., Toyooka, K., Matsuoka, K., Jinbo, T., and Kimura, T. (2007) Development of series of gateway binary vectors, pGWBs, for realizing efficient construction of fusion genes for plant transformation. *Journal of Bioscience and Bioengineering* **104**, 34-41
148. Love, A. J., Geri, C., Laird, J., Carr, C., Yun, B.-W., Loake, G. J., Tada, Y., Sadanandom, A., and Milner, J. J. (2012) *Cauliflower mosaic virus* Protein P6 Inhibits Signaling Responses to Salicylic Acid and Regulates Innate Immunity. *PLoS ONE* **7**, e47535
149. Voinnet, O., Rivas, S., Mestre, P., and Baulcombe, D. (2003) An enhanced transient expression system in plants based on suppression of gene silencing by the p19 protein of tomato bushy stunt virus. *The Plant Journal* **33**, 949-956
150. Kaniga, K., Delor, I., and Cornelis, G. R. (1991) A wide-host-range suicide vector for improving reverse genetics in Gram-negative bacteria: inactivation of the blaA gene of *Yersinia enterocolitica*. *Gene* **109**, 137-141
151. Fyfe, J. A., Harris, G., and Govan, J. R. (1984) Revised pyocin typing method for *Pseudomonas aeruginosa*. *J. Clin. Microbiol.* **20**, 47-50
152. Clarke, T. B., Kawai, F., Park, S.-Y., Tame, J. R. H., Dowson, C. G., and Roper, D. I. (2009) Mutational analysis of the substrate specificity of *Escherichia coli* penicillin binding protein 4. *Biochemistry* **48**, 2675-2683
153. Lloyd, A. J., Gilbey, A. M., Blewett, A. M., De Pascale, G., El Zoeiby, A., Levesque, R. C., Catherwood, A. C., Tomasz, A., Bugg, T. D. H., Roper, D. I., and Dowson, C. G.

- (2008) Characterization of tRNA-dependent peptide bond formation by MurM in the synthesis of *Streptococcus pneumoniae* peptidoglycan. *J. Biol. Chem.* **283**, 6402-6417
154. Ramm, M., Lobe, M., and Hamburger, M. (2003) A simple method for preparation of D-rhamnose. *Carbohydr Res* **338**, 109-112
 155. Chaudhuri, R. R., Loman, N. J., Snyder, L. A. S., Bailey, C. M., Stekel, D. J., and Pallen, M. J. (2008) xBASE2: a comprehensive resource for comparative bacterial genomics. *Nucleic Acids Res.* **36**, D543-D546
 156. Rivera, M., Bryan, L. E., Hancock, R. E. W., and McGroarty, E. J. (1988) HETEROGENEITY OF LIPOPOLYSACCHARIDES FROM PSEUDOMONAS-AERUGINOSA - ANALYSIS OF LIPOPOLYSACCHARIDE CHAIN-LENGTH. *J Bacteriol* **170**, 512-521
 157. Studier, F. W. (2005) Protein production by auto-induction in high-density shaking cultures. *Protein Expr. Purif.* **41**, 207-234
 158. Saleem, M., Moore, J., and Derrick, J. (2012) Expression, Purification, and Crystallization of Neisserial Outer Membrane Proteins. in *Neisseria meningitidis* (Christodoulides, M. ed.), Humana Press. pp 91-106
 159. Gorrec, F. (2009) The MORPHEUS protein crystallization screen. *J. Appl. Crystallogr.* **42**, 1035-1042
 160. Kabsch, W. (2010) XDS. *Acta Crystallogr. Sect. D.* **66**, 125-132
 161. Evans, P. (2006) Scaling and assessment of data quality. *Acta Crystallogr. Sect. D.* **62**, 72-82
 162. McCoy, A. J., Grosse-Kunstleve, R. W., Adams, P. D., Winn, M. D., Storoni, L. C., and Read, R. J. (2007) Phaser crystallographic software. *J. Appl. Crystallogr.* **40**, 658-674
 163. Bricogne, G., Vonrhein, C., Flensburg, C., Schiltz, M., and Paciorek, W. (2003) Generation, representation and flow of phase information in structure determination: recent developments in and around SHARP 2.0. *Acta Crystallogr. Sect. D.* **59**, 2023-2030
 164. Vonrhein, C., Blanc, E., Roversi, P., and Bricogne, G. (2007). in *Macromolecular crystallography protocols* (Doubl  , S. ed.), Humana Press. pp 215-230
 165. Sheldrick, G. (2010) Experimental phasing with SHELXC/D/E: combining chain tracing with density modification. *Acta Crystallogr. Sect. D.* **66**, 479-485
 166. Langer, G., Cohen, S. X., Lamzin, V. S., and Perrakis, A. (2008) Automated macromolecular model building for X-ray crystallography using ARP/wARP version 7. *Nat. Protoc.* **3**, 1171-1179
 167. Cowtan, K. (2008) Fitting molecular fragments into electron density. *Acta Crystallogr. Sect. D.* **64**, 83-89
 168. Emsley, P., Lohkamp, B., Scott, W. G., and Cowtan, K. (2010) Features and development of Coot. *Acta Crystallogr. Sect. D.* **66**, 486-501
 169. Murshudov, G. N., Skubak, P., Lebedev, A. A., Pannu, N. S., Steiner, R. A., Nicholls, R. A., Winn, M. D., Long, F., and Vagin, A. A. (2011) REFMAC5 for the refinement of macromolecular crystal structures. *Acta Crystallogr. Sect. D.* **67**, 355-367
 170. Winn, M. D., Ballard, C. C., Cowtan, K. D., Dodson, E. J., Emsley, P., Evans, P. R., Keegan, R. M., Krissinel, E. B., Leslie, A. G. W., McCoy, A., McNicholas, S. J., Murshudov, G. N., Pannu, N. S., Potterton, E. A., Powell, H. R., Read, R. J., Vagin, A., and Wilson, K. S. (2011) Overview of the CCP4 suite and current developments. *Acta Crystallogr. Sect. D.* **67**, 235-242

171. Lovell, S. C., Davis, I. W., Arendall, W. B., de Bakker, P. I. W., Word, J. M., Prisant, M. G., Richardson, J. S., and Richardson, D. C. (2003) Structure validation by $\text{C}\alpha$ geometry: φ, ψ and $\text{C}\beta$ deviation. *Proteins* **50**, 437-450
172. Dong, A., Xu, X., and Edwards, A. M. (2007) In situ proteolysis for protein crystallization and structure determination. *Nat. Meth.* **4**, 1019-1021
173. Incardona, M.-F., Bourenkov, G. P., Levik, K., Pieritz, R. A., Popov, A. N., and Svensson, O. (2009) EDNA: a framework for plugin-based applications applied to X-ray experiment online data analysis. *J Synchrotron Radiat* **16**, 872-879
174. Adams, P. D., Afonine, P. V., Bunkoczi, G., Chen, V. B., Davis, I. W., Echols, N., Headd, J. J., Hung, L.-W., Kapral, G. J., Grosse-Kunstleve, R. W., McCoy, A. J., Moriarty, N. W., Oeffner, R., Read, R. J., Richardson, D. C., Richardson, J. S., Terwilliger, T. C., and Zwart, P. H. (2010) PHENIX: a comprehensive Python-based system for macromolecular structure solution. *Acta Crystallogr. Sect. D.* **66**, 213-221
175. Chen, V. B., Arendall, W. B., III, Headd, J. J., Keedy, D. A., Immormino, R. M., Kapral, G. J., Murray, L. W., Richardson, J. S., and Richardson, D. C. (2010) MolProbity: all-atom structure validation for macromolecular crystallography. *Acta Crystallogr D Biol Crystallogr* **66**, 12-21
176. Laskowski, R. A., Macarthur, M. W., Moss, D. S., and Thornton, J. M. (1993) PROCHECK - A program to check the stereochemical quality of protein structures. *J Appl Crystallogr* **26**, 283-291
177. Gorrec, F. (2009) The MORPHEUS protein crystallization screen. *J Appl Crystallogr* **42**, 1035-1042
178. Long, F., Vagin, A. A., Young, P., and Murshudov, G. N. (2008) BALBES: a molecular-replacement pipeline. *Acta Crystallogr D Biol Crystallogr* **64**, 125-132
179. Adams, P. D., Afonine, P. V., Bunkoczi, G., Chen, V. B., Davis, I. W., Echols, N., Headd, J. J., Hung, L.-W., Kapral, G. J., Grosse-Kunstleve, R. W., McCoy, A. J., Moriarty, N. W., Oeffner, R., Read, R. J., Richardson, D. C., Richardson, J. S., Terwilliger, T. C., and Zwart, P. H. (2010) PHENIX: a comprehensive Python-based system for macromolecular structure solution. *Acta Crystallogr D Biol Crystallogr* **66**, 213-221
180. Emsley, P., Lohkamp, B., Scott, W. G., and Cowtan, K. (2010) Features and development of Coot. *Acta Crystallogr D Biol Crystallogr* **66**, 486-501
181. Murshudov, G. N., Skubak, P., Lebedev, A. A., Pannu, N. S., Steiner, R. A., Nicholls, R. A., Winn, M. D., Long, F., and Vagin, A. A. (2011) REFMAC5 for the refinement of macromolecular crystal structures. *Acta Crystallogr D Biol Crystallogr* **67**, 355-367
182. McCoy, A. J., Grosse-Kunstleve, R. W., Adams, P. D., Winn, M. D., Storoni, L. C., and Read, R. J. (2007) Phaser crystallographic software. *J Appl Crystallogr* **40**, 658-674
183. Schuttelkopf, A. W., and van Aalten, D. M. F. (2004) PRODRG: a tool for high-throughput crystallography of protein-ligand complexes. *Acta Crystallogr D Biol Crystallogr* **60**, 1355-1363
184. Mori, S., Abeygunawardana, C., Johnson, M. O., and vanZijl, P. (1996) Improved sensitivity of HSQC spectra of exchanging protons at short interscan delays using a new fast HSQC (FHSQC) detection scheme that avoids water saturation (vol 108, pg 94, 1995). *J Magn Reson B* **110**, 321-321
185. Vranken, W. F., Boucher, W., Stevens, T. J., Fogh, R. H., Pajon, A., Llinas, P., Ulrich, E. L., Markley, J. L., Ionides, J., and Laue, E. D. (2005) The CCPN data model for NMR spectroscopy: Development of a software pipeline. *Proteins* **59**, 687-696

186. Mori, S., Abeygunawardana, C., Johnson, M. O., and Vanzijl, P. C. M. (1995) Improved Sensitivity of HSQC Spectra of Exchanging Protons at Short Interscan Delays Using a New Fast HSQC (FHSQC) Detection Scheme That Avoids Water Saturation. *Journal of Magnetic Resonance, Series B* **108**, 94-98
187. Vranken, W. F., Boucher, W., Stevens, T. J., Fogh, R. H., Pajon, A., Llinas, M., Ulrich, E. L., Markley, J. L., Ionides, J., and Laue, E. D. (2005) The CCPN data model for NMR spectroscopy: Development of a software pipeline. *Proteins: Structure, Function, and Bioinformatics* **59**, 687-696
188. Schuck, P. (2000) Size-Distribution Analysis of Macromolecules by Sedimentation Velocity Ultracentrifugation and Lamm Equation Modeling. *Biophysical Journal* **78**, 1606-1619
189. Konarev, P. V., Volkov, V. V., Sokolova, A. V., Koch, M. H. J., and Svergun, D. I. (2003) PRIMUS: a Windows PC-based system for small-angle scattering data analysis. *Journal of Applied Crystallography* **36**, 1277-1282
190. Rambo, R. P., and Tainer, J. A. Characterizing flexible and intrinsically unstructured biological macromolecules by SAS using the Porod-Debye law. *Biopolymers* **95**, 559-571
191. Durand, D., Vivès, C., Cannella, D., Pérez, J., Pebay-Peyroula, E., Vachette, P., and Fieschi, F. NADPH oxidase activator p67phox behaves in solution as a multidomain protein with semi-flexible linkers. *Journal of Structural Biology* **169**, 45-53
192. Svergun, D. (1992) Determination of the regularization parameter in indirect-transform methods using perceptual criteria. *Journal of Applied Crystallography* **25**, 495-503
193. Rai, N., Nöllmann, M., Spotorno, B., Tassara, G., Byron, O., and Rocco, M. (2005) SOMO (SOLUTION MOdeler): Differences between X-Ray- and NMR-Derived Bead Models Suggest a Role for Side Chain Flexibility in Protein Hydrodynamics. *Structure* **13**, 723-734
194. Svergun, D., Barberato, C., and Koch, M. H. J. (1995) CRY SOL - a Program to Evaluate X-ray Solution Scattering of Biological Macromolecules from Atomic Coordinates. *J. Appl. Crystallogr.* **28**, 768-773
195. Trott, O., and Olson, A. J. (2010) AutoDock Vina: Improving the speed and accuracy of docking with a new scoring function, efficient optimization, and multithreading. *Journal of Computational Chemistry* **31**, 455-461
196. Pettersen, E. F., Goddard, T. D., Huang, C. C., Couch, G. S., Greenblatt, D. M., Meng, E. C., and Ferrin, T. E. (2004) UCSF Chimera—A visualization system for exploratory research and analysis. *Journal of Computational Chemistry* **25**, 1605-1612
197. Zhang, X., Henriques, R., Lin, S.-S., Niu, Q.-W., and Chua, N.-H. (2006) Agrobacterium-mediated transformation of *Arabidopsis thaliana* using the floral dip method. *Nat. Protocols* **1**, 641-646
198. Zeth, K., Römer, C., Patzer, S. I., and Braun, V. (2008) Crystal structure of colicin M, a novel phosphatase specifically imported by *Escherichia coli*. *J. Biol. Chem.* **283**, 25324-25331
199. Barreteau, H., Bouhss, A., Gérard, F., Duché, D., Boussaid, B., Blanot, D., Lloubès, R., Mengin-Lecreulx, D., and Touzé, T. (2010) Deciphering the catalytic domain of colicin M, a peptidoglycan lipid II-degrading enzyme. *J. Biol. Chem.* **285**, 12378-12389

200. Helbig, S., and Braun, V. (2011) Mapping functional domains of colicin M. *J. Bacteriol.* **193**, 815-821
201. Holm, L., and Sander, C. (1993) Protein structure comparison by alignment of distance matrices. *J. Mol. Biol.* **233**, 123-138
202. Zheng, H., Chruszcz, M., Lasota, P., Lebioda, L., and Minor, W. (2008) Data mining of metal ion environments present in protein structures. *J. Inorg. Biochem.* **102**, 1765-1776
203. Katz, A. K., Glusker, J. P., Beebe, S. A., and Bock, C. W. (1996) Calcium ion coordination: A comparison with that of beryllium, magnesium, and zinc. *J. Am. Chem. Soc.* **118**, 5752-5763
204. Moncrief, M. B. C., and Maguire, M. E. (1999) Magnesium transport in prokaryotes. *J. Biol. Inorg. Chem.* **4**, 523-527
205. Jones, H. E., Holland, I. B., and Campbell, A. K. (2002) Direct measurement of free Ca²⁺ shows different regulation of Ca²⁺ between the periplasm and the cytosol of *Escherichia coli*. *Cell Calcium* **32**, 183-192
206. Schaller, K., Dreher, R., and Braun, V. (1981) Structural and functional properties of colicin M. *J. Bacteriol.* **146**, 54-63
207. Killmann, H., Videnov, G., Jung, G., Schwarz, H., and Braun, V. (1995) Identification of receptor binding sites by competitive peptide mapping: phages T1, T5, and phi 80 and colicin M bind to the gating loop of FhuA. *J. Bacteriol.* **177**, 694-698
208. Loubens, I., Debarbieux, L., Bohin, A., Lacroix, J. M., and Bohin, J. P. (1993) Homology between a genetic locus (*mdoA*) involved in the osmoregulated biosynthesis of periplasmic glucans in *Escherichia coli* and a genetic locus (*hrpM*) controlling pathogenicity of *Pseudomonas syringae*. *Mol. Microbiol.* **10**, 329-340
209. Höltje, J. V., Fiedler, W., Rotering, H., Walderich, B., and van Duin, J. (1988) Lysis induction of *Escherichia coli* by the cloned lysis protein of the phage MS2 depends on the presence of osmoregulatory membrane-derived oligosaccharides. *J. Biol. Chem.* **263**, 3539-3541
210. Böhringer, J., Fischer, D., Mosler, G., and Hengge-Aronis, R. (1995) UDP-glucose is a potential intracellular signal molecule in the control of expression of sigma S and sigma S-dependent genes in *Escherichia coli*. *J. Bacteriol.* **177**, 413-422
211. Bohin, J.-P. (2000) Osmoregulated periplasmic glucans in Proteobacteria1. *FEMS Microbiol. Lett.* **186**, 11-19
212. Pilsl, H., Glaser, C., Groß, P., Killmann, H., Ölschläger, T., and Braun, V. (1993) Domains of colicin M involved in uptake and activity. *Mol. Gen. Genet.* **240**, 103-112
213. Holm, L., and Sander, C. (1997) Decision support system for the evolutionary classification of protein structures. *ISMB97: Proc. Int. Conf. Intell. Syst. Mol. Biol.* **5**, 140-146
214. Wiener, M., Freymann, D., Ghosh, P., and Stroud, R. M. (1997) Crystal structure of colicin Ia. *Nature* **385**, 461-464
215. Smith, E. E., Sims, E. H., Spencer, D. H., Kaul, R., and Olson, M. V. (2005) Evidence for diversifying selection at the pyoverdine locus of *Pseudomonas aeruginosa*. *J. Bacteriol.* **187**, 2138-2147
216. Tümmler, B., and Cornelis, P. (2005) Pyoverdine receptor: a case of positive darwinian selection in *Pseudomonas aeruginosa*. *J. Bacteriol.* **187**, 3289-3292
217. Bajaj, M., and Blundell, T. (1984) Evolution and the tertiary structure of proteins. *Annu. Rev. Biophys. Bioeng.* **13**, 453-492

218. Wernimont, A., and Edwards, A. (2009) *In situ* proteolysis to generate crystals for structure determination: An update. *PLoS ONE* **4**, e5094
219. Fukuyama, K. (2004) Structure and Function of Plant-Type Ferredoxins. *Photosynth Res* **81**, 289-301
220. Briat, J. F. (2007) Iron dynamics in plants. in *Advances in Botanical Research* (Jean-Claude, K., and Michel, D. eds.), Academic Press. pp 137-180
221. Briat, J.-F., Duc, C., Ravet, K., and Gaymard, F. (2010) Ferritins and iron storage in plants. *Biochimica et Biophysica Acta (BBA) - General Subjects* **1800**, 806-814
222. Franza, T., and Expert, D. (2010) Iron up-take in soft rot *Erwinia*. in *Iron uptake and homeostasis in microorganisms* (Cornelius Piere, A. S. ed.), Caister Academic Press., Norfolk. pp 101–116
223. Monson, R., Burr, T., Carlton, T., Liu, H., Hedley, P., Toth, I., and Salmond, G. P. C. (2012) Identification of genes in the VirR regulon of *Pectobacterium atrosepticum* and characterization of their roles in quorum sensing-dependent virulence. *Environ. Microbiol.*, no-no
224. Toth, I. K., Pritchard, L., and Birch, P. R. J. (2006) Comparative Genomics Reveals What Makes An Enterobacterial Plant Pathogen. *Annual Review of Phytopathology* **44**, 305-336
225. Thomine, S., and Lanquar, V. (2011) Iron transport and signaling in plants transporters and pumps in plant signaling. in *Transporters and Pumps in Plant Signaling* (Geisler, M., and Venema, K. eds.), Springer Berlin Heidelberg, Berlin. pp 99-131
226. Shirvanyants, D., Ding, F., Tsao, D., Ramachandran, S., and Dokholyan, N. V. (2012) Discrete Molecular Dynamics: An Efficient And Versatile Simulation Method For Fine Protein Characterization. *The Journal of Physical Chemistry B* **116**, 8375-8382
227. Petoukhov, M. V., Franke, D., Shkumatov, A. V., Tria, G., Kikhney, A. G., Gajda, M., Gorba, C., Mertens, H. D. T., Konarev, P. V., and Svergun, D. I. (2012) New developments in the ATSAS program package for small-angle scattering data analysis. *Journal of Applied Crystallography* **45**, 342-350
228. Flores, S., Echols, N., Milburn, D., Hespeneide, B., Keating, K., Lu, J., Wells, S., Yu, E. Z., Thorpe, M., and Gerstein, M. (2006) The Database of Macromolecular Motions: new features added at the decade mark. *Nucleic Acids Res.* **34**, D296-D301
229. Ivo S. Ridder, B. W. D. (1999) Identification of the Mg²⁺-binding site in the P-type ATPase and phosphatase member of the HAD (haloacid dehalogenase) superfamily by structural similarity to the response regulator protein CheY. *Biochem. J.* **339**, 223-226
230. Lu, Z., Dunaway-Mariano, D., and Allen, K. N. (2008) The catalytic scaffold of the haloalkanoic acid dehalogenase enzyme superfamily acts as a mold for the trigonal bipyramidal transition state. *Proc. Natl. Acad. Sci. U. S. A.* **105**, 5687-5692
231. Cai, S. J., and Inouye, M. (2002) EnvZ-OmpR Interaction and Osmoregulation in *Escherichia coli*. *J. Biol. Chem.* **277**, 24155-24161
232. Yoshida, T., Phadtare, S., and Inouye, M. (2007) Functional and Structural Characterization of EnvZ, an Osmosensing Histidine Kinase of *E. coli*. in *Methods Enzymol.* (Melvin I. Simon, B. R. C., and Alexandrine, C. eds.), Academic Press. pp 184-202

233. Mizuno, T., Wurtzel, E. T., and Inouye, M. (1982) Osmoregulation of gene expression. II. DNA sequence of the *envZ* gene of the *ompB* operon of *Escherichia coli* and characterization of its gene product. *J. Biol. Chem.* **257**, 13692-13698
234. Stock, A. M., Robinson, V. L., and Goudreau, P. N. (2000) TWO-COMPONENT SIGNAL TRANSDUCTION. *Annu. Rev. Biochem.* **69**, 183-215
235. Elfarash, A., Wei, Q., and Cornelis, P. (2012) The soluble pyocins S2 and S4 from *Pseudomonas aeruginosa* bind to the same FpvA1 receptor. *MicrobiologyOpen*, n/a-n/a
236. Denayer, S., Matthijs, S., and Cornelis, P. (2007) Pyocin S2 (Sa) Kills *Pseudomonas aeruginosa* Strains via the FpvA Type I Ferripyoverdine Receptor. *J. Bacteriol.* **189**, 7663-7668
237. Loftus, S. R., Walker, D., Maté, M. J., Bonsor, D. A., James, R., Moore, G. R., and Kleanthous, C. (2006) Competitive recruitment of the periplasmic translocation portal TolB by a natively disordered domain of colicin E9. *Proceedings of the National Academy of Sciences* **103**, 12353-12358
238. Faraldo-Gomez, J. D., and Sansom, M. S. P. (2003) Acquisition of siderophores in Gram-negative bacteria. *Nat. Rev. Mol. Cell Biol.* **4**, 105-116
239. Noinaj, N., Easley, N. C., Oke, M., Mizuno, N., Gumbart, J., Boura, E., Steere, A. N., Zak, O., Aisen, P., Tajkhorshid, E., Evans, R. W., Gorringer, A. R., Mason, A. B., Steven, A. C., and Buchanan, S. K. (2012) Structural basis for iron piracy by pathogenic *Neisseria*. *Nature* **483**, 53-58
240. Wandersman, C., and Stojiljkovic, I. (2000) Bacterial heme sources: the role of heme, hemoprotein receptors and hemophores. *Curr. Opin. Microbiol.* **3**, 215-220
241. Moraes, T. F., Yu, R.-h., Strynadka, N. C. J., and Schryvers, A. B. (2009) Insights into the Bacterial Transferrin Receptor: The Structure of Transferrin-Binding Protein B from *Actinobacillus pleuropneumoniae*. *Mol. Cell* **35**, 523-533
242. Anderson, J. E., Sparling, P. F., and Cornelissen, C. N. (1994) Gonococcal transferrin-binding protein 2 facilitates but is not essential for transferrin utilization. *J. Bacteriol.* **176**, 3162-3170
243. Lee, B. C., and Schryvers, A. B. (1988) Specificity of the lactoferrin and transferrin receptors in *Neisseria gonorrhoeae*. *Mol. Microbiol.* **2**, 827-829
244. Cornelissen, C. N., Kelley, M., Hobbs, M. M., Anderson, J. E., Cannon, J. G., Cohen, M. S., and Sparling, P. F. (1998) The transferrin receptor expressed by gonococcal strain FA1090 is required for the experimental infection of human male volunteers. *Mol. Microbiol.* **27**, 611-616
245. Rohde, K. H., Gillaspay, A. F., Hatfield, M. D., Lewis, L. A., and Dyer, D. W. (2002) Interactions of haemoglobin with the *Neisseria meningitidis* receptor HpuAB: the role of TonB and an intact proton motive force. *Mol. Microbiol.* **43**, 335-354
246. Krewulak, K. D., and Vogel, H. J. (2008) Structural biology of bacterial iron uptake. *Biochimica et Biophysica Acta (BBA) - Biomembranes* **1778**, 1781-1804
247. Tong, Y., and Guo, M. (2009) Bacterial heme-transport proteins and their heme-coordination modes. *Arch. Biochem. Biophys.* **481**, 1-15
248. Alontaga, A. Y., Rodriguez, J. C., Schönbrunn, E., Becker, A., Funke, T., Yukl, E. T., Hayashi, T., Stobaugh, J., Moënné-Loccoz, P., and Rivera, M. (2008) Structural characterization of the hemophore HasA from *Pseudomonas aeruginosa*: NMR spectroscopy reveals protein-protein interactions between holo-HasA and hemoglobin. *Biochemistry* **48**, 96-109

249. Arnoux, P., Haser, R., Izadi-Pruneyre, N., Lecroisey, A., and Czjzek, M. (2000) Functional aspects of the heme bound hemophore HasA by structural analysis of various crystal forms. *Proteins* **41**, 202-210
250. Krieg, S., Huché, F., Diederichs, K., Izadi-Pruneyre, N., Lecroisey, A., Wandersman, C., Delepelaire, P., and Welte, W. (2009) Heme uptake across the outer membrane as revealed by crystal structures of the receptor–hemophore complex. *Proc. Natl. Acad. Sci. U. S. A.* **106**, 1045-1050
251. Ajioka, R. S., Phillips, J. D., and Kushner, J. P. (2006) Biosynthesis of heme in mammals. *Biochimica et Biophysica Acta (BBA) - Molecular Cell Research* **1763**, 723-736
252. Espinas, N. A., Kobayashi, K., Takahashi, S., Mochizuki, N., and Masuda, T. (2012) Evaluation of unbound free heme in plant cells by differential acetone extraction. *Plant Cell Physiol.* **53**, 1344-1354
253. Im, S.-c., Liu, G., Luchinat, C., Sykes, A. G., and Bertini, I. (1998) The solution structure of parsley [2Fe-2S]ferredoxin. *Eur. J. Biochem.* **258**, 465-477
254. Kelley, L. A., and Sternberg, M. J. E. (2009) Protein structure prediction on the Web: a case study using the Phyre server. *Nat. Protocols* **4**, 363-371
255. Strop, P., and Brunger, A. T. (2005) Refractive index-based determination of detergent concentration and its application to the study of membrane proteins. *Protein Sci.* **14**, 2207-2211
256. Grimm, C., Chari, A., Reuter, K., and Fischer, U. (2010) A crystallization screen based on alternative polymeric precipitants. *Acta Crystallogr. Sect. D.* **66**, 685-697
257. Seddon, A. M., Curnow, P., and Booth, P. J. (2004) Membrane proteins, lipids and detergents: not just a soap opera. *Biochimica et Biophysica Acta (BBA) - Biomembranes* **1666**, 105-117
258. Braun, V. (1995) Energy-coupled transport and signal transduction through the Gram-negative outer membrane via TonB-ExbB-ExbD-dependent receptor proteins. *FEMS Microbiol. Rev.* **16**, 295-307
259. Amorim, G. C. d., Prochnicka-Chalufour, A., Delepelaire, P., Lefèvre, J., Simenel, C., Wandersman, C., Delepierre, M., and Izadi-Pruneyre, N. (2013) The Structure of HasB Reveals a New Class of TonB Protein Fold. *PLoS ONE* **8**, e58964
260. Zhao, Q., and Poole, K. (2000) A second tonB gene in *Pseudomonas aeruginosa* is linked to the exbB and exbD genes. *FEMS Microbiol. Lett.* **184**, 127-132
261. Postle, K. (1990) TonB and the Gram-negative dilemma. *Mol. Microbiol.* **4**, 2019-2025
262. Stojiljkovic, I., and Hantke, K. (1994) Transport of haemin across the cytoplasmic membrane through a haemin-specific periplasmic binding-protein-dependent transport system in *Yersinia enterocolitica*. *Mol. Microbiol.* **13**, 719-732
263. Taylor, A. B., Smith, B. S., Kitada, S., Kojima, K., Miyaura, H., Otwinowski, Z., Ito, A., and Deisenhofer, J. (2001) Crystal Structures of Mitochondrial Processing Peptidase Reveal the Mode for Specific Cleavage of Import Signal Sequences. *Structure* **9**, 615-625
264. Subashchandrabose, S., Smith, S. N., Spurbeck, R. R., Kole, M. M., and Mobley, H. L. T. (2013) Genome-Wide Detection of Fitness Genes in Uropathogenic *Escherichia coli* during Systemic Infection. *PLoS Pathog.* **9**, e1003788
265. Dziva, F., Hauser, H., Connor, T. R., van Diemen, P. M., Prescott, G., Langridge, G. C., Eckert, S., Chaudhuri, R. R., Ewers, C., Mellata, M., Mukhopadhyay, S., Curtiss, R., Dougan, G., Wieler, L. H., Thomson, N. R., Pickard, D. J., and Stevens, M. P.

- (2013) Sequencing and Functional Annotation of Avian Pathogenic *Escherichia coli* Serogroup O78 Strains Reveal the Evolution of *E. coli* Lineages Pathogenic for Poultry via Distinct Mechanisms. *Infect. Immun.* **81**, 838-849
266. Boyce, J. D., Wilkie, I., Harper, M., Paustian, M. L., Kapur, V., and Adler, B. (2002) Genomic Scale Analysis of *Pasteurella multocida* Gene Expression during Growth within the Natural Chicken Host. *Infect. Immun.* **70**, 6871-6879
267. Paustian, M. L., May, B. J., and Kapur, V. (2001) *Pasteurella multocida* Gene Expression in Response to Iron Limitation. *Infect. Immun.* **69**, 4109-4115
268. Okinaka, Y., Yang, C.-H., Perna, N. T., and Keen, N. T. (2002) Microarray Profiling of *Erwinia chrysanthemi* 3937 Genes That are Regulated During Plant Infection. *Mol. Plant. Microbe Interact.* **15**, 619-629
269. Ivanov, R., Fobis-Loisy, I., and Gaude, T. (2010) When no means no: guide to Brassicaceae self-incompatibility. *Trends Plant Sci.* **15**, 387-394
270. Tsutsui, S., Tasumi, S., Suetake, H., and Suzuki, Y. (2003) Lectins Homologous to Those of Monocotyledonous Plants in the Skin Mucus and Intestine of Pufferfish, *Fugu rubripes*. *J. Biol. Chem.* **278**, 20882-20889
271. Van damme, E. J. M., Nakamura-tsuruta, S., Smith, D. F., Ongenaert, M., Winter, H. C., Rougé, P., Goldstein, I. J., Mo, H., Kominami, J., Culierrier, R., Barre, A., Hirabayashi, J., and Peumans, W. J. (2007) Phylogenetic and specificity studies of two-domain GNA-related lectins: generation of multispecificity through domain duplication and divergent evolution. *Biochem. J.* **404**, 51-61
272. Parret, A. H. A., Wyns, L., De Mot, R., and Loris, R. (2004) Overexpression, purification and crystallization of bacteriocin LlpA from *Pseudomonas* sp. BW11M1. *Acta Crystallogr. Sect. D.* **60**, 1922-1924
273. Egan, A. J. F., and Vollmer, W. (2013) The physiology of bacterial cell division. *Ann. N. Y. Acad. Sci.* **1277**, 8-28
274. Lewis, K. (2000) Programmed Death in Bacteria. *Microbiol. Mol. Biol. Rev.* **64**, 503-514
275. Mahoney, T. F., and Silhavy, T. J. (2013) The Cpx Stress Response Confers Resistance to Some, but Not All Bactericidal Antibiotics. *J. Bacteriol.*
276. Heeb, S., and Haas, D. (2001) Regulatory Roles of the GacS/GacA Two-Component System in Plant-Associated and Other Gram-Negative Bacteria. *Mol. Plant. Microbe Interact.* **14**, 1351-1363
277. Wolanin, P. M., Webre, D. J., and Stock, J. B. (2003) Mechanism of Phosphatase Activity in the Chemotaxis Response Regulator CheY[†]. *Biochemistry* **42**, 14075-14082
278. Burrows, L. L., Urbanic, R. V., and Lam, J. S. (2000) Functional Conservation of the Polysaccharide Biosynthetic Protein WbpM and Its Homologues in *Pseudomonas aeruginosa* and Other Medically Significant Bacteria. *Infect. Immun.* **68**, 931-936
279. Rocchetta, H. L., and Lam, J. S. (1997) Identification and functional characterization of an ABC transport system involved in polysaccharide export of A-band lipopolysaccharide in *Pseudomonas aeruginosa*. *J. Bacteriol.* **179**, 4713-4724
280. Rocchetta, H. L., Burrows, L. L., Pacan, J. C., and Lam, J. S. (1998) Three rhamnosyltransferases responsible for assembly of the A-band D-rhamnan polysaccharide in *Pseudomonas aeruginosa*: a fourth transferase, WbpL, is required for the initiation of both A-band and B-band lipopolysaccharide synthesis. *Mol. Microbiol.* **30**, 1131-1131

281. Lam, J. S., Taylor, V. L., Islam, S. T., Hao, Y., and Kocincova, D. (2011) Genetic and Functional Diversity of *Pseudomonas aeruginosa* Lipopolysaccharide. *Front Microbiol* **2**, 118-118
282. Hao, Y., King, J. D., Huszczyński, S., Kocincova, D., and Lam, J. S. (2013) Five New Genes Are Important for Common Polysaccharide Antigen Biosynthesis in *Pseudomonas aeruginosa*. *Mbio* **4**
283. Jacobs, M. A., Alwood, A., Thaipisuttikul, I., Spencer, D., Haugen, E., Ernst, S., Will, O., Kaul, R., Raymond, C., Levy, R., Liu, C. R., Guenther, D., Bovee, D., Olson, M. V., and Manoil, C. (2003) Comprehensive transposon mutant library of *Pseudomonas aeruginosa*. *Proc Natl Acad Sci U S A* **100**, 14339-14344
284. Ovod, V., Rudolph, K., Knirel, Y., and Krohn, K. (1996) Immunochemical characterization of O polysaccharides composing the alpha-D-rhamnose backbone of lipopolysaccharide of *Pseudomonas syringae* and classification of bacteria into serogroups O1 and O2 with monoclonal antibodies. *J Bacteriol* **178**, 6459-6465
285. Ovod, V. V., Knirel, Y. A., Samson, R., and Krohn, K. J. (1999) Immunochemical characterization and taxonomic evaluation of the O polysaccharides of the lipopolysaccharides of *Pseudomonas syringae* serogroup O1 strains. *J Bacteriol* **181**, 6937-6947
286. Abdel-Mawgoud, A. M., Lepine, F., and Deziel, E. (2010) Rhamnolipids: diversity of structures, microbial origins and roles. *Appl Microbiol Biotechnol* **86**, 1323-1336
287. Caffall, K. H., and Mohnen, D. (2009) The structure, function, and biosynthesis of plant cell wall pectic polysaccharides. *Carbohydr Res* **344**, 1879-1900
288. Knirel, Y. A., Shashkov, A. S., Senchenkova, S., Ajiki, Y., and Fukuoka, S. (2002) Structure of the O-polysaccharide of *Pseudomonas putida* FERM p-18867. *Carbohydr Res* **337**, 1589-1591
289. Molinaro, A., Silipo, A., Lanzetta, R., Newman, M. A., Dow, J. M., and Parrilli, M. (2003) Structural elucidation of the O-chain of the lipopolysaccharide from *Xanthomonas campestris* strain 8004. *Carbohydr Res* **338**, 277-281
290. Vinion-Dubiel, A. D., and Goldberg, J. B. (2003) Lipopolysaccharide of *Burkholderia cepacia* complex. *J Endotoxin Res* **9**, 201-213
291. Wang, L., Wang, Q., and Reeves, P. R. (2010) The variation of O antigens in gram-negative bacteria. in *Endotoxins: Structure, Function and Recognition*, Springer. pp 123-152
292. Coggan, K. A., and Wolfgang, M. C. (2012) Global regulatory pathways and cross-talk control *Pseudomonas aeruginosa* environmental lifestyle and virulence phenotype. *Curr. Issues Mol. Biol.* **14**, 47
293. Bravo, A., Likitvivatanavong, S., Gill, S. S., and Soberón, M. (2011) *Bacillus thuringiensis*: A story of a successful bioinsecticide. *Insect Biochem. Mol. Biol.* **41**, 423-431
294. Galitsky, N., Cody, V., Wojtczak, A., Ghosh, D., Luft, J. R., Pangborn, W., and English, L. (2001) Structure of the insecticidal bacterial [delta]-endotoxin Cry3Bb1 of *Bacillus thuringiensis*. *Acta Crystallogr. Sect. D.* **57**, 1101-1109
295. Kathage, J., and Qaim, M. (2012) Economic impacts and impact dynamics of Bt (*Bacillus thuringiensis*) cotton in India. *Proceedings of the National Academy of Sciences* **109**, 11652-11656
296. Wu, K.-M., Lu, Y.-H., Feng, H.-Q., Jiang, Y.-Y., and Zhao, J.-Z. (2008) Suppression of Cotton Bollworm in Multiple Crops in China in Areas with Bt Toxin-Containing Cotton. *Science* **321**, 1676-1678

297. Bravo, A., Gill, S. S., and Soberón, M. (2007) Mode of action of *Bacillus thuringiensis* Cry and Cyt toxins and their potential for insect control. *Toxicon* **49**, 423-435
298. Bravo, A., and Soberón, M. (2008) How to cope with insect resistance to Bt toxins? *Trends Biotechnol.* **26**, 573-579
299. Thomma, B., Cammue, B., and Thevissen, K. (2002) Plant defensins. *Planta* **216**, 193-202
300. Montesinos, E. (2007) Antimicrobial peptides and plant disease control. *FEMS Microbiol. Lett.* **270**, 1-11
301. Păcurar, D. I., Thordal-Christensen, H., Păcurar, M. L., Pamfil, D., Botez, C., and Bellini, C. (2011) *Agrobacterium tumefaciens*: From crown gall tumors to genetic transformation. *Physiological and Molecular Plant Pathology* **76**, 76-81
302. Gotham, S. M., Fryer, P. J., and Paterson, W. R. (1988) The measurement of insoluble proteins using a modified Bradford assay. *Anal. Biochem.* **173**, 353-358
303. Zhang, J., and Zhou, J.-M. (2010) Plant Immunity Triggered by Microbial Molecular Signatures. *Mol. Plant* **3**, 783-793
304. Hann, D. R., and Rathjen, J. P. (2007) Early events in the pathogenicity of *Pseudomonas syringae* on *Nicotiana benthamiana*. *The Plant Journal* **49**, 607-618
305. Dangl, J. L., and Jones, J. D. G. (2001) Plant pathogens and integrated defence responses to infection. *Nature* **411**, 826-833
306. Kohanski, M. A., Dwyer, D. J., Hayete, B., Lawrence, C. A., and Collins, J. J. (2007) A Common Mechanism of Cellular Death Induced by Bactericidal Antibiotics. *Cell* **130**, 797-810
307. Ishiga, Y., Ishiga, T., Uppalapati, S. R., and Mysore, K. S. (2011) Arabidopsis seedling flood-inoculation technique: a rapid and reliable assay for studying plant-bacterial interactions. *Plant methods* **7**, 32

11 Publications related to this work

Protein Structure and Folding:
**The Crystal Structure of the Lipid
II-degrading Bacteriocin Syringacin M
Suggests Unexpected Evolutionary
Relationships between Colicin M-like
Bacteriocins**



Rhys Grinter, Aleksander W. Roszak, Richard
J. Cogdell, Joel J. Milner and Daniel Walker
J. Biol. Chem. 2012, 287:38876-38888.
doi: 10.1074/jbc.M112.400150 originally published online September 20, 2012

Access the most updated version of this article at doi: [10.1074/jbc.M112.400150](https://doi.org/10.1074/jbc.M112.400150)

Find articles, minireviews, Reflections and Classics on similar topics on the [JBC Affinity Sites](http://www.jbc.org/).

Alerts:

- [When this article is cited](#)
- [When a correction for this article is posted](#)

[Click here](#) to choose from all of JBC's e-mail alerts

Supplemental material:

<http://www.jbc.org/content/suppl/2012/09/20/M112.400150.DC1.html>

This article cites 58 references, 20 of which can be accessed free at
<http://www.jbc.org/content/287/46/38876.full.html#ref-list-1>

Ferredoxin Containing Bacteriocins Suggest a Novel Mechanism of Iron Uptake in *Pectobacterium* spp.

Rhys Grinter¹, Joel Milner², Daniel Walker^{1*}

1 Institute of Infection, Immunity and Inflammation, College of Medical, Veterinary and Life Sciences, University of Glasgow, Glasgow, United Kingdom, **2** Institute of Molecular Cell and Systems Biology, College of Medical, Veterinary and Life Sciences, University of Glasgow, Glasgow, United Kingdom

Abstract

In order to kill competing strains of the same or closely related bacterial species, many bacteria produce potent narrow-spectrum protein antibiotics known as bacteriocins. Two sequenced strains of the phytopathogenic bacterium *Pectobacterium carotovorum* carry genes encoding putative bacteriocins which have seemingly evolved through a recombination event to encode proteins containing an N-terminal domain with extensive similarity to a [2Fe-2S] plant ferredoxin and a C-terminal colicin M-like catalytic domain. In this work, we show that these genes encode active bacteriocins, pectocin M1 and M2, which target strains of *Pectobacterium carotovorum* and *Pectobacterium atrosepticum* with increased potency under iron limiting conditions. The activity of pectocin M1 and M2 can be inhibited by the addition of spinach ferredoxin, indicating that the ferredoxin domain of these proteins acts as a receptor binding domain. This effect is not observed with the mammalian ferredoxin protein adrenodoxin, indicating that *Pectobacterium* spp. carries a specific receptor for plant ferredoxins and that these plant pathogens may acquire iron from the host through the uptake of ferredoxin. In further support of this hypothesis we show that the growth of strains of *Pectobacterium carotovorum* and *atrosepticum* that are not sensitive to the cytotoxic effects of pectocin M1 is enhanced in the presence of pectocin M1 and M2 under iron limiting conditions. A similar growth enhancement under iron limiting conditions is observed with spinach ferredoxin, but not with adrenodoxin. Our data indicate that pectocin M1 and M2 have evolved to parasitise an existing iron uptake pathway by using a ferredoxin-containing receptor binding domain as a Trojan horse to gain entry into susceptible cells.

Citation: Grinter R, Milner J, Walker D (2012) Ferredoxin Containing Bacteriocins Suggest a Novel Mechanism of Iron Uptake in *Pectobacterium* spp.. PLoS ONE 7(3): e33033. doi:10.1371/journal.pone.0033033

Editor: Pierre Cornelis, Vrije Universiteit Brussel, Belgium

Received: November 17, 2011; **Accepted:** February 9, 2012; **Published:** March 9, 2012

Copyright: © 2012 Grinter et al. This is an open-access article distributed under the terms of the Creative Commons Attribution License, which permits unrestricted use, distribution, and reproduction in any medium, provided the original author and source are credited.

Funding: RG is supported by a Kelvin-Smith Studentship from the University of Glasgow. The funders had no role in study design, data collection and analysis, decision to publish, or preparation of the manuscript.

Competing Interests: The authors have declared that no competing interests exist.

* E-mail: Daniel.Walker@glasgow.ac.uk

Introduction

Bacteriocins are highly potent narrow-spectrum antibacterial protein toxins produced by a variety of Gram-negative bacteria that are active against bacteria closely related to the producing strain [1]. The best characterised of the bacteriocins are the colicins from *E. coli* and genes encoding putative bacteriocins with cytotoxic domains highly homologous to cytotoxic domains of the colicins can be identified in the genomes of a wide variety of Gram-negative bacteria. The cytotoxic activity of colicin-like bacteriocins is housed in a C-terminal domain, with central and N-terminal domains encoding receptor-binding and translocation functions [2]. Colicin cytotoxic domains take the form of a specific nuclease domain that hydrolyses DNA, tRNA or 16S rRNA, a pore-forming domain that depolarises the cytoplasmic membrane, or as in the case of colicin M, inhibits cell wall production through degradation of undecaprenyl-phosphate-linked peptidoglycan precursors [3,4]. The C-terminal domain is also the site of binding for a specific immunity protein that protects the producing cell from the lethal effects of the toxin [5,6]. To gain entry into target cells, colicins initially bind to a specific outer membrane receptor and cross this membrane through recruitment of host proteins of the TolABQR-Pal or TonB-ExbBD complexes in the periplasmic space [7,8]. A number of the receptors for colicins and

for the closely related pyocins are TonB dependent with a normal physiological role in iron siderophore uptake [9,10]. Unlike the colicins, little is known about the receptors and mechanisms of entry used by bacteriocins from plant pathogenic bacteria.

The genus *Pectobacterium* contains necrotrophic plant pathogens, characterised by their ability to secrete cell wall degrading enzymes including pectinases, cellulases, proteases and xylanases. These enzymes are produced in greater abundance in *Pectobacterium* spp. than in other phytopathogenic bacteria and give the genus its distinctive soft rot phenotype. The genus *Pectobacterium* is divided into four species *atrosepticum*, *betavasculorum*, *carotovorum* and *wasabiae* [11,12]. Strains of *carotovorum* and *wasabiae* have a broad host range, while *atrosepticum* and *betavasculorum* are restricted to potato and sugar beet respectively [13]. *P. atrosepticum* is the causative agent of black leg in potato, one of the most economically important diseases of any temperate crop [14].

Iron acquisition mechanisms of *Pectobacterium* have not yet been studied extensively, however the genus has been shown to acquire iron by diverse mechanisms including siderophore, haem iron and ferric-citrate production/absorption [15,16]. The closely related soft rot pathogen *Dickeya dadantii* (formerly *Erwinia chrysanthemi*) has been shown to possess two high affinity iron siderophores (achromobactin and chrysobactin) and mutants impaired in the production of these siderophores are less virulent, suggesting iron

acquisition is an important virulence determinant in infection [17]. Additionally, transcription of pectolysin genes responsible for degradation of the host cell wall during infection, has been shown to be triggered by iron limitation, suggesting a link between iron limitation and pathogenesis [18].

Plant-type ferredoxins are a super family of proteins containing a single [2Fe-2S] cluster. They are predominantly present in the chloroplasts, where they primarily function as electron carriers from photosystem one to enzymes responsible for carbon, nitrogen and sulphur assimilation [19]. Plant-type ferredoxins are also present in the non-photosynthetic tissues of plants suggesting a wider physiological relevance. Genes very closely related to those encoding plant-type ferredoxins are also present, seemingly uniquely among heterotrophic bacteria, in the genomes of a number of *Pectobacterium* species. These genes were likely acquired by horizontal gene transfer [20]. [2Fe-2S] ferredoxins more distantly related to plant-type ferredoxins are widely distributed through prokaryotic and eukaryotic kingdoms [21].

In this work we have purified and characterised two novel bacteriocins from *Pectobacterium* species. These bacteriocins, named pectocin M1 and M2, contain a predicted N-terminal domain with high levels of sequence similarity to plant ferredoxins and a C-terminal domain highly homologous to the catalytic domain of the *E. coli* bacteriocin, colicin M. The cytotoxic activity of these bacteriocins is limited to *Pectobacterium* spp. and is dependent on iron availability. Our data indicate that the ferredoxin domain acts as a receptor binding domain and that these bacteriocins have evolved to gain entry into susceptible cells through parasitisation of a previously unreported iron uptake system in *Pectobacterium* spp.

Results

Identification of pectocin M genes in the genomes of *Pectobacterium* spp.

As part of a wider study into the identification and potential use of bacteriocins as biocontrol agents we searched the genome sequences of plant pathogenic bacteria for genes encoding putative colicin-like bacteriocins. Two putative colicin M-like bacteriocin genes were identified in the genomes of *P. carotovorum* subsp. *carotovorum* PC1 (*Pcc* PC1) and *P. carotovorum* subsp. *brasiliensis* BPR1692 (*Pcb* BPR1692). These genes encode proteins that we have named pectocin M1 and pectocin M2, respectively. Pectocin M1 and M2 have an N-terminal domain with approximately 60% identity to spinach ferredoxin I and a C-terminal domain with approximately 46% identity to the catalytic domain of colicin M (Figure 1a and b). The colicin M-like domains of both proteins contain all residues that have previously been shown to be important for the catalytic activity and consequently cytotoxicity of colicin M [22]. A linker region of approximately 20 amino acids, which is not conserved between pectocin M1 and M2 connects the two domains and overall these proteins share 58% sequence identity.

Phylogenetic analysis of the ferredoxin domains of these pectocins show they cluster with a number of other ferredoxin and ferredoxin-domain containing proteins from *Pectobacterium* species (Figure 1c). This cluster of sequences is most similar to [2Fe-2S] ferredoxins from plants and cyanobacteria, with ferredoxins from the genus *Arabidopsis* sharing the highest sequence identity. This cluster is much more distantly related to typical bacterial ferredoxins (Figure 1c). The cysteine residues of plant ferredoxins that coordinate the [2Fe-2S] cluster in the active centre of these proteins are conserved in the pectocins, indicating that these proteins may also contain the [2Fe-2S] cluster (Figure 1b).

Evolution of the pectocin M1 gene through gene duplication and recombination

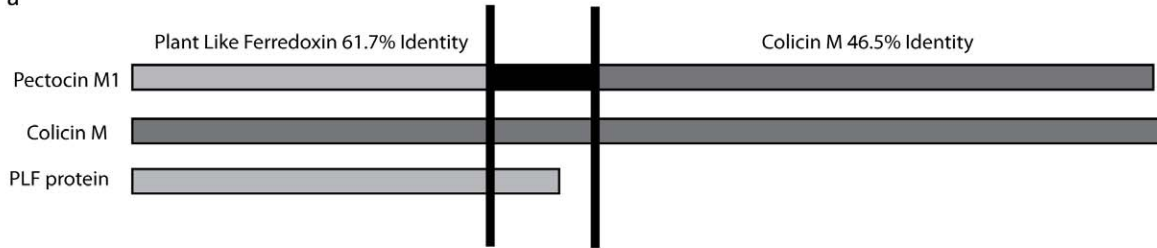
Analysis of the genomic context of pectocin M1 gives clues to its evolutionary origin. As shown in Figure 2a, approximately 3000bp upstream of the gene coding for pectocin M1, is a predicted open reading frame encoding a plant-like ferredoxin with 52% amino acid identity to the ferredoxin domain of pectocin M1. Alignment of the nucleotide sequences of these regions (Figure 2b) shows high nucleotide conservation (>50%) that encompasses the area of sequence similarity between pectocin M1 and the plant-like ferredoxin, as well as part of a hypothetical open reading frame present in both regions, but truncated in the pectocin M1 region. High levels of similarity and truncation of the adjacent open reading in the pectocin M1 region strongly suggests a gene duplication event. Evolution of the gene encoding the active bacteriocin is therefore likely to have occurred after this gene duplication event, through recombination between the duplicated ferredoxin gene and an ancestral bacteriocin carrying a colicin M-like cytotoxic domain. An open reading frame directly upstream of the pectocin M1 gene encodes a likely pectocin M1 immunity protein, which shares 24% amino acid identity with the immunity protein of colicin M. Pectocin M2 does not share this genomic context, however the open reading frame directly upstream codes for a bacteriocin closely related to carocin S2 [23], suggesting it may have been recruited to a genomic island.

Purification and characterisation of pectocin M1 and M2

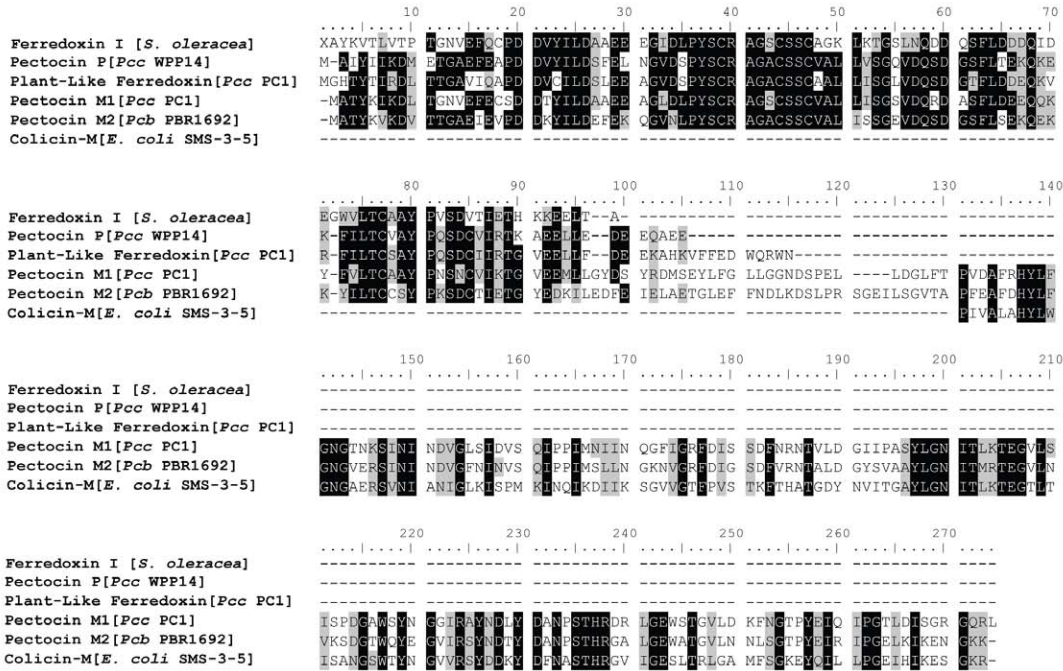
Pectocin M1 and M2 were expressed in *E. coli* BL21 (DE3) and purified by anion exchange chromatography and gel filtration to >90% homogeneity based on analysis by SDS PAGE (Figure 3a). The purified recombinant proteins were red-brown in colour and the absorption spectra of both proteins displayed maxima at 330 nm, 423 nm, and 466 nm (Figure 3b), which are characteristic of plant ferredoxins [21]. These data show both pectocins M1 and M2 contain a [2Fe-2S] cluster.

Initially the killing spectrum of pectocin M1 and pectocin M2 was tested against five *P. atrosepticum* and five *P. carotovorum* isolates using the agar overlay spot test method on LB agar. Under these experimental conditions pectocin M1 was found to be active against three *atrosepticum* strains and one *carotovorum* strain. The zones of inhibition in this experiment while distinct, were hazy (Figure 3c). Pectocin M2 did not show activity against any of the strains tested under these conditions. Since a number of bacteriocins utilise outer membrane receptors involved in iron uptake [2] we tested the activity of the pectocins under iron limiting conditions induced by addition of the iron chelator 2,2'-bipyridine to the LB agar. Under these conditions, the activity of pectocin M1 was greatly enhanced (Figure 3c), with seven of ten *Pectobacterium* spp. being inhibited. For pectocin M2, three of the ten strains were weakly inhibited (Table 1, Table S1). The minimum inhibitory concentration of pectocin M1 under iron-limiting conditions was calculated using the above method with serial dilutions of pectocin M1 and varied from 14.5–145 nM among susceptible strains. The cytotoxic effect of pectocin M1 in liquid culture was tested by adding varying concentrations of pectocin M1 to an iron limited log-phase culture of the susceptible strain *P. atrosepticum* LMG 2386. A concentration-dependent reduction in growth was observed upon the addition of pectocin M1 (Figure 3d). To determine if pectocin M1 and M2 might be active against more distantly related bacterial species, pectocin M1 and pectocin M2 were tested for inhibitory activity against strains of *E. coli*, *Pseudomonas syringae*, *Pseudomonas aeruginosa* and *Ervinea rhapontici* (see Table S2). None of these more distantly related bacteria showed any susceptibility to pectocin M1 or M2 (at 1.2 and

a



b



c

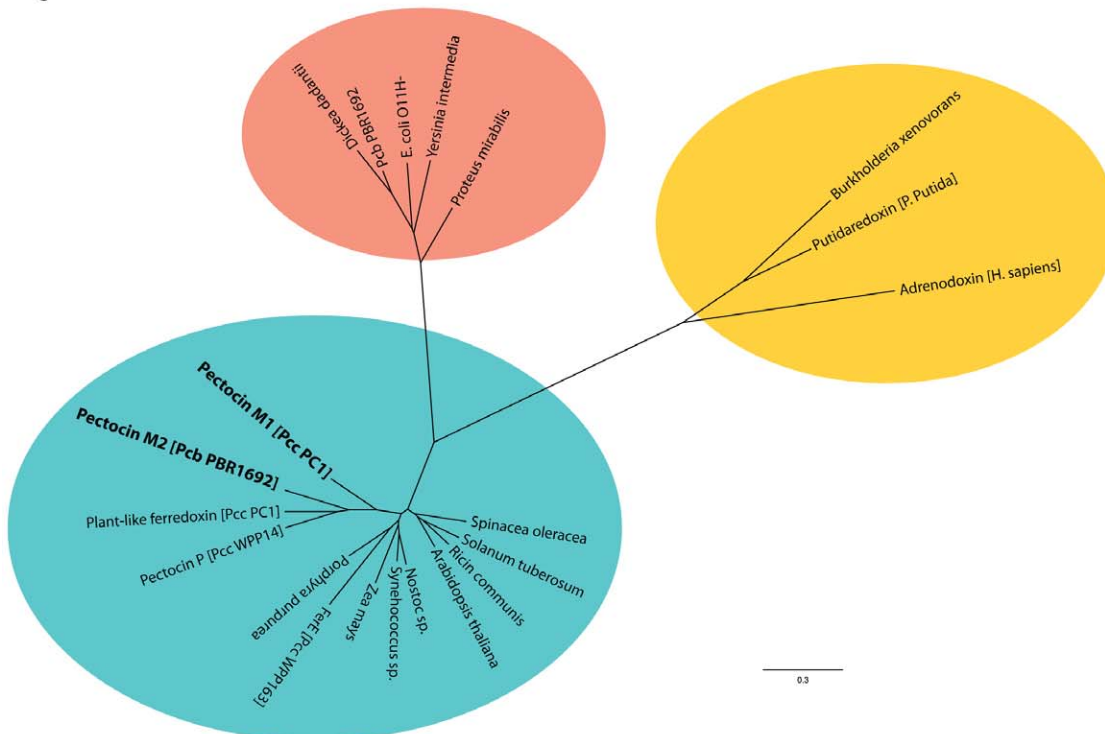


Figure 1. Domain structure, homology and molecular phylogeny of pectocins M1 and M2. a) Domain structure of pectocin M1 and relationship to colicin M and plant ferredoxin. b) Sequence alignment of pectocin M1, M2 and pectocin P (see discussion) with [2Fe-2S] ferredoxin type proteins and colicin M. For clarity of presentation prior to alignment pectocin P was truncated to amino acids 1–101 (N-terminal domain) and colicin M was truncated to amino acids 128–271 (C-terminal domain). Genbank/PDB accession numbers are as follows: Ferredoxin I [*S. oleracea*] 1704156A, plant-like ferredoxin [*Pcc* PC1] YP_003017870, pectocin M1 [*Pcc* PC1] YP_003017875, pectocin M2 [*Pcb* BPR1692] ZP_03825528, colicin M [*E. coli* SMS-3-5] YP_001739994, pectocin P [*Pcc* WPP14] ZP_03830397. Invariant residues are highlighted in black, residues with similar properties in gray b) Nearest neighbour joining molecular phylogenetic tree of [2Fe-2S] ferredoxins and pectocin ferredoxin domains. Bootstrap values (%) at major nodes are indicated. Species names represent independent ferredoxin proteins from listed species, typifying the class of ferredoxin. Proteins discussed in the study are named with species designation in brackets. Plant ferredoxins and adrenodoxin were aligned with signal peptides removed, pectocin sequences were trimmed to minimum region on homology with plant-like ferredoxin from *Pcc* PC1. Ellipses designate the following: blue=plant-type ferredoxins, red=ferredoxins found predominately in γ -proteobacteria, yellow=ferredoxins involved in electron transport to cytochrome P450. Scale represents substitutions per amino acid site.
doi:10.1371/journal.pone.0033033.g001

10 mg/ml respectively) suggesting that the activity of these pectocins is limited species of *Pectobacterium* closely related to the producing strain.

The ferredoxin domain of pectocins M1 and M2 mediate receptor binding

As ferredoxin is a potential iron source for phytopathogenic *Pectobacterium* species we hypothesised that pectocins M1 and M2 were parasitising an existing iron uptake system by using their ferredoxin domain to bind to a cell surface receptor, which has a normal physiological role in iron acquisition from ferredoxin. If this is the case, the addition of a plant ferredoxin at sufficient concentration should abolish pectocin M1 binding to its receptor and therefore abolish its cytotoxic activity. To test this hypothesis spinach ferredoxin was spotted adjacent to pectocin M1 in an agar overlay spot test. Clear inhibition of cell killing was observed in the region where the diffusion zone of spinach ferredoxin overlaps with the pectocin M1 diffusion zone (Figure 4a). Indeed, for all 7 susceptible strains cytotoxicity of pectocin M1 could be abolished to a similar extent by the addition of spinach ferredoxin. This effect was not observed with adrenodoxin, a more distantly related mammalian [2Fe-2S] cluster containing ferredoxin, indicating a level of specificity for plant ferredoxins (Figure 4a). Additionally, in five pectocin M1 susceptible strains that are not sensitive to pectocin M2 the cytotoxicity of pectocin M1 could be abolished by the addition of pectocin M2, indicating these two bacteriocins utilise the same receptor.

To determine if the activity of the colicin M-like domain of pectocin M1 is essential for its cytotoxicity, we made a mutant protein in which Asp222 is replaced by Ala. The equivalent Asp of colicin M has been shown to be essential for the catalytic activity and consequent cytotoxicity of colicin M [22]. Purified pectocin

M1 Asp222Ala had no detectable cytotoxicity, but was able to abolish cytotoxicity of wild-type pectocin M1 indicating that it is fully functional in binding to its receptor (Figure 4a). Taken together, these data indicate that receptor recognition occurs through the ferredoxin domain of pectocin M1 and M2 and that the normal physiological role of pectocin M1/M2 receptor is to bind plant ferredoxins.

Growth enhancement under iron limiting conditions by pectocins and spinach ferredoxin

During spot tests on iron limiting media to determine the killing spectrum of pectocin M1 and M2 we observed that the growth of a number of insensitive *Pectobacterium* strains was observably enhanced where the pectocins were spotted onto the plate. Additionally, some strains that were inhibited by pectocin M1 displayed a zone of enhanced growth peripheral to the zone of inhibition. Four and five of the ten *Pectobacterium* isolates exhibited enhanced growth in the presence of pectocin M1 and M2 respectively. The enhancement of growth due to pectocin M1 was significantly more pronounced than that due to pectocin M2, with strongest enhancement present at 200 μ M 2,2'-bipyridine for both pectocin M1 and pectocin M2 (Table S1). This observation led us to hypothesise that *Pectobacterium* strains are able to utilise these ferredoxin domains as an iron source under iron limiting conditions.

To test this idea further, and to test the specificity of this growth enhancement, related plant and mammalian ferredoxin-type proteins (spinach ferredoxin I and human adrenodoxin) as well as syringacin M, a colicin M homologue from *Pseudomonas syringae* which contains an active colicin M catalytic domain but an unrelated N-terminal region [24] (unpublished data) were tested for their ability to enhance the growth of *Pectobacterium* spp.

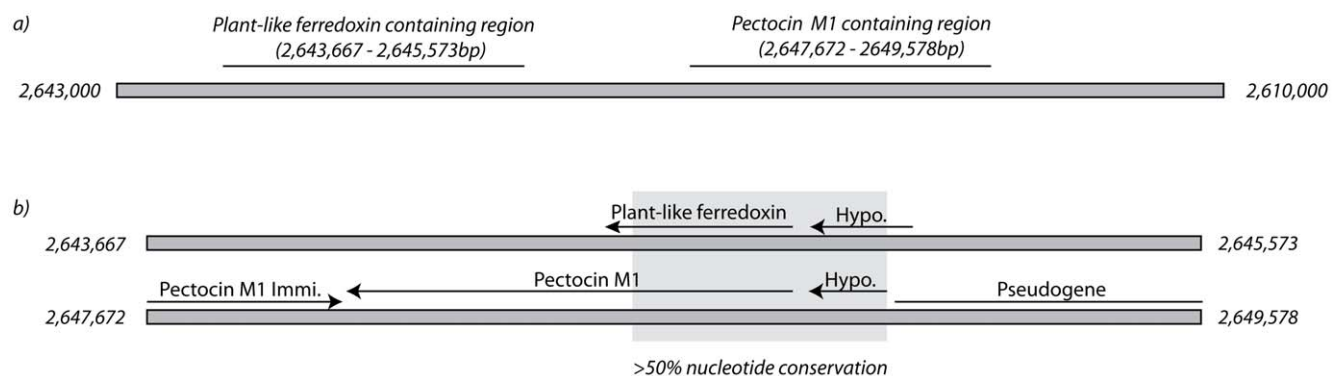


Figure 2. Genomic context of the pectocin M1 gene. a) Position of genomic regions on the chromosome of *Pcc* PC1 containing the pectocin M1 gene and a related plant-like ferredoxin gene. b) Alignment of genomic regions from above, containing the pectocin M1 gene and the related plant-like ferredoxin gene showing annotated open reading frames and nucleotide homology shared between the two regions.
doi:10.1371/journal.pone.0033033.g002

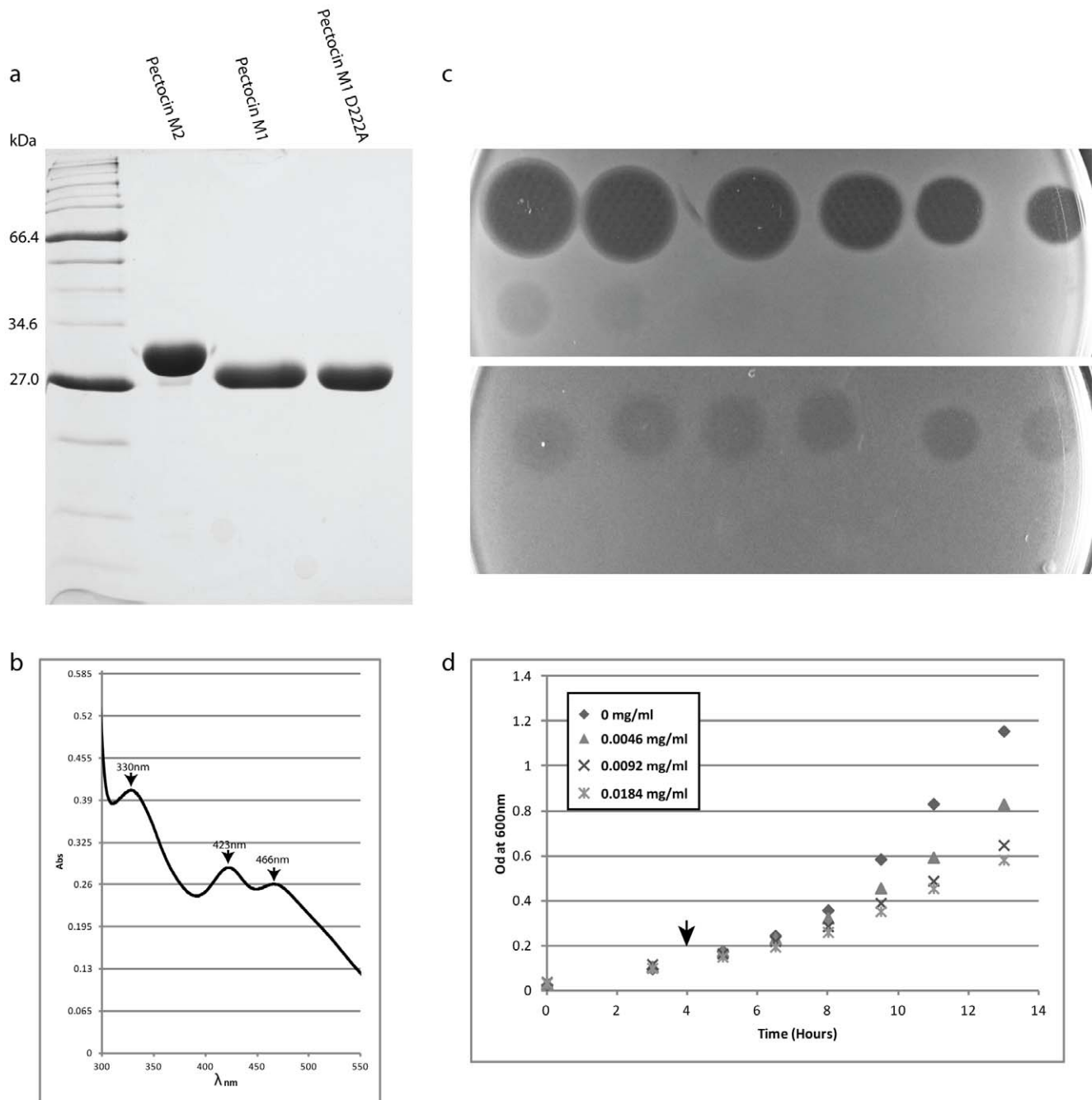


Figure 3. Purification and characterisation of pectocin M proteins. a) SDS PAGE of purified pectocin M2, M1 and M1 D222A b) Absorbance spectrum of pectocin M1 at a concentration 1.2 mg ml^{-1} . Maxima at 330, 423 and 466 nm, identical to those observed in plant ferredoxins, indicate the presence of a $[2\text{Fe-2S}]$ cluster in pectocin M1. Spectra with identical absorbance peaks were obtained for the pectocin D222A mutant and pectocin M2. c) Agar overlay spot tests of a 3-fold serial dilution ($68 \text{ }\mu\text{M}$ - 0.385 nM) of pectocin M1 spotted onto overlay of *P. atrosepticum* LMG 2386 cells grown in the presence (top) and absence (bottom) of the iron chelator 2,2'-bipyridine ($200 \text{ }\mu\text{M}$). d) Liquid growth inhibition assay, test strain LMG 2386, grown in LB broth with $200 \text{ }\mu\text{M}$ 2,2'-bipyridine. Purified PM1 was added when indicated. doi:10.1371/journal.pone.0033033.g003

under iron-limiting conditions. Five strains exhibited strongly enhanced growth due to the spinach ferredoxin at either 20 or 2 mg ml^{-1} (Figure 4b), this enhanced growth was dependent on the concentration of the iron chelator 2,2'-bipyridine, with the strongest enhancement at $400 \text{ }\mu\text{M}$ (Table S1). No enhanced growth was observed with the $[2\text{Fe-2S}]$ cluster containing protein adrenodoxin at 30 mg ml^{-1} or syringacin M at 5 mg ml^{-1} .

Discussion

In this work we have identified, purified and characterised two novel bacteriocins, pectocin M1 and M2, which are active against selected strains of *Pectobacterium* spp. These bacteriocins share a common domain structure, with an N-terminal ferredoxin domain containing a $[2\text{Fe-2S}]$ cluster and a C-terminal cytotoxic domain homologous to colicin M. Activity of pectocin M1 was inhibited by

Table 1. Susceptibility of *Pectobacterium* strains to pectocin M1 and M2.

Species	No. Strains tested	No. Strains susceptible to indicated Pectocin	
		M1	M2
<i>Pb. atrosepticum</i>	5	5	1
<i>Pb. carotovorum</i>	5	2	1

doi:10.1371/journal.pone.0033033.t001

the addition of spinach ferredoxin, which strongly suggests that the ferredoxin domain mediates binding to a receptor on the surface of sensitive *Pectobacterium* strains. The mammalian ferredoxin adrenodoxin was unable to elicit this effect, even at a concentration 15 times higher than the lowest tested spinach ferredoxin concentration. This suggests that the pectocin M receptor is specific for plant-type ferredoxin and is not merely binding due to the presence of an iron sulphur cluster. The inhibition of bacteriocin cytotoxicity as an indicator of competition is well established by previous studies of bacteriocin-receptor interactions in *E. coli*. For example, colicin M, which gains entry to the cell via the

ferrichrome receptor FhuA, can be blocked by the addition of ferrichrome, the normal physiological ligand of FhuA. In addition, colicin M is able to block albomycin activity, an antibiotic which also uses FhuA as a receptor [22,25,26]. Similarly vitamin B₁₂, the substrate of the BtuB receptor, is able to inhibit cytotoxicity of the E group colicins which also bind this receptor [27].

The cytotoxicity and spectrum of killing of pectocin M1 and M2 is greatly enhanced under iron limiting conditions suggesting that production of their receptor is unregulated and that this receptor likely plays a role in iron acquisition. This idea is supported by the observation that some strains of *Pectobacterium* spp. are able to exhibit enhanced growth under iron limiting conditions in the presence of a plant-like ferredoxin, either in the form of spinach ferredoxin or the pectocins themselves. The growth enhancement is specific to the extent that adrenodoxin does not elicit this effect. The enhanced growth observed under iron limiting conditions in the presence of the pectocins and spinach ferredoxin, suggests that the iron contained in plant-like ferredoxins can be specifically utilised by *Pectobacterium* species. Taken together, these data strongly suggest that the pectocin M receptor has a normal physiological role in iron acquisition from plant ferredoxin.

The importance of iron acquisition in bacterial pathogenesis of animals is well established and the ability to acquire sufficient iron often determines the success or failure of an infection [28]. The dynamics of iron availability during bacterial pathogenesis of plants is less well understood, although a number of studies have strongly correlated iron acquisition and virulence in *planta* [17,18,29]. During infection, *Pectobacterium* species release large quantities of pectinases and cellulases which macerate host tissues creating the distinctive soft rot associated with the genus. This disease phenotype results in cell lysis and the release of intracellular nutrients for absorption by the bacteria [11]. Since ferredoxin is the major iron containing protein in plants it undoubtedly represents an attractive potential source of iron in an environment of low iron availability [30]. As such, the ability of *Pectobacterium* spp. to acquire iron from ferredoxin may represent an important virulence mechanism, although this remains to be tested.

A number of iron acquisition systems involving absorption from iron containing proteins have been identified in pathogenic bacteria [28]. The best studied system involves the transferrin-binding proteins TbpA and TbpB of *Neisseria* spp. These outer membrane proteins bind transferrin with a preference for the holoprotein, strip the protein of its two iron atoms before releasing the apoprotein into the extracellular environment. These proteins have been shown to be specific for the transferrin of the host and are essential for virulence [31]. Whether the entire ferredoxin protein or simply the iron which it contains is taken into the cell by *Pectobacterium* is currently unknown.

The ferredoxin domain of pectocin M1 is closely related to plant ferredoxins and the pectocin M1 gene has seemingly evolved through duplication of a horizontally acquired plant ferredoxin gene and subsequent recombination with an ancestral colicin M-like bacteriocin. The presence of ferredoxin genes in *Pectobacterium* spp. that appear to have been acquired through horizontal gene transfer from plants has been previously noted [20]. In addition to pectocin M1 and M2, we have identified a further putative bacteriocin that contains an N-terminal ferredoxin domain. Analysis of the genome sequence of *Pectobacterium carotovorum* subsp. *carotovorum* WPP14 revealed a gene encoding a putative bacteriocin (designated pectocin P, Figure 1b) with an N-terminal ferredoxin domain and a C-terminal domain with 41% identity to the C-terminal 187 amino acids of pectocin, a peptidoglycan degrading bacteriocin with muramidase activity from *Yersinia pestis*

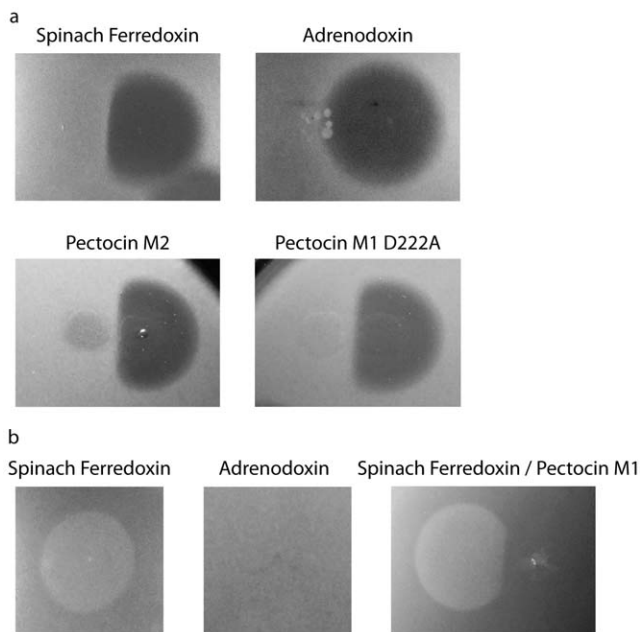


Figure 4. Asymmetric pectocin M1 spot test inhibition zones and growth enhancement due to plant-like ferredoxin, but not adrenodoxin a) Asymmetric pectocin M1 inhibition zones against *P. atrosepticum* LMG2386 due to plant-like ferredoxin containing proteins. Protein concentration for spots were as follows: pectocin M1 1.2 mg ml⁻¹, spinach ferredoxin 20 mg ml⁻¹, adrenodoxin 30 mg ml⁻¹, pectocin M2 10 mg ml⁻¹, pectocin M1 D222A 5.6 mg ml⁻¹ b) Growth enhancement of *P. carotovorum* subsp. *carotovorum* LMG 2410 by plant-like ferredoxin containing proteins. Protein concentrations for spots were as follows: spinach ferredoxin 20 mg ml⁻¹, adrenodoxin 30 mg ml⁻¹, Spinach ferredoxin 20 mg ml⁻¹:pectocin M1 1.2 mg ml⁻¹. Pectocin M1 causes asymmetry in zone of enhancement due to spinach ferredoxin in LMG 2410 (400 μM 2,2'-bipyridine) presumably through competition for a common receptor. Pectocin M1 does not enhance growth of this strain under these conditions.

doi:10.1371/journal.pone.0033033.g004

[32,33,34]. Like colicin M the cellular target of pesticin is located in the periplasm and as such a receptor binding and translocation domain sufficient to deliver a colicin M catalytic domain to its site of action would also be sufficient to deliver the cytotoxic domain of a pesticin-like bacteriocin. Recombination and gene duplication have been well established as evolutionary mechanisms for generating bacteriocins with new specificities [1]. Many of the colicins and related bacteriocins identified to date are mosaics of related receptor binding, translocation and catalytic domains [2,35]. However, the evolution of ferredoxin containing bacteriocins seems to be unprecedented in that *Pectobacterium* spp. has successfully utilised a horizontally acquired host gene for competition against closely related bacterial strains.

Methods

Bacterial strains and media

Strains of *Pectobacterium* spp. used in this study are listed in Table 2. Other bacterial strains are listed in Table S2. All bacterial strains were grown in LB broth with the exception of *Pseudomonas syringae* pathovars which were grown in Kings B Broth. All strains were grown at 28°C, with the exception of *E. coli* and *P. aeruginosa* which were grown at 37°C. Media was supplemented with ampicillin 100 µg ml⁻¹, kanamycin 50 µg ml⁻¹, isopropyl-β-D-thiogalactopyranoside (IPTG) 0.1–1 mM or 2,2'-bipyridine 100–400 µM when required.

Plasmid construction and DNA manipulation

Plasmids used in this study are outlined in Table 2. pJMPCI and pJMBPR which contain the open reading frames of pectocin M1 and M2 and unique NdeI and XhoI sites at the start codons and

directly after the stop codons of the pectocin genes were synthesized by DNA 2.0. Plasmids pETMPCI and pMBPR, used for expression of the pectocin M1 and M2, respectively were created by subcloning the NdeI/XhoI fragments of pJMPCI and pJMBPR into the corresponding sites of pET-21a. The D222A mutant of pectocin M1 was created using the QuikChange Site Directed Mutagenesis Kit (Stratagene) utilising pETMPCI as a template and the following primers, (5'-GCA TCC GCG CAT ATA ACG CTC TGT ATG ATG CTA ATC CG-3', 5'-CGG ATT AGC ATC ATA CAG AGC GTT ATA TGC GCG GAT GC-3') to give the D222A pectocin M1 encoding plasmid pETMPCID222A.

Protein expression and purification

Pectocin M1 and M2 were expressed in *E. coli* BL21 (DE3) carrying the plasmid pETPCI or pETBPR, respectively. Cells were grown at 37°C and protein expression was induced by the addition of IPTG at an OD₆₀₀ of approximately 0.6. Cultures were grown for a further six hours at 28°C. Cells were harvested and resuspended in 50 mM Tris-HCl, pH 7.5, 20 mM NaCl and Complete EDTA free protease inhibitor cocktail tablets (Roche) were added. After disruption by sonication the supernatant was clarified by centrifugation and applied to a DE-52 anion exchanged column (Whatman) equilibrated in 50 mM Tris-HCl, pH 7.5, 20 mM NaCl. Bound protein was eluted with a linear gradient of 20–600 mM NaCl in lysis buffer. Pectocin containing fractions were identified based on colour and analysis by SDS-PAGE. Pectocin containing fractions were pooled and dialysed into 50 mM Tris-HCl, pH 7.5, 20 mM NaCl and loaded onto a Superdex S75 26/60 column, (GE Healthcare). To obtain homogenous protein a final purification step using a Mono Q

Table 2. Strains and plasmids used in this study.

Strain or Plasmid	Relevant Characteristic(s)	Source or Reference
<i>P. carotovorum</i> subsp. <i>carotovorum</i>		
LMG 2410	Isolated from <i>Cucumis sativus</i>	BCCM
LMG 2412	Isolated from <i>Hyacinthus orientalis</i>	BCCM
LMG 2442	Isolated from <i>Brassica oleracea</i>	BCCM
LMG 2444	Isolated from <i>Solanum tuberosum</i> (tuber soft rot)	BCCM
LMG 2913	Isolated from soil	BCCM
<i>P. atrosepticum</i>		
LMG 2374	Isolated from <i>Apium graveolens</i> var. <i>dulce</i>	BCCM
LMG 2375	Isolated from <i>Solanum tuberosum</i> (tuber soft rot)	BCCM
LMG 2386	Isolated from <i>Solanum tuberosum</i> (stem rot)	BCCM
LMG 2391	Isolated from soil	BCCM
SCRI 1043	Isolated from <i>Solanum tuberosum</i> (tuber soft rot)	[37]
Plasmids		
pJexpress411	Kan ^r cloning/expression vector, T7 promoter	this study
pJexpress404	Amp ^r cloning/expression vector, T5 promoter	this study
pET21-a(+)	Amp ^r cloning/expression vector, T7 promoter	Novagen
pJMPC1	Kan ^r pJexpress411 with Pectocin M1 inserted into NdeI/XhoI sites	this study
pJMBPR	Kan ^r pJexpress411 with Pectocin M2 inserted into NdeI/XhoI sites	this study
pETMPCI	Amp ^r pET21-a(+) with Pectocin M1 inserted into NdeI/XhoI sites	this study
pETMPCID222A	Amp ^r pET21-a(+) with Pectocin M1 D222A inserted into NdeI/XhoI sites	this study
pETMBPR	Amp ^r pET21-a(+) with Pectocin M2 inserted into NdeI/XhoI sites	this study

BCCM = Belgian Co-ordinated Collections of Micro-organisms, NCPPB = National Collection Plant Pathogenic Bacteria, SCRI = Scottish Crop Research Institute.
doi:10.1371/journal.pone.0033033.t002

(GE Healthcare) anion exchange column was employed with bound protein eluted with a linear gradient of 20–700 nM NaCl in 50 mM Tris-HCl, pH 7.5. Fractions were pooled as above and dialysed into 50 mM Tris-HCl, pH 7.5, 100 mM NaCl. Dialysed fractions were aliquoted and frozen at -80°C . The absorption spectrum of purified pectocins was determined using a UV-1700 Pharma Spec, UV-VIS spectrophotometer (Shimadzu). Spinach ferredoxin was obtained from Sigma-Aldrich. Adrenodoxin was provided as a gift from Ms Alette Brinth (University of Glasgow) and was judged as >90% holoprotein, based on the ratio of absorbance at 414 nm and 276 nm.

Growth inhibition/enhancement assays

Inhibition of growth on solid media was determined using the soft agar overlay method [36]. 100 μl of mid-log phase culture of the test strain was added to 5 ml of 0.6% agar in dH_2O melted and cooled to 42°C . The molten agar was then overlaid onto LB medium with or without 100–400 μM 2,2'-bipyridine. Purified protein was spotted directly onto the surface of the overlay once solidified. To observe inhibition interference proteins were spotted within the others zone of diffusion on the plate. Plates were incubated for a further 12 hours and zones of inhibition/enhancement observed. For inhibition of growth in liquid culture cells were grown in LB broth with 200 μM 2,2'-bipyridine purified pectocin M1 was added to at mid-log phase and the OD_{600} was monitored throughout the experiment.

Identification of pectocins and bioinformatic analysis

Putative pectocins were identified by interrogating the National Center for Biotechnology (NCBI) non-redundant protein database

References

- Parret A, De Mot R (2002) Bacteria killing their own kind: novel bacteriocins of *Pseudomonas* and other γ -proteobacteria. *Trends Microbiol* 10: 107–12.
- Cascales E, Buchanan SK, Duche' D, Kleanthous C, Lloube's R, et al. (2007) Colicin Biology. *Microbiol Mol Biol Rev* 71: 159–229.
- El Ghachi M, Bouhss A, Barreteau H, Touze' T, Auger G, et al. (2006) Colicin M Exerts Its Bacteriolytic Effect via Enzymatic Degradation of Undecaprenyl Phosphate-linked Peptidoglycan Precursors. *J Biol Chem* 281: 21761–21772.
- Barreteau H, Bouhss A, Gerard F, Duche' D, Boussaid B, et al. (2010) Deciphering the Catalytic Domain of Colicin M, a Peptidoglycan Lipid II-degrading Enzyme. *J Biol Chem* 285: 12378–12389.
- Walker D, Moore MR, James R, Kleanthous C (2003) Thermodynamic consequences of bipartite immunity protein binding to the ribosomal ribonuclease colicin E3. *Biochemistry* 42: 4161–71.
- Kleanthous C, Walker D (2001) Immunity proteins: enzyme inhibitors that avoid the active site. *Trends Biochem Sci* 26: 624–31.
- Loftus SR, Walker D, Maté MJ, Bonsor DA, James R, et al. (2006) Competitive recruitment of the periplasmic translocation portal by Tol B by the natively disordered domain of colicin E9. *Proc Natl Acad Sci USA* 103: 12353–8.
- Kleanthous C (2010) Swimming against the tide: progress and challenges in our understanding of colicin translocation. *Nat Rev Micro* 8: 843–848.
- Baysse C, Meyer J, Plesiat P, Geoffroy V, Michel-Briand Y, et al. (1999) Uptake of Pyocin S3 Occurs through the Outer Membrane Ferripyoverdine Type II Receptor of *Pseudomonas aeruginosa*. *J Bacteriol* 181: 3849–3851.
- Zeth K, Römer C, Patzer SI, Braun V (2008) Crystal Structure of Colicin M, a Novel Phosphatase Specifically Imported by *Escherichia coli*. *J Biol Chem* 283: 25324–25331.
- Kim HS, Ma B, Perna NT, Charkowski AO (2009) Phylogeny and Virulence of Naturally Occurring Type III Secretion System-Deficient *Pectobacterium* Strains. *Appl Environ Microbiol* 75: 4539–4549.
- Koiv V, Andresen L, Mac A (2010) AcpA of *Pectobacterium* is not involved in the regulation of extracellular plant cell wall degrading enzymes production. *Mol Genet Genom* 283: 541–549.
- Ma B, Hibbing ME, Kim HS, Reedy RM, Yedidia I, et al. (2010) Host Range and Molecular Phylogenies of the Soft Rot Enterobacterial Genera *Pectobacterium* and *Dickeya*. *Phytopath* 97: 1150–1163.
- Pérombelon MCM (2002) Potato diseases caused by soft rot erwinias: an overview of pathogenesis. *Plant Pathol* 51: 1–12.
- Franza T, Expert D (2010) Iron up-take in soft rot Erwinia. In: Cornelius P, Andrews SC, eds. Iron uptake and homeostasis in microorganisms. Norfolk: Caister Academic Press. pp 101–116.
- Ishimaru CA, Loper LE (1992) High-affinity iron uptake systems present in *Erwinia carotovora subsp. carotovora* include the hydroxamate siderophore aerobactin. *J Bacteriol* 174: 2993–3003.
- Expert D (2006) Genetic Regulation of Iron in *Erwinia chrysanthemi* as Pertains to Bacterial Virulence. In: Barton LL, Abadia J, eds. Iron Nutrition in Plants and Rhizospheric Microorganisms. Dordrecht: Springer. pp 215–227.
- Franza T, Sauvage C, Expert D (1999) Iron Regulation and Pathogenicity in *Erwinia chrysanthemi* 3937: Role of the Fur Repressor Protein. *Mol Plant Microbe Interact* 12: 119–128.
- Fukuyama K (2004) Structure and Function of Plant-Type Ferredoxins. *Photosynth Res* 81: 289–301.
- Sjöblom S, Harjupää H, Brader G, Palva ET (2008) A Novel Plant Ferredoxin-Like Protein and the Regulator Hor Are Quorum-Sensing Targets in the Plant Pathogen *Erwinia carotovora*. *Mol Plant Microbe Interact* 7: 967–978.
- Hall DO, Cammack R, Rao KK (1972) The plant ferredoxins and their relationship to the evolution of ferredoxins from primitive life. *Pure and Applied Chem* 34: 553–578.
- Helbig S, Braun V (2011) Mapping functional domains of colicin M. *J Bacteriol* 193: 815–821.
- Chan Y, Wu J, Wu H, Tzeng K, Chuang D (2011) Cloning, purification, and functional characterization of Carocin S2, a ribonuclease bacteriocin produced by *Pectobacterium carotovorum*. *BMC Microbiol* 11: 99.
- Barreteau H, Bouhss A, Fourgeaud M, Mainardi J, Touze' T, et al. (2009) Human- and Plant-Pathogenic *Pseudomonas* Species Produce Bacteriocins Exhibiting Colicin M-Like Hydrolase Activity towards Peptidoglycan Precursors. *J Bacteriol* 191: 3657–3664.
- Wayne R, Frick K, Neilands JB (1976) Siderophore protection against colicins M, B, V, and Ia in *Escherichia coli*. *J Bacteriol* 126: 7–12.
- Ferguson AD, Coulton JW, Diederichs K, Wolfram W, Braun V, et al. (2000) Crystal structure of the antibiotic albomycin in complex with the outer membrane transporter FhuA. *Protein Sci* 9: 956–963.
- Cavard D (1994) Rescue by vitamin B₁₂ of *Escherichia coli* cells treated with colicins A and E allows measurement of the kinetics of colicin binding on BtuB. *FEMS Microbiol Lett* 1: 37–42.
- Ratledge C, Dover LG (2000) Iron metabolism in pathogenic bacteria. *Annu Rev Microbiol* 54: 881–941.
- Expert D, Toussaint A (1985) Bacteriocin-resistant mutants of *Erwinia chrysanthemi*: possible involvement of iron acquisition in phytopathogenicity. *J Bacteriol* 163: 221–227.

with the protein sequence for colicin M from *E. coli*, using the pBlast algorithm. Genomic regions containing proteins of interest were then investigated using the NCBI graphic interface. Sequences were saved in FASTA format and analysed using Bioedit, ClustalW multiple sequence alignment tool and CLC genomics workbench.

Supporting Information

Table S1 Enhancement/Inhibition of growth of *Pectobacterium spp.* at differing concentrations of 2,2'-bipyridine. (DOC)

Table S2 Non-*Pectobacterium* species tested for susceptibility to pectocins M1 and M2. (DOC)

Acknowledgments

We would like to thank Ms. Alette Brinth for kindly supplying purified human adrenodoxin, Dr Nick Tucker (Strathclyde) for *P. aeruginosa* strains and Philip Younger for creation and characterisation of pectocin M1 D222A. The authors would also like to thank members of the Walker group for critical reading of the manuscript.

Author Contributions

Conceived and designed the experiments: RG JJM DW. Performed the experiments: RG. Analyzed the data: RG DW. Contributed reagents/materials/analysis tools: RG DW. Wrote the paper: RG DW.

30. Terauchi AM, Lu S, Zaffagnini M, Tappa S, Hirasawa M, et al. (2009) Pattern of Expression and Substrate Specificity of Chloroplast Ferredoxins from *Chlamydomonas reinhardtii*. *J Biol Chem* 284: 25867–25878.
31. Parker Siburt CJ, Roulhac PL, Weaver KD, Noto JM, Mietzner TA, et al. (2009) Hijacking transferrin bound iron: protein–receptor interactions involved in iron transport in *N. gonorrhoeae*. *Metalomics* 1: 249–255.
32. Pils H, Killmann H, Hantke K, Braun V (1996) Periplasmic location of the pesticin immunity protein suggests inactivation of pesticin in the periplasm. *J Bacteriol* 178: 2431–2435.
33. Vollmer W, Pils H, Hantke K, Höltje JV, Braun V (1998) Pesticin displays muramidase activity *J Bacteriol* 179: 1580–1583.
34. Fetherston JD, Bearden SW, Perry RD (1996) YbtA, an AraC-type regulator of the *Yersinia pestis* pesticin/yersiniabactin receptor. *Mol Microbiol* 22: 315–325.
35. Michel-Briand Y, Baysse C (2002) The pyocins of *Pseudomonas aeruginosa*. *Biochimie* 84: 499–510.
36. Fyfe JM, Harris G, Govan JR (1984) Revised Pyocin Typing Method for *Pseudomonas aeruginosa*. *J Clin Microbiol* 20: 47–50.
37. Bell KS, Sebahai M, Pritchard L, Holden MTG, Myman LJ, et al. (2004) Genome sequence of the enterobacterial phytopathogen *Erwinia carotovora* subsp. *atroseptica* and characterization of virulence factors. *Proc Natl Acad Sci U S A* 30: 11105–11110.

Structure of the atypical bacteriocin pectocin M2 implies a novel mechanism of protein uptake

Rhys Grinter,^{1†} Inokentijis Josts,^{1†} Kornelius Zeth,^{2,3}
Aleksander W. Roszak,⁴ Laura C. McCaughey,¹
Richard J. Cogdell,⁵ Joel J. Milner,⁶
Sharon M. Kelly,⁵ Olwyn Byron⁶ and Daniel Walker^{1*}

¹Institute of Infection, Immunity and Inflammation,

⁵Institute of Molecular Cell and Systems Biology and

⁶School of Life Sciences, College of Medical, Veterinary
and Life Sciences, University of Glasgow, Glasgow G12
8QQ, UK.

⁴WestCHEM, School of Chemistry, College of Science
and Engineering, University of Glasgow, Glasgow G12
8QQ, UK.

²Unidad de Biofísica (CSIC-UPV/EHU), Barrio Sarriena
s/n, 48940, Leioa, Vizcaya, Spain.

³IKERBASQUE, Basque Foundation for Science, Bilbao,
Spain.

Summary

The colicin-like bacteriocins are potent protein antibiotics that have evolved to efficiently cross the outer membrane of Gram-negative bacteria by parasitizing nutrient uptake systems. We have structurally characterized the colicin M-like bacteriocin, pectocin M2, which is active against strains of *Pectobacterium* spp. This unusual bacteriocin lacks the intrinsically unstructured translocation domain that usually mediates translocation of these bacteriocins across the outer membrane, containing only a single globular ferredoxin domain connected to its cytotoxic domain by a flexible α -helix, which allows it to adopt two distinct conformations in solution. The ferredoxin domain of pectocin M2 is homologous to plant ferredoxins and allows pectocin M2 to parasitize a system utilized by *Pectobacterium* to obtain iron during infection of plants. Furthermore, we identify a novel ferredoxin-containing bacteriocin pectocin P, which possesses a cytotoxic domain homologous to lys-ozyme, illustrating that the ferredoxin domain acts as

a generic delivery module for cytotoxic domains in *Pectobacterium*.

Introduction

It is a dogma of colicin biology that after binding tightly to their cognate outer membrane (OM) receptor, colicins utilize an intrinsically unstructured translocation domain (IUTD) to recruit the inner membrane-bound Tol or Ton complex (Kleanthous, 2010; Housden *et al.*, 2013). These complexes, which are responsive to the proton motive force (pmf), mediate translocation of the bacteriocin across the OM (Cascales *et al.*, 2007; Housden *et al.*, 2010). The formation of a colicin translocon has recently been visualized directly for the DNase-type colicin E9 through the isolation and imaging of the colicin in complex with its primary receptor BtuB, the trimeric porin OmpF, which allows passage of the IUTD across the OM and the periplasmic protein TolB, which is a component of the cell envelope-spanning TolABQR-Pal complex (Housden *et al.*, 2013). Similarly, the TonB-dependent pore-forming colicin, colicin IA, uses one copy of the TonB-dependent receptor Cir as its primary receptor and a second copy as a translocation pathway for its IUTD to cross the OM to deliver a TonB-binding epitope to the periplasm (Jakes and Finkelstein, 2010). In addition to the colicins, which show a potent narrow spectrum of killing activity against strains of *E. coli* and other closely related bacteria, other colicin-like bacteriocins have also been characterized. These include the S-type pyocins from *Pseudomonas aeruginosa*, klebicins from *Klebsiella pneumoniae* and syringacin M from *P. syringae* (Riley *et al.*, 2001; Michel-Briand and Baysse, 2002; Barreteau *et al.*, 2009). The recently determined structures of the M-class bacteriocins pyocin M and syringacin M showed that like colicin M, these bacteriocins possess a 30- to 40-amino-acid IUTD, which is essential for translocation, indicating that translocation across the OM likely occurs through the same mechanism as the colicins (Zeth *et al.*, 2008; Barreteau *et al.*, 2012a,b; Grinter *et al.*, 2012b).

We recently described the novel M-class bacteriocins pectocin M1 and M2, which are produced by and active against strains of the soft-rot phytopathogens *Pectobacte-*

Accepted 23 May, 2014. *For correspondence. E-mail Daniel.Walker@glasgow.ac.uk; Tel. (+44) 141 3305082; Fax (+44) 141 3304297. †These authors contributed equally.

rium atrosepticum (*Pba*) and *Pectobacterium carotovorum* (*Pbc*) (Grinter *et al.*, 2012a; 2013). The domain structure of these proteins suggested that they challenge the dogma that an IUTD is the universal mechanism by which colicin-like bacteriocins achieve translocation. Pectocin M1 and M2 consist of an M-class cytotoxic domain with lipid II degrading activity, fused to a plant-like ferredoxin domain (Grinter *et al.*, 2012a; 2013). This ferredoxin domain, which contains an intact [2Fe-2S] iron–sulphur cluster, substitutes for the helical receptor binding domain and IUTD of the M-class bacteriocins discussed above, that are required to deliver the cytotoxic domain to the periplasm. Further to this, we observed that the addition of plant ferredoxin to strains of *Pba* and *Pbc* exposed to the pectocins inhibited bacteriocin-induced killing (Grinter *et al.*, 2012a). These observations show first, that *Pba* and *Pbc* possess an OM receptor able to bind ferredoxin and second, that pectocins M1 and M2 parasitize this receptor to target and ultimately gain entry to susceptible cells. The role of ferredoxin binding for these plant pathogens is apparent under iron-limiting conditions where, in the presence of plant ferredoxin, some strains of *Pectobacterium* spp. show strongly enhanced growth (Grinter *et al.*, 2012a). This effect is not observed on addition of the mammalian ferredoxin homologue, adrenodoxin, which also contains a [2Fe-2S] iron–sulphur cluster (even at greatly increased concentrations), indicating a high level of specificity for plant ferredoxin. Similarly, adrenodoxin is not able to rescue cells from pectocin M-induced killing (Grinter *et al.*, 2012a). Thus, like other colicin-like bacteriocins, pectocins M1 and M2 parasitize an existing nutrient uptake system to gain entry into target cells. However, for these bacteriocins the mechanism is overt and unprecedented, with the direct utilization of ferredoxin, a protein from which *Pectobacterium* spp. is able to directly acquire iron, as the targeting region of the bacteriocin (Grinter *et al.*, 2013).

In order to gain further insight into the mechanism through which pectocins M1 and M2 gain entry into target cells, we have used X-ray crystallography and small angle X-ray scattering along with *in silico* modelling approaches to characterize the structural and dynamic properties of pectocin M2. Our data show that there is a high degree of conformational flexibility between the ferredoxin and colicin M-like cytotoxic domain through movement of a linking helix and definitively show that the protein lacks the flexible IUTD that is characteristic of all other characterized colicin-like bacteriocins. The lack of an IUTD indicates that the ferredoxin-containing pectocins utilize an existing ferredoxin uptake mechanism to cross the OM, without direct interaction with the Tol or Ton complexes in the periplasm. Additionally, we have determined the existence of an additional ferredoxin-containing bacteriocin, pectocin P, which possesses a cytotoxic domain that is a structural homologue of lysozyme, illustrating that ferre-

doxin can act as a generic module for the delivery of structurally diverse cytotoxic proteins to the periplasm.

Results

The crystal structure of pectocin M2

In initial crystallization trials for pectocin M2, characteristic red-brown crystals of this ferredoxin-containing bacteriocin formed with PEG 3350 and ammonium sulphate as the precipitants. Data from these crystals were collected to 2.3 Å in the space group *P2*₁ and phased using anomalous scattering data from the metal centres of the [2Fe-2S] iron–sulphur cluster. The structure of pectocin M2 revealed an N-terminal domain with the predicted ferredoxin-fold (residues 2–94, in red), separated from the colicin M-like cytotoxic domain (residues 116–271, in blue) by a linker region (residues 95–115, in green) that forms an α -helix (Fig. 1A and B). There is a significant difference in the orientation of the cytotoxic and ferredoxin domains of the two pectocin M2 molecules in the asymmetric unit (ASU) with a root mean square deviation (r.m.s.d.) of 3.4 Å, between main-chain atoms (Fig. S1). The fold of the pectocin M2 ferredoxin domain is identical (r.m.s.d. 0.60 Å) to that of spinach ferredoxin (PDB ID = 1A70) and the C-terminal cytotoxic domain is highly similar to the lipid II-cleaving catalytic domains of colicin M (PDB ID = 2XMX, r.m.s.d. 1.7 Å) (Fig. 1C and D) (Zeth *et al.*, 2008). The crystal structure of pectocin M2 adds to a growing body of structural and biochemical data on colicin M-like cytotoxic domains (Zeth *et al.*, 2008; Barreteau *et al.*, 2010; 2012b; Helbig and Braun, 2011; Grinter *et al.*, 2012b). We confirmed the enzymatic activity of pectocin M1 and M2 by a lipid II hydrolysis assay (Fig. S2). In the recently solved structures of pyocin M (PaeM) and syringacin M a divalent metal ion (Ca²⁺ or Mg²⁺) is co-ordinated by a key catalytic aspartic acid side-chain in conjunction with two backbone carbonyls. Mg²⁺, Ca²⁺ or Mn²⁺ ions are required for catalytic activity of M-class bacteriocins, and analysis of these proteins has shown co-ordination at this position to be essential for activity (Grinter *et al.*, 2012b). In the pectocin M2 structure this key aspartate (D226) adopts an analogous conformation. However, no density for a metal ion is observed in this position, which is occupied by a water molecule (Fig. 2A). The absence of a metal ion is unsurprising given the lack of divalent ions and the high ionic strength of the crystallization conditions.

Comparative analysis of the catalytic domains of colicin M homologues reveals significant variation between the structures. In the structures of pyocin M and syringacin M a key conserved arginine is located distant from other conserved residues creating an open active-site cleft. In contrast, in the pectocin M2 structure this residue (R236) is orientated towards the other key catalytic residues

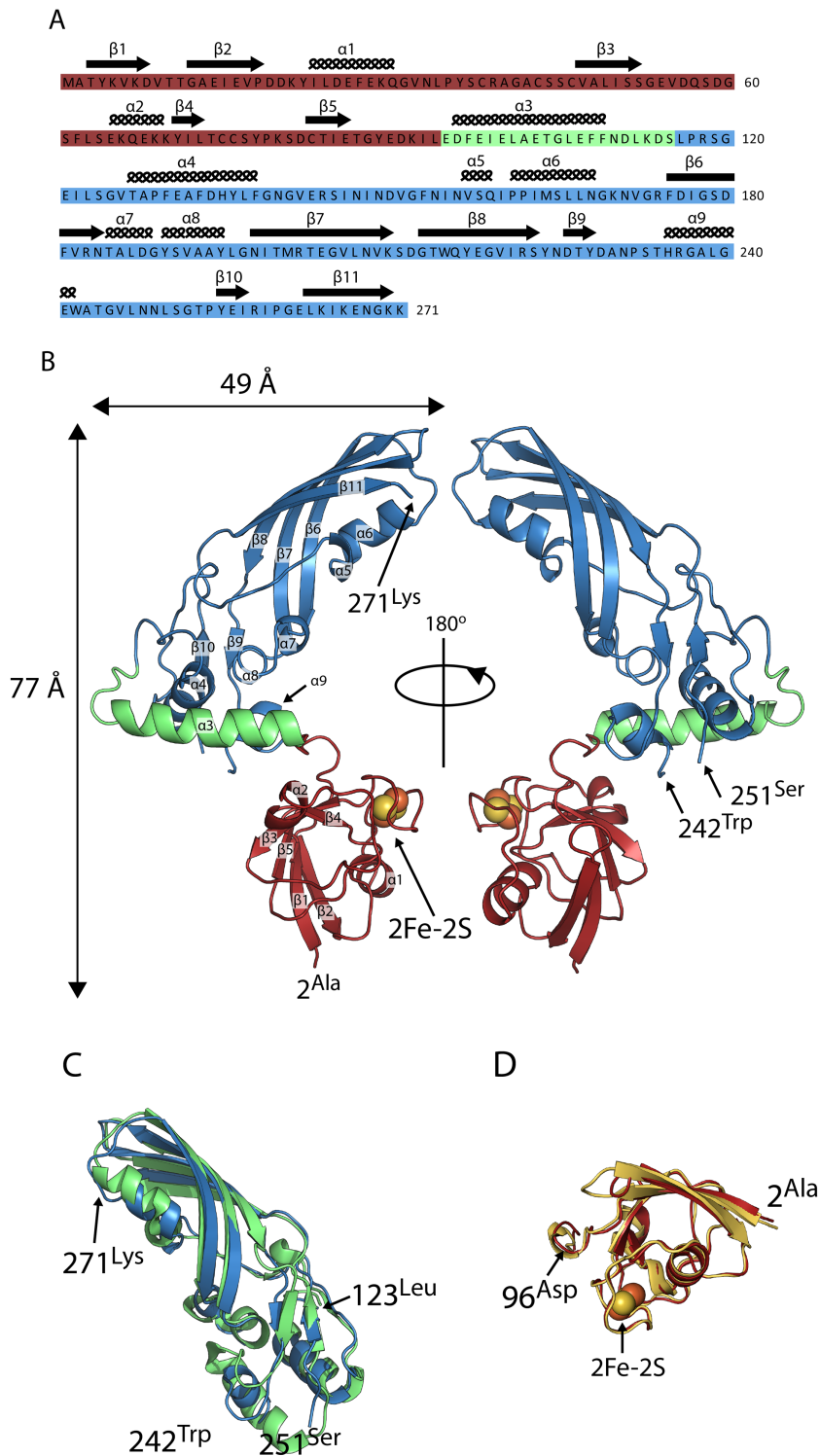


Fig. 1. The crystal structure of pectocin M1 reveals a ferredoxin-containing colicin-like bacteriocin that lacks an IUTD.

A. Amino acid sequence of pectocin M2, showing structural domains (ferredoxin domain = red, linker helix = green, catalytic domain = blue) and annotated with secondary structure.

B. Schematic of the crystal structure of pectocin M2 observed in the $P2_1$ crystal form, with the cytotoxic domain in blue, plant-like ferredoxin domain in red and linker helix in green. The [2Fe-2S] iron-sulphur cluster is represented by spheres.

C. Schematic of cytotoxic domain of pectocin M2 aligned with that of colicin M (PDB ID = 2XMX) (backbone r.m.s.d. = 1.65 Å, pectocin M2 residues = 123–271, colicin M residues = 123–271).

D. Schematic of the ferredoxin domain of pectocin M2 aligned with that of spinach ferredoxin (PDB ID = 1A70) (backbone r.m.s.d. = 0.6 Å, pectocin M2 residues = 2–96, spinach ferredoxin residues = 2–96).

(Fig. 2B). The electron density for R236 permitted modelling of two conformations, one within hydrogen bonding distance of the aspartic acid co-ordinated water and the other forming a hydrogen bond with N184. In this conformation, R236 creates a defined active site tunnel which

would enable co-ordination of the lipid II and positioning of the pyrophosphate group in close proximity to all key catalytic residues (Fig. 2A and B).

In contrast to the compact structures of the homologous bacteriocins, colicin M, pyocin M and syringacin M, where

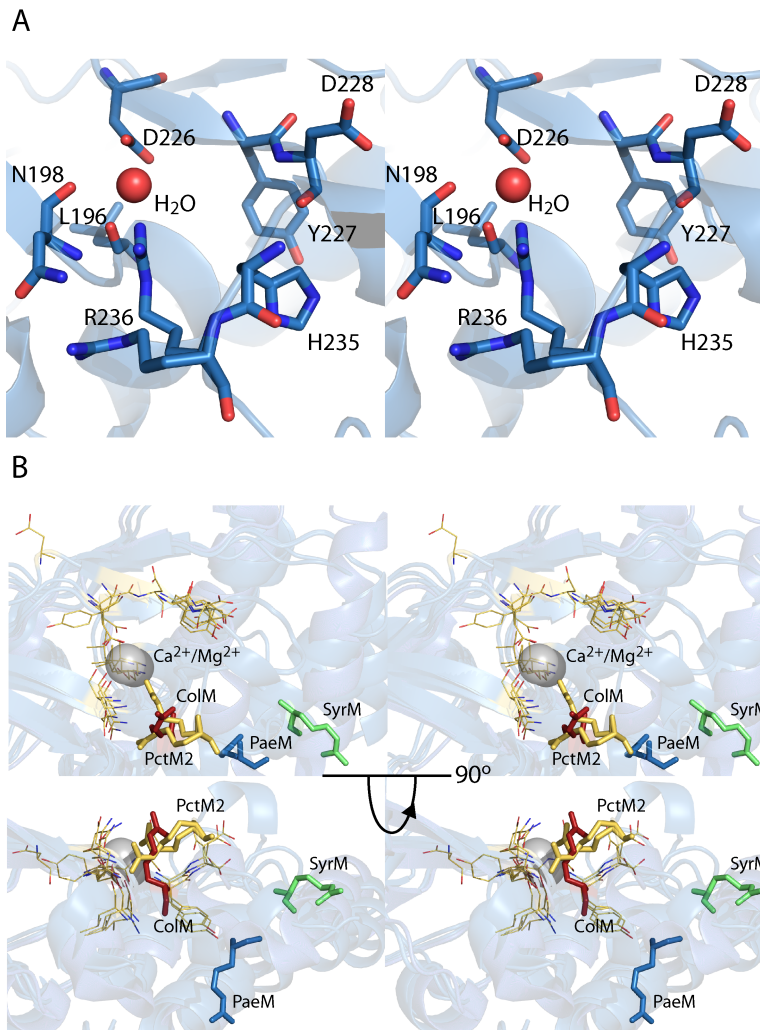


Fig. 2. Colicin M-class bacteriocins possess a highly flexible active site.

A. A stereo view of a stick model of the key active site residues of pectocin M2, showing a water molecule occupying the key metal binding site of the enzyme.

B. A stereo view of the overlay of the catalytic site from all structurally characterized colicin-M class bacteriocins, showing conformational variability of the key catalytic arginine. Key arginine shown as sticks and colour coded according to structure; green = syringacin M (PDB ID = 4FZL), blue = pyocin M (PDB ID = 4G75), red = colicin M (PDB ID = 2XMX) and yellow = pectocin M2 (PDB ID = 4N58). All other catalytically important residues shown as lines in yellow.

the receptor binding and catalytic domains are not separated by linker regions and do not form obviously structurally distinct elements (Zeth *et al.*, 2008; Barreteau *et al.*, 2012b; Grinter *et al.*, 2012b), the catalytic and receptor binding domains of pectocin M2 do not form extensive interactions. The relative orientation of the ferredoxin domain, linker region and cytotoxic domain gives rise to a non-linear dog-leg structure. Interestingly, and again in contrast to colicin M, pyocin M and syringacin M, the N-terminal region of pectocin M2 lacks a disordered or flexible IUTD that is otherwise characteristic of the colicin-like bacteriocins, with the entire N-terminus being integral to the globular ferredoxin domain. These data suggest a mechanism of uptake distinct from closely related colicin-like bacteriocins.

Pectocin M2 is flexible

Given that pectocin M2 lacks an IUTD required to contact the Tol or Ton complexes in the periplasm and mediate

translocation of this protein across the outer membrane, alternative mechanisms of uptake must be considered. One possibility is that the entire bacteriocin passes through the lumen of its OM receptor. Since proteins involved in iron uptake are invariably TonB-dependent receptors that possess large 22-stranded β -barrels this may be plausible. However, such a mechanism would only be feasible if pectocin M2 were flexible and significant rearrangement of the dog-leg configuration observed in the crystal structure could be achieved. The observation that there is a relatively large difference in orientation between the cytotoxic and ferredoxin domains in the monomers of the ASU (Fig. S1) is suggestive of such flexibility and indicates that the crystal structure may not be wholly representative of pectocin M2 in solution.

To assess the conformational flexibility of pectocin M2 we performed small angle X-ray scattering (SAXS). SAXS data were obtained for a range of pectocin M2 concentrations. Comparison of these data with a theoretical scattering curve generated, using CRYSOLO (Svergun *et al.*,

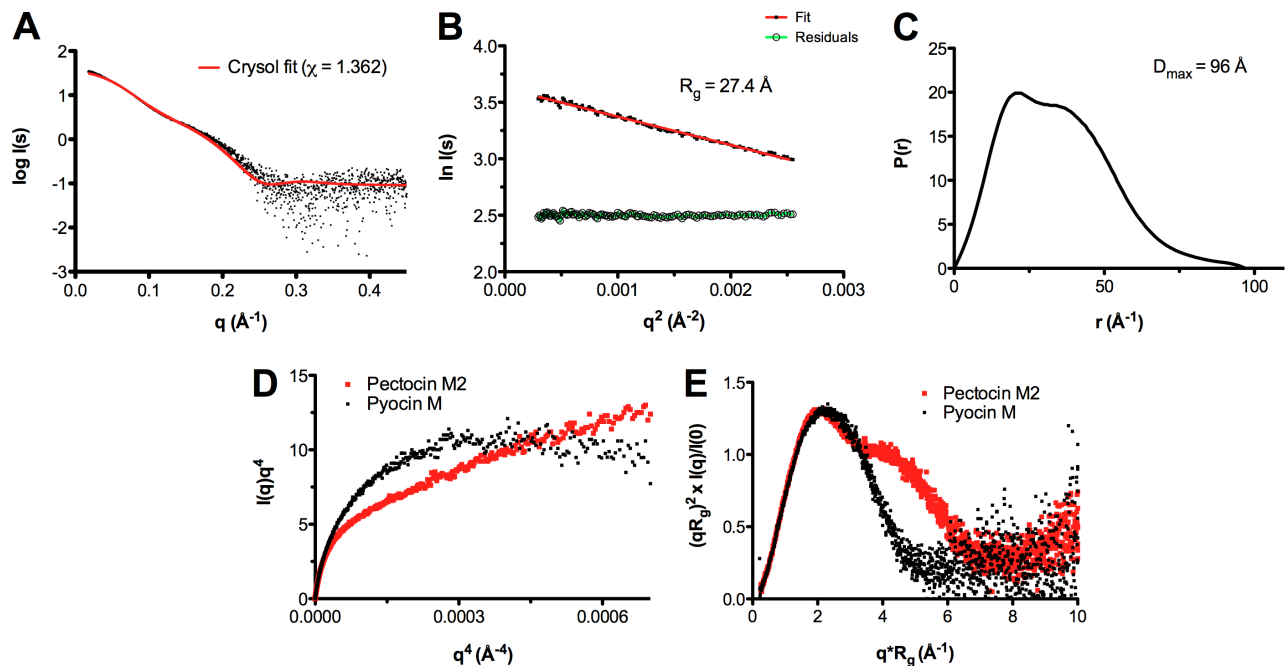


Fig. 3. SAXS shows pectocin M2 is flexible.

A. Overlay of the experimentally determined pectocin M2 SAXS curve (black points) with the scattering curve computed with CRYSOLOG from the $P2_1$ crystal structure (red line) produces a fit ($\chi^2 = 1.362$) with visible deviations between the data, especially evident at low angles, suggesting that the crystal structure is more compact than that of pectocin M2 in solution.

B. Derivation of R_g from a Guinier analysis (red) of the scattering curve; residuals of the fit are in green.

C. Pair-distance distribution plot from experimental scattering data for pectocin M2 exhibiting two maxima which highlights the bimodal character of the molecule in solution. The D_{max} of the particle is 96 Å.

D. Porod-Debye and (E) normalized Kratky plots for pectocin M2 imply increased flexibility of the protein in solution (red). Pyocin M (black), a protein of similar molecular weight with a relatively rigid structure and strong inter-domain contacts is used as a control.

1995), from the pectocin M2 crystal structure shows there are obvious differences between the theoretical curve and experimental scattering data (Fig. 3A). In addition, the radius of gyration ($R_g = 27$ Å) obtained from Guinier analysis of the experimental scattering data is somewhat larger than that calculated from the pectocin M2 crystal structure ($R_g = 24$ Å) using SOMO (Rai *et al.*, 2005) (Fig. 3B). Consistent with this, the $p(r)$ function, which describes the paired set of vectors between all the electrons within the protein, indicates a maximum particle size ($D_{max} = 96$ Å, Fig. 3C) that is much greater than the maximum dimension of the pectocin M2 crystal structure (77 Å, Fig. 1B). These data suggest that the pectocin M2 crystal structure is not wholly representative of the conformational ensemble present in solution and that this protein adopts an elongated conformation, implying inter-domain flexibility.

To test this idea further, we examined the Porod-Debye plot for pectocin M2, where scattering decay is examined as $I(q)q^4$ as a function of q^4 . This analysis reports directly on particle flexibility and typically for compact globular particles an asymptotic plateau is reached for the low q part of the data. However, for pectocin M2 no discernible plateau was observed (Fig. 3D). For comparison, we also obtained

scattering data for pyocin M which, as with colicin M and syringacin M, forms a compact structure and similarly analysed these data (Barreteau *et al.*, 2012b). In contrast to the curve obtained for pectocin M2, the Porod-Debye plot for pyocin M reached a plateau confirming its rigidity and compactness (Fig. 3D). In addition, the Kratky plot [$I(q)q^2$ versus q] for pectocin M2 normalized to the scattering intensity $I(0)$ and R_g , has two maxima with increasing scattering at higher angles. The Kratky plot reports directly on inter-domain flexibility and for pectocin M2 is consistent with a two-domain protein connected by a flexible linker (Fig. 3E). In comparison, there is a single maximum in the pyocin M Kratky plot, consistent with its single domain-like globular structure. Taken together these analyses indicate that pectocin M2 is flexible and adopts conformations distinct from that observed in the crystal structure.

Pectocin M2 can adopt a highly extended conformation and exists as two distinct subpopulations in solution

To determine if the SAXS data for pectocin M2 could be better described by an ensemble of conformations we first used discrete molecular dynamics (DMD) simulations

(Shirvanyants *et al.*, 2012) to explore the accessible conformational states of pectocin M2 and generated a random pool of 5000 possible conformations using the crystal structure of pectocin M2. Next, we used a genetic algorithm implemented in the program GAJOE (Petoukhov *et al.*, 2012) to select for ensembles of these models that would better describe our SAXS data. Model selection was successful as judged by the close correlation of the theoretical scattering curve generated from the selected ensemble with the experimental SAXS data (Fig. 4A), indicating that our scattering data are best described by an ensemble of pectocin M2 conformers in solution. Interestingly, the selected ensembles show a bimodal distribution in comparison with the random pool of DMD-generated pectocin M2 models when the population frequency is plotted against R_g or D_{max} (Fig. 4B and C). Thus, in the population of selected conformations, we frequently find a compact conformation described by the first peak (with maxima at approximately 23 and 75 Å for R_g and D_{max} respectively) that approximates closely to the conformation found in the pectocin M2 $P2_1$ crystal structure for which R_g and D_{max} were calculated as 24 and 77 Å respectively. The second peak represents an ensemble of pectocin M2 conformers in an extended conformation with D_{max} values ranging up to 98 Å, which correlates closely with the experimentally determined value of D_{max} (96 Å). These analyses suggest that pectocin M2 can adopt both bent and elongated linear conformations in solution.

The bimodal distribution of the selected ensembles suggests discrete populations in solution, the more compact of which is similar to the conformation observed in the $P2_1$ crystals of pectocin M2. In an attempt to capture the more elongated conformation *in crystallo*, thus validating our solution scattering and modelling data, we repeated crystallization of pectocin M2. A custom re-crystallization screen was devised exploiting information from the initial trails. Crystals were obtained in a number of conditions from this screen and were tested for diffraction as well as space group and unit cell variation, which is indicative of novel packing. A form with the radically different space group of $P3_121$ was chosen for optimization, which yielded crystals diffracting to 1.86 Å. As an alternative domain arrangement to the $P2_1$ form was expected, data from this crystal form were again phased using anomalous data from the metal centres of the [2Fe-2S] cluster. During model building from these data it was immediately apparent that in this crystal form pectocin M2 did indeed adopt an elongated conformation (Fig. 5A). The calculated R_g and D_{max} for this structure were 28 and 97 Å respectively. These values correlate well with the extended population from the DMD simulation, suggesting that this structure is representative of the second elongated pool identified by our modelling. Alignment of this elongated ($P3_121$) form and the original $P2_1$ form, based on their cytotoxic or ferredoxin

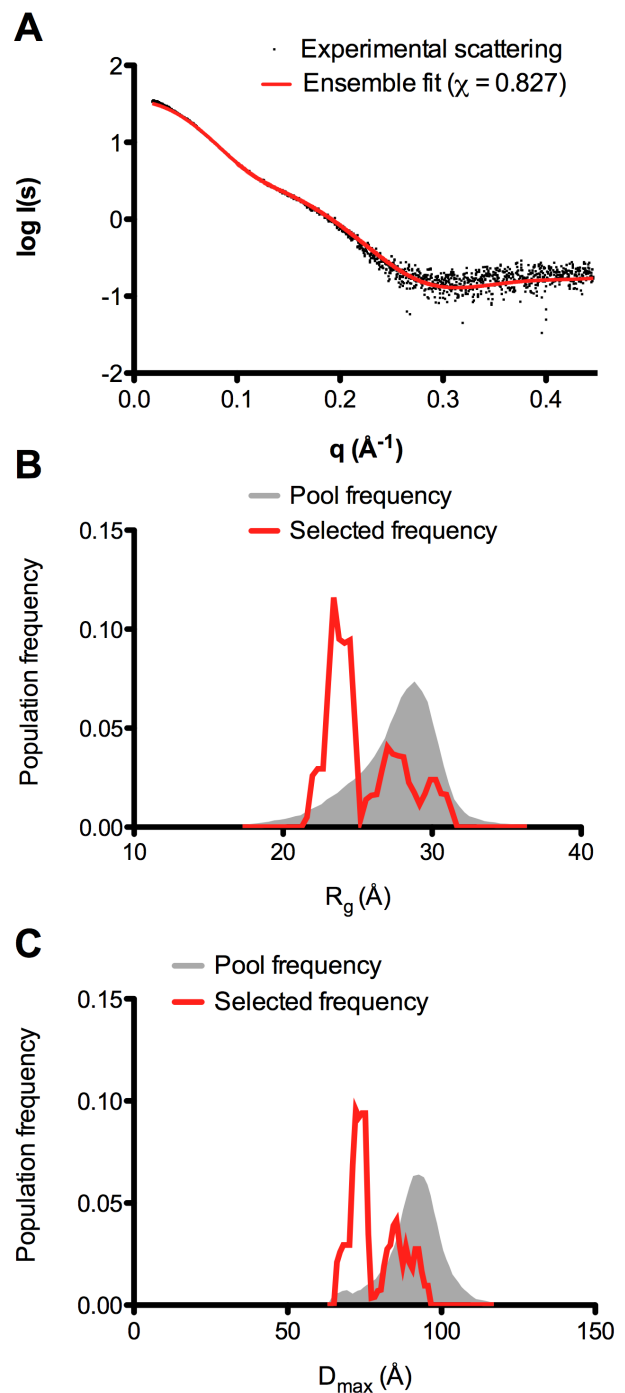


Fig. 4. Analysis of conformational heterogeneity of pectocin M2 reveals compact and extended ensembles in solution. A. Overlay of scattering curves of pectocin M2 between experimental data and the best ensemble selected by GAJOE indicates improved fit to the scattering data ($\chi = 0.827$). B and C. R_g (B) and D_{max} (C) distribution of solution ensembles selected by a genetic algorithm using GAJOE from a pool of 5000 random conformers of pectocin M2. Compact and elongated molecule were both selected implying that the protein is conformationally heterogeneous in solution allowing for significant inter-domain re-arrangements about the linker helix (residues 96–115).

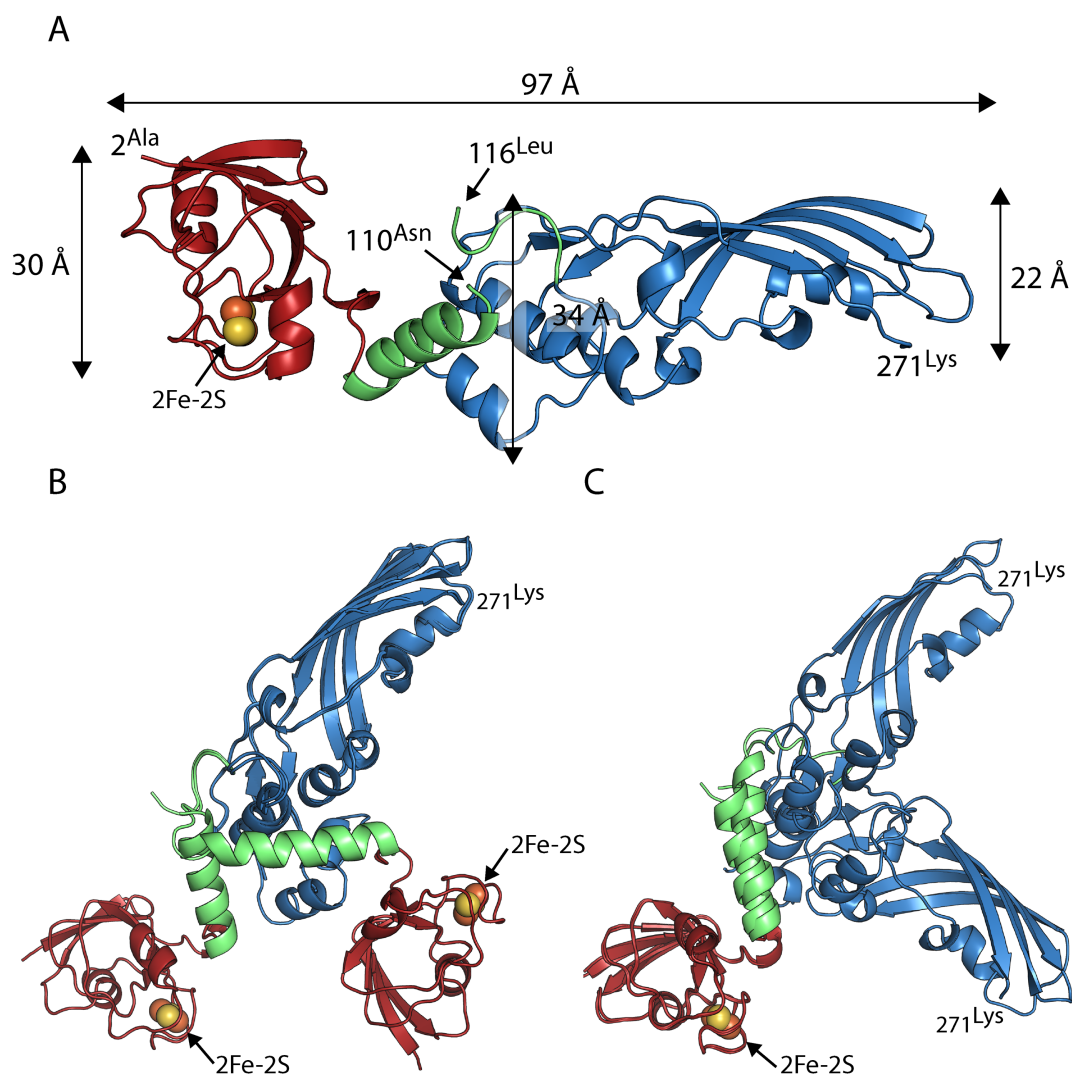


Fig. 5. Pectocin M2 P_{3;21} structure confirms extended conformation predicted by solution scattering.

A. Pectocin M2 in P_{3;21} crystal form is highly elongated, consistent with the extended conformation predicted from solution scattering and DMD simulations.

B. Alignment of the catalytic domains of the P_{2;1} and P_{3;21} crystal forms of pectocin M2, illustrating the difference in orientation between the ferredoxin and linker regions.

C. Alignment of the ferredoxin domains of the P_{2;1} and P_{3;21} crystal forms of pectocin M2, illustrating the difference in orientation of the catalytic domains.

domains, show a major difference in the relative orientations of these domains (Fig. 5B and C).

The ferredoxin domain is a generic module for the delivery of cytotoxic domains to the periplasm

In addition to pectocin M1 and M2, we previously identified a putative third member of the ferredoxin-containing bacteriocin family, designated pectocin P (Grinter *et al.*, 2012a). The open reading frame for pectocin P, identified in the genome of *Pectobacterium carotovorum* subsp. *carotovorum* WPP14, consists of an N-terminal ferredoxin

domain, connected to a pectocin-like cytotoxic domain, which is analogous to T4 lysozyme. Similar to pectocins M1 and M2, there is no sequence N-terminal of the ferredoxin domain, so this bacteriocin also lacks an IUTD. To confirm that this open-reading frame encodes an active bacteriocin, we tested the cytotoxic activity of recombinantly expressed and purified pectocin P against diverse *Pectobacterium* isolates. For this test we utilized a solid growth inhibition assay conducted in parallel with pectocins M1 and M2 (Fyfe *et al.*, 1984). As with pectocins M1 and M2, limited inhibition of growth was observed under iron-replete conditions (LB agar). However, under iron-limiting

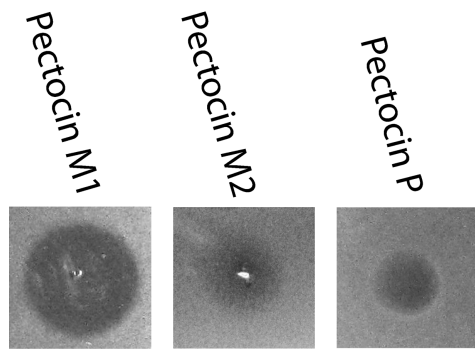


Fig. 6. Activity of pectocin P against *Pectobacterium atrosepticum* LMG 2386. Purified pectocins M1, M2 and P (2 mg ml^{-1}) were spotted onto a soft agar overlay seeded with *Pba* LMG 2386. Clear zones indicate inhibition of growth due to the cytotoxic effect of pectocins on cells.

conditions, inhibition of growth was observed for 17 of the 19 strains (Fig. 6, Table S1). The existence of pectocin P, an additional ferredoxin-containing bacteriocin with no N-terminal IUTD and a pesticin-like cytotoxic domain, provides strong supporting evidence that the ferredoxin domain acts as a generic module for the delivery of cytotoxic domains to the periplasm in *Pectobacterium* spp. The cytotoxic domains of both M-class bacteriocins and pesticin have been studied extensively and there is no indication that they possess any intrinsic capacity to cross the OM (Barreteau *et al.*, 2010; Helbig and Braun, 2011; Lukacik *et al.*, 2012; Patzer *et al.*, 2012), indicating that ferredoxin uptake represents an unprecedented example of receptor-mediated protein uptake for nutrient acquisition in bacteria.

Discussion

In this work we present the structure and solution properties of the atypical bacteriocin pectocin M2, which consists of a fusion between a colicin M-like cytotoxic domain and a plant-derived ferredoxin domain. We have previously demonstrated that *Pectobacterium* spp. are able to acquire iron directly from plant ferredoxin under iron-limiting conditions through a receptor mediated process and that the bacteriocins pectocin M1 and M2 parasitize this system for cell entry through presentation of a ferredoxin domain (Grinter *et al.*, 2013). In this study we provide an insight into how this uptake occurs by showing that pectocin M2 has an unprecedented structure among bacteriocins in that it lacks an IUTD. Additionally, we definitively show that pectocin M2 is highly flexible in solution fluctuating between compact and extended conformations.

All iron-uptake systems identified to date in Gram-negative bacteria, either siderophore based or targeting a

protein substrate, utilize a TonB-dependent receptor to transport iron across the outer membrane (Faraldo-Gomez and Sansom, 2003). Likewise, binding and parasitization of these receptors for cell entry is a characteristic trait of colicin M, and other characterized colicins and pyocins, including the E-type colicins (E1-E9), colicins A, B, D, IA and IB and pyocins S1-S5 (Loftus *et al.*, 2006; Buchanan *et al.*, 2007; Cascales *et al.*, 2007; Denayer *et al.*, 2007; Devanathan and Postle, 2007; Elfarash *et al.*, 2012). As such, while it is yet to be confirmed that a TonB-dependent receptor is responsible for mediating ferredoxin iron and pectocin uptake, this class of protein is by far the most likely candidate.

In bacteriocins the IUTD normally functions to deliver an epitope to the periplasm, which mediates binding to the Tol or Ton complexes. This direct interaction occurs between the colicins and TolB for group A colicins and TonB for group B colicins and is essential for uptake of these bacteriocins. In addition to their subversion for bacteriocin import, Tol and Ton complexes have a general physiological role in the bacterial cell. The Ton complex provides the energy required for the import of iron containing siderophores and related substrates through TonB-dependent receptors, by interaction with the receptor plug domain subsequent to binding of the substrate on the outer surface of the receptor (Noinaj *et al.*, 2010). Given the universal role of TonB-dependent receptors in iron transport across the outer membrane and their parasitization by colicin-like bacteriocins, it is reasonable to speculate that the ferredoxin/pectocin receptor is a member of this class of protein.

Since pectocin M1 and M2 lack an IUTD they are unable make direct contact with the Tol or Ton complexes in the periplasm and thus are unable to directly utilize the pmf for cell entry. However, the fact that these proteins parasitize a system for which the receptor binding and translocation domains are structurally analogous to the substrate provides an intuitive solution to this problem. A number of TonB-dependent receptors have been identified, which obtain iron from host proteins during infection. In all of these systems the iron or iron containing compound is liberated from the protein on the cell surface and transported into the cell, potentially because all of the proteins identified are too large pass through the lumen of their receptor (Wandersman and Stojiljkovic, 2000; Faraldo-Gomez and Sansom, 2003; Noinaj *et al.*, 2012). Plant ferredoxin, however, is a small globular protein, which is in fact comparable in dimensions to the plug domain that ordinarily occludes the pore of a TonB-dependent receptor (Fig. 7A and C). This creates the possibility that the ferredoxin is imported intact into the periplasm. If this were the case it could readily explain the pectocins lack of an IUTD as the energy required for cell entry would still be provided by the Ton complex, but

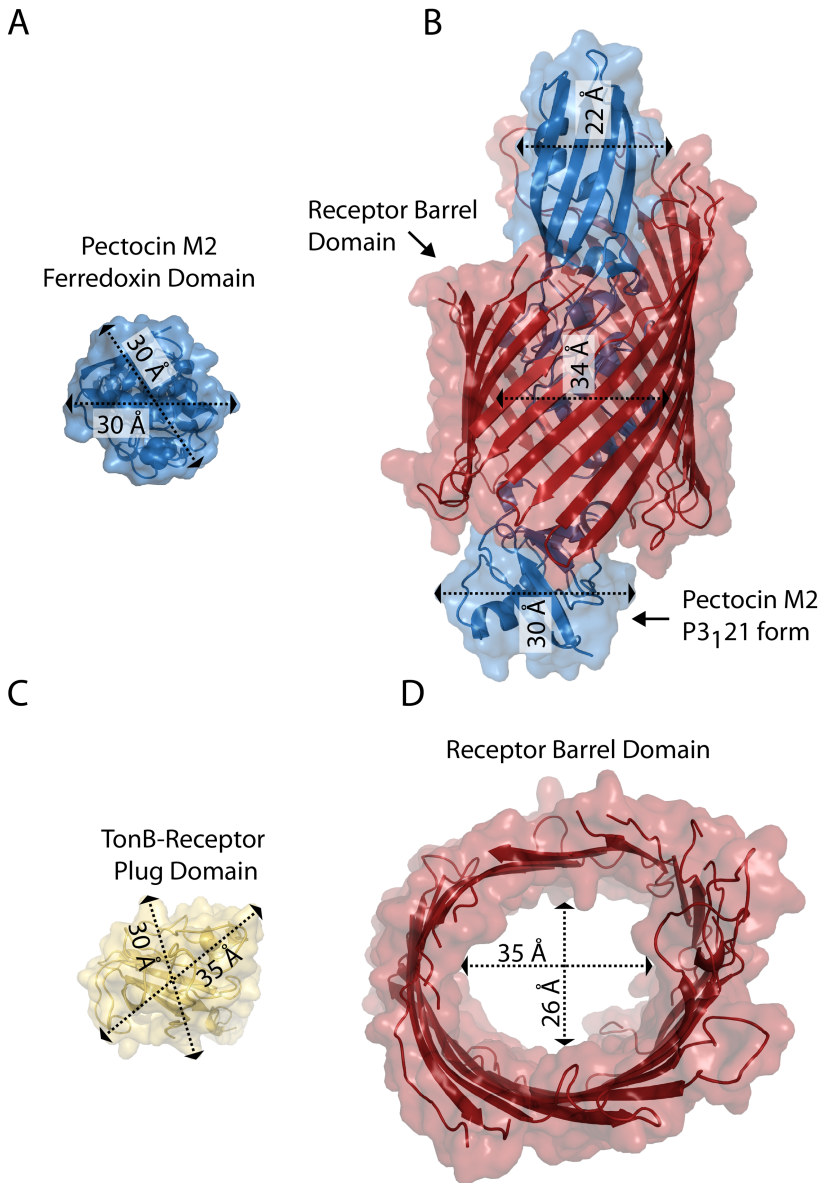


Fig. 7. The extended conformation of pectocin M2 has dimensions compatible with passage through the lumen of a TonB-dependent receptor.

A. The extended conformation of pectocin M2 (blue cartoon and surface), fitted into the pore of the barrel of HasR from *Serratia marcescens* PDB ID = 3CLS, illustrating that the extended conformation of pectocin M2 is conducive to transport through the lumen of a TonB-dependent receptor without unfolding. B. Dimensions of the ferredoxin domain of pectocin M2. C. The width of the plug domain, which ordinarily blocks the lumen of the receptor barrel, is similar to that of the elongated conformation of pectocin M2. D. Top-down view of the HasR barrel showing the internal dimensions of the barrel domain.

transduced through receptor plug domain, as with ordinary substrate importation.

As the elongated conformation of pectocin M2 has comparable dimensions along its length (Fig. 5A) we manually docked this model into the barrel domain of the hemophore receptor HasR, a TonB-dependent receptor shown to be responsible for importation of the relatively bulky substrate, haem (Fig. 7B and D). This docking illustrates that pectocin M2 in its elongated conformation could traverse the lumen of such a receptor to gain entry to the cell, with the flexibility of pectocin M2 observed in solution allowing the protein to adapt to the shape of the lumen of its transporter during importation. In the case of the transport of iron-siderophores, it is generally thought that there

are two possibilities with respect to the role of TonB in stimulating substrate transport. Either TonB induces a rearrangement of the plug domain within the barrel that is sufficient to allow passage of the substrate or it directly pulls the plug domain completely from the barrel (Usher *et al.*, 2001; Udho *et al.*, 2009; 2012). However, for an intact protein such as ferredoxin to be translocated directly through the lumen of a TonB-dependent receptor, it would be necessary for the plug domain to completely exit the barrel during substrate transport and it has not as yet been directly demonstrated that this occurs in TonB-dependent receptors. The identification of this receptor and the testing of this importation hypothesis represents an intriguing question for future work.

Experimental procedures

Expression and purification of ferredoxins and pectocins

A list of bacterial strains and plasmids used in this work is provided in Table S1. The open reading frame for pectocin P minus stop codon was synthesized by DNA 2.0 and ligated into the expression vector pJ404 (T5 promoter, C-terminal His₆-tag). The resulting vector was designated pJPP1. Vectors for expression of pectocins M1 and M2 were as previously described (Grinter *et al.*, 2012a). All proteins were expressed and purified as previously described (Grinter *et al.*, 2012a). Proteins were concentrated to 5–15 mg ml⁻¹ using a centrifugal concentrator and stored at -80°C in this buffer until required. For pectocins M1 and P, 5% glycerol was added to all buffers as it was found to enhance protein stability.

Cytotoxicity assays

The cytotoxicity of purified pectocins was tested using the soft agar overlay method (Fyfe *et al.*, 1984). 200 µl of mid-log phase culture of the test strain was added to 6 ml of 0.6% agar melted and cooled to 42°C. The molten agar was then overlaid onto LB medium with or without 100–400 µM 2,2'-biyridine. Purified pectocins (2 mg ml⁻¹) were spotted directly onto the surface of the overlay, once solidified. Plates were incubated at 28°C for 16 h, and monitored for zones of growth inhibition.

SAXS data collection and analysis

SAXS data were collected on the X33 beamline at the Deutsches Elektronen Synchrotron (DESY, Hamburg, Germany). Pectocin M2 and pyocin M concentrations between 0.4 and 4.0 mg ml⁻¹ were used. Average buffer scattering was subtracted from the sample scattering. The first 200 points (low angle data) of the scattering curve obtained for 1 mg ml⁻¹ protein were merged with the rest of the high angle data from the 4 mg ml⁻¹ sample to avoid the influence on the data of any inter-particle interference. All data processing was performed using PRIMUS (Konarev *et al.*, 2003). Porod-Debye [$I(q)q^4$ versus q^4] and normalized Kratky [$I(q)q^2$ versus q] plots were used to assess particle flexibility as described in the *Results* section (Durand *et al.*, 2010; Rambo and Tainer, 2011). The distance distribution function, $p(r)$, was obtained by indirect Fourier transform of the scattering intensity using GNOM (Svergun, 1992). A Guinier plot [$\ln I(s)$ versus q^2] was used to determine the radius of gyration, R_g , of pectocin M2 and pyocin M. US-SOMO (Rai *et al.*, 2005) was used to determine hydrodynamic parameters based on the crystal structures of pectocin M2. CRY SOL (Svergun *et al.*, 1995) was used to compute theoretical scattering curves from high-resolution X-ray structures.

DMD and EOM simulations

Discrete molecular dynamics simulations of the pectocin M2 linker region (residues 96–116) were undertaken with

US-SOMO (Brookes *et al.*, 2010; Shirvanyants *et al.*, 2012) in order to explore pectocin M2 conformational space. The Andersen thermostat temperature (T) was set to 0.5 kcal mol⁻¹ K⁻¹ to allow for sufficient sampling of conformational dynamics around the native state without melting the structure of the linker. The run time and pdb output step were adjusted in order to generate 5000 models. Next, the pool of 5000 'random' pectocin M2 conformers generated was refined by a genetic algorithm implemented in the program GAJOE as part of the ensemble optimization method (Bernadó *et al.*, 2007; Petoukhov *et al.*, 2012).

Pectocin M2 crystallization and diffraction data collection

Initial crystallization trials were performed at the high throughput crystallization facility of the University of Zurich using the vapour diffusion method (reservoir volume of 50 µl, drop size: 100 nl protein, 100 nl reservoir solution) with pectocin M2 at a final concentration of 15 mg ml⁻¹. Pectocin M2 formed crystals or spherulites in a number of conditions containing ammonium sulphate and PEG 3350. Crystals were extracted from one of these conditions [15% PEG 3350, 0.2 M ammonium sulphate, 3% 2-methyl-2,4-pentanediol (MPD), 0.1 M bis-tris pH 6.5], cryoprotected by increasing PEG 3350 to 30% and data were collected at 100 K to 2.3 Å in the space group $P2_1$, at the SLS (Zurich). Re-crystallization screening of pectocin M2 was performed, using a custom screen with variations in the concentration/ratio of precipitants from the original condition (ammonium sulphate and PEG 3350), pH and additives. Clusters of large rod-shaped crystals formed at high ammonium sulphate concentrations. This was optimized giving a final condition of 1.8 M ammonium sulphate, 3% MPD, 0.1 M MES, pH 6.5. These crystals were manually separated and cryoprotected with 15–20% glycerol. Data were collected at 100 K on beamlines I02 and I03 at the Diamond Light Source (Oxfordshire, UK). Automatic data-processing was performed with Xia2 within the EDNA package (Incardona *et al.*, 2009). Datasets for experimental phasing using the iron–sulphur cluster of pectocin M2 were collected at the iron K-edge (1.7433 Å) and high-resolution data were collected at 0.9796 Å. Data collection statistics from both crystal forms are reported in Table 1.

Pectocin M2 structure solution and refinement

Phases for the $P2_1$ and $P3_121$ datasets were obtained from the anomalously scattering substructure from the pectocin–ferredoxin domain iron–sulphur cluster, determined for the iron-edge dataset using the Hybrid Substructure Search from the Phenix package (Adams *et al.*, 2010). Four positions were located per ASU corresponding to two iron–sulphur clusters (correlation coefficient = 0.5) from two pectocin M2 molecules. These positions were then utilized by Phaser-EP (McCoy *et al.*, 2007; Adams *et al.*, 2010; Winn *et al.*, 2011) phases were improved using RESOLVE density modification from the Phenix package, and the initial model was built and refined using Phenix Autobuild (Adams *et al.*, 2010). The model was then built and refined manually using Coot 0.7 and Refmac5

Table 1. Crystallographic data collection and refinement statistics.

		High resolution dataset	Iron edge dataset
Data collection^a			
Space group	<i>P2</i> ₁	<i>P3</i> ₁ 21	<i>P3</i> ₁ 21
Cell dimensions			
<i>a</i> , <i>b</i> , <i>c</i> (Å)	44.65, 116.75, 60.78	117.45, 117.45, 128.45	117.26, 117.26, 128.53
α , β , γ (°)	90, 94.96, 90	90, 90, 120	90, 90, 120
Resolution (Å)	50.00–2.30 (2.44–2.30)	64.22–1.86 (1.91–1.86)	43.31–2.01 (2.06–2.01)
<i>R</i> _{merge} (%)	5.0 (59.9)	3.4 (68.3)	3.8 (69.3)
<i>R</i> _{pim} (%) ^b	–	0.9 (15.7)	2.0 (31.0)
Mean <i>I</i> / σ (<i>I</i>)	12.41 (1.85)	47.1 (5.5)	28.9 (3.1)
Completeness (%)	96.6 (95.7)	100.0 (99.9)	99.4 (98.7)
Redundancy	3.2 (2.8)	20 (20.8)	8 (6.6)
Refinement			
Resolution (Å)	50.00–2.30 (2.44–2.30)	64.22–1.86 (1.91–1.86)	
No. of reflections	52652 (8438)	86092 (6304)	
<i>R</i> _{work} / <i>R</i> _{free} (%)	21.0/27.2	16.8/19.1	
No. of atoms			
Protein	4093	4175	
Ligand/ion	34	388	
Water	49	438	
<i>B</i> factors			
Protein	69.1	45.5	
2Fe-2S	74.6	35.4	
SO ₄ ²⁻ /Cl ⁻	95	68.2	
Glycerol/MPD	–	70.7	
Water	42.4	56.0	
Root mean square deviations			
Bond lengths (Å)	0.016	0.024	
Bond angles (°)	1.757	2.55	
PDB identifier	4N59	4N58	

a. Values in parentheses refer to the highest resolution shell.

b. $R_{pim} = \sum_{hkl} [1/(N-1)^{1/2} \sum_l I(hkl) - \langle I(hkl) \rangle] / \sum_{hkl} I(hkl)$

(McCoy *et al.*, 2007; Emsley *et al.*, 2010; Murshudov *et al.*, 2011). Validation of refined structures was performed using the Molprobity web server and Procheck from CCP4i (Laskowski *et al.*, 1993; Chen *et al.*, 2010). Refinement statistics for both datasets are reported in Table 1.

Lipid II cleavage assay

Lipid II hydrolysis assays were performed and visualized as previously described by (Grinter *et al.*, 2012b), with non-radiolabelled lipid II substrate obtained from the UK Bacterial Cell Wall Biosynthesis Network (Lloyd *et al.*, 2008; Clarke *et al.*, 2009). A band corresponding to lipid II was observed with an *R*_f of 0.7 as reported previously (Barreteau *et al.*, 2009).

Acknowledgements

We thank the Diamond Light Source for access to beamlines I02 and I03 (proposal numbers MX6638 and MX8659). We acknowledge funding from P-CUBE for initial crystallization trials performed at HT-X Zurich and were are grateful to Beat Blattmann for technical assistance. R.G. is supported by a Kelvin-Smith Scholarships from the University of Glasgow. I.J. and L.M. are supported by studentships from the Wellcome Trust, award numbers 093592/Z/10/Z and 093597/Z/10/Z respectively.

References

- Adams, P.D., Afonine, P.V., Bunkoczi, G., Chen, V.B., Davis, I.W., Echols, N., *et al.* (2010) PHENIX: a comprehensive Python-based system for macromolecular structure solution. *Acta Crystallogr D Biol Crystallogr* **66**: 213–221.
- Barreteau, H., Bouhss, A., Fourgeaud, M., Mainardi, J.-L., Touzé, T., Gérard, F., *et al.* (2009) Human- and plant-pathogenic pseudomonas species produce bacteriocins exhibiting colicin M-like hydrolase activity towards peptidoglycan precursors. *J Bacteriol* **191**: 3657–3664.
- Barreteau, H., Bouhss, A., Gérard, F., Duché, D., Boussaid, B., Blanot, D., *et al.* (2010) Deciphering the catalytic domain of colicin M, a peptidoglycan lipid II-degrading enzyme. *J Biol Chem* **285**: 12378–12389.
- Barreteau, H., Ghachi, M.E., Barnéoud-Arnoulet, A., Sacco, E., Touzé, T., Duché, D., *et al.* (2012a) Characterization of colicin M and its orthologs targeting bacterial cell wall peptidoglycan biosynthesis. *Microb Drug Resist* **18**: 222–229.
- Barreteau, H., Tiouajni, M., Graille, M., Josseume, N., Bouhss, A., Patin, D., *et al.* (2012b) Functional and structural characterization of PaeM, a colicin M-like bacteriocin produced by *Pseudomonas aeruginosa*. *J Biol Chem* **287**: 37395–37405.
- Bernadó, P., Mylonas, E., Petoukhov, M.V., Blackledge, M., and Svergun, D.I. (2007) Structural characterization of flex-

- ible proteins using small-angle X-ray scattering. *J Am Chem Soc* **129**: 5656–5664.
- Brookes, E., Demeler, B., Rosano, C., and Rocco, M. (2010) The implementation of SOMO (SOLution MOdeller) in the UltraScan analytical ultracentrifugation data analysis suite: enhanced capabilities allow the reliable hydrodynamic modeling of virtually any kind of biomacromolecule. *Eur Biophys J* **39**: 423–435.
- Buchanan, S.K., Lukacik, P., Grizot, S., Ghirlando, R., Ali, M.M.U., Barnard, T.J., *et al.* (2007) Structure of colicin I receptor bound to the R-domain of colicin Ia: implications for protein import. *EMBO J* **26**: 2594–2604.
- Cascales, E., Buchanan, S.K., Duché, D., Kleanthous, C., Llobès, R., Postle, K., *et al.* (2007) Colicin biology. *Microbiol Mol Biol Rev* **71**: 158–229.
- Chen, V.B., Arendall, W.B., III, Headd, J.J., Keedy, D.A., Immormino, R.M., Kapral, G.J., *et al.* (2010) MolProbity: all-atom structure validation for macromolecular crystallography. *Acta Crystallogr D Biol Crystallogr* **66**: 12–21.
- Clarke, T.B., Kawai, F., Park, S.-Y., Tame, J.R.H., Dowson, C.G., and Roper, D.I. (2009) Mutational analysis of the substrate specificity of *Escherichia coli* penicillin binding protein 4. *Biochemistry* **48**: 2675–2683.
- Denayer, S., Matthijs, S., and Cornelis, P. (2007) Pyocin S2 (Sa) kills *Pseudomonas aeruginosa* strains via the FpvA Type I ferripyoverdine receptor. *J Bacteriol* **189**: 7663–7668.
- Devanathan, S., and Postle, K. (2007) Studies on colicin B translocation: FepA is gated by TonB. *Mol Microbiol* **65**: 441–453.
- Durand, D., Vivès, C., Cannella, D., Pérez, J., Pebay-Peyroula, E., Vachette, P., and Fieschi, F. (2010) NADPH oxidase activator p67phox behaves in solution as a multi-domain protein with semi-flexible linkers. *J Struct Biol* **169**: 45–53.
- Elfarash, A., Wei, Q., and Cornelis, P. (2012) The soluble pyocins S2 and S4 from *Pseudomonas aeruginosa* bind to the same FpvA receptor. *MicrobiologyOpen* **1**: 268–275.
- Emsley, P., Lohkamp, B., Scott, W.G., and Cowtan, K. (2010) Features and development of Coot. *Acta Crystallogr D Biol Crystallogr* **66**: 486–501.
- Faraldo-Gomez, J.D., and Sansom, M.S.P. (2003) Acquisition of siderophores in Gram-negative bacteria. *Nat Rev Mol Cell Biol* **4**: 105–116.
- Fyfe, J.A., Harris, G., and Govan, J.R. (1984) Revised pyocin typing method for *Pseudomonas aeruginosa*. *J Clin Microbiol* **20**: 47–50.
- Grinter, R., Milner, J., and Walker, D. (2012a) Ferredoxin containing bacteriocins suggest a novel mechanism of iron uptake in *Pectobacterium* spp. *PLoS ONE* **7**: e33033.
- Grinter, R., Roszak, A.W., Cogdell, R.J., Milner, J.J., and Walker, D. (2012b) The crystal structure of the lipid II-degrading bacteriocin syringacin M suggests unexpected evolutionary relationships between colicin M-like bacteriocins. *J Biol Chem* **287**: 38876–38888.
- Grinter, R., Milner, J., and Walker, D. (2013) Beware of proteins bearing gifts: protein antibiotics that use iron as a Trojan horse. *FEMS Microbiol Lett* **338**: 1–9.
- Helbig, S., and Braun, V. (2011) Mapping functional domains of colicin M. *J Bacteriol* **193**: 815–821.
- Housden, N.G., Wojdyla, J.A., Korczynska, J., Grishkovskaya, I., Kirkpatrick, N., Brzozowski, A.M., and Kleanthous, C. (2010) Directed epitope delivery across the *Escherichia coli* outer membrane through the porin OmpF. *Proc Natl Acad Sci USA* **107**: 21412–21417.
- Housden, N.G., Hopper, J.T.S., Lukyanova, N., Rodriguez-Larrea, D., Wojdyla, J.A., Klein, A., *et al.* (2013) Intrinsically disordered protein threads through the bacterial outer-membrane porin OmpF. *Science* **340**: 1570–1574.
- Incardona, M.-F., Bourenkov, G.P., Levik, K., Pieritz, R.A., Popov, A.N., and Svensson, O. (2009) EDNA: a framework for plugin-based applications applied to X-ray experiment online data analysis. *J Synchrotron Radiat* **16**: 872–879.
- Jakes, K.S., and Finkelstein, A. (2010) The colicin Ia receptor, Cir, is also the translocator for colicin Ia. *Mol Microbiol* **75**: 567–578.
- Kleanthous, C. (2010) Swimming against the tide: progress and challenges in our understanding of colicin translocation. *Nat Rev Microbiol* **8**: 843–848.
- Konarev, P.V., Volkov, V.V., Sokolova, A.V., Koch, M.H.J., and Svergun, D.I. (2003) PRIMUS: a Windows PC-based system for small-angle scattering data analysis. *J Appl Crystallogr* **36**: 1277–1282.
- Laskowski, R.A., Macarthur, M.W., Moss, D.S., and Thornton, J.M. (1993) PROCHECK – a program to check the stereochemical quality of protein structures. *J Appl Crystallogr* **26**: 283–291.
- Lloyd, A.J., Gilbey, A.M., Blewett, A.M., De Pascale, G., El Zoeiby, A., Levesque, R.C., *et al.* (2008) Characterization of tRNA-dependent peptide bond formation by MurM in the synthesis of *Streptococcus pneumoniae* peptidoglycan. *J Biol Chem* **283**: 6402–6417.
- Loftus, S.R., Walker, D., Maté, M.J., Bonsor, D.A., James, R., Moore, G.R., and Kleanthous, C. (2006) Competitive recruitment of the periplasmic translocation portal TolB by a natively disordered domain of colicin E9. *Proc Natl Acad Sci USA* **103**: 12353–12358.
- Lukacik, P., Barnard, T.J., Keller, P.W., Chaturvedi, K.S., Seddiki, N., Fairman, J.W., *et al.* (2012) Structural engineering of a phage lysin that targets Gram-negative pathogens. *Proc Natl Acad Sci USA* **109**: 9857–9862.
- McCoy, A.J., Grosse-Kunstleve, R.W., Adams, P.D., Winn, M.D., Storoni, L.C., and Read, R.J. (2007) Phaser crystallographic software. *J Appl Crystallogr* **40**: 658–674.
- Michel-Briand, Y., and Baysse, C. (2002) The pyocins of *Pseudomonas aeruginosa*. *Biochimie* **84**: 499–510.
- Murshudov, G.N., Skubak, P., Lebedev, A.A., Pannu, N.S., Steiner, R.A., Nicholls, R.A., *et al.* (2011) REFMAC5 for the refinement of macromolecular crystal structures. *Acta Crystallogr D Biol Crystallogr* **67**: 355–367.
- Noinaj, N., Guillier, M., Barnard, T.J., and Buchanan, S.K. (2010) TonB-dependent transporters: regulation, structure, and function. *Annu Rev Microbiol* **64**: 43–60.
- Noinaj, N., Easley, N.C., Oke, M., Mizuno, N., Gumbart, J., Boura, E., *et al.* (2012) Structural basis for iron piracy by pathogenic *Neisseria*. *Nature* **483**: 53–58.
- Patzer, S.I., Albrecht, R., Braun, V., and Zeth, K. (2012) Structure and mechanistic studies of pesticin, a bacterial homolog of phage lysozymes. *J Biol Chem* **287**: 23381–23396.
- Petoukhov, M.V., Franke, D., Shkumatov, A.V., Tria, G., Kikhney, A.G., Gajda, M., *et al.* (2012) New developments

- in the ATSAS program package for small-angle scattering data analysis. *J Appl Crystallogr* **45**: 342–350.
- Rai, N., Nöllmann, M., Spotorno, B., Tassara, G., Byron, O., and Rocco, M. (2005) SOMO (SOLution MOdeler): differences between X-ray- and NMR-derived bead models suggest a role for side chain flexibility in protein hydrodynamics. *Structure* **13**: 723–734.
- Rambo, R.P., and Tainer, J.A. (2011) Characterizing flexible and intrinsically unstructured biological macromolecules by SAS using the Porod-Debye law. *Biopolymers* **95**: 559–571.
- Riley, M.A., Pinou, T., Wertz, J.E., Tan, Y., and Valletta, C.M. (2001) Molecular characterization of the klebicin B plasmid of *Klebsiella pneumoniae*. *Plasmid* **45**: 209–221.
- Shirvanyants, D., Ding, F., Tsao, D., Ramachandran, S., and Dokholyan, N.V. (2012) Discrete molecular dynamics: an efficient and versatile simulation method for fine protein characterization. *J Phys Chem B* **116**: 8375–8382.
- Svergun, D. (1992) Determination of the regularization parameter in indirect-transform methods using perceptual criteria. *J Appl Crystallogr* **25**: 495–503.
- Svergun, D., Barberato, C., and Koch, M.H.J. (1995) CRYSQL – a program to evaluate X-ray solution scattering of biological macromolecules from atomic coordinates. *J Appl Crystallogr* **28**: 768–773.
- Udho, E., Jakes, K.S., Buchanan, S.K., James, K.J., Jiang, X., Klebba, P.E., and Finkelstein, A. (2009) Reconstitution of bacterial outer membrane TonB-dependent transporters in planar lipid bilayer membranes. *Proc Natl Acad Sci USA* **106**: 21990–21995.
- Udho, E., Jakes, K.S., and Finkelstein, A. (2012) TonB-dependent transporter FhuA in planar lipid bilayers: partial exit of its plug from the barrel. *Biochemistry* **51**: 6753–6759.
- Usher, K.C., Özkan, E., Gardner, K.H., and Deisenhofer, J. (2001) The plug domain of FepA, a TonB-dependent transport protein from *Escherichia coli*, binds its siderophore in the absence of the transmembrane barrel domain. *Proc Natl Acad Sci USA* **98**: 10676–10681.
- Wandersman, C., and Stojiljkovic, I. (2000) Bacterial heme sources: the role of heme, hemoprotein receptors and hemophores. *Curr Opin Microbiol* **3**: 215–220.
- Winn, M.D., Ballard, C.C., Cowtan, K.D., Dodson, E.J., Emsley, P., Evans, P.R., *et al.* (2011) Overview of the CCP4 suite and current developments. *Acta Crystallogr D Biol Crystallogr* **67**: 235–242.
- Zeth, K., Römer, C., Patzer, S.I., and Braun, V. (2008) Crystal structure of colicin M, a novel phosphatase specifically imported by *Escherichia coli*. *J Biol Chem* **283**: 25324–25331.

Supporting information

Additional supporting information may be found in the online version of this article at the publisher's web-site.

Lectin-Like Bacteriocins from *Pseudomonas* spp. Utilise D-Rhamnose Containing Lipopolysaccharide as a Cellular Receptor

Laura C. McCaughey^{1,9}, Rhys Grinter^{1,9}, Inokentijis Josts¹, Aleksander W. Roszak^{2,3}, Kai I. Waløen^{1,4}, Richard J. Cogdell³, Joel Milner³, Tom Evans¹, Sharon Kelly³, Nicholas P. Tucker⁵, Olwyn Byron⁴, Brian Smith³, Daniel Walker^{1*}

1 Institute of Infection, Immunity and Inflammation, College of Medical, Veterinary and Life Sciences, University of Glasgow, Glasgow, United Kingdom, **2** WestCHEM, School of Chemistry, College of Science and Engineering, University of Glasgow, Glasgow, United Kingdom, **3** Institute of Molecular Cell and Systems Biology, College of Medical, Veterinary, and Life Sciences, University of Glasgow, Glasgow, United Kingdom, **4** School of Life Sciences, College of Medical, Veterinary and Life Sciences, University of Glasgow, Glasgow, United Kingdom, **5** Strathclyde Institute for Pharmaceutical and Biomedical Sciences, University of Strathclyde, Glasgow, United Kingdom

Abstract

Lectin-like bacteriocins consist of tandem monocoat mannose-binding domains and display a genus-specific killing activity. Here we show that pyocin L1, a novel member of this family from *Pseudomonas aeruginosa*, targets susceptible strains of this species through recognition of the common polysaccharide antigen (CPA) of *P. aeruginosa* lipopolysaccharide that is predominantly a homopolymer of D-rhamnose. Structural and biophysical analyses show that recognition of CPA occurs through the C-terminal carbohydrate-binding domain of pyocin L1 and that this interaction is a prerequisite for bactericidal activity. Further to this, we show that the previously described lectin-like bacteriocin putidacin L1 shows a similar carbohydrate-binding specificity, indicating that oligosaccharides containing D-rhamnose and not D-mannose, as was previously thought, are the physiologically relevant ligands for this group of bacteriocins. The widespread inclusion of D-rhamnose in the lipopolysaccharide of members of the genus *Pseudomonas* explains the unusual genus-specific activity of the lectin-like bacteriocins.

Citation: McCaughey LC, Grinter R, Josts I, Roszak AW, Waløen KI, et al. (2014) Lectin-Like Bacteriocins from *Pseudomonas* spp. Utilise D-Rhamnose Containing Lipopolysaccharide as a Cellular Receptor. PLoS Pathog 10(2): e1003898. doi:10.1371/journal.ppat.1003898

Editor: Guy Tran Van Nhieu, Collège de France, France

Received: July 18, 2013; **Accepted:** December 10, 2013; **Published:** February 6, 2014

Copyright: © 2014 McCaughey et al. This is an open-access article distributed under the terms of the Creative Commons Attribution License, which permits unrestricted use, distribution, and reproduction in any medium, provided the original author and source are credited.

Funding: LCM and IJ are supported by 4-year studentships from the Wellcome Trust. RG is supported by a Kelvin Smith Scholarship from the University of Glasgow. We would like to acknowledge the Diamond Light Source for access to I04, I04-1 and I24 (proposal number MX6683). The funders had no role in study design, data collection and analysis, decision to publish, or preparation of the manuscript.

Competing Interests: The authors have declared that no competing interests exist.

* E-mail: Daniel.Walker@glasgow.ac.uk

⁹ These authors contributed equally to this work.

Introduction

The ability to target a subgroup of pathogenic bacteria in a complex bacterial community has potential applications in medicine and agriculture where the maintenance of a 'normal' microbiome is beneficial. For example, the use of broad spectrum antibiotics to treat bacterial infections is known to cause a range of complications associated with collateral damage to the microbiome, including antibiotic associated diarrhea and *Clostridium difficile* infection [1,2]. In addition, there is growing evidence to suggest that microbial dysbiosis may play a role in a range of chronic diseases such as inflammatory bowel disease, diabetes, obesity and rheumatoid arthritis [3,4,5,6]. Indeed, for Crohn's disease, where the link with dysbiosis is well established, the administration of multiple courses of antibiotics is associated with an increased risk factor for the development of this chronic form of inflammatory bowel disease [7,8,9].

In contrast to the broad spectrum antibiotics that are widely used in medicine and agriculture, protein antibiotics known as bacteriocins often target a specific bacterial species or a group of closely related bacterial species [10,11,12,13]. Well characterised

bacteriocins include the S-type pyocins from *P. aeruginosa* and the closely related colicins of *E. coli* [12,13]. The colicin-like bacteriocins form a diverse family of multidomain protein antibiotics which share similar mechanisms of uptake and kill cells through either a pore-forming activity, a specific nuclease activity against DNA, tRNA or rRNA or through inhibition of cell wall synthesis [14,15,16,17]. In the case of S-type pyocins it is thought that their activity is limited to strains of *P. aeruginosa*, whereas colicins show activity against *E. coli* and some strains of closely related bacteria such as *Salmonella* spp. [18]. In the case of colicins and S-type pyocins, killing specificity is primarily determined by the presence of a specific outer membrane receptor on the cell surface. For example, the well characterised E group colicins utilise the TonB-dependent BtuB receptor, which has a normal physiological role in vitamin B₁₂ uptake [19]. Colicin-like bacteriocins have also been shown to have a potent antibiofilm activity, indicating their potential as useful therapeutics for the treatment of chronic biofilm mediated infections [20,21]. In the case of the opportunistic human pathogen *P. aeruginosa* there is an urgent requirement for the development of novel therapeutic options since its ability to form drug-resistant biofilms in

Author Summary

Due to rapidly increasing rates of antibiotic resistance observed among Gram-negative pathogens, such as *Pseudomonas aeruginosa*, there is an urgent requirement for novel approaches to the treatment of bacterial infections. Lectin-like bacteriocins are highly potent protein antibiotics that display an unusual ability to kill a select group of bacteria within a specific genus. In this work, we show how the lectin-like protein antibiotic, pyocin L1, can kill *Pseudomonas aeruginosa* with extraordinary potency through specific binding to the common polysaccharide antigen (CPA) of *P. aeruginosa* lipopolysaccharide. The CPA is predominantly a homopolymer of the sugar D-rhamnose that although generally rare in nature is found frequently as a component of the lipopolysaccharide of members of the genus *Pseudomonas*. The targeting of D-rhamnose containing polysaccharides by pyocin L1 and a related lectin-like protein antibiotic, putidacin L1, explains the unusual genus-specific killing activity of the lectin-like bacteriocins. As we learn more about the link between changes to the microbiome and a range of chronic diseases there is a growing realisation that the ability to target specific bacterial pathogens while maintaining the normal gut flora is a desirable property for next generation antibiotics.

combination with the presence of an outer membrane that is highly impermeable to many classes of antibiotics can make this pathogen essentially untreatable in some groups of patients. This is exemplified in cystic fibrosis patients where chronic lung infection with *P. aeruginosa* is the leading cause of mortality [22].

An interesting addition to this group of protein antibiotics is the recently discovered lectin-like bacteriocins that contain two carbohydrate-binding domains of the monocot mannose-binding lectin (MMBL) family [23,24,25,26,27]. Lectin-like bacteriocins from *P. putida* (putidacin L1 or LlpA_{BW}) *P. syringae* (LlpA_{Pss642}) and *P. fluorescens* (LlpA_{1PF-5}) have been characterised and have the unprecedented ability to kill strains of a broad range of bacterial species within the genus *Pseudomonas*, but are not active outside this genus [24,26,27]. Similarly the lectin-like bacteriocin LlpA_{Xcm761} from *Xanthomonas citri* pv. *malvacearum* LMG 761 has the ability to kill various species within the genus *Xanthomonas* [24]. The molecular basis of this unusual genus specific activity has not been explained.

Lectins are a structurally and evolutionarily diverse class of proteins produced widely by prokaryotes and eukaryotes and are defined by their ability to recognise and bind carbohydrates. This binding is generally highly specific and mediates a range of diverse functions, including cell-cell interaction, immune recognition and cytotoxicity [28,29]. MMBLs represent a structurally conserved lectin subclass, of which the mannose-binding *Galanthus nivalis* agglutinin (GNA) was the first to be characterised [30]. The MMBL-fold consists of a three sided β -prism; each face of which contains a sugar binding motif with the conserved sequence QxDxNxVxY [31]. While originally identified in monocots like *G. nivalis* or *Allium sativum*, it is now recognised that proteins of this class are distributed widely throughout prokaryotes and eukaryotes, where they have evolved to mediate diverse functions [30,32,33,34]. Structural and biochemical analysis of MMBLs has shown that they are generally translated as a single polypeptide chain containing tandem β -prism domains that are then proteolytically processed into monomers. These domains often form homo- or hetero-dimers by strand exchange and π -stacking [35].

The lectin-like bacteriocins are not proteolytically processed and thus consist of a single peptide chain, containing tandem β -prism domains. Sequence alignments of members of this class from *Pseudomonas* spp. show complete conservation of two sugar binding motifs on the C-terminal domain and partial conservation of two sites on the N-terminal domain [23]. Recent work by Ghequire *et al* [23] on the characterisation of putidacin L1 shows these motifs to be important for cytotoxicity. Mutagenesis of the first C-terminal motif has the most dramatic effect on activity, while mutagenesis of the second C-terminal and first N-terminal sugar binding motifs leads to a synergistic reduction in activity. This study also showed low-affinity binding between putidacin L1 and methyl- α -D-mannose or a range of mannose containing oligosaccharides. However, K_{d} s for these protein-carbohydrate complexes were reported in the range from 46 mM for methyl- α -D-mannose to 2 mM for a mannose containing pentasaccharide [23]. An extensive search for high affinity carbohydrate binding through the use of glycan arrays failed to detect high affinity carbohydrate binding for this lectin-like bacteriocin [23].

Despite progress in our understanding of the structure and host range of MMBL-like bacteriocins, the mechanism by which these bacteriocins target susceptible strains and exert their antimicrobial effects is unknown. Here we report on the discovery of a novel member of this family, pyocin L1 from *P. aeruginosa*, and show that it utilises lipopolysaccharide (LPS) as a surface receptor, specifically targeting the common polysaccharide antigen (CPA) that is a conserved homopolymer of D-rhamnose. Structural and biophysical analysis shows that the C-terminal carbohydrate binding motifs are responsible for D-rhamnose recognition and that these sites are specific for this sugar over D-mannose. Further to this, we show that the previously described putidacin L1 also selectively binds LPS from susceptible, but not from resistant, *P. syringae* isolates and shows selectivity for D-rhamnose over D-mannose. This work shows that the physiologically relevant ligand for the QxDxNxVxY carbohydrate binding site of the lectin-like bacteriocins is indeed D-rhamnose and not D-mannose as previously thought. As such, the genus-specific activity of lectin-like bacteriocins from *Pseudomonas* spp. can be attributed to the widespread inclusion of the rare D-rhamnose in the LPS of members of the genus *Pseudomonas*.

Results

Identification and characterisation of pyocin L1

As part of a wider project, aimed at identifying bacteriocins that could be used as novel therapeutics in the treatment of *P. aeruginosa* infections, we searched the genomes of 10 recently sequenced clinical and environmental isolates of *P. aeruginosa* for genes with homology to known bacteriocins. One putative bacteriocin gene identified in strain C1433, an isolate from a patient with cystic fibrosis, encodes a protein with 31% identity to the lectin-like bacteriocin LlpA_{1PF-5}, from *P. fluorescens*. This protein, designated pyocin L1, contained 256-amino acids with a predicted molecular mass of 28413 Da. Alignment of the pyocin L1 protein sequence with other lectin-like bacteriocins, LlpA_{1PF-5}, LlpA_{Pss642}, putidacin L1 (LlpA_{BW}), LlpA_{Au1504} from *Burkholderia cenocepacia* and LlpA_{Xcm761} from *Xanthomonas citri* pv. *malvacearum* shows that pyocin L1 contains tandem MMBL domains with three conserved QxDxNxVxY MMBL sugar-binding motifs (Figure S1). Two of these motifs are located in the C-terminal domain of the protein and one in the N-terminal domain. Comparison with the sequences of other lectin-like bacteriocins shows that the C-terminal QxDxNxVxY motifs are highly conserved, with only LlpA_{Xcm761} lacking one C-terminal motif. In contrast the

N-terminal sugar-binding motifs are less well conserved with only LlpA_{Au1504} possessing two fully conserved QxDxNxVxY motifs (Figure S1).

In order to determine the killing spectrum of pyocin L1 we cloned the pyocin L1 open reading frame into the pET21a vector and expressed and purified the protein by nickel affinity, anion exchange and size exclusion chromatography. Purified pyocin L1 was tested for its ability to inhibit the growth of 32 environmental and clinical isolates of *P. aeruginosa* using an overlay spot plate method on LB agar [36]. Under these conditions, pyocin L1 showed killing activity against nine of the *P. aeruginosa* strains tested. Strain E2, an environmental isolate from a tomato plant for which the genome sequence is available, and strain P8, a clinical isolate from a cystic fibrosis patient, showed the greatest sensitivity to pyocin L1 with killing observed down to concentrations of 27 nM and 7 nM, respectively. Pyocin L1 also showed activity against 5 of the 11 *P. syringae* strains tested, although the effect was much weaker, with cell killing observed at high μ M concentrations.

Pyocin L1 targets the common polysaccharide antigen (CPA) of *P. aeruginosa* LPS

In order to gain insight into the bacteriocidal activity of pyocin L1, we subjected *P. aeruginosa* E2 to high concentrations of recombinant protein and recovered mutants with greatly increased tolerance to pyocin L1 (Figure 1A). The genomes of two of these mutants were sequenced and comparative analysis with the genome of wild-type E2 revealed a dinuclear deletion, C710 and T711, of the 1146-bp *wbpZ* gene. This deletion was common to both mutants. *wbpZ* encodes a glycosyltransferase of 381 amino acids that plays a key role in lipopolysaccharide synthesis, specifically in the synthesis of the common polysaccharide antigen (CPA) also known as A-band LPS [37], (Figure S2). Most strains of *P. aeruginosa* produce two distinct LPS-types that differ in their O-antigen, but share the same core oligosaccharide. The CPA is predominantly a homopolymer of D-rhamnose and the O-specific antigen contains a heteropolymeric repeating unit that varies widely among strains [38]. Consistent with mutation of *wbpZ*, we found that production of CPA, as determined by immunoblotting with a CPA-specific monoclonal antibody [39], in both M4(E2) and M11(E2) was reduced to undetectable levels (Figure 1B). Visualisation of LPS from these strains was performed via silver staining and comparable quantities of LPS were shown to be present. These observations suggest that pyocin L1 may utilise CPA as a cellular receptor. To test this idea further, we obtained two transposon insertion mutants of *P. aeruginosa* PAO1, which is sensitive to pyocin L1, with insertions in the genes responsible for the transport of CPA to the periplasm [40]. These two genes, *wzt* and *wzm*, encode the ATP-binding component and membrane component of a CPA dedicated ABC transporter [38]. Pyocin L1, which shows good activity against PAO1 showed no activity against strains with insertions in *wzm* and *wzt* (Figure 1C) and immunoblotting with a CPA-specific antibody confirmed the absence of the CPA in these pyocin L1 resistant strains (Figure 1D). Thus, the presence of CPA on the cell surface is required for pyocin L1 killing.

In order to determine if the requirement for CPA is due to a direct interaction with pyocin L1 we purified LPS from wild-type PAO1 and from the pyocin L1 resistant, *wzm* and *wzt* mutants (which produce no CPA but do produce the O-specific antigen) and analysed the pyocin-CPA interaction by isothermal titration calorimetry (ITC). Titration of pyocin L1 into isolated LPS-derived polysaccharides (a mixture of CPA and the O-specific antigen containing polysaccharides) from PAO1 gave rise to strong

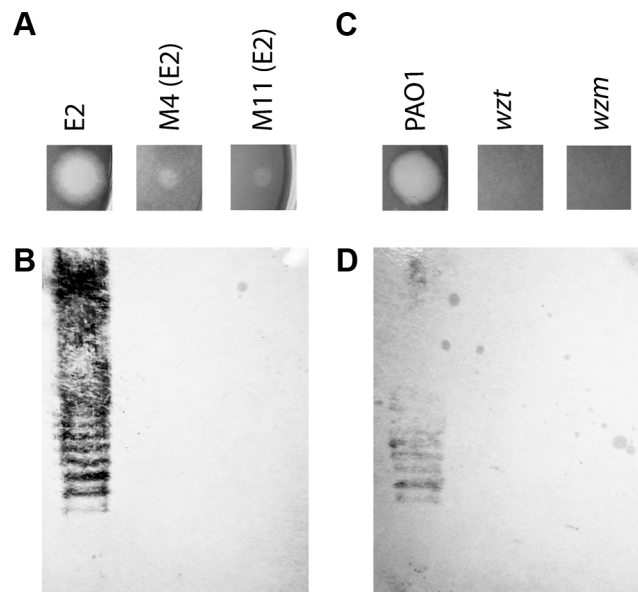


Figure 1. CPA production correlates with pyocin L1 killing. (A) Inhibition of growth of *P. aeruginosa* E2 and tolerant mutants M4 and M11 by pyocin L1, as shown by a soft agar overlay spot-test. 5 μ l of purified pyocin L1 (1.5 mg ml⁻¹) was spotted onto a growing lawn of cells. Clear zones indicate cell death. (B) Expression of CPA by *P. aeruginosa* E2 and tolerant mutants, visualised by immunoblotting with the CPA specific antibody N1F10. (C) Inhibition of growth of *P. aeruginosa* PAO1 and PAO1 *wzm* and *wzt* mutants by pyocin L1 (details as for A). (D) Expression of CPA by PAO1 and *wzm* and *wzt* strains (details as for B).
doi:10.1371/journal.ppat.1003898.g001

saturable exothermic heats of binding (Figure 2A), whereas no binding was detected on titration of pyocin L1 into an equivalent concentration of LPS carbohydrates from PAO1 *wzt*, which produces the O-specific antigen but not the CPA (Figure 2B). These data show that pyocin L1 binds directly to the CPA and that this interaction is required for killing. The CPA is therefore likely to be the cellular receptor for pyocin L1.

Pyocin L1 binds the monosaccharide D-rhamnose

The evolutionary relationships between MMBL-like bacteriocins and the originally identified mannose-binding members of this protein family, led to the assumption that carbohydrate binding of polysaccharides by the lectin-like bacteriocins is primarily mediated through binding of D-mannose at one or more of their conserved QxDxNxVxY carbohydrate binding motifs. Indeed, the recent structures [23] of putidacin L1 bound to mannose-containing monosaccharides adds weight to this idea, although measured affinities between polysaccharides and putidacin L1 are weak (mM) and so may not be physiologically relevant. However, the strong interaction between pyocin L1 and CPA, is incompatible with this and suggests that D-rhamnose and not D-mannose is the likely physiological substrate for the QxDxNxVxY carbohydrate binding motifs.

To determine the affinity of pyocin L1 for D-rhamnose and D-mannose, isothermal titration calorimetry (ITC) was performed. Titration of pyocin L1 into D-rhamnose gave rise to weakly saturable heats of binding that are significantly larger than the heats observed on titration of pyocin L1 into an identical concentration of D-mannose (Figure 3). From this experiment an apparent K_d of 5–10 mM was estimated for the interaction of pyocin L1 with D-rhamnose with apparently weaker binding for

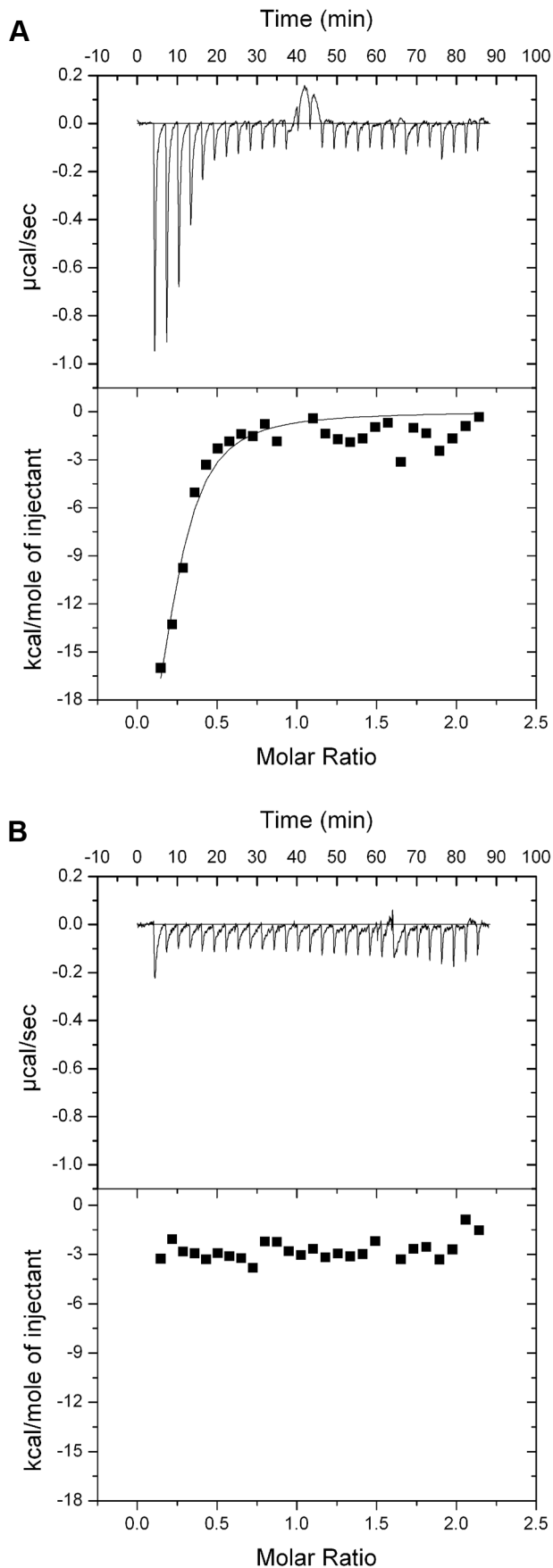


Figure 2. Pyocin L1 binds strongly to CPA from *P. aeruginosa* PAO1. (A) ITC binding isotherm of pyocin L1 (150 µM) titrated into isolated LPS-derived polysaccharide (1 mg ml⁻¹) from wild-type *P. aeruginosa* PAO1. Strong, saturable heats were observed indicative of a strong interaction. Curve fitted with a single binding site model. (B) ITC isotherm of pyocin L1 (150 µM) titrated into isolated LPS-derived polysaccharide (1 mg ml⁻¹) from PAO1 wzt. No saturable binding isotherm was observed.
doi:10.1371/journal.ppat.1003898.g002

D-mannose, $K_d > 50$ mM. The interaction between pyocin L1 and these monosaccharides was also probed using NMR with ¹⁵N labelled pyocin L1, monitoring changes to its ¹⁵N-heteronuclear single quantum correlation (¹⁵N-HSQC) spectra on addition of D-rhamnose or D-mannose. In the absence of added monosaccharide ¹⁵N-HSQC spectra of pyocin L1, which should contain one crosspeak for each non-proline amide NH as well as peaks for the NH groups in various side chains, were well resolved and dispersed, indicative of a folded protein. Chemical shift perturbation monitored by ¹⁵N-HSQC allows the mapping of changes to a protein that occur on ligand binding. Addition of either D-rhamnose or D-mannose up to a concentration of 100 mM did not give rise to large or global changes in chemical shifts (Figure S3). On addition of D-rhamnose significant chemical shift changes were observed for a discrete subset of peaks including some in the amide side chain region of the spectra, while changes of a smaller magnitude were observed on the addition of equal concentrations of D-mannose (Figure S3). Fitting the chemical shift changes that occur on addition of D-rhamnose, for peaks showing strong shifts, to a single site binding model indicates a K_d for the pyocin L1- D-rhamnose complex in the range of 5–20 mM (Figures 3C–F). These data correlated well with the ITC sugar binding data, with low mM binding of pyocin L1 to D-rhamnose and much weaker binding to D-mannose.

D-rhamnose and the CPA bind to the C-terminal QxDxNxVxY motifs of pyocin L1

In an attempt to determine the location of the pyocin L1 D-rhamnose binding site(s) and the structural basis of the D-rhamnose specificity of pyocin L1 we determined the X-ray structures of pyocin L1 with bound D-mannose, D-rhamnose and in the unbound form (Table 1). Pyocin L1, as predicted by sequence homology to MMBL proteins, consists of two tandem β-prism domains characteristic of MMBLs, connected by antiparallel strands propagating from the end of each MMBL domain and lending a strand to the reciprocal β-prism. The strands contain a tryptophan residue which forms π-stacking interactions with two other tryptophans in the β-prism to stabilise the structure (Figure 4A). This interaction is conserved throughout MMBLs, with most members of the class utilising it to form either homo- or heterodimers of single MMBL subunits. However, in pyocin L1, as with the recently described structure of putidacin L1, both domains are from a single polypeptide chain [23]. Other structural elements are also common between the two bacteriocins, namely a C-terminal extension of 30 amino acids and a two-turn α-helix insertion into loop 6 of the N-terminal MMBL domain (Figure 4B). The overall root mean square deviation (rmsd) of backbone atoms for pyocin L1 and putidacin L1 is 7.5 Å, which is relatively high due to a difference in the relative orientation of the two MMBL domains. In contrast, the relative orientation of the tandem MMBL domains of pyocin L1 matches those of the dimeric plant lectins very closely, with alignment of pyocin L1 with the snowdrop lectin homodimer (pdb ID: 1MSA) giving an rmsd of 4.81 Å. Comparison of the respective N- and C- terminal domains from pyocin L1 and

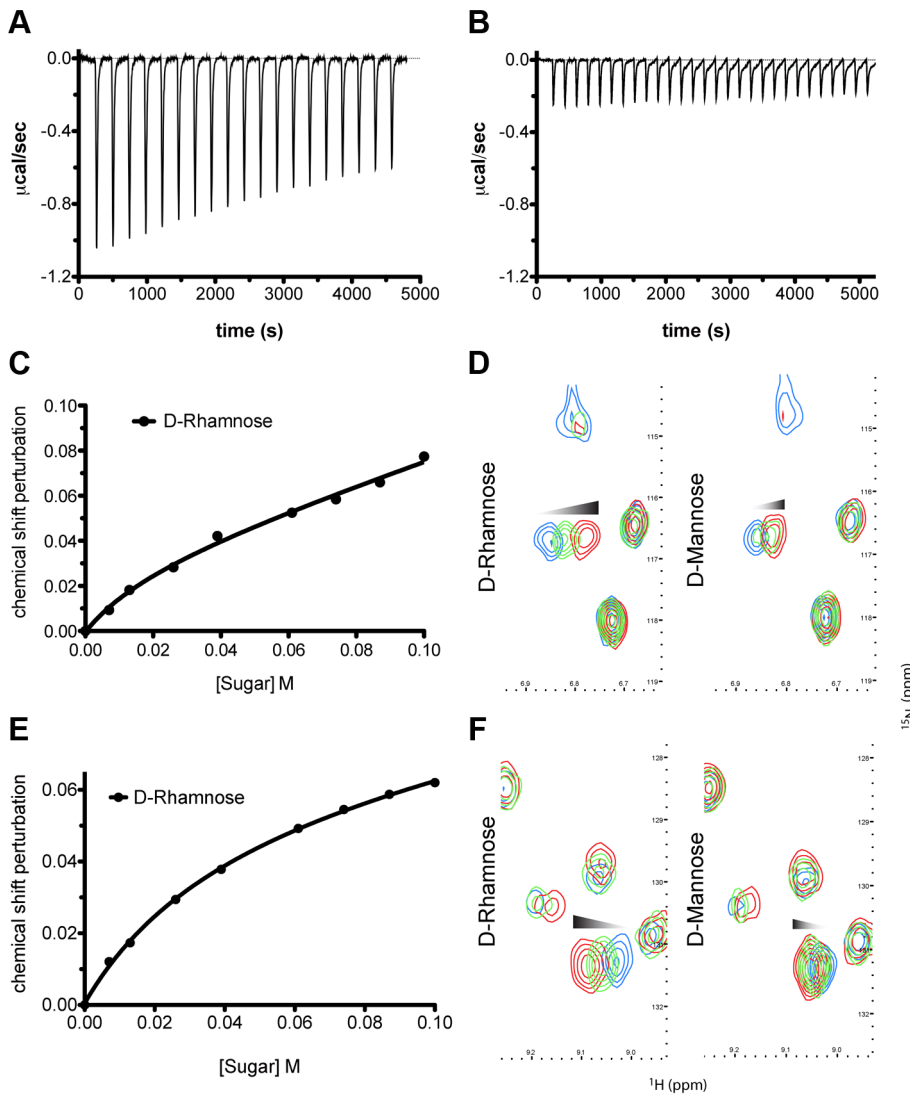


Figure 3. Pyocin L1 shows specificity for D-rhamnose compared with D-mannose. (A) ITC binding isotherm of D-rhamnose (50 mM) titrated into pyocin L1 (100 μM). Weakly saturable heats were observed, indicative of binding with modest affinity ($K_d \sim 5\text{--}10$ mM). (B) ITC binding isotherm of D-mannose (50 mM) titrated into pyocin L1 (100 μM). Small-weakly saturable heats were observed, indicative of very weak interaction ($K_d \sim 50$ mM). Titration of monomeric sugars into ^{15}N -labelled pyocin L1, monitored using ^1H - ^{15}N HSQC NMR spectroscopy. Shifts within spectra were converted to chemical shift perturbation (CSP) values using equation $\Delta_{\text{ppm}} = \sqrt{[\Delta\delta_{\text{HN}} + (\Delta\delta_{\text{N}} \cdot \alpha_{\text{N}})^2]}$. CSP values are plotted against sugar concentration in (C) and (E) and visualised in (D) and (F). Peak positions, which correspond to backbone amide signals, at selected sugar concentrations (blue: no sugar, green: 60 mM, red: 100 mM) are shown. Perturbation of peak position (ppm) is indicative of association between ligand and protein molecules in solution.

doi:10.1371/journal.ppat.1003898.g003

putidacin L1 shows they possess very similar folds with rmsds of 2.77 Å and 2.02 Å, respectively (Figures 4C–D). The higher value for comparison of the N-terminal domains is due to the presence of a 2-strand extension to β-sheet two of the putidacin L1 N-terminal MMBL domain, which is absent from pyocin L1 and other MMBLs. In order to identify protein structures which share a similar fold to pyocin L1 we submitted the structure of the DALI server (http://ekhidna.biocenter.helsinki.fi/dali_server/start). The DALI server searches the protein data bank (PDB) to identify proteins structurally related to the query structure [41]. Significant structural homology was only identified for putidacin L1 and other proteins previously characterised as containing a MMBL fold such as the snowdrop lectin. MMBL dimers of plant origin often form higher order structures, however small angle X-ray scattering of pyocin L1 showed it to be monomeric in solution (Figure S4).

Electron density maps, derived from both D-mannose and D-rhamnose soaked crystals show clear density for sugar moieties in both sites, C1 and C2 (Figure 5). The sugars refined well in these densities at full occupancy, giving B-factors comparable to the surrounding protein side chains. The canonical MMBL hydrogen bonds observed for both D-mannose and D-rhamnose were the same: Gln to O3, Asp to O2, Asn to O2 and Tyr to O4. In addition, O6 of D-mannose forms a hydrogen bond with Tyr169 in C1 and His194 in C2. As D-rhamnose is C6 deoxy D-mannose, it lacks these interactions (Figure 6). The fact that D-mannose forms an additional hydrogen bond is counter-intuitive given that pyocin L1 has a significantly stronger affinity for D-rhamnose, however Val154, Val163 and Ala166 of C1 and Val184 and Ala191 of C2 form a hydrophobic pocket to accommodate the C6-methyl group of D-rhamnose (Figure S5).

Table 1. Crystallographic data collection and refinement statistics.

	Sugar Free Form	D-Rhamnose Soak	D-Mannose Soak
Data collection^a			
Space group	C222 ₁	C222 ₁	C222 ₁
Cell dimensions, <i>a</i> , <i>b</i> , <i>c</i> (Å)	53.41, 158.40, 147.67	52.99, 160.65, 150.57	53.42, 162.1, 152.5
Resolution (Å)	36.42 - 2.09 (2.14 - 2.09)	54.99 - 2.37 (2.43 - 2.37)	55.53 - 2.55 (2.67 - 2.55)
Solvent content (%)	56	55	56
No. of unique observations	37131 (2751)	26242 (1922)	22096 (2901)
Multiplicity	4.8 (4.9)	4.4 (4.5)	5.5 (5.7)
Completeness (%)	99.0 (99.8)	99.1 (99.5)	99.9 (100.0)
R _{merge} (%)	7.2 (59.2)	5.9 (83.0)	7.1 (85.6)
R _{pim} (%) ^b	4.1 (33.0)	3.4 (44.9)	3.3 (39.2)
Mean I/sigma (I)	14.3 (2.1)	19.0 (2.1)	13.3 (2.3)
Refinement statistics			
R _{work} /R _{free} (%)	17.8/22.2	20.9/25.7	19.4/24.8
No. of non-hydrogen atoms	4505	4178	4138
RMSD of bond lengths (Å)	0.02	0.015	0.013
RMSD of bond angles (°)	1.96	1.63	1.70
No. of waters	344	95	27
Mean/Wilson plot B-value (Å ²)	40.2/33.8	54.2/43.6	65.9/59.1
Ramachandran plot (%) ^c			
Favoured/Allowed/Outliers	97.2/2.2/0.6	97.4/2.2/0.4	96.6/3.0/0.4
PDB identifier	4LE7	4LED	4LEA

^aValues in parentheses refer to the highest resolution shell.

^b $R_{pim} = \frac{\sum_{hkl} [1/(N-1)]^{1/2} \sum_i |I_i(hkl) - \langle I(hkl) \rangle|}{\sum_{hkl} \sum_i I_i(hkl)}$

^cPercentages of residues in favored/allowed regions calculated by the program RAMPAGE [68].

doi:10.1371/journal.ppat.1003898.t001

Weak density was observed for both sugars at site N1, however given the high concentrations used in the soak and the overall low binding affinity of pyocin L1 for monomeric sugars, it is unlikely that N1 represents a primary binding site for D-rhamnose (Figure S5). The conserved residues in site N2 form interactions with the C-terminal extension of the protein and as such are inaccessible. Weak density was also observed adjacent to the binding site C1 of mol B in both the soaks and in mol A of the D-rhamnose form. This density may correspond to a peripheral binding site utilised in binding to the carbohydrate chain of LPS, as is observed in the structure of putidacin L1 bound to oligosaccharides [23].

To test the idea that the observed binding of D-rhamnose to sites C1 and C2 is reflective of CPA binding and that this binding is critical to pyocin L1 cytotoxicity, we created pyocin L1 variants in which the conserved aspartic acids of the QxDxNxVxY motifs of the C1 and C2 sugar binding sites were mutated to alanine and compared their cytotoxicity and ability to bind the CPA by ITC with the wild-type protein. Titrations with wild-type pyocin L1 and the D150A (C1) and D180A (C2) variants were performed by titrating protein at a concentration of 100 μM into a solution of LPS-derived polysaccharide (1 mg ml⁻¹) from strain PAO1 (Figure 7). Under these conditions we were able to generate binding isotherms that enabled us to accurately determine an apparent K_d of 0.15 (±0.07) μM for the wild-type pyocin L1-CPA complex. For both the D150A (C1) and D180A (C2) variants, affinity for CPA was reduced. For the pyocin L1 D150A-CPA complex a K_d of 1.52 (±0.51) μM was determined, a 10-fold increase in K_d relative to the wild-type pyocin L1-CPA complex. However, CPA binding to the D180A variant was severely weakened and although heats of

binding were still observed the K_d for this complex, which could not be accurately determined, is likely >500 μM. We also produced a double mutant in which both D150A and D180A mutations were present. For this double mutant, no binding to CPA was observed by ITC. These data show that both the C1 and C2 sugar binding motifs are required for full CPA binding, but that the C2 binding site is the major CPA binding determinant. The killing activity of these sugar binding motif variants showed a good correlation with their ability to bind the CPA. Both the D150A and D180A variants showed reduced cytotoxicity against PAO1 relative to pyocin L1, with the D150A showing a greater reduction in activity and for the D150A/D180A variant very low levels of cytotoxicity were observed (Figure 7).

Putidacin L1 binds to *P. syringae* LPS and D-rhamnose

Pyocin L1 targets sensitive strains of *P. aeruginosa* through binding to LPS and utilises this as a cell surface receptor. To determine if LPS binding is common to the homologous and previously characterised lectin-like bacteriocin putidacin L1, we purified this protein and determined if the susceptibility of a number of strains of *P. syringae* correlated with the ability of putidacin L1 to bind to LPS-derived carbohydrates from these strains.

From the five strains of *P. syringae* tested, LMG 5456 and LMG 2222 were found to be highly susceptible to putidacin L1 with killing down to concentrations of 0.3 and 7.6 nM respectively. DC3000 and NCPPB 2563 showed complete resistance and LMG 1247 was highly tolerant (killing down to 0.6 μM). Binding of putidacin L1 to the isolated LPS-derived polysaccharides of the

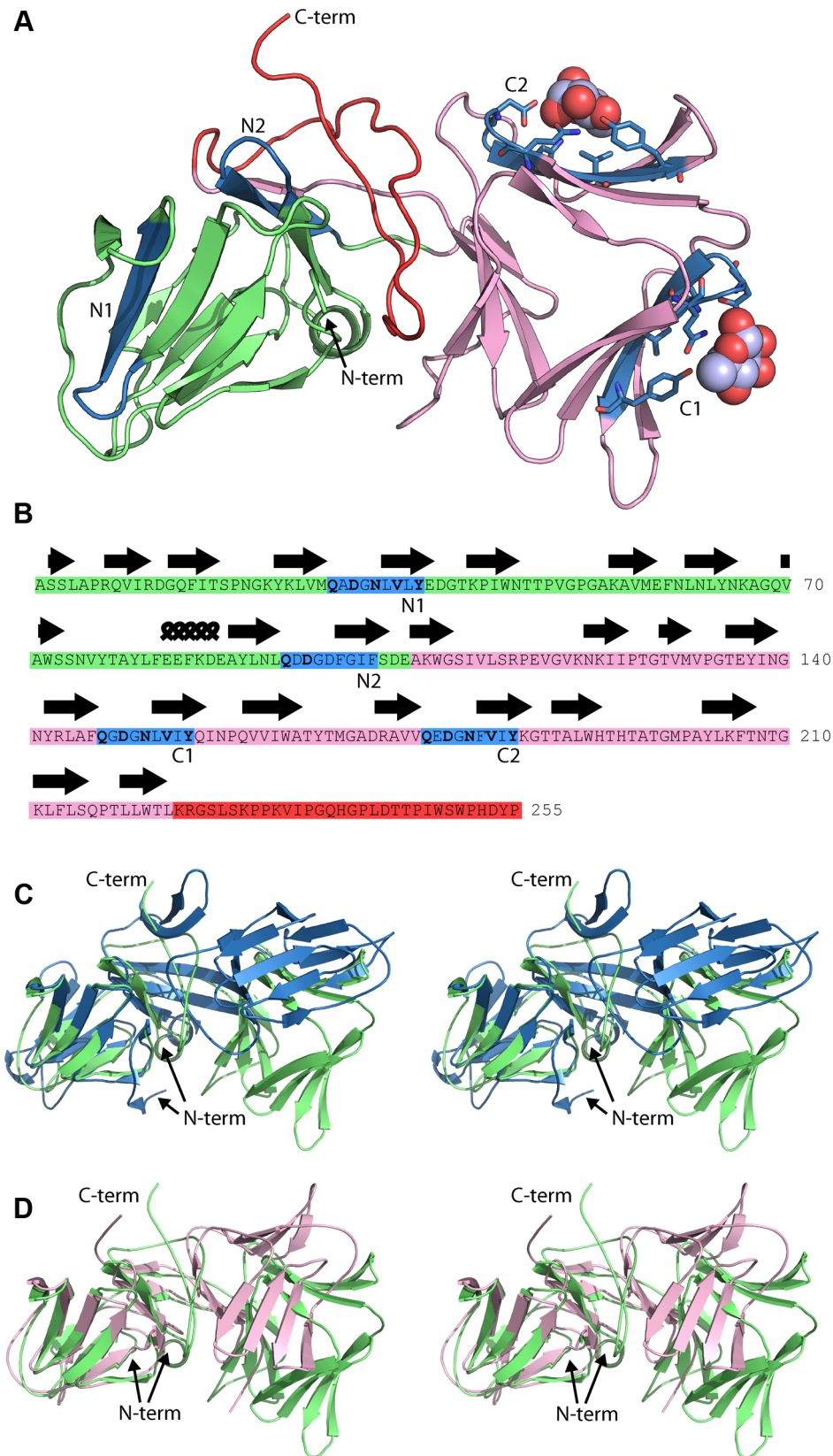


Figure 4. Crystal structure of pyocin L1 reveals tandem MMBL domains and sugar-binding motifs. (A) Ribbon diagram of structure of pyocin L1 in complex with α -D-rhamnose, amino acids 2-256. N-terminal domain (green), C-terminal domain (pink), C-terminal extension (red), α -D-rhamnose (spheres) and sugar binding sites containing the conserved or partially conserved QxDxNxVxY motif are highlighted (blue) and are designated N1, N2 and C1, C2 according to order of appearance in the primary sequence of the N- and C-terminal domains, respectively. Pyocin L1

residues involved in hydrogen bonding with α -D-rhamnose are shown in stick representation. (B) Sequence and secondary structure (β -sheets = arrows, α -helices = coils) of pyocin L1 with colours corresponding to the structure in (A). Residues conserved in sugar binding motifs are shown in bold. (C) Structural alignment of pyocin L1 (green) and putidacin L1 (blue) based on N-terminal MMBL domain in wall-eyed stereo. (D) Structural alignment of pyocin L1 (green) and *Allium sativum* agglutinin (1BWU) (pink) based on N-terminal MMBL domain in wall-eyed stereo. doi:10.1371/journal.ppat.1003898.g004

above mentioned strains was tested by ITC. Large saturable heats of binding were observed for putidacin L1 and the LPS-derived polysaccharides from LMG 5456 and LMG 2222, while no binding was observed between putidacin L1 and the LPS-derived polysaccharides from LMG 1247, 2563 or DC3000 (Figure 8). Thus, there is excellent correlation between putidacin L1 cell killing and the binding of LPS-derived polysaccharide indicating that like pyocin L1, putidacin L1 utilises LPS as a surface receptor.

Although *P. syringae* O-antigens are diverse relative to CPA, the incorporation of D-rhamnose is widespread and seemingly almost universal in strains of this species [42,43]. Interestingly, in cases where D-rhamnose is not a component of *P. syringae* LPS, L-rhamnose is present [42]. As with pyocin L1 we utilised ITC and NMR to characterise the binding affinity of putidacin L1 for D-rhamnose, in comparison with D-mannose and L-rhamnose. Putidacin L1 exhibited

an affinity of 5–10 mM for D-rhamnose, which is comparable to that of pyocin L1, and approximately 10-fold stronger than its affinity for D-mannose (Figure S6). Interestingly, no binding of L-rhamnose to putidacin L1 or pyocin L1 was observed (Figure S7). It is interesting to note that in the strains of *P. syringae* we have tested, the killing spectrum (but not the potency) of pyocin L1 and putidacin L1 is identical. This observation combined with the specificity of putidacin L1 for D-rhamnose, strongly suggests that it also binds to a D-rhamnose containing O-antigen. Indeed branched D-rhamnose O-antigens are common in *P. syringae* [42,43].

Our data for both pyocin L1 and putidacin L1 indicate that D-rhamnose containing O-antigens are utilised as surface receptors for lectin-like bacteriocins from *Pseudomonas* spp. This is an attractive hypothesis since the inclusion of D-rhamnose in the lipopolysaccharides from members of this genus is widespread and

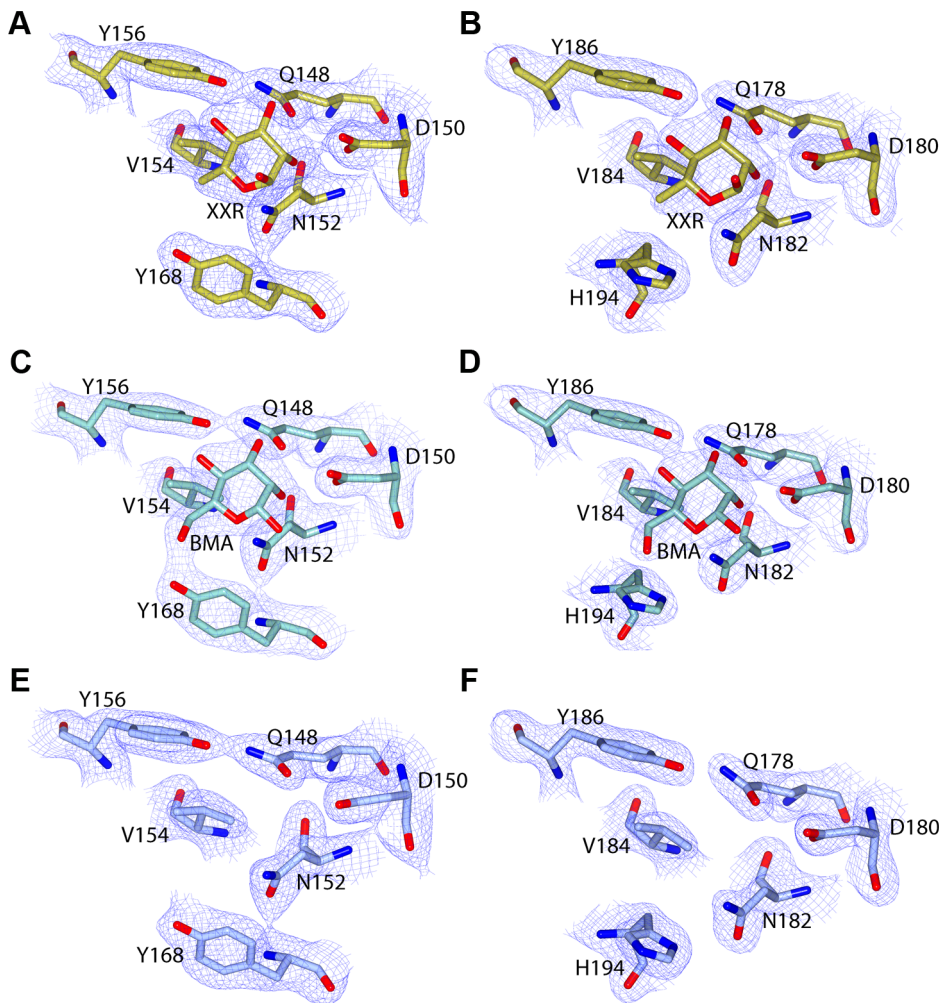


Figure 5. C-terminal MMBL-sugar binding motifs of pyocin L1 bind D-rhamnose and D-mannose. Electron density (at 1.3 σ) with fitted stick model of pyocin L1 MMBL-sugar binding site C1 with: (A) D-rhamnose (XXR), (C) D-mannose (BMA), (E) no bound sugar, and sugar binding site C2 with: (B) D-rhamnose, (D) D-mannose, (F) no bound sugar. For clarity, electron density is clipped to within 1.5 Å of visible atoms. doi:10.1371/journal.ppat.1003898.g005

could form an important component of the genus specific activity of this group of bacteriocins.

Discussion

In this work we have shown that pyocin L1 targets susceptible cells through binding to the CPA component of LPS and that primary recognition of CPA occurs through binding of D-rhamnose at the conserved QxDxNxVxY sugar binding motifs of the C-terminal lectin domain. The ability of both pyocin L1 and putidacin L1 to recognise D-rhamnose containing carbohydrates is an important component of their ability to target sensitive strains of *Pseudomonas* spp. The use of the O-antigen as a primary receptor differentiates the lectin-like bacteriocins from other multidomain bacteriocins such as colicins and S-type pyocins (colicin-like bacteriocins) which utilise outer membrane proteins as their primary cell surface receptors [44]. The colicin-like bacteriocins also possess a flexible, or natively disordered N-terminal region that is thought to pass through the lumen of a coreceptor and interact with the periplasmic Tol or Ton complexes that mediate translocation of the bacteriocin across the outer membrane [11,44]. The lack of such a flexible N-terminal region in the lectin-like bacteriocins suggests that either they do not need to cross the outer membrane in order to mediate their cytotoxicity or they do so by a mechanism that is fundamentally different to the diverse family of colicin-like bacteriocins. Given the extensive structural homology between the lectin-like bacteriocins and plant lectins it seems likely that these bacteriocins share a common ancestor with plant lectins and from an evolutionary perspective are unrelated to the colicin-like bacteriocins.

In addition to O-antigen recognition, additional factors, as yet to be determined, are clearly also important in strain and species specificity among the lectin-like bacteriocins. Indeed, recent work from Ghequire *et al.* has shown through domain swapping experiments that for putidacin L1 (LlpA_{BW}) and the homologous lectin-like bacteriocin LlpA1_{PF-5} from *Pseudomonas fluorescens*, species specificity is governed by the identity of the N-terminal lectin domain [23]. Thus, in view of these data and our own data it seems likely that the C-terminal lectin domain of this class of bacteriocins plays a general role in the recognition of D-rhamnose containing O-antigens, with the N-terminal domain interacting with species-specific factors and thus determining the precise species and strain specificity of these bacteriocins. Although there are few clues as to how the lectin-like bacteriocins ultimately kill

susceptible cells, we have established a clear role for the C-terminal MMBL domain of these proteins. The roles of the N-terminal MMBL domain and the C-terminal extension remain to be discovered [23]. However, from the previous work of Ghequire *et al.*, it is clear that all three of these regions are required for killing of susceptible cells.

Interestingly, although rhamnose is frequently a component of plant and bacterial glycoconjugates, such as the rhamnolipids of *P. aeruginosa* [45] and pectic polysaccharides of plant cell walls [46], it is generally the L-form of this sugar that is found in nature. Although otherwise rare, D-rhamnose is found frequently as a component of the LPS of plant pathogens and plant associated bacteria such as *P. syringae* [42,43], *P. putida* [47], *Xanthomonas campestris* [48] and *Burkholderia* spp. [49], but is a relatively rare component of the O-antigens of animal pathogens such as *E. coli*, *Salmonella* and *Klebsiella*. It is interesting to speculate that since D-rhamnose is a common component of the LPS of bacterial plant pathogens, that some of the many lectins produced by plants may have evolved to target D-rhamnose as part of plant defence to bacterial pathogens.

The specificity of lectin-like bacteriocins suggests that these protein antibiotics may be useful in combating plant pathogenic bacteria, either through the use of bacteriocin expressing biocontrol strains or by the production of transgenic plants engineered to express these proteins. The specific targeting mechanism described here, binding of D-rhamnose containing polymers, indicates that the lectin-like bacteriocins would not interact with either plant or animal cells, since these lack D-rhamnose containing glycoconjugates. In addition, these narrow spectrum antibiotics would leave the majority of the soil microbiome and the gut microbiome of plant-eating animals intact and so would be likely to have minimal environmental impact and minimal impact on animal health. This latter property and the potency of these protein antibiotics could also make the use of lectin-like bacteriocins in the treatment of chronic multidrug-resistant *P. aeruginosa* infections in humans an attractive proposition.

Materials and Methods

Bacterial strains, plasmids and growth conditions

Strains and plasmids utilised in this study are presented in Supplementary Table S1. Strains of *P. aeruginosa* were grown in LB at 37°C, *P. syringae* were grown in King's B Media (KB) (20 g

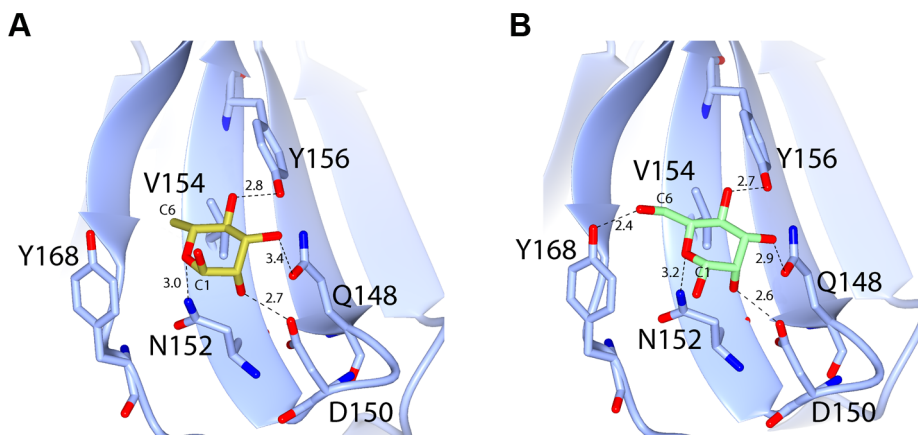


Figure 6. Hydrogen-bonding interactions between pyocin L1 MMBL sugar-binding motif C1 with D-rhamnose and D-mannose. Hydrogen bonds between protein side chains with (A) D-rhamnose and (B) D-mannose are shown; all distances are in Å. doi:10.1371/journal.ppat.1003898.g006

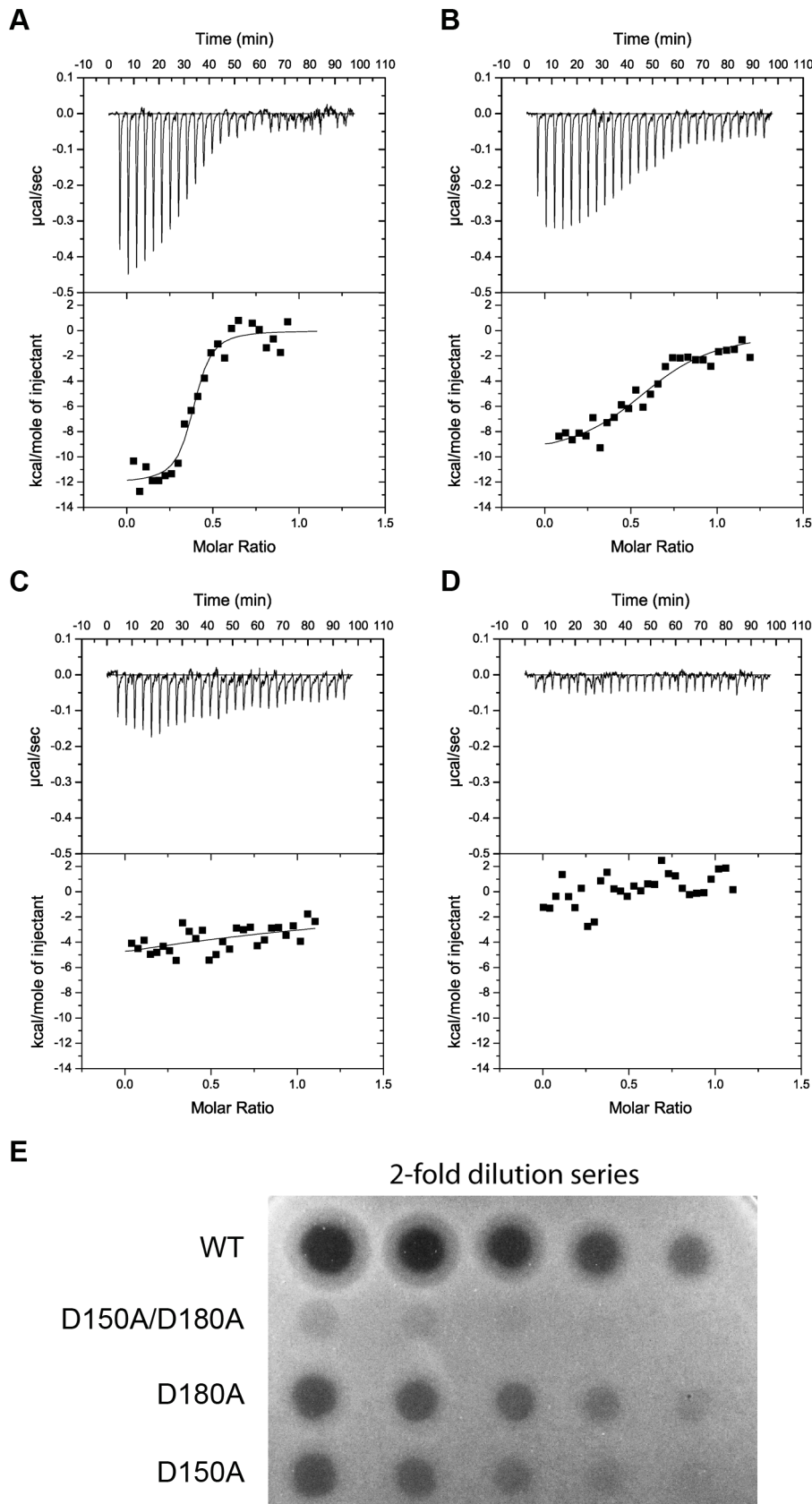


Figure 7. Binding of the CPA at the C-terminal sugar binding motifs, C1 and C2, is critical to pyocin L1 cytotoxicity. ITC binding isotherms of (A) wild-type (B) D180A (C) D150A and (D) D150A/D180A pyocin L1 all at (100 μM) titrated into isolated LPS-derived polysaccharide (1 mg ml^{-1}) from wild-type *P. aeruginosa* PAO1. Fit to a single binding site model is shown. (E) Spot tests to determine cytotoxic activity of wild-type

and pyocin L1 variants against of *P. aeruginosa* PAO1. Purified protein (starting concentration $400 \mu\text{g ml}^{-1}$ with 2-fold sequential dilutions) was spotted onto a growing lawn of *P. aeruginosa* PAO1. Clear zones indicate pyocin L1 cytotoxicity. doi:10.1371/journal.ppat.1003898.g007

peptone, 10 g glycerol, 1.5 g MgSO_4 , 1.5 g K_2HPO_4 per liter adjusted to pH 7.5) at 28°C .

Cloning and purification of lectin-like bacteriocins

Pyocin L1 was amplified from the genomic DNA of the producing strain *P. aeruginosa* C1433 [50] by PCR using primers designed to introduce an NdeI site at the start of the *pyoL1* gene (ACA GAT CAT ATG AAG TCT CCA AAC AAA AGG AGG) and an XhoI site at the end of the gene (ACA GAT CTC GAG GAC CAC GGC GCG CCG TCG TGG ATA GTC GTG GGG CCA A). The PCR product was ligated into the corresponding sites of the *E. coli* expression vector pET21a to give pETPyoL1 which encodes pyocin L1 with a C-terminal His₆ tag separated from the C-terminus of pyocin L1 by a 6 amino acid linker (RRRAVV). Pyocin L1 was overexpressed from *E. coli* BL21(DE3)pLysS carrying the plasmid pETPyoL1. Five litres of LB broth was inoculated (1:100) from an overnight culture and cells were grown at 37°C in a shaking incubator to an $\text{OD}_{600} = 0.6$. Protein production was induced by the addition of 0.3 mM isopropyl β -D-1-thiogalactopyranoside (IPTG), the cells were grown at 22°C for a further 20 h and harvested by centrifugation. Cells were resuspended in 20 mM Tris-HCl, 500 mM NaCl, 5 mM imidazole (pH 7.5) and lysed using an MSE Soniprep 150 (Wolf Laboratories) and the cell debris was separated by centrifugation. The cell-free lysate was applied to a 5-ml His Trap HP column (GE Healthcare) equilibrated in 20 mM Tris-HCl, 500 mM NaCl, 5 mM imidazole (pH 7.5) and pyocin

L1 was eluted over a 5–500 mM imidazole gradient. Pyocin L1 containing fractions were identified by SDS PAGE, pooled and dialyzed overnight into 50 mM Tris-HCl, 200 mM NaCl, pH 7.5 and remaining contaminants were removed by gel filtration chromatography on a Superdex S75 26/600 column (GE Healthcare) equilibrated in the same buffer. The protein was concentrated using a centrifugal concentrator (Vivaspin 20) with a molecular weight cut off of 5 kDa and stored at -80°C until required. The putidacin L1 open reading frame was synthesised (DNA 2.0) and cloned into pET21a via 5' NdeI and 3' XhoI restriction sites. The stop codon was removed in order to utilise the pET21a C-terminal His₆ tag. Purification of putidacin L1 was performed as for pyocin L1. Constructs to express the pyocin L1 mutants D31A, D97A, D150A and D180A were created using the QuikChange Site Directed Mutagenesis Kit (Stratagene) utilising pETPyoL1 as a template. The primers used were CAA ATT GGT CAT GCA AGC GGC TGG CAA CTT GGT CCT TTA CG and CGT AAA GGA CCA AGT TGC CAG CCG CTT GCA TGA CCA ATT TG for D31A, CCG TAC CTG AAT CTT CAA GAT GCT GGG GAC TTC GGT ATA TTT TC and GAA AAT ATA CCG AAG TCC CCA GCA TCT TGA AGA TTC AGG TAC GC for D97A, CGC CTA GCG TTT CAG GGA GCT GGC AAC CTA GTG ATC TAT C and GAT AGA TCA CTA GGT TGC CAG CTC CCT GAA ACG CTA GGC G for D150A and GAT AGA GCA GTA GTG CAA GAG GCT GGA AAT TTT GTT ATC TAC AAA G and CTT TGT AGA TAA CAA AAT TTC CAG CCT CTT GCA CTA CTG CTC

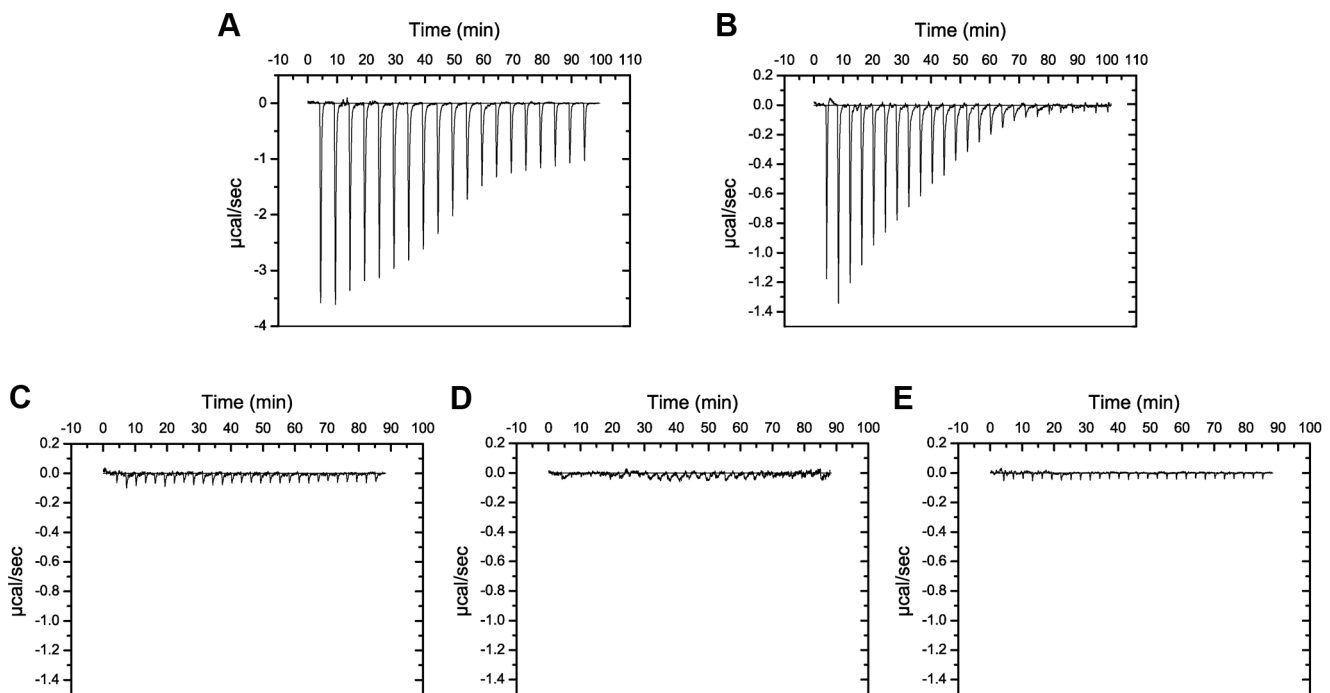


Figure 8. Putidacin L1 binds strongly to LPS-derived polysaccharides from susceptible but not tolerant or resistant *P. syringae* isolates. ITC isotherm of LPS-derived polysaccharides (3 mg ml^{-1}) from strains highly sensitive to putidacin L1: (A) *P. syringae* LMG 2222, (B) *P. syringae* LMG 5456 titrated into putidacin L1 ($60 \mu\text{M}$). Large, saturable heats are indicative of binding. LPS-derived polysaccharides (3 mg ml^{-1}) from strains non-sensitive to putidacin L1: (C) *P. syringae* NCPPB 2563, (D) *P. syringae* DC3000, or highly tolerant (E) *P. syringae* LMG 1247 to putidacin L1, show no heats of binding when titrated into putidacin L1 ($60 \mu\text{M}$). doi:10.1371/journal.ppat.1003898.g008

TAT C for D180A. Mutant proteins were purified as described above for wild-type pyocin L1.

Pyocin sensitivity assays: Overlay spot plate method

Soft agar overlay spot plates were performed using the method of [35]. 150 μ l of test strain culture at $OD_{600} = 0.6$ was added to 6 ml of 0.8% soft agar and poured over an LB or KB agar plate. 5 μ l of bacteriocin at varying concentrations was spotted onto the plates and incubated for 20 h at 37 or 28°C.

Isolation of pyocin L1 tolerant mutants

1.5 ml of a culture of *P. aeruginosa* E2 ($OD_{600} = 0.6$) was centrifuged and resuspended in 100 μ l of LB, to which 100 μ l (8 mg ml⁻¹) of purified pyocin L1 was added. The culture was grown for 1 h, plated onto a LB agar plate and incubated for 20 h at 37°C. Isolated colonies were identified as *P. aeruginosa* using 16S PCR as described previously [51].

Whole genome sequencing

The genomes of *P. aeruginosa* E2 and derived pyocin L1 tolerant mutants were sequenced at the Glasgow Polyomics Facility, generating paired-end reads on an Illumina MiSeq Personal Sequencer. Reads were mapped to the previously sequenced parent genomes of *P. aeruginosa* E2 using the CLC genomics workbench, MAUVE and RAST to create an ordered annotated genome. The CLC genomics workbench was used for genome comparisons and the identification of SNPs/INDELS.

LPS purification and isolation of LPS-derived polysaccharide

LPS was purified from 1 litre cultures of *P. aeruginosa* and *P. syringae* strains as described previously, with modifications including the omission of the final trifluoroacetic acid hydrolysis and chromatography steps [52]. Cells were grown for 20 h at 37°C and 28°C for *P. aeruginosa* and *P. syringae* respectively, pelleted by centrifugation at 6000 g for 20 min, and resuspended in 50 mM Tris, pH 7.5 containing lysozyme (2 mg ml⁻¹) and DNase I (0.5 mg ml⁻¹). Cells were lysed by sonication and the cell lysate was incubated at 20°C for 30 min before EDTA was added to a final concentration of 2 mM. An equal volume of aqueous phenol was added and the solution was heated at 70°C for 20 min, with vigorous mixing. The solution was then cooled on ice for 30 min, centrifuged at 7000 g for 20 min and the aqueous phase extracted. Proteinase K was added to a final concentration of 0.05 mg ml⁻¹ and dialysed for 12 h against 2 \times 5 L H₂O. LPS was pelleted by ultracentrifugation at 100,000 g for 1 h, resuspended in H₂O and heated to 60°C for 30 min to remove residual proteinase K activity. LPS-derived carbohydrates were isolated by heating LPS in 2% acetic acid for 1.5 h at 96°C. Lipid A was removed by centrifugation at 13,500 g for 3 min followed by extraction with an equal volume of chloroform. The aqueous phase was then lyophilised.

SDS-PAGE, silver staining and immunoblotting

Purified LPS from wild-type and mutant samples were resolved by electrophoresis on 12% SDS-polyacrylamide gels. The LPS banding patterns were visualised by the Invitrogen ultrafast silver staining method. For immunoblotting LPS was transferred onto nitrocellulose membranes and western immunoblotting was performed as previously described using the CPA-specific monoclonal antibody N1F10 and alkaline phosphatase-conjugated goat anti-mouse Fab2 as the secondary antibody [39]. The blots were developed using SIGMAFAS BCIP/NBT tablets.

Isothermal titration calorimetry

ITC experiments were performed on a VP-ITC microcalorimeter (MicroCal LLC). For monosaccharide binding, titrations were carried out at 299 K with regular 15 μ l injections of ligands into 60–100 μ M pyocin L1 or putidacin L1 at 300 s intervals. 50 mM D-rhamnose, D-mannose or L-rhamnose were used as titrants and reactions were performed in 0.2 M sodium phosphate buffer, pH 7.5. D-rhamnose (>97%) was obtained from Carbosynth Limited (UK) and D-mannose and L-rhamnose (>99%) from Sigma-Aldrich (UK). For O-antigen-pyocin L1 binding reactions, pyocin L1 or pyocin L1 variants were used as titrant at 100 or 150 μ M with cleaved O-antigen sugars dissolved at 1 mg ml⁻¹ in the chamber. For curve fitting we estimated the molar concentration of LPS-derived CPA containing carbohydrate chains at 20 μ M based on an estimated average molecular weight of 10 kDa for CPA containing polysaccharides and estimating the percentage of total LPS represented by CPA containing carbohydrates as 20% of the total by weight [53]. This value may not be accurate and as such the stoichiometry implied by the fit is likely to be unreliable. However, the use of this estimated value has no impact on the reported parameters of ΔH , ΔS and K_d . For O-antigen-putidacin L1 binding reactions, O-antigen was used as the titrant at 3 mg ml⁻¹ with 60 μ M putidacin L1 in the chamber. Reactions were performed in 20 mM HEPES buffer pH 7.5. All samples were degassed extensively prior to the experiments. Calorimetric data were calculated by integrating the area under each peak and fitted with a single-site binding model with Microcal LLC Origin software. The heats of dilution for each titration were obtained and subtracted from the raw data.

NMR titration experiments

NMR chemical shift perturbation analysis of sugar binding by pyocin L1 and putidacin L1 was carried out at 305 K and 300 K respectively. Fast-HSQC spectra [54] were recorded using ¹⁵N labelled proteins (0.1–0.2 mM) and unlabelled ligands, D-rhamnose and D-mannose (100 mM), on a Bruker AVANCE 600 MHz spectrometer. Protein samples were prepared with and without the sugars present and volumes were exchanged at fixed ratios, making sure the protein concentration remained unchanged. The spectra were processed with Topspin and analysed with CCPNmr analysis [55].

Crystallisation and data collection for pyocin L1

Purified pyocin L1 at a concentration of 15 mg ml⁻¹ was screened for crystallisation conditions using the Morpheus and PGA crystallisation screens (Molecular Dimensions) [56]. Screens were prepared using a Cartesian Honeybee 8+1 dispensing robot, into 96-well, MRC-format, sitting drop plates (reservoir volume of 80 μ l; drop size of 0.5 μ l of protein and 0.5 μ l of reservoir solution). Clusters of needle shaped crystals grew in a number of conditions in each screen over 3 to 7 days. Two of these conditions, condition 1 (20% v/v ethylene glycol, 10% w/v PEG 8000, 0.03 M CaCl₂, 0.03 M MgCl₂, 0.1 M Tris/Bicine, pH 8.5) and condition 2 (20% PEG 550 MME, 20% PEG 20 K, 0.03 M CaCl₂, 0.03 M MgCl₂, 0.1 M MOPS/HEPES, pH 7.5) from the Morpheus screen were selected for optimisation by vapour diffusion in 24 well plates (reservoir volume 500 μ l, drop size 1 μ l protein and 1 μ l reservoir solution). Clusters of needles from these trays grew after 3–7 days and were mechanically separated. The un-soaked crystals were from condition 1, while soaked crystals were from condition 2. Un-soaked crystals were looped and directly cryo-cooled to 110 K in liquid nitrogen; D-mannose and D-rhamnose soaked crystals were soaked for 2–12 min in

artificial mother liquor containing 4 M D-mannose or 2 M D-rhamnose, before cryo-cooling to 110 K. X-ray diffraction data were collected at the Diamond Light Source, Oxfordshire, UK at beam lines I04, I04-1 and I24. Automatic data processing was performed with Xia2 within the EDNA package [57].

Structure solution and refinement for pyocin L1

A dataset from an un-soaked pyocin L1 crystal was submitted to the Balbes pipeline along with the amino acid sequence for pyocin L1 [58]. Balbes produced a partial molecular replacement solution based on the structure of *Galanthus nivalis* agglutinin (PDB ID: 1MSA). Initial phases from Balbes were improved via density modification and an initial model was built using Phase and Build from the Phenix package [59]. The model was then built and refined using REFMAC5 and Coot 0.7 [60,61]. Validation of all models was performed using the Molprobtity web server and Procheck from CCP4-I [62,63]. Two structures of sugar soaked pyocin L1 were solved by molecular replacement using Phaser [64], with the sugar-free pyocin L1 as the search model. Additional electron density corresponding to bound sugars, was observed in both $2F_o - 2F_c$ and $F_o - F_c$ maps [65]. Sugars were fitted and structures refined using Coot 0.7 and REFMAC5. β -D-mannose (PDB ID: BMA) corresponded best to the density of bound D-mannose. The density in the D-rhamnose complex best corresponded to α -D-rhamnose, for which no PDB ligand exists; a model for α -D-rhamnose was prepared by removing the oxygen from carbon 6 of α -D-mannose and submitting these PDB coordinates to the ProDRG server, which generated the model and modeling restraints [65]. The resultant α -D-rhamnose was designated with the PDB ID: XXR.

Small angle X-ray scattering

SAXS was carried out on the X33 beamline at the Deutsches Elektronen Synchrotron (DESY, Hamburg, Germany). Data were collected on samples of Pyocin L1 in the range of 0.5–5 mg ml⁻¹. Buffer was read before and after each sample and an average of the buffer scattering was subtracted from the sample scattering. The data obtained for each sample were analysed using PRIMUS [66], merging scattering data at low angles with high angle data. The distance distribution function, $p(r)$, was obtained by indirect Fourier transform of the scattering intensity using GNOM [67]. A Guinier plot ($\ln I(s)$ vs s^2) was used to calculate the molecular weight at $I(0)$ and radius of gyration, R_g , of PyoL1. *Ab initio* models of the protein in solution were built using DAMMIF [68], averaged with DAMAVER [69] and overlaid with the available crystal structure using SUPCOMB [70].

Supporting Information

Figure S1 Sequence alignment of pyocin L1 and previously reported MMBL-like bacteriocins. Dark blue shading designates sequence identity, light blue designates chemically conserved residues. The three conserved MMBL sugar-binding motifs (N1, C1 and C2) and the partially conserved motif (N2) are boxed in red. (JPG)

Figure S2 Genetics of CPA biosynthesis in *P. aeruginosa*. (A) CPA operon, annotated with location of *P. aeruginosa* E2 tolerant mutant (M4 and M11) deletion and PAO1 transposon insertion mutants. (B) Summary of CPA biosynthetic pathway, showing function performed by genes, shown to induce pyocin L1 tolerance or resistance. (TIF)

Figure S3 ¹H-¹⁵N HSQC spectra of ¹⁵N-labelled pyocin L1 in presence (red) and absence (black) of 100 mM (A) D-rhamnose and (B) D-mannose, showing distinctive chemical shifts upon addition of associating sugars. Chemical shift changes specific to a small number of cross-peaks illustrates association of the sugars with a small subset of amino acids, which likely correspond to the residues within the binding sites. Analogous changes are observed for D-rhamnose and D-mannose titrations indicative that the same sites are binding both ligands. Greater shift magnitude is observed for D-rhamnose, indicative of a greater affinity towards this monosaccharide. Boxed regions include cross-peaks used for chemical shift perturbation analysis as shown in Figure 3. (TIF)

Figure S4 Small angle X-ray scattering of pyocin L1. (A) *Ab initio* model of pyocin L1 computed with DAMMIF overlaid with the crystal structure. (B) Guinier plot of scattering data indicates that the protein is monomeric in solution ($I(0)$ gives a molecular mass of 29.53 kDa) by extrapolation of scattering intensity to zero scattering angle. Radius of gyration is 2.72 nm, indicative of a folded, globular monomeric particle in solution. (TIF)

Figure S5 Coordination of D-rhamnose in C1, C2 and N2 binding sites of pyocin L1. (A) Stereo view of D-rhamnose coordination by binding site C1 (A), C2 (C) and N1 (E), from D-rhamnose soak data. Core binding motif residues (blue) and additional residues contributing to the pocket (white) are shown. Omit map density for D-rhamnose in binding site C1 (B), C2 (D), N1 (F) calculated by refinement of data from D-rhamnose soaked crystal with model built from unsoaked crystal. Density for all sites contoured to 0.15e/Å³. (TIF)

Figure S6 Putidacin L1 shows specificity for D-rhamnose, compared with D-mannose. (A) ITC isotherm of D-rhamnose (50 mM) titrated into putidacin L1 (0.1 mM). Weakly saturable heats are indicative of binding with modest affinity (Kd ~5–10 mM). (B) ITC isotherm of D-mannose (50 mM) titrated into putidacin L1 (0.1 mM). Binding is undetectable under reaction conditions. (TIF)

Figure S7 Putidacin L1 and pyocin L1 do not bind L-rhamnose. ITC isotherms of L-rhamnose (50 mM) titrated into putidacin L1 (A) and pyocin L1 (B) both at (0.1 mM). Binding is undetectable under these conditions. (TIF)

Table S1 Strains and plasmids used in this work. (PDF)

Text S1 References for supplementary information. (DOCX)

Acknowledgments

We thank Joseph Lam and Erin Anderson (University of Guelph) for kindly supplying an anti-CPA monoclonal antibody.

Author Contributions

Conceived and designed the experiments: DW LCM RG IJ. Performed the experiments: LCM RG IJ. Analyzed the data: DW LCM RG IJ NPT SK BS KIW AWR OB. Contributed reagents/materials/analysis tools: DW NPT SK BS. Wrote the paper: DW LCM RG IJ AWR KIW RJC JM TE SK NPT OB BS. Provided strains and genome sequences used in the study: NPT.

References

- Gorkiewicz G (2009) Nosocomial and antibiotic-associated diarrhoea caused by organisms other than *Clostridium difficile*. *International Journal of Antimicrobial Agents* 33: S37–S41.
- Carroll KC, Bartlett JG (2011) *Biology of Clostridium difficile: Implications for Epidemiology and Diagnosis*. *Annual Review of Microbiology* 65: 501–521.
- Manichanh C, Borrrel N, Casellas F, Guamer F (2012) The gut microbiota in IBD. *Nature Reviews Gastroenterology & Hepatology* 9: 599–608.
- Qin J, Li Y, Cai Z, Li S, Zhu J, et al. (2012) A metagenome-wide association study of gut microbiota in type 2 diabetes. *Nature* 490: 55–60.
- Henaoui-Mejia J, Elinav E, Jin C, Hao L, Mehal WZ, et al. (2012) Inflammation-mediated dysbiosis regulates progression of NAFLD and obesity. *Nature* 482: 179–U167.
- Scher JU, Abramson SB (2011) The microbiome and rheumatoid arthritis. *Nature Reviews Rheumatology* 7: 569–578.
- Hviid A, Svanstrom H, Frisch M (2011) Antibiotic use and inflammatory bowel diseases in childhood. *Gut* 60: 49–54.
- Shaw SY, Blanchard JF, Bernstein CN (2011) Association Between the Use of Antibiotics and New Diagnoses of Crohn's Disease and Ulcerative Colitis. *American Journal of Gastroenterology* 106: 2133–2142.
- Spehlmann ME, Begun AZ, Saroglou E, Hinrichs F, Tiemann U, et al. (2012) Risk factors in German twins with inflammatory bowel disease: Results of a questionnaire-based survey. *Journal of Crohns & Colitis* 6: 29–42.
- Grinter R, Milner J, Walker D (2012) Ferredoxin containing bacteriocins suggest a novel mechanism of iron uptake in *Pectobacterium* spp. *PLoS ONE* 7: e33033.
- Grinter R, Roszak AW, Cogdell RJ, Milner JJ, Walker D (2012) The Crystal Structure of the Lipid II-degrading Bacteriocin Syringacin M Suggests Unexpected Evolutionary Relationships between Colicin M-like Bacteriocins. *Journal of Biological Chemistry* 287: 38876–38888.
- Cascales E, Buchanan SK, Duché D, Kleanthous C, Llobès R, et al. (2007) Colicin biology. *Microbiology and Molecular Biology Reviews* 71: 158–229.
- Michel-Briand Y, Baysse C (2002) The pyocins of *Pseudomonas aeruginosa*. *Biochimie* 84: 499–510.
- Walker D, Moshbahi K, Vankemmelbeke M, James R, Kleanthous C (2007) The role of electrostatics in colicin nuclease domain translocation into bacterial cells. *Journal of Biological Chemistry* 282: 31389–31397.
- Ogawa T, Tomita K, Ueda T, Watanabe K, Uozumi T, et al. (1999) A cytotoxic ribonuclease targeting specific transfer RNA anticodons. *Science* 283: 2097–2100.
- Ng CL, Lang K, Meenan NAG, Sharma A, Kelley AC, et al. (2010) Structural basis for 16S ribosomal RNA cleavage by the cytotoxic domain of colicin E3. *Nature Structural & Molecular Biology* 17: 1241–.
- Zeth K, Roemer C, Patzer SI, Braun V (2008) Crystal structure of colicin M, a novel phosphatase specifically imported by *Escherichia coli*. *Journal of Biological Chemistry* 283: 25324–25331.
- Graham AC, Stocker BAD (1977) GENETICS OF SENSITIVITY OF SALMONELLA SPECIES TO COLICIN-M AND BACTERIOPHAGES T5 T1, AND ES18. *Journal of Bacteriology* 130: 1214–1223.
- Kurisu G, Zakharov SD, Zhalnina MV, Bano S, Eroukova VY, et al. (2003) The structure of BtuB with bound colicin E3 R-domain implies a translocon. *Nature Structural Biology* 10: 948–954.
- Smith K, Martin L, Rinaldi A, Rajendran R, Ramage G, et al. (2012) Activity of Pyocin S2 against *Pseudomonas aeruginosa* Biofilms. *Antimicrobial Agents and Chemotherapy* 56: 1599–1601.
- Brown CL, Smith K, McCaughey L, Walker D (2012) Colicin-like bacteriocins as novel therapeutic agents for the treatment of chronic biofilm-mediated infection. *Biochemical Society Transactions* 40: 1549–1552.
- Lyczak JB, Cannon CL, Pier GB (2002) Lung Infections Associated with Cystic Fibrosis. *Clinical Microbiology Reviews* 15: 194–222.
- Ghequire MGK, Garcia-Pino A, Lebbe EKM, Spaepen S, Loris R, et al. (2013) Structural Determinants for Activity and Specificity of the Bacterial Toxin LlpA. *PLoS pathogens* 9: e1003199–e1003199.
- Ghequire MGK, Li W, Proost P, Loris R, De Mot R (2012) Plant lectin-like antibacterial proteins from phytopathogens *Pseudomonas syringae* and *Xanthomonas citri*. *Environmental Microbiology Reports* 4: 373–380.
- Ghequire MGK, Loris R, De Mot R (2012) MMBL proteins: from lectin to bacteriocin. *Biochemical Society Transactions* 40: 1553–U1433.
- Parret AHA, Schoofs G, Proost P, De Mot R (2003) Plant lectin-like bacteriocin from a rhizosphere-colonizing *Pseudomonas* isolate. *Journal of Bacteriology* 185: 897–908.
- Parret AHA, Temmerman K, De Mot R (2005) Novel lectin-like bacteriocins of biocontrol strain *Pseudomonas fluorescens* PF-5. *Applied and Environmental Microbiology* 71: 5197–5207.
- Sharon N (2001) *Lectins*. eLS: John Wiley & Sons, Ltd.
- Sharon N, Lis H (2004) History of lectins: from hemagglutinins to biological recognition molecules. *Glycobiology* 14: 53R–62R.
- Van Damme EJM, Nakamura-Tsuruta S, Smith DF, Ongenaert M, Winter HC, et al. (2007) Phylogenetic and specificity studies of two-domain GNA-related lectins: generation of multispecificity through domain duplication and divergent evolution. *Biochemical Journal* 404: 51–61.
- Chandra NR, Ramachandiraiah G, Bachhawat K, Dam TK, Suroliya A, et al. (1999) Crystal structure of a dimeric mannose-specific agglutinin from garlic: Quaternary association and carbohydrate specificity. *Journal of Molecular Biology* 285: 1157–1168.
- Vasta GR, Nita-Lazar M, Giomarelli B, Ahmed H, Du S, et al. (2011) Structural and functional diversity of the lectin repertoire in teleost fish: Relevance to innate and adaptive immunity. *Developmental and Comparative Immunology* 35: 1388–1399.
- Kurimoto E, Suzuki M, Amemiya E, Yamaguchi Y, Nirasawa S, et al. (2007) Curculin Exhibits Sweet-tasting and Taste-modifying Activities through Its Distinct Molecular Surfaces. *Journal of Biological Chemistry* 282: 33252–33256.
- Shimokawa H, Fukudome A, Yamashita R, Minami Y, Yagi F, et al. (2012) Characterization and cloning of GNA-like lectin from the mushroom *Marasmius oreades*. *Glycoconjugate Journal* 29: 457–465.
- Hester G, Wright CS (1996) The Mannose-specific bulb lectin from *Galanthus nivalis* (snowdrop) binds mono- and dimannosides at distinct sites. Structure analysis of refined complexes at 2.3 angstrom and 3.0 angstrom resolution. *Journal of Molecular Biology* 262: 516–531.
- Fyfe JAM, Harris G, Govan JRW (1984) Revised Pyocin Typing Method For *Pseudomonas-Aeruginosa*. *Journal of Clinical Microbiology* 20: 47–50.
- Rochetta HL, Burrows LL, Pacan JC, Lam JS (1998) Three rhamnosyl-transferases responsible for assembly of the A-band D-rhamnan polysaccharide in *Pseudomonas aeruginosa*: a fourth transferase, WbpL, is required for the initiation of both A-band and B-band lipopolysaccharide synthesis. *Molecular Microbiology* 30: 1131–1131.
- Lam JS, Taylor VL, Islam ST, Hao Y, Kocincova D (2011) Genetic and Functional Diversity of *Pseudomonas aeruginosa* Lipopolysaccharide. *Frontiers in microbiology* 2: 118–118.
- Hao Y, King JD, Huszczyński S, Kocincova D, Lam JS (2013) Five New Genes Are Important for Common Polysaccharide Antigen Biosynthesis in *Pseudomonas aeruginosa*. *Mbio* 4.
- Jacobs MA, Alwood A, Thaipisuttikul I, Spencer D, Haugen E, et al. (2003) Comprehensive transposon mutant library of *Pseudomonas aeruginosa*. *Proceedings of the National Academy of Sciences of the United States of America* 100: 14339–14344.
- Holm L, Rosenström P (2010) Dali server: conservation mapping in 3D. *Nucleic Acids Research* 38: W545–W549.
- Ovod V, Rudolph K, Knirel Y, Krohn K (1996) Immunochemical characterization of O polysaccharides composing the alpha-D-rhamnose backbone of lipopolysaccharide of *Pseudomonas syringae* and classification of bacteria into serogroups O1 and O2 with monoclonal antibodies. *Journal of Bacteriology* 178: 6459–6465.
- Ovod VV, Knirel YA, Samson R, Krohn KJ (1999) Immunochemical characterization and taxonomic evaluation of the O polysaccharides of the lipopolysaccharides of *Pseudomonas syringae* serogroup O1 strains. *Journal of Bacteriology* 181: 6937–6947.
- Kleanthous C (2010) Swimming against the tide: progress and challenges in our understanding of colicin translocation. *Nature Reviews Microbiology* 8: 843–848.
- Abdel-Mawgoud AM, Lepine F, Deziel E (2010) Rhamnolipids: diversity of structures, microbial origins and roles. *Applied Microbiology and Biotechnology* 86: 1323–1336.
- Caffall KH, Mohnen D (2009) The structure, function, and biosynthesis of plant cell wall pectic polysaccharides. *Carbohydrate Research* 344: 1879–1900.
- Knirel YA, Shashkov AS, Senchenkova S, Ajiki Y, Fukuoka S (2002) Structure of the O-polysaccharide of *Pseudomonas putida* FERM p-18867. *Carbohydrate Research* 337: 1589–1591.
- Molinario A, Silipo A, Lanzetta R, Newman MA, Dow JM, et al. (2003) Structural elucidation of the O-chain of the lipopolysaccharide from *Xanthomonas campestris* strain 8004. *Carbohydrate Research* 338: 277–281.
- Vinon-Dubiel AD, Goldberg JB (2003) Lipopolysaccharide of *Burkholderia cepacia* complex. *Journal of Endotoxin Research* 9: 201–213.
- Stewart L, Ford A, Sangal V, Jeukens J, Boyle B, et al. (2013) Draft genomes of twelve host adapted and environmental isolates of *Pseudomonas aeruginosa* and their position in the core genome phylogeny. *Pathogens and Disease* [epub ahead of print]
- Claesson MJ, Wang Q, O'Sullivan O, Greene-Diniz R, Cole JR, et al. (2010) Comparison of two next-generation sequencing technologies for resolving highly complex microbiota composition using tandem variable 16S rRNA gene regions. *Nucleic Acids Research* 38.
- Ramm M, Lobe M, Hamburger M (2003) A simple method for preparation of D-rhamnose. *Carbohydrate Research* 338: 109–112.
- Rivera M, Bryan LE, Hancock REW, McGroarty EJ (1988) Heterogeneity Of Lipopolysaccharides From *Pseudomonas-Aeruginosa* - Analysis Of Lipopolysaccharide Chain-Length. *Journal of Bacteriology* 170: 512–521.
- Mori S, Abeynawardana C, Johnson MO, vanZijl P (1996) Improved sensitivity of HSQC spectra of exchanging protons at short interscan delays using a new fast HSQC (FHSQC) detection scheme that avoids water saturation (vol 108, pg 94, 1995). *Journal of Magnetic Resonance Series B* 110: 321–321.
- Vranken WF, Boucher W, Stevens TJ, Fogh RH, Pajon A, et al. (2005) The CCPN data model for NMR spectroscopy: Development of a software pipeline. *Proteins-Structure Function and Bioinformatics* 59: 687–696.

56. Gorrec F (2009) The MORPHEUS protein crystallization screen. *Journal of Applied Crystallography* 42: 1035–1042.
57. Incardona M-F, Bourenkov GP, Levik K, Pieritz RA, Popov AN, et al. (2009) EDNA: a framework for plugin-based applications applied to X-ray experiment online data analysis. *Journal of Synchrotron Radiation* 16: 872–879.
58. Long F, Vagin AA, Young P, Murshudov GN (2008) BALBES: a molecular-replacement pipeline. *Acta Crystallographica Section D-Biological Crystallography* 64: 125–132.
59. Adams PD, Afonine PV, Bunkoczi G, Chen VB, Davis IW, et al. (2010) PHENIX: a comprehensive Python-based system for macromolecular structure solution. *Acta Crystallographica Section D-Biological Crystallography* 66: 213–221.
60. Emsley P, Lohkamp B, Scott WG, Cowtan K (2010) Features and development of Coot. *Acta Crystallographica Section D-Biological Crystallography* 66: 486–501.
61. Murshudov GN, Skubak P, Lebedev AA, Pannu NS, Steiner RA, et al. (2011) REFMAC5 for the refinement of macromolecular crystal structures. *Acta Crystallographica Section D-Biological Crystallography* 67: 355–367.
62. Chen VB, Arendall WB, III, Headd JJ, Keedy DA, Immormino RM, et al. (2010) MolProbity: all-atom structure validation for macromolecular crystallography. *Acta Crystallographica Section D-Biological Crystallography* 66: 12–21.
63. Laskowski RA, MacArthur MW, Moss DS, Thornton JM (1993) PROCHECK - A program to check the stereochemical quality of protein structures. *Journal of Applied Crystallography* 26: 283–291.
64. McCoy AJ, Grosse-Kunstleve RW, Adams PD, Winn MD, Storoni LC, et al. (2007) Phaser crystallographic software. *Journal of Applied Crystallography* 40: 658–674.
65. Schuttelkopf AW, van Aalten DMF (2004) PRODRG: a tool for high-throughput crystallography of protein-ligand complexes. *Acta Crystallographica Section D-Biological Crystallography* 60: 1355–1363.
66. Konarev PV, Volkov VV, Sokolova AV, Koch MHJ, Svergun DI (2003) PRIMUS: a Windows PC-based system for small-angle scattering data analysis. *Journal of Applied Crystallography* 36: 1277–1282.
67. Svergun DI (1992) Determination Of The Regularization Parameter In Indirect-Transform Methods Using Perceptual Criteria. *Journal of Applied Crystallography* 25: 495–503.
68. Franke D, Svergun DI (2009) DAMMIF, a program for rapid ab-initio shape determination in small-angle scattering. *Journal of Applied Crystallography* 42: 342–346.
69. Volkov VV, Svergun DI (2003) Uniqueness of ab initio shape determination in small-angle scattering. *Journal of Applied Crystallography* 36: 860–864.
70. Kozin MB, Svergun DI (2001) Automated matching of high- and low-resolution structural models. *Journal of Applied Crystallography* 34: 33–41.